



**Geology and Genesis of Dounan Manganese
Deposits, Yunnan Province, P. R. China**

Baohong Hou, M. Sc
Department of Geology and Geophysics
The University of Adelaide
Adelaide, South Australia
Australia 5005



October 1993

A thesis submitted to the University of Adelaide in the fulfilment
of the requirements for the degree of Doctor of Philosophy

Awarded 1994

Contents

Page

Lists of Figures	IX
Lists of Tables	XII
Lists of Photographs	XIII
Abstract	XVII
Statement	XVIII
Acknowledgments	XIX

Chapter 1. General Introduction

1.1 Aims of the Project.....	1
1.2 Geologic Setting.....	2
1.2.1 Introduction.....	2
1.2.2 Regional Tectonics and Stratigraphy.....	2
1.2.3 Igneous Rocks.....	5
1.2.4 Geologic Evolution and Mineralization Period of Southeastern Yunnan.....	8
1.3 Previous Work.....	9
1.4 Terminology of Dounan Mn Ores and Rocks.....	10
1.5 Methods of Study.....	12
1.5.1 Scope and Method of Treatment.....	12
1.5.2 Selected Areas for Study.....	13
1.6 Thesis Layout.....	14

PART I. SEDIMENTARY SEQUENCES AND ENVIRONMENTS**Chapter 2. Stratigraphy**

2.1 Introduction.....	15
2.2 Sampling Locations.....	17
2.3 Regional Structure.....	17
2.4 Regional Stratigraphy, Facies and Microfacies of Southeastern Yunnan.....	21
2.4.1 Baixian Section.....	22
2.4.2 Jiasha Section.....	22
2.4.3 Bapanzai Section.....	25
2.4.4 Yanzijao Section.....	26
2.4.5 Dounan Section.....	29
2.4.6 Laowu Section.....	29
2.4.7 Xinzhuangke Section.....	31
2.4.8 Shiwang Section.....	32
2.4.9 Yangqigou Section.....	33
2.5 Local (Dounan) Stratigraphy, Facies and Microfacies.....	33
2.5.1 Introduction.....	33
2.5.2 Stratigraphy.....	36
2.5.3 Dounan Facies Sequence and Model (Markov Chain) Analysis.....	39
2.5.4 Detailed Stratigraphy of Mn-bearing Series.....	42
2.5.4.1 Upper Ore-bearing Series (T ₂ f ₅₋₂).....	42
2.5.4.2 Lower Ore-bearing Series (T ₂ f ₄₋₁).....	45
2.5.5 Paleontology.....	46
2.5.5.1 Relationship between Fossils and Ores.....	46

	Page
2.5.5.2	Features of Fossils.....46
2.5.5.3	Distribution of Fossils.....48
2.5.6	Sedimentary Cycles, Microfacies and Environments.....49
2.5.6.1	Vertical Variation.....49
2.5.6.2	Sedimentary Environments of Mn-bearing Serie.....52
2.6	Stratigraphic Correlation of Falang Formation.....55
2.6.1	Regional Stratigraphic Correlation.....55
2.6.2	Local (Dounan Area) Stratigraphic Correlation.....59
2.7	Lithofacies-Paleogeographic Environment of Falang Formation.....59
2.7.1	Environmental Analysis.....59
2.7.1.1	Depositional Environments and Lithofacies.....59
2.7.1.2	Transgressive/Regressive Models of the Dounan Sequence.....64
2.7.2	Lithofacies-Paleogeography.....65
2.8	Discussion.....67

Chapter 3. Orebeds

3.1	Introduction.....69
3.2	Distribution of Dounan Orebeds.....70
3.2.1	Gake Area.....70
3.2.2	Kata Area.....72
3.2.3	Daaozi Area.....74
3.2.4	Baigu Area.....75
3.2.5	Milike Area.....79
3.3	Features of Orebeds.....79
3.3.1	Mode of Occurrence, Morphology and Scale of Orebodies.....80
3.3.2	Chemical Features of Orebeds.....80
3.3.3	Hangingwall, Footwall.....80
3.4	Correlation of Orebeds.....84
3.4.1	Correlation of Lower Orebeds, T2f4-1 Mn-bearing Series.....85
3.4.2	Correlation of Upper Orebeds, T2f5-2 Mn-bearing Series.....86
3.5	Paleotectonics and Sedimentation of Orebeds.....88
3.5.1	Sedimentary Center Migration of Manganese Orebeds.....88
3.5.2	Relationship between Paleotectonics and Mineralization.....90
3.6	Discussion.....90

PART II. ROCKS AND ORES

Chapter 4. Petrology and Mineralogy

4.1	Introduction.....92
4.2	Description of Samples.....93
4.2.1	Primary Manganese Ores.....93
4.2.1.1	Manganese Oxide Ores.....93
4.2.1.2	Manganese Carbonate Ores.....96
4.2.1.3	Transitional / Mixed Type (Unsorted Manganese Oxide) Ores.....98
4.2.2	Supergene Oxidized Ores.....99
4.2.3	Alternative Classification and Reserves.....101
4.2.4	Rocks.....103
4.2.4.1	Micrite or Mn-bearing Micrite (Oolitic/Pisolitic).....103
4.2.4.2	Intramicrodite/Intrasparite (Brecciated/Intraclastic).....103
4.2.4.3	Calcarenite.....104

	Page
4.2.4.4 Calcilutite	104
4.2.4.5 Silty Claystone	104
4.2.4.6 Siltstone / Clayey Siltstone	105
4.2.4.7 Sandstone	105
4.2.4.8 Conglomerate	105
4.2.5 Summary	105
4.3 Textural and Structural Features of Ores and Rocks	107
4.3.1 Texture	107
4.3.2 Structure	110
4.3.3 Cathodoluminescence (CL)	112
4.3.4 Scanning Electron Microscopy (SEM)	114
4.3.5 Discussion	115
4.4 Mineralogy	117
4.4.1 X-Ray Diffraction (XRD)	118
4.4.2 Description of Minerals	125
4.4.2.1 Braunite	126
4.4.2.2 Manganite	128
4.4.2.3 Calciorhodochrosite	128
4.4.2.4 Mn-calcite/Mn-bearing Calcite	129
4.4.2.5 Supergene Oxidized Minerals	129
4.4.2.6 Gangue Minerals	131
4.5 Ore Phases	132
4.5.1 Conception and General Features	132
4.5.2 Primary Ore Phases	132
4.5.2.1 Microphases of Ores	132
4.5.2.2 Vertical Variation of Ore Phases	135
4.5.2.3 Horizontal Distribution of Ore Phases	137
4.5.3 Supergene Oxidized Ore Phases	139
4.6 Discussion	139
Chapter 5. Geochemistry	
5.1 Introduction	143
5.2 Chemical Characterization of Ores and Rocks	144
5.2.1 Inter-Element Correlations	144
5.2.2 Bulk Composition of Ores and Rocks	147
5.2.2.1 Major and Minor Elements	147
5.2.2.2 Trace Elements	152
5.2.2.3 Rare Earth Elements (REE)	156
5.2.3 Shale-normalized REE-Patterns	163
5.2.4 Electron Microprobe Analysis (EMPA)	164
5.2.5 Isotopic Characteristics of Ores and Rocks	170
5.2.5.1 Introduction	170
5.2.5.2 Sample Selection	171
5.2.5.3 Isotopic Features	171
5.3 Discussion	173
5.3.1 Relationships between Trace Elements and REEs in Different Materials	173
5.3.2 Vertical Variation of Rare Earth Elements	177
5.3.3 Comparison of REE Patterns from Dounan with Other Mn (Oxide) Deposits	179
5.3.4 Application of Isotopic Analysis	182

Chapter 6. Genesis of the Manganese Deposit

6.1	Introduction	190
6.2	Evidence of Sedimentary and Diagenetic Activity	191
6.2.1	Paleotectonics and Paleogeomorphology	192
6.2.1.1	Regional Tectonic Position and Features of Dounan Area	192
6.2.1.2	Features of Dounan Marine Basin (Dounan-Yanzijiao-Laowu)	192
6.2.1.3	Mn Formation Controls of Paleotectonics and Paleogeomorphology	193
6.2.2	Stratigraphic and Textural Features	193
6.2.2.1	Relations between Orebodies and Enclosing Rocks	193
6.2.2.2	Information on the Primary Sedimentary Origin of Mn Ores	195
6.2.2.3	Variation in Diagenetic Effects	196
6.2.3	Lithofacies-Paleogeographic Conditions	196
6.2.3.1	Relationship between Lithofacies and Mn Deposition	196
6.2.3.2	Lithofacies of Mn-bearing Series	196
6.2.3.3	Paleogeographic Evolution of Mn-bearing Series	197
6.2.3.4	Lithofacies-Paleogeographic Control to the Mn Deposits	197
6.2.3.5	Evolution of Mn Sedimentary Basin and Mn-bearing Series	197
6.2.4	Paleoclimate	198
6.2.5	Environmental Conditions of Mn Mineralization	203
6.2.5.1	Mineral and Rock Indicators	203
6.2.5.2	Relations between Ore Phases	203
6.2.5.3	Primary Fabric Indicators	204
6.2.5.4	Diagenetic Fabric Indicators	204
6.2.5.5	Eh-pH Relations of Manganese Formation	205
6.2.5.6	Redox Interface Controls on Precipitation Environments	205
6.2.6	Biological Activity	206
6.2.6.1	Biological Influences on the Mn Environments	206
6.2.6.2	Environments of Dounan Oncolites and Stromatolites	207
6.2.6.3	Influence of Biological Activity on Mn Mineralization	207
6.2.6.4	Biological Mineralization in Diagenesis	207
6.2.7	Geochemical Conditions	208
6.2.7.1	General Geochemical Natures of Manganese	208
6.2.7.2	Geochemistry of Manganese during Sedimentation	208
6.2.7.3	Relations between Manganese and Other Major or Minor Elements	209
6.2.7.4	REE Evidence of Mn Mineralization	210
6.2.7.5	Isotopic Evidence of Mn Mineralization	211
6.2.7.6	Diagenetic Variations	212
6.3	Source Materials and Weathering Processes	213
6.3.1	Source of Gangues	213
6.3.2	Source of Manganese	214
6.3.3	Weathering Processes	215
6.4	Transport Processes	216
6.4.1	Transport of Detrital Sediments	216
6.4.2	Transport of Carbonate Materials	217
6.4.3	Transport of Manganese	217
6.5	Sedimentation Processes	220
6.5.1	Precipitation of Mn Oxide Minerals	222
6.5.2	Precipitation of Mn Carbonate Minerals	223
6.5.3	Precipitation of Transitional (or Mixing) Mn Ores	225
6.5.4	Precipitation of Gangues	226
6.5.5	Growth Rate and Environment of Mn Ooliths/Pisoliths	226
6.5.6	Hydrodynamic Conditions of Forming Mn Ooliths/Pisoliths	227
6.5.7	Biological Influences on the Precipitation of Mn Ooliths/Pisoliths	228
6.5.8	Depositional Mechanism of Ore Phases	230
6.6	Remobilization Processes and Secondary Enrichment in Diagenesis	231
6.6.1	Dissolution of Quartz and Calcite	233
6.6.1.1	Thermodynamics of the Si-H ₂ O System	233

	Page
6.6.1.2 Thermodynamics of the Ca-CO ₂ -H ₂ O System.....	234
6.6.2 Dissolution of Manganese Oxides.....	234
6.6.2.1 Alteration of Braunite.....	235
6.6.2.2 Redox Reactions between Carbonate Phases and Manganese Oxides.....	235
6.6.3 Dissolution of Manganese Carbonates.....	236
6.6.4 Biological Activity.....	237
6.6.5 Pressure Solution.....	237
6.7 Transport of Dissolved Manganese in Porewater.....	238
6.8 Fixation Processes During Diagenesis.....	240
6.8.1 Reprecipitation of Si- and Ca-minerals.....	241
6.8.2 Reprecipitation of Mn Minerals.....	242
6.8.2.1 Reprecipitation of Mn During Redox Reaction between Mn Oxides and Carbonates.....	242
6.8.2.2 Reprecipitation of Mn as Oxides.....	242
6.8.2.3 Reprecipitation of Mn as Carbonates.....	243
6.8.2.4 Microbial Influences on Mn Reprecipitation.....	243
6.8.2.5 Reprecipitate Dependency upon Mineralogy of Substrate Rocks.....	244
6.9 Discussion.....	245
6.9.1 Discussion of Mn Sedimentation.....	245
6.9.1.1 The Influence of Ocean Chemistry on Ore Formation.....	246
6.9.1.2 Sea Level Influence on Ore Formation.....	248
6.9.1.3 Paleoclimatic Influence on Ore Formation.....	248
6.9.2 Mn Secondary Enrichment in Diagenesis.....	249
6.9.3 Interaction of Processes.....	251
6.9.4 Genetic Overview of Dounan Braunite.....	252
Chapter 7. The Mineralization Model	
7.1 Introduction.....	258
7.2 Primary and Secondary Evolutions of Dounan Ores and Rocks.....	258
7.2.1 Sedimentary Development of Primary Ores and Rocks.....	258
7.2.2 Cyclic Mobility of Diagenetic Products.....	260
7.3 The Profil of Mineralization.....	262
7.4 The Model of Mineralization.....	266
7.5 Review of Sedimentary and Diagenetically Influenced Mn-Deposits.....	268
7.5.1 Nikopol, Ukraine and Chiatura, Georgia.....	269
7.5.2 Groote Eylandt, Australia.....	270
7.5.3 Molango, Mexico.....	271
7.5.4 úrkút/Eplény, Hungary.....	272
7.5.5 Braunite Mn Deposits of India, West and North Africa, Former USSR and Brazil.....	272
7.5.6 Manganese Group of Western Australia.....	273
7.5.7 General Comparison of Sedimentary-Diagenetic Products in Different Areas.....	274
7.6 Discussion.....	275
Chapter 8. Résumé and Conclusions.....	277
References.....	280

	Page
Appendix I. (Methods)*	
I.1 Sampling Technique.....	A I. - 1
I.2 Equipment and Sample Preparation.....	A I. - 1
I.3 Rock and Ore Analyses.....	A I. - 2
I.3.1 X-Ray Fluorescence (XRF).....	A I. - 2
I.3.1.1 Analytical Background.....	A I. - 2
I.3.1.2 Equipment.....	A I. - 2
I.3.1.3 Sample Preparation for Pressed Powder Buttons.....	A I. - 2
I.3.1.4 Sample Preparation for Fusion Beads.....	A I. - 2
I.3.2 X-Ray Diffraction (XRD).....	A I. - 3
I.3.2.1 Analytical Background.....	A I. - 3
I.3.2.2 Equipment and Sample Preparation.....	A I. - 3
I.3.3 Wet Chemical Analyses.....	A I. - 4
I.3.4 Geochemical Environmental Index.....	A I. - 4
I.3.5 Scanning Electron Microscopy (SEM).....	A I. - 4
I.3.5.1 Analytical Background.....	A I. - 4
I.3.5.2 Equipment and Method.....	A I. - 4
I.3.5.3 Sample Preparation.....	A I. - 5
I.3.6 Electron Microprobe Analyses (EMPA).....	A I. - 5
I.3.6.1 Analytical Background.....	A I. - 5
I.3.6.2 Equipment and Method.....	A I. - 5
I.3.6.3 Sample Preparation.....	A I. - 5
I.3.7 Cathodoluminescence (CL).....	A I. - 6
I.3.7.1 Analytical Background.....	A I. - 6
I.3.7.2 Equipment and Method.....	A I. - 6
I.3.7.3 Sample Preparation.....	A I. - 6
I.3.8 Isotope Analyses.....	A I. - 7
I.3.8.1 Analytical Background.....	A I. - 7
I.3.8.2 Sample Preparation and Equipment.....	A I. - 7
I.3.9 REE Analyses by Isotope Dilution (IDA) (REEs).....	A I. - 8
I.3.9.1 Analytical Background.....	A I. - 8
I.3.9.2 Equipment.....	A I. - 9
I.3.9.3 Sample Preparation or Experimental Procedures.....	A I. - 9
 Appendix II. (Stratigraphy)	
II.1 Sample Localities, Sampling Position in Vertical Section; Grainsize.....	A II. - 1
II.2 Geochemical Environmental Index of Dounan Stratigraphy.....	A II. - 5
 Appendix III. (Orebeds)	
III.1 Scale, Morphology and Occurrence of Minor Orebodies.....	A III. - 1
 Appendix IV. (Petrology and Mineralogy)	
IV.1 Ore and Rock Types.....	A IV. - 1

* The Appendix number corresponds to the respective chapter.

Appendix V. (Geochemistry)

V.1	XRF/AA Major and Minor Element Analyses of Ores and Rocks; [%]... A V. - 1
V.2	XRF Trace Element Analyses of Ores and Rocks; [ppm] A V. - 3
V.3	IDMS Rare Earth Element Analyses of Ores and Rocks; [ppm]..... A V. - 4
V.4	Electron Microprobe Analysis (EMPA); [%]..... A V. - 5
V.5	Stable Isotope Composition of Ores and Rocks; [PDB].....A V. - 14

List of Figures

Fig.1.1	Location of Dounan Mn deposits, Yunnan Province, China.....	3
Fig.1.2	Geotectonic sketch map of southeast of Yunnan, China.....	4
Fig.1.3	Geology and manganese distribution in southeastern Yunnan, China.....	6
Fig.1.4	Geological sketch map of the Dounan area.....	7
Fig.2.1	Structural sketch map of the Dounan area.....	18
Fig.2.2	Geological section along prospecting line 56, Dounan Mn mine.....	19
Fig.2.3	Geological section along prospecting line 17, Dounan Mn mine.....	19
Fig.2.4	Geological map of Dounan Mn mine area in the Dounan syncline.....	20
Fig.2.5	Stratigraphic section of Falang Formation, at Baixian.....	23
Fig.2.6	Stratigraphic and facies profile of Falang Formation, at Baixian.....	24
Fig.2.7	Stratigraphic and facies profile of Falang Formation, at Jiasha.....	25
Fig.2.8	Stratigraphic and facies profile of Falang Formation, at Bapanzai.....	26
Fig.2.9	Stratigraphic and facies profile of Falang Formation, at Yanzijiao.....	28
Fig.2.10	Stratigraphic and facies profile of Falang Formation, at Laowu.....	29
Fig.2.11	Stratigraphic and facies profile of Falang Formation, at Xinzuangke.....	31
Fig.2.12	Stratigraphic and facies profile of Falang Formation, at Shiwang.....	32
Fig.2.13	Sedimentary facies and environment, Falang stage of Mid-Triassic, at Dounan.....	35
Fig.2.14	Facies relationship diagram of Dounan: Markov Chain.....	41
Fig.2.15	Sedimentary facies model of Falang Formation at Dounan.....	41
Fig.2.16	Stratigraphic profile of Mn-bearing series of Falang Formation at Dounan.....	43
Fig.2.17	Fe ³⁺ , Fe ²⁺ , Fe ³⁺ /Fe ²⁺ and organic C variations of Falang Formation.....	50
Fig.2.18	Sedimentary environments of Lower ore-bearing series.....	53
Fig.2.19	Detailed geological profiles of orebodies V ₁₋₁ and between V ₁ and V ₂	54
Fig.2.20	Sedimentary environments of Upper ore-bearing series.....	56
Fig.2.21	Correlation of Falang Formation, southeastern Yunnan.....	57
Fig.2.22	Correlation of Falang Formation stratigraphy of Dounan area.....	60
Fig.2.23	Block diagrams of Dounan sedimentary environment and model.....	61
Fig.2.24	Sedimentary facies sketch map of Falang stage, southeastern Yunnan.....	62
Fig.2.25	Lithofacies palaeogeographic map and section of Falang stage, southeastern Yunnan.....	63
Fig.3.1	Vertical geologic profile of Lower ore-bearing series, Gake area.....	71
Fig.3.2	Vertical geologic profile of Lower ore-bearing series, Kata area.....	73
Fig.3.3	Vertical geologic profile of Lower ore-bearing series, Daaози area.....	75
Fig.3.4	Vertical geologic profile of Upper ore-bearing series, Baigu area.....	76
Fig.3.5	Vertical geologic profile of orebeds V ₄ and V ₅ , Baigu area.....	77
Fig.3.6	Vertical geologic profile of orebeds V ₈ and V ₉ , Baigu area.....	78
Fig.3.7	Vertical geologic profile of Lower ore-bearing series, Milike area.....	79
Fig.3.8	Variation between the thickness and Mn content of Dounan orebodies.....	82
Fig.3.9	Relationship between manganese and phosphorus.....	83
Fig.3.10	Correlation diagram V ₁ ore horizons and related beds in the Gake area.....	86
Fig.3.11	Stratigraphic column showing regular intervals between orebeds.....	87
Fig.3.12	Correlation diagram showing stratigraphic positions of V ₇ Mn horizons.....	87
Fig.3.13	Correlation diagram showing stratigraphic positions of V ₈ & V ₉ Mn horizons.....	88
Fig.3.14	Mn metallometric percentage hypsometric curves.....	89
Fig.4.1a	X-ray Diffraction patterns of Mn oxide ores.....	121
Fig.4.1b	X-ray Diffraction patterns of Mn carbonate and unsorted or banded ores.....	122
Fig.4.1c	X-ray Diffraction patterns of rocks associated with Mn ores.....	123
Fig.4.2	Distribution of ore phases of Dounan main orebeds.....	133
Fig.4.3	Distribution and cross sections of ore phases of Dounan orebed V ₈	134
Fig.4.4	Vertical profile of orebed V ₁ , drill hole CK556, Gake area.....	136
Fig.4.5	Vertical profile of orebed V ₈ , drill hole CK2501, Baigu area.....	136
Fig.4.6	Paragenetic sequence of Mn oxide and carbonate and gangue minerals of Dounan ores.....	141

	Page
Fig.5.1	Correlations of components in Dounan ores and rocks.....146
Fig.5.1a	Correlation of Mn and CaO in ores and rocks.
Fig.5.1b	Correlation of CaO and Fe ₂ O ₃ T in ores and rocks.
Fig.5.1c	Correlation of Mn and Ni in ores and rocks.
Fig.5.1d	Correlation of Ni and U in ores and rocks.
Fig.5.1e	Correlation of Mn and SiO ₂ in ores and rocks.
Fig.5.1f	Correlation of Al ₂ O ₃ and TiO ₂ in ores and rocks.
Fig.5.2	Major and minor element concentrations in the Dounan ores and rocks.....151
Fig.5.2a	Major and minor element concentrations in Mn oxide ores.
Fig.5.2b	Major and minor element concentrations in transitional ores.
Fig.5.2c	Major and minor element concentrations in Mn carbonate ores.
Fig.5.2d	Major and minor element concentrations in Mn-bearing rocks.
Fig.5.3	Trace element concentrations in the Dounan ores and rocks.....155
Fig.5.3a	Trace element concentrations in Mn oxide ores.
Fig.5.3b	Trace element concentrations in transitional ores
Fig.5.3c	Trace element concentrations in Mn carbonate ores.
Fig.5.3d	Trace element concentrations in Mn-bearing hosted rocks.
Fig.5.3e	Trace element range of all samples of manganese ores.
Fig.5.3f	Trace element range of all samples, concentrations in Mn-bearing rocks.
Fig.5.4a	Mean REE concentration patterns of Mn oxides161
Fig.5.4b	Mean REE concentration patterns of Mn carbonate and unsorted ores.....161
Fig.5.5a	Scatter plot of total REE and calciorhodochrosite contents161
Fig.5.5b	Scatter plot of Mn minerals and La.....161
Fig.5.5c	Scatter plot of total REE and braunite contents161
Fig.5.5d	Scatter plot of calciorhodochrosite contents and La/Yb ratio.....161
Fig.5.5e	Scatter plot of braunite contents and La/Yb ratio.....161
Fig.5.5f	Scatter plot of Mn minerals and Eu-anomaly.....161
Fig.5.6	Scatter plot of Σ REE and Σ LREE/ Σ HREE162
Fig.5.7a	Shale-normalized REE-patterns of Mn oxides.....163
Fig.5.7b	Shale-normalized REE-patterns of Mn carbonate and unsorted ores163
Fig.5.8a	Distribution of elements in braunite; No.42.....169
Fig.5.8b	Distribution of elements in braunite; No.39.....169
Fig.5.8c	Distribution of elements in braunite; No.46.....169
Fig.5.8d	Distribution of elements in Mn-calcite; No.142.....169
Fig.5.8e	Distribution of elements in calciorhodochrosite; No.142.....169
Fig.5.9a	Distribution of minerals in calciorhodochrosite oolite; No.143169
Fig.5.9b	Distribution of minerals in braunite oolite; No.43169
Fig.5.10	Stratigraphic profile of Mn content and $\delta^{13}\text{C}$ values174
Fig.5.11	Scatter plot of Mn content versus $\delta^{13}\text{C}$ values175
Fig.5.12	REE concentration profiles in the Mn sediments178
Fig.5.13	a) La-Nd and La-Eu plots; b) La-Er and La-Yb plots as per (a).....178
Fig.5.14	Comparison of shale-normalized REE patterns of various manganese oxides.....180
Fig.5.15	Sources and isotopic composition of diagenetic CO ₂ in depth-related diagenetic zones184
Fig.5.16	Plot of oxygen isotope ratio against carbon isotope ratio.....185
Fig.5.17	Plot of calculated precipitation temperatures against carbon isotope ratio185
Fig.5.18	Oxygen-isotope composition, versus percentage of carbonate minerals.....187
Fig.6.1	Lithofacies-isopach map of Lower Mn-bearing series199
Fig.6.2	Lithofacies-isopach map of Upper Mn-bearing series200
Fig.6.3	Global paleogeography at some time in the Triassic Period.....202
Fig.6.4	Palaeogeography of the Middle Triassic of south China.....202
Fig.6.5	Manganese sedimentation in the coastal zone of intracratonic basin.....221
Fig.6.6	Field of stability of solids and solutes and solubility of manganese as functions of pH and redox potential at 25° C and one atm. in the system Mn-H ₂ O.....224
Fig.6.7	Eh-pH diagram for anhydrous Mn compounds at 25° C and 1 atm.....224
Fig.6.8	Field of stability of solids and solutes and solubility of manganese as functions of pH and redox potential at 25° C and 1 atm. in the system Mn-CO ₂ -H ₂ O.....224

	Page
Fig.6.9	Depositional mechanism sketch map of Dounan ore phases232
Fig.6.10	Relationships at a basin margin during marine transgression and regression247
Fig.7.1	Model of mobilization, transportation and precipitation paths for primary minerals in the weathering sedimentary environment of Dounan.....259
Fig.7.2	Model of remobilization and reprecipitation paths for dominant diagenetic minerals in the buried environment of Dounan261
Fig.7.3a	Idealized history of the Dounan Mn deposits263
Fig.7.3b	Detialed sections of Fig.7.3, IV264
Fig.7.4	Idealized model of mineralization through the Dounan manganese deposits267

List of Tables

Table 1.1	Stratigraphy of southeastern Yunnan.....	5
Table 1.2	Terminology for Dounan Mn ores and rocks, including sketches of the most common materials.....	11
Table 2.1	Stratigraphical legend for Dounan manganese ore deposits.....	16
Table 2.2	General stratigraphy of Dounan area.....	34
Table 2.3	Primary transition frequency	40
Table 2.4	Primary transition probability (P _{ij}).....	40
Table 2.5	Mean transition probability (R _{ij})	40
Table 2.6	Transition difference probability (P _{ij} -R _{ij}).....	41
Table 2.7	Statistics of paleobiofossils in Dounan Mn ores	47
Table 3.1	Main features of Dounan Mn orebodies.....	81
Table 3.2	Chemical composition of Dounan Mn orebodies	82
Table 3.3	Mn contents of the hanging wall, footwall and intercalated rocks of main Mn orebodies	83
Table 4.1	Relationship between ores and minerals in Dounan Mn deposits.....	102
Table 4.2	Relationships between ore type and industrial grade in Dounan Mn deposits	102
Table 4.3a	Primary manganese ores.....	106
Table 4.3b	Supergene manganese ores.....	107
Table 4.3c	Rocks associated with manganese ores.....	108
Table 4.4a	Observed d-spacing (Å) and intensity (I) of X-Ray powder analysis.....	118
Table 4.4b	Observed d-spacing (Å) of X-Ray diffraction (XRD) patterns	119
Table 4.5	Minerals of Dounan manganese ores	125
Table 4.6	Chemical analysis of braunite from Dounan and comparison with Wafangzi Mn deposits, China	127
Table 4.7	Chemical analysis of calciorhodochrosite/rhodochrosite from Dounan Mn deposits.....	129
Table 4.8	Electron microprobe analyses of Dounan hausmannite	131
Table 5.1	Elements and methods used for geochemical characterization	144
Table 5.2	Visual cross-correlation of major and trace elements.....	145
Table 5.3	Chemical analyses of major and minor element [%].....	148
Table 5.4a	Correlation matrix of composition of Mn oxide ores.....	148
Table 5.4b	Correlation matrix of composition of transitional (or mixed) ores.....	148
Table 5.4c	Correlation matrix of composition of Mn carbonate ores	148
Table 5.5	Statistics of major and minor elements; [%]	149
Table 5.6	Statistics of trace elements in ores and rocks; [ppm]	153
Table 5.7a	Statistics of Rare Earth Elements in ores and associated rocks; [ppm]	158
Table 5.7b	Statistics of ratios, anomalies and enrichment ratios in REE.....	159
Table 5.8a	Microanalysis of braunite from the Dounan ores [wt.%].....	166
Table 5.8b	Microanalysis of Mn carbonate minerals from the Dounan ores [wt.%].....	167
Table 5.9	Isotopic composition, inferred temperatures and depth of precipitation	172
Table 6.1	Comparison of syngenetic elements (mean) of Dounan Mn ooliths/pisoliths with other places.....	227
Table 7.1	Comparison of sedimentary-diagenetic products from different localities	274

List of Photographs (for detailed explanation see text)

Plate 2.1	Overviews of Dounan Mn mine-areas	17 - 18
Fig.2a	A general (aerial) view of the manganese mine at Dounan.	
Fig.2b	Disconformable relationship between Falang (T2f) and Geju (T2g) Formations.	
Fig.2c	Overview of Gake mine-area.	
Plate 2.2	Overviews of Dounan Mn mine-areas	17 - 18
Fig.2d	Overview of Kata mine-area.	
Fig.2e	Overview of Daaози mine-area.	
Fig.2f	Overview of Baigu mine-area.	
Fig.2g	Overview of Milike mine-area.	
Plate 2.3	Microfossils from Dounan Mn ores and associated rocks	47 - 48
Fig.1a	Braunite oolite composed of mineralizing algal balls.	
Fig.1b	Braunite mineralized algal balls.	
Fig.1c	Mineralizing bluegreen algae or stromatolites, braunite algae.	
Fig.1d	Totally braunite mineralized algal balls oolite or oncolite.	
Fig.2a	Carbonate pisolite core composed of braunite mineralizing stromatolite fragment.	
Fig.2b	Mn-bearing carbonate stromatolites mineralized by braunite.	
Fig.3a	Mineralized crinoidea.	
Fig.3b	Mineralized biofragments.	
Plate 2.4	Fossils from Dounan Mn ores and associated rocks	48 - 49
Fig.4a	Strongly mineralized bivalve.	
Fig.4b	Mineralized ostracoda in siltstone.	
Fig.5a	Foraminifera as oolite core mineralized by braunite oncolites.	
Fig.5b	Slightly mineralized foraminifera, textularia, typical shallow marine product.	
Fig.5c	Calciorhodochrosite oncolites replaced foraminifera.	
Fig.5d	Mn-calcite oncolites replaced foraminifera.	
Fig.6a	Mineralized biofragments.	
Fig.6b	Mineralized biofragments.	
Plate 4.1	Ores and associated rocks	95 - 96
Fig.1a	Inversely graded Mn oxide oolite/pisolite from Gake area.	
Fig.1b	Mn oxide oolites/pisolites cemented by Mn-calcite.	
Fig.1c	Mn oxide oolites/pisolites cemented by calcite Mn-calcite with minor strongly deformed and broken grains.	
Fig.2a	Banded/deformed Mn oxide oolite/pisolite from Gake area.	
Fig.2b	Mn oxide deformed oolites/pisolites with strongly deformed grains.	
Fig.3a	Compact massive Mn oxide oolite/pisolite from Gake area.	
Fig.3b	Compact massive Mn oolites/pisolites largely lacking concentric laminae, but commonly showing relic outlines of oolites/pisolites.	
Fig.4a	Mn carbonate (calciorhodochrosite) oolite/pisolite from Kata area.	
Plate 4.2	Ores and associated rocks	98 - 99

Fig.4b	Mn carbonate (calciorhodochrosite) ooliths/pisoliths cemented by calcite (light colour).	
Fig.4c	Mn carbonate (calciorhodochrosite) ooliths/pisoliths cemented by calciorhodochrosite and Mn-calcite with minor broken grains and replacement texture.	
Fig.5a	Mn carbonate (Mn-calcite) oolite/pisolite from Gake area.	
Fig.5b	Mn carbonate ooliths/pisoliths cemented by braunite and Mn-bearing calcite.	
Fig.5c	Mn carbonate (Mn-calcite) ooliths/pisoliths cemented by calcite and Mn-calcite, slightly deformed grains.	
Fig.6a	Unsorted Mn oxide ooliths/pisoliths.	
Fig.6b	Unsorted Mn oxide ooliths/pisoliths cemented by calcite.	
Fig.6c	Unsorted Mn oxide ooliths/pisoliths.	
Plate 4.3 Ores and associated rocks		103 - 104
Fig.7	Deformed and broken grains in oolitic/pisolitic micrite	
Fig.8	Mn-bearing oolitic/pisolitic micrite.	
Fig.9a	Intramicrodite/intrasparite with poor inverse grading and dark colour cements.	
Fig.9b	Intramicrodite/intrasparite with light grey matrix	
Fig.10	Calcarenite with quartz silts.	
Fig.11	Calcilutite with micrite oncoliths.	
Fig.12	Silty claystone with minor braunite.	
Fig.13	Clayey siltstone.	
Plate 4.4 Ores and associated rocks		109 - 110
Fig.14a	Colloform grains composed of braunite and Mn-calcite.	
Fig.14b	Colloform braunite growing on of a biofragment.	
Fig.14c	Braunite colloform grain showing colloiddally radial structure.	
Fig.14d	Colloidal braunite with two 'nuclei'.	
Fig.15	Braunite microcrystalline texture with relic laminae of primary grain.	
Fig.16	Cryptocrystalline braunite ooliths/pisoliths radially replaced by calcite.	
Fig.17a	Braunite spherulitic texture	
Fig.17b	Braunite spheruliths cemented by Mn-calcite showing different growing processes, implying the presence of two generations of braunite	
Fig.18	Fragmental texture of Mn oxide deformed oolite/pisolite showing broken and abraded grains and preferred orientation	
Fig.19a	Braunite replacing calcite spherulith from outside.	
Plate 4.5 Ores and associated rocks		111 - 112
Fig.19b	Recrystallization of braunite ooliths/pisoliths.	
Fig.19c	Recrystallization of braunite oolith/pisolith.	
Fig.19d	Diagenetically regenerated calciorhodochrosite spherulith.	
Fig.19e	Secondary braunite and Mn-calcite (algal) ooliths/pisoliths replaced each other with relic concentric laminae of primary grains	
Fig.19f	Secondary calcite replacing primary braunite from outside of the ooliths/pisoliths with secondary calcite vien.	
Fig.19g	Secondary calcite (matrix) replacing primary braunite ooliths/pisoliths.	
Fig.20	Deformed bedding structure of banded Mn oxide ore.	
Fig.21	Inverse grading of unsorted Mn oxide ore.	
Plate 4.6 CL photographs of Dounan Mn carbonates and oxides, with composition analyses by EMPA.....		112 - 113

- Fig.22a Plane polarized light photomicrograph of Mn carbonate pisolith.
 Fig.22b CL micrograph of same field of view as Fig. 22a.
 Fig.23 Black and dark brown luminescence in pelletoid braunite.
 Fig.24 Intense orange and black luminescence in Mn-calcite and braunite.
 Fig.25 Black and yellow luminescence in braunite pisolith.
 Fig.26 The CL photograph shows the same features as Fig. 25.
- Plate 4.7 CL photographs of Dounan Mn carbonates and oxides, with composition analyses by EMPA.....113 - 114
- Fig.27 Light orange luminescence in small Mn-bearing calcite ball.
 Fig.28 Concentric zoning in a calciorhodochrosite oolith.
 Fig.29a Plane polarized light photomicrograph of Mn oxide ore.
 Fig.29b CL micrograph of same field of view as Fig. 29a,
 Fig.30 Concentric zoning in a braunite pisolith.
 Fig.31 Concentric braunite pisolith was replaced by yellow luminescent calcite.
 Fig.32 Concentric braunite and pure calcite laminae in a pisolith replaced by dull yellow luminescent Mn-bearing calcite and then replaced again by orange luminescent Mn-calcite.
 Fig.33 Concentrically laminated braunite and very pure calcite pisolith replaced by calcite.
- Plate 4.8 Scanning electron micrographs of Dounan Mn oxide and carbonate ores.....114 - 115
- Fig.34a SEM micrograph of fractured section showing primary colloform braunite in concentric laminae of Mn oxide in pisolith.
 Fig.34b SEM micrograph of fractured section showing cryptocrystalline calciorhodochrosite in concentric laminae of Mn carbonate in pisolith.
 Fig.34c SEM micrograph of fractured section showing concentric laminae of Mn oxide in colloform braunite with Mn-calcite in pisolith.
 Fig.34d SEM micrograph of fractured section showing microcrystalline (octahedron) braunite with Mn-calcite (fine grains) in concentric laminae of Mn oxide in pisolith.
 Fig.35a SEM micrograph of fractured section showing recrystallized braunite spheroids in black Mn carbonates, suspected to be biogenic.
 Fig.35b SEM micrograph of fractured section in the same enlarged area of Fig. 35a showing cryptocrystalline braunite spheroids suspected to be biogenic algae balls.
 Fig.35c SEM micrograph of fractured section showing microcrystalline braunite spheroids; some grains on the surface showing octahedron shape.
 Fig.35d SEM micrograph of fractured section showing braunite spheroid, suspected to be biogenic, in dark Mn carbonate ore, probably biogenic oncolite.
- Plate 4.9 Scanning electron micrographs of Dounan Mn oxide and carbonate ores.....115 - 116
- Fig.35e SEM micrograph of fractured section of calciorhodochrosite spheroids (or oncoliths ?), probably primary and diagenetic.
 Fig.36a SEM micrograph of fractured section showing colloform braunite spherulith, and colloform texture (light outer cycle) in black Mn carbonates; probably primary.
 Fig.36b SEM micrograph of polished section showing primary colloform or cryptocrystalline braunite and Mn-calcite in concentric laminae of Mn oxide in deformed pisolith.
 Fig.36c SEM micrograph of fractured section showing microcrystalline braunite in dark Mn carbonates in tapering concentric laminae deformed pisolith, probably diagenetic.
 Fig.37 SEM micrograph of fractured section showing Mn-calcite crystal in Mn carbonate; probably recrystallized during diagenesis.
 Fig.38 SEM micrograph of polished section showing polycrystalline, recrystallized braunite.
 Fig.39 SEM micrograph of fractured section showing well-microcrystallized calciorhodochrosite.

Fig.40 SEM micrograph of fractured section showing microcrystalline octahedral-like braunite from massive Mn oxide ore.

Plate 4.10 X-ray scanning photographs of Dounan Mn minerals.....128 - 129

Fig.41a Distribution of Mn in braunite; 45 μ x 45 μ ; 16 seconds.

Fig.41b Distribution of Si in braunite; 45 μ x 45 μ ; 80 seconds.

Fig.41c Distribution of Fe in braunite; 45 μ x 45 μ ; 40 seconds.

Fig.42a Distribution of Mn in calciorhodochrosite; 360 μ x 360 μ ; 16 seconds.

Fig.42b Distribution of Ca in calciorhodochrosite; 360 μ x 360 μ ; 50 seconds.

Fig.42c Distribution of Fe in calciorhodochrosite; 360 μ x 360 μ ; 40 seconds.

Fig.42d Distribution of S in calciorhodochrosite; 360 μ x 360 μ ; 40 seconds.

Fig.42e Distribution of Si in calciorhodochrosite; 360 μ x 360 μ ; 80 seconds.

Fig.42f: Distribution of Mg in calciorhodochrosite; 360 μ x 360 μ ; 80 seconds.

Plate 5.1 Analytical area diagrams of electron microprobe analysis168 - 169

Fig.1 Analytical area of braunite from Mn oxide deformed oolite/pisolite.

Fig.2 Analytical area of braunite from Mn oxide oolite/pisolite.

Fig.3 Analytical area of braunite from Massive Mn oxide oolite/pisolite.

Fig.4 Analytical area of calciorhodochrosite from Mn carbonate ore.

Fig.5 Analytical area of calciorhodochrosite oolith from Mn Carbonate ore.

Fig 6 Analytical area of braunite oolith from Mn oxide deformed oolite/pisolite.

Abstract

During the 1990 field session, ore and rock samples were collected from the manganese deposits at Dounan in Yunnan Province of China. Detailed geological examination of several stratigraphic sections allowed a detailed survey of the stratigraphy of the respective sections and a determination of relationships between ore and rock units and their sedimentary facies or environments. Additionally, the studies of the evolution of the Dounan Mn sedimentary basin and ore phases documented typical synsedimentary aspects of three ore phases. Mineralogical/petrological examination and geochemical analyses (especially REE and isotopes) of both ores and associated rocks provide the basis for a better understanding of synsedimentary materials dominating the Dounan deposits. An improved knowledge about upgrading of low-grade manganese ores during diagenesis is very important and significant for the genetic interpretation of the deposits. It is likely that these studies will assist in mine management and further exploration in target areas.

The Dounan manganese deposits of southern China occur as bedded stratiform bodies within Falang marine sediments of Middle Triassic age, and are believed to be of sedimentary-diagenetic origin originally deposited in transitional areas between littoral and shallow marine environments. The manganese occurs primarily as braunite and manganese carbonate minerals. The manganese ores are considered to be a shallow water marine sediments, which predominantly accumulated as accretionary oolites/pisolites, with later modification during diagenesis. The manganese is considered to have mainly been derived from erosion of pre-existing manganese-bearing rocks of oldlands adjacent to the Dounan basin.

The deposits exhibit some unusual characteristics: the major manganese mineral is sedimentary braunite; oolitic/pisolitic, spherulitic, oncolitic, and bioclastic textures or structures are frequently found in the ores; significantly, the formation of braunite and manganese carbonate minerals seems to be, to some extent, influenced by the activities of bacteria, algae and other organisms; and importantly, magmatic or volcanic, hydrothermal and regional metamorphic processes have had no influence on the minerals and ores/rocks of the Mn-bearing series.

An integrated study of the basic geological features (stratigraphy, lithofacies-paleogeography, texture and structure, mineralogy/petrology, and geochemistry) of the Dounan manganese formation suggests that the braunite shows synsedimentary origin with secondary enrichment during diagenesis. Other sedimentary-diagenetic manganese deposits display similar sedimentary-diagenetic processes and thus, these processes described for the Dounan Mn formation are generally applicable for comparable ores. However, in comparison with other braunite deposits, Dounan exhibits a genetic difference and therefore, the sedimentary braunite of the Dounan deposits represents a new type of manganese deposit.

Statement

This thesis contains no material which has been accepted for the award of any other degree or diploma in any university or other tertiary institution and, nor to the best of writer's knowledge and belief, does it contain any copy or paraphrase of previously published or written material by another person, except where due reference has been made in the text.

I give consent to this copy of my thesis, when deposited in the University Library, being available for loan and photocopying.

October 1993, Baohong Hou

Acknowledgements

This thesis greatly benefitted from the help and guidance of numerous people and institutions. I, therefore, wish to express my appreciation and thankfulness to all those who contributed to this study in one way or the other.

I gratefully acknowledge the supervision, encouragement and help given me in all stages of this project by *Professor L. A. Frakes* [Department of Geology and Geophysics, The University of Adelaide (UA)]. I also thank his wife, *Mrs. Esther Frakes*, for her friendly helpfulness to me and my family.

Thank you to:

my dear family for tolerating a massive disruption of our daily life and for moral support;

staff members of the department (UA) for friendly advice or technical assistance; in particular:

Dr. K. Turnbull (geochemistry), *Dr. J. Foden* (REEs), *Dr. V. Gostin* (sedimentology), *Mr. D. Bruce* (laboratory), *Mr. J. Stanley* and *Mr. P. McDuiie* (XRD, XRF), *Mr. W. Mussared* and *Mr. G. Trevelyan* (thin-sectioning), *Mr. J. Willoughby* and *Mr. R. Barrett* (computing and photography);

staff members of the Chinese Ministry of Geology and Mineral Resources (CMGMR), Changchun University of Earth Sciences of China (CUESC), Yunnan Geological School of China (YGSC), Yunnan No.2 Geological Brigade of China (Y2GBC), Dounan Mining Company of Yunnan, China (DMCYC) for providing unrestricted access to the Dounan Mine and associated areas, drill cores, and geological information, practical help and discussion and accommodation; in particular: *Prof. Zhang Yixia* (travel allowance within China, CUESC), *Prof. Zhao Dongpu* (CUESC), *Dr. P. Zhang* (biogeologist, CUESC), *Mr. S. Wang* (CMGMR), *Mr. T. Yan* (CMGMR), *Mr. L. Zhang* (Y2GBC), *Mr. W. Liu* (Y2GBC) and *Mr. F. Zhuang* (DMCYC), and many others;

institutions for providing financial assistance: UA (scholarship and travel allowance), CMGMR and CUESC (travel allowance within China), YGSC, Y2GBC and DMCYC (field travel, accommodation), Department of Geology and Geophysics (UA; travel allowance);

and to all mentioned and to many others who have contributed their help to this work;

again, I wish to especially mention that this study was financed by a Adelaide University Scholarship, for which I am most grateful.



Chapter 1. General Introduction

1.1 Aims of the Project

The present study examines the medium sized sedimentary manganese deposit of Dounan, Yunnan Province of China, to determine the sedimentary environments controlling the distribution of ores and rocks, and to establish the relationships between ore mineralization and changes in the sedimentary environment. The study also aims to work out the sequence of events after the primary ore was formed, to determine which processes led to secondary enrichment of the ore. Until recently, very little was known about the model of formation of braunite, which is the main ore mineral of the Dounan manganese oxide ores. An improved understanding of the sedimentary environment, including a model of braunite formation, is potentially of great benefit for mine management and further exploration projects for new manganese deposits around the southeast of Yunnan, in similar sedimentary and geochemical environments to those of the Dounan manganese deposit.

Deposits of this type, characteristically associated with silt-clay or, rarely, sandy formations and their metamorphosed equivalents, account for the largest share of the Mn-ore reserves of the world (Roy, 1981). Sedimentary processes associated with terrigenous formations seem to have been important in a number of manganese ore deposits, such as at Nikopol and Chiatura in the former U.S.S.R. (Varentsov, 1964), the Cretaceous deposit of Groote Eylandt, Australia (McIntosh et al., 1975; Slee, 1980; Frakes and Bolton, 1984), Liassic manganese deposits at Úrkút and Epleny, Hungary (Cseh-Németh et al., 1980), Riódas Velhas Series and Minas Gerais Mn deposits of the Precambrian in Brazil (Dorr et al., 1956), the Precambrian Franceville Series in Gabon (Weber, 1970), Tangganshan and Wafangzi deposits of the Precambrian in China (Varentsov, 1964; Ye et al., 1988), and many more.

1.2 Geologic Setting

1.2.1 Introduction

Occurrences of the Dounan manganese deposits in the southeast of Yunnan Province, China were primarily investigated during 1958 and 1960 by the Wenshan Geological Brigade. About five years later, No.2 Geological Brigade of Yunnan Geologic Bureau started more intense investigations on the deposits, and it took another 15 years until a detailed geological report on the deposits was submitted, which led to the current mining activities (Zhang et al., 1979). The mixed orebody of manganese oxides and manganese carbonates at Dounan is the largest sedimentary manganese deposit in Yunnan, having reserves estimated in excess of 20 Mts, and a present production of about 40,000 tons per year of metallurgical ore having a manganese content of 23 to 38%. The deposits are found in the Falang Formation of middle Triassic age, and the ores were formed in shallow marine environments. Ores occur as both Mn oxide oolites /pisolites and small amounts of Mn carbonates and hardgrounds, associated with various secondary ores. Zhang et al (1979) noted that the primary sedimentary Mn oxide ores which were formed in shallow marine environments in the middle Triassic, consist mainly of braunite. Although the present study has been oriented so as to include most of the important sedimentary Mn deposits of the Falang Formation in southeastern Yunnan, the observations and interpretations focus on the Dounan, Yanzijiao and Laowu Mn deposits due to the fact that they occur in the same sedimentary basin.

The Dounan manganese deposits are located in the southeast of Yunnan Province (103° 41'-103° 45' E, 23° 35'-23° 37' N, Fig.1.1). The altitude of the study area ranges from about 1600 to 1900 m. The sandstones, mudstones and limestones of the Falang Formation, occur largely in the southwestern part and the lower northeastern part of the area, and have a general 70° E strike. The area has a warm and humid climate (temperature -7.1°C ~ 28.5°C) and has a precipitation rate of 911.5 - 1272.6 mm / year.

1.2.2 Regional Tectonics and Stratigraphy

The tectonic layout of southeastern Yunnan generally delineates the coast line of the Dounan marine basin in the Triassic (Liu et al., 1984; Fig. 1.2). The Dounan manganese deposits lie on the southern margin of the Triassic Kaiyuan-Qiubei sedimentation zone and to the north of the Yuebei oldland; the deposits occur in the middle Triassic fold-system of southern China. The Kangdian oldland lies to the west of the Triassic basin across the Red River fault, and the Ailaoshan uplift lies to the southwest. The basin has a northern boundary with the Nushoushan oldland and a southern boundary with the Ailaoshan uplift and Yuebei oldland. All these oldlands or uplifts supplied sedimentary materials for the Triassic basin.

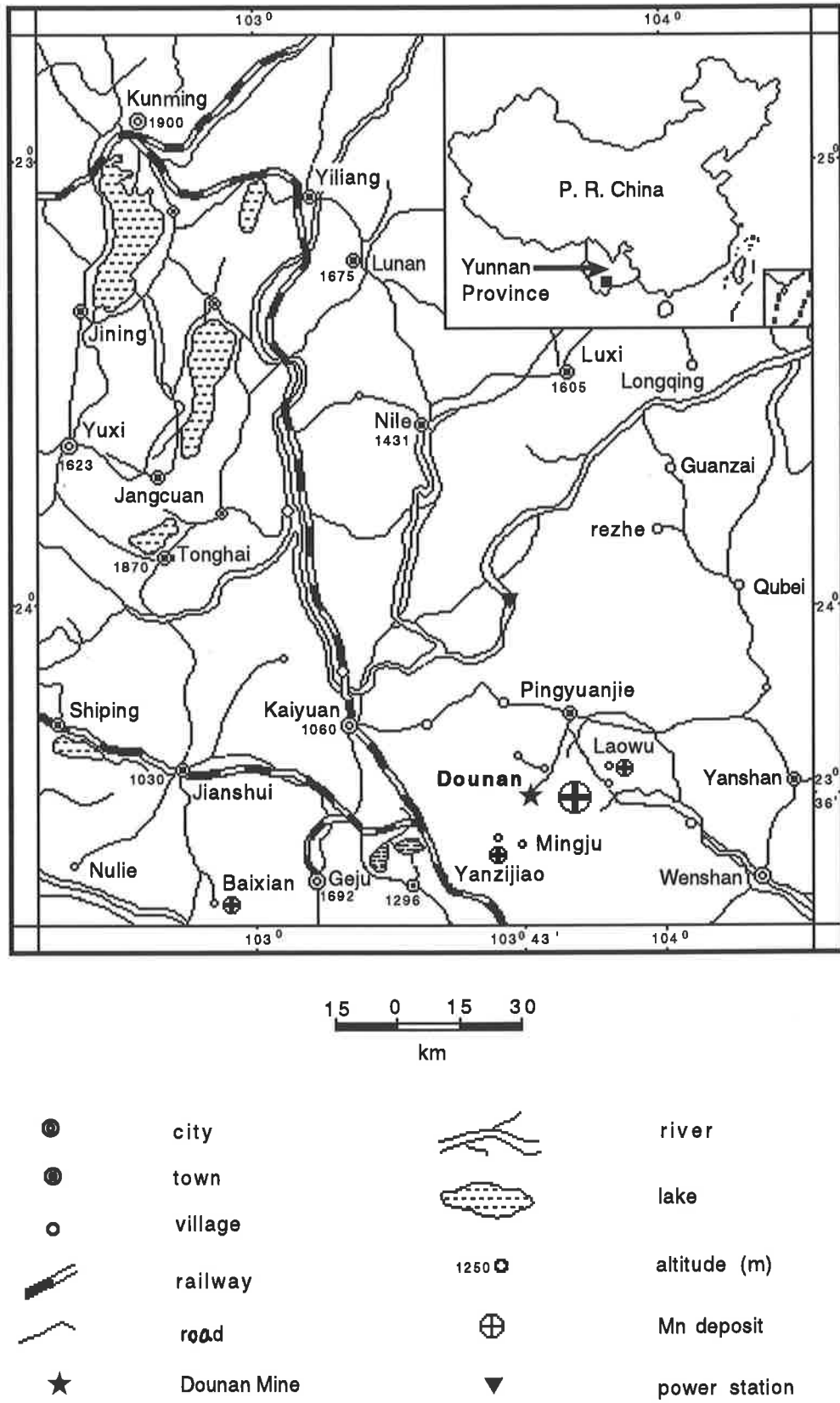


Fig. 1.1 Location of Dounan Mn deposits, Yunnan province, China, modified after Liu et al (1984).

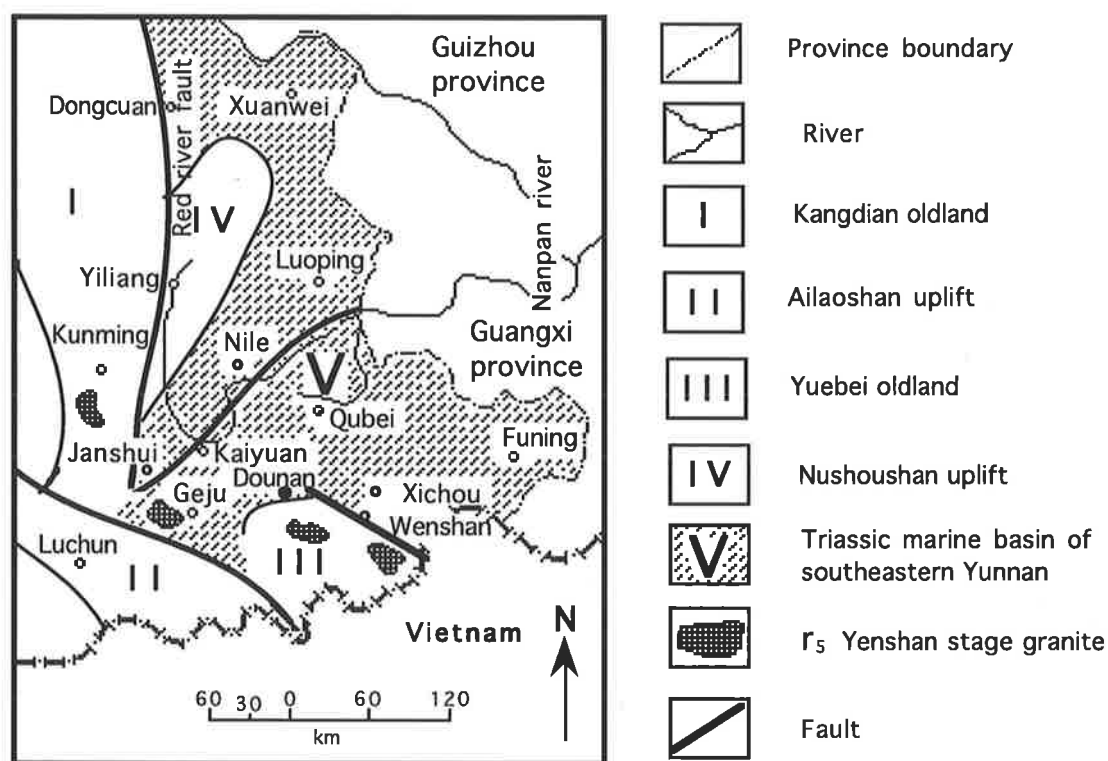


Fig. 1.2 Geotectonic sketch map of southeast of Yunnan, China, modified after Liu et al (1984).

The rocks of the Ailaoshan uplift consist mainly of Proterozoic plagioclase-gneiss, amphibolite and marble. The Kangdian oldland is composed of Proterozoic limestone, slate and some Mn-bearing rocks, whereas the Nushoushan oldland is made up of Proterozoic sandstones, slate, shale, limestone, and dolomite as well as tillite (Zhang et al., 1979). The Yuebei oldland contains Cambrian phyllite, dolomite, limestone and silty shale, thick Ordovician dolomitic limestone and quartz sandstone, granites (fossils determined by Zhang et al., 1979 and Liu et al., 1984). Caledonian movements led to the absence of Silurian sediments in the oldlands, either from erosion of existing sediments or from absence of sedimentation during this time. At the margins of these oldlands, basement rocks are overlain unconformably by shallow-marine sediments of Triassic age; the basin consists mainly of Mesozoic and minor Paleozoic sediments (Table 1.1).

Triassic sediments (sandstones, siltstones, mudstones, and carbonates) overlie the Paleozoic rocks. The Geju Formation, middle Triassic in age, consisting of thick limestone, is disconformably underlain by the Falang Formation. The Mn-bearing series, with a maximum thickness of about 650 m, occurs in both the lower and upper parts of the Falang Formation. Regionally, Triassic sediments can reach up to about 3120 m in thickness. Oxidic manganese oolites/pisolites with small amounts of manganese carbonates exhibit several cycles of normal and inverse grading and they generally are found in both the lower and the upper parts of the Mn-bearing series. Size grading of the oolites/pisolites often ranges between 2-17 mm. over an interval of 0.5-2 meters. The Falang Formation is disconformably overlain by the Niaoge Formation, late Triassic in age. In addition, in the southwestern part of the Dounan basin of the

Table 1.1 Stratigraphy of southeastern Yunnan, modified after Zhang et al (1979).

era- them	system		formation	thickness m	lithology	
Cenozoic	Quaternary			Q	50	loess, clay, sands & gravels
	upper Tertiary		Buzhaoba	N	100	clay or sandy clay, minor brown coal
	lower Tertiary		Lunan	E	300	red & yellow mudstone, sandstone, conglomerate
Mesozoic	Triassic	upper	Huobachong	T ₃ h	214.4	mudstone, siltstone, sandstone, minor coal
			Niaoge	T ₃ n	386.8	shale, siltstone, sandstone, conglomerate
		middle	Falang	T ₂ f	650	mudstone, siltstone, sandstone, limestone, Mn ores, fossils: <i>Daonella indica</i> Bittner
			Geju	T ₂ g	2499.5	limestone, dolomitic limestone, dolostone
		lower	Yangningzhen	T ₁ y	881.7	limestones, fossils: <i>myophoria ovata</i> Goldfuss
			Feixianguan	T ₁ fe	244.8	shale, siltstone sandstone, <i>Claraia aurita</i> Hauer
Palaeozoic	Permian	upper	Longtan	P ₂ l	58	sandstone, shale, chert, coal
			basalt	P ₂ β	286	pyroxene or pyroxene-olivine basalts
		lower	Maokou	P ₁ m	0-291.4	limestone, fossils: <i>Pseudofulina</i> sp.
			Xi xia	P ₁ c	0-333.1	limestone with chert bands, <i>Misellina chaudiae</i>
	Carboniferous	upper	Maping	C ₃ m	180.7	limestone, <i>Rugosofusulina stabilis</i> Rauser
		middle	Weining	C ₂ w	238.3	limestone with chert bands in lower part
		lower	Datang	C ₁ d	450.7	thick limestone, <i>Koninekophyllum</i> sp.
	Devonian	middle	Donggangling	D ₂ d	1179.2	limestone, chert, siltstone, <i>Disphyllum</i> sp.
			Pojiao	D ₂ p	325.3	shale, siltstone, <i>Indospirifer iadukpinensis</i>
	Cambrian	middle	Suanglongtan	Є ₂ s	77.2	dolomitic limestone, shale, <i>Asaphiscus</i> sp.
			Gaota	Є ₂ g	616.1	shale, sandstone, <i>Lisania</i> sp.
lower		Canglangpu	Є ₁ c	130	fine sandstone, shale, <i>Redlichia</i> sp. <i>Paleaolenus</i> cf.	

southeastern Yunnan Triassic sedimentary zone, the Yanzijao manganese deposit, consisting of Mn oxides and carbonates, occurs in the lower part of the Falang Formation, whereas the Laowu manganese deposit in the northeastern part of the basin mainly occurs in the upper part of the Falang Formation. All these manganese deposits are presently being mined (Table 1.1, Figs. 1.3 and 1.4).

Although manganese deposits are widely distributed in southeastern Yunnan province and occur in Cambrian, Devonian, Carboniferous, Permian, and Triassic rocks, only the Triassic deposits possess important industrial scales and values in Mn mining and producing. The Changtian, Yanzijao and Laowu Mn deposits occur at the same stratigraphic level as the Dounan Mn deposit and were formed in the same sedimentary basin (Zhang et al., 1979).

1.2.3 Igneous Rocks

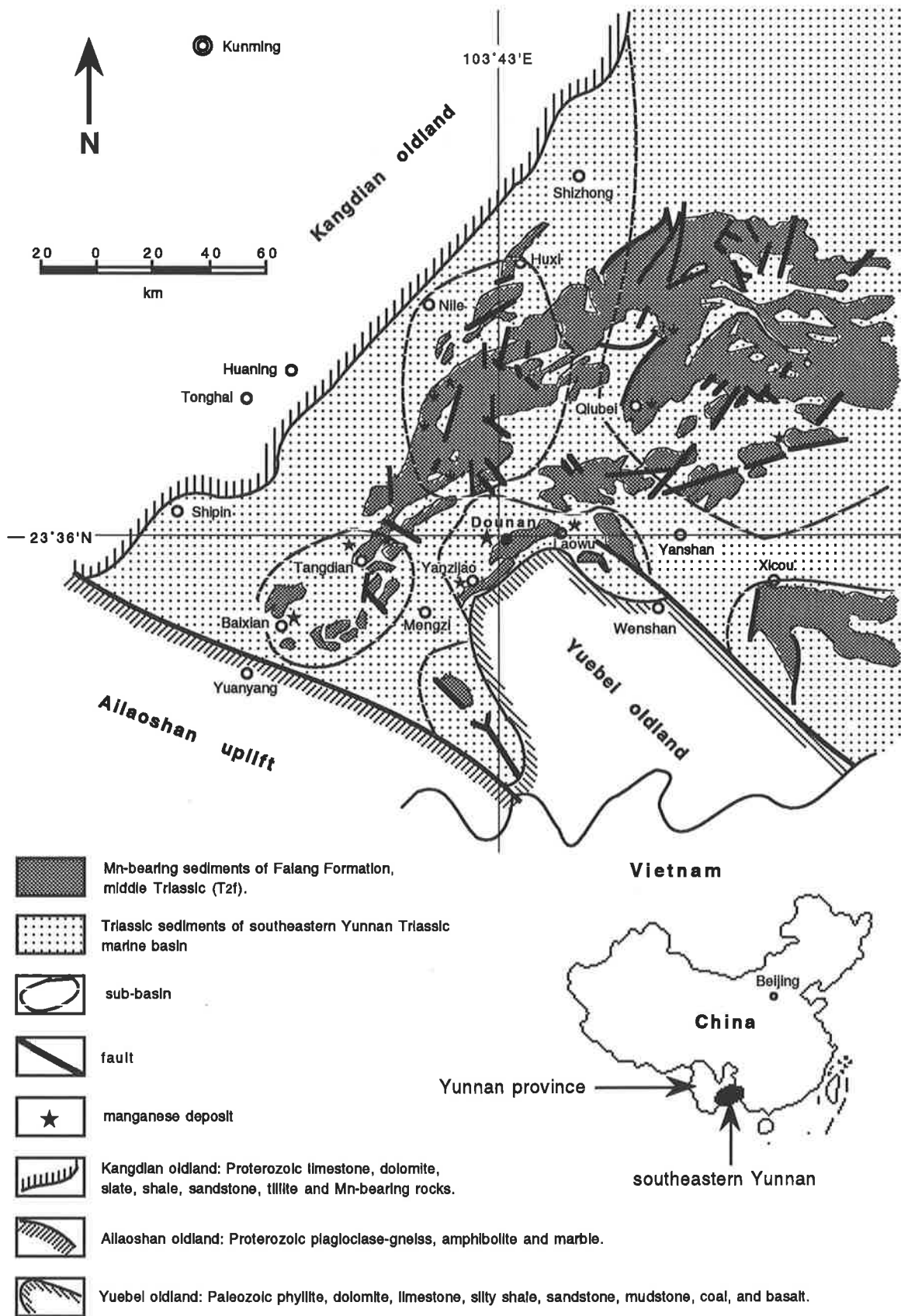


Fig.1.3 Geology and manganese distribution in southeastern Yunnan, China (modified after Su, 1983 and Yang, 1985).

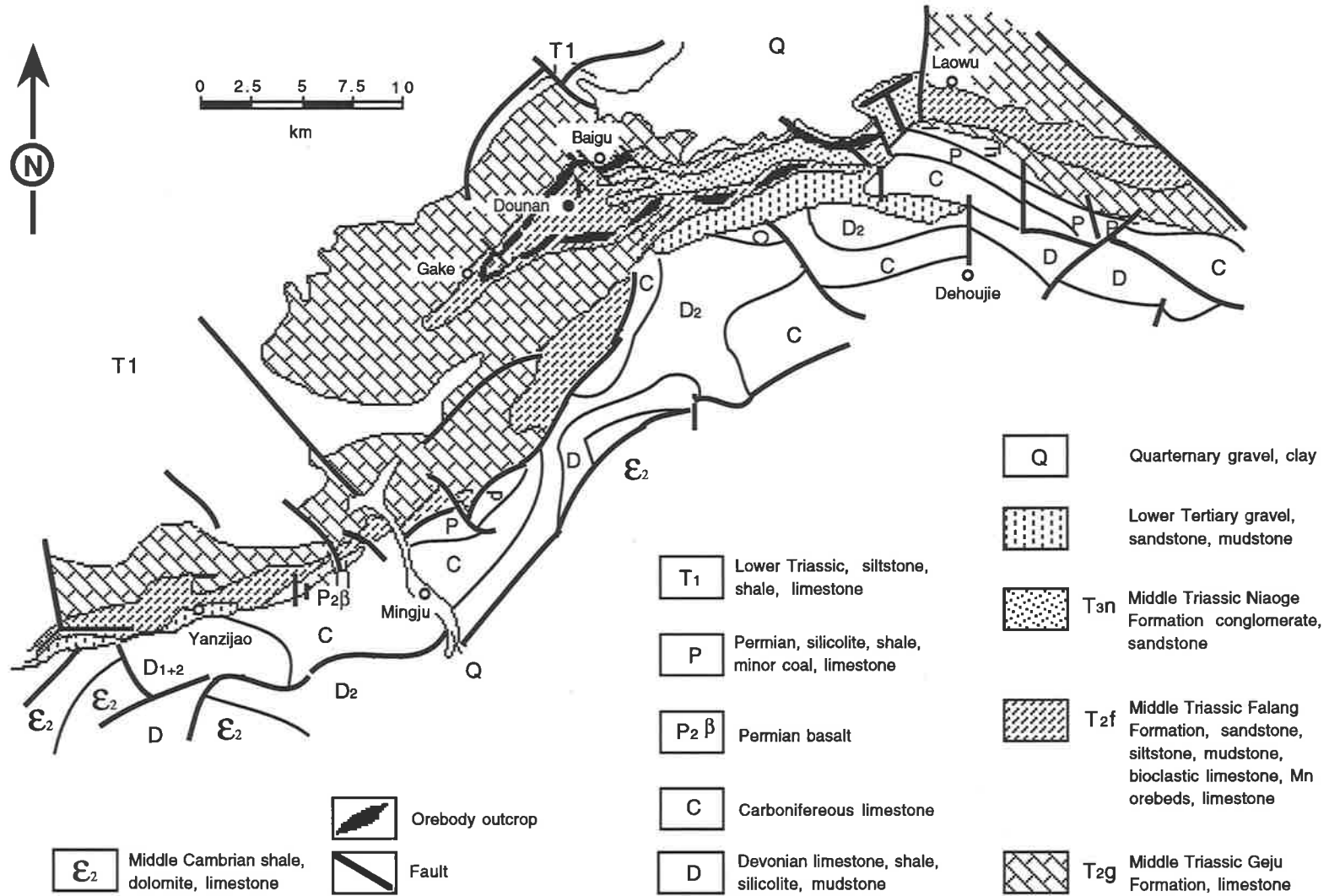


Fig. 1.4 Geological sketch map of the Dounan area (modified after Wang,1981).

There are no outcropping igneous rocks within the Dounan marine basin, but outcrops of Permian basic volcanic rocks are commonly distributed along the Ming-Shu fault at the margin of the Yuebei oldland (Table 1.1 and Fig.1.4). These rocks are principally fissure eruptional basalts and they include dark green augite-olivine basalt and augite basalt, which probably provided weathering materials to the Dounan Triassic Mn deposits (Zhang et al., 1979). Additionally, two granite intrusives crop out in Baozushan (Wenshan county) and Dulong (Madian county) in the south of the Dounan marine basin. According to isotopic age determinations, the age of the Baozushan granite is 115 M. yr., and that of the Dulong granite is 186 M. yr., and they therefore belong to post-Triassic Yenshan movements.

1.2.4 Geologic Evolution and Mineralization Period of Southeastern Yunnan

The absence of Silurian sediments in the northern margin of the Yuebei oldland probably resulted from uplift during the Caledonian orogeny. A transgression area in the Devonian is seen in a disconformity between early Devonian sediments and underlying middle Cambrian strata (Table 1.1). Though there was Mn sedimentation during the Devonian transgression, it was not sufficient to develop an industrial deposit. Thus, the Yuebei oldland was formed and developed after Caledonian movements, and the Wen-Ma fault controlled the eastern boundary of the Yuebei oldland (Zhang et al., 1979). After the Caledonian movements there was no intensive orogenesis, but there were regional regressions and transgressions during the Devonian, Carboniferous and Permian. However, the Tungwu movements took place after deposition of the Maoco Formation limestones (early Permian), and these led to regional uplift, erosion and regression of the shallow sea surrounding the Yuebei oldland. Thus, some of the sediments of the Carboniferous and Permian underwent erosion. An obvious disconformity, for instance, occurs between middle or later Carboniferous limestones and Longtan Formation sediments (early Permian) in areas near the Dounan marine basin, and locally, aluminous shale or coal seams can be found at the base of the Xi Xia Formation (Carboniferous to Permian). Also, an erosional surface occurs between the Omeishan fissure eruptional basalt and Longtan Formation sediments of later Permian age.

Triassic sedimentation followed the late Permian transgression. The transgression reached its peak in the Geju stage of the middle Triassic (i.e. thicker Geju Formation limestone sedimentation). Regression towards the northeast in the later Geju stage, however, exposed local erosional highs (e.g. Yanzijiao, Dounan, Laowu) in the Dounan area, which led to disconformity or sedimentary gap between Falang Formation sediments and the underlying Geju Formation locally. This sedimentary gap is a product of Indo-China movement, though the movement was not active in the Dounan area (Plate 2.1, Fig.2b). During the Falang stage, the sea transgressed from the south along the eastern side of the Yuebei oldland, then moved towards the west into the Dounan sedimentary basin. This second step was a secondary transgression in the middle Triassic, and the scale was smaller than that in the Geju Formation. Significantly, several smaller regressions

and transgressions occurred during the Falang stage and many industrial manganese orebeds were formed in association with these; these represent the most important manganese mineralogical epoch. Up to the Niaoge stage of the late Triassic (i.e. the time of late Indo-China movements), regional regression is indicated by the expansion of continental facies composed of conglomerates/sandstones, and coal. The Dounan area became an area of terrestrial environments due to the final regression and there is an absence of Jurassic and Cretaceous sediments. Tertiary conglomerates, coal and red sediments were formed in local inland basins or fault basins.

1.3 Previous Work

The initial geological survey in this region was carried out by the No.2 Geological Brigade of Yunnan in 1960. Further work (including initial geological exploration) was carried out from 1965 to 1970. The No.2 Brigade did detailed work on the geological setting of the Dounan Mn deposits and their modes of occurrence and on the chemical and mineralogical composition of the ores, as background for exploration and mining. They submitted a geologic report on mining of the Dounan Mn deposits from 1973 to 1979. However, very little research work was done in the Dounan area in this period.

Until recently, the relationship between ore mineralization and changes in the sedimentary environment, especially the sequence of events after the primary ore was formed, and the genesis of braunite in the Dounan area have not been examined or studied systematically (Liu et al., 1984). Although some investigators acknowledge the existence of processes which probably led to secondary enrichment of the ore, emphasis commonly focused on primary sedimentary features and rock types (Su, 1983). Most investigators concluded that the Dounan manganese deposit was formed by sedimentary processes, but that slight metamorphism led to the formation of braunite. However, all previous studies agree that the protore was laid down in a shallow marine environment during marine transgression. It is demonstrated later that this provides only a small part of the overall picture of the deposit.

Zhang et al. (1979) attributed little importance to secondary processes. Their explanation of the ores and rocks with plentiful fossils and variable textures involves deposition of manganese oxides and manganese carbonates in different environments of littoral and shallow marine environments. However, they suggested that the existence of a preferred orientation of some minerals (e.g. hydromica) and the crystalloblastic fabric of braunite supports a slight metamorphic impress.

Wang (1981) concluded that Dounan-type manganese deposits were deposited in a shallow marine environment and belong to a transitional ore formation of primary manganese oxides and carbonates, which he attributed to alteration of the primary sedimentary ore by metamorphic processes. However, he considered primary sedimentary processes to be responsible for the

formation of braunite, and the secondary enrichment of primary Mn oxide ore to have developed by metamorphic process which, however, did not affect the primary manganese carbonate ore except through in-situ recrystallization.

A different idea was presented by J. Su (1983). He stated that the deposit was produced in a shallow open-marine environment during transgression, but that biomineralization was responsible for the formation of braunite in normal sedimentary environments. He suggested that a number of organisms which contributed to biodetritus in the deposits played an important role in the formation of the Dounan Mn deposits. He concluded that the deposit is not a metamorphic product because there is no evidence of metamorphic mineral associations to be found in the ores and rocks, nor is it a product of diagenesis, as the mineral association and ore fabrics (e.g. compaction, shrinkage, cementation, recrystallization) do not strongly support diagenetic processes.

Liu et al (1984) and Liu (1985) presented a slightly different model for the ore formation. They state that there were two stages for the formation of the deposit, which affected both the physical and the chemical character of the mineralization. First was a colloidal process (including biochemical processes) acting in the littoral zone; this is said to be responsible for the formation of oolites and pisolites. The secondary stage was redeposition of the oolites and pisolites in shallow marine environments. The deposit is thought to result from reworking of pre-existing oolites and pisolites. They also suggested a primary sedimentary, not a metamorphic, origin for braunite.




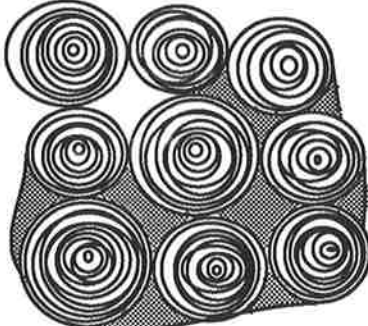
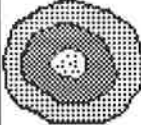
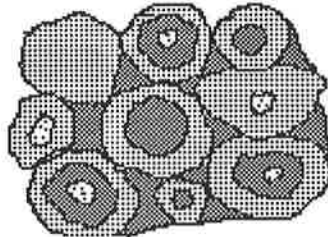


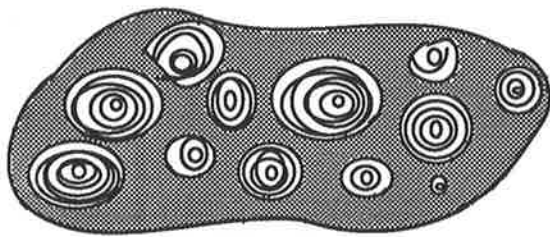

Zhong (1986) agreed that the origin of the deposit was through primary sedimentary processes during transgression. He stated, however, that secondary processes (e.g. diagenetic and slight metamorphic processes) were significant in the development of the sequence, in that they led to secondary enrichment of the ore. The braunite resulted from reworking of pre-existing primary manganese oxides.

Previous studies, of course, are important as a pioneering attempt to decipher some geologic features and their origins, but they provided only a limited interpretation due to the absence of detailed studies on mineralogy, petrology, and geochemistry of Dounan ores and rocks (e.g. microscope-studies, isotopes, REEs).

1.4 Terminology of Dounan Mn Ores and Rocks

The terminology used in this study is proposed by the writer. A brief definition of the main terms and generalized sketches is given here, because of the somewhat confusing descriptions found in the literature (Table 1.2). For example, some geologists (e.g. Zhang et al., 1979; Liu et al., 1984) described Dounan primary sedimentary "mottled" ores as "porphyritic ores" which are easily confused with igneous ores and rocks. The terminology is considered to be important as it

Table 1.2 Terminology for Dounan Mn ores and rocks, including sketches of the most common materials.

Grain	Rock	Terminology, Description
 < 2 mm.		Oolith separate ovoid to spherical grain, concentrically laminated, primary origin Oolite rock composed of ooliths, grain- or matrix-supported
 ≥ 2 mm.		Pisolith separate ovoid to spherical grain, concentrically laminated; primary origin Pisolite rock composed of pisolites, grain- or matrix supported
 3-15 mm.		Spherulith separate ovoid to spherical grain, crudely laminated; primary and/or secondary origin mass of spherulites, matrix supported
 < 2 mm. - ≥ 2		Deformed oolith/pisolith Separate flattened to irregular grain, concentrically laminated. Commonly, grains occur oriented arrangement; diagenetic origin; oolite /pisilite rock composed of oolites/pisolites, grain- or matrix supported.
 grain 0.2 - 15 mm.	Unsorted ores oolith / pisolith separate ovoid to spherical grain, with oolith / pisolith fragments; concentrically or crudely laminated; matrix supported, mostly inversely graded; primary origin.	
 grain < 2 mm. - ≥ 2 mm.	Compact massive ores separate and/or intergrown oolith / pisolith , rounded to ovoid grain, dense; mostly composed of braunite, commonly grains are hard to be seen; diagenetic origin.	

should be applicable to many deposits. Nonetheless, it is necessary to explain and describe further transitional types of primary ores and rocks, which are probably limited to a specific type of deposit and environment. This is done in Chapters 2, 3 and 4 which in detail examine manganese materials identified at Dounan.

1.5 Methods of Study

1.5.1 Scope and Method of Treatment

From a review of the earlier literature on the Triassic sedimentary syngenetic manganese formations of southeastern Yunnan, it is clear that a considerable number of restricted studies have been done on different aspects of these manganese formations, often confined to limited localized areas (e.g. main mining areas). An attempt to tackle the problem on a regional basis has been made only by the No.2 Geological Brigade of Yunnan Geological and Mineral Resources Bureau, though this work is mainly confined to the field relations and distribution of the orebodies. Intensive field and laboratory investigations on restricted areas have been attempted by a few workers (Liu et al., 1984) but no worthwhile attempt has so far been made to determine the detailed relationships between sedimentary environments and mineralization, nor to examine the important sequence of events after the primary ores were formed, which probably led to secondary enrichment of the Mn ores.

In this text, the writer intends to present a comprehensive account of the nature of the manganese ores and manganese silicate rocks of syngenetic/diagenetic types occurring in the Dounan area. In this attempt, the writer will depend primarily on the data collected during his own investigations but will also utilize the observations of other workers in this field. Though the scope more or less emphasizes the study of the origin of the ores and associated rocks, an appreciation of the general geological setting is also essential to fit the problems and the data into the broader background of the geological history of Triassic Mn formation in the Dounan area. Thus, in dealing with Dounan manganese deposits, the writer at the outset presents the geological background of these deposits and their stratigraphic positions in the Triassic manganese formation. This will be followed by a description of the mode of occurrence of the different orebodies and associated rocks in the field, in which sedimentary environment and microfacies analyses will be emphasized. The petrology and mineralogy of the different orebodies will be firmly established. A detailed description of the textural relationships of the ore minerals will follow next and these will be interpreted to determine the paragenetic order. The geochemistry of the ores will be discussed for the purposes of ore genesis, and braunite will be treated particularly in this context. The nature of the interesting mineral assemblages has been carefully studied and the petrogenetic aspects of this ore type will be thoroughly discussed. In the light of the field and laboratory data, the model for origin of the manganese orebodies will be discussed in detail. The textural data and the results of phase-equilibrium studies of systems involving manganese, silica, and calcium, have been utilized to determine the mode of formation and transformation of

manganese oxide and manganese carbonate phases in changing temperature conditions with diagenesis. Finally, a comparative study of the sedimentary/diagenetic origin of manganese (braunite) from all parts of the world has been attempted and critically analyzed, and a method utilizing the minerogenetic trends and province distributions is suggested for the purpose of further prospecting in the future.

At the instigation of this project, the Dounan Mn mine was operational and consequently, factual and interpretive maps of Dounan geology, produced by geologists of the No.2 Geological Brigade, were available. Despite this, the writer re-mapped the surface outcrops of mine and regional (southeastern Yunnan province) workings, re-measured and modified 9 geological sections, and re-logged a number of drill cores for the study of regional and local sedimentary environments. This information was used to select specific lines of section for detailed study, with the requirements that the sections chosen must allow continuous sampling of the freshest material of each rock or ore type at varying stratigraphic positions. Each line of section was then subjected to two sampling approaches. In the first approach, hand-specimen samples were collected, taking care to sample all mesoscopic variations in texture and mineralogy, whereas in the second approach samples were taken at regular intervals (see also Appendix I). This bipartite sampling approach has proven to be ideal, with the first set of samples being used to document textural and mineralogical variations, whilst the second set of samples has revealed variations in composition and micro-texture which might otherwise have been unnoticed.

About 200 samples, encompassing all rock and ore types and textural variations, were sectioned and examined with a petrographic microscope. For each rock or ore type all variations were carefully documented with reference to their stratigraphic position. The characteristics of each rock or ore type, and of each distinctive texture, were used to evaluate various hypotheses for their genesis. The detailed study of these samples throughout the Mn-bearing series (the Falang Formation, middle Triassic) was used to analyze the Dounan evolution of sedimentation and to understand the lithofacies-palaeogeography of the Falang stage. Also, the detailed study of different orebed sections revealed different features of sedimentation related to the evolution of the sedimentary basin, and this plays an important role in the genetic interpretation of the Dounan manganese deposits.

A number of analytical techniques were employed for rock and ore analyses. The equipment, sample preparation and analytical background are described in Appendix I. For further information see also Table of Contents.

1.5.2 Selected Areas for Study

The present study has been so oriented as to include most of the important deposits of sedimentary manganese formations of the Dounan area (including Yanzijiao and Laowu, see

Figs. 1.1, 1.3, and 1.4), so that the observations and interpretations thereof are representative and reasonable. Accordingly, for the purpose of the present study the southeastern manganese belt of Yunnan has been divided into several sectors, each of which has been treated individually in the study of sedimentary environments (Chapter 2 Stratigraphy), and the observations have been ultimately utilized to build up a generalised sedimentary picture.

1.6 Thesis Layout

The thesis is divided into three parts. Part I encompasses the stratigraphic and sedimentary aspects (including microfacies, facies, and environmental analyses) of the Falang Formation. Regionally, each major geological measured section/association is discussed separately, with the order of discussion corresponding to their position within the sedimentary basin. Further, local stratigraphy, facies and microfacies of the Dounan area are discussed in detail. This is necessary to establish the relationship between ore mineralization and changes in the sedimentary environments. Orebeds are discussed specifically as to their distributions and their important features (Chapter 3), with the order of discussion corresponding to their distributions in Dounan Mn deposit. Based on the examination of different orebeds, an evolution of orebed formation and development is outlined.

Part II deals specifically with the rocks and ores of Dounan, including the sequence of events after the primary ore was formed, as some processes led to secondary enrichment of the ore. This part is in turn subdivided into two major sections, namely a petrographic and mineralogical one (Chapter 4) and a geochemical one (Chapter 5). In each of these sections description and data are presented and then interpreted in terms of the genesis of the Dounan Mn deposit; these studies of the ore sequence are also directed at understanding the formation of braunite, which provides information on the history of ore formation.

Part III emphasizes the genesis of the manganese deposits. Chapters 6 and 7 summarize and discuss various aspects of the study. In particular, these Chapters are devoted to the genesis of Dounan Mn deposits, and summarize what the writer believes to be the most important aspects of the deposits and their implications. Chapter 8 gives the résumé and conclusions of this study.

PART I

SEDIMENTARY SEQUENCES AND ENVIRONMENTS

Chapter 2 Stratigraphy

2.1 Introduction

The general stratigraphy of the southeast of Yunnan is outlined in the previous description on the geological setting in Chapter 1 and thus, emphasis focuses here on individual vertical geological sections for the detailed study of sedimentary environments, especially in the Dounan area. Since a number of authors have briefly examined the rocks and ores of Dounan and related areas and have correlated some geological sections (Zhang et al., 1979, Liu et al., 1984), redescrptions will be made in detail (locations, stratigraphic positions, and grainsize data are given in Appendix II, Table II.1). The main concern of this study is to provide important information supporting interpretations drawn from field observations and determining the sedimentary environments of the rocks and ores. All of the localities which could control the analysis of the sedimentary environments in southeastern Yunnan discussed here were subjected to detailed descriptions and analysis.

More than eight measured geological sections (mostly ore-bearing sections) were examined in the southeast of Yunnan. However, the Dounan (including Yanzijiao and Laowu) area is discussed in detail in this Chapter as it is the main manganese-mine studied in this thesis. As an introduction to this Chapter, a detailed legend for all figures (except for the diagrams already indicated) is listed in Table 2.1. For locations of measured stratigraphic sections see Figs. 1.1 and 1.3. Also, all fossils described here have been determined by Zhang et al (1979).

To extend a facies analysis to the entire (southeastern Yunnan) basin it is necessary to come to grips with problems of stratigraphic correlation and to apply various basin techniques. Stratigraphic methods are described first, and basin mapping, including the use of facies ratio and isopach maps, paleocurrent analysis, and so on, is dealt with later. The end product of this work









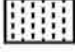



















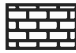
















Falang Formation, middle Triassic	T _{3n}	Niaoge Formation, upper Triassic		Mn-bearing limestone		wavy bedding
	T _{2f6}	member 6		intraspartite or intramicrudite		slump bedding or turbidite
	T _{2f5}	member 5		Mn-bearing intraspartite		massive bedding
	T _{2f4}	member 4		Mn ore bed		ripple marks
	T _{2f3}	member 3		chert		desiccation crack
	T _{2f2}	member 2		Mn-bearing mudstone		birdseye
	T _{2f1}	member 1		Mn-bearing siltstone		stromatolite
T _{2g}	Geju Formation, middle Triassic		disconformity		burrows	
T _{2t}	Tuowei Formation, middle Triassic	ST	supratidal		foraminifera	
V ₇	Mn orebed number	IT	intertidal		algae	
	conglomerate	SBT	subtidal		scouring	
	sandstone	LG	lagoonal		bioturbation	
	siltstone/clayey siltstone	BR	barrier		ammonoidea	
	mudstone/silty claystone	SL	slope		ostropoda	
	shale	OM	open marine neritic		gastropoda	
	limestone	EF	evaporite flat		anthozoa	
	calcilutite	TF	tidal flat		bivalvia	
	calcarenite or oolitic micrite	TR	transgression		crinoidea	
	dolostone	RE	regression		bioclastic debris	
	dolomitic limestone	CS	cycle of sedimentation		exotic blocks	
	siliceous micrite		lamination or horizontal bedding		fish fossils	
	dolocalcarenite		low-angle cross-bedding			
	Mn-bearing dolocalcilutite		cross-bedding			

Table 2.1 Stratigraphic legend for Dounan manganese ore deposits.

is a paleogeographic synthesis, depicting an interpretation of the stratigraphic and geographic evolution of the basin through Falang time (Miall, 1984).

2.2 Sampling Locations

An overview of southeastern Yunnan geology is given in the previous Chapter (Table 1.1, Figs. 1.3 and 1.4), and the locations and geology of mining areas in the Dounan basin are present in Fig. 2.4. The mining areas at Dounan are named after local villages such as Gake, Baigu (Zhang et al., 1979). Plates 2.1 and 2.2 (Figs. 2a-g) briefly present the main oolite and pisolite ore units and two large-scale Triassic measured geological sections (i.e. Gake and Baigu sections) which are representative for all parts of the deposit.

An areal view of the Dounan Mn deposit depicts the large Dounan syncline geomorphology (Plate 2.1, Fig. 2a) and underground operations typical for mining activities at Dounan. Though the thick outcropping sections of the Falang Formation can be seen in detail (the lower part in Gake and upper part in Baigu mining areas), all samples were taken from underground and from drill cores in order to obtain fresh material. In all mining areas (Plate 2.1, Fig. 2c and Plate 2.2, Figs. 2d-g), the main mining activities are operating underground though there are some small open operations on the surface. Deep weathering outcrops are widespread at Dounan.

Detailed photos of orebeds and ores which are of particular importance for genetic interpretations are shown in the following Chapters

2.3 Regional Structure

There are two groups of faults in the Dounan area, i. e. NNE thrust structures and NW thrust-torsion structures (Fig. 2.1). A representative NW strike structure is the Wen-Ma fault, which begins in northwestern Pingyuanjie, trends through Wenshan and Malipo to Vietnam, and is over 150 km long. This fault is a major structure in the region. The Wen-Ma fault underwent long-term movements and its southwestern (or upfaulted) block moved as a thrust towards the NE, as well as torsionally with a right-lateral wrench component. It plays a significant role as the eastern boundary of the Yuebei oldland due to long-term uplift of the southwestern block. In addition, another NW oriented fault is the Kai-Ming (Fig. 2.1), starting from Kaiyuan in the northwest and extending for 60 km to Shidong and Mingjiu. The NNE structural belt is mainly made up of the Dounan arcuate syncline and the Ming-Shu (Mingjiu-Shuzu) arcuate fault zone, starting in eastern Wen-Ma and continuing to western Yanzijao (Fig. 1.4 and Fig. 2.1).

The Dounan arcuate syncline is about 40 km long. In eastern Laowu district, the axis of the syncline strikes N 60° W in surface rocks of the Falang Formation, with a northern limb mainly

Plate 2.1 Overviews of Dounan Mn mine-areas.

Fig. 2a: A general (aerial) view of the manganese mine at Dounan, showing the morpho-structure of Dounan syncline.

Fig. 2b: Disconformable relationship between Falang (T2f) and Geju (T2g) Formations, Gake area.

Fig. 2c: Overview of Gake mine-area.

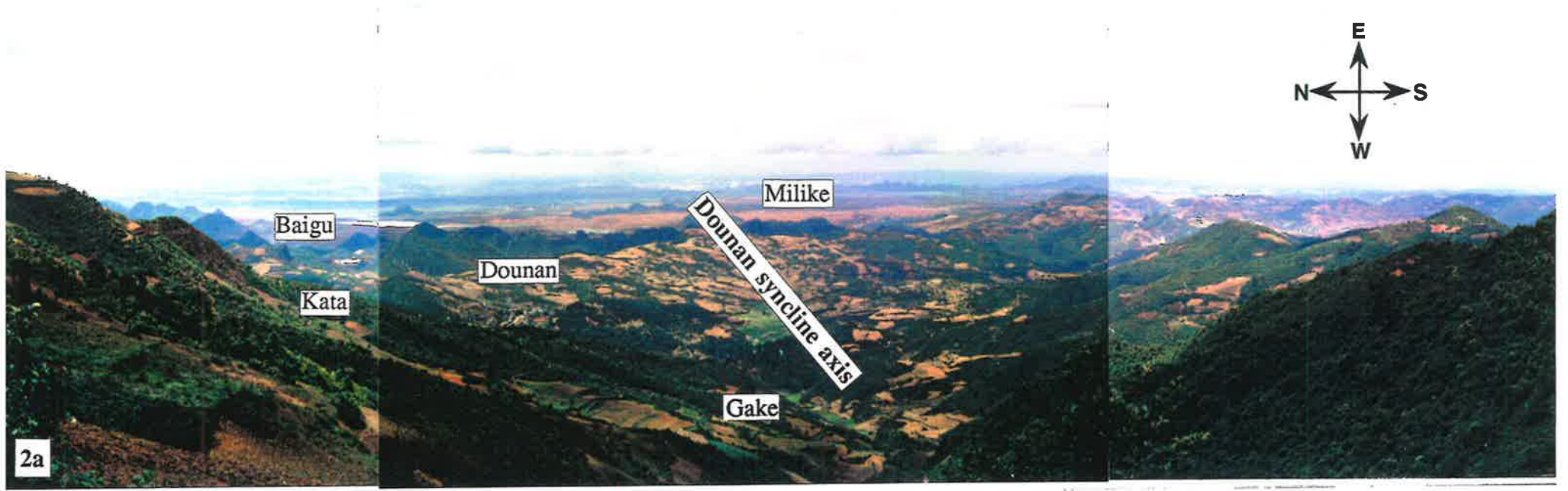
Plate 2.2 Overviews of Dounan Mn mine-areas.

Fig. 2d: Overview of Kata mine-area.

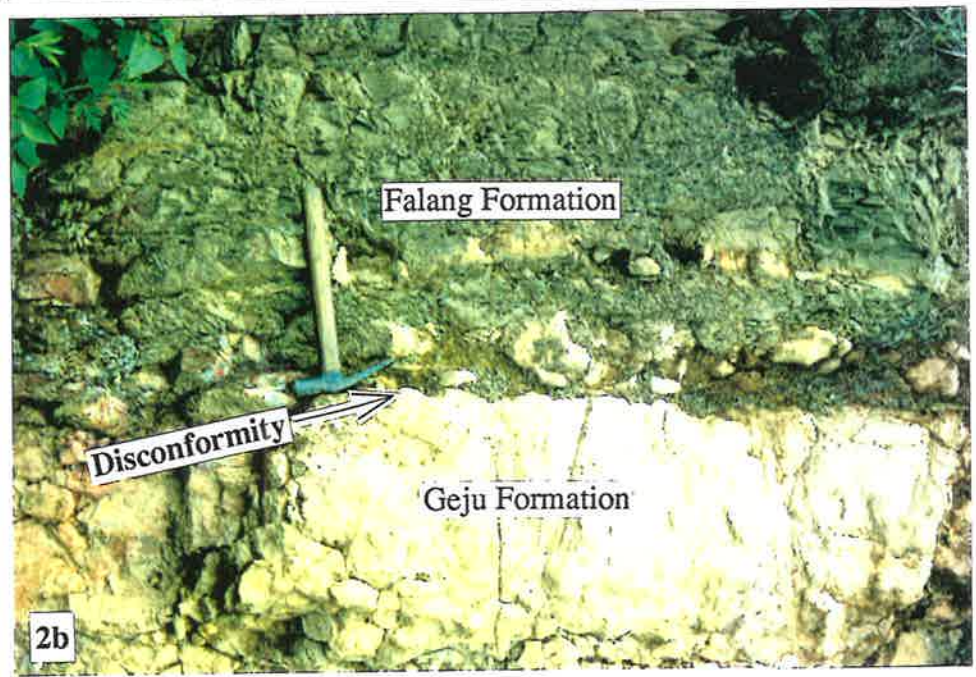
Fig. 2e: Overview of Daaози mine-area.

Fig. 2f: Overview of Baigu mine-area.

Fig. 2g: Overview of Milike mine-area.



2a



2b



2c



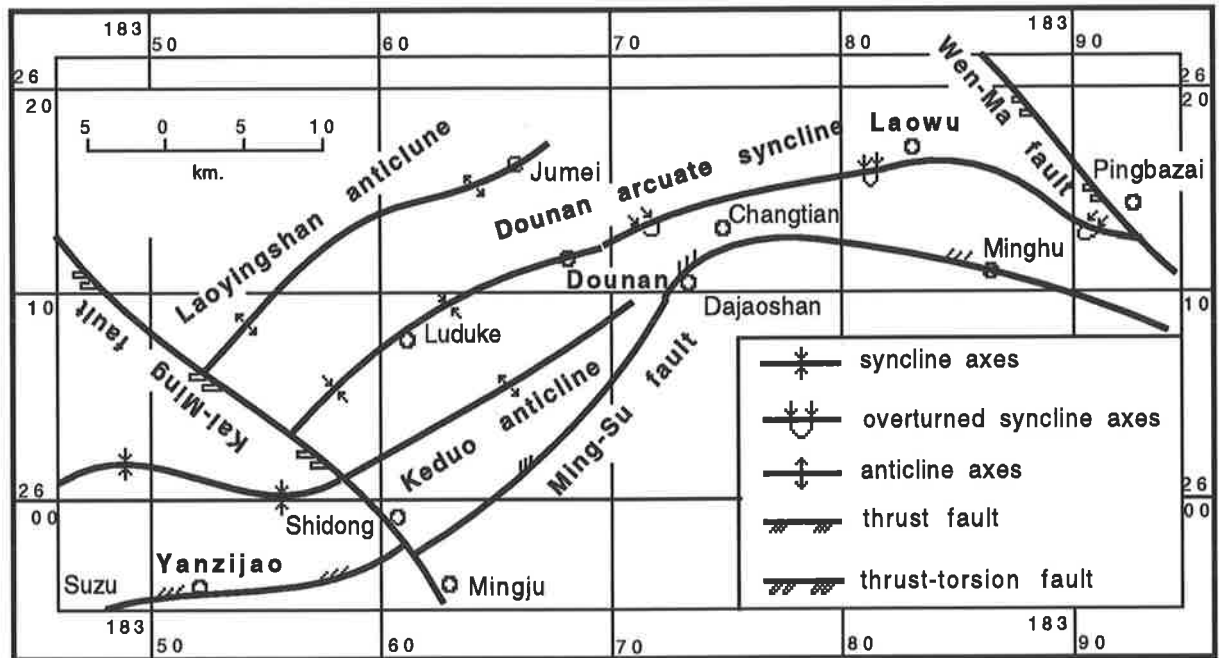


Fig. 2.1 Structural sketch map of the Dounan area, modified after Zhang et al (1979).

composed of the Geju Formation, also middle Triassic, and an overturned southern limb underlain by Carboniferous and Permian sediments. Between Laowu and Dounan, the axis of the fold strikes E-W and contains the Niaoge Formation of later Triassic age in the center, with limbs of Falang and Geju Formations of (Fig. 2.2), commonly with an overturned southern limb (Figs. 2.2 and 2.3). In the Dounan area, however, the axis of the fold strikes N 50°-60° E, and another two anticlines occur on both northern and southern limbs of the Dounan arcuate syncline, i. e. Laoyingshan and Keduo anticlines (Fig. 2.1). The axis of the Laoyingshan anticline exposes the Longtan Formation (later Permian), whereas the axis of the Keduo anticline consists of the Geju Formation of middle Triassic age (Table 1.1). The Ming-Shu arcuate fault zone is located to the south of and is parallel to the Dounan syncline; it is about 60 km long. The southern block is thrust towards the northern limb, which led to a series of Tertiary paternoster faulted basins along the arcuate fault zone (Zhang et al., 1979).

The Dounan Mn deposits are located in the Dounan syncline, which strikes N 50°- 70° E (Fig. 2.4). The northern limb of the syncline dips generally to the south at between 20°-30°, whereas its southern limb dips to the north at an angle between 50°-80°; in some places the syncline is overturned toward the NW. The Dounan syncline is known to affect the Niaoge Formation, and the Falang and Geju Formations, and is divided into five mining areas, i. e. Gake, Kata, Daozi, Baigu, and Milike (Fig. 2.4). In the Gake and Daozi areas, the south-limb strata dip to the north at between 50°-70°, with some parts at 90° or overturned; whereas in the Milike area the southern limb of the syncline is overturned. In addition, there are a few small folds in the Dounan area, i. e., a composite fold parallel to the Dounan syncline farther south, and a composite cross-fold with a vertical axial plane near prospecting line 25 in the Baigu area. Neither of these greatly influenced the orebodies (Fig. 2.4).

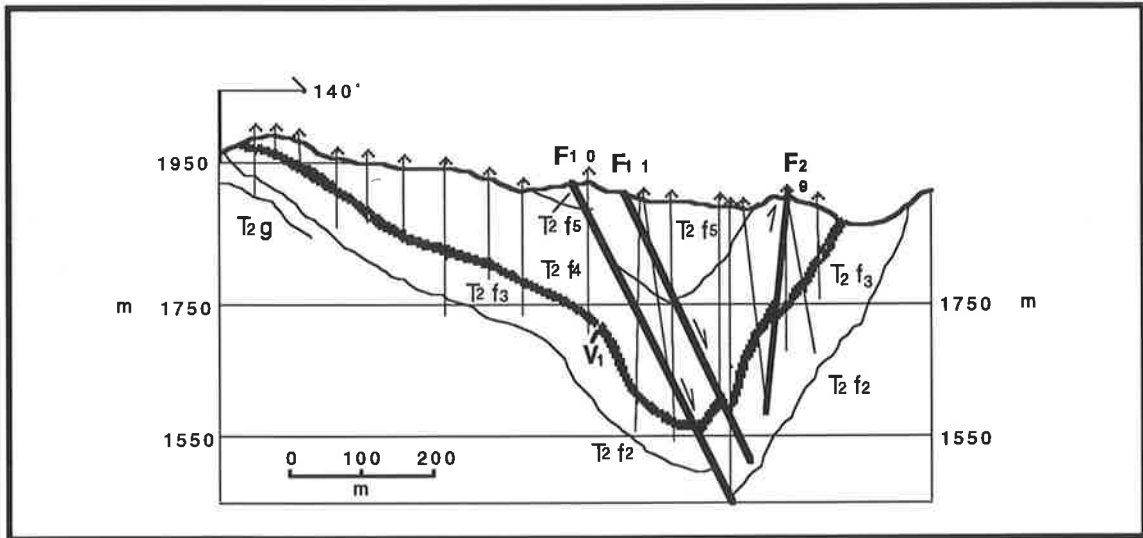


Fig. 2.2 Geological section along prospecting line 56, Dounan manganese mine, modified after Liu et al (1984; also see Fig. 2.4).

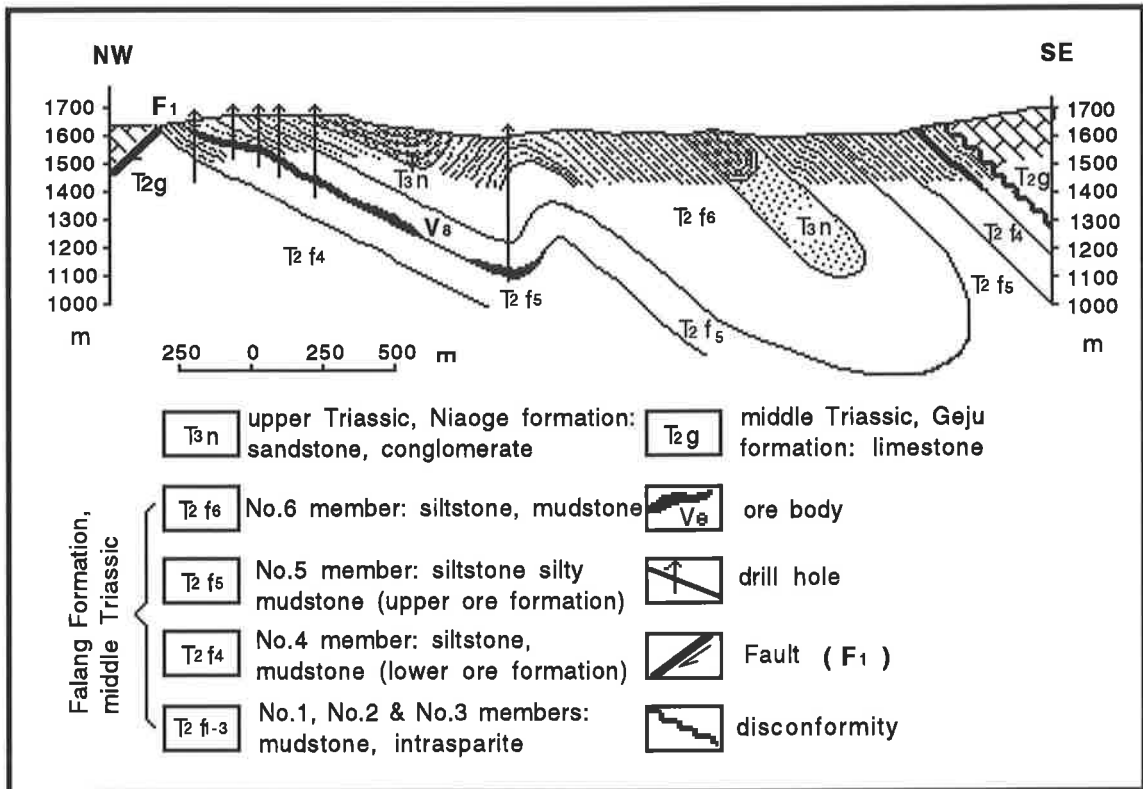


Fig. 2.3 Geological section along prospecting line 17, Dounan manganese mine, modified after Liu et al (1984; also see Fig. 2.4).

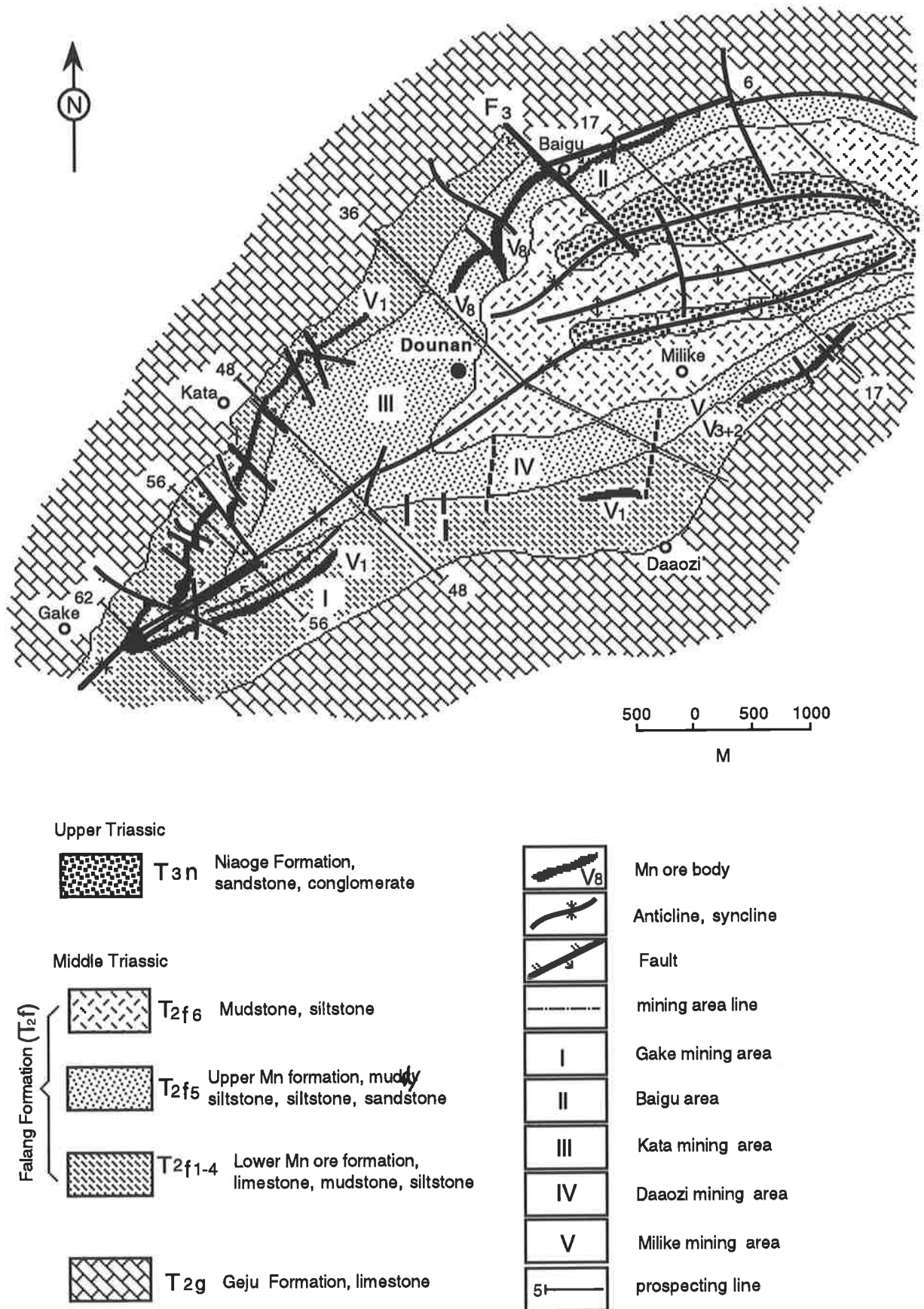


Fig. 2.4 Geological map of Dounan Mn mine area in the Dounan syncline of southeastern Yunnan, modified after Liu et al (1984).

The rocks comprising the Dounan syncline are intensely faulted, especially in the Gake area, and cross-faults (WNW-ESE) are common. Generally, there are four groups of faults in the Dounan manganese deposits:

- (1). ENE-WSW reverse faults mainly distributed near the axis of the Dounan syncline and parallel with the latter; they intensely affect orebodies in the Gake area, but have little influence in other mining areas, which normally are cut by cross-faults.
- (2). NW-SE dipping normal faults striking N 30°-40° W and dipping W at 70°-80°; the zone of fracturing is about 10 meters wide. They intensely influence orebodies and cut NE trending thrust faults.
- (3). WNW-ESE trending normal cross-faults dipping SW at ~ 70°, with a fracture zone 0.1-several meters wide. They are distributed throughout the Dounan syncline, cut other groups of faults, and also have destroyed some orebodies.
- (4). NS trending normal faults dipping to the east at 70°-80°, with a 1-10 meters wide fracture zone, occasionally up to 20 meters. Some orebodies are highly fractured by this group of faults.

2.4 Regional Stratigraphy, Facies and Microfacies of Southeastern Yunnan

The sedimentary manganese ore deposits of middle Triassic age, as already stated, occur in several districts of southeastern Yunnan. The most important and extensive deposits occur in the Yanzijao-Dounan-Laowu ore-forming belt confined to the Falang Formation of middle Triassic age. In addition there is another manganese ore belt in the western area of southeastern Yunnan (i.e. Baixian). There is, however, a great difference in rock association of the Falang Formation between the two sedimentary basins due to the different sedimentary facies/environments. The western basin mainly consists of carbonates with minor Mn-bearing clastic sediments; whereas the eastern basin is composed of terrigenous clastic rocks intercalated with intraclastic carbonates and Mn-bearing formation. In addition, turbidite facies clastic rocks occur in Yangqigou, the northeastern part of the area.

Generally, the Mn-bearing sequence consists of three or four sedimentary cycles. Mn orebeds occur in the middle and/or upper cycles, and mainly in the mixed association of clastic and carbonate rocks. Detailed measured sections from different districts are given from the southwest to the northeast of southeastern Yunnan in the following sections (see Figs. 1.1 and 1.3).

The study and interpretation of the textures, sedimentary structures, fossils and lithologic associations of the Falang Formation sedimentary rocks in some localities adjacent to the Dounan sub-basin, well section or small segment of southeastern Yunnan marine basin comprise the subject of facies analysis. In writing this section the several excellent texts (e.g. Walker, 1979; Wilson, 1975; Reading, 1978; Blatt et al., 1980; Leeder, 1982; Miall, 1984; Einsele, 1992) that deal exclusively with facies analysis have been reviewed. This section focuses on a discussion of

the Dounan facies analysis on a regional basis. This discussion will provide an introduction to the Dounan facies modeling analysis.

2.4.1 *Baixian (in Jianshui) Section*

The sedimentary features and microfacies analysis of Baixian geological section suggest that the sediments of the Falang Formation can be divided into four sedimentary cycles (Figs. 2.5 and 2.6): Cycle I lacks a transgression phase and consists of a half sedimentary cycle; cycles II, III, and IV are complete.

Cycle I: this includes T2fa1-3 members which consist of shale, calcilutite, and dolosparite, characterized by lamination, burrows, and foraminifera in the lower part; lamination and algae in the middle part; and desiccation cracks in the upper part, which suggests a microfacies association of lagoon-intertidal flat-evaporite flat environments.

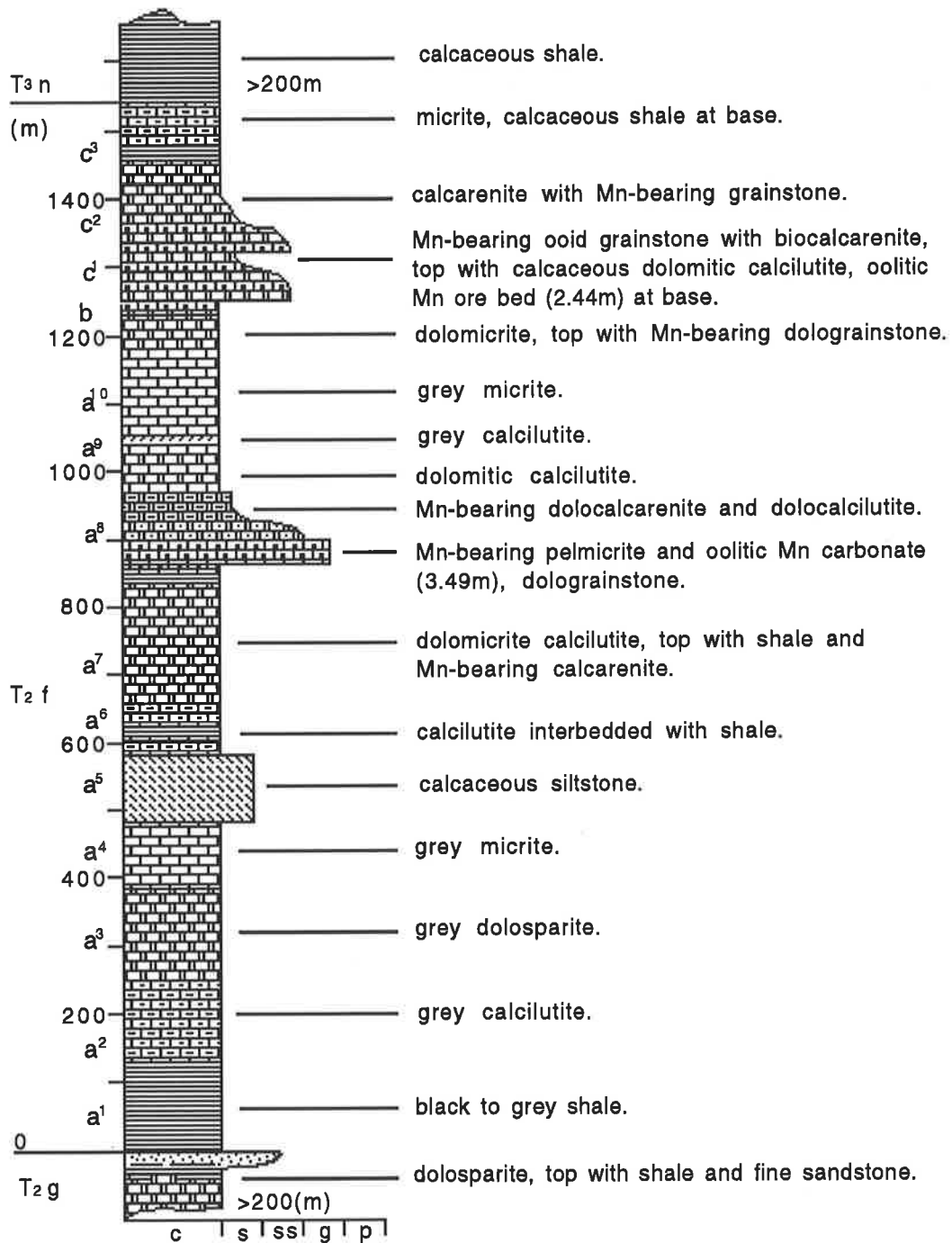
Cycle II: this includes T2fa4-7 members composed of micrite, muddy and calcareous siltstone, calcilutite, dolomicrite, and minor Mn-bearing calcarenite, characterized by cross-bedding, lamination, stromatolites, bivalves, and foraminifera in the lower part, foraminifera, and burrows in the middle, followed by cross-bedding, stromatolites, and birdseye structures in the upper parts, which indicates a microfacies evolution of tidal flat-lagoon-tidal flat-evaporite flat environments.

Cycle III: this includes T2fa8-10 members consisting of micrite, calcilutite, dolomitic calcilutite, and calcarenite, with Mn-bearing limestone and Mn orebeds at the base (~3.49 m), characterized by low-angle cross bedding, wavy bedding, algae and anthozoa fossils in the lower part; lamination, desiccation cracks and birdseye structures, foraminifera and crinoids in the upper part, suggesting a microfacies evolution of tidal flat-lagoon-tidal flat-evaporite flat environments.

Cycle IV: this contains T2fb and T2fc1-3 members composed of micrite, calcareous shale, and dolomicrite. The lower part has calcarenite, biocalcarenite, an oolitic Mn orebed (~2.44 m) and is characterized by lamination, stromatolites, bivalves, crinoids, with desiccation cracks and birdseye structures near the top. The middle part is characterized by wavy bedding, stromatolites, gastropodes, bivalves, and crinoids, following lamination and desiccation cracks. The upper part is rich in lamination, stromatolites, and crinoids. All these suggest a microfacies evolution of three sub-cycles from tidal flat to evaporite flat.

This section, therefore, contains two Mn orebeds which both occur in the initial period of regressions, and a total of ~1445 m of sediments. Its representative fossils are *Daonella aff. indica* Bittner, *Halobia cf. plamicosta* Yin et Hsu. The Falang Formation is conformable with both underlying Geju and overlying Niaoge Formations.

2.4.2 *Jiasha (in Geju) Section*

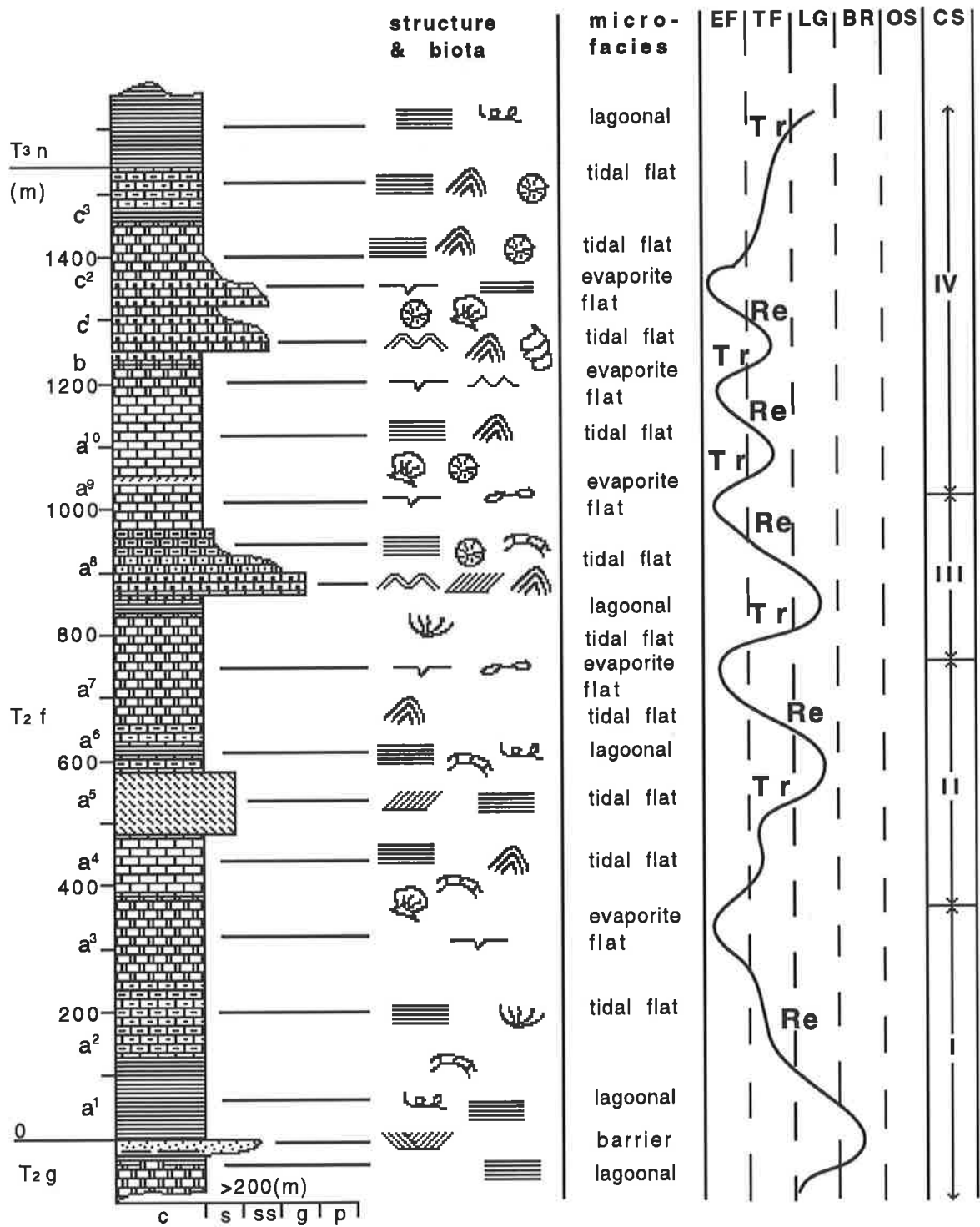


(grainsize)

c - clay, s - silt, ss - sand

g - granule, p - pebble

Fig. 2.5 Stratigraphic section, Falang Formation, at Baixian of southeastern Yunnan, data from Liu et al (1984). For legend see Table 2.1.



(grainsize)

c - clay, s - silt, ss - sand
g - granule, p - pebble

Fig. 2.6 Stratigraphic and facies profile of Falang Formation at Baixian of southeastern Yunnan, data from Liu et al (1984). For legend see Table 2.1.

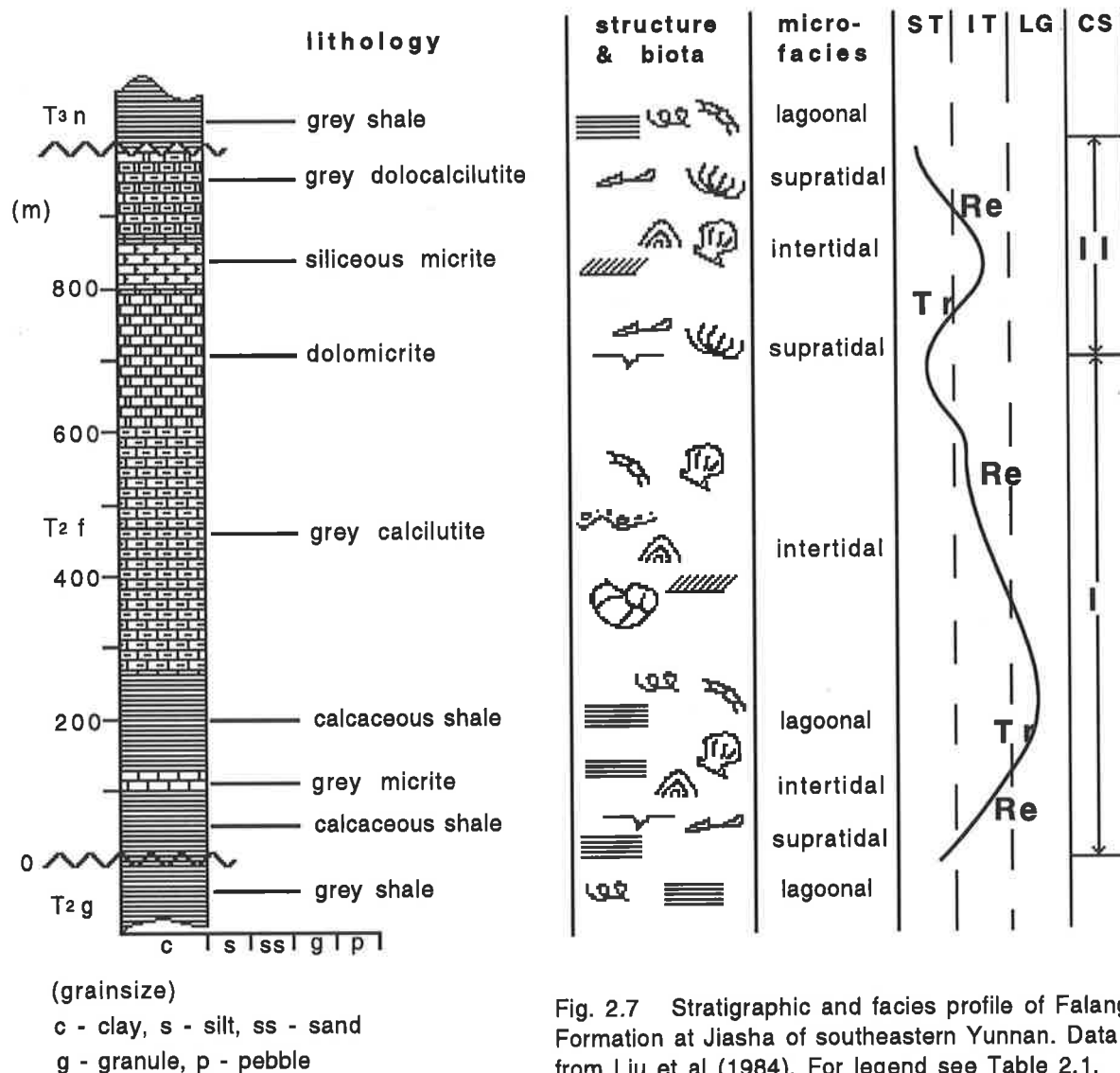


Fig. 2.7 Stratigraphic and facies profile of Falang Formation at Jiasha of southeastern Yunnan. Data from Liu et al (1984). For legend see Table 2.1.

Two sedimentary cycles can be recognized in the 1000 m thick Jiasha section of the Falang Formation (Fig. 2.7):

Cycle I: the lower cycle is composed of calcareous shale and calcilutite, and is disconformable over the underlying Geju Formation. It is characterized by desiccation cracks and birdseye structures, lamination, foraminifera, ostracods, stromatolites, and bivalves at the base; lamination, foraminifera, and burrows in the middle; and low-angle cross bedding, scouring, desiccation cracks and birdseye structures, stromatolites, ammonoids, bivalves, and algae at the top, which suggests a microfacies evolution of supratidal-intertidal-lagoon-intertidal-supratidal environments.

Cycle II: the upper cycle consists of dolomicrite, siliceous micrite, and dolocalcilutite, and also is overlain disconformably by the Niaoge Formation. It is characterized by desiccation cracks and birdseye structures, low-angle cross bedding, algae, stromatolites, and bivalves, which indicates a microfacies development of supratidal-intertidal-supratidal environments.

2.3.4 Bapanzai (in Kaiyuan) Section

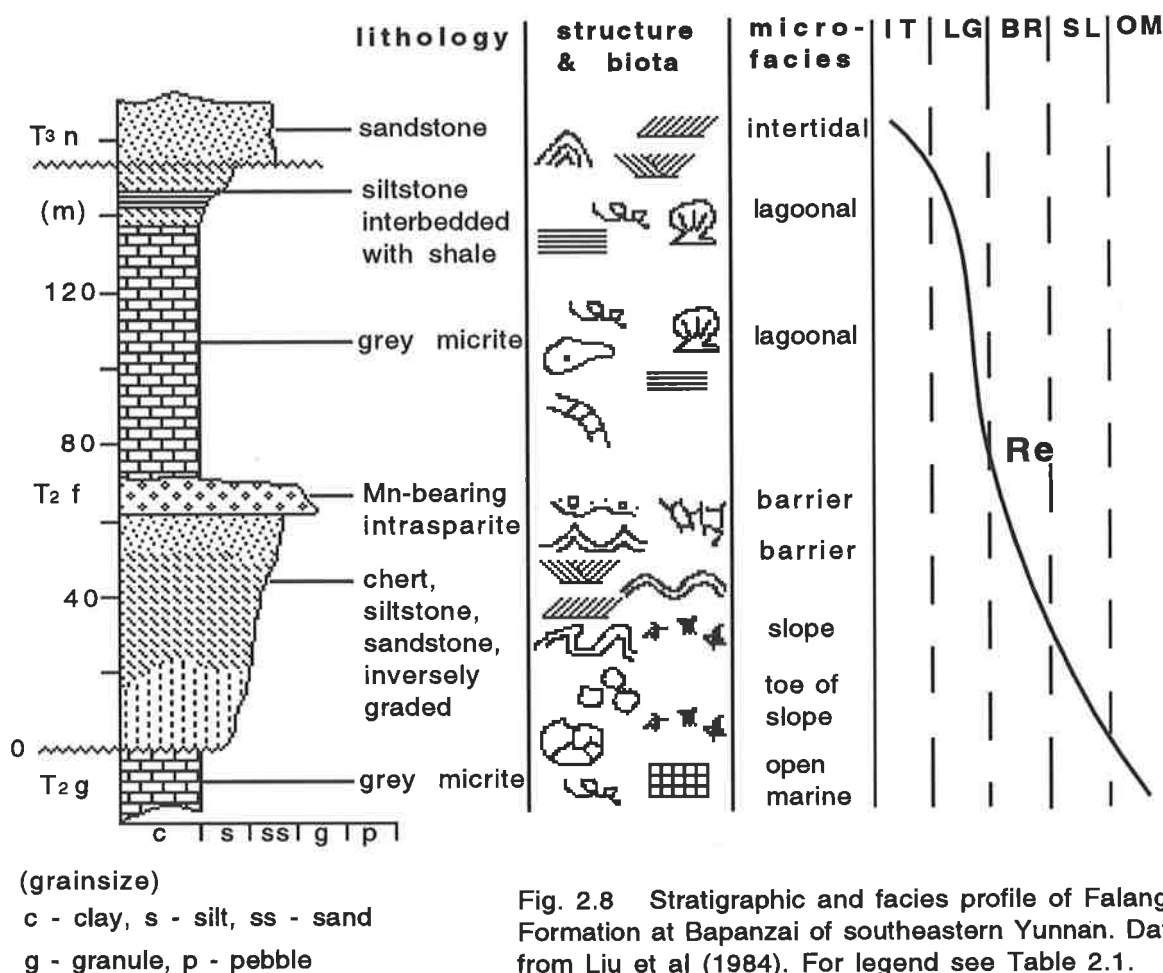


Fig. 2.8 Stratigraphic and facies profile of Falang Formation at Bapanzai of southeastern Yunnan. Data from Liu et al (1984). For legend see Table 2.1.

At Bapanzai, the Falang Formation is thin (~148.5 m) and probably incomplete, consisting of a simple regressive sedimentary cycle (Fig. 2.8). The lower part is composed of chert, quartz siltstone, and fine quartz sandstone, and shows a disconformity with the underlying Geju Formation. It is characterized by massive bedding, exotic blocks, slump bedding, and bioclastic debris. The middle part consists of quartz sandstone and Mn-bearing intrasparite, characterized by wavy bedding, cross-bedding, and anthozoan fossils. The upper part is made up of micrite, siltstone, and shale, and also has a disconformable relationship with the overlying Niaoge Formation. It is characterized by lamination, low-angle cross bedding, burrows, foraminifera, ostracods, and bivalves. The sedimentary features suggest a regressive microfacies evolution of open marine-slope-barrier-lagoon-intertidal environments.

2.4.4 Yanzijiao (in Mengzi) Section

The Falang Formation is well represented in Yanzijiao, Dounan, and Laowu which belong to the Dounan marine basin. The important concentrations of manganese ores have been found in this Formation in these three districts. The broad stratigraphic succession of the Falang Formation at Yanzijiao is given as follows (298.83 m total thickness):

Tertiary red conglomerate

----- Disconformity -----

- 9) Grey or light grey dolomicrite, mostly occurring as lenticular layers, characterized by stromatolites, low-angle cross bedding, scouring, desiccation cracks and birdseye structures, ~75 m in thickness.
- 8) Dark red mudstone with micrite lenses, lamination, containing bivalve and burrow fossils: *Daonella ex. gr. Gevillia sp. Posidonia aff. Wengensis* Wissmann, ~12.30 m in thickness.
- 7) Light yellow mudstone, with Mn-bearing oolitic mudstone at top, characterized by cross-bedding, wavy bedding, and lamination, and bivalves [e.g. *Daonella lommeli* (Wissmann)], anthozoa, foraminifera, and gastropod fossils, ~7.70 m in thickness.
- 6) Brownish red mudstone with low-angle cross bedding and lamination, and stromatolites, foraminifera, and bivalves: *Daonella lommeli* (Wissmann), ~36.80 m in thickness.
- 5) Yellow mudstone with brown mudstone intercalations, and minor sandy Mn oxides at base, containing lamination, burrows, foraminifera, and bivalves: *Daonella lommeli* (Wissmann), *Posidonia cf. Wengensis* (Wissmann), ~32.80 m in thickness.
- 4) Black massive and banded Mn oolitic oxide ores consisting mainly of psilomelane and pyrolusite being divided two layers: upper layer ~0.20 m and lower layer ~0.33 m with 1.20 m intervening gangue ~1.73 m total thickness.
- 3) Grey or light grey intrasparite, brecciated structure, both clasts (1-3 cm) and matrix (cement) consisting of micrite, characterized by wavy bedding, minor ostracods and anthozoans, ~30.80 m in thickness.
- 2) Dark red mudstone with lamination, burrows, and foraminifera, ~17.60 m in thickness.
- 1) Yellow-green mudstone with fossiliferous intrasparite at base, characterized by cross-bedding, ripple marks, and bivalves: *Daonella lommeli* (Wissmann), ~34.10 m in thickness.

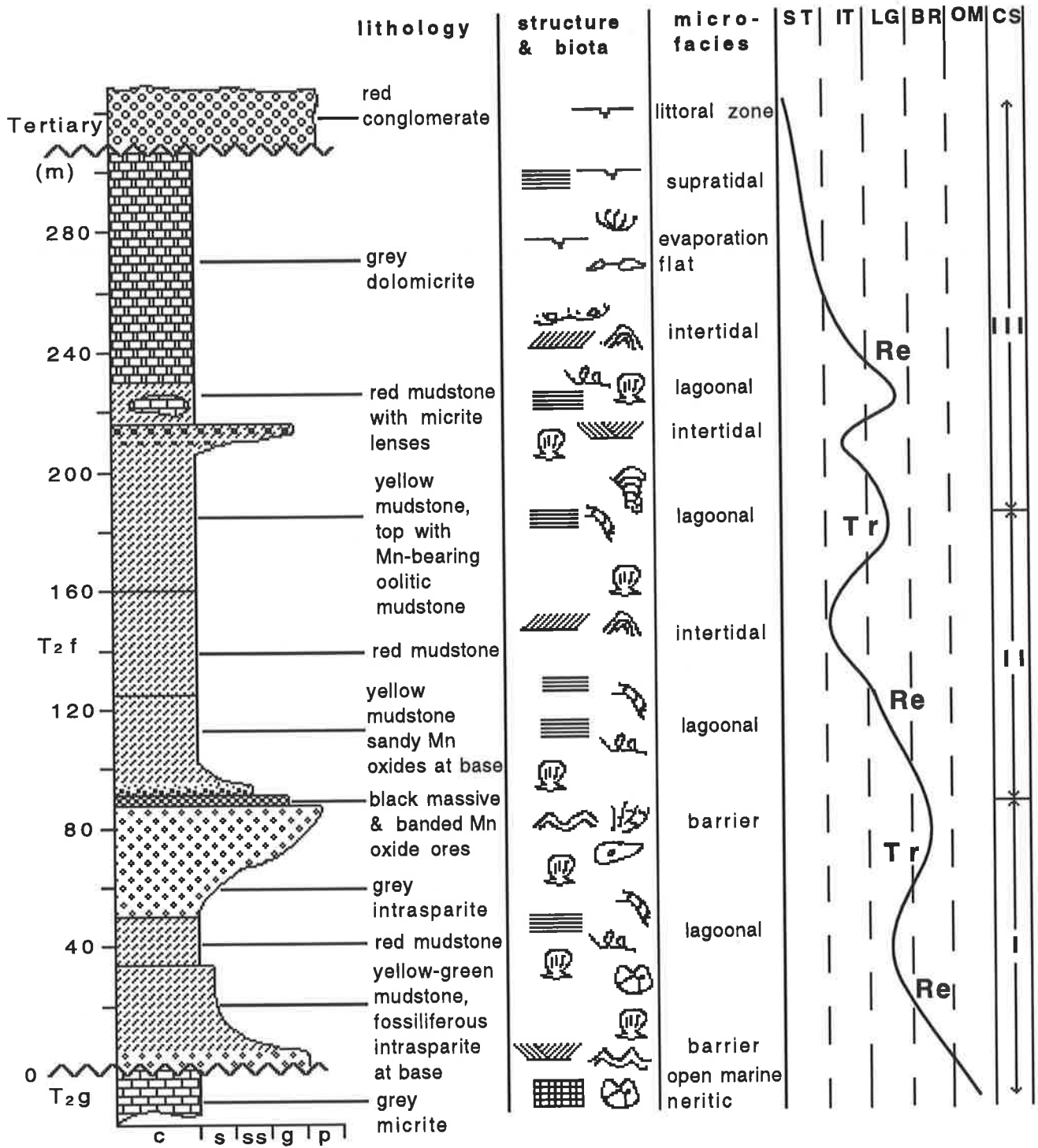
----- Disconformity -----

Geju Formation (T_{2g}) grey micrite with massive bedding and ammonoids

In summary, the Yanzijao stratigraphic sequence of the Falang Formation, the sequence varies from silty claystone, intrasparite, Mn-bearing micrite, and Mn orebeds to dolomicrite from the base to the top, the thickness varies from 81.81 m to 514.10 m and the unit contains plentiful fossils such as: *Danonella bulogensis bifurcata*, *D. lommel* (Wissmann), *Posidonia Wengensis*, *Myophoria sp.*, *Halobia aff. rugosodes Hsu*, *Anodontopnora sp.*, *Pratrachycgras douvillei*, *Trachyceras sp.* (Liu et al., 1984). Thus the characteristics described above suggest that the sedimentation can be divided into three cycles (Fig. 2.9):

Cycle I: including T_{2f1-3} members, with microfacies development of barrier-lagoon-barrier.

Cycle II: including T_{2f4-6} members, with microfacies association of lagoon-intertidal-lagoon, the lower Mn orebeds formed at base.



(grainsize)

c - clay, s - silt, ss - sand

g - granule, p - pebble

Fig. 2.9 Stratigraphic and facies profile of Falang Formation, at Yanzijao of southeastern Yunnan. Data from Liu et al (1984). For legend see Table 2.1.

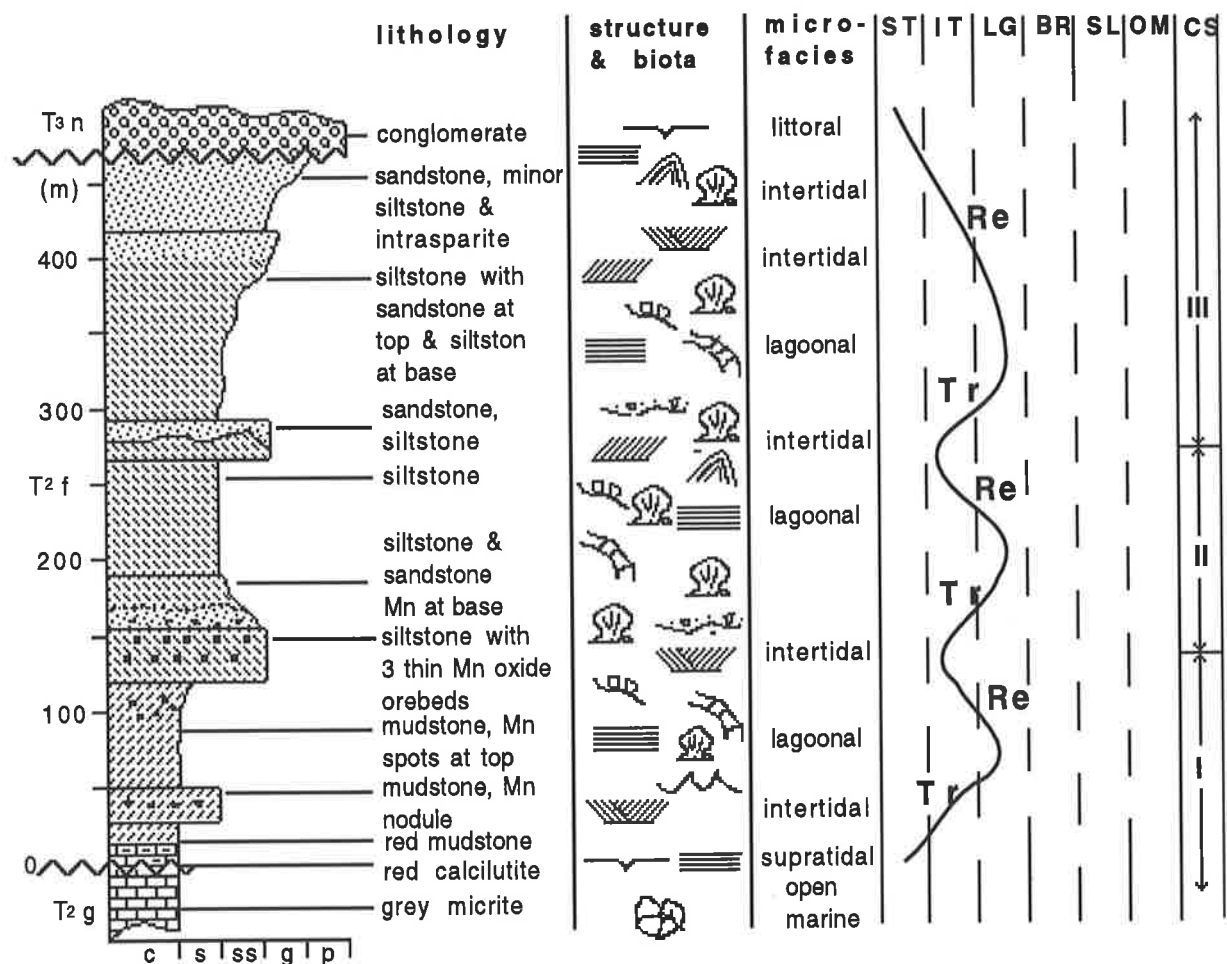
Cycle III: including T2f7-9 members, with microfacies evolution of intertidal-lagoon-intertidal-
evaporation flat/supertidal, the upper Mn orebeds formed at the base.

2.4.5 Dounan Section

The Dounan Falang Formation consists of mudstones, siltstones, intraclastic limestones, and Mn orebeds (~10 layers), and contains plentiful fossils. This section will be described in detail in section 2.5 due to its importance in the studied area.

2.4.6 Laowu (in Wenshan) Section

This section lies to the NE of Dounan and totals to 433.44 m in thickness. The stratigraphic succession is divided into 10 members as follows (Fig. 2.10):



(grainsize)
 c - clay, s - silt, ss - sand
 g - granule, p - pebble

Fig. 2.10 Stratigraphic and facies profile of Falang Formation, at Laowu of southeastern. Data from Liu et al (1984). For legend see Table 2.1.

Niaoge Formation (T_{3n}): conglomerate and sandy conglomerate which consist mainly of quartz sandstone, quartzite and chert, with desiccation structures.

----- **Disconformity** -----

- 10) Yellow sandstone with siltstone and intrasparite intercalations. Cross-bedding, stromatolites, and bivalves are common, ~53.19 m in thickness.
- 9) Yellow sandstone and siltstone at top, muddy siltstone at the middle and base, commonly with bivalves, foraminifera, burrows, and low-angle cross bedding at top and lamination at base, ~128.28 m in thickness.
- 8) Light yellow sandstone and siltstone with low-angle cross bedding, scouring, stromatolites, and bivalves, ~18.77 m in thickness.
- 7) Yellow siltstone. lamination, burrows, foraminifera, and bivalves are common. ~73.17 m in thickness.
- 6) Yellow fine sandstone and siltstone, with abundant Mn matrix and spots at base, characterized by low-angle cross bedding, wavy bedding, and bivalves, ~29.99 m in thickness.
- 5) Yellow siltstone and mudstone, with 3 thin granular Mn orebeds. The major orebed (at base) consists of psilomelane and pyrolusite (~1.15 m), and has oolitic, banded, and some typical supergene (e.g. honey, reniform and botryoidal) structures. Two other orebeds occur as lenticular layers and poor quality ores. Cross-bedding and wavy bedding are common. ~17.89 m in thickness.
- 4) Yellow mudstone, with minor black Mn oxide spots, lamination, burrows, foraminifera, and bivalves. ~70.08 m in thickness.
- 3) Yellow mudstone with Mn oxide pisolites which can be correlated with Dounan Lower ore-bearing series (T_{2f4-1}). Cross-bedding and ripple marks are common. ~20.43 m in thickness.
- 2) Dark red mudstone with lamination, desiccation and birdseye structures, ~5.13 m in thickness.
- 1) Dark red calcilutite with desiccation and birdseye, ~12.61 m in thickness.

----- **Disconformity** -----

Geju Formation: grey micrite with massive bedding and annonoids.

The characteristics described above suggest the following three sedimentary cycles:

Cycle I: including the members 1-4 which indicate a microfacies association of supratidal-intertidal-lagoon-intertidal, grading upward into

Cycle II: including the members 5-7 which suggest a microfacies evolution of intertidal-lagoon-intertidal, Mn deposit formed at the base of the cycle, grading upward into

Cycle III: including the members 8-10, evolving lagoon-intertidal-supratidal environments.

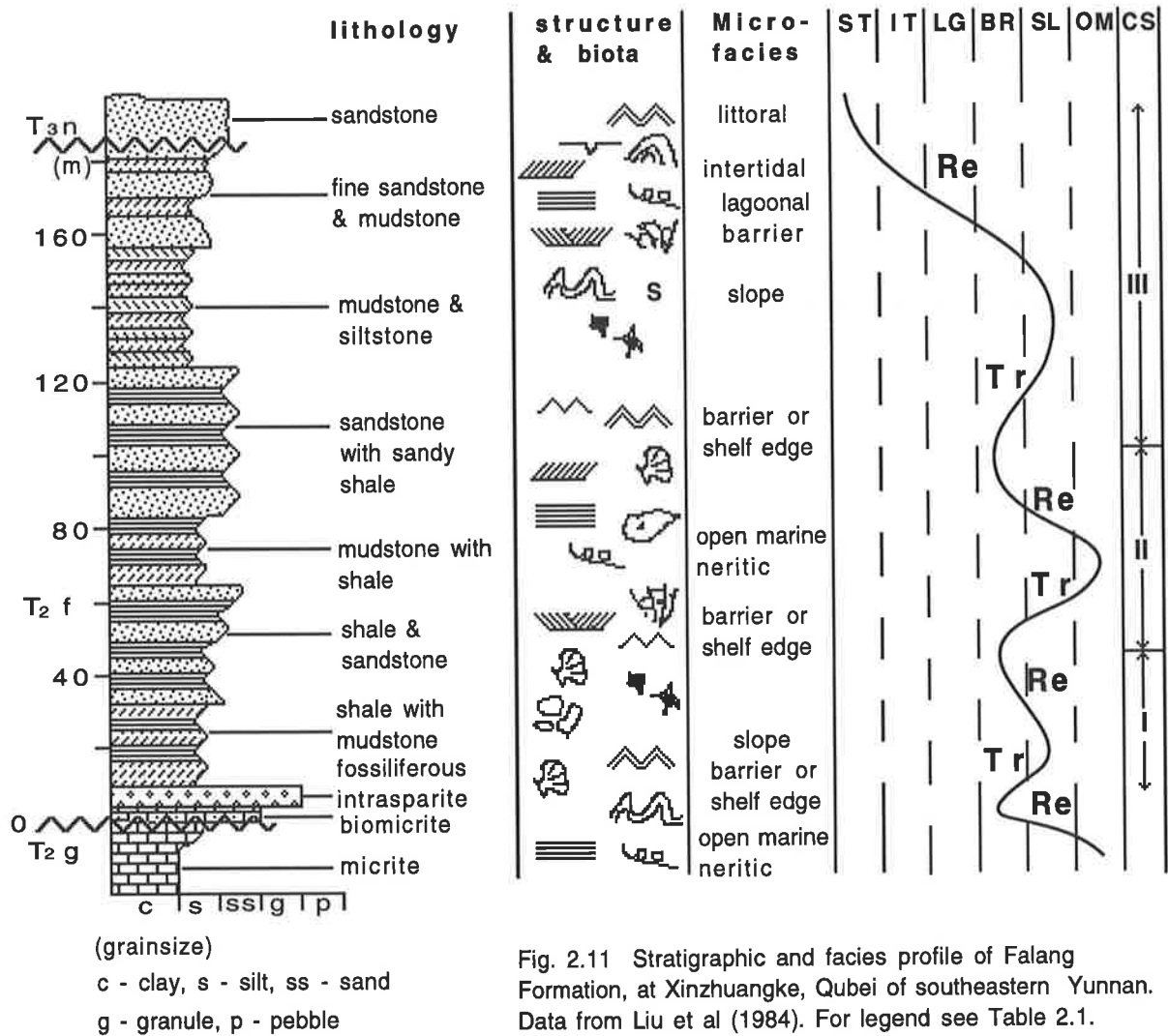


Fig. 2.11 Stratigraphic and facies profile of Falang Formation, at Xinzhuangke, Qubei of southeastern Yunnan. Data from Liu et al (1984). For legend see Table 2.1.

2.4.7 Xinzhuangke (in Qubei) Section

The stratigraphy and microfacies of the Falang Formation at Xinzhuangke are shown in Fig. 2.11. Here, the Falang Formation has a thickness of ~182.50 meters, and has disconformable relationships with both the overlying Niaoge and underlying Geju Formations. Three sedimentary cycles have been worked out as follows:

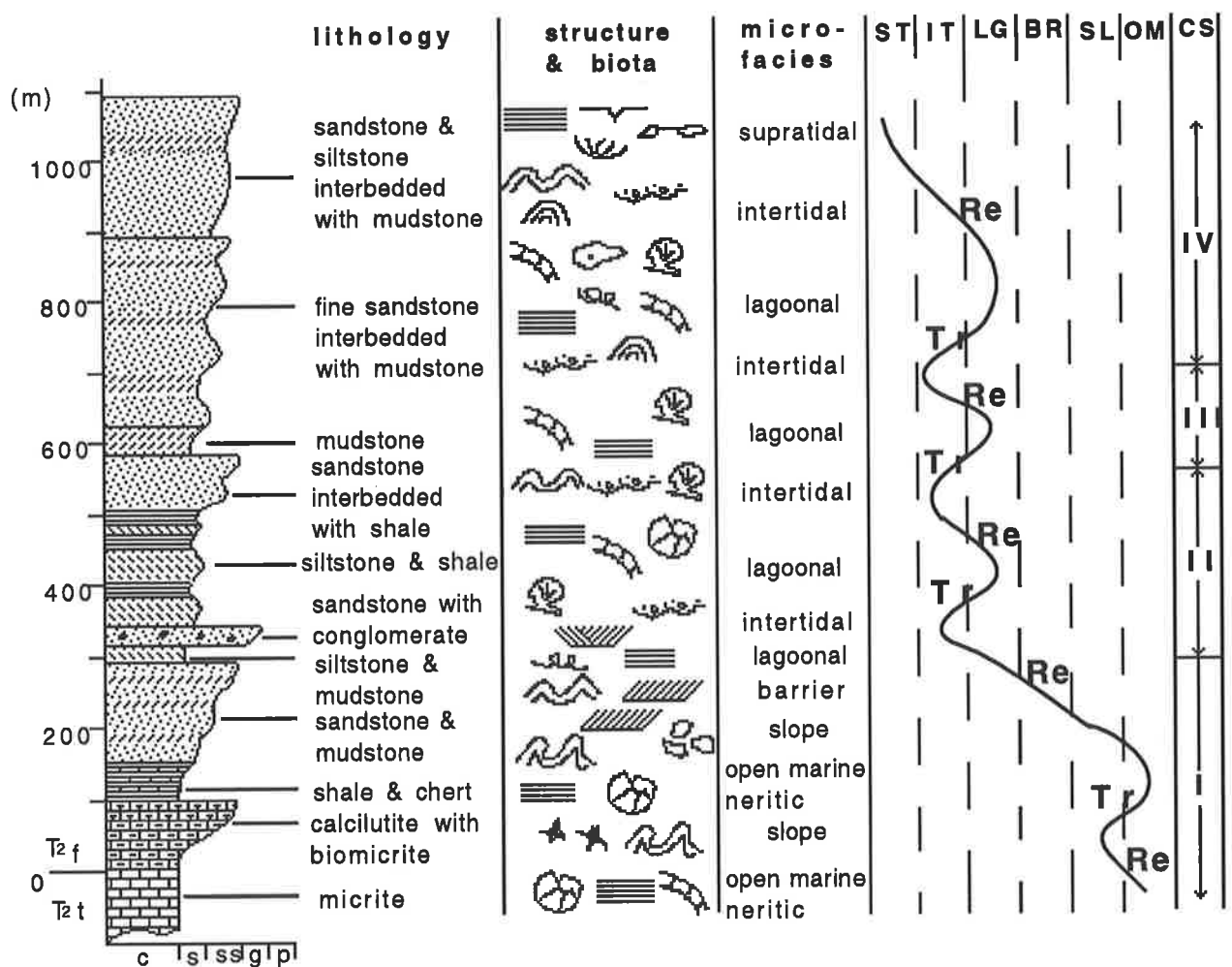
Cycle I: from the bottom to the top, consisting of biomicrite, fossiliferous intrasparite, shale with mudstone intercalations, shale interbedded with fine quartz sandstone. Wavy bedding, slump bedding, turbidites, cross-bedding, ripple marks, exotic blocks, bioclastic debris, anthozoans, and bivalves are common. The microfacies development is suggested as barrier-slope-barrier, grading upward into

Cycle II: from the bottom to the top, composed of silty sandstone with shale intercalations, fine quartz sandstone with shale, mudstone/siltstone, characterized by lamination, turbidite, oblique bedding, wavy bedding, ripple marks, slump bedding, burrows, ostracods, and bivalves, indicating a microfacies association of open marine neritic-slope-barrier, developing upward into

Cycle III: from the bottom to the top, made up of mudstone, siltstone, fine sandstone with mudstone, characterized by slump bedding, turbidites, bioclastic debris, cross-bedding, lamination, low-angle cross bedding, desiccation forms, burrows, and stromatolites, suggesting a microfacies development of slope-barrier-lagoon-intertidal environments.

2.4.8 Shiwang (in Qubei) Section

The Niaoge Formation (T3n) cannot be seen in this section probably due to erosion or to poor outcrop. The Falang Formation is over 1000 meters thick and shows a disconformity with underlying the Tuowei (T2t) Formation, and is characterized by turbidites. The study of the measured section allows the following environmental analysis from the bottom to the top (Fig. 2.12):



(grainsize)
 c - clay, s - silt, ss - sand
 g - granule, p - pebble

Fig. 2.12 Stratigraphic and facies profile of Falang Formation, at Shiwang of southeastern Yunnan. Data from Liu et al (1984). For legend see Table 2.1.

Cycle I: consisting of calcilutite with biomicrite, shale, chert, mudstone, and quartz sandstone, characterized by typical Bouma sequences, slump bedding, lamination, wavy bedding, exotic blocks, bioclastic debris, and ammonoids, suggesting a microfacies evolution of slope-open sea-slope-barrier, followed by

Cycle II: composed of mudstone, siltstone, quartz sandstone with conglomerate, siltstone interbedded with shale, characterized by lamination, wavy bedding, scouring, stromatolites, foraminifera, ammonoids, and bivalves, indicating a microfacies association of lagoon-intertidal-lagoon-intertidal-lagoon, grading upward into

Cycle III: made up of fine quartz sandstone, mudstone, siltstone, and sandstone, characterized by lamination, wavy bedding, scouring, desiccation, birdseye, stromatolites, burrows, foraminifera, algae, and bivalves, suggesting a microfacies development of intertidal-lagoon-intertidal-supratidal environments.

2.4.9 Yangqigou (in Qubei) Section

The Falang Formation of this section has disconformable relationships with both overlying T_{3n} and underlying T_{2b} Formations, and possesses a rock association of grey calcareous mudstone interbedded with siltstone and fine sandstone, characterized by grading bedding, ripple marks, cross-bedding, and typical Bouma sequence (turbidite), ~3142.82 m in thickness, with determined fossils: *Protrachyceras costulatum*, *P. Ladinum*, *Trachyceras Sinense*, *Halobia rugosoides*, *H. Planicosta*, *Daonella lommeli* (Wissmann), which suggest a regressive microfacies evolution of open sea-slope-barrier-lagoon-intertidal-supratidal environments from the bottom to the top.

2.5 Local (Dounan) Stratigraphy, Facies and Microfacies

2.5.1 Introduction

This section focuses on a discussion of facies, microfacies or environments based on the kinds of examined information. It is hoped that this examination will provide a significant facies model or sedimentary environment of the Dounan Mn deposits, so that it can be applied to interpret the genesis of the deposits. The major Triassic sediments at Dounan are distributed on a relatively wide scale (Fig. 2.4). The Dounan stratigraphy is simply composed of Triassic Geju, Falang, and Niaoge Formations. Of these, the Geju Formation consists of limestone, and the Falang Formation contains a relatively complex rock association of both clastic rocks and carbonates, whereas the Niaoge Formation consists solely of coarse clastic rocks. Fossils are plentiful in the latter two units. The stratigraphic classification of the Falang Formation as suggested by Zhang et al (1979) is given in Table 2.2 for detailed study to be analyzed in the following sections (Fig. 2.13).

Table 2.2 General stratigraphy of Dounan area, modified after Zhang et al (1979).

System	Formation	Member	Sub-member	Key	Thickness (m)			
					Min.	Max.	Ave.	
Quaternary alluvial and eluvial series					Q	2	12	6
Upper Triassic	Niaoge	sandstone mudstone		T _{3n2}		>130		
		sandstone conglomerate		T _{3n1}	188	200	195	
Disconformity								
Middle Triassic	Falang	laminated siltstone mudstone		T _{2f6}	66	172	110	
		upper ore-containing series	fissile siltstone with limestone	T _{2f5-3}	110	137	115	
			Baigu ore-bearing series	T _{2f5-2}	45	72	60	
			sideritic siltstone	T _{2f5-1}	29	62	45	
		lower ore-containing series	fissile mudstone	T _{2f4-4}	29	53	40	
			Mn-bearing mudstone	T _{2f4-3}	22	40	37	
			laminated calcareous siltstone	T _{2f4-2}	11	37	34	
			Gake ore-bearing series	T _{2f4-1}	21	35	23	
		dark red beds	brecciated limestone	T _{2f3-2}	5	30	26	
			mudstone	T _{2f3-1}	11	43	28	
		grey-green mudstone		T _{2f2}	16	203	132	
		grey intraclastic carbonates		T _{2f1}	5	11	8	
		Disconformity						
	Geju	grey limestone		T _{2g}	2499.5			

2.5.2 Stratigraphy

The stratigraphy of the Dounan area is divided as follows (from base; Fig. 2.13):

1) *Middle Triassic Geju Formation (T_{2g})*: grey micrite but with minor quartz silts and dolomite in Gake, containing crinoids and ammonoids such as *Protachyceras? sp.* *Dagnoceras sp.*

----- **Disconformity** -----

2) *The Middle Triassic Falang Formation (T_{2f})* can be divided into six members (one to six in ascending order). Of these the members 3 (T_{2f3}), 4 (T_{2f4}) and 5 (T_{2f5}) can further be divided into a number of sub-members:

(1) *5 to 11 meters. Member 1 (T_{2f1})*: grey intraclastic limestone can be divided into two sub-members:

- i. *Clay and conglomerate*: only occur on the disconformity face with underlying Geju Formation (Plate 2.1, Fig. 2d), conglomerate (0.5-5 cm) consisting of micrite with red colour.
- ii. *Grey intraclastic micrite and calcilutite with minor pyrite*, grains varying 1-5 cm and lying parallel to the layer; characterized by bivalves, foraminifera, ostracods, gastropods, spherical algae.

(2) *16 to 203 meters. Member 2 (T_{2f2})*: dark grey mudstone with bioclastic calcarenite intercalation characterized by lamination and massive bedding and fossils such as: *Daonella aff. sturi* Benecke, *D. cf. dubia* Gabb, *D. lommeli* (Wissmann), *Dagnoceras tinae* Spath, *Posidonia cf. wengensis* Wissmann. Commonly, the petrology and thickness of this member change greatly from the southwest to the northeast, e. g. mudstone in Gake (~200 m in thickness), to the northeast (Kata), mudstone interbedded with micrite (~100 m in thickness), and to eastern Baigu carbonates (~20 to 50 meters).

(3) *Member 3 (T_{2f3} ~50 m in thickness)* dark red 'brecciated' rocks. Two sub-members can be recognized:

- i. *11 to 43 meters. Red and green mudstone (T_{2f3-1})*, with siltstone intercalations, composed of argillaceous hydromica clay, kaolin, and minor silts, and characterized by massive bedding, ostracods, foraminifera, crinoids, spherical algae, and bivalves such as: *Posidonia cf. wengensis* Wissmann and *Protrachyceras doprati* Mansuy.
- ii. *5 to 30 meters. Dark red intraclastic limestone (T_{2f3-2})*: primary 'brecciated' micrite, irregular brecciated texture (0.2-15 cm), composed of bioclastic micrite and quartz silts, mainly Fe oxide-bearing micrite and argillaceous materials and biofragments which are cemented by quartz silts (10-15%), calcarenite (~20%), Fe oxide-bearing argillaceous cement (~10%). The grains mostly do not show orientated arrangement but inverse grading. Significantly, this layer is the under-

lying key bed of lower (Gake) ore-bearing series; It is characterized by crinoids, foraminifera, ostracods, gastropods, spherical algae, e.g. *Protrachyceras* or *Trochyceras* sp.

(4) *Member 4* (T2f4, ~130 m in thickness) lower ore-bearing member mainly distributed in all mining areas but minor in Baigu area. Laterally, clastic rocks mainly occur in the western part (e.g. Gake and Kata areas), whereas intraclastic carbonates dominate the eastern part (e.g. Baigu area). This unit can be divided into four sub-members;

i. *21 to 35 meters*. Gake ore-bearing series (T2f4-1): grey fissile mudstone or siltstone with oolitic/pisolitic micrite, intraclastic micrite, and thin Mn orebed intercalations in the upper part; the lower part contains intraclastic micrite with siltstone, Mn-bearing limestone, and Mn orebed intercalations. There are usually oncolites and catagraphias in micrite. The ores and rocks are characterized by ooliths/pisoliths, brecciation, normal and inverse grading, lamination, low-angle tabular cross-bedding, ripple marks, scouring, and ostracods, foraminifera, gastropods, algae, bioclastic debris, and bivalves, e.g. *Posidonia* cf. *wengensis* (Wissmann), *Clionites* sp. *Daonella lommeli* (Wissmann). The T2f4-1 sub-member contains five economic orebeds (i.e. V1, V2, V3, V3+1, and V3+2), and three uneconomic orebeds (i.e. V1+1, V1-1, and V1-2). Mostly, the orebeds change laterally into Mn-bearing rocks from the southwest (e.g. Gake) to the northeast (e.g. Baigu).

ii. *11 to 37 meters*. Grey laminated calcareous siltstone (T2f4-2), with calcilutite, calcarenite, and lenticular bioclastic micrite intercalations, and characterized by lamination, cross-bedding, wavy bedding, and fossils such as *Posidonia* cf. *ovalis* Kittl, *Daonella lommeli* Wissmann *D. cf. indica* Bittner, *Trachyceras sinensis* Mansuy.

iii. *22 to 40 meters*. Grey Mn-bearing mudstone (T2f4-3), with a number of layers (2-13) of intraclastic micrite intercalations, and a local poor manganese orebed; characterized by lamination, deformed bedding, wavy bedding, cross-bedding, and fossils such as: *Daonella lommeli* Wissmann, *Posidonia* sp., *Hectoria* sp. and *Clionites* sp.

iv. *29 to 53 meters*. Grey fissile mudstone (T2f4-4), with siltstone or siltstone intercalations, and characterized by lamination, wavy bedding, low-angle cross bedding, slump bedding, small ripple marks and bivalves. Towards eastern Baigu the unit changes laterally into calcarenite, bioclastic limestone and minor Mn-bearing micrite.

(5) *Member 5* (T2f5) upper ore-bearing member which is mainly distributed in the Baigu and Milike areas and can be divided into three sub-members from the base:

i. *29 to 62 meters*. Sideritic siltstone sub-member (T2f5-1): grey calcareous siltstone and mudstone with sideritic nodules which show dark grey orientated grains (0.3-1.5 cm), but laterally changing into calcarenite and bioclastic micrite; characterized by lamination, low-angle tabular and wedge-shaped bedding, occasional wavy bedding and scouring, and also plentiful gastropods, ammonoids, and bivalve fossils such as: *Daonella spitiensis* Bittner, *D. lommeli* Wissmann, *Daonella* cf. *lommeli* Wissmann, *Daonella* sp., *Unionites* (?) sp., *Halobia planicosta* Tin et Hsu, *Protrachyceras* sp. *Daonella indica* Bittner, *Daonella consobrina* Yin et Hsu, *Daonella* aff. *moussoni* (Merian) *Halobia* sp., *spelionites* sp. Significantly, this unit has a layer of Mn-

bearing micrite at the top boundary with overlying sub-member T2f5-2, containing ~10% manganese and considered to be an uneconomic orebed (V4).

ii. 45 to 72 meters. Baigu (or upper) ore-bearing series (T2f5-2): siltstone, mudstone, calcarenite, micrite, algal dolomitic calcarenite, oolitic/pisolitic micrite, Mn-bearing oolitic/pisolitic micrite, and Mn oxides and carbonates; characterized by wavy cross-bedding, low-angle tabular cross-bedding, lamination, involution and lenticular cross-bedding, normal and inverse grading, ripple marks and scouring occurring at the top of orebeds such as V7, V8 and V9, commonly plentiful fossils in both rocks and ores such as ostracods, crinoids, foraminifera fish fragments, algae, and bivalves: *Daonella spitiensis* Bittner, *D. indica* Bittner, *D. lommeli* Wissmann, *Posidonia wen-gensis* Wissmann. This unit has five commercial orebeds (i.e. V9, V8, V7b, V7a, and V6) and two uncommercial orebeds (V10 and V5) (see Chapter 3).

iii. (T2f5-3): 110 to 137 meters. Grey fissile siltstone and mudstone with fissile calcarenite, bioclastic and oolitic/pisolitic micrite intercalations, and with quartz sandstone (0.1-2.0 m in thickness) at base, characterized by lamination in mudstone, tabular and wedge-shape and low-angle cross bedding, ripple marks, and minor involution and wavy and lenticular bedding, and fossils such as: gastropods, ostracods, foraminifera, algae, and fish fragments in intraclastic limestones; *Daonella aff. subarcitica* (?) Popow, *D. india* Bittner, *Halobia cf. Charlyana* var. *Pirivadiata* (?) Reed in terrigenous clastic rocks..

(6) 66 to 172 meters. Member 6 (T2f6) Laminated mudstone-siltstone: upper grey fissile mudstone with calcarenite intercalations; lower grey calcareous quartz siltstone with calcarenite, bioclastic and pisolitic limestone intercalations, characterized by lamination, low-angle cross-bedding, minor wavy and lenticular bedding, and plentiful ammonoid and bivalve fossils such as: *Daonella sturi* (Bencke), *Posidonia* sp., *Anodontophora* sp., *Halobia* sp. *Halobia cf. Pluriradiata* Reed, *H. cf. moluccana* Wanner, *H. cf. charlyana* var. *Pulriadiata* Reed, *Gorvillia* (Angustella) *angulata* Munster, *Spiriferina bifurcata yang et yin*, *S. yang et yin*, *Montlivaltia norica* Frech, *Clionites* sp., *Trachyceras sinense* Mansuy, *T. aff. fascigerum* Mansuy, *Protrachyceras douvillei* (Mansuy), *P. costulatum* (Mansuy). *Trachyceras* sp. *Spiriferina* sp.

----- Disconformity -----

3) > 300 meters. Upper Triassic Niaoge Formation (T3n) can be divided into two members:

(1) 188 to 200 meters. Lower sandstone-conglomerate member (T3n1): three interbeddings of mudstone, siltstone, sandstone, and conglomerate; characterized by brownish red sandy conglomerate which is composed of quartz, chert, and limestone clasts varying in size up to 1-7 cm. cemented by argillaceous, siliceous and silty cements.

(2) Over 130 meters. Upper sandstone-mudstone member (T3n2): fissile mudstone with quartz fine sandstone, occasional calcarenite lenticular intercalations.

The Niaoge Formation is mainly distributed in the Dounan syncline axis, the eastern part of Baigu and the northern part of Milike mining areas (Fig. 2.4), and significantly has plentiful ammonoids and bivalve fossils such as: *Angustella angulata* Munst, *Halobia yunnanensis* Reed, *Halobia cf. pluriradiata* Reed, *Daonella sp.*, *Daonella cf. arzelensis* Kittl, *Andontophora munsteri* Wissmann, *Palaeopharas sp.*, *Protrachyceras douvillei* (Mansuy), *Pratrachyceras costulatum* (Mansuy).

4) 2 to 12 meters. Quaternary alluvial and elluvial sandy clay, clay, sands, and gravels.

2.5.3 Dounan Facies Sequence and Model (Markov Chain) Analysis

The first edition of *Facies Models* (Walker, 1979) advocated a method for constructing facies models based on transition frequencies. The method is objective and powerful, yet easy to apply and later on was improved by Harper (1984). According to them, the method consists of: 1) tabulating observed numbers of transitions, and 2) converting these to relative frequencies relative to low totals. The 3), a matrix is calculated assuming the null hypothesis that such transitions are random, and depend only on the relative abundance of facies in the successions. Finally, 4), the random probabilities are subtracted from the observed probabilities to produce a matrix emphasizing differences from random which are large.

The following methods or procedures are used to analyze the Dounan facies model (Walker, 1984; Harper, 1984):

- 1) The measured sections are examined in detail according to Walther's facies law.
- 2) Eight genetic facies are worked out based on petrology, texture, structure, fossils and microfacies analysis of the section. Those are identified as follows:
 - A. dark red intramicrudite / intrabrecciated micrite with low-angle cross bedding and ripple marks;
 - B. green-grey siltstone intercalated with bioclastic micrite, with slump bedding, exotic blocks, and bioclastic debris;
 - C. grey-green mudstone with massive bedding or poor laminations;
 - D. dark red or black oolitic/pisolitic micrite, manganese oxide and/or carbonate oolites/pisolites with tabular cross-bedding, low-angle cross bedding, and ripple marks;
 - Ss. Breccias associated with and scouring granules or pebbles;
 - E. dark grey siltstone intercalated with calcarenite, with laminations;
 - F. light grey sandstone and intraclastic micrite with cross-bedding, low-angle cross bedding, lenticular bedding, and stromatolites;
 - G. light grey mudstone and mudstone intercalated with dolomitic micrite, with lamination, desiccation forms, and birdseye structure.
- 3) According to possible transitions (i to j) (e.g., facies C overlain by facies B), a primary transitional frequency is given in Table 2.3, i.e. the observed numbers of successes occurring.

Table 2.3 Primary transition frequency

	A	B	C	D	Ss	E	F	G	Σ
A		5	1	3	4	8			2
B	5		5	1					11
C	1	4							5
D	7				1	1	1		30
Ss	2	3		2		10			17
E	8	1		12			4		2
F					2	1		3	6
G							1		1
Σ	2	13	6	18	16	31	6	3	116

Table 2.4 Primary transition probability (P_{ij})

A		0.238	0.048	0.143	0.190	0.381			1.000
B	0.455		0.455	0.091					1.000
C	0.200	0.800							1.000
D	0.234				0.333	0.400	0.033		1.000
Ss	0.118	0.176		0.118		0.588			1.000
E	0.320	0.040		0.480			0.160		1.000
F					0.333	0.167		0.500	1.000
G							1.000		1.000

Table 2.5 Mean transition probability (R_{ij})

A		0.140	0.065	0.194	0.172	0.333	0.065	0.032
B	0.223		0.058	0.175	0.155	0.301	0.058	0.029
C	0.209	0.118		0.164	0.145	0.282	0.055	0.027
D	0.235	0.133	0.061		0.163	0.316	0.061	0.031
Ss	0.230	0.130	0.060	0.180		0.310	0.060	0.030
E	0.271	0.153	0.071	0.212	0.188		0.071	0.035
F	0.209	0.118	0.055	0.164	0.145	0.282		0.027
G	0.204	0.115	0.053	0.159	0.142	0.274	0.053	

Table 2.6 Transition difference probability (P_{ij} - R_{ij})

	A	B	C	D	Ss	E	F	G
A		+0.098	-0.017	+0.051	+0.018	+0.048	-0.065	-0.032
B	+0.232		+0.397	-0.084	-0.155	-0.301	-0.058	-0.029
C	-0.009	+0.682		-0.164	-0.145	-0.282	-0.055	-0.027
D	-0.001	-0.133	-0.061		+0.170	+0.084	-0.028	-0.031
Ss	-0.112	+0.046	-0.060	-0.062		+0.278	-0.060	-0.030
E	+0.049	-0.113	-0.071	+0.268	-0.188		+0.089	-0.035
F	-0.209	-0.118	-0.055	-0.164	+0.188	-0.115		+0.473
G	-0.204	-0.115	-0.053	-0.159	-0.142	-0.274	+0.947	

Fig. 2.14 Facies relationship diagram for Dounan data, derived from Table 2.6. Heavy lines show relationships significant at big number level, light lines at middle number level, and dashed at low number lines level.

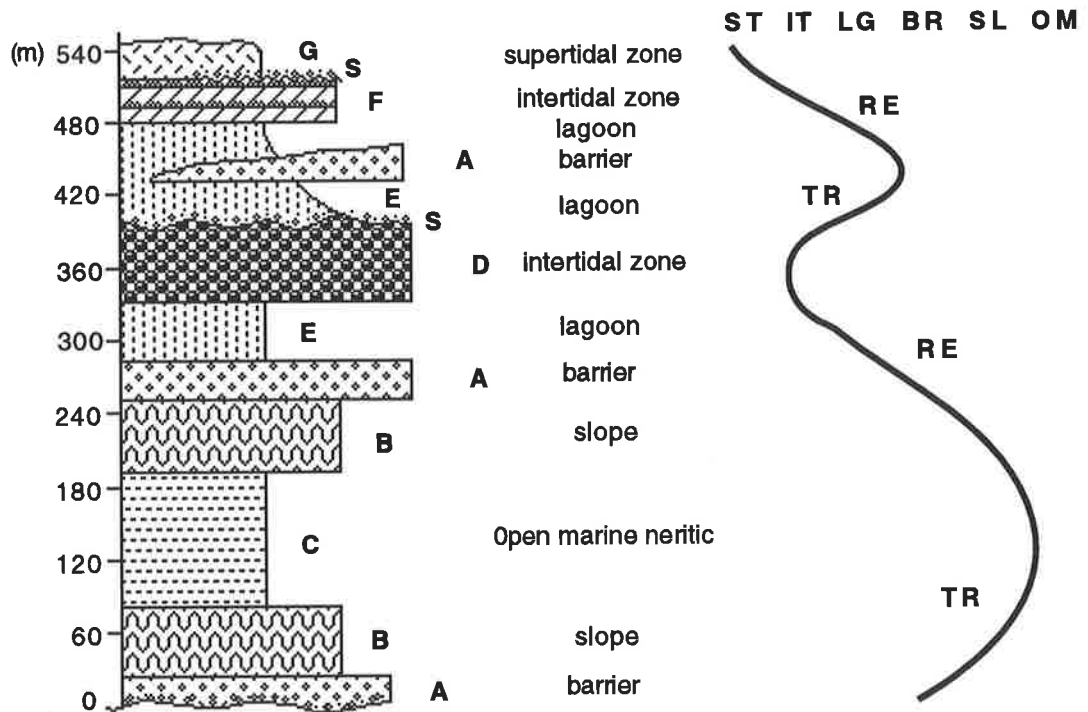
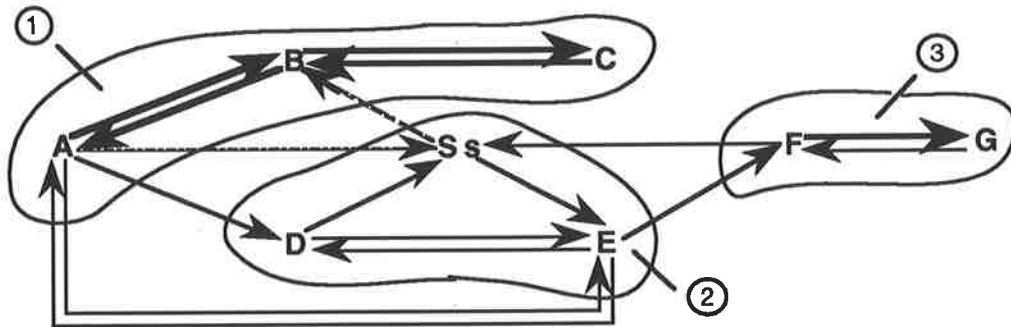


Fig. 2.15 Sedimentary facies model of Falang Formation at Dounan.

4) The observed transitions (Table 2.3) are converted into primary transitional probability (P_{ij} , Table 2.4) by computing the probabilities associated with the observed numbers of successes in the Falang Formation.

5) Then, the mean (or random) transitional probability (R_{ij} , Table 2.5) can be computed based on the hypothesis that the facies transition occurs at random. The transition is given by

$$R_{ij} = n_j / (N - n_i)$$

where R_{ij} = random (sequence) transition probability, n_i and n_j = the numbers of facies i and facies j occurring respectively, N = total number of facies (Walker, 1979).

6) Importantly, a difference probability ($P_{ij} - R_{ij}$, Table 2.6) can be computed by using observed transition probability (P_{ij}) subtracting random sequence probability (R_{ij}), and then using the differences as the basis for a facies model.

7) A Dounan facies relationship (Markov chain, Fig. 2.14) can be worked out in terms of the data from Table 2.6. However, it is important to distinguish the single facies sequence from repeat facies sequences (cycles). According to Fig. 2.14 three genetic associations of micro-facies can be identified. Group 1 represents a transgressive-regressive sedimentary cycle from barrier, slope to open marine and then again slope and barrier; group 2 shows an ore-forming cycle of alternations of lagoonal and intertidal environments; group 3 indicates a regressive tidal flat facies sequence. Scouring (Ss) represents the end of the ore-forming cycle. Thus, the result (Fig. 2.14) illustrates that the interpretation of microfacies and sedimentation of the Falang Formation described above is reasonable, and that deposition of the Falang Formation followed transgression-regression cycles.

8) Finally, the Dounan sedimentary facies model of the Falang Formation is given in Figure 2.15, based on the facies relationships (Fig. 2.14). The lower part of the facies model consists of the first sedimentary cycle (group 1 in Fig. 2.14) formed in relatively low energy marine environments; the middle part of the model is composed of the second cycle (group 2) formed during alternation of lagoonal and intertidal environments; whereas the upper part of the model is made up of the tidal flat environments (group 3) in which manganese ores formed near the end of regressive intertidal and associated (e.g. the upper subtidal zone) environments.

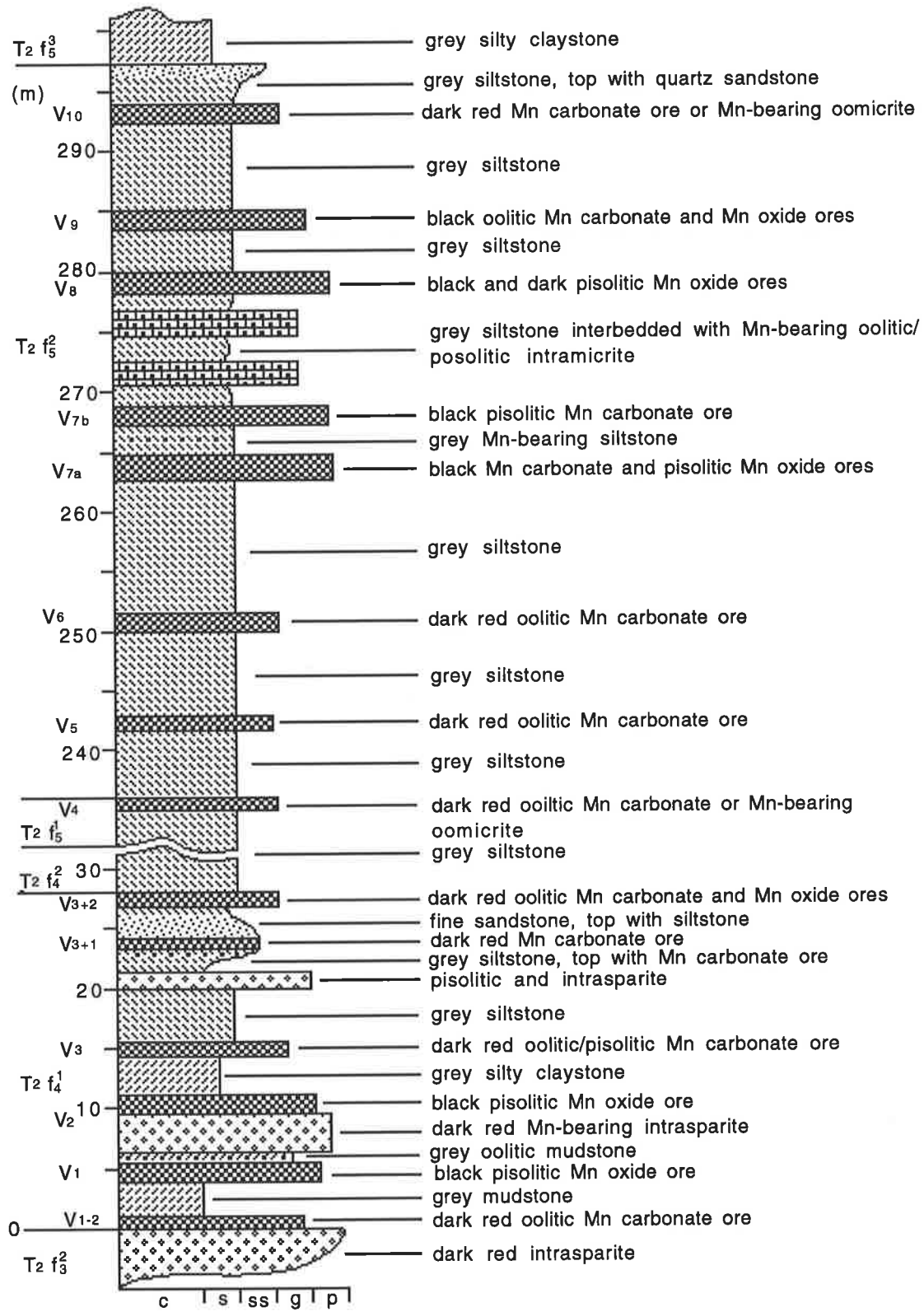
2.5.4 Detailed Stratigraphy of Mn-bearing Series

There are two ore-bearing series in Dounan area, as stated above, i. e. the upper (Baigu) ore-bearing series (T2f5-2) mainly formed in Gaigu and the lower (Gake) ore-bearing series (T2f4-1), mainly formed in other mining areas (Figs. 2.4 & 2.16).

2.5.4.1 Upper Ore-bearing Series (T2f5-2)

The series can be divided into 15 layers, and described from the base as follows:

0.85 to 1.16 meters. Underlying T2f5-1 dark red oolitic/pisolitic Mn carbonates (V4), poor ores.



(grainsize)
 c - clay, s - silt, ss - sand
 g - granule, p - pebble

Fig. 2.16 Stratigraphic profile of Mn-bearing series, Falang Formation at Dounan of southeastern Yunnan. For legend see Table 2.1.

Conformity

- 1) ~6.00 meters. Grey laminated siltstone, with quartz fine sandstone at base.
- 2) 0.30 to 0.65 meters. Dark red Mn carbonates (V5), poor quality.
- 3) ~8.60 meters. Grey laminated siltstone.
- 4) 0.23 to 2.12 meters. Dark red Mn carbonates (V6), poor quality.
- 5) 8.00 to 12.50 meters. Grey siltstone with intraclastic micrite.
- 6) 0.08 to 4.70 meters. Black or dark red Mn oxides and carbonates (V7a).
- 7) 0.5 to 2.5 meters. Grey laminated siltstone, laterally changing into Mn-bearing intraclastic micrite.
- 8) 0.13 to 1.95 meters. Black or dark red lenticular Mn oxides and carbonates (V7b).
- 9) 8.00 to 10.00 meters. Grey laminated siltstone with oolitic/pisolitic micrite intercalations, and with minor pyrite spots or nodules, and with increasing carbonates towards the east.
- 10) 0.10 to 2.98 meters. Black massive/banded Mn oxides and dark red Mn carbonates (V8).
- 11) 0.43 to 5.32 meters. Grey siltstone with oolitic/pisolitic Mn-bearing micrite as base.
- 12) 0.13 to 2.10 meters. Black and dark red unsorted or banded Mn oxides and carbonates (V9), laterally changing into Mn-bearing limestone towards the east.
- 13) 6.00 to 8.00 meters. Grey laminated siltstone with bioclastic limestone and bivalves at base.
- 14) 0.49 to 1.36 meters. Dark red, grey, and black Mn carbonates (V10), mostly occur as Mn-bearing limestone lenticular bodies.
- 15) 2.00 to 4.00 meters. Grey siltstone with calcarenite at top, characterized by lamination and wavy bedding.

Conformity

0.20 to 4.00 meters. Overlying T2f5-3 grey quartz sandstone (key bed)

The upper ore-bearing series, therefore, possesses the following features:

- (1) This Mn-bearing series mainly consists of siltstone with intraclastic or oolitic/pisolitic micrite and manganese orebed intercalations.
- (2) The thickness varies between 45 and 72 meters, being mostly about 60 meters.
- (3) Mn orebeds are distributed regularly in the series, with ~10 m intervals between orebeds.
- (4) The footwall and hangwall rocks of orebeds mainly are siltstone or Mn-bearing micrite.
- (5) This Mn-bearing series is mainly distributed in the Baigu area, where it is divided into two parts by the F3 fault (Fig. 2.4). The petrology of the two parts is obviously different, i.e. carbonates dominate in the eastern part where the orebeds are thin and of poor quality; siltstone dominates in the western part, along with thicker and good quality orebeds, which probably indicates that the stratigraphy, facies and orebeds are all influenced by the F3 fault.

(6) The main orebeds (e.g. V8 & V7) are often accompanied by some small lenticular orebodies (usually < 0.5 m in thickness).

2.5.4.2 Lower Ore-bearing Series (T2f4-1)

This unit can be divided into 19 layers and described from the base as follows:

Underlying T2f3-2 dark red brecciated micrite.

Conformity

- 1) 0.31 to 0.93 meters. Dark red Mn carbonates or Mn-bearing micrite (Mn 6-8%) (V1-2).
- 2) ~0.50 meter. Grey and green laminated mudstone.
- 3) 0.05 to 0.20 meters. Black / dark red unsorted Mn oxides and carbonates (V1-1).
- 4) 0.20 to 1.00 meters. Dark red brecciated micrite (0.1-2.5 cm).
- 5) 0.07 to 4.01 meters. Black Mn oxides (V1).
- 6) 0.05 to 0.20 meters. Black oolitic mudstone / calcilutite (keybed)
- 7) 0 to 0.5 meters. Dark red or grey Mn carbonates or Mn-bearing micrite (V1+1).
- 8) 0.40 to 0.50 meters. Grey calcilutite with minor syngenetic breccia and dark red Fe oxide spots at base.
- 9) ~0.70 meter. Dark red brecciated quartz silty micrite (0.5-1.0 cm), with bioclastic debris (key bed).
- 10) ~0.50 meter. Mudstone with brecciated micrite, red colour at top and grey at base.
- 11) 0.03 to 1.93 meters. Black and dark red Mn oxides and carbonates (V2).
- 12) 2.00 to 3.00 meters. Grey laminated silty claystone with calcarenite.
- 13) 0.50 to 0.95 meters. Dark red Mn carbonates (V3).
- 14) 4.00 to 5.00 meters. Grey laminated siltstone.
- 15) 0.20 to 1.50 meters. Grey brecciated or oolitic/pisolitic (0.1- 1.5 cm) micrite (key bed), with bioclastic debris, pyrite, chlorite, and Mn 2-4%.
- 16) ~1.77 meters. Grey siltstone with silty claystone intercalation.
- 17) 0.10 to 0.38 meters. Dark red Mn carbonates or Mn-bearing micrite (Mn 2-15%).
- 18) 1.30 to 1.70 meters. Grey siltstone and fine sandstone with Mn-bearing micrite (~0.2 m) intercalation.
- 19) 0.12 to 1.32 meters. Black and dark red unsorted Mn oxides and carbonates (V3+2).

conformity

Overlying T2f4-2 grey laminated calcareous siltstone.

Thus, the lower ore-bearing series has the following features:

(1) The lower ore-bearing series consists of mudstone, siltstone, intraclastic limestone, and manganese ores.

(2) The major orebeds (e.g. V₁) mainly occur in the lower part of the series, and show upward trends towards poor quality and larger intervals between orebeds.

(3) The Dounan syncline has a thicker ore-bearing series (40-50 m) along its southern limb and a thinner ore-bearing series (20-25 m) along the northern limb.

(4) The lenticular orebeds V₁₋₂ and V₁₋₁ occur between orebed V₁ and T_{2f3-2} dark red brecciated micrite, but wherever orebeds V₁₋₂ and V₁₋₁ do not occur, the orebed V₁ is directly underlain by T_{2f3-2}, which suggests that the brecciated micrite was formed in barrier environments, whereas orebeds V₁₋₂ and V₁₋₁ were formed in small submarine depressions.

2.5.5 Paleontology

Detailed studies at Dounan show that there exist plentiful algae and biofossils in the ores and rocks of the Falang Formation, and importantly they are partly or totally mineralized or "replaced" by manganese materials (Liu et al., 1984). This fact is emphasized not only in hand specimen but also in micro-observation (e.g. microscopy and SEM).

2.5.5.1 Relationship between Fossils and Ores

Commonly, fossils such as bivalves, ammonoids, gastropods, foraminifera, ostracods, and crinoids can be found in Dounan manganese ores and associated rocks. Also, algae, oncolites, and biofragments often occur in the ores and associated rocks (Plates 2.3 and 2.4). The determined algae include *dacycladaceae* of blue-green algae, *Plaeomicroystis sp.* and *calcispheres*. Observations show the following relationships between biofossils and Mn ores:

- Manganese ores occur as intraclastic biograins such as braunite oncolites (Plate 2.3, Figs. 1a-1d, 2a-2b), calciorhodochrosite oncolites (Plate 2.3, Fig. 3a; Plate 2.4, Figs. 5c-d), and ore biofragments (Plates 2.3 and 2.4, Figs. 3a-3b, 6a-6b), cemented by braunite, calciorhodochrosite, and other carbonate materials.
- Fossils are partly or totally replaced or filled by manganese minerals (all Figures in Plates 2.3 and 2.4).
- Oncolites, mostly composed of braunite or calciorhodochrosite, have cores of mineralized fossil material.

2.5.5.2 Features of Fossils

Since the fossils in the strata of the Falang Formation have been described in previous sections, this description focuses on the features of fossils. Generally, all orebeds in Dounan area contain fossils (Table 2.7), of these a lot occur as oncoliths in oolites/pisolites. Thus, the activities of

Table 2.7 Statistics of paleobiofossils in Dounan Mn ores, modified after Liu et al (1984).

fossils	orebeds							
	V1	V2	V6	V7 b	V7 a	V8	V9	
Osagia dounan f. nov. (new type)	+		-	-	+	-	-	
Osagia lamellosa f. nov. (new type)			-		-	+		
Paraosagia columnaria Gr. et f. nov. (new type)			-		-	+		
Osagia f. (not typed)					-		+	
DACYCLADACEAE of dasycladales of Chlorophyta, Dasycladales of blue-green algae			+	+	+	+	+	
CODIACERE of blue-green algae						+	+	
Siphonales of Chlorophyta				-			-	
Palaeolyngbya sp. (not sorted)					-			
RHODOPHYTA of Rhodophyta (not sorted)					-		-	
CALCISPHERES				-	-	-	-	
Stromatolites	+	+	-	-	+	++	-	
Palaeomicrocystis (not sorted)						-		
Oncolites of braunite	++	++	+	++	++	++	+	
Oncolites of calciorhodochrosite	+	+	++	+	+	+	+	
Oncolites of chert laminea				-	-		-	
Bivalve	-	-	+	+	+	-	-	
Foraminifera	+	+	+	+	+	+	-	
Ostracoda	+	-	-	-	-	+	-	
Ammonoidea		-		+		-		
Gastropoda			-		+		-	
Crinoidea	-		+		-		-	
Anthozoa			-		-			
Bioclastic debris	-	-	+	+	-	-	+	
++ major, + minor, - trace								

Plate 2.3 Microfossils from Dounan Mn ores and associated rocks.

Fig. 1a: Braunite oolite composed of mineralized algal balls; Gake area; light colour: braunite; dark colour: Mn-calcite; sample 958-39; polished section; parallel polarizers; the bar equals 400 μ .

Fig. 1b: Braunite mineralized algal balls; Gake area; white mineral: braunite; black colour: organic-bearing calcite; grey colour: calcite; sample 958-42; polished section; parallel polarizers; the bar equals 10 μ .

Fig. 1c: Mineralized bluegreen algae or stromatolite, braunite algae; light colour: braunite; dark colour: calcite; Gake area; sample 958-38; polished section; parallel polarizers; the bar equals 2 mm.

Fig. 1d: Totally mineralized algal ball oolites or oncolites braunite-(black colour) cemented by Mn-calcite; recemented and replaced by sparite (white); the secondary generation of manganese oxide cement replaced by secondary braunite (black); Kata area; sample 958-60; thin section; parallel polarizers; the bar equals 300 μ .

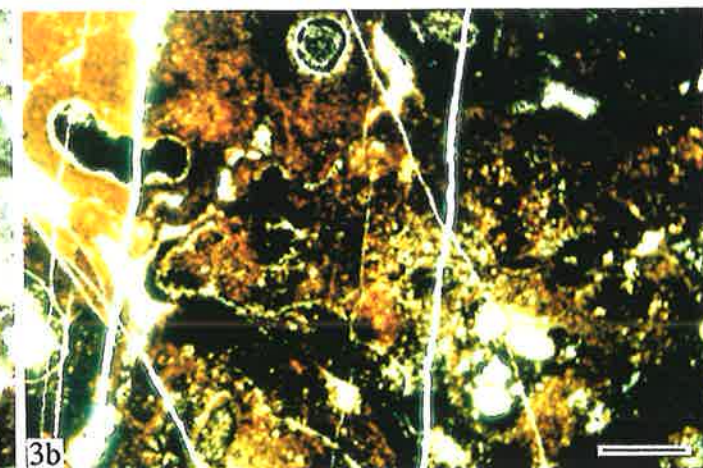
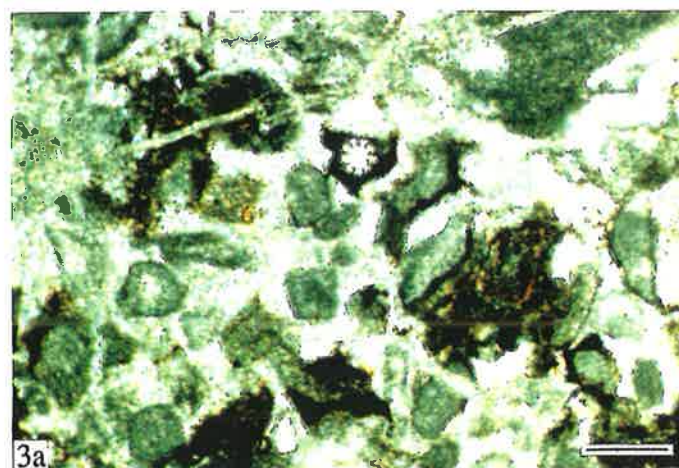
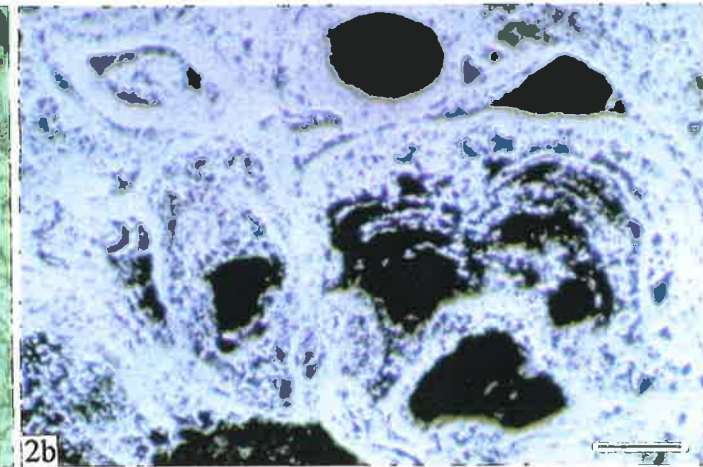
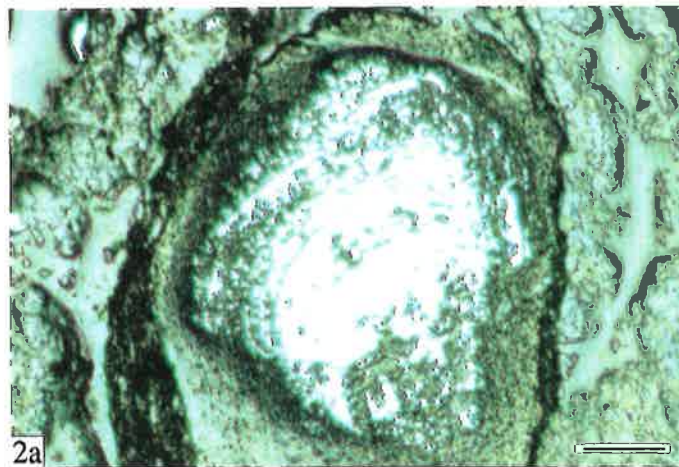
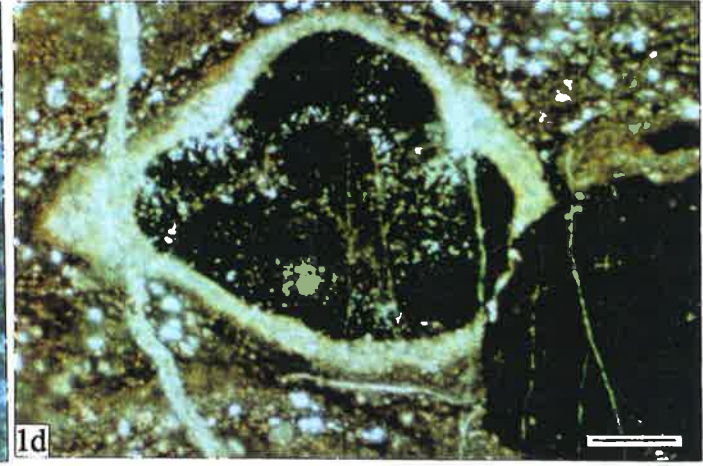
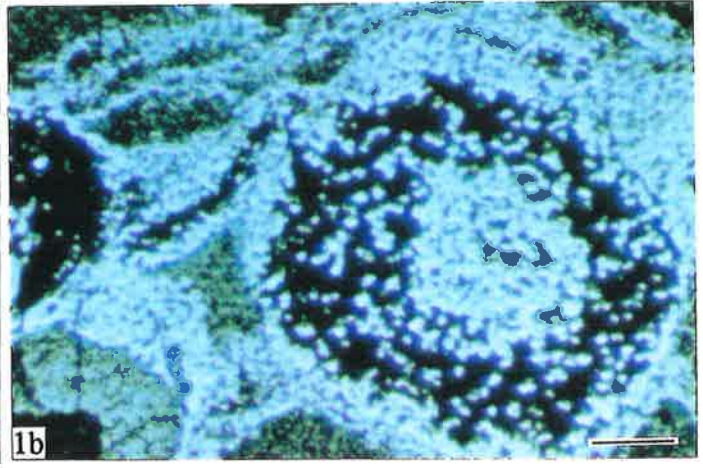
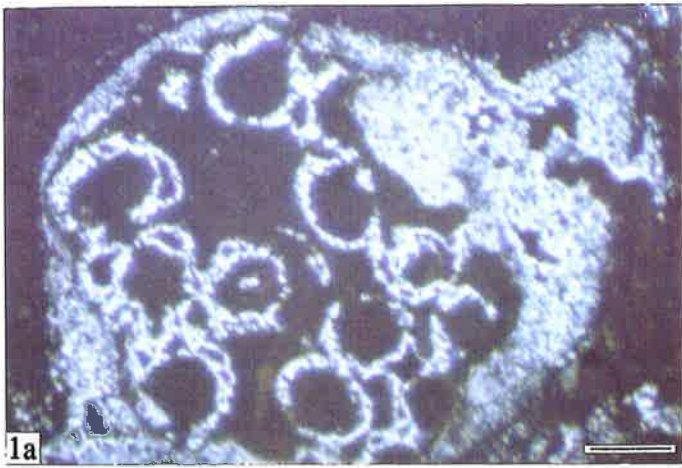
Fig. 2a: Carbonate pisolite core composed of braunite mineralized stromatolite fragment (white); Kata area; sample 958-61; polished section; parallel polarizers; the bar equals 1 cm.

Fig. 2b: Mn-bearing carbonate stromatolites (dark colour) mineralized by braunite (light colour); dark colour: braunite oncolites; Gake area; sample 958-49; polished section; crossed polarizers; the bar equals 1 cm.

Fig. 3a: Mineralized crinoid; black colour: braunite; dark colour: calciorhodochrosite; light colour: calcite; Daaazi area; sample 958-78; thin section; parallel polarizers; the bar equals 10 μ .

Fig. 3b: Mineralized biofragments (at top); dark colour: braunite oncolites; light colour: calcite; Gake area; sample 958-68; thin section; parallel polarizers; the bar equals 10 μ .

Plate 2.3



algae and oncolites seem to have played important roles in the formation of Dounan primary manganese ores. Based on detailed studies, the oncolites in Dounan manganese ores can be divided into the following types:

- In terms of the "core" features, there exist four kinds of oncolite, i. e. single core oncolites (Plate 2.3, Fig.2a; Plate 2.4, Figs. 5a and 6b); multi-core oncolites determined as *Osagia f.* (Plate 2.3, Figs. 1a, 1b, 1d and 2b); non-fossil core oncolites (Plate 2.3, Fig. 1c); and non-core oncolites (Plate 2.3, Figs. 2b and 3a; Plate 2.4, Fig. 5d).
- According to the types of laminae, there are two types of microstromatolite. These are (1) *Paraosagia columnaria Gr. et f. nov.* and *Osagia lamellosa f. nov.* replaced by braunite, calciorhodochrosite or chert (e.g., Plate 2.3, Fig. 2b) and (2) *Osagia dounan f. nov.* (e.g., Plate 2.3, Figs. 1b, 1c) (Zhang et al., 1979 and Liu et al., 1984).
- Based on the mineralogical components, three kinds of oncolites are common, i.e. braunite oncolites (Plate 2.3, Figs. 1d, 2b and 3b; Plate 2.4, Figs. 4a, 4b and 5a); manganese carbonate oncolites (Plate 2.4, Figs. 5c, 5d, 6a and 6b); and braunite-Mn carbonate oncolites (Plate 2.3, Figs. 1c and 3a).

In addition, foraminifera, ostracods, bivalves, and anthozoans replaced or filled by braunite or manganese carbonate minerals are commonly found in Dounan manganese ores (Plate 2.3, 3a and 3b; Plate 2.4, Figs. 4a, 4b, 5a-d, 6a and 6b). Generally, the shapes of oncolites or oololiths/pisoliths simply follow those of their cores (all Figures in Plates 2.3 and 2.4), probably due to their primary development based on the cores. Thus, the paleontology of Dounan sequence is important not only in the formation of the manganese deposits but also in understanding the microfacies of the Dounan basin.

2.5.5.3 Distribution of Fossils

It is generally considered that types of algae are controlled by water depth: (from shallow to deep) blue algae, green algae, and red algae (Liu et al., 1984). Commonly, blue algae grow in supratidal and intertidal areas to form algae flats; green algae form in the lower intertidal or lagoonal zones; and red algae occur from low tidal level to subtidal barrier reef (e.g., Ginsburg, 1971). Oncolites develop in relatively high intertidal or upper subtidal zones.

The distribution of animal fossils can also indicate environmental variation. Generally, the supratidal zone lacks marine fossils except for minor ostracods, gastropods, and shell fragments moved by large waves. Relatively poor fossils occur in the upper intertidal area, but variety increases downward to the lower intertidal zone, e.g. bivalves. The subtidal zone has plentiful and various fossils such as crinoids, bivalves, etc. However, foraminifera are widely distributed in marine environments.

Plate 2.4 Fossils from Dounan Mn ores and associated rocks.

Fig. 4a: Strongly mineralized bivalve; black colour: braunite; white colour: calcite; Gake area; sample 958-46; thin section; parallel polarizers; the bar equals 2 cm.

Fig. 4b: Mineralized ostracod in siltstone (light colour); dark colour: braunite; Baigu area; sample 958-142; thin section; parallel polarizers, the bar equals 2 cm.

Fig. 5a: Foraminifera as oolite core mineralized by braunite oncolites (black colour); white colour: calcite; brownish colour: secondary mineralizing braunite replacing primary braunite; Gake area; sample 958-56; thin section; parallel polarizers; the bar equals 5 mm.

Fig. 5b: Slightly mineralized foraminifera, *Textularia* (biserial form), typically shallow marine; dark colour: braunite; white colour calcite; brownish colour: Mn-calcite; Baigu area; sample 958-152; thin section; parallel polarizers; the bar equals 2 mm.

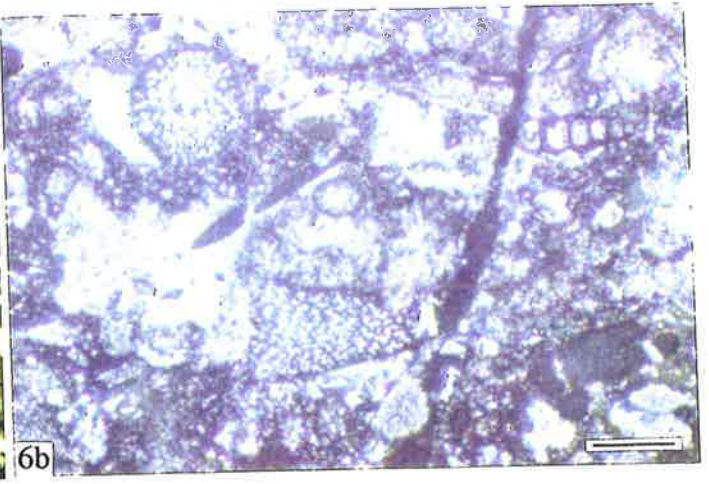
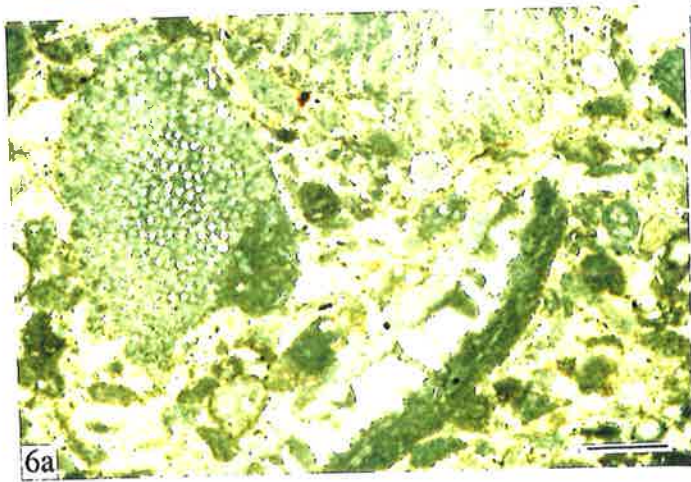
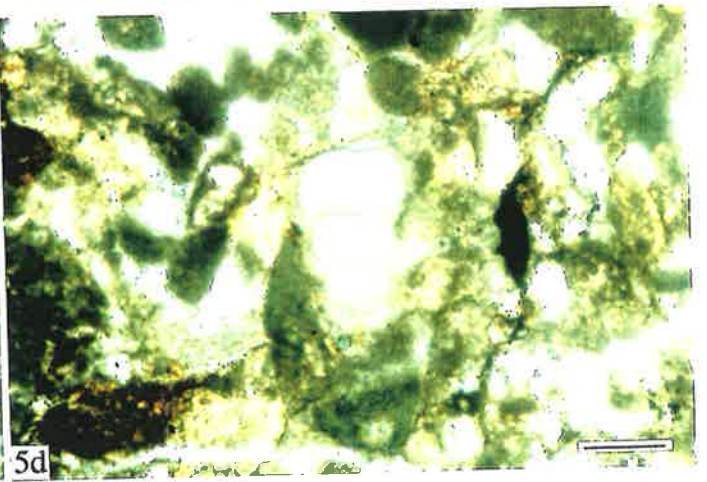
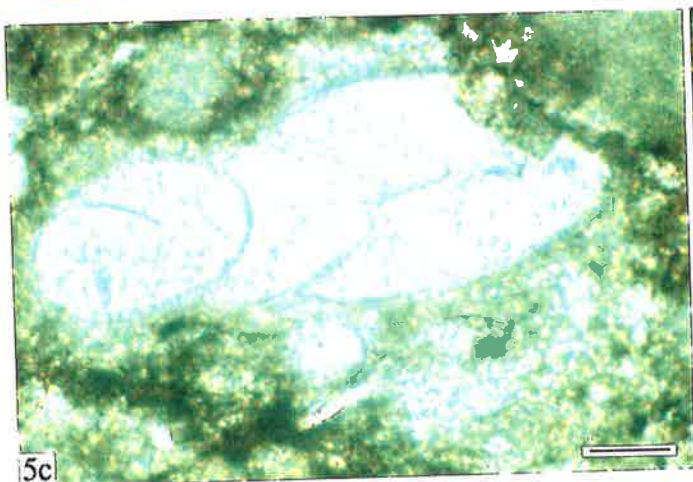
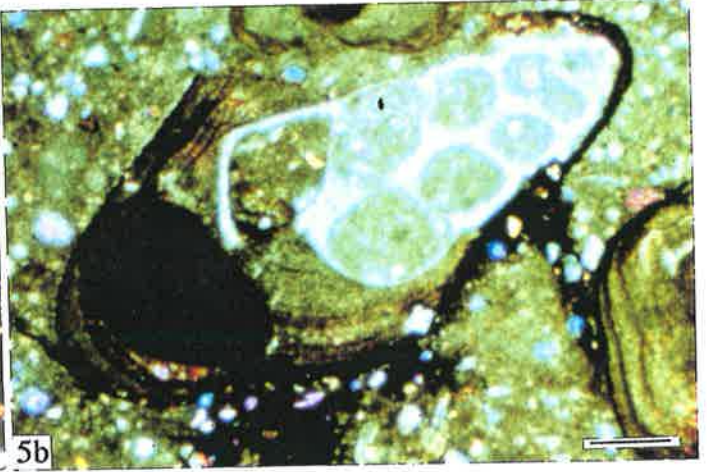
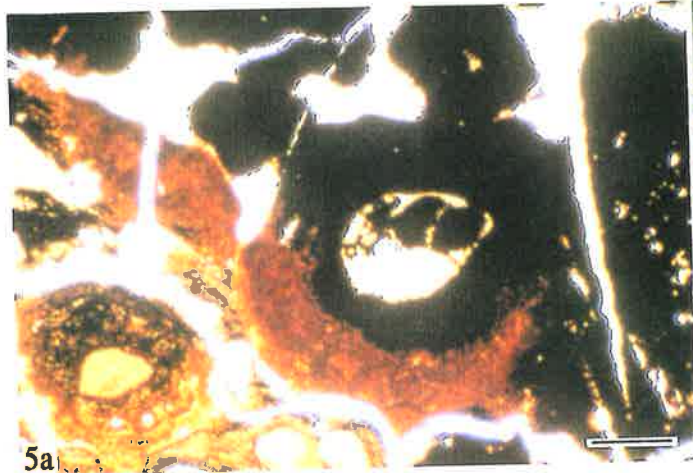
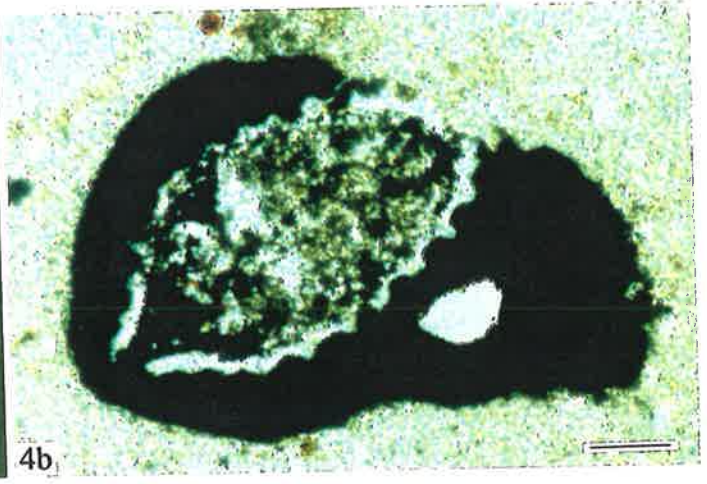
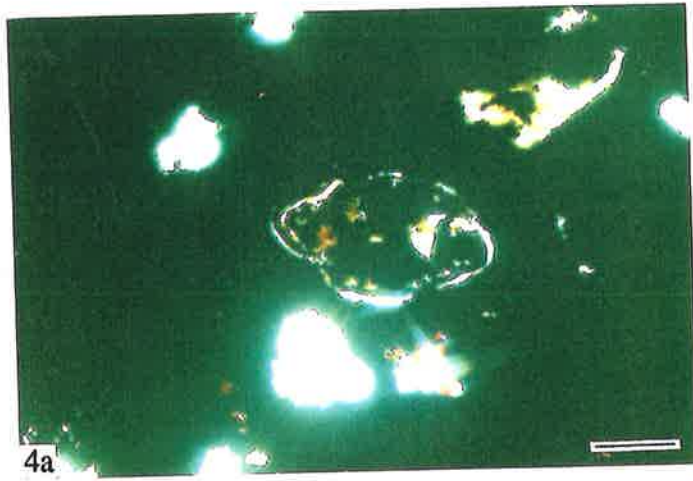
Fig. 5c: Calciorhodochrosite oncolites (dark colour) replaced foraminifera; light colour: calcite; Baigu area; sample 958-156; thin section; crossed polarizers; the bar equals 1 mm.

Fig. 5d: Mn-calcite oncolites (green) replacing foraminifera; light colour: calcite; Baigu area; sample 958-171; thin section; parallel polarizers; the bar equals 5 mm.

Fig. 6a: Mineralized biofragments [e.g. foraminifera (bottom), algae (top left), and crinoid (top right)]; dark colour: calciorhodochrosite; light colour: calcite; Baigu area; sample 958-173; thin section; parallel polarizers; the bar equals 2 mm.

Fig. 6b: mineralized biofragments [e.g. bivalve (top left), foraminifera (top right), and algae (bottom)]; dark colour: calciorhodochrosite; light colour: calcite; Baigu area; sample 958-172; thin section; crossed polarizers; the bar equals 5 mm.

Plate 2.4



In most cases, in Dounan manganese ores, fossils, except that some whole-bodied ammonoids, bivalves, and foraminifera, occur as fragments, and these represent a mixed association from intertidal to subtidal zones. Significantly, the distribution of fossils in the Dounan manganese deposits (from orebeds V₁ to V₁₀) indicates that the deposits formed in regressive sequences, i.e. the sedimentary environments represent relatively shallow marine processes.

2.5.6 Sedimentary Cycles, Microfacies and Environments

2.5.6.1 Vertical Variation

Figure 2.13 suggests that the Dounan Falang Formation, with a rock association of terrigenous clastic-carbonate rocks, formed in shallow marine environments. The vertical variation of Dounan sedimentation, as reflected in textures, structures and biota, suggests alternating transgression-regression which can be divided into three sedimentary cycles, i. e. a lower microfacies association of barrier-slope-open marine; a middle development of intertidal-lagoon-barrier-slope-open sea; evolving upward into lagoon-intertidal flat and finally, the supratidal zone. Manganese ores were deposited during the transitional period from transgression to regression, i.e. the bottoms of sedimentary cycles II and III. Stratigraphic variations in geochemistry are shown in Figure 2.17.

1) Lower cycle (I): Cycle I comprises several sub-cycles composed of T_{2f1} - T_{2f3-1} beds. The continuous sedimentation of siltstone and mudstone (T_{2f2}) follows T_{2f1} intraclastic micrite, and with a colour variation from red to light grey, grey-green to dark red, which suggests that climates varied from humid to dry. The following microfacies association is suggested:

a The barrier facies is characterized by bioclastic intramicrutite (T_{2f1}), mixed biotas of the intertidal and subtidal zones, and micrite matrix, and by geochemical features (Fe³⁺ 0.09% - 0.60%, Fe²⁺ 0.40% - 1.31%, organic carbon 0.03% - 0.09%) which suggest that sediments originally deposited in the subtidal zone were redeposited in high energy, slightly oxidizing marine barrier environments.

b The slope facies are identified in T_{2f2} and T_{2f3-1} siltstone and mudstone characterized by slump bedding, exotic blocks, bioclastic debris, euryhaline bivalves and ammonoids, and geochemical features (Fe³⁺ 0.17% - 1.98%, Fe²⁺ 0.81% - 2.25%, organic carbon 0.03% - 0.10%) suggesting reducing to slightly reducing marine environments.

c The open marine neritic facies consists of grey or grey-green laminated and massive clay-rich siltstone and mudstone with minor glauconite, characterized by euryhaline bivalves, ammonoids, and geochemical features (Fe³⁺ 0.15% - 1.99%, Fe²⁺ 0.84% - 2.46%, organic carbon 0.09% - 0.13%) suggesting reducing and brackish environments.

2) Middle cycle (II): This cycle includes T_{2f3-2} - T_{2f5-1} beds with various rocks/ores found in the Dounan area. Both normal and inverse size grading can be found in this cycle. The colour

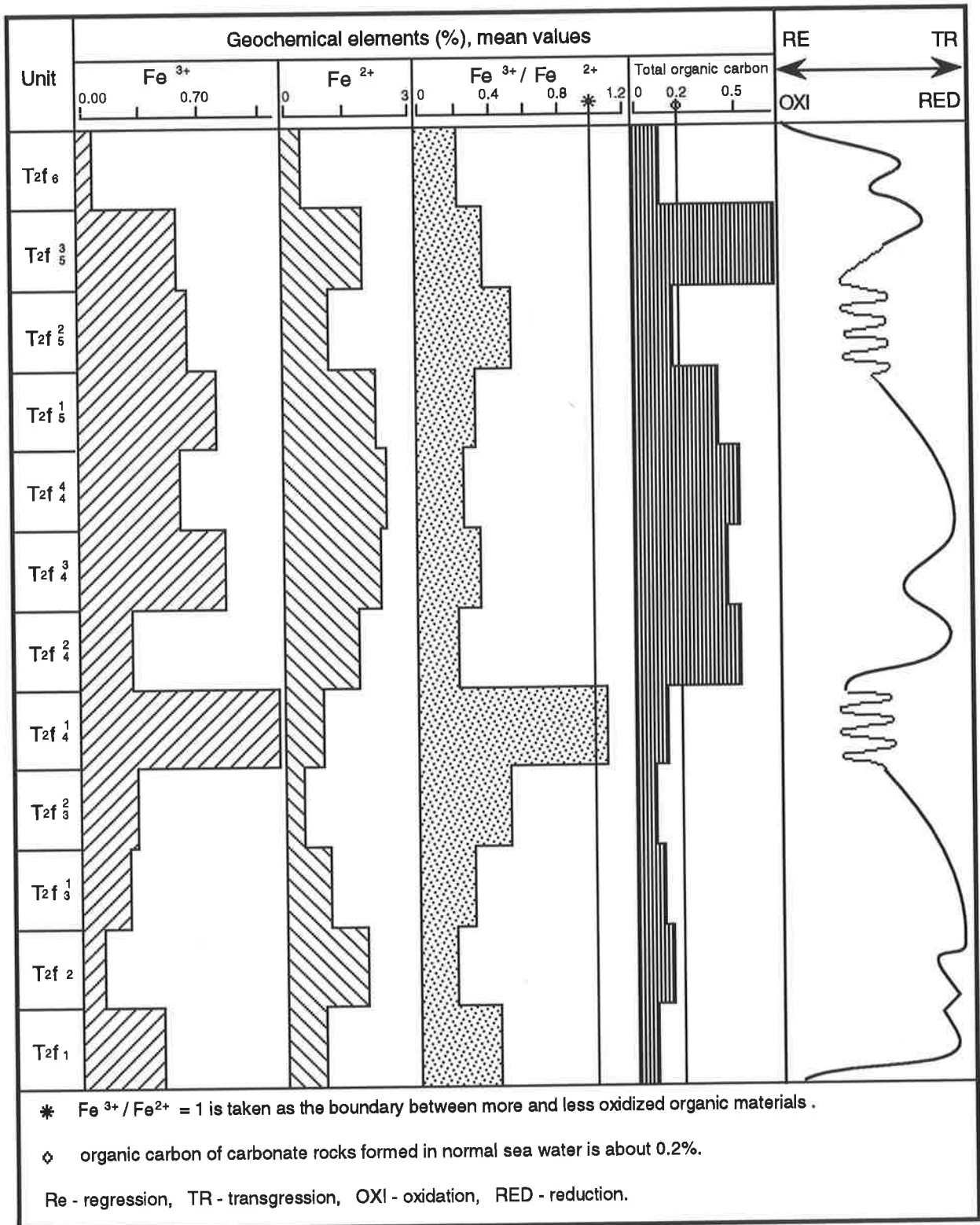


Fig. 2.17 Fe³⁺, Fe²⁺, Fe³⁺ / Fe²⁺ and organic C variations in the Falang Formation, Dounan manganese deposit. Data from Table II.2.

varies from dark red through grey-green to black, reflecting a variation from arid to humid climates. These suggest the following microfacies development:

a Barrier: the features of T2f3-2 beds are similar to those of cycle I (T2f1 beds), including geochemical features, and thus also suggest high energy, slightly oxidizing marine environments. Also, the barrier facies occur in the middle (T2f4-3) and the top (T2f5-1) of this cycle, but here they include oolitic/pisolitic micrite.

b The lagoonal facies mainly occurs in the lower part (T2f4-1) of the cycle. The siltstone, mudstone, and calcilutite are characterized by dark grey colours, lamination, concentric oncolites which contain *Cyanophyta*, *Chlorophyta* and *Bodophyta*, foraminifera, ostracods, pyrite, collophanite, glauconite, and plentiful organic matter, which suggest low energy reducing environments.

c The intertidal facies is mainly composed of manganese oxide and/or carbonate oolites/pisolites and Mn-bearing oolitic/pisolitic micrite (T2f4-1 bed). Oolite/pisolite is characterized by mostly inverse size grading, tabular cross-bedding, ripple marks, scouring, and various intertidal-subtidal fossils. High energy environments are indicated.

Thus, two microfacies (lagoon and intertidal) and several sub-cycles composed of these two facies are identified in the lower ore-containing series (T2f4-1). The ores thus can be reasonably considered as geochemical products of lagoonal and intertidal sedimentation. The geochemical features from the foot-wall calcilutite (Fe^{3+} 1.55%, Fe^{2+} 1.37%, suggesting slight oxidation) and from the hanging-wall calcilutite and mudstone (Fe^{3+} 0.24%, Fe^{2+} 0.98%, indicating reduction) when compared with those of the manganese ores, suggest a transition from first slightly oxidizing to strongly oxidizing and finally to reducing marine environments (see Fig. 2.18).

d The slope facies mainly occurs in the upper part (e.g. T2f4-3, T2f4-4, T2f5-1) of the cycle and shows similar features to the slope facies in cycle I, but with slightly different geochemical features (Fe^{3+} 0.19% - 0.36%, Fe^{2+} 1.24% - 1.87%, organic carbon 0.16% - 0.42%), which suggests reducing marine environments.

e The open marine siltstone and mudstone facies (T2f4-4) is characterized by grey-green colour, lamination and massive bedding, occasionally small scale low-angle cross-bedding, glauconite and siderite nodules, and geochemical features (Fe^{3+} 0.81%, Fe^{2+} 2.72%, organic carbon 0.48%) suggesting strongly reducing marine environments.

3) Upper cycle (III). This cycle contains T2f5-2 and T2f6 sub-members. The features of microfacies association of the upper ore-bearing series (T2f5-2) are extremely similar to those of the lower ore-bearing series (T2f4-1) in cycle II, but the former contains relatively more sedimentary structures and fossils (determined by previous workers) than the latter. However, the greater abundance of broken ooliths and pisoliths in the upper ore-bearing series indicates shallower intertidal environments with higher energy than those of the lower ore-bearing series.

The lower part of this cycle also shows mineralogical replacement of lagoonal and intertidal facies though the rocks are mainly composed of fine clastic materials. Supratidal products dominate the upper part of bed T2f6, which indicates the end of Falang Formation sedimentation.

2.5.6.2 Sedimentary Environments of Mn-bearing Series

1) Environments of Lower Mn-bearing Series (T2f4-1)

Based on the petrology, texture, structure and grainsize or grain-grading, the lower Mn-bearing series can be ascribed as following eleven cyclothems (Fig. 2.18):

In the lower part of cyclothem I (CS1) the intraclastic or bioclastic facies is characterized by intertidal features, then followed by transgressive laminated (0.4-6.6 m in thickness) calcareous siltstone and micrite (lagoonal). Importantly, the manganese oxides/carbonates mostly with inverse grading (V1-1, Fig. 2.19, A) were formed locally near the end of CS1 regression (intertidal facies). During CS2, however, the high energy intertidal environments led to a thicker accumulation of manganese oxide oolites/pisolites (V1), which is followed by typically normal and then inverse gradings with several red to grey-green interbedded layers (Fig. 2.19, B). In CS3, orebed V2 shows not only inverse grading but also scouring and ripple marks, which indicates a regressive intertidal sedimentation. The orebed V2, however, shows lateral facies variation, e.g. mixed manganese oxides and carbonates occur in southern Gake, whereas manganese carbonates appear in northern Gake exposures, reflecting a variable oxidation interface in different places. Then, the intraclastic micrite facies is followed by laminated siltstone, which marks the end of cyclothem 3 transgression (lagoon). The calcarenite and oolitic micrite facies of cyclothem 4 are followed by inversely graded manganese oolites/pisolites (V3) formed in high energy intertidal environments. Following this, the basin was supplied continuously with silty or muddy sediments but only a very small amount of manganese. Only thin or lenticular manganese orebeds (e.g. V3+0, V3+1) occur in these cyclothems (CS5-CS10). High energy intertidal (CS11) manganese oolites (V3+2) mark the final regression of the lower Mn-bearing series.

In summary, the sedimentation of the lower Mn-bearing series in the subtidal lagoon and intertidal zones shows the following features:

- (1) Mixed manganese oxide and carbonate orebeds mainly occur in the lower part of the lower Mn-bearing series, i.e. in the last period of regression, whereas manganese carbonates dominant orebeds mainly formed in the upper part of the series, mostly in the transitional zone of regression and transgression.
- (2) The thicker manganese orebeds mainly formed in high energy environments, whereas thin and lenticular manganese orebeds occur in relatively low energy zones such as the transitional zone between intertidal and subtidal areas.
- (3) The various intertidal and/or subtidal structures with normal and/or inverse size grading can be found in the orebeds, which reflects shifts between lagoonal and intertidal environments.

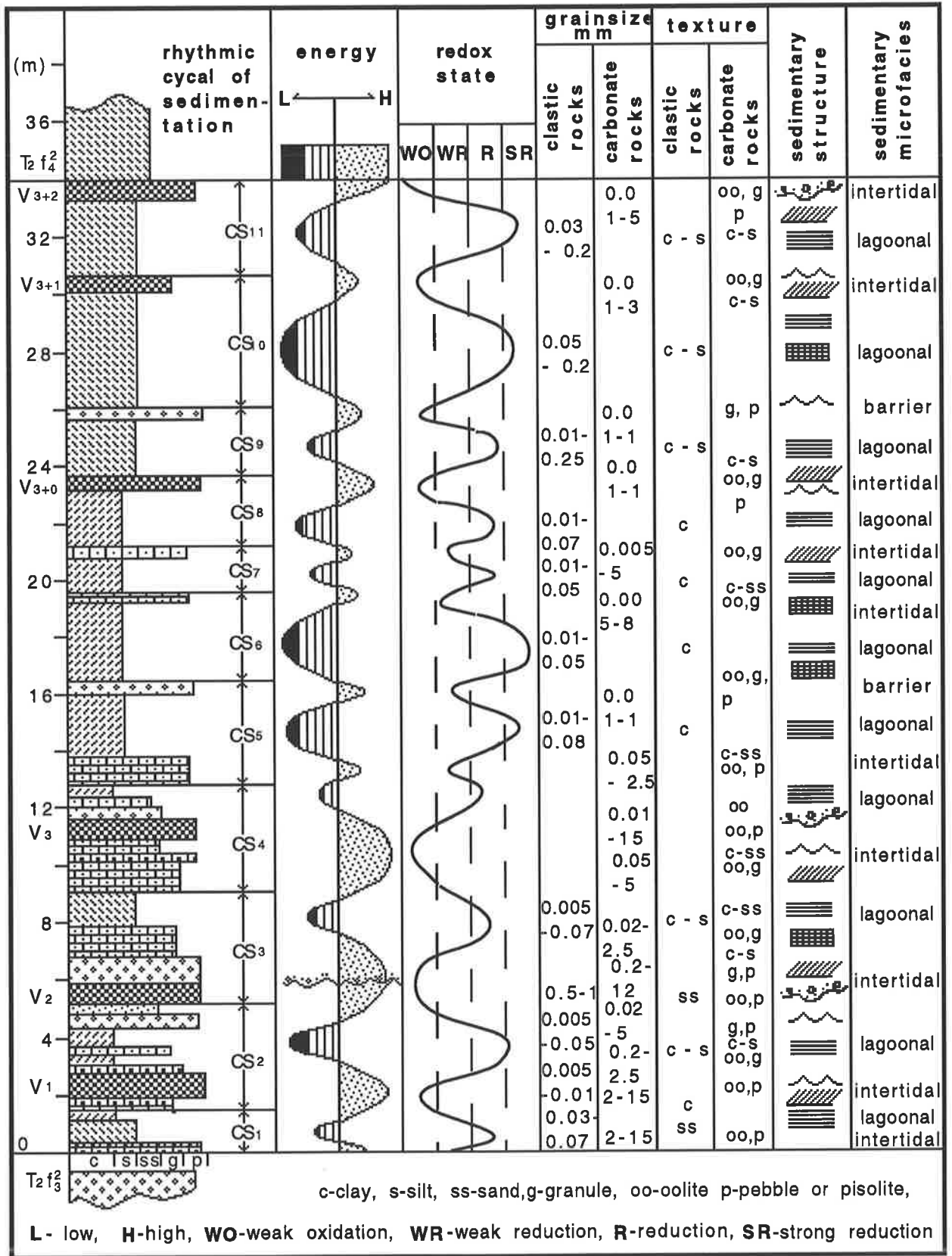


Fig. 2.18 Sedimentary environments, Lower ore-bearing series (T₂ f₄₋₁), Falang formation, at Dounan, Yunnan. For legend see Table 2.1.

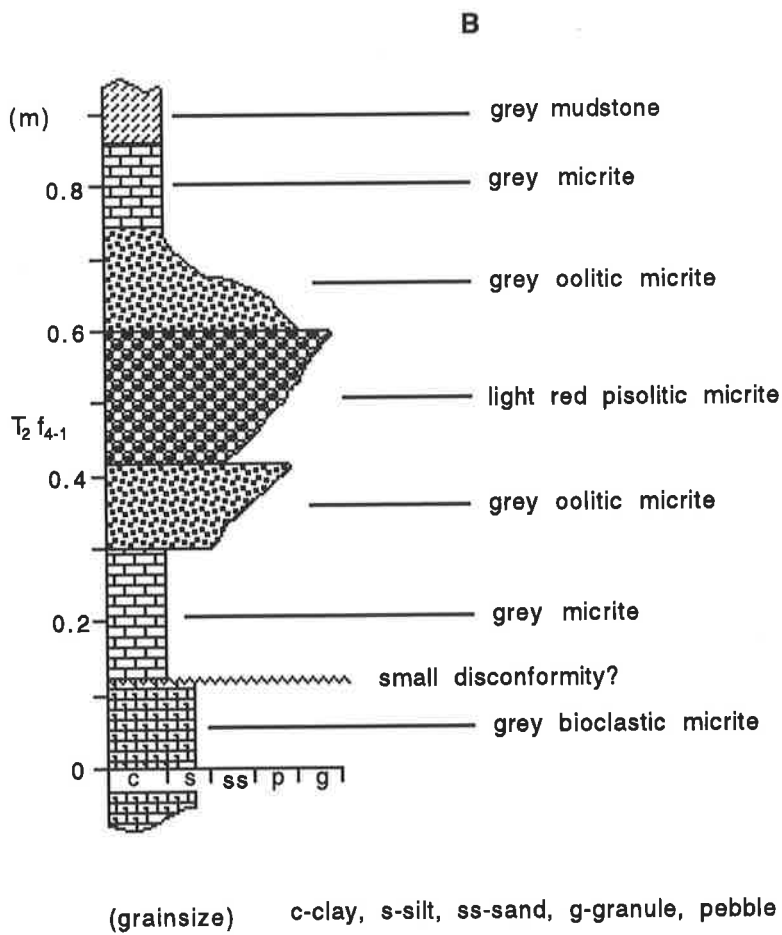
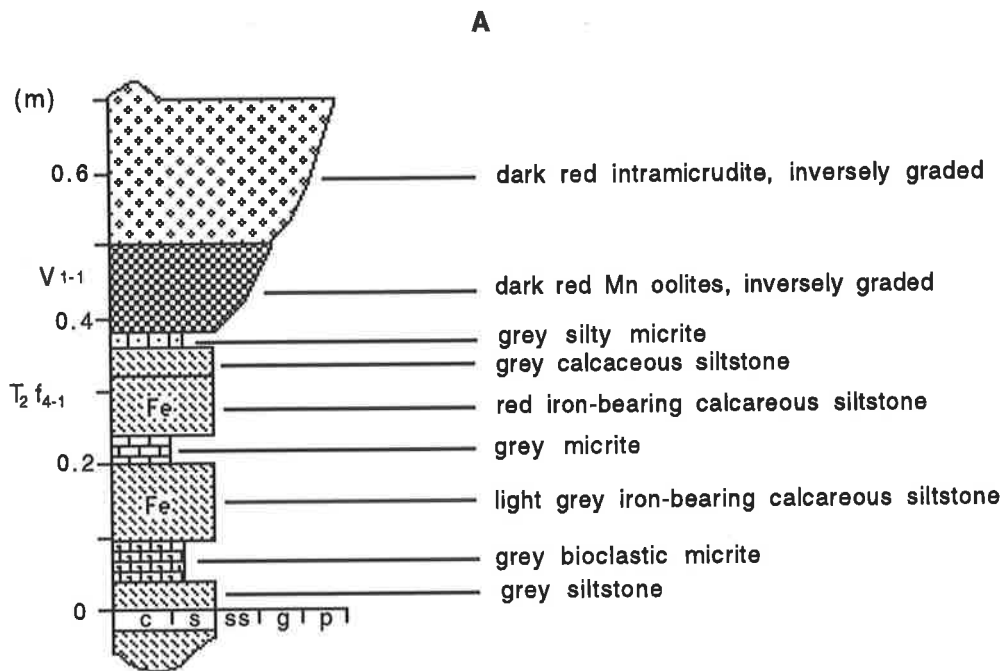


Fig. 2.19 Detailed geological profiles of V₁₋₁ (A), and between V₁ and V₂ (B), in Dounan Mn deposits, Yunnan.

2) *Environments of Upper Mn-bearing Series (T_{2f5-2})*

Six cyclothems in the upper Mn-bearing series can be described as follows according to the petrology, fabrics, and grain size (Fig. 2.20). All cyclothems, except for cyclothem 6, are composed of manganese orebeds, intraclastic carbonates, siltstone or silty claystone, and contain relatively more clastic rocks than intraclastic carbonates and manganese ores. In the vertical sequence three manganese ore groups (i.e. lower V₅, middle V_{6-V7}, and upper V_{8-V10}) generally show reverse size grading of oolites/pisolites.

In the facies sequence of the upper Mn-bearing series, barrier sandstone with wavy bedding is followed by laminated lagoonal siltstone, and then by an inversely graded intertidal manganese orebed (V₅) at the end of the first regression (CS₁). This grades upward into lagoonal siltstone characterized by lamination, which reflects a transgression, and is then followed by the second manganese ore group (V_{6-V7}) mainly formed in the transitional period between transgression and regression. The beds underlying the orebeds, for instance, show lamination, whereas the hanging walls of the orebeds contain wavy bedding and low-angle cross-bedding, inverse grading in orebeds, and importantly, scouring on the tops of orebeds, which reflects an environmental evolution from low to high energy (CS₃). Next, a transgressive lagoonal facies is characterized by laminated or massive silty claystone facies (CS₄). The sedimentary environments of the overlying third manganese group (CS₄-CS₅) are similar to those of the second manganese group. Commonly, the manganese ores facies are characterized by oolitic/ pisolitic structures; ripple marks of the hanging wall of orebed V₈ indicate a regression from lagoonal to intertidal environments. Following the transgression during the early part of cyclothem 5 (characterized by laminated silty claystone with calcarenite intercalation), manganese orebeds (V_{9-V10}) again were formed during the regression of cyclothem 5. Several transgression/regression sub-cycles are indicated by inverse grading in the orebeds and scouring on the top of the orebeds. The suggestion is that they probably formed during general regression from lagoonal to intertidal environments. Finally, sedimentation ends with a long-term transgression characterized by laminated and massive siltstone facies (CS₆), without any manganese deposition.

2.6 *Stratigraphic Correlation of Falang Formation*

2.6.1 *Regional Stratigraphic Correlation*

To extend a facies analysis to the entire southeastern Yunnan basin it is necessary to come to grips with problems of stratigraphic correlation and apply various basin mapping techniques. The Falang Formation in which the manganiferous orebeds are intercalated shows various rock facies from place to place in the southeast of Yunnan. Correlation of the manganiferous formations at different places is shown in Figure 2.21, and roughly four lithologic associations of

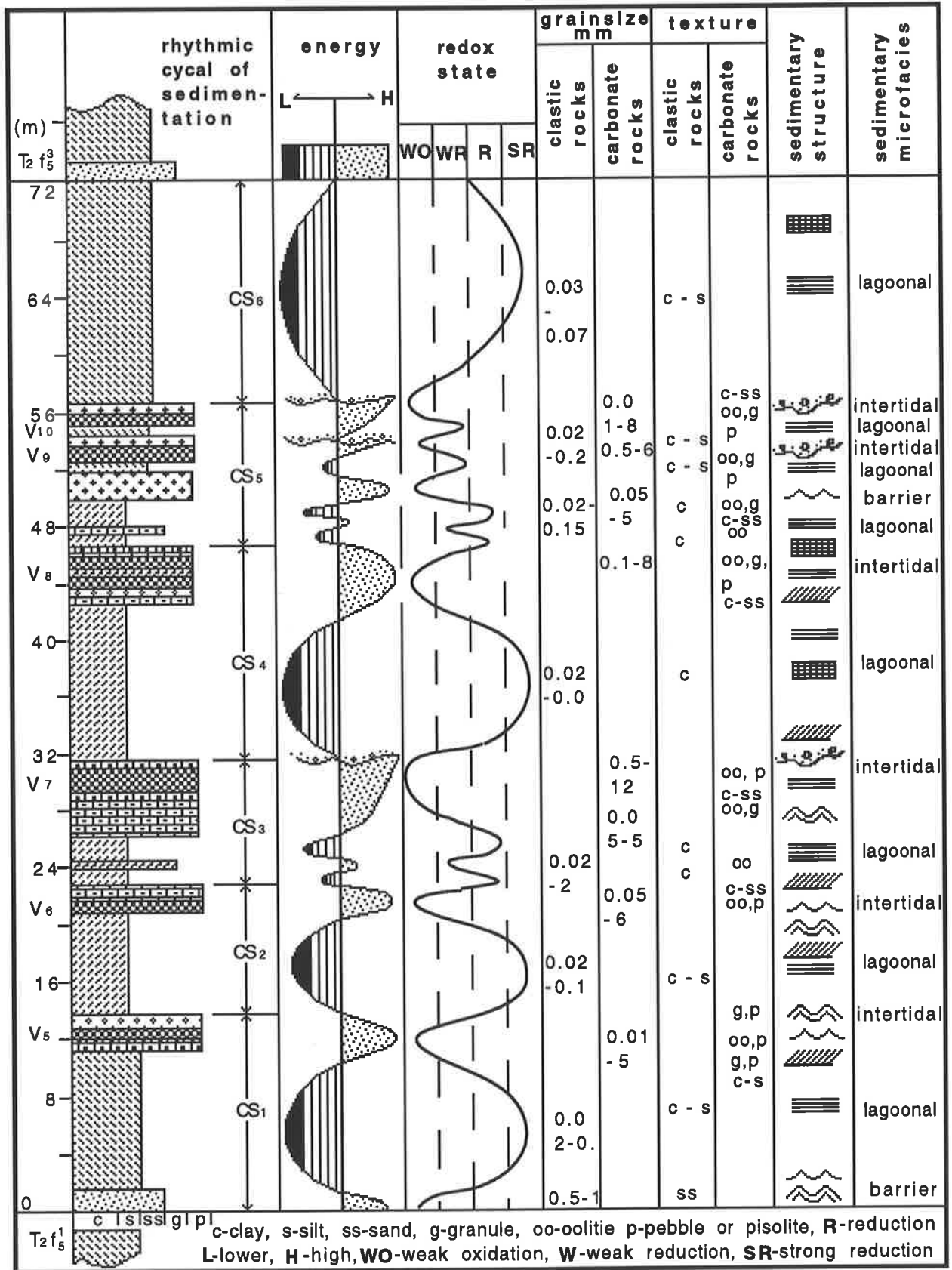


Fig. 2.20 Sedimentary environments of Upper ore-bearing series (T₂f₅-2), Falang Formation at Dounan. For legend see Table 2.1.

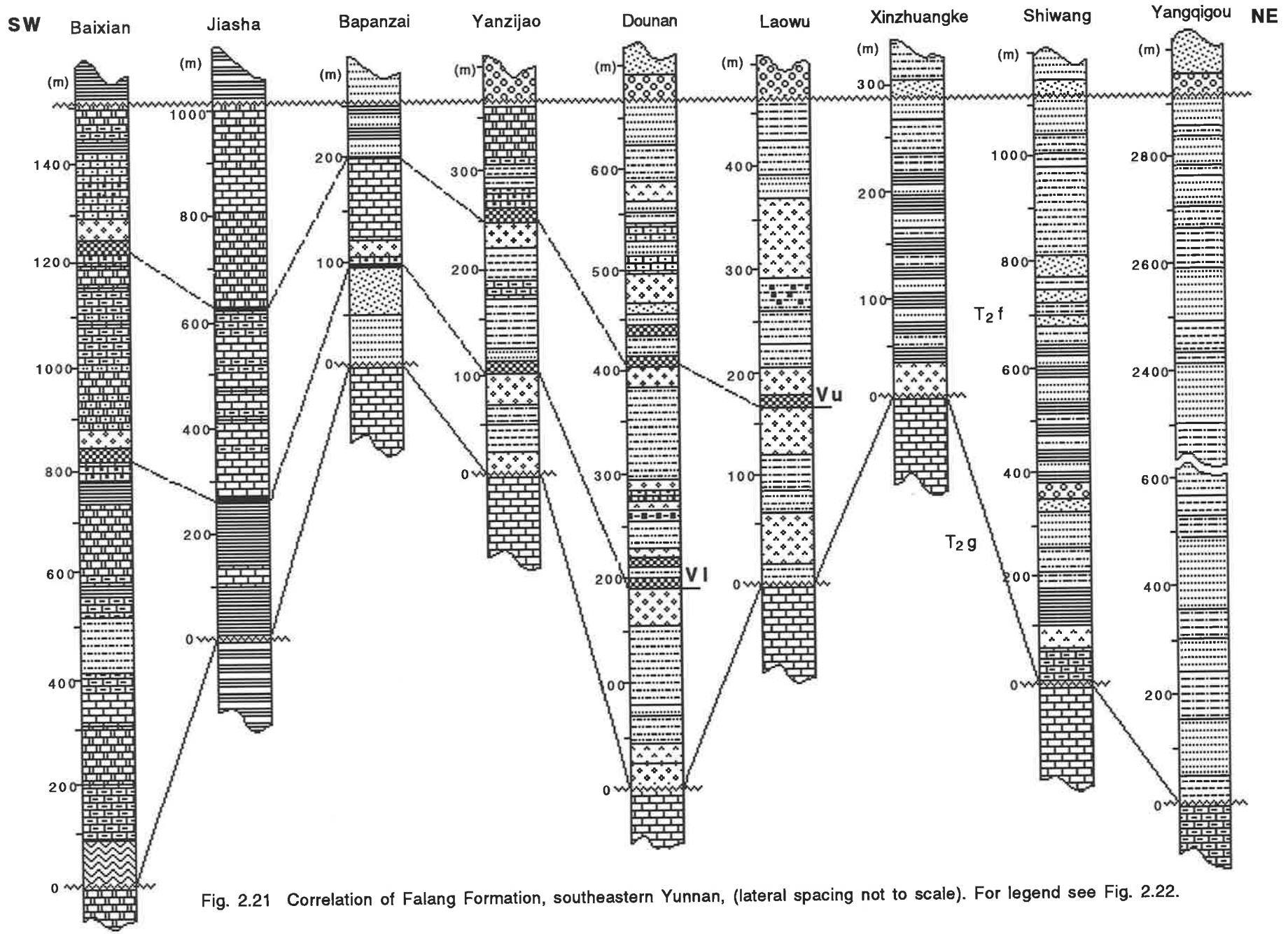


Fig. 2.21 Correlation of Falang Formation, southeastern Yunnan, (lateral spacing not to scale). For legend see Fig. 2.22.

sedimentary rocks from bottom to the top of the Falang Formation can be identified and correlated as follows:

1) *Grey-green argillaceous rocks*. This mainly includes T2f1 - T2f2 strata, and is mainly composed of shale, calcilutite and dolostone at Baixian (400-500 m in thickness); shale intercalated with micrite at Jasha (120-130 m); siltstone at Bapanzai (40-70 m); siltstone, calcilutite and intramicrudite at Yanzijiao (4.48-52.77 m); mudstone and silty claystone with intraclastic micrite at base at Dounan (103-132 m); mudstone or silty claystone at Laowu (25-50 m); bioclastic micrite at Xinzhuangke (12-34 m); calcilutite and shale intercalated with micrite and silty claystone at Shiwang (250-300 m); and silty claystone and siltstone at Yangqigou (600-800 m). Thus, the sections of Baixian, Jasha and Bapanzai show similar petrology and sedimentary features, and a petrological variation from shale to calcilutite to siltstone. Sediment thickness decreases from SW to NE, in the Baixian marine sub-basin, with a depositional center at Baixian. In the NE Dounan area (Yanzijiao-Dounan-Laowu), the rocks vary from calcareous mudstone to carbonates with thicker sediments at Dounan and thinner sediments at Yanzijiao and Laowu, defining another marine sub-basin, i.e. the Dounan sub-basin with a depositional center at Dounan. These rocks are absent at Mingju, between Yanzijiao and Dounan, probably due to an uplift consisting of the Geju Formation limestone. Farther NE again, the rocks in the Qubei area (Xinzhuangke-Shiwang-Yangqigou) vary from calcilutite to algal micrite, and to mudstone or siltstone with increasing thickness, slump bedding and Bouma sequence structures, which reflects relatively deep water (slope-open sea) deposition.

2) *Dark red argillaceous-intraclastic-micrite carbonate rocks*. This mainly contains T2f3 beds with a description from SW to NE as follows: the rocks vary from limestone and dolostone to shale, and to sandstone with decreasing thickness from Baixian to Jasha and Bapanzai in the Baixian sub-basin; the dark-red rock association of siltstone and intramicrudite in the Dounan sub-basin possibly reflecting dry climate. Significantly, there is an obvious lateral variation, from intramicrudite/intrasparite in the area of Yanzijiao-Gake, into netted micrite to the NE in the area of Laowu-Baigu, indicating shallow environments with high energy in the western part of the Dounan sub-basin and relatively quiet water with low energy in the east. Also, the thickness variation (e.g. 5.5-24 m at Yanzijiao, 16-73 m at Gake, ~45 m at Baigu, ~20.5 m at Laowu) implies a sedimentary center near Dounan; Qubei has thicker mudstone and siltstone (> 200 m in thickness).

3) *Mn-bearing siltstone-intraclastic carbonate rocks*. This includes T2f4-1 - T2f5-2 beds, generally composed of siltstone, intraclastic micrite, and oolitic/pisolitic manganese orebeds. The Baixian sub-basin shows a regressive sequence and contains both the lower and upper ore series. Although the Dounan basin also possesses regressive features, only the upper ore-bearing series is seen at Laowu. To the NE, manganese deposition is not known but micrite, silty claystone and siltstone dominate the sequence in the Qubei area. The variation in thickness (310-470 m at Baixian, 195-340 m at Jasha, 75-210 m at Bapanzai, 62-287 m at Yanzijiao, 261-300 m

at Gake, 193-240 m at Baigu, ~153 m at Laowu, ~20 m at Xinzhuangke, 300-400 m at Shiwang, 55-600 m at Yangqigou) in these rocks also indicates increasing water depth from SW to NE, but with some higher areas, such as between Bapanzai and Yanzijao, and between Laowu and Shiwang.

4) *Grey siltstones (intercalated with intraclastic micrite and calcarenite)*. This includes T2f5-3 and T2f6 strata. Grey calcarenite, clay and dolostone, characterized by tidal flat features, dominate at Baixian and Jasha; supratidal siltstone and mudstone occur at Bapanzai, whereas fine terrigenous clastic rocks with tidal-flat structures and shallow marine fossils dominate in the Dounan sub-basin. Generally, this belt is not everywhere developed, due to an obvious discontinuity with the overlying Niaoge Formation of upper Triassic age.

2.6.2 *Local (Dounan Area) Stratigraphic Correlation*

In the Dounan area, the lower part of the Falang Formation shows complete development in the western Yanzijao and Gake areas except for an absence of the T2f6 bed. In the eastern Baigu and Laowu areas the upper part of the Falang Formation is completely developed; in the lower part, T2f1 - T2f3 strata are absent or incomplete (Fig. 2.22). The grey argillaceous rocks at the base show complete development in the Yanzijao and Gake areas, and are relatively thick at Gake, implying a depositional center nearby during this stage. The dark red argillaceous-intraclastic-micrite belt dominates everywhere except the western Laowu area, although with maximum thickness at Dounan. Importantly, the Mn-bearing belt shows different developments at different areas. For example, the lower ore-containing series is mainly developed at Yanzijao and Gake, whereas the upper ore-bearing series is well developed at Baigu and eastern Laowu, which suggesting a northeastward migration of the depocenter.

2.7 *Lithofacies-Paleogeographic Environment of Falang Formation*

2.7.1 *Environmental Analysis*

2.7.1.1 *Depositional Environments and Lithofacies*

The Triassic marine basin of southeastern Yunnan was divided into two submarine sub-basins (i.e. Baixian and Dounan submarine sub-basins) by the Kaiyuan submarine uplift which is an extension of the Yuebei oldland (Zhang et al., 1979). The three or four main environments of the Dounan barrier-island system (i. e. open sea-slope, barrier beach, lagoon, and tidal flat) are made up of a number of sub-environments, each of which is characterized by distinct lithofacies (Figs. 2.23, 2.24, 2.25). The regional sedimentation of southeastern Yunnan is mainly of a terrigenous clastic type, except for the Geju area, which is mainly composed of carbonate platform facies.

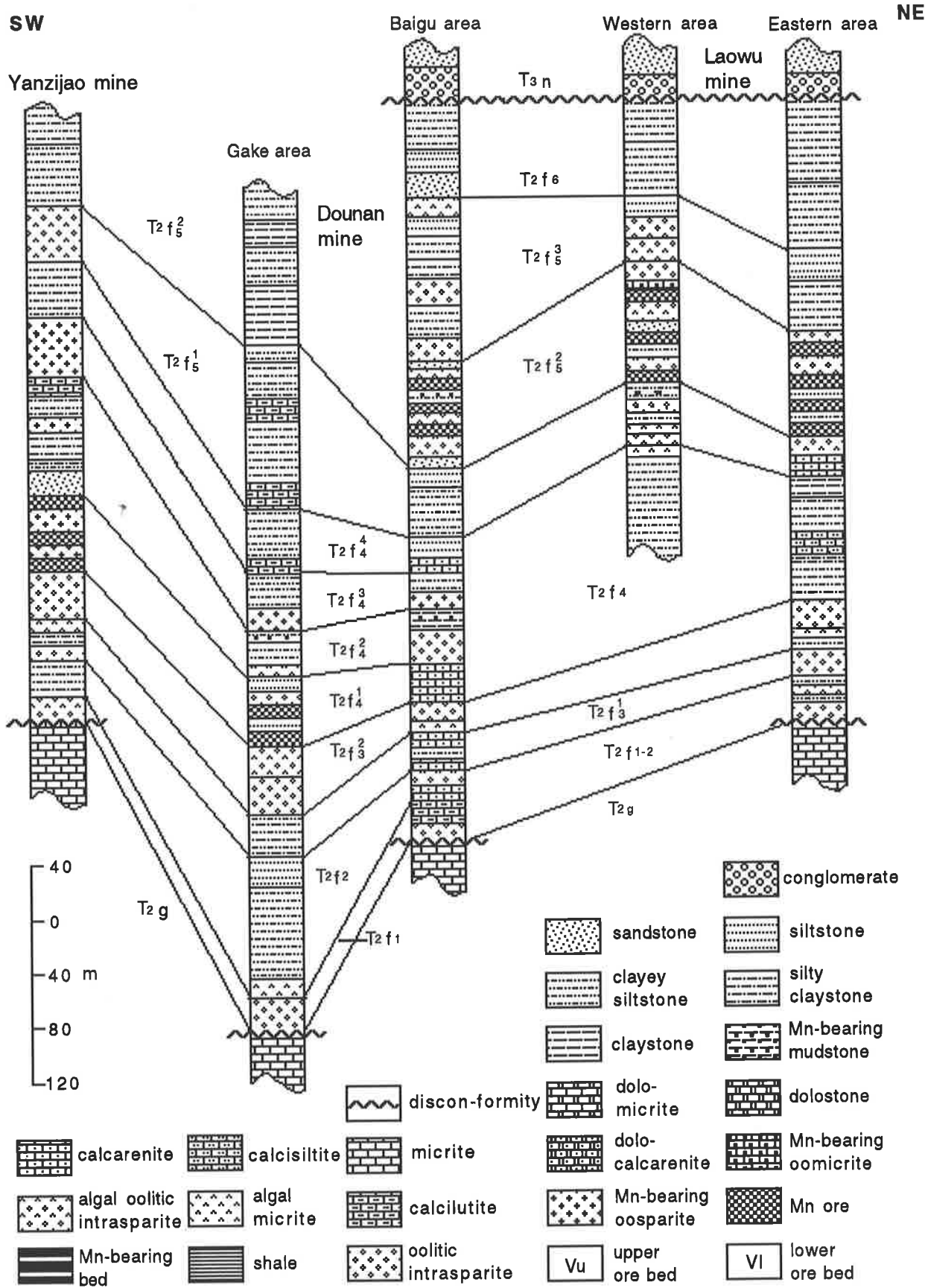


Fig. 2.22 Correlation of Falang Formation stratigraphy, middle Triassic, in Dounan area of southeastern Yunnan (lateral spacing not to scale). Note that the upper ore-bearing series is absent in the Gake area, indicating that it has been eroded or was never deposited. Note also that the lower ore-bearing series has correlations in the Baigu area, but that ores are poor or not present.

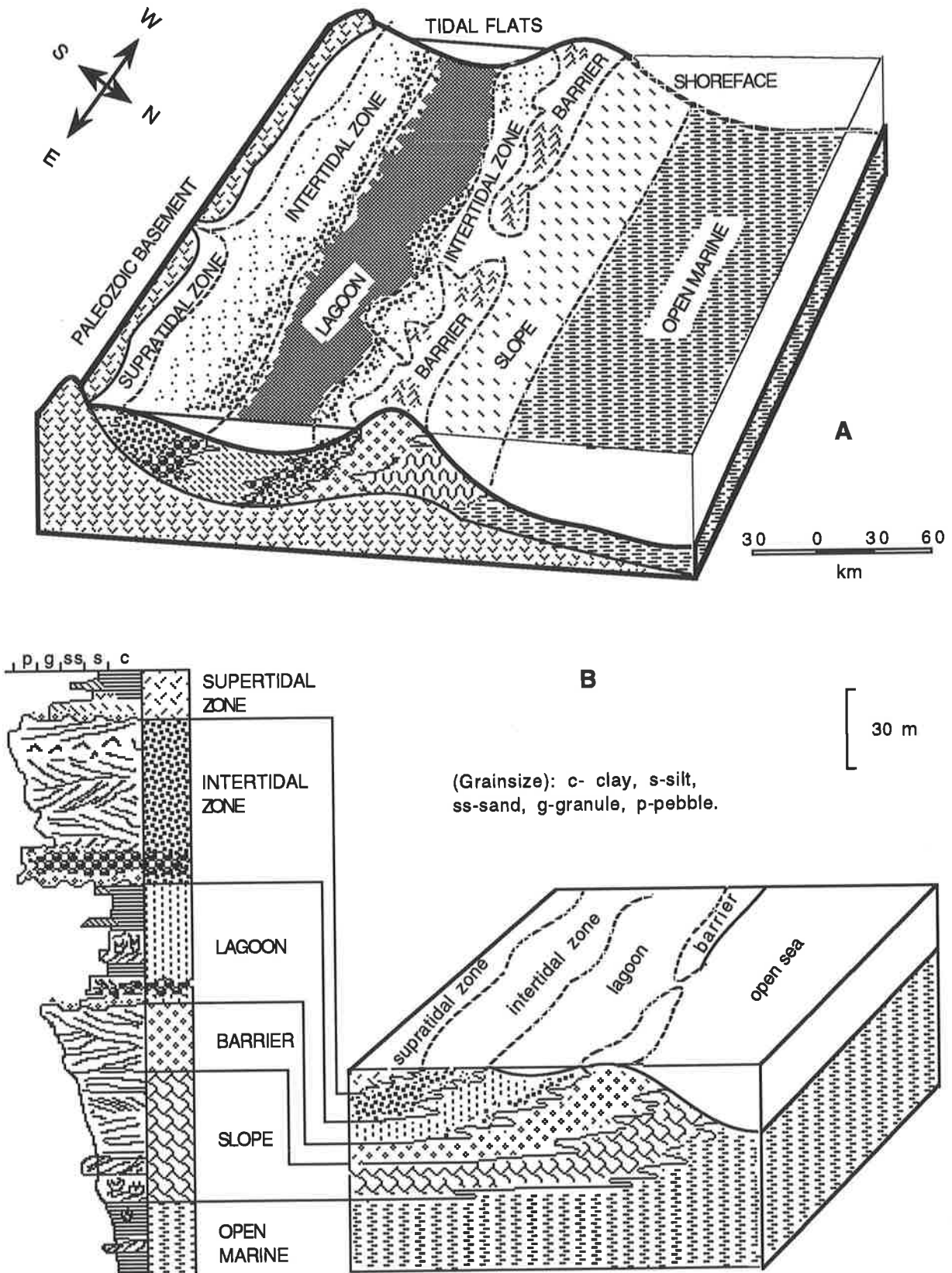


Fig. 2.23 Block diagrams illustrating the various subenvironments in the Dounan barrier-island system (A) and the depositional model of the Dounan Mn sequences (B).

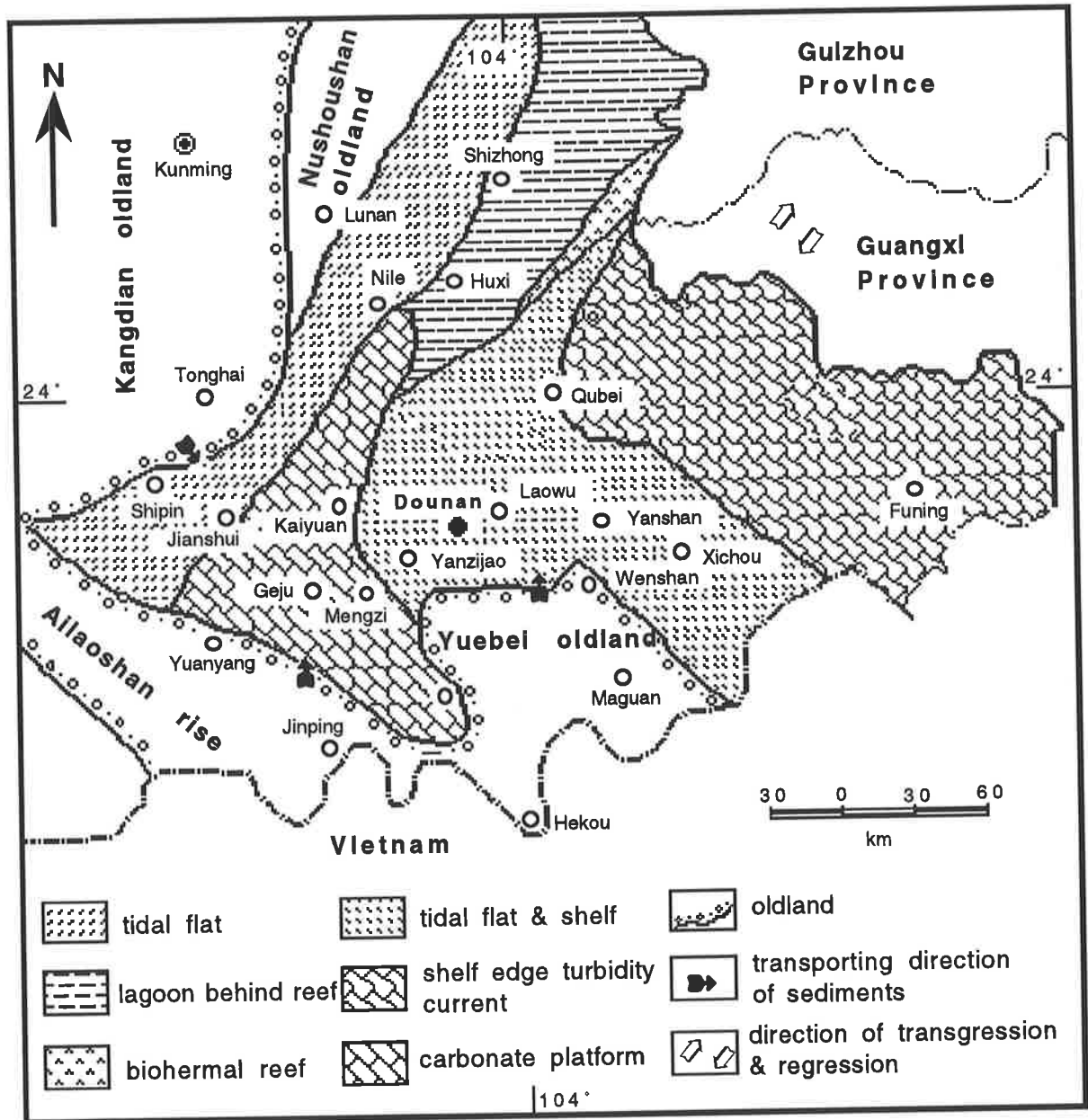


Fig. 2.24 Sedimentary facies sketch map of Falang stage, middle Triassic, in southeastern Yunnan (modified after Liu et al., 1984).

The Baixian sequence, as representative of the Baixian sub-basin, shows a facies association of lagoonal and evaporite flat deposition mainly composed of shale, dolomicrite and/or calcilutite with lagoon and tidal flat structures (Fig. 2.6). Also, the primary ores are mainly manganese carbonates, which suggests that the sediments mainly formed in a reducing-alkaline, low energy environment.

The Dounan sequence, a representative suite of the Dounan sub-basin, is composed of a number of shallow marine microfacies including a barrier-island system characterized by typically distinct lithofacies structures and biota fossils (Fig. 2.13). Generally, the facies of barrier and intertidal environments are characterized by intraclastic limestones and manganese oolites/pisolites, whereas the lagoonal (including back-barrier) deposits consist of mudstones and

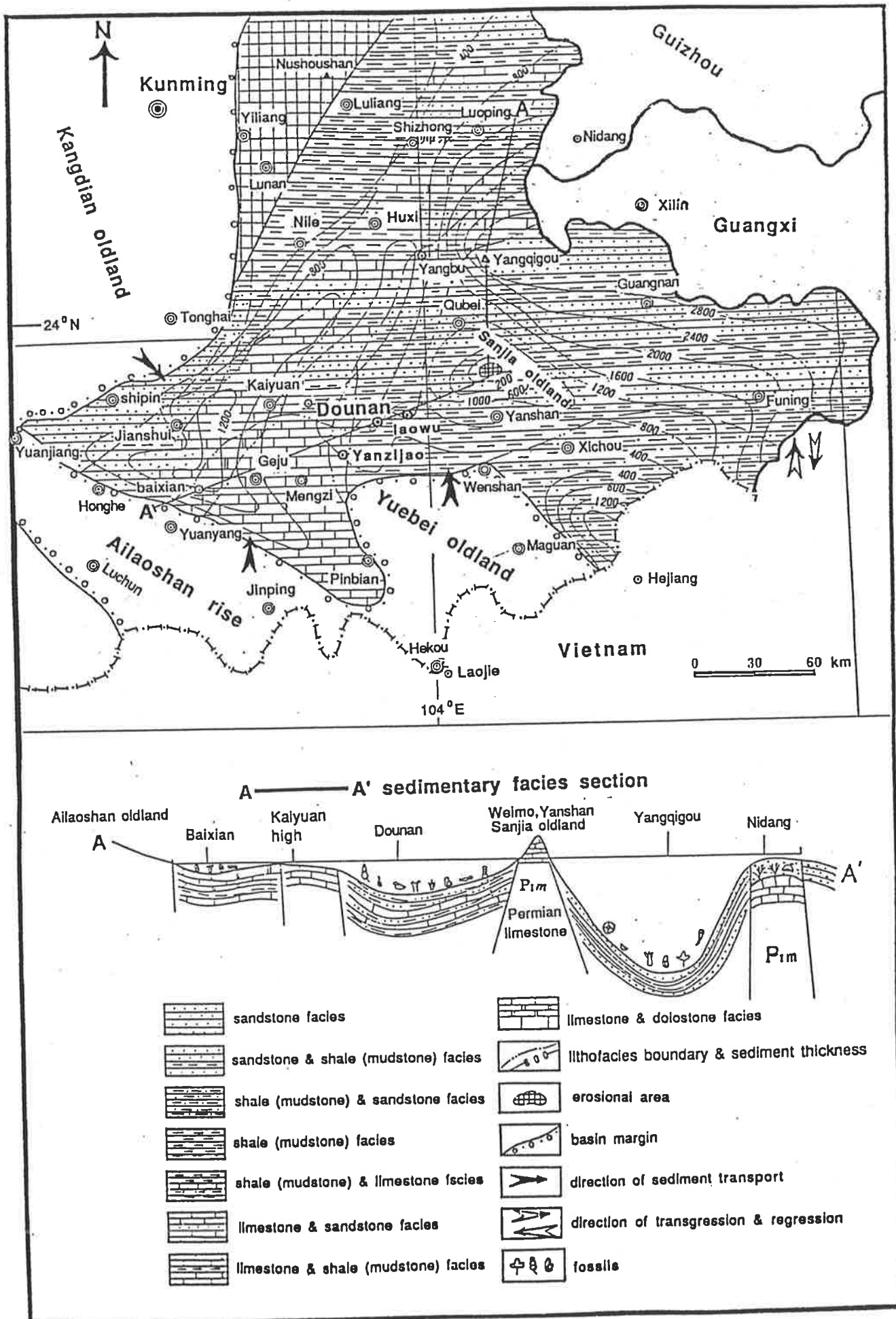


Fig. 2.25 Lithofacies palaeogeographic map and section of Falang stage, middle Triassic, in the southeast of Yunnan province, modified after Liu et al (1984).

siltstones. Manganese deposition mainly consists of mixed ore facies of both manganese oxides and carbonates as oolite/pisolite. Significantly, the Dounan ore-forming environments are confined to the intertidal zone and subtidal lagoon, the former being the zone of wave swash, the surge of water caused by incoming plunging breakers in the surge zone (Fig. 2.23). Lagoonal sequences generally consist of interbedded and interfingering fine intraclastic carbonates, siltstone and mudstone facies; these are characteristic of a number of overlapping subenvironments (see Figures in Chapter 2.4 and 2.5).

Reinson (1984) stated that the lateral and vertical extent and the occurrence of specific facies within a barrier-island system is dependent upon tidal range and the relative importance of tidal-current versus wave generated processes. For example, tidal-flat deposits will not be an important facies in microtidal environments because of the limited tidal range, whereas they may be extensive in mesotidal environments because of the stronger tidal currents generated by the larger tidal range. Thus, the thicker Falang Formation (including manganese orebeds) and typical structures in the Dounan area indicate that they formed in mesotidal environments. The evolution of the sedimentary facies and sedimentation discussed previously, strongly suggests an environmental variation from semi-deep to shallow marine and littoral facies. The manganese deposits mainly formed early in small-scale regressive sequences, while relative sea level was low.

Generally, the shoreface environment is defined as the area seaward of the barrier and the shoreface is an environment in which depositional processes are governed by wave energy (Reinson, 1984). The sedimentary facies in the Qubei area suggest nearshore environments but also including slope and open sea facies (Fig. 2.23) characterized by poorly laminated or massive fine sandstone, siltstone and mudstone. Typical Bouma structures and slump structures indicate the existence of turbidite or slope facies. These sediments are considered as correlative with the Bianyang and Jiangdonggou Formations of Guizhou province (Liu et al., 1984), but of different facies (Figs. 2.24, 2.25).

2.7.1.2 Transgressive / Regressive Models of the Dounan Sequence

The concepts of transgression and regression as used by geologists usually refer to the overlapping of deeper water deposits onto more landward or shallower water deposits (transgressive sequence), or shallow water deposits over more seaward or deep water facies (regressive sequence) (Reinson, 1984). The terms "transgression" and "regression" are also used to imply the process of migration of the shoreline of a water body, in a landward direction (transgression), or a seaward direction (regression) (Curry, 1964).

Commonly, transgressive and regressive barrier-shoreline migrations of the study area produce corresponding transgressive and regressive overlapping in not only "regional" but also "local" areas (see Figures in Chapter 2.4 and 2.5). The Falang ore-bearing series mainly formed in regressive sequences, though several sedimentary cycles have already been recognized in the

evolution of the Falang Formation (Fig. 2.23). Dominantly transgressive shorelines can have "local" regressive segments within them. Such situations are caused by short-term temporal variations in depositional conditions along the barrier-island strandline. Longshore sediment supply, local wave climate, and number and location of tidal inlets are some of the conditions which can change significantly and can affect both progradational and erosional trends in near juxtaposition. This is illustrated by the beach sequences observed on Kiawah island (South Carolina) (Barwis, 1978), the landward sequence being transgressive and the seaward sequence progradational or suggestive of regression. Thus, from the examples of not only modern, but some ancient sequences (Harper, 1984) it is obvious that there cannot be just one generalized facies model for barrier-island deposits.

If we apply the facies model criteria of Walker (1984), at least two "end-member" models (indicating a barrier-inlet model) for Dounan barrier-island stratigraphic sequences can be recognized: the transgressive model and the regressive (prograding) model, though the Mn-bearing series mainly formed in the latter (Fig. 2.23). The regressive facies model in Figure 2.23 serves as a norm for interpreting Falang stage regressive sequences in the Dounan area only. It yields a gradational and coarsening-upwards sequence, dominated by facies of the shoreface, barrier, back-barrier tidal flat, lagoon and tidal flat of barrier-beach complex. However, the transgressive model is more complicated than the regressive model in terms of interbedding of facies and alternating lithologies. It is characterized by subtidal, back-barrier, barrier and shoreface facies and does not show an obvious fining-upwards or coarsening-upwards trend. The contact between some facies may be sharp or erosional. Harper (1984) stated that many ancient sequences will deviate substantially from the normative model, because the facies stacking in transgressive sequences is quite variable, due to the rapid response of depositional environments to change in sediment supply and inlet conditions in transgressive situations. Importantly, one of the main differences between the regressive model and the transgressive model lies in the relationship with lagoonal facies (Harper, 1984). In the regressive sequence lagoonal deposits would overlies the barrier facies, whereas in the transgressive model lagoonal facies underlie barrier deposits within the lower or middle positions of the Dounan sequence.

2.7.2 Lithofacies-Paleogeography

Based on the previous description and analysis the Falang stage lithofacies-paleogeography of southeastern Yunnan can generally be outlined. The biggest transgression of the Triassic took place in the Geju stage, in the initial part of the middle Triassic; the sea then retreated towards the northeast near the end of the Geju stage, which led to some local erosion in areas such as Baixian, Dounan and Laowu. Some areas remained underwater continuously and received sediments (Zhang et al., 1979), but a local disconformity between the Geju and Falang Formations developed in most areas of southeastern Yunnan. The second transgression of middle Triassic age took place in the initial period of Falang (Ladinian) deposition. This transgression was

smaller than the first one, and led to formation of the large Falang stage sedimentary basin of southeastern Yunnan, semi-surrounded by Nioushoushan, Kangdian, Ailaoshan and Yuebei erosional oldlands or uplifts, which provided sedimentary materials (including manganese) for the Falang Formation. Following this, a series of small scale regressions and transgressions led to the lower Mn-bearing sedimentary cycles. After a third large transgression, small-scale regressions and transgressions took place again and led to development of the upper Mn-bearing sequence. The evolution of Falang sedimentation in the southeastern Yunnan marine basin led to a series of manganese deposits along the shallow marine zone of the southeastern Yunnan sedimentary basin (Figs. 2.23 and 2.25).

The Kaiyuan topographic high, which trends NW and represents a submarine connection between the Kangdian and Yuebei oldlands, limited seawater access to the Geju (Baixian) sub-basin which then became more saline, accumulating thick dolomitic limestone and argillaceous dolostone (Figs. 2.24, 2.25). The Baixian manganese deposit formed in a sub-basin of the southern sedimentary zone of the Geju basin (Zhang et al., 1979). About 100 meters of Falang sediments were deposited on the Kaiyuan submarine high. When compared with the stratigraphy of the central Geju basin it is obvious that the lower sedimentary cycle of the Falang Formation is missing.

To the east of the Kaiyuan submarine high, there existed shallow marine environments with a barrier-island system along the northern margin of the Yuebei oldland, where a series of terrigenous clastic rocks, carbonates and manganese ores were deposited. It is in this Dounan marine sub-basin that a sedimentary complex, 800 m thick, of terrigenous clastic and intraclastic rocks and manganese oxides and/or carbonates (Dounan manganese deposits) were deposited. To the north of the Dounan basin, in the Jiangbian basin (Huxi area, Fig. 2.25), thicker (>1000 m) siliceous mudstones and limestones were deposited, and a series of small-scale manganese deposits (mostly poor ores) were formed along the northern and western shorelines of this basin. To the east of both the Dounan and Jiangbian basins, thinner sequences (only 174 m in thickness in Xinzhuangke) composed of thin mudstone, siltstone and sandstone and also some small-scale manganese deposits were deposited on the Yanshi (Yanshan-Shizhong) submarine high, which trends nearly S-N (Figs. 2.21, 2.25). Again, to the east of the Yanshi high, the water became deep, and shoreface mudstone, siltstone and fine sandstone (but no Mn deposits) were deposited; this indicates a disadvantageous environment for manganese deposition, probably because the area was distant from the oldlands and the manganese supply was low.

Although the Falang lithofacies-paleogeography of southeastern Yunnan is characterized by shallow marine, the sedimentary facies show variable features due to the differences in the paleo-topography in the depositional areas. Generally, from the southwest to the northeast, the facies varied from dolomitic limestones to siltstones and then mudstones. The western Geju basin is characterized by three oldlands and one submarine high, on which salinized tidal-flat argillaceous or dolomitic limestone facies commonly accumulated; these conditions constituted an

advantage for the formation of manganese carbonate ores, when the paleotopography was suitable and when there was sufficient Mn supply (e.g., Baixian manganese deposit). Towards the east, on the western Kaiyuan submarine high, environments were suitable for shallow water sandstone, siliceous calcarenite facies, but not Mn deposits, to form, but some small manganese deposits could still be formed such as at Bapanzai. To the east of Kaiyuan, the thicker limestone and mudstone intercalated with siltstone facies (150-1500 m in thickness) could have been an advantage for the formation of manganese deposits when the material supply and paleobathymetry were ideal, e.g. Yanzijiao manganese deposit. Still farther the east, the shallow marine shelf is characterized by mudstones and siltstones intercalated with intraclastic carbonate facies, and suitable conditions for the formation of large-scale Mn deposits (e.g. paleobathymetry, manganese material supply, pH and Eh values), especially along the tidal-flat zones close to the shoreline of the Yuebei oldland, such as the Dounan and Laowu manganese deposits, and the Tangde and Guohua small manganese deposits. Although the tidal-flat sandstone, siltstone and mudstone facies were also deposited in shallow water along the Nushoushan and Kangdian oldlands, manganese deposits are not found in this area, probably because Mn supply and paleobathymetry were not suitable. In addition, the southeastern area of southeastern Yunnan (e.g. Xichou) was located in relatively open marine conditions and the siltstone and mudstone environments were suitable for forming manganese deposits, as long as manganese supply was present, such as in small deposits at Baishiya and Shieroun. This area is considered to be prospective for manganese.

2.8 Discussion

The information in the stratigraphical profiles can be used to generalize the important lithofacies-paleogeographic features of southeastern Yunnan. Especially, detailed Dounan sequences identify primary sedimentary environments in the Dounan sub-basin suitable for accumulation of ores, which probably means that the primary sedimentary mineralization played an important role in the genesis of Dounan manganese deposits relative to secondary events such as diagenetic and supergene processes. Grainsize variations in the vertical sequences are indicative of manganese depositional events during regressions and interruption of the manganese input during transgressions. This fact is emphasized by the textural and structural variations of both stratigraphic sections and vertical profiles of the orebeds (see Chapter 3) in the field (e.g. Gake and Baigu mine-areas). Importantly, the scouring observed at the top of orebeds suggest short (submarine) erosional events during sedimentation, especially regressions. Here, the tops of inverse graded parts of the profiles show higher energy environments than the lower parts. In contrast, the normally graded indicate that the energy levels decreased upward.

Other genetic information includes the fact that the manganese ores are always associated with complex mixed associations of terrigenous clastic and intraclastic carbonate sediments. Ob-

viously, the Dounan ores do not form in "pure" clastic or carbonate rock facies, but rather in areas and times of changing environments.

Two manganese groups are identified in the Dounan sequence of the Falang Formation: i.e. the upper part (T2f5-2) and the lower part (T2f4-1) of the sequence. Although the two manganese groups formed in different sedimentary cycles, they have similar sedimentary features, and both resulted from the interactive sedimentation of intertidal and lagoonal facies. Similarly, though many manganese ore layers occur in the Falang Formation and in different positions in the vertical sequences, they testify to similar geochemical and sedimentary environments. Tidal flats (including the back-barrier area) are preferred sites for primary manganese ores. The variable thicknesses of manganese oxides/carbonates indicate varying rates of ore-formation, perhaps due to variable timespans of environmental stability. Compared with very fine materials, these coarse grained manganese ores enclose large biofragments such as bivalves and ammonoids. The importance of oxygen in the formation of manganese oxides is demonstrated by the fact that the biota in Mn-bearing units is abundant and varied but is less so above and below. The association of terrigenous clastic and carbonate rocks with manganese oxides and carbonates may have been a factor in the formation of braunite and calciorhodochrosite, which are the dominant manganese minerals in the Dounan ores.

Paleontology may play a considerable role in the formation of Dounan manganese ores. This fact is emphasized by microscopic observations of the manganese ores or orebeds, in where the fossils are often partly or totally "replaced" by manganese minerals, as seen particularly well in the ores of the Gake and Baigu areas. In many cases this "replacement" is found not only in manganese ores but in Mn-bearing rocks.

Importantly, the migration of the sedimentary centers of Dounan manganese orebeds indicates that the Dounan manganese deposits formed in regressive sequences. This interpretation is strongly supported by mostly inversely graded structures in the orebeds (see Chapter 3).

Chapter 3 Orebeds

3.1 Introduction

The stratigraphy of both regional and local areas has been described in detail in the previous Chapter and here emphasis focuses on the individual vertical profiles which include orebeds. Descriptions will be kept brief (localities, stratigraphic positions, and grainsize data are given in Appendix II, Table II.1).

There are about ten manganese orebeds in the Dounan middle Triassic Falang Formation; these were named V₁, V₂, V₁₀ by Zhang et al (1979). Some additional small orebeds will also be described, such as V₁₋₁ and V₃₊₂. The main purpose of this study is to provide further background information on the genetic interpretation of Dounan manganese ores drawn from field observations. Most of the localities discussed here were subjected to a small-scale sampling procedure (see Appendix I.1) to allow a stratigraphically oriented geochemical analysis of the materials.

Three incomplete vertical profiles of orebeds were examined in the Kata, Daaazi and Milike mine-areas, which will be only briefly discussed in this Chapter as they are still being prospected and are not in the main mine-areas. In many aspects, however, the ores in these minor mine-areas are similar to those occurring in the Gake area, and also can be correlated to each other; they are slightly different from those occurring in the Baigu area, mostly in details of their stratigraphy. The ore sections examined in Gake and Baigu mine-areas discussed below are typical representatives for the respective localities, in that most ores/associated rocks are laterally continuous over large distances, except for lensoid intercalations and very thin units such as orebed V₁₋₂ and V₃₊₁. Since this study deals with manganese oxide and carbonate oolites and pisolites, the grainsize of these materials is emphasized. This approach illustrates gradients of ore components within orebeds, and thus provides information on genesis.

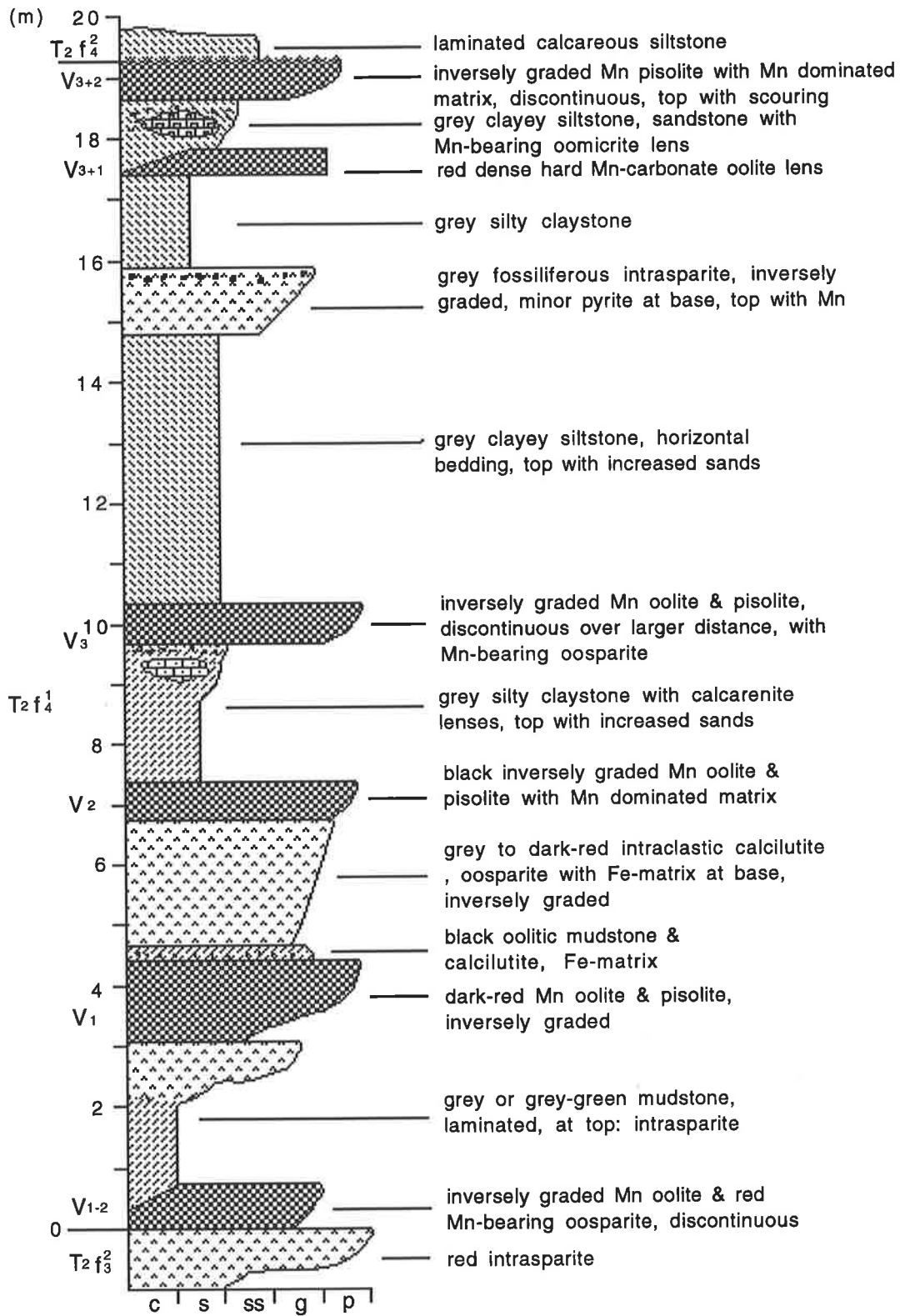
3.2 Distribution of Dounan Orebeds

The section descriptions were made in five mine-areas from the southwest to the northeast of the Dounan deposit. The common legend for all ore sections in this Chapter is shown in Table 2.1 and locations are shown on Fig. 2.4.

3.2.1 Gake Area

This area covers the SW flank of the Dounan syncline (Fig. 2.4) and includes the three main manganese orebeds of i.e. V₁, V₂ and V₃ and the 5 subsidiary orebeds, i.e. V₁₋₂, V₁₋₁, V₁₊₁, V₃₊₁ and V₃₊₂ (Figs. 3.1). This area, together with the Baigu area, were first investigated systematically by the No.2 Geological Brigade of Yunnan Province in the 1970s. Mostly, the orebeds here can be traced throughout the deposit within sub-member T_{2f4-1} with a thickness of ~20 meters; they have been called "Gake orebeds" by Zhang et al (1979), due to their occurrence mainly in the Gake area. Commonly, the manganese oxide and carbonate horizons in the Gake area show inverse (occasionally normal) grading, and are underlain by intraclastic calcilutite/micrite which is also inversely graded.

Generally, orebed V₁ has three components, i.e. V₁₋₂, V₁₋₁ and V₁₊₁. Orebed V₁₋₂ generally occurs at the base of sub-member T_{2f4-1}, and the ores are commonly composed of manganese oxide and carbonate oolites/pisolites and show dark red and black colours, massive structure and three grades of manganese tenor, i.e. Mn 6-8% (Mn-bearing micrite); Mn ~15% (Mn carbonate ores); and Mn ~21% (Mn oxide ores) (e.g. drilling core CK532). This unit is 0.31-0.93 m thick, and is discontinuously distributed. Orebed V₁₋₁ is mainly composed of unsorted manganese oxide or carbonate oolites/pisolites, commonly shows massive and banded structures, and is inversely graded. Content is Mn 8-25% and the unit is 0.05-0.2 m in thickness but discontinuous over large distances. V₁₋₁ increases in thickness (e.g. 2.32 meters at drill core CK31) in the northern limb of the Dounan syncline. Generally, grey laminated mudstone (~1 m in thickness) occurs between orebeds V₁₋₂ and V₁₋₁, showing sharp contacts. Red Mn-bearing intrasparite overlies orebed V₁₋₁, and a sharp boundary separates the intrasparite from the overlying orebed V₁, which shows black inversely graded manganese oolites/pisolites with manganese dominated matrix, intercalated with dark-red manganese carbonate oolites/pisolites, and banded and massive structures. Orebed V₁ is considered to be the most important orebed in the Gake area, with Mn 12-38% (average Mn 24.36%) and a thickness of 0.07-4.01 m. The overlying black oolitic mudstone or calcilutite with ferruginous spots (0.1-0.3 cm) above orebed V₁ is one of the easily recognizable key beds in the Dounan sequence. Still higher is intraclastic calcilutite intercalated with quartz silty intraclastic oomicrite (~0.7 m in thickness) which is a key bed between orebeds V₁ and V₂.



(grainsize)

c - clay, s - silt, ss - sand
g - granule, p - pebble

Fig. 3.1 Vertical geological profile of Lower ore-bearing series, Gake area.

Orebed V₂ (Fig. 3.1) is the second main ore unit; it consists of inversely graded manganese oolites/pisolites which is matrix-dominated (0.07-1.93 m in thickness). The ores are composed of black Mn oxides and dark red Mn carbonates or Mn-bearing micrite, mainly showing massive and banded structures. Above V₂ is grey silty claystone with intercalated calcarenite lenses near the top (totalling 2-3 m in thickness). Dark red, inversely graded Mn carbonate oolites/pisolites (0.5-0.95 m in thickness), commonly containing broken grains and occasionally containing black braunite ooliths/pisoliths, next occur as orebed V₃. These are mostly poor quality ores, which are distributed only on the northern limb of the Dounan syncline (e.g. prospecting line 55-57, Figs. 2.4); they change laterally into Mn-bearing oolitic/pisolitic micrite. Again, an easily recognized key bed composed of grey brecciated or oolitic/pisolitic (0.5-1.5 cm) calcilutite (0.2-1.5 m in thickness) with bioclastic debris and minor chlorite and pyrite, occurs between grey laminated siltstone (underlying layer 4-5 m in thickness) and grey silty claystone (overlying layer ~1.77 m in thickness). Generally, this mudstone is overlain by orebed V₃₊₁ which consists of dark red manganese or Mn-bearing carbonate oolites lenses (0.10-0.38 m in thickness). Commonly, the ores of orebed V₃₊₁ show poor quality and occur only locally in the Dounan deposit (e.g. drill cores CK56A7 and CK56B2); they change laterally into Mn-bearing oolitic micrite, overlain by grey siltstone and sandstone with Mn-bearing oomicrite lenses at the top. Above this unit, orebed V₃₊₂ occurs at the top of T_{2f4-1} sediments as the last layer of this sub-member, and consists of dark red or black Mn carbonate and oxide oolites/pisolites, with inverse grading and scouring on the top; they are of poor quality and are discontinuously distributed.

3.2.2 *Kata Area*

This section was examined in the northwestern part of the Dounan Mn deposit, adjacent to the western Gake mine-area, where additional excavation provided a relatively complete profile through orebeds V₁, V₂ and V₃, including V₁₊₁ which is not present in the Gake area. The top and bottom parts of ore-containing sub-member T_{2f4-1} at this location could not be found due to poor outcrops. The ores of this section are very similar to those of the Gake area except that orebeds are thinner and more cemented than at Gake (Fig. 3.2). Generally, this section can be well correlated with units in the Gake and Daozi areas.

In contrast to the Gake area, here the underlying units of both orebeds V₁ and V₂ are mudstones (showing sharp contacts with the two orebeds), which reflect relatively low energy environments, but the grey layer underlying orebed V₁ indicates a deeper lagoon site, whereas the red beds with desiccation structures underlying orebed V₂ suggests a shallower tidal-flat environment. Orebed V₁₊₁ overlies an early recognizable key bed of oolitic mudstone, and consists of dark-red manganese carbonate or Mn-bearing (Mn 4-8%) micritic oolites (0-0.5 m in thickness), commonly containing braunite ooliths/pisoliths and bands; it is of poor quality,

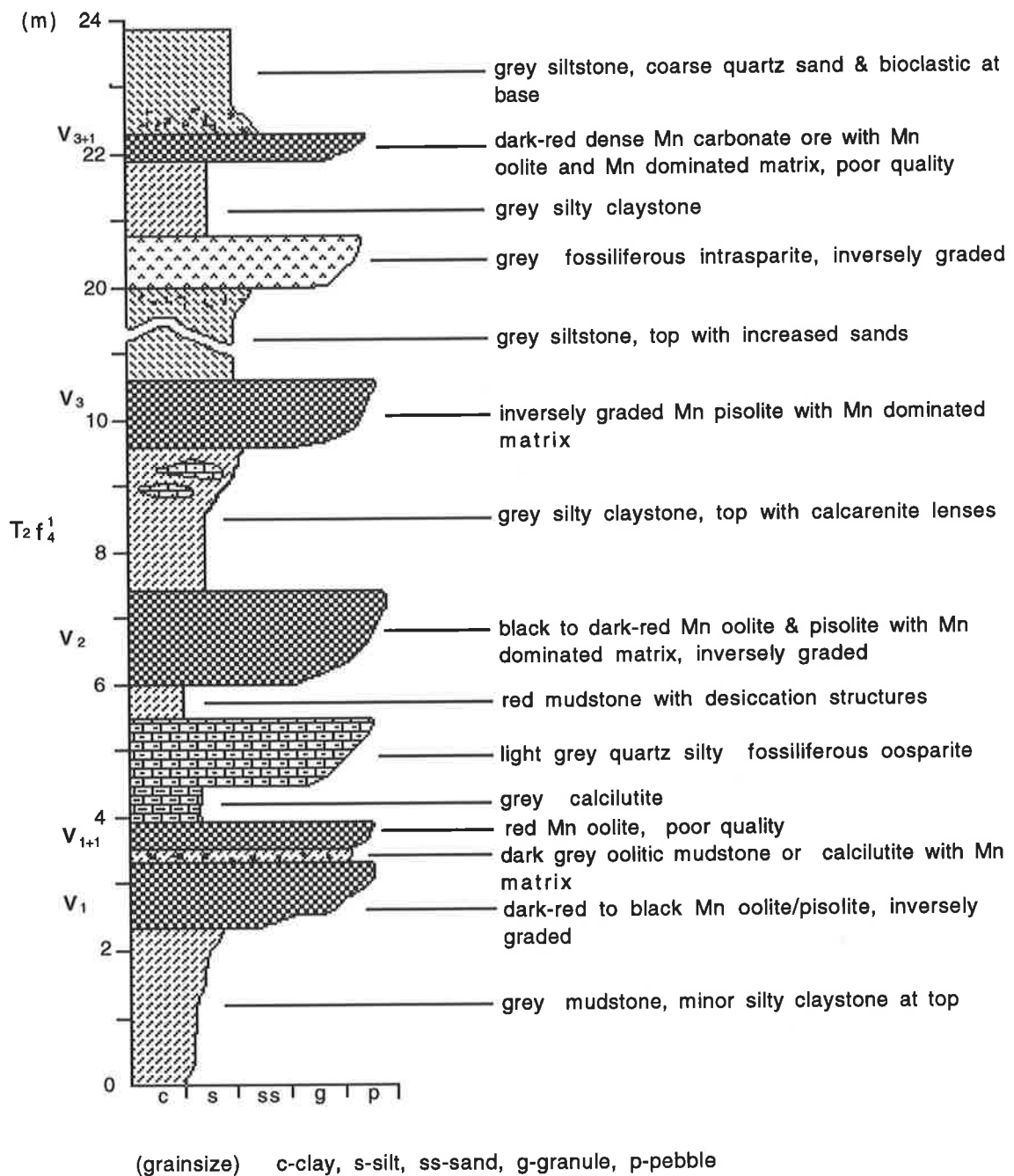


Fig. 3.2 Vertical geological profile of Lower ore-bearing series , Kata area.

laterally discontinuous, and shows occasional inverse or normal grading. The key bed underlying orebed V_{1+1} consists of thin red oolitic mudstone or calcilutite with manganese matrix, which is underlain by inversely graded manganese oolites/pisolites (V_1). Sharp boundaries separate both orebeds V_1 and V_{1+1} from this key bed which differs lithologically from its correlate in the Gake area (commonly intraclastic calcilutite).

A fossiliferous oosparite unit occurs between V_{1+1} and the red mudstone, which shows sharp contact with overlying orebed V_2 . Although orebed V_2 is also composed of both Mn oxide and carbonate oolites/pisolites, it contains relatively more oolites and shows inverse grading. It is separated from orebed V_3 by 2-3 m of grey silty claystone which contains calcarenite lenses at the top and shows sharp boundaries with both underlying orebed V_2 and overlying orebed V_3 . The second main orebed (V_3) of this area is characterized by normal and inverse grading, and Mn oolites/pisolites consisting of both manganese oxides and carbonates. V_3 is followed by a thick grey mudstone and then a grey inversely graded fossiliferous intrasparite. Still higher is silty claystone followed by orebed V_{3+1} with a sharp base. Commonly, orebed V_{3+1} is overlain by grey siltstone which contains coarse quartz sands and bioclastic debris at the base, and is composed of Mn carbonate and minor Mn oxide oolites /pisolites, with inverse grading, dark red colour and poor ore quality.

3.2.3 Daaazi Area

In the Daaazi mine-area, the stratobound manganese ores of the Dounan syncline trend east-west throughout the southeastern part of the Dounan manganese deposit. The geological section of the Daaazi area is poorly exposed; excavations and test trenches provide only an incomplete profile (Fig. 3.3). This includes only orebeds V_1 and V_2 in a relatively thin sequence.

Orebed V_1 is mainly composed of inversely graded manganese oxide and minor carbonate as oolites/pisolites in a Mn-dominated matrix of black and dark red colours. The presence of the thin manganese oolite horizon overlying orebed V_1 suggests that the precipitation of manganese oxide and carbonate orebodies must have continued over a considerable time span after orebed V_1 was deposited. The observation of continuous grain size gradients over 0.2-0.5 meters near the boundary between these two units supports this view. A sharp boundary separates orebed V_1 from the underlying grey mudstone.

Generally, orebed V_2 is composed of inversely graded black manganese oxide (containing minor Mn carbonate) as oolites/pisolites set in a manganese-dominated matrix. A relatively sharp boundary separates orebed V_2 from the underlying dark-red oolitic calcarenite, in which intercalated relatively thin pisolitic calcarenite horizon mostly at the top. The dark-brown Mn-bearing micrite with a thin manganese oolite horizon at the base separates its underlying orebed

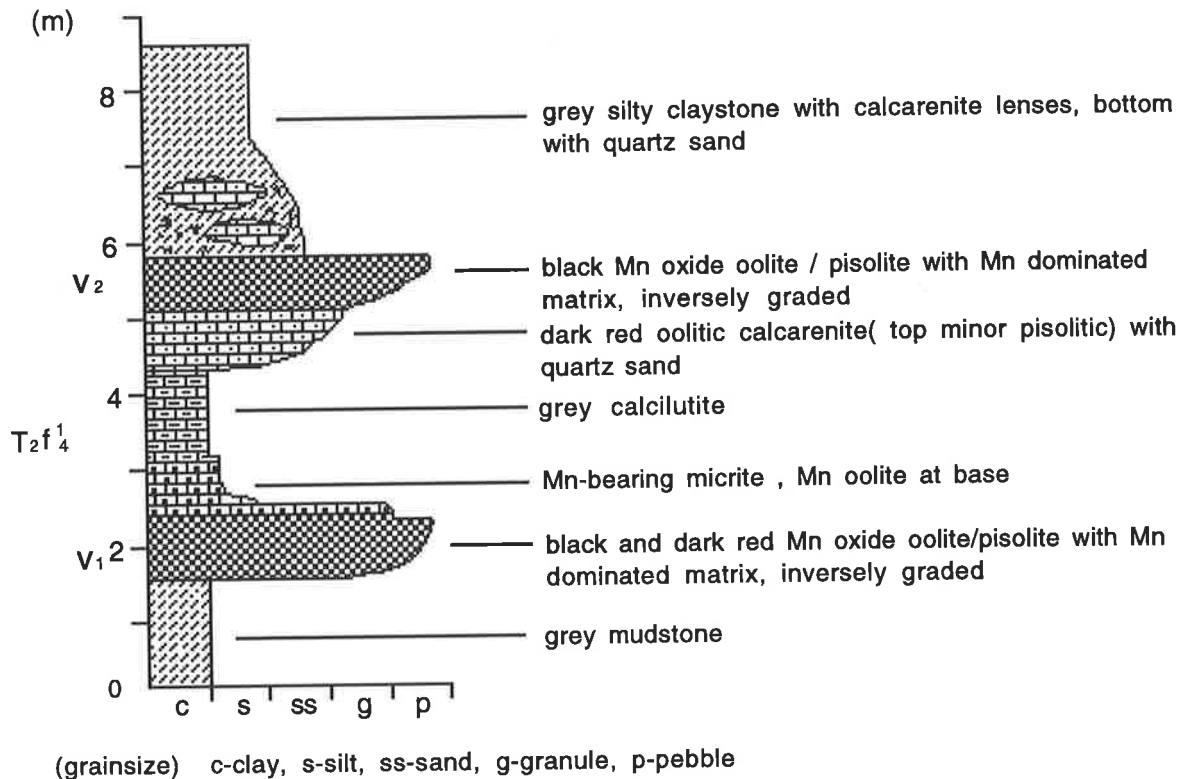


Fig. 3.3 Vertical geological profile of Lower ore-bearing series, Daozi area .

V₁ from overlying grey calcilutite. The unit is overlain by grey silty claystone intercalated with calcarenite lenses and quartz sands at the base.

3.2.4 Baigu Area

There are a number of manganese orebeds in this area, including those affected by fault F₃ (Fig. 2.4). These orebeds are mostly confined to the Baigu area in the northern and northeastern part of the deposit. The Baigu area contains a relatively thick development of sub-member T_{2f5-2} with ~8 inversely (occasionally normally) graded manganese oolite/pisolite orebeds (i.e. V₄ - V₁₀) (Fig. 3.4). Significantly, throughout ~60 m of the upper ore-bearing section of the Dounan Mn deposit, the oolitic/pisolitic but very hard siliceous manganese oxide and calcareous manganese carbonate horizons occur at regular intervals. Description will be from the bottom to the top of the Baigu profile.

Orebed V₄ occurs between two siltstone layers and is mainly composed of dark-red oolitic/pisolitic manganese carbonate ores. The unit shows a number of normally and inversely graded ores with abrupt variations in grainsize at the top; it is of poor quality, discontinuous and non-commercial. The ores of orebed V₅ are similar to those of orebed V₄, are mostly non-commercial, and are underlain by laminated siltstone. The top contains oolitic/pisolitic micrite and minor

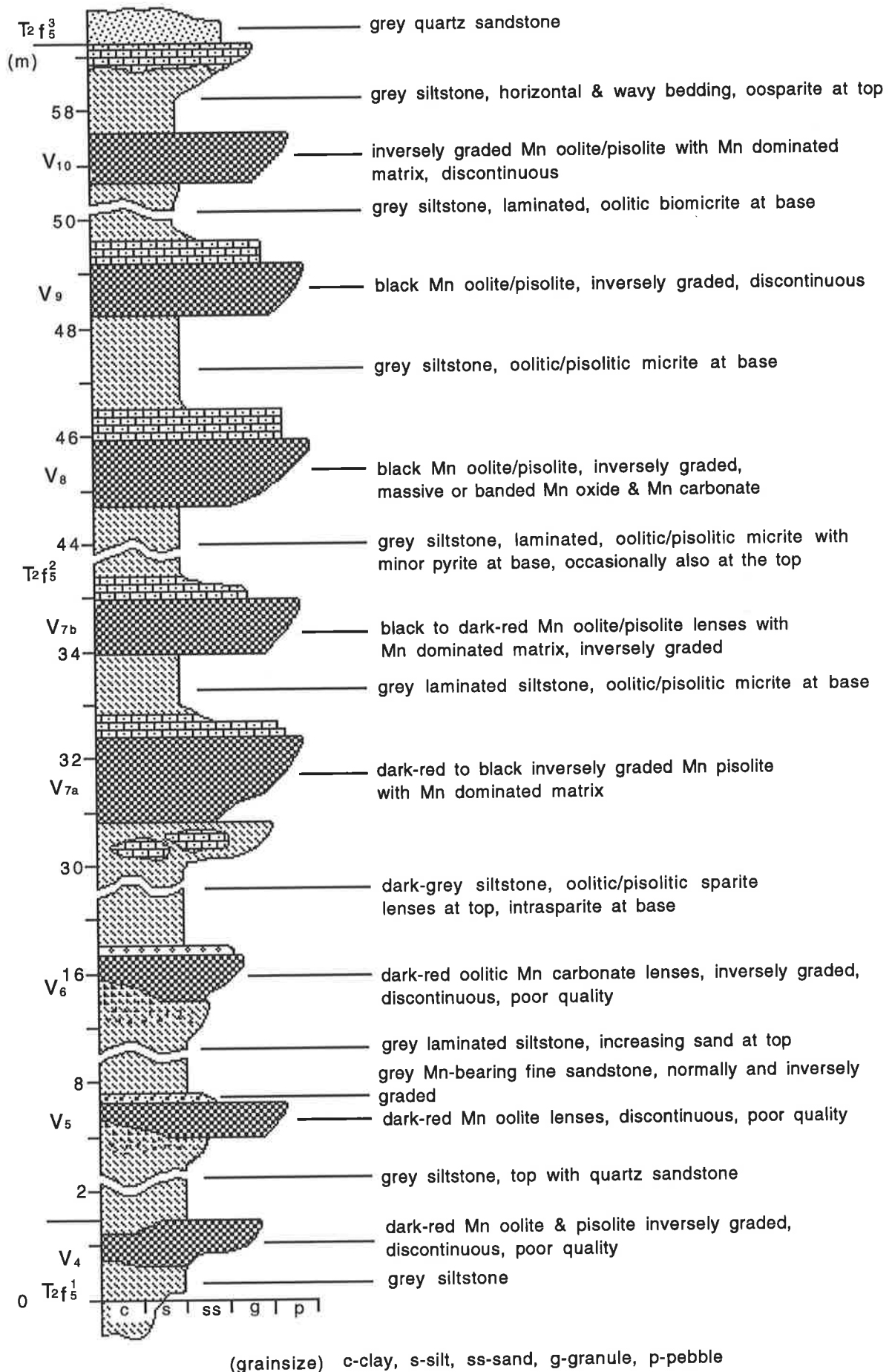


Fig. 3.4 Vertical geological profile of Upper ore-bearing series, Baigu area.

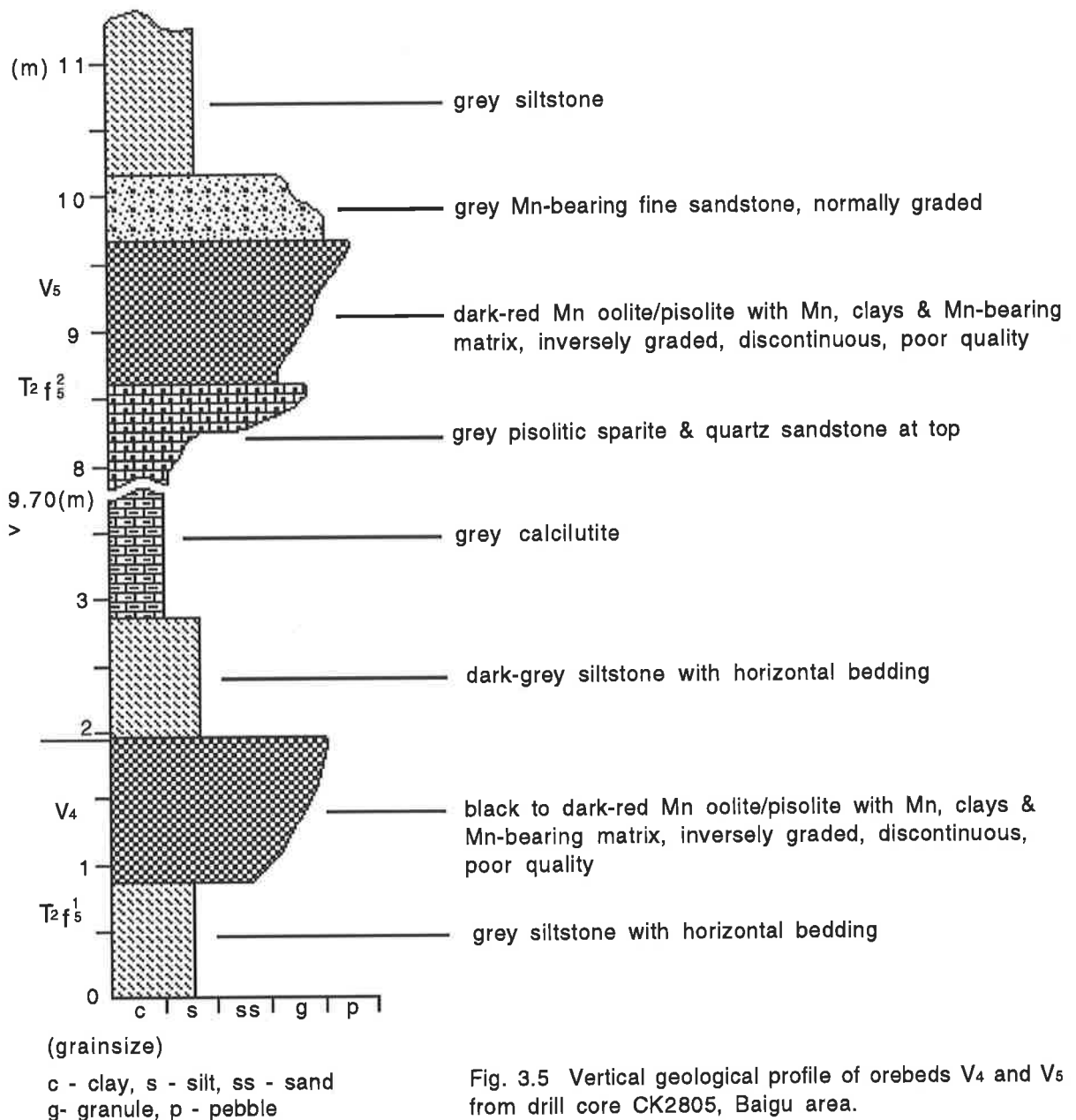


Fig. 3.5 Vertical geological profile of orebeds V₄ and V₅ from drill core CK2805, Baigu area.

sandstone. V₅ is overlain by normally graded Mn-bearing sandstone. Locally, orebeds V₄ and V₅ (~2 m) are commercial; these consist of manganese carbonate ores (e.g. prospecting line 28, drill core CK2805, Fig. 3.5), but they laterally change into Mn-bearing micrite. This probably reflects relatively complex depositional sub-environments during these stages. Orebed V₆ is mainly composed of dark-red oolites/pisolites of manganese carbonate (with minor oxides) set in a Mn and clay micrite matrix. The ore is of poor quality and is laterally discontinuous. It is underlain by laminated siltstone (~8 m in thickness) with minor sandstone at the top; above the ore is siltstone with intrasparsite at the base.

Orebed V₇ is separated into two horizons, i.e. V_{7a} and V_{7b} by a thin layer (~1.5 m) of siltstone with oolitic/pisolitic micrite at the bottom. Compared with orebed V_{7a}, the upper orebed, V_{7b}, is a relatively thin layer, but both orebeds have similar manganese ores composed of inversely graded manganese oxide and carbonate oolite/pisolite with manganese dominated matrix.

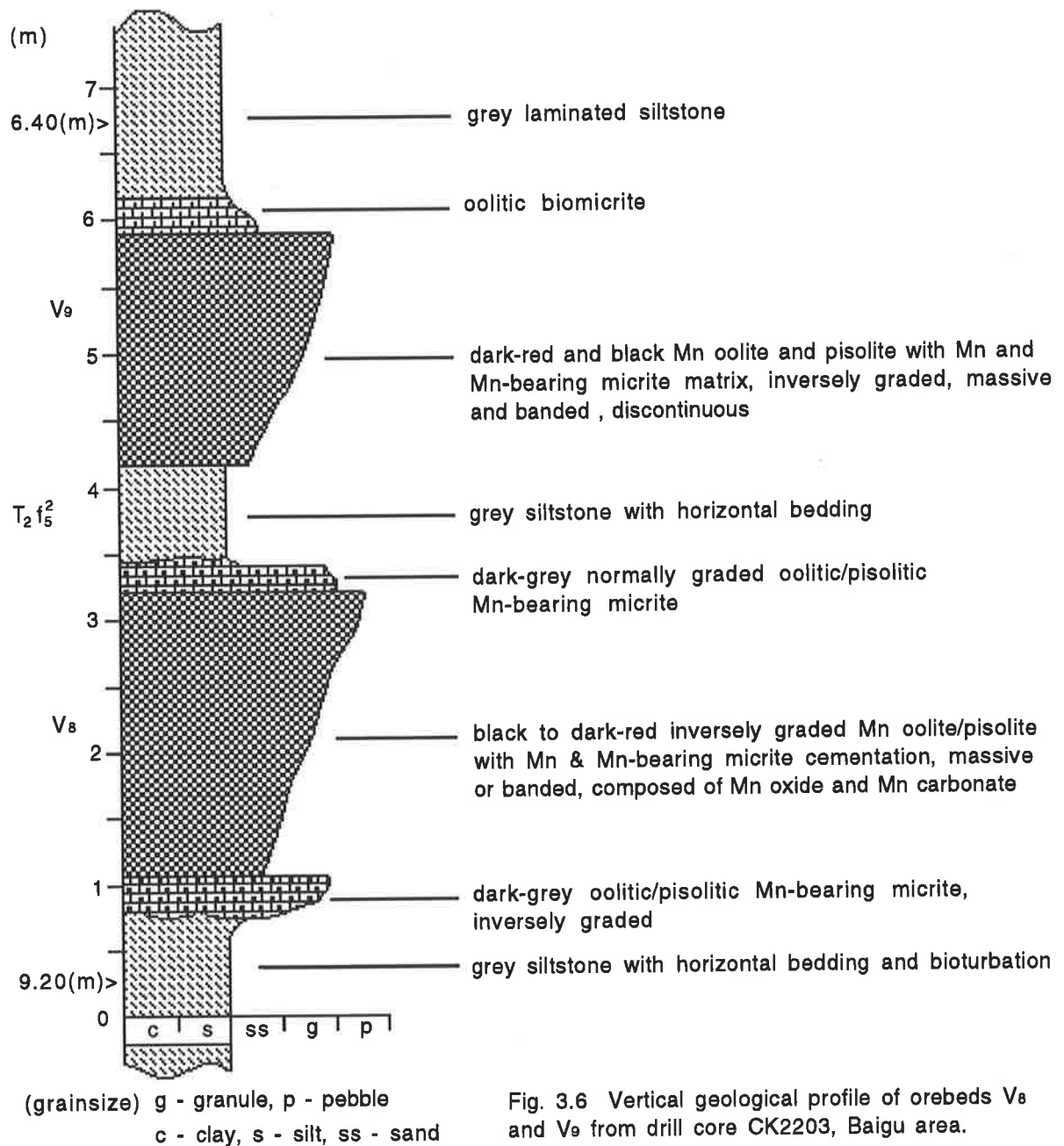
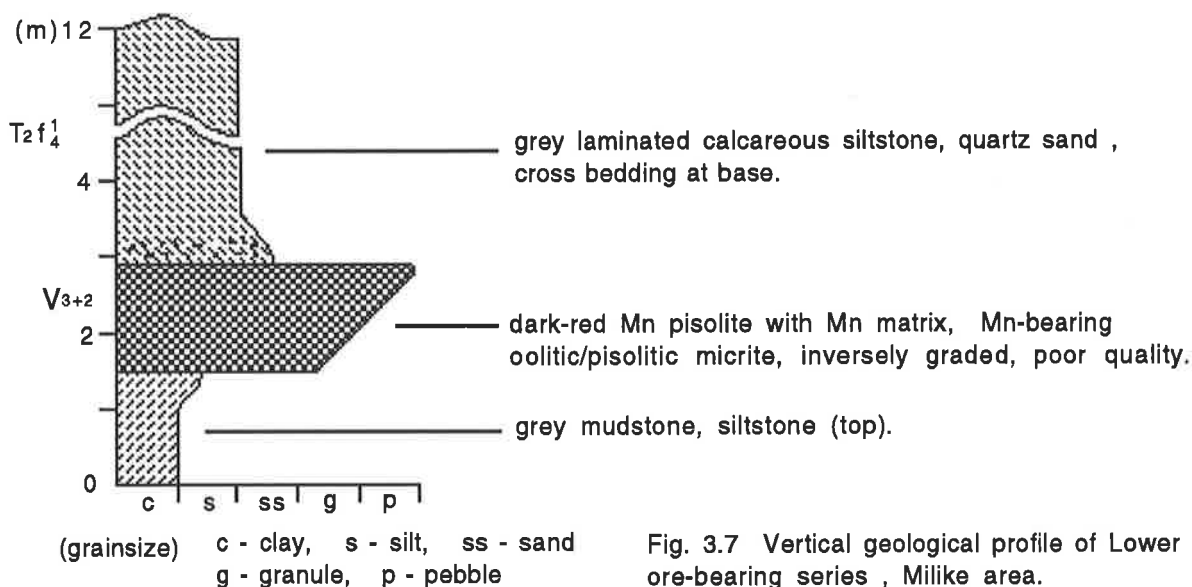


Fig. 3.6 Vertical geological profile of orebeds V_8 and V_9 from drill core CK2203, Baigu area.

Orebed V_{7b} is laterally discontinuous. Similarly, both orebeds V_{7a} and V_{7b} are overlain by siltstone with oolitic/pisolitic micrites at the base. Generally, orebed V_8 is the most continuous and important orebody in the Baigu mine-area and is composed of black to dark-red, massive or banded, manganese oxide and carbonate oolites/pisolites, showing good quality and inverse grading. Occasionally, orebed V_8 is directly underlain by reversely graded oolitic/pisolitic Mn-bearing micrite but with abrupt variation in grainsize at the boundary (Fig. 3.6). It is commonly overlain by oolitic/pisolitic Mn-bearing micrite and laminated siltstone, ~2 m thick. Above this unit, orebed V_9 consists mainly of manganese carbonate oolites with minor pisolitic Mn oxides showing both normal and inverse grading. Above V_9 is the overlying oolitic biomicrite and laminated siltstone (~10 m in thickness, Figs. 3.4 and 3.6). Finally, orebed V_{10} shows poor quality manganese carbonate oolites/pisolites, but mostly occurs as Mn-bearing intraclastic



micrite and calcarenite with manganese, clay and Mn-bearing carbonate matrix, typically distributed discontinuously and showing scouring on the top.

3.2.5 Milike Area

The stratigraphy here is poorly known and only orebed V₃₊₂ (Fig. 3.7) has been examined in the Milike area due to poor exposures. Orebed V₃₊₂ consists of dark-red manganese carbonate (minor Mn oxide) oolite/pisolite with manganese and Mn-bearing matrix; it is laterally discontinuous, but can be correlated with occurrences in the Gake, Kata and Daaози areas.

At present, prospecting work is still being carried out in the Milike and Daaози areas. Thus, both of these areas are considered to be possible manganese-mineralized areas (Liu, et al., 1984).

3.3 Features of Orebeds

At this point in time, Gake and Baigu are the two main mine-areas. There are about 8 main and minor orebeds (V₁₋₂ to V₃₊₂, Fig. 3.1) in the Gake area, all of which are bedded or stratiform; these make up the so called "Gake (or lower) ore-bearing series" (Liu, et al., 1984). Of these, orebed V₁ is the thickest and of the best quality for commercial purposes. Orebeds V₂, V₃ and V₃₊₂ are next in quality, whereas others show non-commercial ores because of their small thicknesses and low grade. The Baigu ore-bearing section also contains about 8 main and minor orebeds (V₄ to V₁₀, Figs. 3.4, 3.5 and 3.6), which also are bedded or stratiform. These occur in sub-member T_{2f5-2}, the so called "upper ore-bearing series" and among them, orebed V₈ shows greatest thickness and highest grade. All orebeds in the deposit are located in the Dounan syncline (Fig. 2.4), but at depth the orebodies become considerably thinner or even disappear.

3.3.1 Mode of Occurrence, Morphology and Scale of Orebodies

The major features of the main commercial manganese orebeds in the Dounan area are separately summarized in Table 3.1.

3.3.2 Chemical Features of Orebeds

Chemical analyses of the Dounan main orebeds (Table 3.2) show that the Dounan ores contain high manganese and low phosphorus, sulfur and iron. The primary ores average to Mn 23.63%, Fe 1.15%, Mn/Fe = 15.01, S 0.096%, whereas secondary oxidized ores average to Mn 39.25%, Fe 3.31%, Mn/Fe = 11.94, S 0.032%. Other relationships seen in Table 3.2 and Figs. 3.8 and 3.9 include:

- Generally, the thickness of orebeds varies inversely with the manganese content (tenor), but in some places the two co-vary (Fig. 3.8).
- Manganese content (tenor) is inversely related to phosphorus content (Fig. 3.9), especially when P shows extreme values, but Mn otherwise appears to be independent.
- Commonly, manganese content (tenor) also has an inverse relationship to other components such as Fe, SiO₂, Al₂O₃, CaO and MgO (Table 3.2).
- Compared with primary oxide ores, the secondary oxidized ores contain on average nearly twice as much (x1.7) manganese, (x2.1) iron, (x1.5) SiO₂ and (x2.3) Al₂O₃. They also contain less CaO (x0.4), phosphorus (x0.7), MgO (x0.4) and sulfur (x0.3) than do primary ores.

3.3.3 Hangingwall, Footwall

1) Lithologic Proportions

In the Dounan Mn-bearing series, intraclastic or brecciated micrite (~38.9% in hangingwall rocks) commonly dominates in the hangingwall, with siltstone making up ~23%, mudstone or silty claystone ~22.1%, and Mn-bearing micrite ~16%. Footwall rocks mainly consist of (intraclastic) micrite (~42.3%) and minor Mn-bearing micrite (~13.9%), mudstone or silty claystone (~20.6%) and siltstone (~23.1%). Gangue rocks (>0.5 m in thickness) are mainly composed of Mn-bearing micrite (~48.5%), minor micrite (~21.2%), mudstones (~12.1%) and siltstones (~18.2%) (Liu et al., 1984). Thus, the (intraclastic) carbonates dominate both hangingwall and footwall of the Dounan orebeds and are minor components, terrigenous clastic rocks whereas Mn-bearing carbonates are an important constituent of gangue rocks (~50%).

Looking specifically at the lower Mn-bearing series in the Dounan sequence, the hangingwall and footwall are generally composed of (intraclastic) micrite (~50.3%), Mn-bearing micrite (~

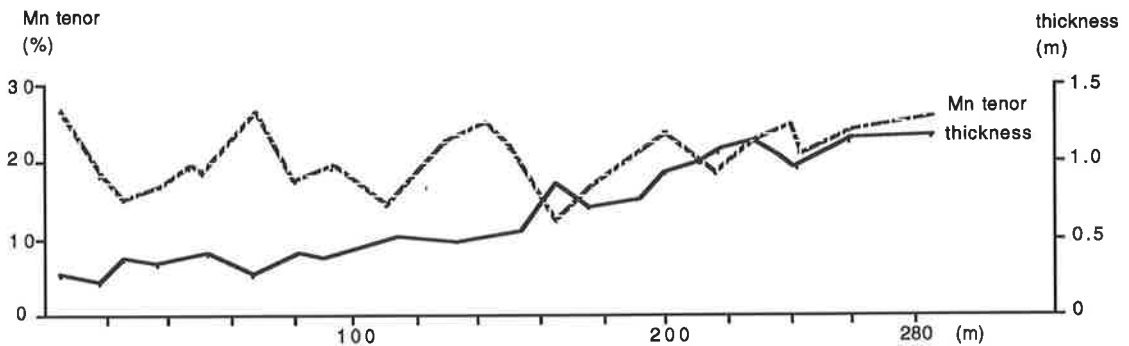
mine-area	orebody	length (m.)			thickness (m.)		shape of orebody	interval between orebeds Min.-Max. ----- mean (m.)	ore reserves (x10,000 tons)	percentage of total reserves
		strike length	dip length		Min.-Max.	mean				
			Min.-Max.	mean						
Baigu	V ₉	840	160-590	340	0.49-2.10	0.94	wavy bedded	0.43-5.32	71.437	4.3
	V ₈	2320	155-1035	541	0.53-2.98	1.26	stratiform	2.66 6.10-12.31	476.964	28.8
	V _{7b}	360	32-370	158	0.39-1.95	0.92	lenticular	8.96 0.53-3.07	14.286	0.8
	V _{7a}	2080	70-650	284	0.35-4.70	1.52	wavy bedded	1.51 5.88-14.86	115.294	9.0
	V ₆	510	66-382	184	0.32-2.12	0.89	lenticular	11.13	15.359	0.9
Gake	V ₃₊₂	460	40-302	132	0.52-1.32	0.74	lenticular	5.20-16.5	4.209	0.2
	V ₃	600	58-191	113	0.50-0.95	0.69	lenticular	10.22 1.43-4.97	0.241	0.1
	V ₂	1560	18-706	217	0.33-1.26	0.71	wavy bedded	2.66 0.60-5.00	48.762	2.8
	V ₁	2154	51-762	371	0.50-4.01	1.31	stratiform	2.27	640.997	39.6
Kata	V ₃₊₂	140	280	280	0.25-1.15	0.71	lenticular	2-7	currently prospecting	2.2
	V ₃₊₁	930	60-500	300	0.19-1.35	0.69	lenticular	5		1.3
	V ₃	620	20-240	100	0.21-1.51	0.80	lenticular	4-7 6		1.4
	V ₂	800	80-270	200	0.12-2.74	0.87	stratiform	5-8 6		2.1
	V ₁	900	70-400	250	0.21-2.76	1.04	stratiform	1-4 2		3.9
Daaozi	V ₁	700	60-150	80	0.15-0.76	0.53	wavy bedded			0.6
Milike	V ₃₊₂	900			0.15-1.92	0.93	wavy bedded			2.1

Table 3.1 Main features of Dounan Mn orebodies (modified after Liu, 1985).

Table 3.2 Chemical composition of Dounan Mn orebodies (after Liu et al., 1984).

orebed	type of ores	elements (%)									Mn Fe	P/per 1% of Mn	
		Mn	Fe	SiO ₂	Al ₂ O ₃	CaO	MgO	P	S	LOI			
V ₉	primary	20.60	1.72	14.78	3.38	20.85	2.97	0.046	0.131	24.56	11.98	0.0022	
V ₈	oxidized	34.37	2.66	17.33	4.71	11.65	1.80	0.071	0.090	16.44	12.92	0.0021	
	primary	23.51	1.48	14.64	3.24	17.51	2.84	0.060	0.127	23.26	15.89	0.0026	
V _{7b}	primary	19.25	2.01	23.20	5.21	15.16	3.12	0.050	0.060	19.85	9.85	0.0026	
V _{7a}	oxidized	30.33	6.18	32.19	9.06	0.74	0.68	0.020	0.020	7.00	4.91	0.0007	
	primary	19.75	1.55	14.38	3.23	22.53	2.85	0.050	0.083	26.12	12.74	0.0025	
V ₂	oxidized	39.74	3.27	18.69	7.09	1.43	1.03	0.041	0.019	13.08	12.15	0.0010	
	primary	16.60	1.71	14.24	3.17	25.30	3.05	0.057	0.163	28.27	9.71	0.0034	
V ₁	oxidized	44.45	2.50	15.57	5.71	2.48	0.89	0.051	0.061	11.06	17.78	0.0011	
	primary	25.33	1.31	12.54	2.75	19.57	3.06	0.057	0.099	22.62	19.34	0.0023	
whole Dounan area	oxidized	I	43.71	3.22	18.38	6.85	1.72	0.79	0.038	0.021	12.52	13.57	0.0009
		II	32.42	3.48	25.29	7.97	6.77	1.59	0.044	0.053	13.55	9.32	0.0014
		ave.	39.52	3.31	20.68	7.23	3.40	1.06	0.040	0.032	12.86	11.94	0.0010
	primary	I	31.31	1.35	10.36	2.35	14.77	2.47	0.060	0.060	20.41	23.19	0.0019
		II	26.90	1.35	12.14	2.72	19.02	2.19	0.052	0.071	21.92	19.93	0.0019
		III	22.97	1.49	12.41	2.85	19.52	3.01	0.058	0.129	24.57	15.42	0.0025
		poor	17.79	1.95	17.73	4.03	20.32	3.06	0.055	0.086	25.50	9.12	0.0031
		ave.	23.26	1.55	13.60	3.06	19.23	2.76	0.056	0.096	23.78	15.01	0.0024

(A). Orebody V₁ from mining quarry B 406, Gake area



(B). Orebody V₈ from mining quarry K1, Baigu area

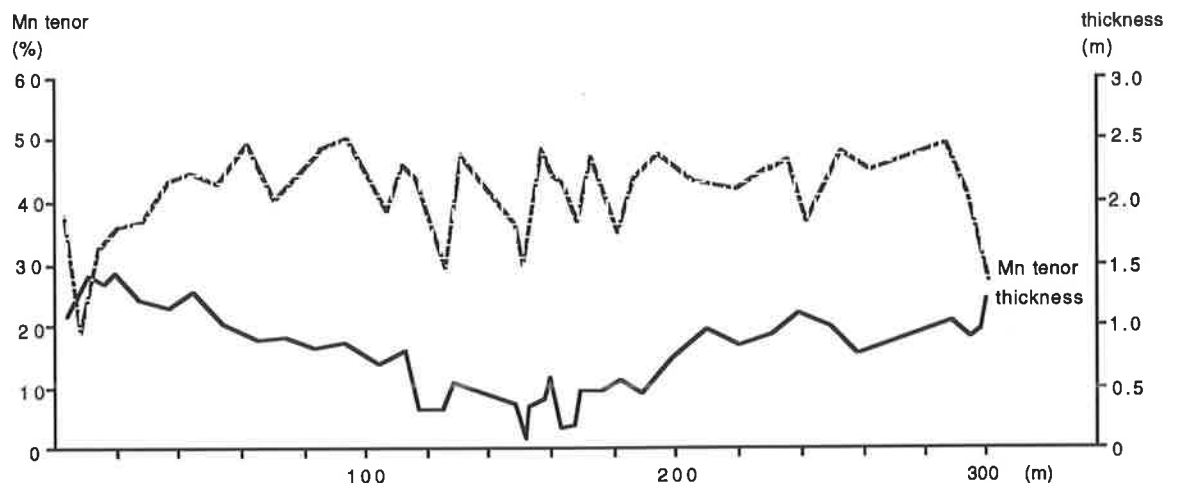
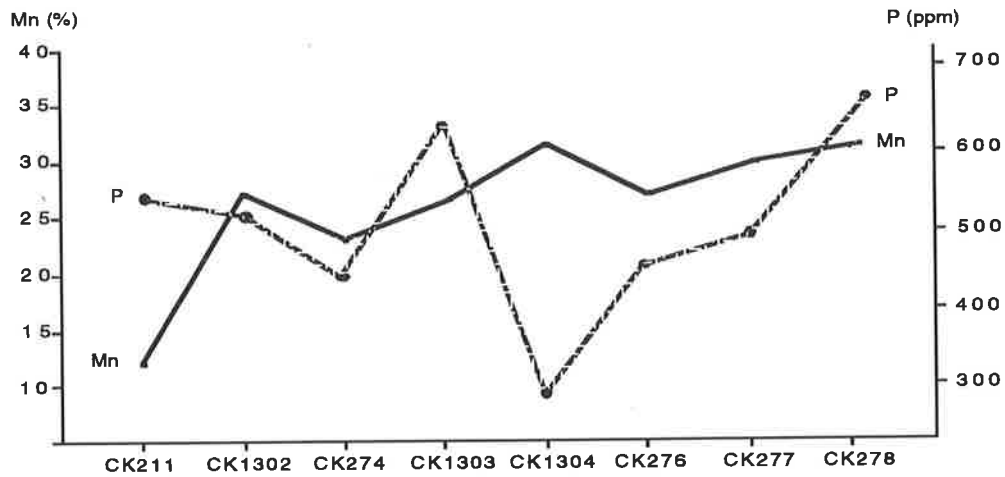


Fig. 3.8 Variation between the thickness and Mn content of Dounan orebodies (after Zhang et al., 1979).

(A). Prospecting line 13, Balgu mine-area



(B). Prospecting line 52, Gake mine-area

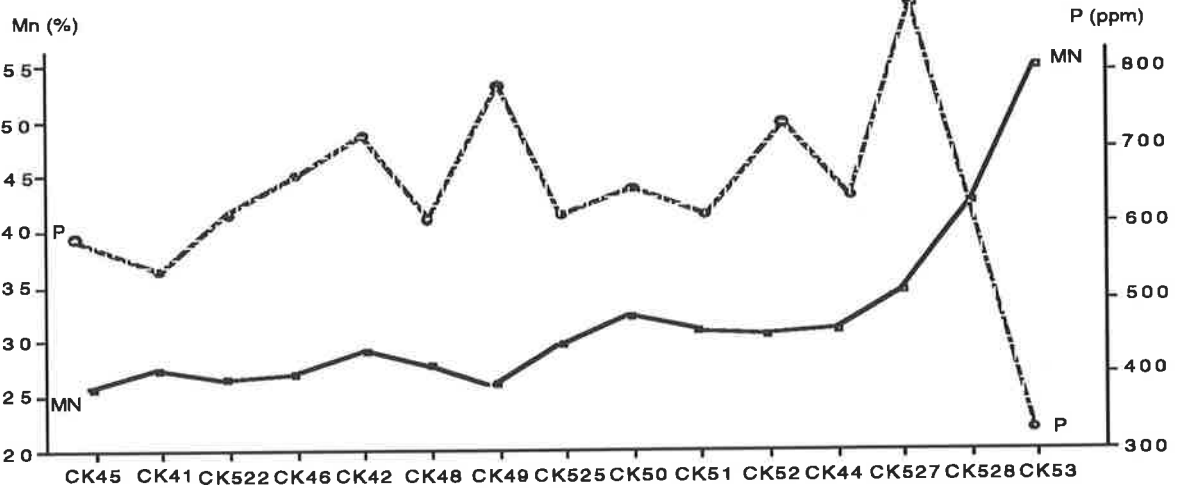


Fig. 3.9 Relationship between manganese and phosphorus (after Zhang et al., 1979).

Table 3.3 Mn contents of the hanging wall, footwall and intercalated rocks of main Mn orebodies of the Dounan deposits (after Zhang et al., 1979).

lithology	average Mn content (%)					
	hangingwall		footwall		intercalation	
siltstone/clayey siltstone	2.45		3.07		4.27	
silty claystone/mudstone	4.32		4.66		2.53	
Mn-bearing limestones	6.32		6.47		6.12	
other limestones	2.55		2.18		2.69	
lithology \ orebed	V ₁	V ₂	V ₁	V ₂	V ₁	V ₂
	1.44	2.12	1.33	3.33		3.74
siltstone/clayey siltstone	4.62	2.26	4.31	7.27		2.53
silty claystone/mudstone	6.41	6.07	7.12	5.94	5.67	6.07
Mn-bearing limestones	2.74	2.51	2.06	3.07		2.35
other limestones						

15.7%), mudstones (~21.9%) and siltstones (~4.9%); whereas those of the upper Mn-bearing series mainly consist of siltstones (~50.4%), and carbonates (~26.1%), Mn-bearing carbonates (~13.9%) and mudstones (~9.6%). This indicates a trend of increasing terrigenous clastic rocks and decreasing carbonates through the evolution of Falang Formation sedimentation. This reflects an overall regressive process during deposition of the Dounan Mn-bearing series.

2) *Manganese Distribution in Hangingwall, Foot wall and Gangue*

The main manganese minerals of the primary ores are braunite and then calciorhodochrosite, and the tenor (Mn content) of the ores is in direct proportion to the content of braunite. The mean manganese contents of hangingwall, footwall and gangue rocks of the Dounan orebeds are given in Table 3.3. These data lead to the following conclusions:

- (1) Manganese content in the hangingwall and footwall is highest in Mn-bearing (including intraclastic or brecciated) micrite, followed by mudstones and then siltstones; but siltstones contain more manganese than mudstones in the gangue rocks.
- (2) The lower manganese contents in siltstones and micrite reflect a poor supply of manganese material to the depositional basin during these stages.
- (3) The main orebeds V₁ and V₈ have different gangue rocks. Orebed V₁ is characterized by Mn-bearing micrite, whereas the gangue in orebed V₈ contains a relatively complex rock association. This reflects an increasing trend of terrigenous clastic materials and regressive sedimentation during evolution of the Dounan sequence.
- (4) Both hanging wall and footwall of orebed V₈ are mainly composed of siltstones and some carbonates, and the hanging wall of orebed V₁ mainly consists of mudstones and some carbonates. However the footwalls of both orebeds V₁ and V₈ are mainly made up of intraclastic carbonates and minor mudstones, which reflects variable sedimentation in intertidal and lagoonal facies during manganese deposition.

3.4 *Correlation of Orebeds*

The main orebeds of the Dounan deposits are in many cases divided and in some cases accompanied by a number of thinner orebeds. For example, orebed V₁ comprises three small orebeds (V₁₋₂, V₁₋₁ and V₁₊₁); and orebed V₇ is divided into two parts (V_{7a} and V_{7b}). A detailed correlation of orebeds is made to allow interpretation of regional Dounan depositional environments. The following factors influence the correlation of orebeds:

- 1) The succession of strata as indicated by the petrology of ores.
- 2) The features and relationships of key beds with orebeds in ore-containing series.
- 3) The locations of orebeds and the intervals between orebeds.
- 4) The petrology of the hanging wall and foot wall of orebeds.
- 5) The features of gangue horizons.
- 6) The texture of orebeds, the type and fabric of ores and their variations.

3.4.1 Correlation of Lower Orebeds, T2f4-1 Mn-bearing Series

The series has an average thickness of 21.29 m (Fig. 3.1). Overlying the series is key bed (T2f4-2), which consists of laminated calcareous siltstone, whereas the underlying key bed (T2f3-2) is dark-red intramicrudite/intrasparite. In this Mn-bearing series orebeds V₁ and V₂ are the principal orebodies, whereas others are small scale. All orebeds in this series can be correlated on the following bases:

- 1) Both the overlying and underlying key beds of T2f4-1 Mn-bearing series have sharp contacts, with orebeds V₃₊₂ and V₁ respectively. The ores are continuous over large areas, and thus can themselves be correlated from place to place.
- 2) Interbeds between ores maintain nearly constant thicknesses and can be correlated in all Dounan deposits, e.g. ~2.27 meters between orebeds V₁ and V₂; ~2.66 meters between orebeds V₂ and V₃; and 2.5 - 3.0 meters between orebeds V₃₊₁ and V₃₊₂.
- 3) A widespread horizon of grey pisolitic micrite, with bioclastic debris, in places brecciated, and ~1.72 m in thickness occurs ~5 meters above orebed V₃. This key bed can be correlated at least around the Gake and Kata areas.
- 4) A key bed of red, brecciated (~1 cm), quartz-rich silty intraclastic micrite occurs between orebeds V₁ and V₂, which can be correlated in all localities due to its wide development.
- 5) Commonly, the hangingwall of orebed V₃ consists of oolitic/pisolitic micrite; the hangingwall of orebed V₁ is composed of calcareous oolitic mudstone; and the surface of orebed V₂ is characterized by asymmetric ripple marks and scouring. All these features can be recognized and correlated throughout the region.

In addition to the correlation by key beds, orebeds occupy similar homotaxial positions and their textures, structures and compositions are consistent and thus correlative over large areas, as below:

- (1) orebeds V₃, V₃₊₁ and V₃₊₂ are everywhere mainly composed of manganese carbonates and minor braunite oololiths/pisoliths.
- (2) Orebed V₃₊₂, the topmost orebody in the lower Mn-bearing sequence, is made up of manganese carbonates and unsorted manganese oxides.
- (3) Generally, orebed V₃₊₁ changes laterally into Mn-bearing intraclastic micrite. It also contains small braunite oololiths (~1 mm), which easily distinguish it from orebed V₃₊₂.
- (4) Orebed V₃ consists of manganese carbonates mostly composed of calciorhodochrosite, which distinguishes it from orebeds V₁ and V₂.
- (5) Both orebeds V₁ and V₂ are main orebodies in this Mn sequence, but the ores of V₂ show mainly unsorted or banded and minor massive structures, have relatively poor quality and are thinner than in orebed V₁, which shows mainly massive and minor banded structures with traces of calciorhodochrosite. Importantly, the key bed above orebed V₁ (composed of oolitic

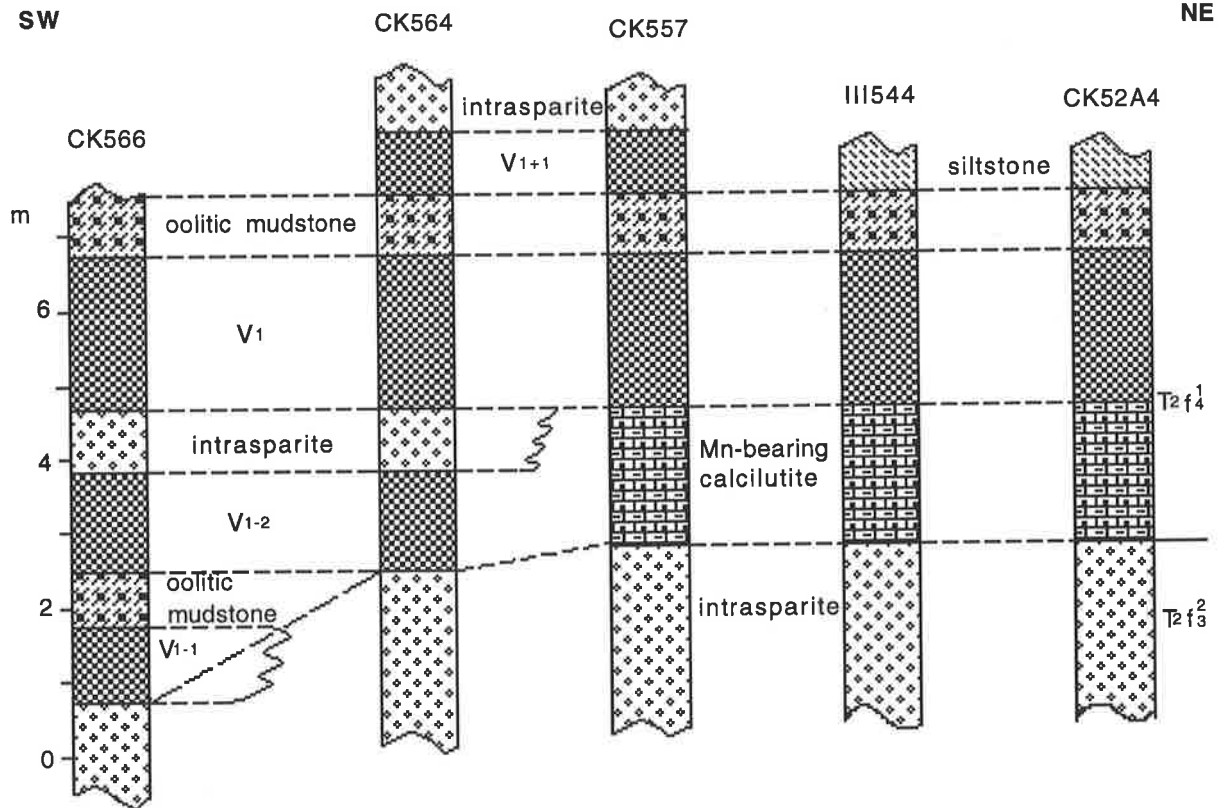


Fig. 3.10 Correlation diagram V1 ore horizons and related beds in the Gake area (lateral extent not to scale; between prospecting lines 56 and 48; see Fig. 2.4).

mudstone 0.1-0.2 m in thickness) and the key bed between orebeds V1 and V2, allow the two to be easily distinguished.

(6) It is necessary to make correlation within orebed V1 due to the association of several small orebodies, such as V1-1 and V1-2 in the southwestern Gake area. Also, the highest small orebed (V1+1) instead occurs in the northeastern area of Gake. Figure 3.10 gives the correlation of the orebed V1 group (Gake).

3.4.2 Correlation of Upper Orebeds, T2f5-2 Mn-bearing Series

This Mn-bearing sequence has an average thickness of about 50 m, and is overlain by quartz sandstone and underlain by Mn-bearing micrite or manganese carbonates (V4). There are three orebed groups in this vertical profile, i.e. upper group orebeds V9 and V8, middle group orebeds V7 and V6, and lower group orebed V5, all which can be correlated as follows:

- 1) The overlying sandstone of this Mn-bearing series is an important key bed which can be recognized and correlated over all the deposits.
- 2) The orebeds occur at regular intervals (~10 m) in the vertical profile (Fig. 3.11).
- 3) The rocks both below and above orebed V7 are mostly composed of siltstone (Fig. 3.12); whereas those of orebeds V9 and V8 generally consist of intraclastic micrite (Fig. 3.13).
- 4) In addition, the features of orebeds themselves can be correlated and distinguished from each other. Orebeds mainly consist of massive or minor banded manganese oxides; orebed V7 is

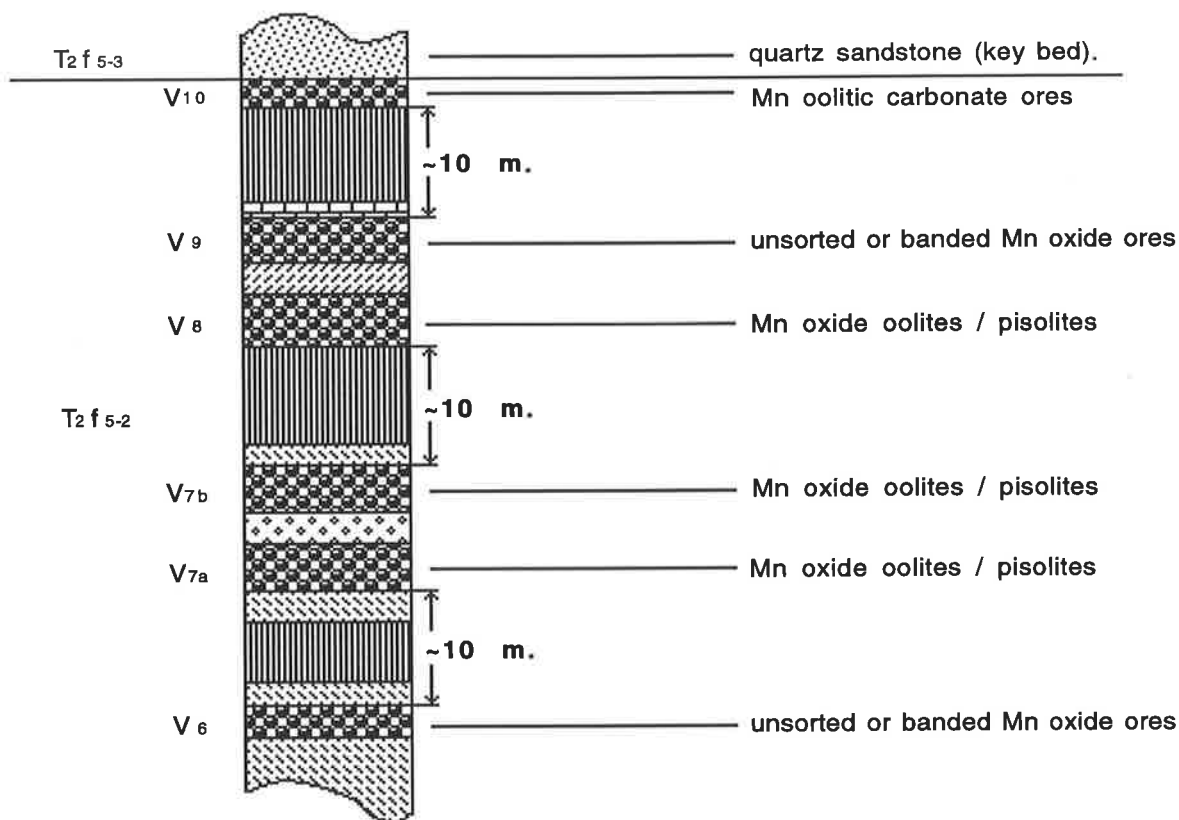


Fig. 3.11 Stratigraphic column showing regular intervals between orebeds in the vertical sequence (V₆ to V₁₀), Baigu area.

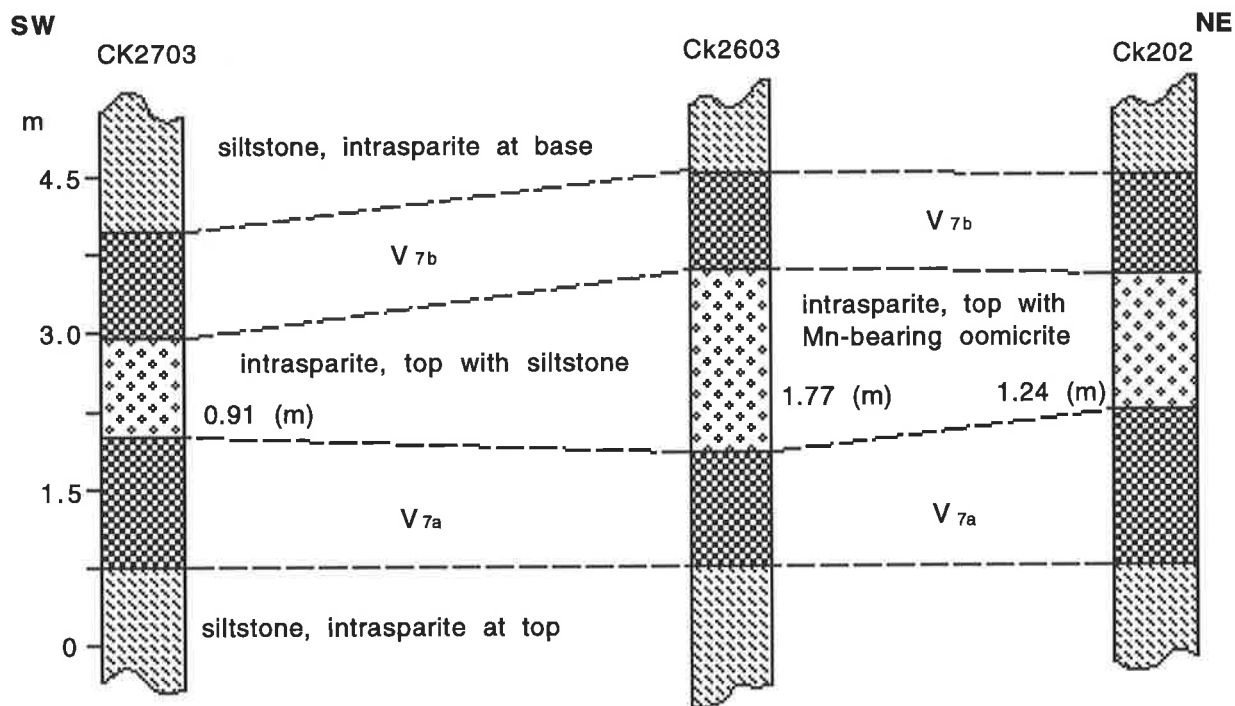


Fig. 3.12 Correlation diagram showing stratigraphic positions of V₇ Mn ore horizons in the Baigu area (lateral extent not to scale; between prospecting lines 17 and 36, see Fig. 2.4).

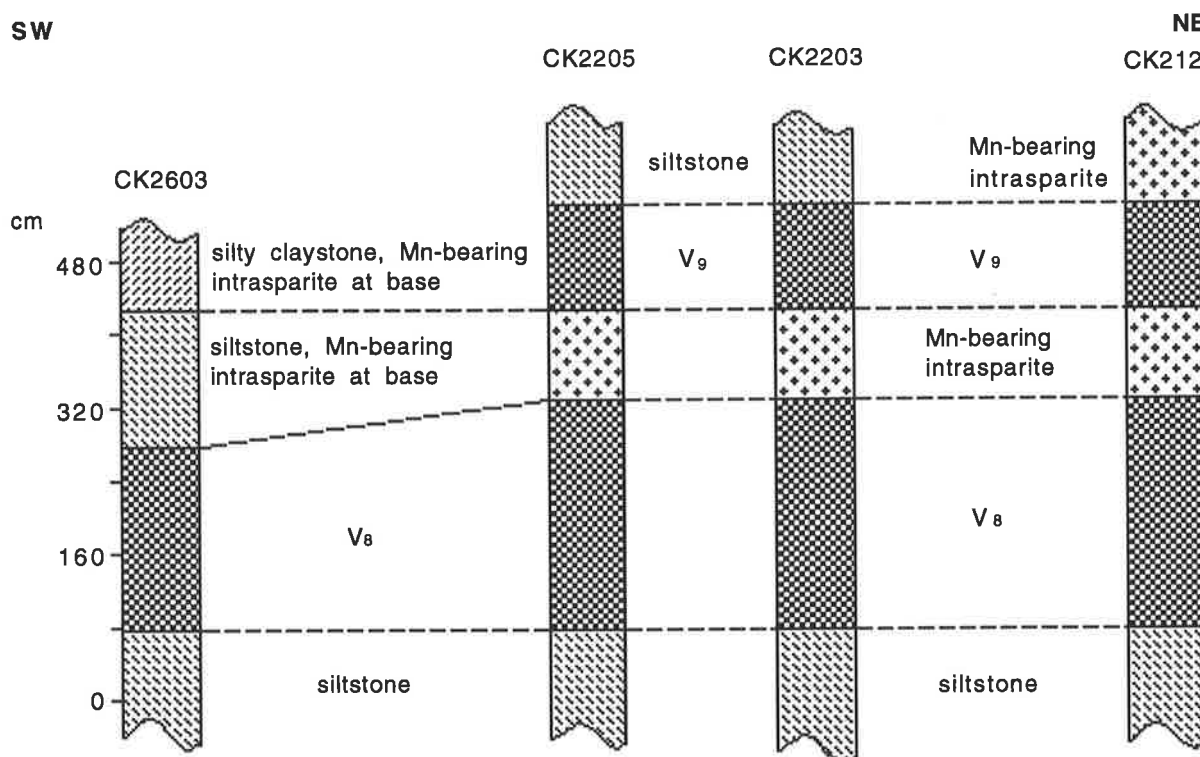


Fig. 3.13 Correlation diagram showing stratigraphic positions of V_8 & V_9 ore horizons in the Baigu area (lateral extent not to scale; between prospecting lines 17 and 36, see Fig. 2.4).

mainly composed of banded and unsorted manganese oxides and orebed V_6 of manganese carbonates and minor unsorted manganese oxides. These units can be recognized and correlated throughout the deposits.

5) Orebed V_9 is mostly composed of unsorted manganese ores (calciorhodochrosite and minor braunite oolites), but is of poor quality and laterally discontinuous (Fig. 3.13). Orebed V_8 shows massive and banded manganese oxide oolites / pisolites mainly composed of braunite, is of good quality, has ripple marks on the surface, and is continuous over large areas (Fig. 3.13). Orebed V_7 consists of two orebodies, V_{7a} and V_{7b} , with a thin brecciated micrite intercalation between them (Fig. 3.12). Orebed V_6 mainly consists of poor quality, banded and unsorted manganese oolites (braunite and calciorhodochrosite), while orebed V_5 everywhere shows non-commercial ores.

3.5 Paleotectonics and Sedimentation of Orebeds

3.5.1 Sedimentary Center Migration of Manganese Orebeds

Significantly, the spatial distribution of orebeds in the Dounan area is characterized by an offlapping from the southwest to the northeast (Fig. 3.14). For example V_{1-1} and the intrasparite above V_{1-2} are formed only in the SW (Fig. 3.10), while V_9 is limited to the NE (Fig. 3.14). This seems to reflect that the depocenters of the manganese orebeds migrated from the southwest to the northeast during Falang sedimentation. The manganese metallometric percentage

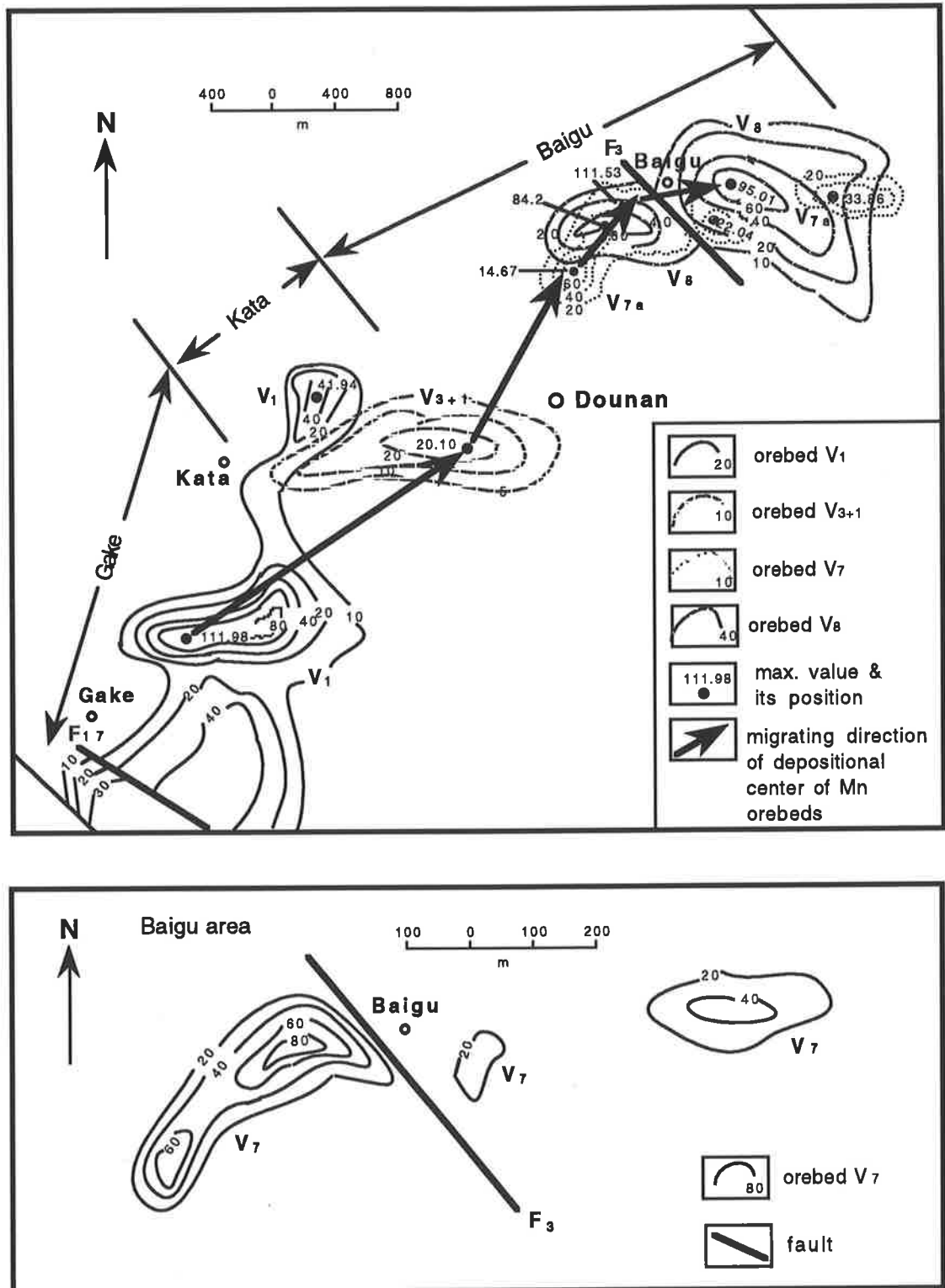


Fig. 3.14 Mn metallometric percentage hypsometric curves (Mn tenor % x thickness of orebeds) of Dounan area (modified after Zhang et al., 1979).

hypsothetic curves (i.e. Mn tenor % x thickness of orebed; Zhang et al., 1979) of Dounan manganese deposits show that each orebed has a depositional center (the maximum value, Fig. 3.14). For instance, the depositional center of orebed V₁ is located at Gake (the maximum value is 111.98); for orebed V₃₊₁, the manganese depositional center is located in the Kata area; and V₇ was concentrated in western Baigu area. Finally, the centers for orebeds V₈ (and V₉, Fig. 3.14) migrated to the eastern Baigu area.

3.5.2 Relationship between Paleotectonics and Mineralization

As stated above, sedimentation of the Dounan sequence during marine regression is characterized by the offlapping distribution of orebeds towards the NE. The Gake lower orebeds (e.g. V₁) can be followed regionally to the southwestern Yanzijiao area (about 20 km SW the Gake area), but not into the northeastern Baigu area. In contrast the upper orebeds (e.g. V₇ and V₈) mainly occurring at Baigu, spread northeastwardly to the northeastern Laowu area (about 18 km from Baigu area), but not into the southwestern Kata area (Figs. 2.21 and 2.22). The interpretation that is the Yanzijiao and Gake areas probably were located on tidal flat environments which was an advantage for the formation of manganese oolites and pisolites, whereas at V₁ - V₃₊₁ time, the northeastern part of the Dounan basin was just located on the shoreface, which was a disadvantage for the deposition of manganese oolites and pisolites. Later, when the upper orebeds (e.g. V₇ and V₈) were deposited, the environments favourable for formation of manganese oolites and pisolites shifted to the Baigu and Laowu areas. This was due either to uplift of the southwestern part of the Dounan basin, or to marine regression towards the northeast, or to a combination of both.

Importantly, as described in Chapter 1, structural movements during the Triassic had both regional and local effects. Tilting of the Dounan syncline towards the northeast took place during the initial period of Falang deposition. After the deposition of orebed V₁, the southwestern part of the Dounan basin started to rise, which led to later migration of the manganese depositional centers towards the northeast and the offlapping distribution of Dounan manganese orebeds. In addition, the faults themselves to some extent controlled the distribution of sedimentary environments for manganese accumulation. For example orebed V₇, distributed on both sides of fault F₃ in the Baigu area, is separated into thick, continuous and high quality ore to the west of the fault and thin, discontinuous and poor quality ore to the east (Fig. 3.14). It is thus likely that vertical movements on fault F₃ led to changing sedimentary environments during the deposition of orebed V₇.

3.6 Discussion

Detailed information on the Dounan orebeds in the five mine-areas can be used to generalize about some primary and secondary features of the orebodies. The observed gaps in the distribution of ore between neighboring mine-areas probably are indicative of local uplifts and sub-basin subsidence events or to irregular basin filling during sedimentation. Manganese layers in some cases also tend to be cyclic and occur as offlapping tongues as seen in the distribution of orebeds V₁₋₂, V₁₋₁, V₁, and V₁₊₁ in the Gake area (Figs. 3.10 and 3.14), orebeds V₂, V₃, and V₃₊₁ in the Kata area (Fig. 3.14), as well as orebeds V_{7a}, V_{7b}, V₈, and V₉ in the Baigu area (Figs. 3.12, 3.13 and 3.14). Such variations in orebed distribution reflect the shift of preferred sites for sedimentation from SW to NE, indicating a general regressive process.

The lack of large variations in the chemistry of the different manganese orebeds suggests similar geochemical environments during accumulation. The quality of the primary manganese ores relates directly to the amount of manganese oxides (braunite) present. However, the relatively thin high-grade orebeds probably formed in weakly oxidizing environments, thus implying rapidly changing environmental conditions. Importantly, the low phosphorus and sulfur contents of the manganese orebeds suggest that the ores mainly formed in brackish environments, removed from significant sources of phosphorus and sulfur. Increasing Mn and SiO₂ and decreasing CaO and MgO in secondary oxidized ores strongly support a supergene process.

Other important genetic information for the development of Dounan orebeds is found when the ores and their host materials are examined. The primary ores are always associated with mixed terrigenous clastic-intraclastic carbonate sediments, i.e., mudstones intercalated with siltstones and intraclastic micrite in the lower series (T_{2f4-1}); and siltstones intercalated with intraclastic micrite and mudstones in the upper ore-bearing series (T_{2f5-2}). Thus, changing nearshore conditions were most favourable for manganese deposition.

PART III

ROCKS AND ORES

Chapter 4 Petrology and Mineralogy

4.1 Introduction

The previous chapters presented the stratigraphy of those part of the deposits selected for detailed study. Below, the materials of Dounan profiles are examined to provide further descriptive and analytical information to assist in the interpretation of mode of origin of the deposits. Therefore, emphasis is concentrated on primary and diagenetic features related to the field observations. Earlier detailed work focused on supergene products which are now nearly mined out (Zhang et al., 1979). Gangue minerals and some superficial ores associated with the deposits are not incorporated into the geological profiles both for technical reasons and because they occur in very small quantities. Descriptions of supergene products are briefly outlined in the hand-specimen descriptions below. Handspecimen and microscopic descriptions illustrate the general composition of ores and rocks; the important rock types are discussed first.

Although some ores and rocks discussed below are of minor importance in quantity, many of them are important diagenetic products which might otherwise be excluded from consideration because of their relative scarcity. As mentioned before, oolitic and pisolitic Mn ores predominate over all other ore types at Dounan, and mudstone, siltstone and limestone are the main rocks associated with the deposits. The ore phases of Dounan deposits can be divided into primary/diagenetic and supergene products: the first includes primary Mn oxide and carbonate as well as mixed phases, and represents about 95% of the total reserves of Dounan ores; the second type represents less than 5%. Though oolites/pisolites can be divided into oxide and carbonate ores, transitional (or mixed) products between the two types commonly occur, and the structure of ore materials is important in the genetic interpretation of the ores. Fabric, texture, and structure of Dounan ores and rocks are examined in this chapter. The geographic and stratigraphic distribution and variation of the ore phases in the Dounan area are significant for interpretation of the deposits and these are also included in this chapter. Importantly, the results of several types of

microanalysis (e.g. scanning electron microscope, cathodoluminescence and scanning X-ray diagrams) are included here and utilized in distinguishing the primary from diagenetic products. A summary of the examined ores and rocks is presented in Table 4.1.

The minerals from these ores and rocks are examined in detail to provide further and important descriptive and analytical information for genetic interpretations, especially for the main ore minerals - braunite and calciorhodochrosite. The X-ray diffraction (XRD) study that follows the descriptive part of this chapter examines most of the ores and rocks, with the exception of some rocks that are of minor importance for the development of the deposits (e.g. supergene products). With this technique, about 50 samples were scanned for their main components, and minor peaks in the spectra were also checked for trace minerals. A detailed description of the analytical techniques is provided in Appendix I and a listing of the sample specifications (ore / rock types) is given in Appendix IV, Table IV.1.

4.2 Description of Samples

4.2.1 Primary Manganese Ores

4.2.1.1 Manganese Oxide Ores

(1) Mn Oxide Oolite / Pisolite

Handspecimen

(Plate 4.1, Fig. 1a)

Mn oxide oolite/pisolite occurs as bedded units throughout the deposits. Several cycles of normal and reverse gradings can be recognized in various locations and small to medium scale cross-bedding can also be identified. Such ores are concentrated in orebeds V₁, V₂, V₇ and V₈ or as a minor component in other orebeds.

The ore mineralogy is relatively simple with the main mineral being braunite and minor calciorhodochrosite, Mn-calcite and calcite associated with braunite. On paragenesis, minerals which may be syngenetic include traces of manganite (1-3%) and hausmannite (~1%), both concentrated in the matrix. Generally, the ores are black to dark-brown in colour and are well cemented. The grains are spherical to ovoid, sometimes flattened, and their sizes vary between <1 mm and 15 mm. Braunite ooliths/pisoliths are generally cemented by carbonate minerals such as calciorhodochrosite, Mn-calcite or Mn-bearing calcite or calcite. The structure of the orebeds is generally massive. Sorting varies from good to poor, and occasionally the oolite/pisolite size range is bimodal.

Microscopy

(Plate 4.1, Figs. 1b and 1c)

As above, oolites and pisolites are discussed together, because they are only distinguished by an artificial size boundary. Internally, the grains are laminated concentrically and individual laminae, often less than 10 μ thick, consist of crystallites that are oriented tangentially and/or radially.

With the exception of some ores in which a number of poorly crystallized manganese oxides occur, most ores show a dominance of braunite, with calciorhodochrosite and/or Mn-calcite or Mn-bearing calcite and/or calcite alternating as laminae in ooliths and pisoliths. Generally, the thickness of the laminae seems to increase in outer parts of the grains. Occasionally, abraded and truncated features (micro-unconformities) indicate erosional processes during the growth of the grains. Rarely, silt-sized detrital materials are accommodated between the manganiferous laminae.

Although ooliths and pisoliths generally do not exhibit nuclei, they occasionally contain centrally-located detrital materials. Such nuclei consist of poorly rounded to angular quartz, calcite, albite, biofragments or organic remains, or argillaceous materials. The contours of these materials tend to be leveled out by a few laminae so that the overall morphology of nuclei is mostly not reflected in the shape of the ooliths and pisoliths.

Within ooliths and pisoliths, the matrix between crystallites often consists of extremely fine-grained manganese oxides ($\ll 5 \mu$) which are well cemented, and with diffuse calciorhodochrosite and Mn-calcite or calcite impregnations and traces of manganite. Generally, micritic calcite and calciorhodochrosite are the main matrix components. Locally, silt-sized quartz can become an important matrix component. The angular shape of these grains indicates a short distance of transport, and they are also poorly sorted (size ranging between $\sim 50 \mu$ and 500μ).

(2) Mn Oxide Deformed Oolite / Pisolite

Handspecimen

(Plate 4.1 Fig. 2a)

Deformed oolite/pisolite of Mn oxides occur as stratiform or wavy bed units throughout the deposits, alone or together with Mn oxide oolite/pisolite to a greater or lesser extent. Characteristic is the morphologically distinct deformation of the ooliths/pisoliths. Deformation is of three types: broken fragments of ooliths/pisoliths; contorted laminae within ooliths/pisoliths; and those which appear to have grown irregularly (Plate 4.1, Fig. 1b, right of center). Individual grains are ovoid to lens-shaped, in some cases flattened, and occasionally closely fitted polygonal grains are found. In many cases grains within a layer display a preferred orientation, suggesting soft-compaction during sedimentation or possibly a diagenetic process. The sorting is poor to good, depending on the precursor (undeformed Mn oxide oolite/pisolite). Stratigraphically, Mn oxide deformed oolite/pisolite is mostly developed in the lower parts of Mn-bearing series in vertical geological profile. Several cycles of normal and inverse grading can be distinguished in many places. Small to medium scale cross-bedding and low angle cross-bedding are also seen.

As with Mn oxide oolites/pisolites, braunite dominates this ore. The crystallinity of the matrix visibly increases with increased size of matrix materials, as does calciorhodochrosite or Mn-calcite content. Primary grains are in some cases replaced by manganiferous materials. The

ores are mostly black to dark-brown, are very hard and dense, and occur in massive or banded structures. The description above already seems to suggest that the origin of this ore type is diagenetic and that undeformed units are overprinted. As a possible further step in diagenesis, the cementation occasionally is superimposed on all primary sedimentary features and the ore grades into compact massive Mn oxides, which will be described below.

Microscopy

(Plate 4.1, Fig. 2b)

The relative simple mineralogy of this ore results in soft materials that were easily deformed. In extreme cases the oolites and pisolites show sutured contacts and compressed grains have angular shapes; less frequently they are fractured. Thus, the appearance of this ore indicates that the precipitating material was very soft during and after at least shortly after deposition. Oolitic and pisolitic structures and textures were examined in the previous section; therefore, emphasis here is on the manganiferous matrix. The dominant mineral of the matrix is cryptocrystalline, and its slightly dark-grey color (brownish tint) helps to distinguish it from the black or dark-brown of the braunite in the adjacent oolites/pisolites. Often the extremely fine grained ($< 5 \mu$), cryptocrystalline matrix tends to crystallize into larger idiomorphous crystals (200 μ or more). In ores influenced by overburden pressure during sedimentary and diagenetic processes, oolites/pisolites become elongate and matrix cementation proceeded parallel to bedding. This leads to ore with banded or massive structure, which often contains relic outlines of primary laminae.

(3) *Compact Massive Mn Oxide Oolite / Pisolite*

Handspecimen

(Plate 4.1, Fig. 3a)

Compact massive Mn oxide oolite/pisolite ores (very well cemented) are observed throughout the Gake area and also around Baigu, overprinting the earlier Mn oxide (and/or deformed) oolites/pisolites to a greater or lesser extent. These ores, together with other Mn oxides, mostly occur in the main orebeds such as V₁, V₂, V₇ and V₈, and form laterally continuous but wavy-bedded bodies and rare lenses. The ore consists predominantly of braunite with trace amounts of calciorhodochrosite, Mn-calcite and manganite, and sometimes overprinted or replaced Mn oxide (or deformed) oolites/pisolites. Massive Mn oxide ore appears to be the final stage in the development of Mn oxide ores during sedimentary and diagenetic processes, but rarely it also appears to present a primary sedimentary product. The ore is black, very hard and dense. Most structures and textures observed in this ore, such as fine lamination consisting of oolites and pisolites, or small/medium scale cross-bedding of the same material, are identical to those found in unaffected ore. Individual grains are spherical to ovoid, occasionally elongated and flattened; sorting and grading also depend upon the precursor. Grainsize varies between < 1 mm and about 8 mm. Commonly, the shape or outline of oolites/pisolites can be seen, but in some cases relicts are totally absent. Generally, the ore shows massive structure and belongs to grade I (rich ore), however it commonly contains minor thin layers of Mn carbonates, which define banded structure.

Plate 4.1 Ores and associated rocks.

Fig. 1a: Inversely graded Mn oxide oolite/pisolite from Gake area; sample 958-38; dark colour: braunite; dark red colour: calciorhodochrosite. Top is to left; pen for scale.

Fig. 1b: Mn oxide ooliths/pisoliths cemented by Mn-calcite with minor slightly deformed grains; white colour: braunite; brown concentric laminae: calciorhodochrosite; Gake area; sample 958-39; polished section; parallel polarizers; the bar equals 200 μ .

Fig. 1c: Mn oxide ooliths/pisoliths cemented by calcite and Mn-calcite with strongly deformed and broken grains; other features similar to the sample in Figure 1b; sample 958-41; the bar equals 100 μ .

Fig. 2a: Banded/deformed Mn oxide oolite/pisolite from Gake area; sample 958-61; black colour: braunite; darkred colour: calciorhodochrosite; pen for scale.

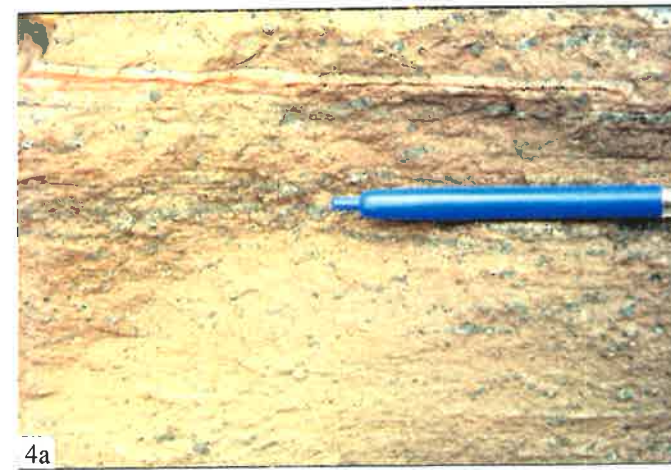
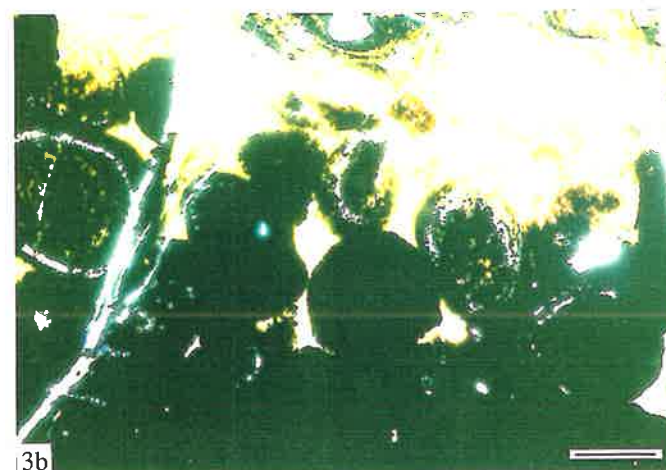
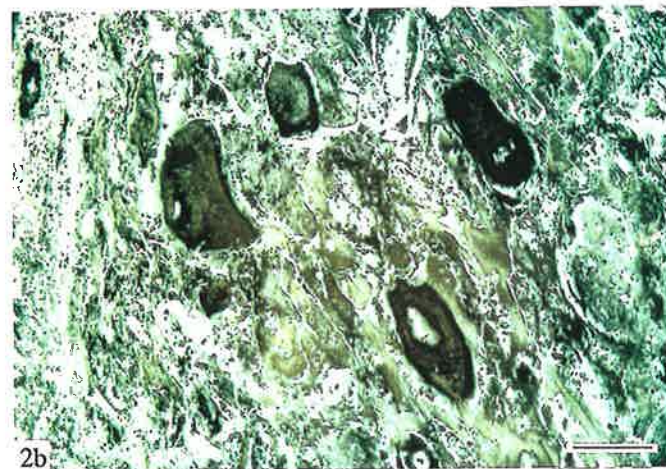
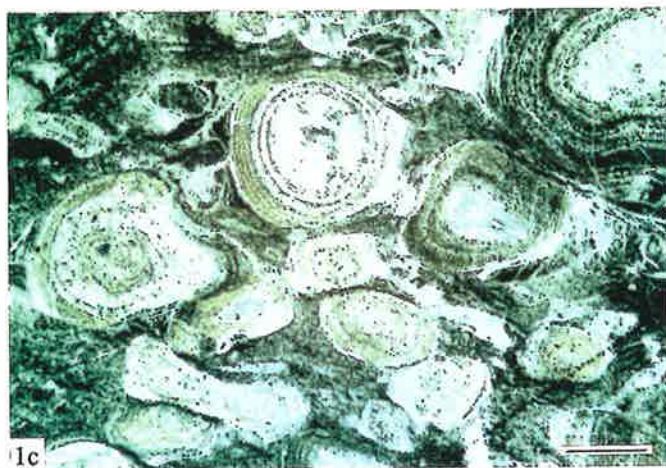
Fig. 2b: Mn oxide deformed ooliths/pisoliths with strongly deformed (elongate) grains; light colour: braunite; dark colour: Mn-calcite; Gake area; sample 958-43; polished section; parallel polarizers; the bar equals 50 μ .

Fig. 3a: Compact massive Mn oxide oolite/pisolite from Gake area (underground mine); sample 958-46. Note calcite vein (yellow); pen for scale.

Fig. 3b: Compact massive Mn ooliths/pisoliths largely lacking concentric laminae, but commonly showing relic outlines of ooliths/pisoliths; black colour: braunite; light colour: calcite; note that cross-cutting carbonate enhances pisolith lamination (left center). Gake area; sample 958-48; thin section; parallel polarizers; the bar equals 100 μ .

Fig. 4a: Mn carbonate (calciorhodochrosite) oolite/pisolite from Kata area; sample 958-74; black colour: braunite; dark red : calciorhodochrosite; pen for scale.

Plate 4.1



*Microscopy**(Plate 4.1, Fig. 3b)*

Most oololiths and pisoliths are composed of hypautomorphic or automorphic granular braunite and minor carbonate detrital materials, and this is common in deformed oololiths and pisoliths as well. Though this ore appears to be diagenetic, it nonetheless exhibits all primary features such as grain size, shape, laminae and cross-bedding, recognizable not only in hand specimens but also in thin or polished sections; overprinting by manganese cementation of the materials is pervasive. As an example of such successive overprinting, a pisolith is shown which is cross-cut by carbonate replacement products. This grain contains very dense and highly reflective Mn oxides, and although a fine lamination is apparent, it is weak and without much contrast. The replacing material, on the other hand, enhances the visibility of one lamina of the primary manganese grain.

Rarely, the matrix seems to enhance textural deformation structures, such as those of closely fitted polygonal grains. Pressure solution at contacts between grains led to partial dissolution of oololiths and pisoliths and to successive cementation in adjoining open pore spaces. Thus, grains appear to fit closely with their neighbours. The amount of detrital material such as silt-sized quartz varies from sample to sample ($\leq 10\%$). However, gangues generally do not play a large role in cemented manganese materials. This ore type is strongly dominated by manganese oxides (braunite), both in oololiths/pisoliths and in matrix.

*4.2.1.2 Mn Carbonate Ores**(1) Calciorhodochrosite Oolite / Pisolite**Handspecimen**(Plate 4.1, Fig. 4a)*

Calciorhodochrosite oolite/pisolite is found in all parts of the deposits, and is relatively more abundant in ores in the northeast (Baigu area) than in the southwest (Gake area). In places it occurs at various stratigraphic levels, but most frequently is developed as stratiform units of the upper ore-bearing series. It occurs interbedded with Mn oxide ores in vertical profiles, and exhibits dark grey or dark brown colours depending on the amount of calciorhodochrosite. The ore mineralogy is relatively simple with calciorhodochrosite being the dominant Mn carbonate phase, with minor Mn-calcite, Mn-bearing calcite, and gangue minerals calcite, quartz, dolomite and albite. Several cycles of normal and inverse grading are found at various locations, and small to medium scale cross-bedding and laminations are also recognized. Individual grains are ovoid to elongated and flattened, in some cases spherical. Grain size varies between 0.4 - 8 mm. Sorting is poor to good, and bimodal units were not observed. Normally, the ores are very hard and dense, show massive or banded structures, and are mostly of low grade. It seems likely that the origin of this ore type is primary but diagenetic overprinting is common.

*Microscopy**(Plate 4.2, Figs. 4b and 4c)*

The colour of oolite and pisolite units is grey or light brown. Internally, the grains are laminated concentrically; individual laminae are mostly less than 10 μ thick. The thickness of laminae increases in the outer part of many grains. However, some ooliths and pisoliths also show pseudo-oolitic/pisolitic textures (spheruliths lacking apparent concentric lamination). Micrite and silt-size detrital materials are commonly accommodated between the manganiferous laminae. Ooliths and pisoliths generally do not show nuclei in this ore type. A few such nuclei consist of calcite, dolomite, poorly rounded to angular quartz grains or biofragments.

The matrix of ooliths/pisoliths in many cases is composed of extremely fine grained manganese carbonates ($\ll 5 \mu$) of very hard cementation, Mn-bearing micrite, clay, calcite, and traces of quartz, albite and dolomite. The matrix enhances textural deformation structures, such as those of closely fitted grains showing preferred orientation. The amount of gangue materials such as calcite, quartz, dolomite or albite varies from 20% - 40%. Thus, gangues play an important role in this ore which is dominated by Mn carbonates, both in oolith/pisolith and in the matrix.

*(2) Mn-calcite Oolite / Pisolite**Handspecimen**(Plate 4.2, Fig. 5a)*

Mn-calcite (including Mn-bearing calcite) oolites/pisolites occur in laterally continuous beds over large areas throughout the deposits. In most cases, it occurs with calciorhodochrosite oolite/pisolite, and exists at various stratigraphic levels. Its handspecimen features are extremely similar to those of calciorhodochrosite oolite/pisolite, but this type contains less manganese. Mineralogically, Mn-calcite or Mn-bearing calcite dominates this ore and gangue minerals are extremely similar to those of calciorhodochrosite oolite/pisolite. The ores are mostly dark-grey or dark-brown. Individual grains are ovoid to elongated or flattened, and closely fitted polygonal grains are common, suggesting compaction during sedimentation and/or diagenesis. Grainsize varies between 0.4 - 5.0 mm and sorting is poor to good. The ores are hard and dense and show massive or banded structures.

*Microscopy**(Plate 4.2, Figs. 5b and 5c)*

Although ooliths and pisoliths dominate the ore, the amount of matrix in this ores is more than that in the calciorhodochrosite oolite/pisolite. Oolitic and pisolitic textures are very similar to those of the latter, but they differ compositionally. The dominant minerals of the matrix are cryptocrystalline manganiferous carbonates (micrite or calcilutite). The light-grey color (or brownish tint) helps to distinguish matrix from the light grey Mn-calcite in the adjacent ooliths and pisoliths. The extremely fine-grained cryptocrystalline matrix locally tends to crystallize into larger idiomorphic crystals (200 μ or more).

Though structures in the Mn-calcite oolite/pisolite appear to be primary (grainsize, shape, laminae, bedding, recognizable in both handspecimens and polished/thin sections), this rock type also exhibits some diagenetic structures and textures that irregularly overprint primary materials. Oololiths and pisoliths in some cases are cross-cut by recrystallized or introduced products.

4.2.1.3 Transitional / Mixed Type (Unsorted Mn Oxide) Ores

Handspecimen

(Plate 4.2, Fig.6a)

Unsorted Mn oxide ore is a mixture of the same Mn oxides and Mn carbonates described in previous sections. This ore is found throughout the deposits, with greatest abundances in the Kata and Baigu areas. It occurs at various stratigraphic levels in the Mn-bearing series, and frequently it is developed as wavy bedded units between Mn oxide and Mn carbonate phases. Generally, this ore is laterally continuous over large area, and is composed of Mn oxide oololiths/pisoliths and Mn carbonate matrix, and often with normal and inverse grading sequences. Small to medium scale cross-bedding can be recognized in some locations.

The ore mineralogy is relatively complex in most cases, with braunite being the dominant oxide phase and calciorhodochrosite dominating the matrix. Minor and trace other minerals such as Mn-calcite, Mn-bearing calcite, calcite and quartz silts, are also identified. Although the textures and structures are similar to those of other oololiths/pisolites, the difference is that black oololiths and pisoliths mainly composed of braunite are heterogeneously distributed in dark-brown Mn carbonate matrix, which mainly consists of cryptocrystalline calciorhodochrosite, Mn-calcite and calcite. These features constitute a unique unsorted structure (so-called unsorted ore). The relative proportions of these oololiths/pisoliths and matrix materials resulted in ores that are black, dark-brown or a mixture of both colors. The grains are spherical to ovoid, sometimes flattened or irregularly ovoid, and their sizes vary (« 1 mm and 20 mm). Locally, the sorting is poor.

Microscopy

(Plate 4.2, Figs. 6b and 6c)

The oolitic and pisolitic structures and textures are very similar to those of Mn oxide oolite/pisolite, the only difference being that the oololiths and pisoliths of unsorted ores are larger and contain multiple nuclei, some of which consist of dark-brown Mn carbonate materials. The dominant mineral of the matrix is cryptocrystalline calciorhodochrosite or Mn-calcite which locally replaces oololiths and pisoliths. Commonly, the concentrically laminated grains consist of alternating laminae of braunite and calciorhodochrosite. The black color of braunite easily helps to distinguish it from the brown or dark-brown color of calciorhodochrosite in the oololiths and pisoliths. Often, cryptocrystalline or extremely fine-grained matrix tends to crystallize into larger idiomorphic crystals.

Plate 4.2 Ores and associated rocks.

Fig. 4b: Mn carbonate (calciorhodochrosite) ooliths/pisoliths cemented by calcite (light colour); dark colour: calciorhodochrosite; black spots: braunite; with secondary calcite vein crossing both ooliths/pisoliths and matrix; Baigu area; sample 958-142; thin section; parallel polarizers; the bar equals 200 μ .

Fig. 4c: Mn carbonate (calciorhodochrosite) ooliths/pisoliths cemented by calciorhodochrosite and Mn-calcite with minor broken grains and replacement texture; note grains showing 'secondary' Mn-rich margins (brown); Baigu area; sample 958-144; thin section; parallel polarizers; the bar equals 200 μ .

Fig. 5a: Mn carbonate (Mn-calcite) oolite/pisolite from Gake area; sample 958-45; black: braunite; white: calcite; darkred colour: Mn-calcite; hammer for scale.

Fig. 5b: Mn carbonate (Mn-calcite) ooliths/pisoliths cemented by braunite (white) and Mn-bearing calcite; the grains are characterized by both good and poor concentric laminae; Gake area; sample 958-45; polished section; parallel polarizers; the bar equals 100 μ .

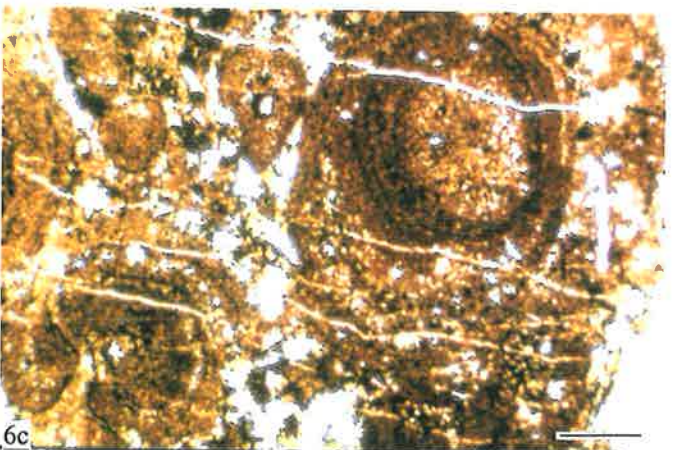
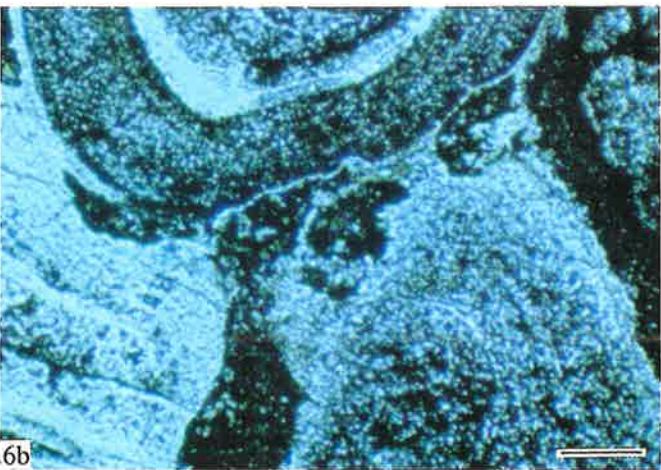
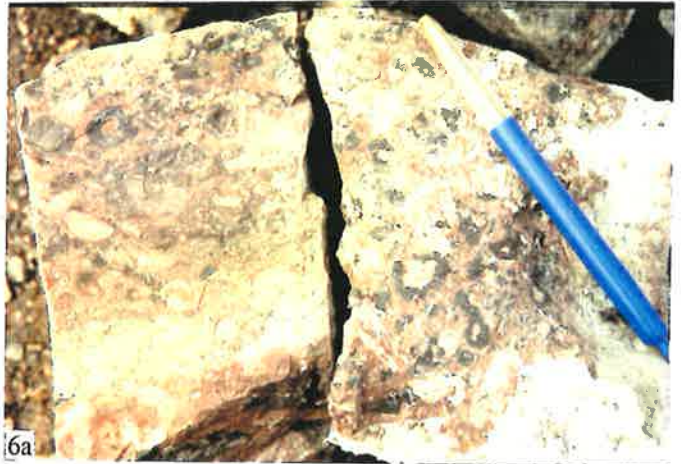
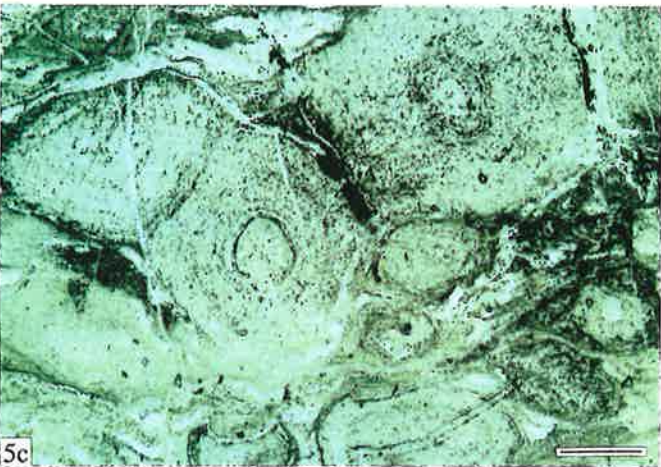
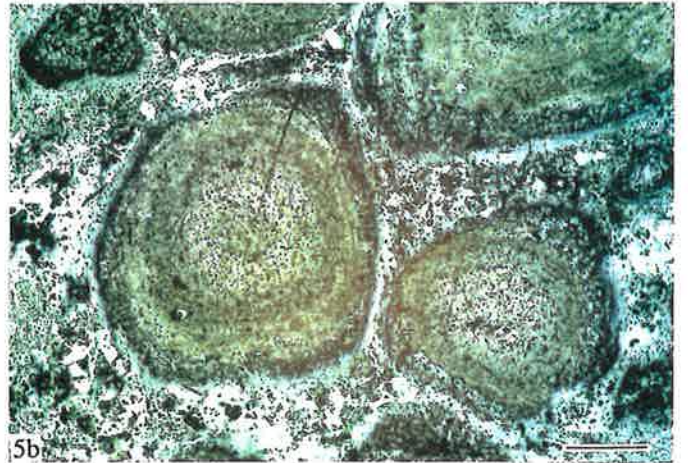
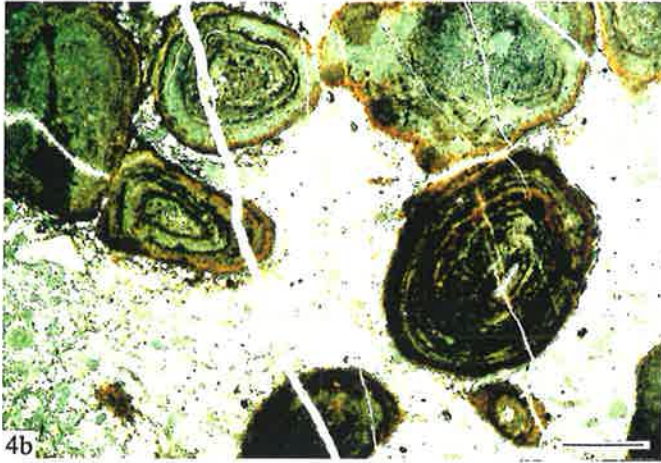
Fig. 5c: Mn carbonate (Mn-calcite) ooliths/pisoliths cemented by calcite (dark colour) and Mn-calcite, slightly deformed grains; Baigu area; sample 958-236; polished section; parallel polarizers; the bar equals 100 μ .

Fig. 6a: Unsorted Mn oxide ooliths/pisoliths cemented by calciorhodochrosite and minor Mn-calcite; black: braunite; darkred: calciorhodochrosite and minor Mn-calcite; the large pisoliths depict some angular calciorhodochrosite, Mn-calcite, and calcite as nuclei; the matrix also contains these minerals and minor amount of quartz silt as well as biofragments; Baigu area; sample 958-204; pen for scale.

Fig. 6b: Unsorted Mn oxide ooliths/pisoliths cemented by calcite (black); the pisoliths are composed of braunite (light colour) and calciorhodochrosite or calcite (dark colour) concentric laminae; note braunite spherulith (top); Gake area; sample 958-63; polished section; parallel polarizers; the bar equals 200 μ .

Fig. 6c: Unsorted Mn oxide ooliths/pisoliths cemented by calcite (white) and cut by calcite veins; the grains (braunite) contain varying Mn contents (Mn 45% - 20%); Gake area; sample 958-82; thin section; parallel polarizers, the bar equals 30 μ .

Plate 4.2



4.2.2 Supergene Oxidized Ores

(1) Massive Psilomelane Ore

Handspecimen

Although massive psilomelane ore is the main supergene product in most parts of the deposits, it is much rarer than primary materials and it is also restricted in distribution near the surface in most mining areas. Generally, the ore is laterally discontinuous over tens of meters and it is associated with primary Mn oxides. The ore is dark-grey to black, fine grained, and very hard and dense. In places, it contains thin subparallel and horizontal veins of recrystallized psilomelane which show crystallites oriented perpendicular to the elongation of the veins. The ore consists predominantly of cryptocrystalline or colloidal psilomelane and small amounts of pyrolusite and a trace of braunite. Rarely, it occurs in crystalline granular, and abundantly as relic outlines of oolites and pisolites. These ores overprint and replace primary Mn oxides and thus their appearance varies according to the precursor to a greater or lesser extent. Because psilomelane is seen to replace braunite, the ore is considered to be a secondary oxidized product of primary Mn oxides, which points to a supergene origin.

Microscopy

The minerals of the ore are generally extremely fine grained ($\sim 1 \mu$ or slightly larger) and they contain relic detrital materials such as quartz and oolites/pisolites of partly replaced braunite. These minerals have been partially replaced by oxidized manganese phases and in some cases only the outlines and/or cleavages structures are preserved. When the ore is strongly overprinted by recrystallization and replacement processes, the primary structures are partially or completely destroyed. The reflectance color of the ore indicates a dominance of psilomelane. Cryptocrystalline or colloidal psilomelane contains small amounts of diffuse pyrolusite, braunite and gangue minerals, and the fine grained and granular psilomelane successively fills the remaining open spaces in cracks.

(2) Spherulitic Psilomelane Ore

Handspecimen

This ore is restricted to the top of orebeds near the surface in most parts of the deposits, and it overlies primary Mn oxide ores. It is less abundant than massive psilomelane ore. Generally, the ore is not laterally continuous and is associated with Mn oxide (or deformed) oolite/pisolite. Normally, this ore type consists of dense spherulitic, very fine-grained psilomelane, with minor pyrolusite, quartz silt and clay. The ore is dark-grey or black and has massive structure. The grains are ovoid or flattened. The replacement of primary Mn oxide ore and gangue minerals is clearly recognized in sections. The ore is of supergene origin, representing alteration of pre-existing oxides.

Microscopy

Oolitic and pisolitic structures and textures are similar to those of primary Mn oxide (or deformed) oolite/pisolite, but the grainsize varies between 0.08 and 8 mm and the thickness of individual laminae of ooliths and pisoliths varies between 0.085 - 0.17 mm. This ore is very fine grained and the concentric laminae in ooliths or pisoliths consist mainly of psilomelane and minor pyrolusite, quartz silt and clay, which are also finely disseminated in the matrix. Deformed and/or fractured ooliths or pisoliths are also distributed irregularly in the matrix.

(3) Banded Psilomelane Ore

Handspecimen

Banded psilomelane ores are locally distributed on primary Mn oxides and they occur near the surface in most deposits. The ores are not laterally continuous (over tens of meters) though some are up to 2-4 cm thick. A broad subhorizontal banding is conspicuous. Rare blocky, reworked fragments of Mn-oxides are found within the ore, which have characteristics indicating a primary origin. The black and dark-brown colours of the ore define interbedded thin layers of psilomelane and silt or clay (banded structure). Generally, the bands vary between 0.5 and 1.0 cm thick with minor brownish pyrolusite intercalations. The ore is fine grained, hard and dense.

Microscopy

Polished sections illustrate that the upper parts of the ores possess an undulating fine sub-horizontal lamination, whereas only the lower parts become increasingly more massive, as in banded structure. Replacement of primary Mn oxides is apparant in many ore samples. Although the ores are dominated by psilomelane, pyrolusite increasingly appears to gain importance in some discontinuous laminations. Psilomelane and pyrolusite overprint and replace previous minerals (e.g. braunite), structures and textures.

(4) Reniform Psilomelane Ore

Handspecimen

Reniform psilomelane ores are locally restricted in most parts of the deposits. Stratigraphically, they occur approximately at the same level as the secondary Mn oxidized products described above, that is, at the top of primary Mn oxides near the surface. Psilomelane gives the ore a black luster. The ore consists of hard and dense cryptocrystalline or colloidal psilomelane containing yellowish silt and clay materials; it generally shows reniform structures, which are reaccumulation features resulting from the weathering process. A local geochemical micro-environment (supergene) played an important role in the development of these ores.

Microscopy



Apart from psilomelane, only minor pyrolusite and traces of braunite have been identified. The ores are colloidal and cryptocrystalline or extremely fine grained. Occasionally, relic ooliths/pisoliths are also incorporated.

(5) Earthy Nsutite Ore

Generally, the distribution of earthy nsutite ore is not restricted to specific ore types, and thus, this ore can be identified near or at the surface in most locations of the Dounan deposits. However, depending on the geological environment of the surrounding ores, earthy nsutite ores vary in their development and they can be overlooked in places where primary Mn carbonates are developed. Here, environmental factors led to the development of small karst features.

As the name suggests, the ores consist mainly of nsutite and minor pyrolusite, silt or clay. They show powdery or earthy textures, and also are characterized by a low density, softness and porous features. The dull and lustreless dark-brown color of the material indicates that nsutite is the main manganese mineral, though minor pyrolusite also presents a similar colour. Commonly, the ores show relic primary structures and textures such as oolith/pisolith, lamination and cross-bedding. The description above strongly suggests that earthy nsutite ores are supergene products of the primary Mn carbonates.

4.2.3 Alternative Classification and Reserves

The major ores of Dounan can also be divided into the following types in terms of value for commercial purposes (Zhang et al., 1979). The primary manganese ores can be divided into three types: i.e. calcareous Mn oxide ores, Mn carbonate ores, and transitional unsorted calcareous Mn oxide ores; whereas the supergene Mn oxidized ores also consist of three types: i.e. massive Mn oxidized ores, banded Mn oxidized ores, and earthy Mn oxidized ores. A summary correlation of the ore types and grades is presented in Table 4.1 and Table 4.2.

In summary, primary calcareous Mn oxides are the main ore type, comprising about 72% of the total Mn reserves; Mn carbonate ores are about 25% of total reserves and the supergene oxidized ores total to only 3% of total reserves (Zhang et al., 1979). The supergene ores occur near the surface and still preserve primary textures and structures with relatively few supergene (e.g. botryoidal, crusty and honeycomb) structures, which indicates that alteration of the ore from braunite to psilomelane is an oxidizing process. On the other hand, when Mn carbonate and some unsorted ores underwent secondary oxidation, the primary structures were mostly destroyed and replaced by supergene (e.g. reniform and honeycomb) structures, which suggests reaccumulation of materials during weathering.

Table 4.1 Relationship between ores and minerals in Dounan manganese deposits (in part after Zhang et al., 1979).

genetic type	ores			mineral *										
	ore phase	ore type	structural type	braunite	Ca-rhodochrosite	Mn-calcite	psilomelane	pyrolusite	nsutite	manganite	hausmannite	calcite	quartz	clay
primary manganese ores	manganese oxides	Mn oxide deformed oolite/pisolite	banded calcareous Mn oxide ore	+++	++	+				-		++	-	-
		Mn oxide oolite/pisolite	massive calcareous Mn oxide ore	+++	+	+				-		+	-	-
		massive Mn oxide oolite/pisolite		+++	-	-				-		-	-	-
	mixed type	unsorted Mn ₂ oxide oolite/pisolite	unsorted calcareous Mn oxide ore	+++	+++	+				-		++	++	-
	manganese carbonates	Ca-rhodochrosite oolite/pisolite	oolitic/pisolitic rhodochrosite ore		+++	++						+	+	-
		Mn-calcite oolite/pisolite	Mn-bearing carbonate ore		++	+++						++	+	-
supergene manganese ores	manganese oxidized phase	massive psilomelane ore	massive Mn oxidized ores	-			+++	+				-	+	+
		psilomelane oolite/pisolite		-			+++	+					+	+
		reniform or cellular psilomelane		-			+++	+					+	+
		banded psilomelane ore	banded Mn oxidized ores	-			+++	+					+	+
		earthy nsutite ore	earthy Mn oxidized ores				-	+	+++				+	++

* +++ major; ++ minor; + poor; - trace

Table 4.2 Relationships between ore type and industrial grade in Dounan manganese deposits (after Liu, 1984).

type	grade		Mn (%)	ores
primary Mn ores	good quality	I	≥ 29	massive Mn oxide ore (major); banded ore (minor)
		II	≥ 25	banded calcareous Mn oxide ore
		III	≥ 20	unsorted and/or banded Mn oxide ore
	poor quality	12-20	unsorted Mn oxide ore ; Mn carbonate ore	
	poorer quality	8-12	Mn carbonate and/or Mn-bearing carbonate ore	
supergene Mn ores	good quality	I	≥ 35	massive (major) and/or banded (minor) Mn oxidized ore
		II	20-35	earthy (major) and/or banded (minor) Mn oxidized ore

4.2.4 Rocks

Although a variety of properties are available for classifying limestones such as colour, grain or crystal size, composition and texture-fabric, most simple petrographic analyses of limestones are for the purpose of environmental interpretation and the most useful classification would be one which relates grain properties and fabric to some environmental property such as energy level during the deposition of the limestone (Tucker and Wright, 1990). Thus, the most widely used classification of Folk (1959, 1962) is used in this text, in which three main constituents in limestones are recognized: allochem (grains), matrix (micrite) and sparite (cement).

4.2.4.1 *Micrite or Mn-bearing Micrite (Oolitic / Pisolitic)* (Plate 4.3, Figs. 7 and 8)

As they accompany the manganese ores, the micrite or Mn-bearing micrite of different types (mainly oolitic and pisolitic) are distributed in all mine-areas in the deposits. They are laterally discontinuous over extensive areas, either in the fine clastic rocks that overlie the orebody, as thick layers underlying the orebed, or occurring in the orebody as gangue rocks. Mn-bearing micrites are also dominant phases in some orebeds (e.g. V4, V5, V6 and V10), where poor quality ores such as Mn-bearing carbonate ores are commonly observed. Small scale cross-bedding can be seen in the many micrites..

The main minerals of the Mn-bearing limestones are extremely fine manganocalcite, Mn-bearing calcite or calcite. The rocks are mainly micrite or Mn-bearing micrite to clay or silt sized with oolitic/pisolitic structures. They are dark-grey and grey and some ores contain dolomite. Clay or relatively fine quartz grains (e.g. silts) are commonly dispersed in the micrite matrix (e.g. calcilutite or calcarenite) or they are accumulated in subhorizontal layers. Primary Mn carbonate and unsorted Mn oxide ores are developed within some Mn-bearing limestones or Mn-bearing limestone-rich horizons. On average, micrites contain 6-7% Mn, and are characterized by concentrically laminated ooliths / pisoliths or spherulites well cemented by microcrystalline calcite, indicating a primary origin (intertidal or barrier environments).

4.2.4.2 *Intramicrodite / Intrasparite (Intraclastic / Brecciated)* (Plate 4.3, Figs. 9a-b)

The intramicrudites/intrasparites of different fabrics are encountered over all of the deposits, but are mainly distributed in the southwestern area. They are generally concentrated in the areas where T2f4-1 ore-bearing rocks occur and are laterally continuous over extensive areas, either as thick or thin layers underlying the orebeds (e.g. T2f3-2 submember), or as gangue layers in the orebody. The main mineral of the rock is microcrystalline or microcryptocrystalline calcite, but

Plate 4.3 Ores and associated rocks,

Fig. 7: Deformed and broken grains in oolitic/pisolitic micrite; dark colour: organic rich carbonate materials; light colour: braunite; Gake area; sample 958-91; polished section; parallel polarizers; the bar equals 100 μ .

Fig. 8: Mn-bearing oolitic/pisolitic micrite; the grains are mostly spheruliths or structures with concentric laminae; white colour: braunite; dark colour: organic rich carbonate materials; Gake area; sample 958-72; polished section; parallel polarizers; the bar equals 100 μ .

Fig. 9a: Intramicrudite/intrasparite with poor inverse grading and dark cements from Gake area; sample 958-21; pen for scale.

Fig. 9b: Intramicrudite/intrasparite with light grey matrix from Kata area; sample 958-94; pen for scale.

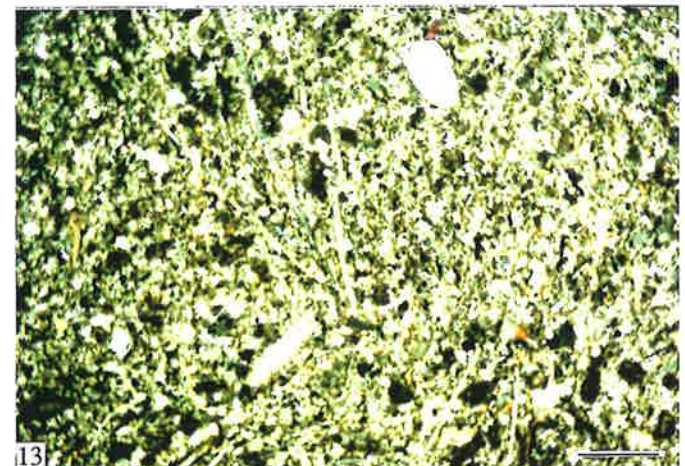
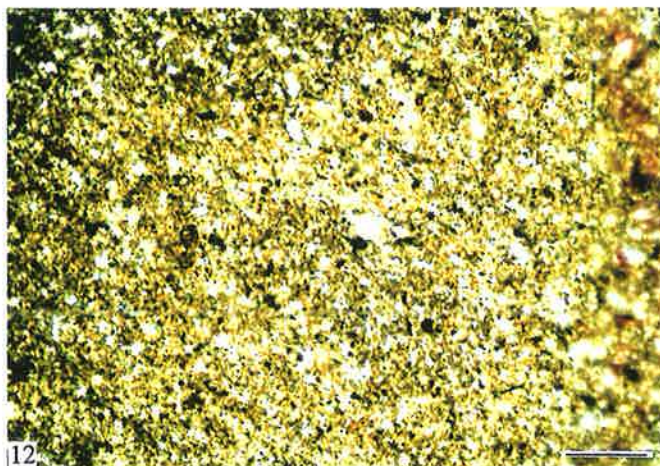
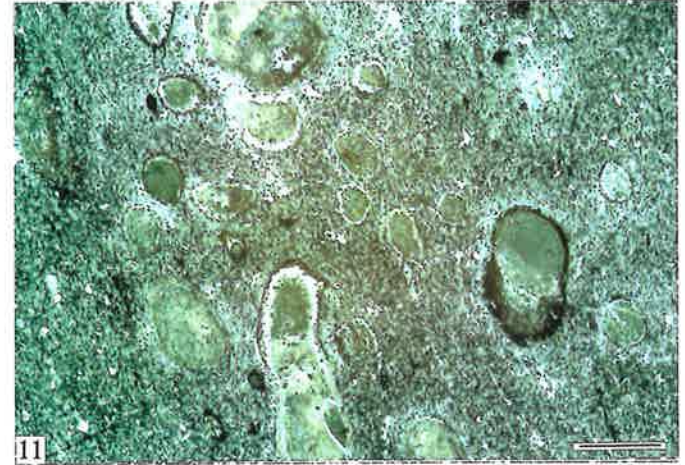
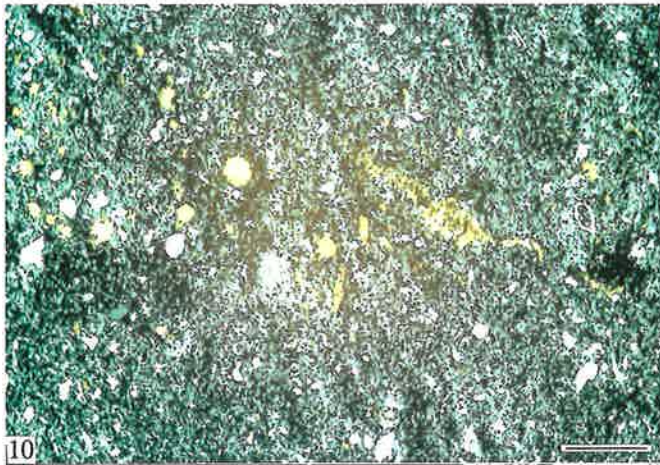
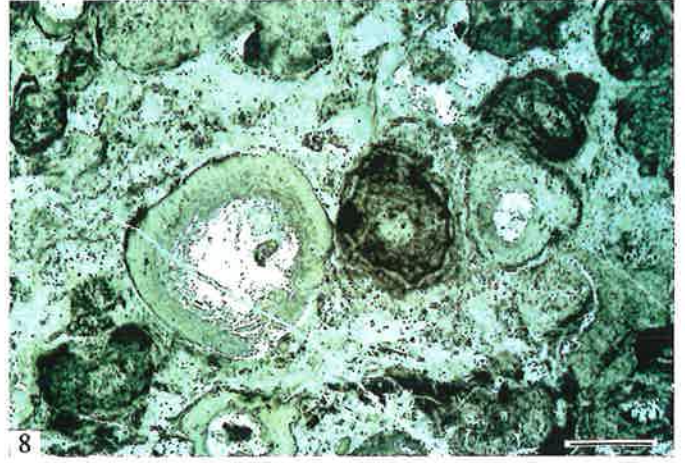
Fig. 10: Calcarenite with quartz silts; Baigu area; sample 958-132; thin section; crossed polarizers; the bar equals 200 μ .

Fig. 11: Calcilutite with micrite oncoliths; Baigu area; sample 958-180; polished section; parallel polarizers; the bar equals 200 μ .

Fig. 12: Silty claystone with minor braunite (black colour); Gake area; sample 958-59; thin section; parallel polarizers; the bar equals 200 μ .

Fig.13: Clayey siltstone from Gake area; sample 958-36; thin section; parallel polarizers; the bar equals 200 μ .

Plate 4.3



minor manganese (3-6%; Mn-bearing intramicrudite / intrasparite) may be present. Usually, the rocks occur in intraclastic / brecciated (0.5-15 cm) structures, with irregularly distributed grains composed of micrite or calcilutite. Such rocks are well cemented by microcryptocrystalline calcite or minor clay and one of primary origin, i.e. sediments formed in low energy (e.g. lagoonal) environments and redeposited in higher energy (e.g. intertidal or barrier) environments after redistribution by waves.

4.2.4.3 *Calcarenite*

(Plate 4.3, Fig. 10)

Calcarenite is found in most areas of the deposits and in most members of the Falang Formation in vertical geologic profiles, except for member 6 (T2f6). The calcarenite tends to decrease in both thickness and abundance from southwest to northeast, and from the bottom to the top in vertical profiles. It is also common as thin layers (0.1 - 1.0 m thick) between orebeds in Mn-bearing members (T2f4-1 and T2f5-2).

Calcarenite is mainly composed of microcryptocrystalline calcite and contains some fine quartz sands or silts (0.2 - 2.0 mm), and minor manganese. Commonly, small scale low-angle cross-bedding, lamination, and sometimes wavy bedding and slump bedding can be seen in the rocks. These are considered to be primary sedimentary products of intertidal or slope environments.

4.2.4.4 *Calcilutite*

(Plate 4.3, Fig. 11)

Calcilutite is distributed in varying quantities throughout the deposits. It is found in minor amounts in the Mn-bearing series, though these locations favour the formation of different types of ores. The units are bedded (0.5 - 1.0 m) and often occur in the lower and upper but less often in the middle part of the Falang Formation and with mudstone or silty claystone. The rock is generally structureless or massive, but in some cases lamination or low angle cross-bedding occurs. The main mineral of calcilutite is cryptocrystalline calcite, but minor micritic dolomite also is present. Generally, muddy materials (silt and clay silicates) are present in minor amounts. Calcilutites formed either in intertidal or open marine neritic environments.

4.2.4.5 *Silty Claystone*

(Plate 4.3, Fig. 12)

Silty claystone is well developed in all parts of the deposits, where it occurs below, above and within the orebeds as thin or thick layers (0.5 - 40 m in thick). They are common rocks in the deposits and are laterally continuous over large areas. The rocks are light to dark grey in colour, and are mainly composed of clay and contain minor quartz silt. Many samples contain minor amounts of manganese (Mn 3-5%) and they also show oolitic structure when formed within

Mn-bearing sections. Structure ranges from laminated to massive, occasionally desiccation forms are found. The rocks formed in lagoonal, open marine or supratidal environments.

4.2.4.6 *Siltstone / Clayey Siltstone*

(Plate 4.3, Fig. 13)

Siltstone or clayey siltstone occurs in all places where silty claystone are developed and also are laterally continuous over large areas as thick or thin layers (0.5 - 40 m). They show light to dark grey colours and occur in all parts of the Falang Formation in vertical geological profiles. The main mineral of the rocks is silt-sized quartz, and clay-sized materials can be present in amounts up to 15%. Dark-grey rocks often contain minor amounts of manganese (Mn 2-5%). Small to medium scale cross-bedding, wavy bedding or oblique bedding is common, and rarely, slump bedding or graded bedding. Silt grains are generally angular to sub-angular in shape. The rocks associated with ores often occur as thin layers (10 to 60 cm) with oolitic mudstones and limestones. The rocks mainly formed in intertidal, barrier, slope or open marine environments.

4.2.4.7 *Sandstone*

Sandstones are concentrated in the central part of the Dounan syncline and crop out in the north-eastern part of the deposits. They are limited stratigraphically to the upper part of the Falang (T₂f₆, 5%) and Niaoge formations in vertical geological profiles. The material is relatively well cemented, and some structures such as oblique bedding, planar bedding and ripple mark can be discerned. The predominant mineral is quartz; only trace amounts of other materials are found. The rocks are usually very light in color, and the fine to medium grains are rounded to sub-angular. Falang sandstones are almostly of intertidal or supratidal origin.

4.2.4.8 *Conglomerate*

Irregular lenses and pockets of conglomerate associated with erosional features are found mainly near the base of the Niaoge Formation in the central part of the Dounan syncline. These units are laterally discontinuous, but large bodies (up to 5 m thick) appear occasionally. Generally, the conglomerate consists of pebbles and cobbles of well rounded quartzite, with a matrix of quartz sand. They are interpreted as supratidal products.

4.2.5 *Summary*

Based on the descriptions above, the main characteristics of the Dounan manganese ores and associated rocks are listed in Table 4.3 (a, b, c).

Table 4.3a: Primary manganese ores

Name	Structure / Geometry	Mineralogy/texture
Braunite oolite / pisolite (Mn oxide)	Normal and inverse grading, grains rounded or sub-rounded, stratiform or wavy bedded, very well cemented, small / medium scale cross-bedding to massive.	Braunite, calciorhodochrosite, Mn-calcite, calcite, manganite, nuclei composed of calcite, albite, silt or sand grains and biofragments.
Deformed braunite oolite / pisolite (Mn oxide)	Normal and inverse grading, grains irregular sub-rounded or ellipsoidal, stratiform or wavy bedded, very well cemented, small / medium scale cross-bedding, grains in preferred orientation, banded or massive.	Braunite, calciorhodochrosite, Mn-calcite, calcite, manganite, nuclei contain calcite, albite, silt or sand grains and biofragments.
Massive braunite oolite / pisolite (Mn oxide)	Poor normal and inverse grading, grains rounded or sub-rounded, poorly concentric laminae but with clear outlines of ooliths / pisoliths, very well cemented, small / medium cross-bedding or, compact massive.	Braunite, calciorhodochrosite, Mn-calcite, calcite, dolomite, manganite, nuclei contain calcite, albite, silt or sand grains and biofragments.
Calciorhodochrosite oolite / pisolite (Mn carbonate)	Normal and inverse grading, grains sub-rounded or irregularly sub-rounded very well cemented, stratiform or wavy bedded, lamination and small scale cross-bedding, massive and banded.	Calciorhodochrosite, Mn-calcite, Mn-bearing calcite, calcite, dolomite, albite, quartz, nuclei contain calcite, albite, quartz and biofragments.
Mn-calcite oolite / pisolite (Mn carbonate)	Normal and inverse grading, grains sub-rounded or irregularly shape, very well cemented, stratiform or lenticular, lamination and small scale cross-bedding, massive and banded.	Mn-calcite, Mn-bearing, calciorhodochrosite, calcite, calcite, dolomite, quartz, nuclei contain calcite, albite, quartz and biofragments.
Unsorted Mn oxide ore (transitional or mixed type)	Varying in size with mostly inverse grading, braunite ooliths / pisoliths or spheruliths irregularly distributed in Mn carbonate (mostly calciorhodochrosite) matrix, grains rounded to sub-rounded, very well cemented, stratiform and wavy bedded, low-angle cross-bedding and lamination, massive or banded.	Calciorhodochrosite, braunite, Mn-calcite, Mn-bearing calcite, manganite, calcite, nuclei contain calcite, albite, silt or sand grains and biofragments.

Table 4.3b: Supergene manganese ores

Name	Structure / geometry	Mineralogy/texture
Massive psilomelane ore	Poorly oolitic or pisolitic, very hard, massive, generally subhorizontal, occasional relic features.	Psilomelane, pyrolusite, braunite, calcite, quartz silt.
Oolitic / pisolitic psilomelane ore	Oolitic / pisolitic, sub-rounded to irregularly sub-rounded, very well cemented in oolite / pisolite, relic features, horizontal to sub-horizontal, massive.	Psilomelane, pyrolusite, braunite, quartz silt.
Banded psilomelane ore	Banded and laminated, well to very well cemented.	Psilomelane, pyrolusite, braunite, quartz silt.
Reniform psilomelane ore	Strongly leached, irregularly reniform or cellular structures which were filled with silts and clay.	Psilomelane, pyrolusite, braunite, quartz silt, clay minerals.
Earthy nsutite ore	Loose, laminated, earthy, containing loose ooliths / pisoliths, often with relic features.	Nsutite, pyrolusite, psilomelane, quartz silt, clay minerals.

4.3 Textural and Structural Features of Ores and Rocks

The manganese oxide and carbonate minerals constituting the orebodies under consideration in this text, exhibit interesting textural and structural features, indicating varying conditions of formation during sedimentation as well as the nature of post-sedimentary changes. These features are recorded and an attempt is made to interpret them to determine the mode of origin and paragenetic trends for minerals and ores/rocks. The textural and structural features of the ores and rocks are described first and the special micro-behaviour or characteristics (e.g. CL and SEM) of the different ore minerals will then be discussed.

4.3.1 Texture

1) Colloform Texture

(Plate 4.4, Figs. 14a-d)

The most interesting feature noted in some Mn oxide ores is the relict colloform texture exhibited by braunite and minor manganite in oolite/pisolite. In slightly deformed concentric rings, manganite occupies the core and braunite the outer ring, or vice versa. Healed shrinkage cracks have been detected and oxides of manganese in veins have been crystallized to braunite and manganite. Apparently braunite and manganite colloform bodies in the original sediments were transformed to crystalline braunite and manganite at higher temperature during diagenesis, though outwardly or inwardly the texture remained intact. Importantly, the presence of the relict

Table 4.3c: Rocks associated with manganese ores

Name	Structure / Geometry	Mineralogy/texture
Mn-bearing limestone (oolitic / pisolitic)	Oolitic and pisolitic, grains rounded to sub-rounded, normal and inverse grading, stratiform, lamination, small / medium scale cross-bedding, massive.	Micrite, calcilutite, calcarenite, silt, clay minerals, calcite, dolomite.
Intramicrodite / intrasparite (intraclastic / brecciated)	Intraclastic or brecciated, grains irregular or angular, very well cemented, stratiform, low-angle cross-bedding, massive.	Micrite, calcilutite, calcarenite, silt, clay minerals, calcite, dolomite.
Calcarenite	Stratiform or wavy bedded, fine quartz grains sub-rounded to angular (0.2-2.0 mm), lamination, small / medium scale cross-bedding, wavy bedding, slump bedding, massive.	Micritic calcite, quartz, silt and sands, calcite.
Calcilutite	Stratiform, lamination, small low-angle cross-bedding.	Micritic calcite, dolomite, clay minerals.
Claystone / Silty claystone	Stratiform, lamination or massive bedding, sometimes oolitic texture with grains rounded to sub-rounded.	Clay minerals, quartz silt or sands, micritic calcite.
Siltstone / clayey siltstone	Stratiform, lamination, small / medium scale cross-bedding, wavy bedding, sometimes structureless, grains angular to sub-angular, massive.	Quartz silt, clay minerals, micritic calcite.
Sandstone	Dense, cross-bedding, planar bedding, ripple mark, grains rounded to sub-angular.	Quartz
* Conglomerate	Lenses, discontinuous.	Sand, quartzite pebbles, silt, clay minerals.

* Not associated with manganese ores.

colloform structure of braunite emphasizes the primary sedimentary origin of braunite, though this texture is rather limited in comparison to crystalline braunite.

2) *Cryptocrystalline Texture*

(Plate 4.4, Figs. 14d and 16)

This texture is mainly exhibited by braunite, calciorhodochrosite and Mn-calcite or Mn-bearing calcite. It constitutes laminations and oncolites, is commonly associated with ores of dark colour, and contains organic materials. It is widespread in various ores of Dounan but mostly in Mn carbonate ores and in the matrix of manganese oolites/pisolites.

3) *Microcrystalline-Granular Texture*

(Plate 4.4, Fig. 15)

This texture, mainly composed of automorphic or hypautomorphic granular braunite, with varying grain size from 0.001 to 0.05 mm (generally 0.005 - 0.01 mm), is one of the main textures of Mn oxide ores in the Dounan area. Generally, braunite is present in the ore in two generations. The first generation braunite occurs as colloform texture or as cryptocrystalline grains which are intensely shattered and elongated; both exhibit a concentrically laminated arrangement in oolites/pisolites, indicating precrystalline early sedimentation. This braunite is less abundant than those of the second generation. In some cases second generation braunite also shows concentrically laminated arrangement in oolites/pisolites, but in other cases relatively coarse crystals of octahedral shapes replacing the first generation braunite led to the disappearance of concentrically laminated structure. This texture can commonly be found in massive Mn oxide ores.

4) *Oolitic / Pisolitic Texture*

(e.g. Plates 4.1-4.2)

This texture is universally present in the Dounan manganese ores, and is mainly composed of colloform and cryptocrystalline or microcrystalline Mn oxide and/or carbonate minerals in concentric laminations. Componently, the manganese ores can broadly be divided into a number of types:

- (a). The oolites/pisolites consist mainly of braunite with minor Mn-calcite or calcite;
- (b). The oolites/pisolites consist mainly of calciorhodochrosite with minor braunite;
- (c). The oolites/pisolites consist mainly of both braunite and calciorhodochrosite; and
- (d). The oolites/pisolites consist mainly of Mn-calcite with minor calciorhodochrosite and/or calcite.

Commonly, the oolites/pisolites show spherical to ovoid appearance, and their nuclei are composed of calcite, quartz, albite and biofragment grains (0.3-15.0 mm), and mostly the shapes of oolites/pisolites follow those of the nuclei. Grains are mostly concentrically laminated, in some cases, of alternating mineralogy. Laminae range in thickness from 0.1 to 3.5 mm.

5) *Deformed Oolitic / Pisolitic Texture*

(e.g. Plate 4.1, Figs. 1c and 2b)

Plate 4.4 Ores and associated rocks.

Fig. 14a: Colloform grains composed of braunite (light colour) and Mn-calcite (dark colour), which occur between the concentric laminae of braunite pisolith as laminae; Gake area; sample 958-62; polished section; parallel polarizers; the bar equals 30 μ .

Fig. 14b: Colloform braunite (black) growing on of a biofragment; brown: Mn-calcite; Kata area; sample 958-49; thin section; parallel polarizers; the bar equals 100 μ .

Fig. 14c: Braunite (white) colloform grain showing colloiddally radial structure probably due to collocrystallization; dark colour: cryptocrystalline carbonate materials; Daaози area; sample 958-78; polished section; parallel polarizers; the bar equals 100 μ .

Fig. 14d: Colloidal braunite (light colour) with two 'nuclei'; dark colour: cryptocrystalline carbonate materials which cut through the colloform body; Baigu area; sample 958-170; polished section; parallel polarizers; the bar equals 30 μ .

Fig. 15: Braunite (light colour) microcrystalline texture with relic laminae of primary grain; dark colour: calcite; Gake area; sample 958-50; polished section; crossed polarizers; the bar equals 0.2 mm.

Fig. 16: Cryptocrystalline braunite ooliths/pisoliths (black) radially replaced by calcite (light colour); Baigu area; sample 958-172; thin section; parallel polarizers; the bar equals 0.5 mm.

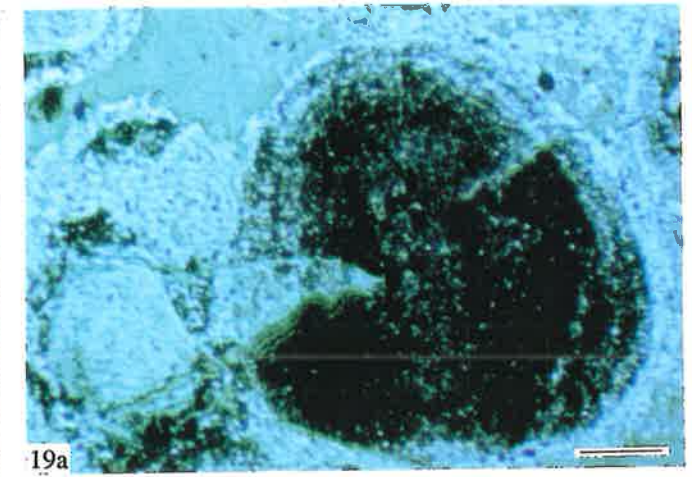
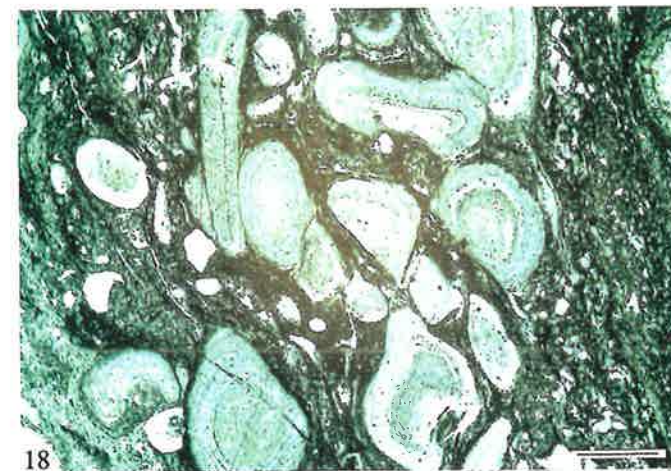
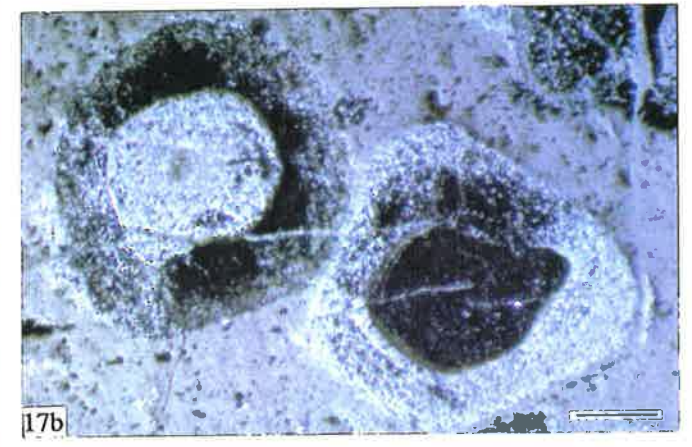
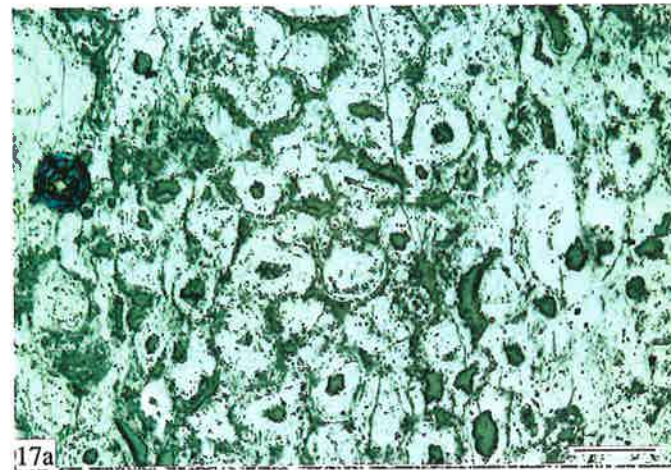
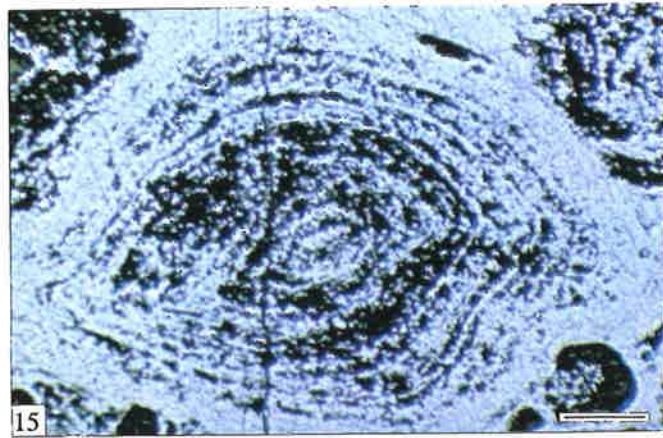
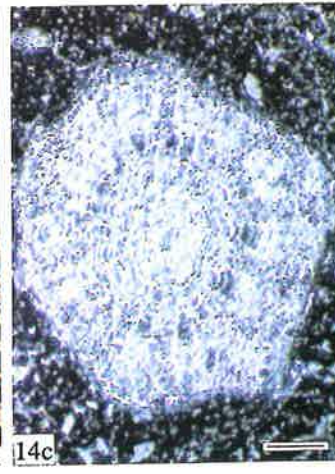
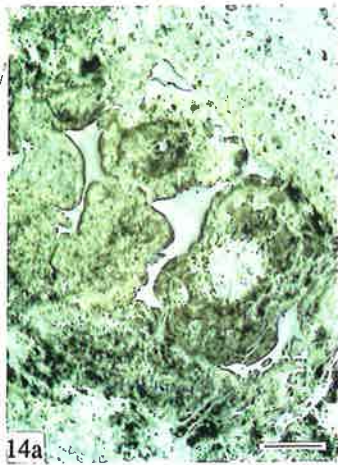
Fig. 17a: Braunite (light colour) spherulitic texture; dark colour: calcite; Gake area; sample 958-73; polished section; crossed polarizers; the bar equals 0.5 cm.

Fig. 17b: Braunite (light colour) spheruliths cemented by Mn-calcite showing different growing processes, implying the presence of two generations of braunite; black: organic matter-bearing calcite; Baigu area; sample 958-232; polished section; crossed polarizers; the bar equals 1 mm.

Fig. 18: Fragmental texture of Mn oxide deformed oolite/pisolite showing broken and abraded grains and preferred orientation; white: braunite; light grey colour: calciorhodochrosite and Mn-calcite; dark grey colour: calcite; Gake area; sample 958-42; polished section; parallel polarizers; the bar equals 1 cm.

Fig. 19a: Braunite (white) replacing calcite spherulith (black) from outside; the cements (blue): Mn-calcite (black); Baigu area; sample 958-172; polished section; parallel polarizers; the bar equals 30 μ .

Plate 4.4



This texture is mainly present in the Mn oxide deformed oolite/pisolite and occasionally in other ore types. Generally, its features and constituting components are the same as those of the oolitic/pisolitic ores, but the shapes of ooliths/pisoliths vary from ovoid to flattened grains which are commonly oriented in direction mostly parallel to each other and to the layers. This latter condition is interpreted as resulting from diagenetic alteration, including compaction.

6) *Spherulitic Texture*

(Plate 4.4, Figs. 17a-b)

Rarely, this texture is present in the mass of spherulites which mainly consist of braunite or Mn carbonate minerals. Commonly, the spherulith is composed of 1-3 concentric laminae, and the inner lamina in many cases is made up of cryptocrystalline braunite or Mn carbonate minerals. Biofragments of the nucleus may be surrounded or enveloped by secondary crystalline braunite or Mn carbonate minerals.

7) *Fragmental Texture*

(Plate 4.4, Fig.18)

This texture is generally composed of various fragments such as broken ooliths/pisoliths or spheruliths of Mn oxides or carbonates, bioclastic fragments, sands or silts, and Mn-bearing brecciated micrite, which are well cemented by cryptocrystalline Mn oxide and/or carbonate materials. Commonly, fragmental texture occurs in unsorted Mn oxide, banded or Mn carbonate ores.

8) *Replacing and Recrystalline Textures*

(Plate 4.4, Fig.19a; Plate 4.5, Figs.19b-g)

Importantly, various replacing and recrystalline textures are common in the Dounan manganese ores. They are observed in the ore minerals, or among ore and gangue minerals. Two, and in some places, three, generations of both ore and gangue minerals can be recognized in most Dounan manganese ores, which indicates that post-depositional alteration was extensive.

4.3.2 *Structure*

1) *Massive Structure*

(Plate 4.1, Figs. 3a-b)

This structure is present in most ore types of the Dounan deposits, especially in altered Mn oxide or carbonate oolites/pisolites. However, compact massive oxide ores show strong diagenetic crystallization in the form of ooliths/pisoliths in close contact as well as the disappearance of concentric laminae and the development of indistinct margins of ooliths and pisoliths in the ores. Massive structure also is the main structure of supergene psilomelane ores.

2) *Banded Structure*

(Plate 4.1, Fig. 2a)

This structure is mainly characterized by interbedded black Mn oxide deformed oolite/pisolite and dark red Mn carbonate ores (occasionally Mn-bearing intraclastic limestones). The width of the banding varies from 0.5 to 2.0 cm, occasionally to 4.0 cm, and the two ore types occur in roughly equal amounts. Mn oxide deformed oolite/pisolite and some Mn carbonate ores commonly feature banded structure.

3) *Unsorted Structure*

(Plate 4.2, Fig. 6a)

This particular ore structure is characterized by black braunite ooliths/pisoliths, spheruliths and small lenses (2-15 mm) scattered heterogeneously in dark-red Mn carbonate matrix. This is the typical structure of unsorted Mn oxide ores, and it often occurs with inverse grading.

4) *Stylolites (Liu et al., 1984)*

Rarely, stylolites are present in Mn carbonate ores or in the contact area between Mn oxide ooliths/pisoliths and Mn-bearing intraclastic micrite. Boundaries between grains are compressed and show local truncation of oolite/pisolite concentric lamination, indicating early diagenetic pressure solution.

5) *Deformed Bedding Structure*

(Plate 4.5, Fig. 20)

Rarely, this structure can be found in banded and Mn carbonate ores, and is characterized by deformed Mn laminae (5-8 cm thick). It probably results from slipping and the action of gravity on sediments in a slope zone (e.g. the zone between intertidal and lagoon) during sedimentation or early diagenesis.

6) *Brecciated Structure*

(Plate 4.3, Fig. 9b; Plate 4.4, Fig. 18)

Broken oolitic/pisolitic or laminated braunite and Mn carbonate ores (1-10 cm thick) are commonly present as angular grains (< 2 - 15 cm), which are randomly oriented on a base of Mn-bearing micrite or calcilutite. Redeposition of sediments in high energy environments is indicated.

7) *Size Grading*

(Plate 4.1, Figs. 1a and 4a; Plate 4.5, Fig. 21)

Inverse and normal grading (5-50 cm thick) is very often found in the Dounan manganese oolite/pisolite (grainsize varies from < 2 to 15 cm). The structure is taken to indicate variations of transport energy during ore deposition.

Plate 4.5 Ores and associated rocks.

Fig. 19b: Recrystallization of braunite ooliths/pisoliths showing regenerated cycles and recrystallized calcite nuclei; black: primary braunite; brown: secondary braunite; light colour: calcite; Kata area; sample 958-54; thin section; parallel polarizers; the bar equals 100 μ .

Fig. 19c: Recrystallization of braunite oolith/pisolith showing regenerated braunite (black) replacing recrystallized radial oolith (typical diagenetic product) composed of Mn-calcite (brown colour), cemented by calcite; Baigu area; sample 958-202; thin section; crossed polarizers; the bar equals 200 μ .

Fig. 19d: Diagenetically regenerated calciorhodochrosite spherulith; black: calcite; Baigu area; sample 958-144; polished section; crossed polarizers; the bar equals 1 mm.

Fig. 19e: Secondary braunite (black) and Mn-calcite (white) (algal) ooliths/pisoliths replaced by each other with relic concentric laminae of primary grains; Kata area; sample 958-65; thin section; parallel polarizers; the bar equals 10 μ .

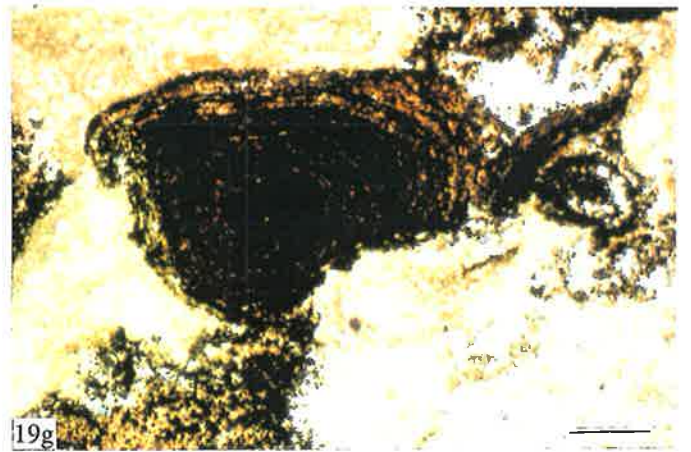
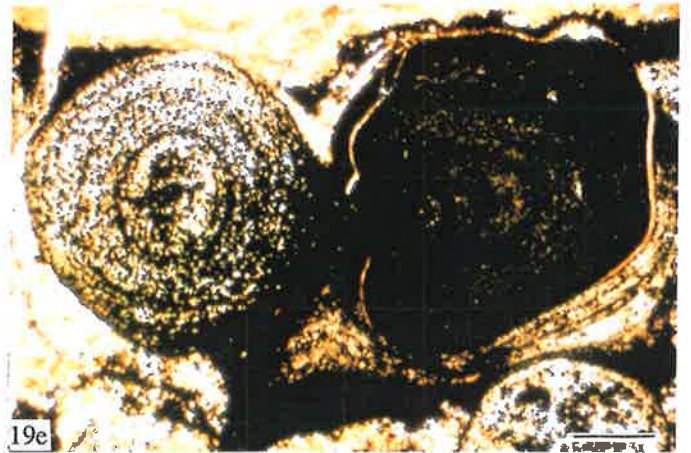
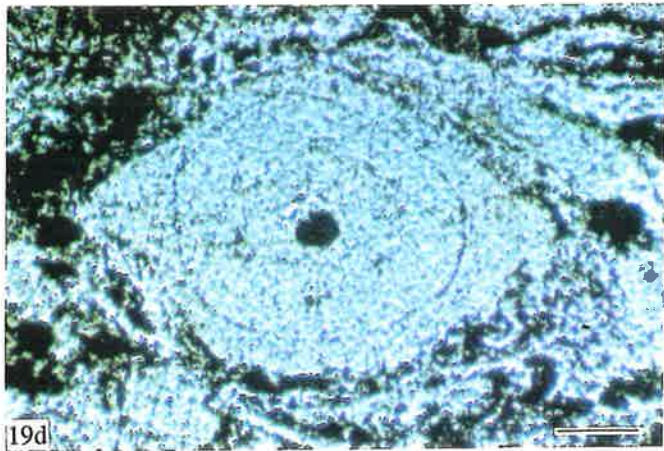
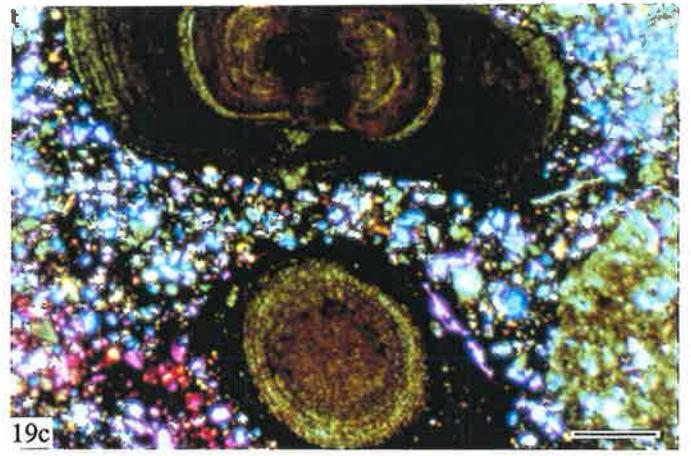
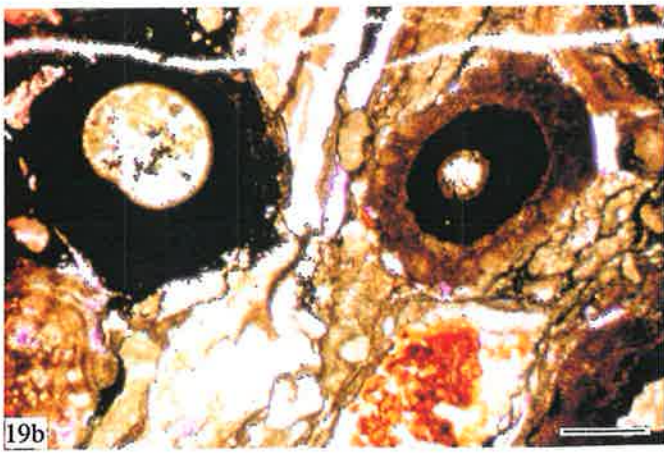
Fig. 19f: Secondary calcite (white) replacing primary braunite (black) from outside of the ooliths/pisoliths, with secondary calcite vein; brown: Mn-calcite; Baigu area; sample 958-173; thin section; parallel polarizers; the bar equals 30 μ .

Fig. 19g: Secondary calcite (matrix, white) replacing primary braunite ooliths/pisoliths (black); Gake area; sample 958-64; thin section; parallel polarizers; the bar equals 30 μ .

Fig. 20: Deformed bedding structure of banded Mn oxide ore; black: braunite; darkred: calciorhodochrosite and Mn-calcite; Baigu area; sample 958-205.

Fig. 21: Inverse grading of unsorted Mn oxide ore, top to left; black: braunite; darkred: calciorhodochrosite and Mn-calcite; Baigu area; sample 958-204.

Plate 4.5



4.3.3 Cathodoluminescence (CL)

Luminescence microscopy and spectroscopy are being employed in wider array of geological studies. Luminescence studies allow better interpretation of diagenetic, mineralization, and alteration events because of the control and discrimination of crosscutting relationships and subtle changes in chemistry that often become obvious using luminescence (Charles et al., 1991). Thus, Cathodoluminescence (CL) microscopy has become an essential and important tool in petrological, ore deposit and mineralogical studies (Walker and Burley, 1991), and Cathodoluminescence (CL) petrography of Dounan ores provides essential information on provenance, growth, fabrics, diagenetic textures and mineral zonation, in addition to enabling more precise quantification of constituents and fabrics.

Generally, the most widespread use of CL is in studies of carbonate diagenesis. (Meyers, 1974; Frank et al., 1982; Grover and Read, 1983; Niemann and Read, 1988; and many others). They considered that the most important activator of luminescence in *natural* calcite and dolomite is Mn^{2+} because it is relatively abundant and generates intense emission, and the most important quencher of Mn^{2+} -activated luminescence is Fe^{2+} . Substituting for calcium in carbonate minerals, Mn^{2+} emission is yellow-to-red; very pure calcite often luminesces blue and exhibits a broad blue emission band which is thought to be due to an intrinsic defect center, although impurities such as Pd can also give rise to a blue emission band. However, very rarely, line emission is due to equivalent rare earths such as Eu^{3+} , Sm^{3+} , Dy^{3+} (e.g. Machel, 1985; Machel et al., 1991; Marshall, 1988).

Cathodoluminescence in carbonates is primarily a result of diagenesis; unaltered carbonate sediments may be cathodoluminescent, but this is quite rare. Thus, cathodoluminescence is most commonly the result of postdepositional precipitation or recrystallization (Machel and Burton, 1991). However, the Dounan Mn carbonates of which are some biogenic, strongly cathodoluminesce even though some of them do not show apparent evidence of diagenesis (Plate 4.6, Figs. 22a-b). In the nucleus of a pisolith, a group of circular structures interpreted as algal balls are clearly visible in plane polarized light photomicrographs; they gave red luminescence in calciorhodochrosite. The concentric laminae of the pisolith are composed of both calciorhodochrosite and calcite (yellow luminescence) and possess the same primary sedimentary features as the algal ball group. Recrystallization as microcrystalline calcite is seen only in the cement among algal balls.

Generally, marine biogenic carbonates are noncathodoluminescent (e.g. Czerniakowski et al., 1984; Popp et al., 1986a, 1986b.). However, the amount of manganese in a carbonate mineral lattice sufficient to produce cathodoluminescence depends largely on the presence of other cathodoluminescence activators and quenchers, notably iron acting as a common cathodoluminescence quencher (Gies, 1975; Frank et al., 1982; Hemming et al., 1989). Since Dounan carbonates contain very little Fe^{2+} (mostly not detected), cathodoluminescence in biogenic

Plate 4.6 CL photographs of Dounan Mn carbonates and oxides, with composition analyses by EMPA.

Fig. 22a: Plane polarized light photomicrograph of Mn carbonate pisolith (calciorhodochrosite) from sample 958-204 unsorted Mn oxide ore illustrating the relationship of nuclei algal balls (A) group and concentric laminae (B). Algal balls (calciorhodochrosite) contain spherical structures interpreted as individual algae, and nuclei (top left). Calcite cement (C); the scale bar equals 0.5 mm.

Fig. 22b: CL micrograph of same field of view as Fig. 22a, illustrating clear definition of algal balls group-cement relationship and additional details not revealed by transmitted light microscopy; calciorhodochrosite: Mn, EMPA analysis of the red areas (A) gave ~34% Mn, Fe is nearly below detection (up to 2%); yellow zones indicate Mn-bearing calcite (~5% Mn) (B), but the dark areas contain slightly more Mn, and blue luminescing areas represent pure calcite (C); calciorhodochrosite algal balls were cemented by primary calciorhodochrosite (dull-red) (D) which has replaced by calcite (yellow) (E); concentric laminae are composed of calciorhodochrosite and calcite (F); the photograph was taken in conditions of 20kv, 200UA, and 5.46 seconds; the scale bar equals 0.5 mm.

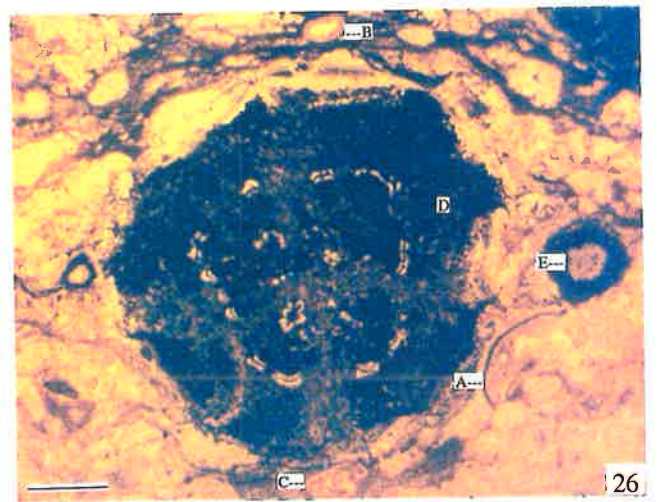
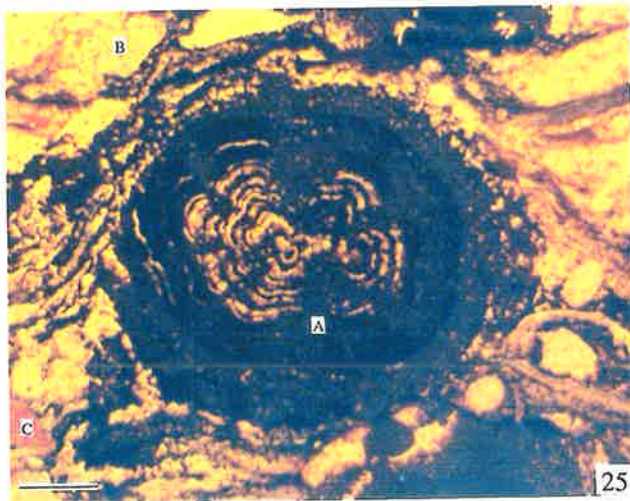
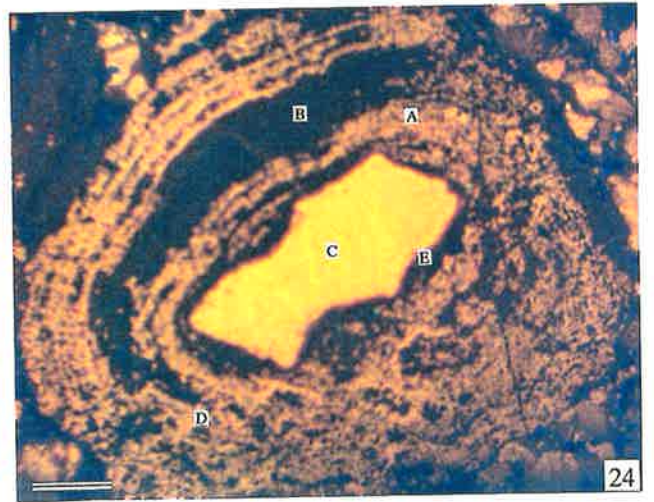
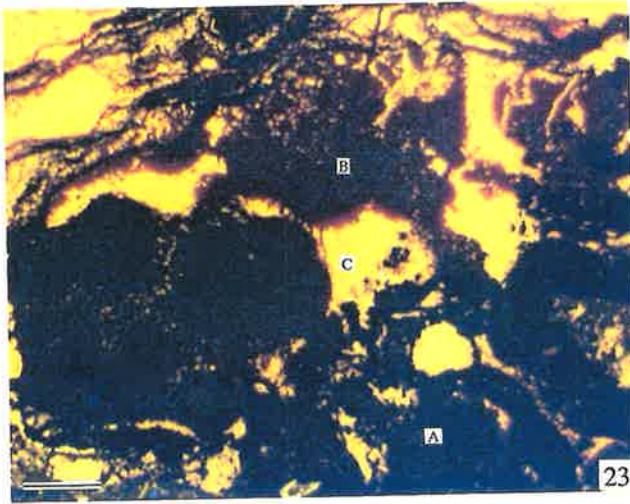
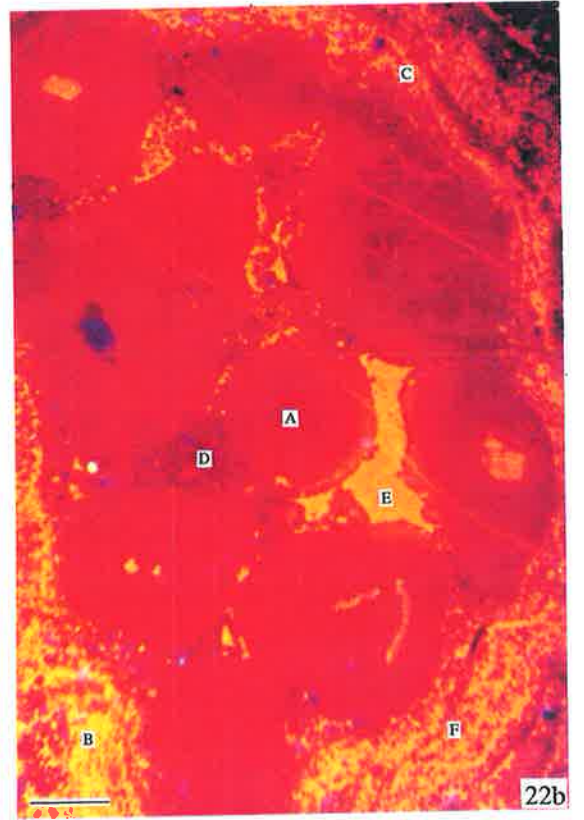
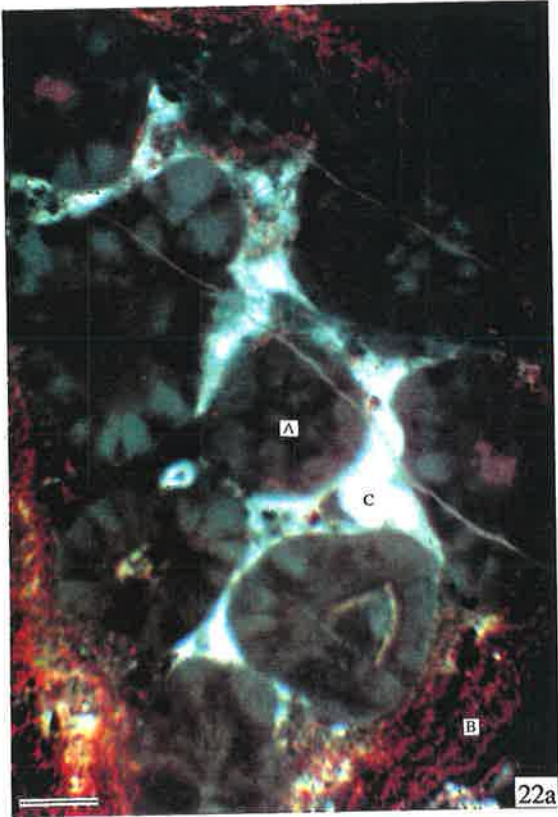
Fig. 23: Black and dark brown luminescence in pelletoid braunite [Mn, EMPA analysis of the black areas gave 55% Mn (A), those of the dark brown areas gave 35% Mn (B), Fe is mostly below 2%]; the yellow luminescent mineral is calcite (C) filling pores because braunite (possibly algal) pellets; sample from 958-38; under 19 kv, 200UA and 8.46 seconds, the scale bar equals 0.1 mm.

Fig. 24: Intense orange (EMPA analysis gave 17% Mn) and black (EMPA analysis gave 40% Mn) luminescence in Mn-calcite (A) and braunite (B) in an Mn carbonate oolite; the yellow CL area in this sample is a detrital calcite grain (C, nucleus of oolite); the braunite replaces orange luminescing Mn-calcite, which leads to discontinuous concentric laminae of braunite (D); braunite in the core replaces yellow luminescing calcite (nucleus) (C) giving an intense red luminescing calciorhodochrosite zone (E); sample 958-64; under 20 kv, 200 UA and 4.43 seconds; the scale bar equals 0.3 mm.

Fig. 25: Black and yellow (A) luminescence in braunite pisolith which are cemented by yellow luminescing calcite (B) and orange luminescing calciorhodochrosite (C) showing clear colloidal texture. Orange luminescing calcite colloidal cycles within structure suggest primary origin; sample 958-39; under 20 kv, 200 UA and 14.75 seconds; the scale bar equals 0.5 mm.

Fig. 26: The CL photograph shows the same features as Fig. 25; however, the difference is that orange luminescing intraclasts [e.g. bivalve (A) and foraminifera (B & C)]; calcite replaces braunite colloids (D); some intraclasts occur as colloidal nuclei of braunite (E); sample 958-63; under 20 kv, 200 UA and 12.97 seconds; the scale bar equals 0.5 mm.

Plate 4.6



carbonates depends largely on the presence of the amount of manganese in carbonate mineral lattices.

What appear to be braunite algal balls cemented by calcite are abundant in the Dounan Mn deposits (Plate 4.6, Fig. 23). Although there are no published reports of cathodoluminescence in braunite for comparison, the large difference in Mn-content between brown and black luminescent algal balls probably represents both primary and early diagenetic environments. Adams and Schofield (1983) reported cathodoluminescent magnesian calcite cements from a water depth of 8 m in mixed siliciclastic/carbonate gravels in the temperate water adjacent to the island of Islay in southern Scotland. Another example from Dounan mixed siliciclastic/carbonate ore provides obvious evidence of diagenetic replacement between braunite and orange luminescent Mn-calcite (Plate 4.6, Fig. 24). This is strongly supported by the discontinuous concentric laminae of braunite and the near-nucleus, intense-red luminescing calciorhodochrosite rim, which likely represents replacement by braunite of yellow luminescing calcite. Commonly, recrystallization of primary colloidal braunite led to orange luminescing concentric colloidal Mn-calcite zones (plate 4.6, Figs. 25 and 26). Despite a lack of obvious replacement or recrystallization, the calciorhodochrosite, including matrix, still exhibits orange cathodoluminescence. However, braunite colloids in biogenic carbonates (e.g. foraminifera and bivalves) are apparently replaced by orange luminescing Mn-calcite (Plate 4.6, Fig. 26). The observation of uniform bright-orange cathodoluminescence in biological carbonate is probably a good indicator of recrystallization (Glover, 1977), or is probably a result of the carbonates having had more opportunities to encounter low-Eh nonmarine carbonate-saturated diagenetic environments, which are environments in which cathodoluminescence is commonly produced (Major, 1991).

Commonly, Dounan Mn carbonates show different types of growth zoning patterns in relation to growth interfaces. The latter separate the growing crystal or oolite / pisolite from either an aqueous solution or another solid phase. Primary manganocalcite spherulites are concentrically enclosed by secondary enrichment zones (Plate 4.7, Fig. 27). Similarly, concentric zoning in a calciorhodochrosite oolite shows varying CL intensity (Plate 4.7, Fig. 28), which reflects different generations, i.e. primary and secondary enrichment zones. Zoning is one of the most distinctive features that is commonly observed in petrographic studies of minerals, and also records a wealth of information regarding the conditions and environments in which it formed, thus zoning is an especially important aspect because it reflects either changing growth conditions or variations in growth mechanism (cf. Veizer, 1983). The concentric zoning in carbonate grains is also clearly revealed in CL micrographs though it is not seen in plane polarized light photomicrographs (Plate 4.7, Figs. 29a-b). Manganese composition shows an increasing trend from inner to outer zones, and the braunite surrounding the grain is highly enriched in manganese, which, given the replacement textures observed, suggests an evolution from primary sedimentary to early and late diagenetic stages. Concentric zoning probably results from changing fluid properties, and it can be exactly defined where compositional changes are abrupt or discontinuous (Reeder, 1991).

Plate 4.7 CL photographs of Dounan Mn carbonates and oxides, with composition analysis by EMPA.

Fig. 27: Light orange luminescence in small Mn-bearing calcite ball (A) (EMPA analysis gave 9.8% Mn) indicates primary origin, but orange luminescence in Mn-calcite (EMPA analysis gave 16% Mn) which surround the former (A) suggests secondary enrichment (B). Yellow luminescence (calcite) mostly constitutes the nuclei of oololiths of both minerals (C). Dark mineral is braunite (D) replaced by calciorhodochrosite of red luminescence (E). Blue luminescing minerals are very pure calcite. Sample 958-142; under 20 kv, 200 UA and 6.31 seconds; the scale bar equals 0.1 mm.

Fig. 28: Concentric zoning in a calciorhodochrosite oololith. The overall difference in CL intensity of the two concentric zones represents different generations. The light orange luminescing inner zone (A) indicates primary origin (EMPA analysis gave 30% Mn); whereas red luminescing external zone (B) suggests secondary enrichment (EMPA analysis gave 43% Mn). Yellow is calcite nucleus. Sample 958-143; under 20 kv, 200 UA and 0.78 seconds; the scale bar equals 0.5 mm.

Fig. 29a: Plane polarized light photomicrograph from sample 958-43 Mn oxide ore, illustrating the obscure nature of carbonate pellet (A) in braunite (B) (black) ore; the scale bar equals 0.1 mm.

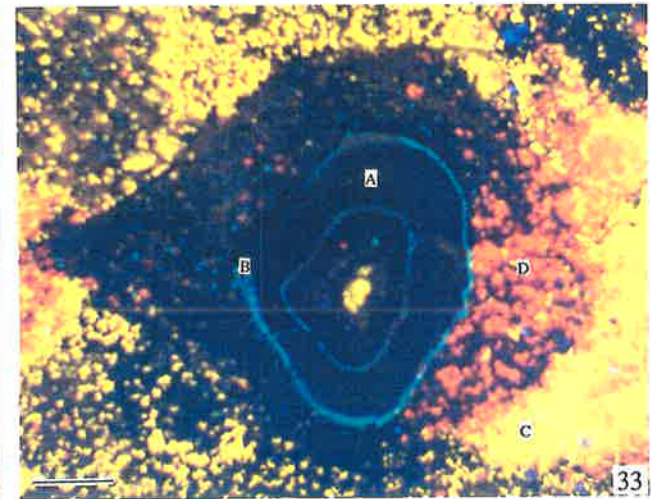
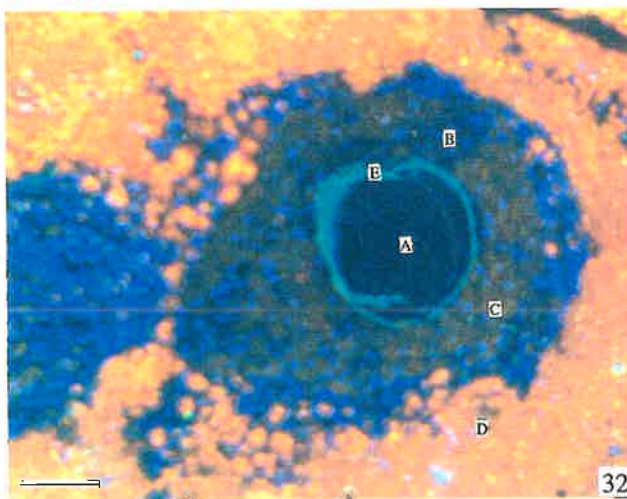
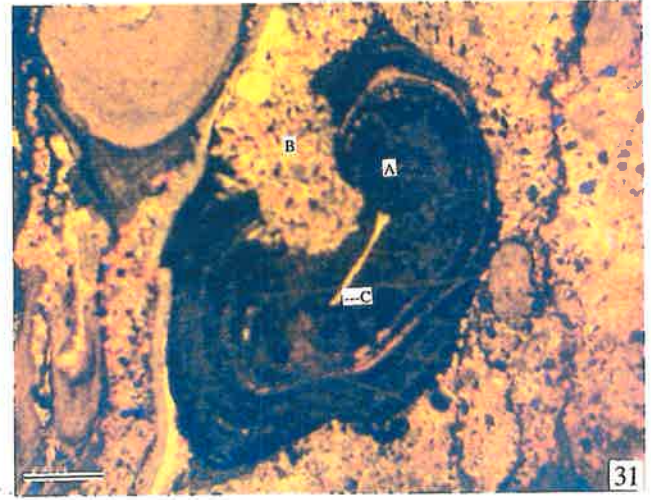
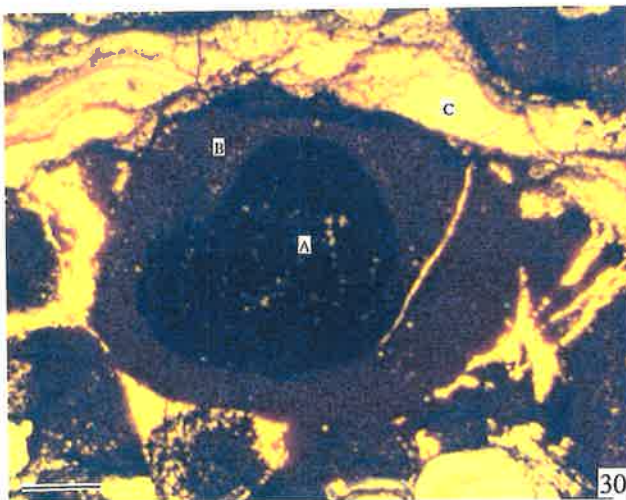
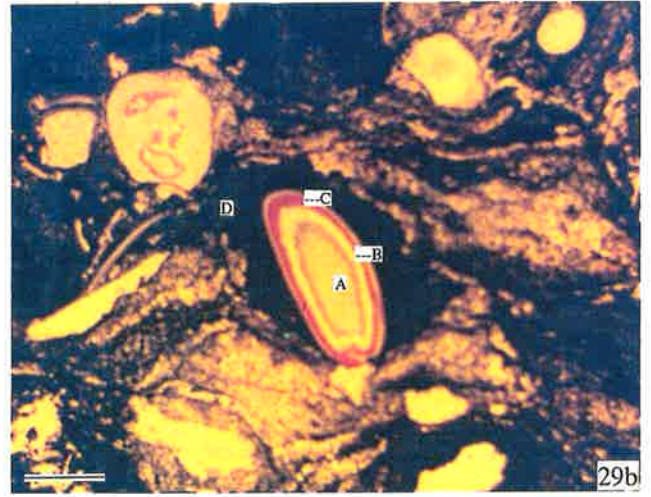
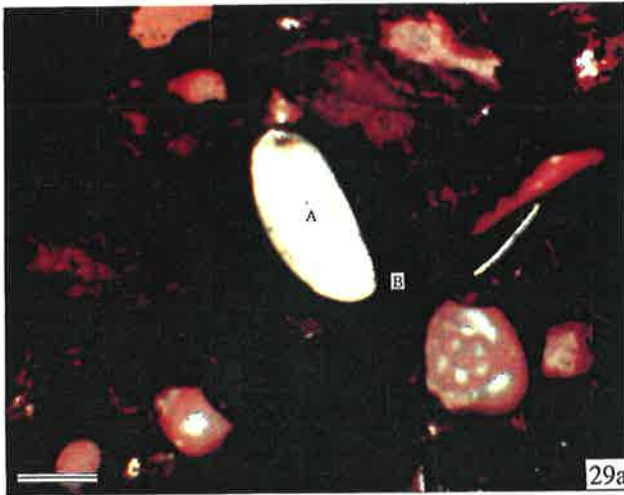
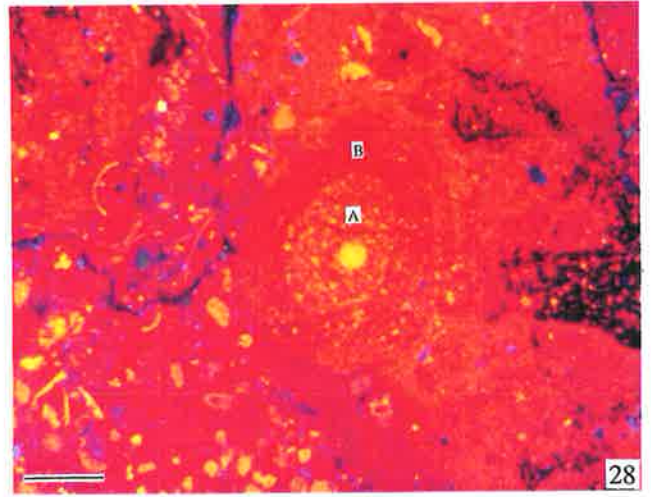
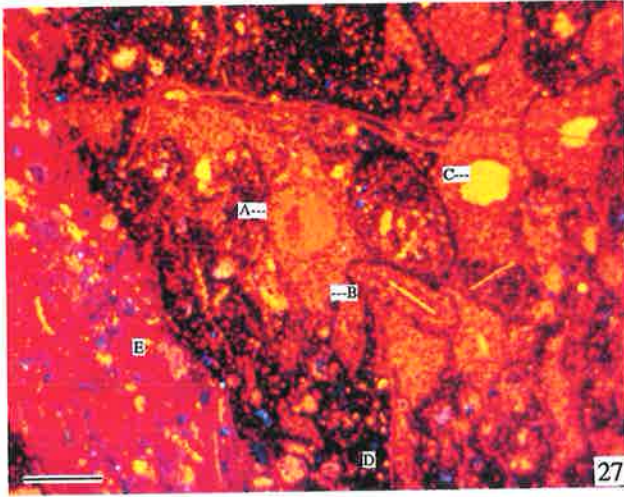
Fig. 29b: CL micrograph of same field of view (but reversed) as Fig. 29a, illustrating clear concentric zoning in carbonate pellet. The dull yellow luminescing nucleus is Mn-calcite (A) (EMPA analysis gave 17% Mn); yellow luminescing zone surrounding the nucleus is calcite (B) which probably represents early diagenesis; red luminescing zone contains 41% Mn (by EMPA analysis), and might represent late diagenetic calciorhodochrosite (C). Black mineral is braunite (D). With 20 kv, 200 UA and 5.44 seconds; the scale bar equals 0.1 mm.

Fig. 30: Concentric zoning in a braunite pisolith. Black braunite pisolith (A) (EMPA analysis gave 57% Mn) is surrounded and replaced by brown luminescing braunite (B) (EMPA analysis gave 36% Mn). Pisoliths are cemented by yellow luminescent calcite (C) which appears to replace primary braunite, leading to secondary braunite (B). Sample 958-50; under 20 kv, 200 UA and 11.15 seconds; the scale bar equals 2 mm.

Fig. 31: Concentric braunite pisolith (A) (blackcolour) was replaced by yellow luminescent calcite (B). Notice that the shape of pisolith followed detrital calcite nuclei (C), which indicates that braunite pisolith is of primary sedimentary origin. Sample 958-42 ; under 20 kv, 200 UA and 11.25 seconds; the scale bar equals 3.5 mm.

Fig. 32: Concentric braunite (A) (dark blue) and pure calcite (B) (blue) laminae in a pisolith replaced by dull yellow luminescent Mn-bearing calcite (C) and then replaced again by orange luminescent Mn-calcite (D) (matrix). Calcite with over 500 ppm Tb shows very distinctive green colour (E) (Machel, et al., 1991). Sample 958-143; under 20 kv, 200 UA and 21.14 seconds; the bar equals 3.5 mm.

Fig. 33: Concentricly laminated (dark blue) braunite (A) and very pure calcite (B) (green) pisolith replaced by yellow luminescing calcite (C) (EMPA analysis gave 1% Mn), which led to formation of orange luminescent Mn-calcite (D) (EMPA analysis gave 15% Mn). sample 958-205; under 20 kv, 200 UA and 31.14 seconds; the bar equals 3.5 mm.



Some Dounan braunite grains show not only concentric zoning but also replacement between the zones (Plate 4.7, Fig. 30). As with many carbonate cements, the textural evidence suggests these are true growth zones. Zonal fabrics in carbonates and braunite certainly provide useful information about the history and type of grain growth, but there still remain enormous problems regarding the geological interpretation that can be placed on such fabrics. Despite this, application of cathodoluminescence to the Dounan Mn deposits at least provides important new information on both primary and diagenetic processes. Concentric braunite pisoliths replaced by carbonate matrix not only indicate the presence of primary braunite (Plate 4.7, Fig. 31) but also suggest more than one generation of replacement (Plate 4.7, Figs. 32 and 33). A wide variety of authigenic minerals occur as cement and as replacements of other minerals in most sedimentary rocks, and for spectroscopic techniques to be successfully applied to these minerals, it is necessary to be able to collect a spectrum from not only an individual mineral type, but also an individual generation (successive generations may have precipitated under different conditions and therefore have different lattice configurations or chemical compositions - their CL characteristics may thus also be different). Additionally, in some cases, each generation may exhibit internal growth zonation, and each individual zone ideally merits study (Reeder, 1991). Unfortunately, the authigenic minerals tend to be rather small, typically of the order of a few tens of microns in size, and in the case of individual growth zones, often considerably smaller. However, cathodoluminescence study of authigenic mineral groups can provide important genetic information.

4.3.4 *Scanning Electron Microscopy (SEM)*

In the descriptions above, results of the polarizing and cathodoluminescence microscopic studies of Mn oxide and carbonate ores in the Dounan area have revealed a number of structures which could reflect various genetic types. Further, scanning electron microscopy carried out on fractured or polished sections of Dounan Mn oololiths/pisoliths, revealed other interesting structures which may also be of various origins. Particularly, many microstructures, which not seen clearly by other means, can be observed in SEM, such as the relationship between concentric laminae in Mn oololiths/pisoliths, the features of biogenic spheroids, and recrystallization of the manganese minerals. The following observations indicate that the oololiths and pisoliths supplement previous examinations of thin and polished surfaces by optical and CL techniques:

1) The oololiths and pisoliths are composed of concentric laminae of primary colloform or cryptocrystalline braunite and Mn carbonate minerals, and the different concentric laminae show synsedimentary paragenetic relationships as indicated in Plate 4.8, Figs. 34a-b. The structures originated in undoubted sedimentary rocks, and more specifically, in shallow marine environments.

Plate 4.8 Scanning electron micrographs of Dounan Mn oxide and carbonate ores.

Fig. 34a: SEM micrograph of fractured section showing primary colloform braunite (light colour) in concentric laminae of Mn oxide in pisolith; dark colour: cryptocrystalline Mn-calcite; Gake area; sample 958-62.

Fig. 34b: SEM micrograph of fractured section showing cryptocrystalline calciorhodochrosite in concentric laminae of Mn carbonate in pisolith; light colour: braunite; Gake area; sample 958-45.

Fig. 34c: SEM micrograph of fractured section showing concentric laminae of Mn oxide in collocrystalline braunite (light coloured laminae) with Mn-calcite (dark coloured laminae) in pisolith; the braunite seems to crystallize into Mn carbonate laminae; Baigu area; sample 958-170.

Fig. 34d: SEM micrograph of fractured section showing microcrystalline (octahedron) braunite (coarse grains) with Mn-calcite (fine grains) in concentric laminae of Mn oxide in pisolith; Gake area; sample 958-50.

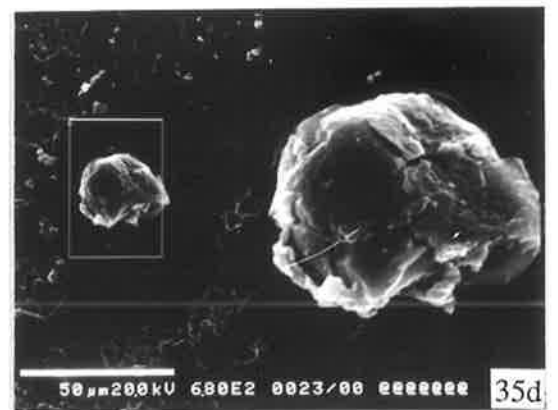
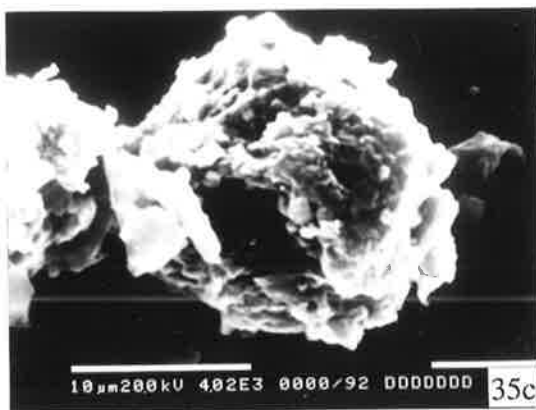
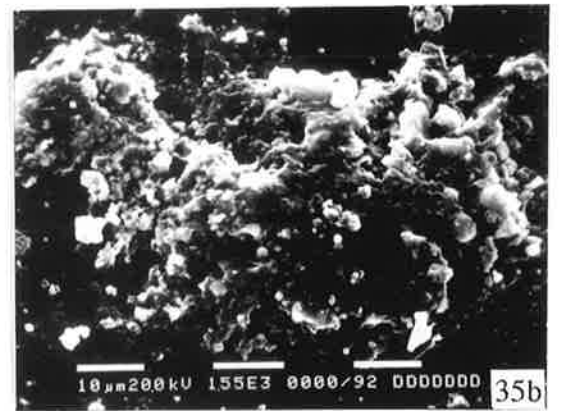
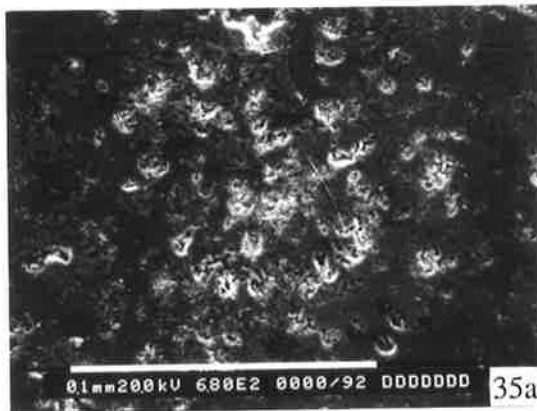
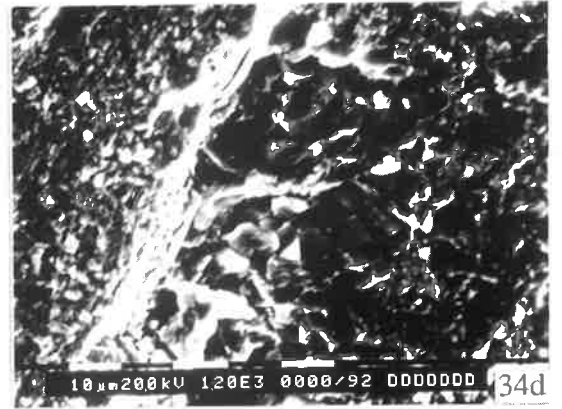
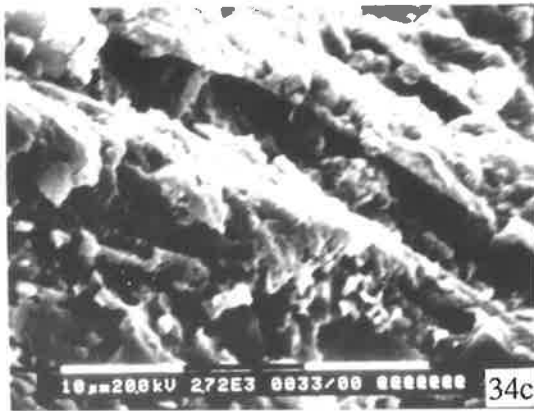
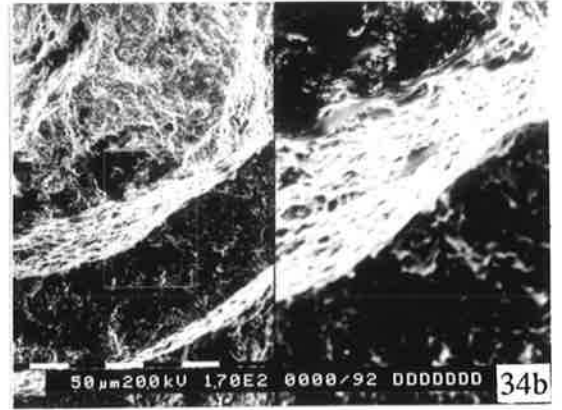
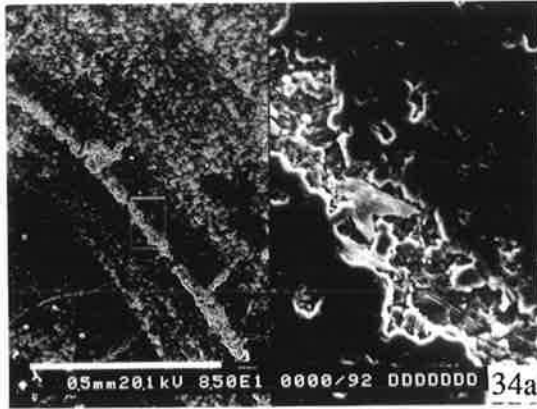
Fig. 35a: SEM micrograph of fractured section showing recrystallized braunite spheroids (light colour) in black Mn carbonates, suspected to be biogenic; Baigu area; sample 958-204.

Fig. 35b: SEM micrograph of fractured section in an enlarged area of Fig. 35a, showing cryptocrystalline braunite spheroids (light colour) suspected to be biogenic algae balls.

Fig. 35c: SEM micrograph of fractured section showing microcrystalline braunite spheroids; some grains on the surface showing octahedral shape; Gake area; sample 958-38.

Fig. 35d: SEM micrograph of fractured section showing braunite spheroid, suspected to be biogenic, in dark Mn carbonate ore, probably biogenic oncolite; Baigu area; sample 958-142.

Plate 4.8



2) Some oololiths and pisoliths show collocrystallized concentric laminae composed of braunite and Mn carbonate minerals, but the braunite seems to collocrystallize into Mn carbonate laminae, as shown in Plate 4.8, Fig. 34c. This suggests that the structure is metasynsedimentary and that enclosing rocks are early diagenetic.

3) Some oololiths and pisoliths exhibit microcrystallized concentric laminae texture consisting of relatively coarse (octahedral) braunite and fine Mn carbonate minerals, but with an obvious replacing trend between the two concentric laminae (Plate 4.8, Fig. 34d). This is suspected to have formed during diagenetic transition from colloform to cryptocrystalline, then to microcrystalline textures.

4) Braunite spheroids (Plate 4.8, Figs. 35a-b) abound in manganese oolites/pisolites in the Dounan area. These spheroids occasionally show an advanced state of recrystallization (Plate 4.8, Figs. 35c-d). It is not difficult to see how the biogenic cryptocrystalline spheroids changed into microcrystalline texture during diagenesis.

5) Calciorhodochrosite spheroids or oncolite microstructures show typically radial texture (Plate 4.9, 35e), which indicates a typical diagenetic process.

6) The deformed concentric laminae structures in the deformed manganese oololiths and pisoliths most commonly appear as collocrystallizing braunite and cryptocrystalline Mn carbonate minerals as shown in Plate 4.9, Figs. 36a-b. The crystallizing trend probably resulted from diagenetic piezocrystallization, during an advanced state of recrystallization which obliterated the concentric laminae in deformed oolith/pisolith (Plate 4.9, Fig. 36c).

7) The well-crystallized Mn-calcite also shows an advanced state of recrystallization on the surface (Plate 4.9, Fig. 37), suspected to be diagenetic.

8) As an undoubted diagenetic product, the well-crystallized massive manganese oxide oolites/pisolites commonly show a microstructure of polycrystalline braunite (Plate 4.9, Fig. 38). The relatively coarse grain size, often greater than 10 μ m, suggests recrystallization.

9) The well-microcrystallized calciorhodochrosite between concentric laminae in pisoliths (Plate 4.9, Fig. 39) also suggests a post-depositional event.

10) The well-microcrystallized (octahedron) braunite (Plate 4.9, Fig. 40) commonly occurs in massive Mn oxide oolite/pisolite in which the concentric laminae have mostly disappeared. This is suspected to be the result of early diagenetic processes.

4.3.5 Discussion

Plate 4.9 Scanning electron micrographs of Dounan Mn oxide and carbonate ores.

Fig. 35e: SEM micrograph of fractured section of calciorhodochrosite spheroids (or oncoliths ?), probably primary and diagenetic; Baigu area; sample 958-205.

Fig. 36a: SEM micrograph of fractured section showing colloform braunite spherulith and collocrystalline texture (light outer cycle) in black Mn carbonates; probably primary; Gake area; sample 958-41.

Fig. 36b: SEM micrograph of polished section showing primary colloform or cryptocrystalline braunite (light colour) and Mn-calcite (dark colour) in concentric laminae of Mn oxide in deformed pisolith; Gake area; sample 958-43.

Fig. 36c: SEM micrograph of fractured section showing microcrystalline braunite (light colour) in dark Mn carbonates in tapering concentric laminae deformed pisolith, probably diagenetic; Gake area; sample 958-47.

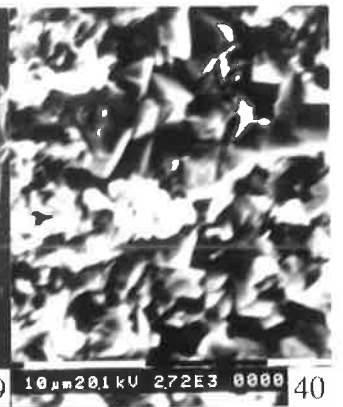
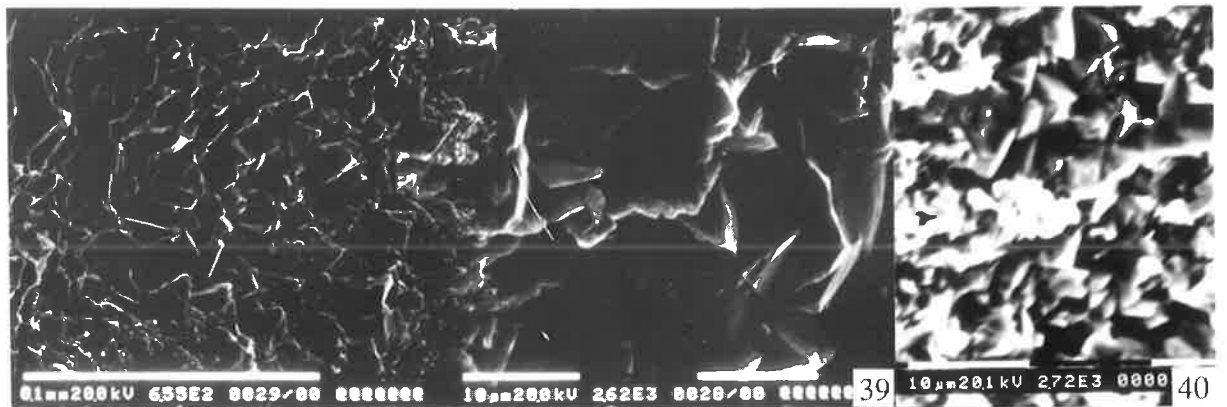
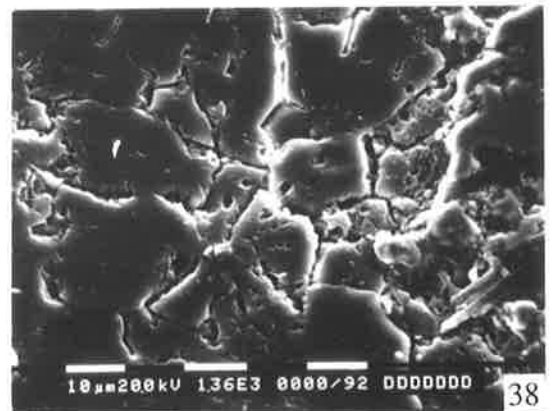
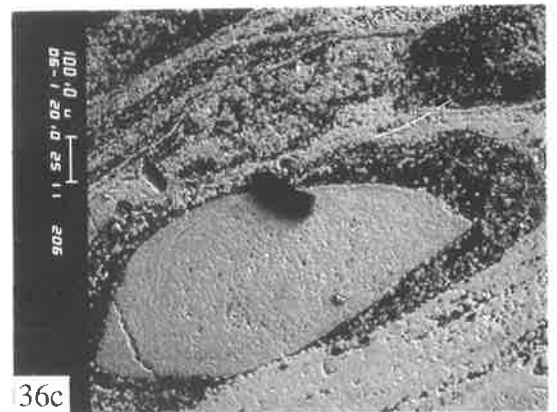
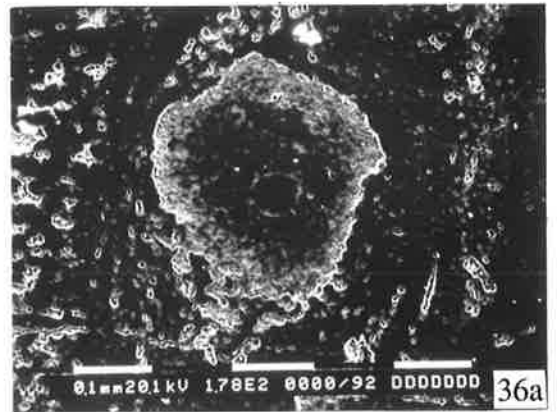
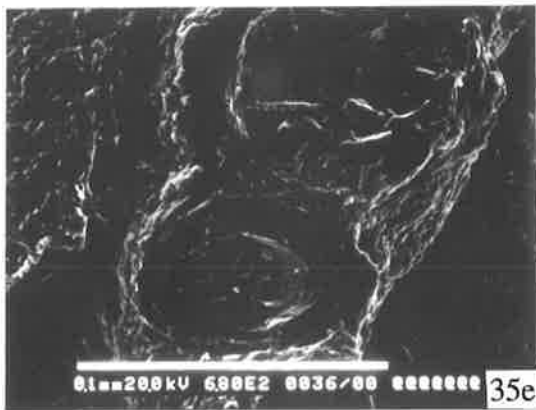
Fig. 37: SEM micrograph of fractured section showing Mn-calcite crystal in Mn carbonate; probably recrystallized during diagenesis; Gake area; sample 958-236.

Fig. 38: SEM micrograph of polished section showing polycrystalline, recrystallized braunite; Gake area; sample 958-48.

Fig. 39: SEM micrograph of fractured section showing well-microcrystallized calciorhodochrosite; Baigu area; sample 958-144.

Fig. 40: SEM micrograph of fractured section showing microcrystalline octahedral-like braunite from massive Mn oxide ore; Gake area; sample 958-50.

Plate 4.9



The fabric study of the Dounan ores discussed above, yields a generalised picture of the behavior of the manganese oxide and carbonate minerals under varying sedimentary and diagenetic conditions. Examination of the Dounan manganese oxide and carbonate oololiths/ pisoliths by conventional macro- or microscopic methods but also by CL, optical and scanning electron microscopy of thin or polished and fractured sections, satisfy the synsedimentary, metasynsedimentary (early diagenetic) and diagenetic interpretation. In summary, braunite is universally present in manganese ores of all mine-areas, from synsedimentary to diagenetic stages. Concentric laminations of manganese oxide and carbonate oololiths/pisololiths are characteristic both in macro- and microscale, and contacts of the laminae are generally sharp except where replacement and admixture of the components occur. The Mn-oxide or Mn-carbonate inter-laminations are often obscured by recrystallization. The manganese oxide and carbonate laminae generally demonstrate collo- to crypto- to micro-crystalline fabrics consisting dominantly of braunite, calciorhodochrosite and Mn-calcite. These manganese minerals also constitute macro- (> 1mm size) or micro- (< 1mm size) oncolites or spheruliths of spherical to elliptical shape, with or without nuclei. The spheruliths lack concentric layering and are restricted to specific Mn oxide or carbonate beds. Commonly, these manganese minerals, constituting the oololiths/ pisoliths, spheruliths or oncolites, retain evidence of diagenetic recrystallization and replacement. In the initial stage of recrystallization, aggregates show an obvious crystallizing evolution from collocrystalline to crypto- to microcrystalline textures.

In the final stage of recrystallization the outer form and the interlaminations of the grains are obliterated and very fine but discrete grains of braunite, calciorhodochrosite, Mn-calcite, etc. have evolved. These latter minerals were also transformed to other generations of manganese oxide or carbonate phases by replacement during diagenesis. The evidence of conversion from one mineral to another is mostly retained frozen in the ores. Commonly, such conversion started from the core, periphery and crystallographic planes of the pre-existing phases. In many samples, grains of ore or gangue minerals are observed to be partially or totally transformed to others. Relatively coarse grains of braunite or Mn carbonate minerals generally formed along the contacts of concentric laminae of crypto- and micro-crystalline braunite or Mn carbonate minerals and they also occur as euhedral crystals in sharp contact with calcite gangue. Minor manganite commonly shows conversion to braunite by further reaction with available silica. The conversion generally occurs along the grain margins or on crystallographic planes. The ores show only local restricted supergene alteration, as demonstrated by minor (only 3% of total reserves of the Dounan ores) oxidation of braunite and Mn carbonate minerals to psilomelane or pyrolusite and only local development of nsutite.

The manganese ore horizons in the Dounan sequence are comfortably enclosed in unaltered sedimentary rocks; this relationship eliminates the possibility of metamorphic and supergene origins for the Dounan Mn oxides and carbonates. Similarly, typical synsedimentary fabrics such as extremely fine concentric laminations composed of braunite and Mn carbonate minerals

laminae, collo- crypto- micro-crystalline grain size, oolites and pisolites as well as spherulites (including oncolites), fine laminations (or wavy laminations), and normal or inverse gradings, all indicate a synsedimentary origin for these ores in the mixed deposition of clastic and intraclastic carbonate rocks. In addition, the fragmental and brecciated fabrics also show synsedimentary features. In the total absence in the ores of recrystallization, metamorphism and replacement due to hydrothermal activity, all the ores could only be of synsedimentary origin. Furthermore, some typical diagenetic fabrics such as euhedral to subhedral recrystallized grains from colloform minerals, deformed oolites and pisolites with recrystallization, sutured and deformed bedding structures, and various replacement structures, all suggest diagenetic alteration. Significantly, the spherulitic texture with enlarged recrystallized margins indicates an important evolution from sedimentary to diagenetic processes.

Besides $< 100 \mu$ spheroids or oncolites of braunite or Mn carbonate minerals, there are other smaller $< 10 \mu$ micro-spheroids or larger $> 400 \mu$ spheroids or oncolites, all suspected to be sedimentary in origin. The colloform or cryptocrystalline or extremely fine microcrystalline grains generally occur in the central part of the spheroid or oncolite, whereas relatively coarse euhedral crystals commonly occur in the outer parts of the spheroids due to recrystallization, again indicating an evolution from sedimentation to diagenesis. In stable thermodynamical conditions, a crystal composed of the same material possesses minimal internal energy compared with an amorphous body (Jin and Li, 1981). Thus, the amorphous body exists in an unstable state and inclines to conversion to the crystal form. The evidence of conversion from collo- to crypto- and to microcrystalline grains is very abundantly distributed in the Dounan Mn deposits, and the equilibrium texture of recrystallization can be demonstrated by the equigranular cyclopean braunite crystals with $\sim 120^\circ$ crystallographic angles (Plate 4.9, Fig. 38). Although the supergene ores show some typical supergene (e.g. reniform, cellular and earthy) structures, it is not difficult to find a number of relic primary sedimentary fabrics in the supergene ores.

4.4 Mineralogy

The manganese ores of the areas mentioned in the previous chapters do not vary very widely in their physical and chemical characters. Generally, the primary ores are colloform or cryptocrystalline or extremely fine grained, whereas diagenetic products show pronounced relict primary sedimentary textures or structures and are recrystallized into fine to medium grained ores. Below, bulk samples representative for the various ore and rock types are analyzed by X-Ray Diffraction (XRD) to determine the dominant mineralogy of the samples. The patterns illustrated are chosen as typical from some 50 spectra and provide information on the full range of ore/rock types in the deposits.

Table 4.4a Observed d-spacings (Å) and intensity (I) of X-Ray powder analysis from Dounan manganese ores (modified after Zhang et al., 1979).

Braunite				Ca-rhodochrosite				Manganite				Hausmannite			
Dounan		A•S•T•M		Dounan		A•S•T•M		Dounan		A•S•T•M		Dounan		A•S•T•M	
d	I	d	I	d	I	d	I	d	I	d	I	d	I	d	I
		4.65	5	4.25	5			3.40	100	3.40	100	4.85	40	4.86	70
3.45	20	3.46	10	3.70	20			2.63	40	2.63	60	3.30	20		
		3.33	5	3.35	40			2.53	20	2.53	40	3.05	50	3.05	50
		2.96	5	3.02	40			2.41	60	2.41	70	2.88	10	2.87	20
2.71	100	2.69	100	2.90	100	2.95	100	2.27	30	2.26	40	2.73	80	2.74	90
2.35	30	2.34	20	2.41	30	2.40	30	2.19	30			2.47	100	2.47	100
1.87	10	1.87	5	2.26	10			1.78	40	1.77	50	2.35	10	2.34	50
1.82	10	1.82	5	2.20	50			1.71	40	1.71	40	2.03	20	2.02	60
		1.80	5	2.09	10			1.67	70	1.68	70			1.812	10
1.75	10	1.76	5	2.02	30	2.04	40	1.64	10	1.64	20	1.79	20	1.779	50
1.65	70	1.65	70	1.92	10			1.50	20	1.50	40	1.70	10	1.689	20
1.53	20	1.53	10	1.87	10	1.85	80	1.44	20	1.44	40			1.629	15
1.50	20	1.50	10	1.81	60	1.81	70					1.57	30	1.571	60
1.46	20	1.46	10	1.57	5							1.54	70	1.537	80
1.42	50	1.42	30	1.55	30	1.56	40					1.46	10	1.462	10
1.37	5	1.37	5	1.47	10	1.48	40					1.44	20	1.434	50
1.35	20	1.35	10	1.39	10	1.40	40							1.405	10
		1.27	5			1.37	5							1.378	10
1.17	10	1.17	5	1.30	3	1.30	10							1.340	20
1.16	10	1.15	5	1.25	10	1.25	30							1.323	30
1.08	30	1.08	20											1.238	10
1.05	20	1.05	10												

* A•S•T•M - standard section of minerals.

The lattice dimensions of many manganese minerals, especially manganese oxides, can vary considerably, depending on substitution effects altering the cell structure. Therefore, analyses of the samples were mainly based on mineralogical studies from Dounan Mn deposits to guarantee sample compatibility (Zhang, et al., 1979; Liu, et al., 1984). In some cases, it was necessary to use additional mineral data such as microscopy, chemical analyses and electron microprobe analyses of minerals for the interpretation of mineral descriptions, because some spectra of the present study did not match with results of the previous study (Liu, et al., 1984). The d-spacings and identity of some Mn minerals are listed in Table 4.4.

4.4.1 X-Ray Diffraction (XRD)

The X-ray diffraction patterns of the most common ores, which are mostly of primary origin, together with some ores strongly overprinted by diagenetic processes (e.g. compact massive or deformed Mn oxide oolites/pisolites) are illustrated in Figure 4.1a. The following figures show

Table 4.4b: Observed d-spacings (Å) of X-Ray diffraction (XRD) patterns from Dounan Mn ores and associated rocks (see Figs. 4.6 a-c.).

Braunite	Manganite	Calciorhodochrosite	(Mn-) calcite	Dolomite	Quartz	Feldspar	Mica
4.71						6.49	10.32 5.07 4.54
			3.86	4.07	4.31 4.26	4.06 3.80	
3.50	3.42	3.69		3.71 3.69		3.71	
			3.03 2.96		3.37 3.34		3.37
			2.90 2.86	2.93 2.92		3.21	
2.73		2.88 2.85				2.73 2.66	
	2.65			2.58			2.61
	2.53		2.50				
	2.42				2.46		
		2.41 2.40	2.40				
2.36			2.28 2.24				
	2.28						
	2.21	2.22		2.21 2.19			
2.15		2.18				2.13	
		2.04 2.01	2.09		2.03		
			1.91 1.88 1.87			1.99	
1.88							
1.82		1.83	1.82			1.82	
	1.78			1.81			
1.75		1.77					
	1.71 1.67					1.67	
1.66			1.62 1.60				
		1.55					
1.54				1.54		1.54	
1.50	1.50		1.52				

the patterns of Mn carbonate and unsorted or banded ores (Figs. 4.1b). Additionally, some of these primary (or diagenetic) products are examined in the final plot (Fig. 4.1c) of this section to investigate the mineralogy of the gangue minerals. The d-spacings of the diffractograms are listed in Table 4.4.

Mn oxide oolite/pisolite and compact massive oolite/pisolite are shown first because the samples are almost monomineralic (Fig. 4.1a). Only small quantities of calciorhodochrosite or Ca-calcite are detected in addition to the high braunite contents. For this reason, the XRD-trace can be used for comparison with other ore samples. Similarly, Mn oxide deformed oolite/pisolite contains insignificant amounts of Mn carbonate minerals, together with abundant braunite. The XRD-patterns of the Mn oxide deformed oolite/pisolite closely resemble the diagrams of Mn oxide oolite/pisolite, and in the field, the former type is found mostly within the units of the latter; the mineralogical similarities are therefore not surprising. However, the deformed type exhibits small amounts of gangue minerals such as quartz and feldspar, which are lacking in Mn oxide oolite/pisolite. Some of this ore sampled from the same geological sections possesses minor Mn carbonate minerals such as calciorhodochrosite. The gangue minerals exist as the matrix between the grains.

In the diffractograms of some Mn oxide oolite/pisolite, manganite gains importance although braunite is still the dominant mineral, and calcite appears in small amounts; with the exception of a very small calciorhodochrosite peak no other ore and gangue minerals can be identified. Mn oxide oolite/pisolite is less well-crystallized than the massive Mn oolite/pisolite; the major peaks of braunite are relatively smaller and quartz or feldspar peaks are lacking in both ore types. The massive Mn oxide oolite/pisolite exhibits similar, but still relatively low Ca-rhodochrosite, Mn-calcite or calcite concentrations. The several different peaks for the main manganite lines between 30° and 70° 2θ indicate the presence of this mineral in some Mn oxide oolites/pisolites. Moreover, when compared with the other Mn phases of this sample it is an important component, because the quantities of all manganese minerals, with the exception of braunite, are generally low while the manganite peaks are still visible.

Mn carbonate ores seem to have relatively low crystallinities compared with the Mn oxides, which is illustrated by the relatively low intensities of the reflections. Calciorhodochrosite and Mn-calcite are the main ore minerals and occasionally, braunite is of comparably high concentration, although its dominant peak sometimes overlaps with a dolomite line. The gangue minerals, such as calcite, dolomite, quartz and feldspar, all exhibit relatively small peaks; occasionally, quartz shows a stronger peak (Fig. 4.1b). The mineralogy of oolitic/pisolitic rhodochrosite ore appears to be similarly complicated as different mineral lines, such as Ca-rhodochrosite, Mn-calcite, calcite, dolomite, braunite, quartz and feldspar, can be identified (manganite appears to be lacking). Oolitic/pisolitic Mn-calcite ore, of similar paragenesis as oolitic/pisolitic calciorhodochrosite ore, also has similar mineralogical composition, but Mn-calcite dominates in the sample and more braunite peaks are recognized. Also, strong lines are

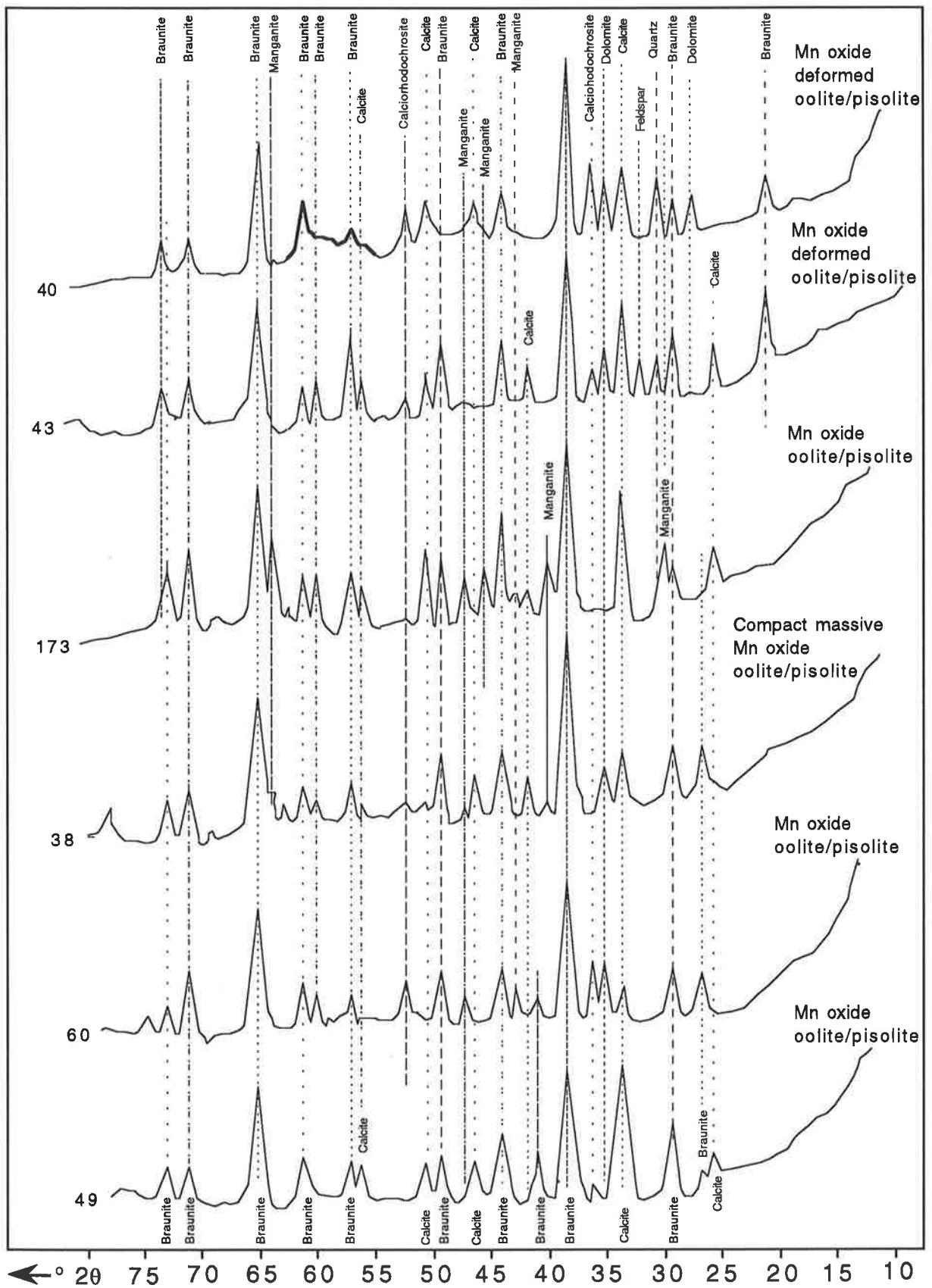


Fig. 4.1a X-ray Diffraction patterns of Mn oxide ores; sample numbers are indicated at the left of the respective spectra; all samples have the common prefix 958.

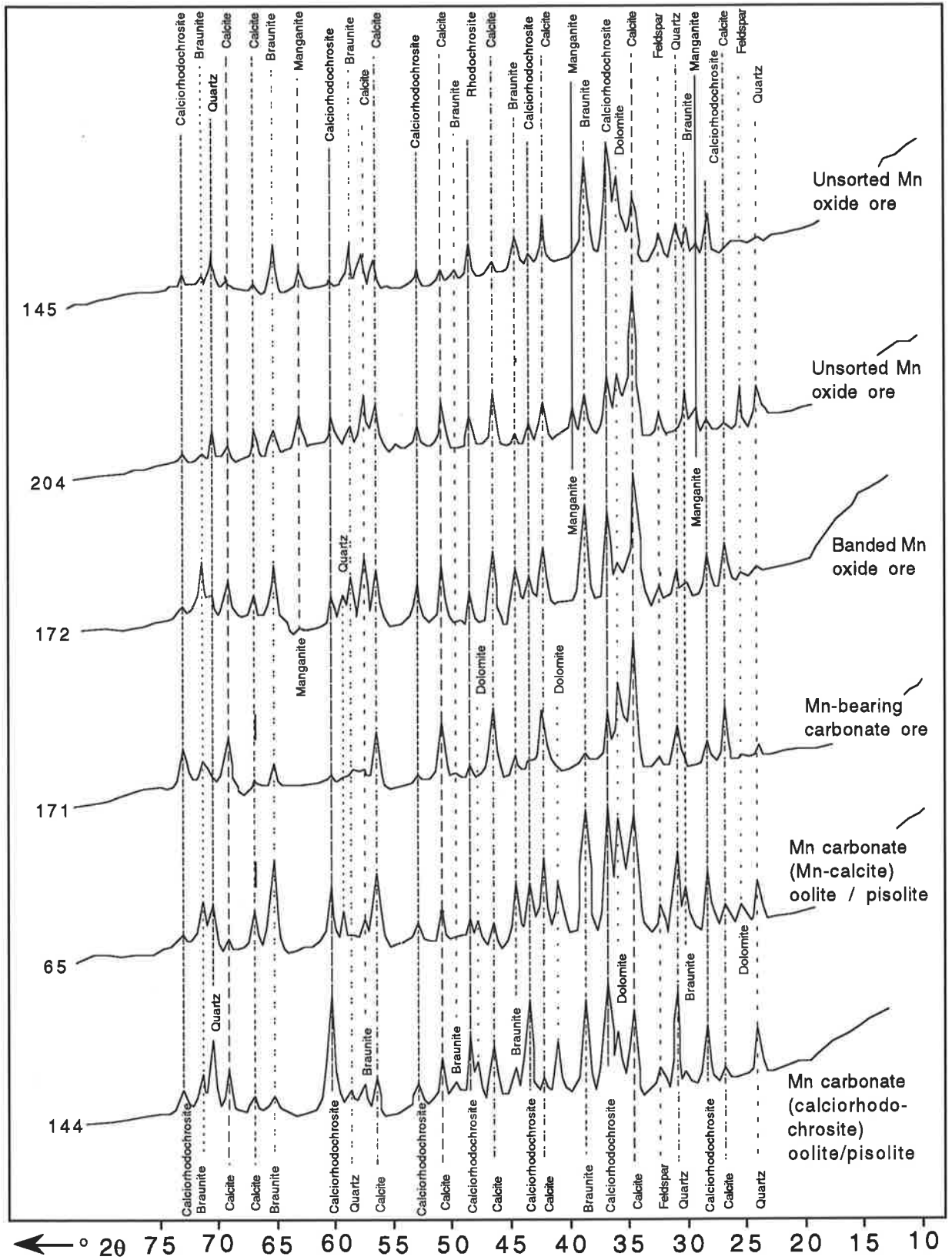


Fig. 4.1b X-ray Diffraction patterns of Mn carbonate and unsorted or banded Mn oxide ores; sample numbers are indicated at the left of the respective spectra; all samples have the common prefix 958.

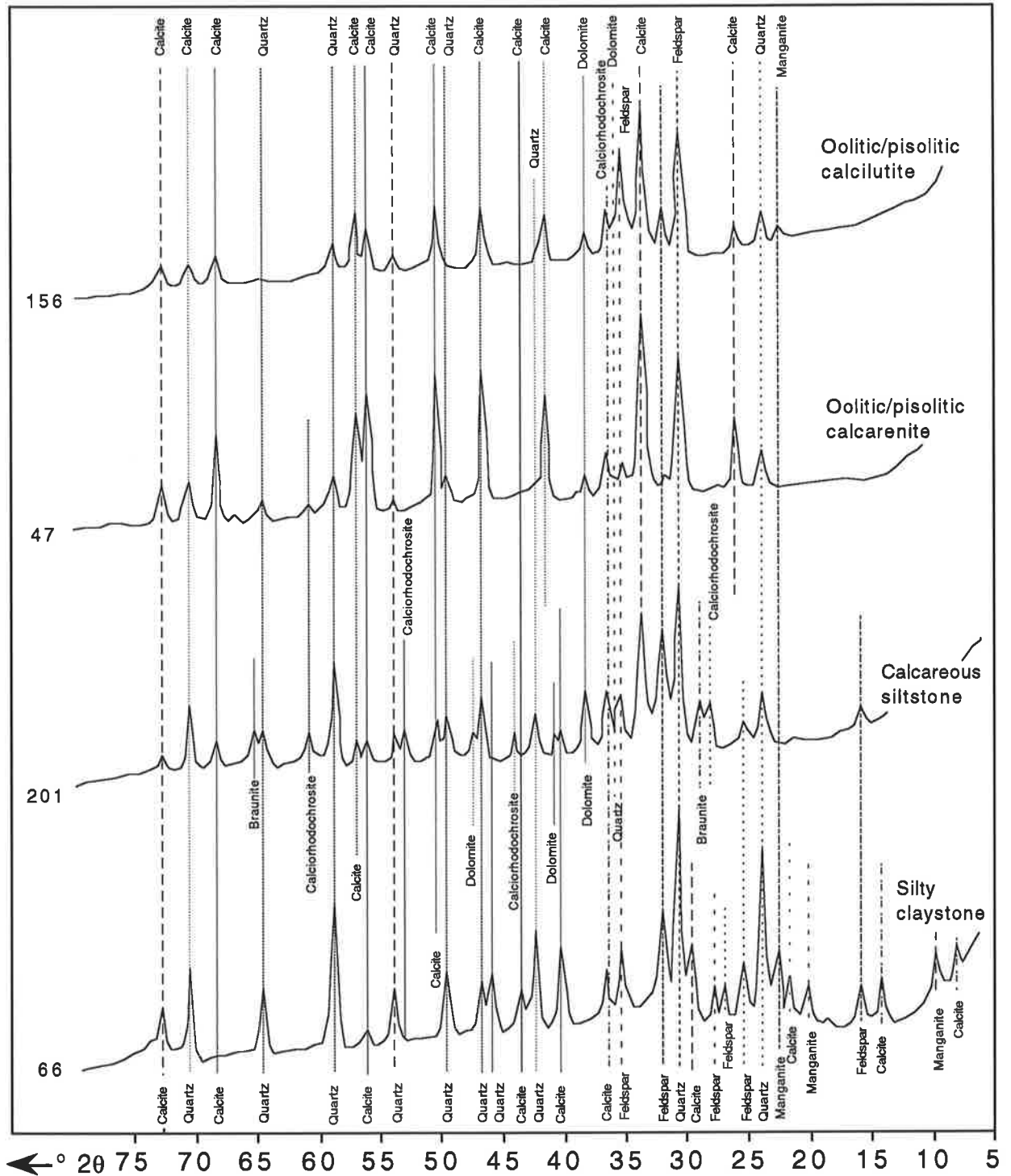


Fig. 4.1c X-ray Diffraction patterns of rocks associated with Mn ores; sample numbers are indicated at the left of the respective spectra; all samples have the common prefix 958.

observed for quartz and less important peaks show feldspar in these two ore types. These two gangue minerals generally constitute the matrix between the grains. The last example in Figure 4.1b is Mn-bearing oolitic/pisolitic carbonate ore. Though this ore type is rare, it is shown for comparison. The crystallinity of Mn carbonate is very low, calcite seems to dominate over Mn-calcite, braunite sometimes is one of the main constituents of the sample, and dolomite and quartz are of minor importance.

Transitional ore types possess comparably complex mineralogies (Fig. 4.1b), and the patterns show variable quantities of braunite, calciorhodochrosite, Mn-calcite and calcite; less abundant manganite, dolomite, quartz and feldspar are also indicated. The gangue minerals either occur within the ooliths and pisoliths or form the matrix between the grains. Depending on the ore type, one or other mineral dominates over the other phases. The structures constitute another important feature of these ore types and their close association with the sedimentary environments is reflected in their mineralogical composition. Commonly, Mn carbonate minerals constitute the matrix, whereas braunite forms the grains in the ores. Fine Mn carbonate minerals strongly color the matrix (pink) and lead to the conclusion that Mn carbonate minerals (reduction) are the dominant phase in the matrix; whereas braunite makes the grains black and indicates that Mn oxide is the main phase of grains (oxidation). The line scans reveal that these colorations are indeed due to an effect of mineralogical composition in the ores. However, in banded Mn oxide ore, black bands and pink bands individually indicate the presence of braunite and Mn carbonate minerals. Commonly, some amounts of terrigenous clastic materials such as quartz and feldspar exist in light-colored bands but these are minor in dark bands. Therefore, these mixed ore types suggest the presence of a transitional sedimentary environment between oxidation and reduction. Although in appearance the unsorted Mn oxide ore differs greatly from the banded Mn oxide ore, the mineral assemblages are comparable (although the crystallinity of braunite seems to have increased), the amounts of quartz and feldspar are similar, and only trace quantities of manganite are present.

The four main rock types associated with Mn ores are similar in their mineralogical composition (Fig. 4.1c). Quartz dominates, and feldspar and mica have higher concentrations in silty claystone, some reflections indicate small amounts of calcite, but Mn minerals cannot be found. Calcareous siltstone possesses well developed quartz lines and calcite or dolomite is also a dominant part of the rock; calciorhodochrosite and braunite are indicated by small peaks. The XRD-pattern of oolitic/pisolitic calcarenite is dominated by calcite, whereas quartz shows a number of relatively weak lines. Very weak peaks indicate the presence of dolomite, and Mn-minerals cannot be identified. The oolitic/pisolitic calcilutite exhibits calcite and quartz peaks relatively smaller than in calcarenite. Also, these two mineral lines are prominent relative to very small peaks for braunite, calciorhodochrosite and dolomite. The mineralogical composition of calcilutites is relatively simple and manganese phases are almost undetectable. Thus, calcilutite samples seem to stand out from all other ore and rock types analyzed in that they hardly contain Mn minerals. Therefore, it must be pointed out again that the relatively 'pure' rocks (e.g. siltstone

and limestone) hardly contain Mn minerals, whereas the mixed types (e.g. calcareous clayey siltstone, clayey or silty limestone) possess well developed Mn-mineral phases.

4.4.2 Description of Minerals

The mineralogy of the Dounan manganese oxides and carbonates has long been considered to be most interesting but at the same time presents a very enigmatic problem. With some superfluous names, created on the basis of inadequate data, misconceptions about the nomenclature of manganese minerals were widely prevalent for a long time. This widely conflicting nomenclature has, however, been somewhat straightened out recently and the review work done by Zhang et al (1979) and Liu et al (1984) has contributed much in this direction. The comprehensive work on individual mineral phases performed by them have clarified and systematised the nomenclature of individual mineral species to a great extent. The writer, however, still feels that the nomenclature used in this text should be clarified at the outset. Out of about twenty valid species examined in manganese and gangue (Zhang et al., 1979, and Liu et al., 1984), only about five, i.e. braunite, calciorhodochrosite, Mn-calcite, calcite and quartz, are found as main or minor minerals; others are seen in minor or trace amounts in the Dounan manganese deposits. The minerals examined in the deposits are listed in Table 4.5.

The name braunite has been used in this text on the basis of its composition $[\text{Mn}(\text{Mn}, \text{Si})\text{O}_3$ or $(\text{Mn}^{+2}_{1.0} \text{Mn}^{+4}_{0.92} \text{Si}^{+4}_{0.08})_{2.0} \cdot \text{O}_3]$ and tetragonal symmetry or orthorhombic structure (Zhang et al., 1979; Liu et al., 1984). Roy (1981) stated that natural braunite is related to α - Mn_2O_3 ("C" type cubic structure, Pauling and Shappel, 1930; revised as orthorhombic with space group *Pcab*, Geller, 1971) with partial substitution by silica in the structure of the latter. But there is controversy about the valence state of manganese in the α - Mn_2O_3 structure. Some

Table 4.5 Minerals of Dounan manganese ores

primary products				supergene products	
manganese oxides		manganese carbonates			
Mn-mineral	gangue	Mn-mineral	gangue	Mn-mineral	gangue
braunite*	quartz^	Calciorhodochrosite*	calcite#	psilomelane*	limonite^
manganite^	calcite^		quartz^	pyrolusite#	hydromica^
Calciorhodochrosite^	albite^	Mn-calcite*	albite^	nsutite#	chlorite^
Mn-calcite^	dolomite^		dolomite^	hausmannite^	
	chalcedony^	Mn-bearing calcite#	chlorite^		
Mn-bearing calcite^	pyrite^	braunite^	chalcedony^		
	mica^				
	glauconite				

* - major; # - minor; ^ - trace in individual ore type.

workers concluded that the manganese in α - Mn_2O_3 is entirely in Mn^{3+} state (e.g. Mason, 1943; Klingsberg and Roy, 1959), while others are of the opinion that it is in Mn^{2+} and Mn^{4+} states (e.g. Krishnan and Banerjee, 1939; Muan, 1959a). In the case of Dounan, the latter view has been accepted by previous workers, so that the entry of silica and Fe^{2+} with little or Fe^{3+} free in the structure of braunite is easily explained and the formula of braunite can be written as $\text{Mn}^{2+}(\text{Mn}^{4+} \text{Si}^{4+}) \text{O}_3$.

The name manganite was proposed on the basis of its composition [$\text{Mn}_2\text{O}_3 \cdot \text{H}_2\text{O}$ or $\text{Mn}(\text{OH})_2 \cdot \text{MnO}_2 \cdot \text{H}_2\text{O}$] and monoclinic symmetry; it is related to the γ - MnOOH structure (Zhang et al., 1979; Liu et al., 1984).

There is not much controversy about the minerals Mn-calcite ($\text{Mn} > 12\%$) or Mn-bearing calcite ($\text{Mn} < 12\%$), identification of which is based on its simple composition [(Ca, Mn) CO_3] and rhombohedral cell. Calciorhodochrosite, characterizing the MnCO_3 phases, on the other hand, presents certain problems. The name rhodochrosite was first suggested by the Wenshan Geological Team of Yunnan Province in the 1960s. Zhang et al (1979) and Liu et al (1984), however, later agreed to refer to the mineral calciorhodochrosite on the basis of the considerable calcium content, which varies from 5 to 28%, so that the formula can be written as [Mn, Ca] CO_3] (Liu et al., 1984).

X-ray powder patterns for primary gangue minerals (Table 4.5) were earlier reported by Zhang et al (1979) and Liu et al (1984). These two groups of workers also contributed work on the poorly crystallized supergene manganese minerals such as psilomelane, pyrolusite, nsutite and hausmannite, and there is controversy about these minerals.

In the Dounan Mn deposits, braunite is the predominant manganese mineral present, and calciorhodochrosite is the next most abundant Mn mineral. Mn-calcite or/and Mn-bearing calcite sometimes assume importance, which is considered to be a very rare example in Chinese manganese deposits (e.g. Zhang et al., 1979; Wang, 1981; Liu et al., 1984; Yue, 1985; Su, 1983). As stated above, generally, in sedimentary-diagenetic processes the Mn oxide ores are composed of braunite alone or of braunite plus Mn carbonate minerals (e.g. unsorted and banded ores) assemblage. In the diagenetic products, commonly both Mn oxide and carbonate minerals are recrystallized and assume a polycrystalline texture, and the secondary enlarging margins and replacement of grains are prevalent. The higher Mn oxidized minerals, such as psilomelane, pyrolusite and nsutite, occur only as supergene products and their preponderance varies with the degree of alteration. The specific characteristics of each of the Mn oxide and carbonate minerals present in the Dounan orebodies are discussed below, but the chemistry of the minerals (e.g. electron microprobe analysis) will be discussed in detail in Chapter 5.

4.4.2.1 BRAUNITE

As stated earlier, this mineral is the most abundant in all the orebodies of Mn oxides. In no case has braunite been found to be a supergene product in the Dounan deposits, though Hewett and Fleischer (1960) pointed out its supergene derivation in Globe, Arizona, and Patagonia. Two generations (primary and diagenetic) of braunite have been universally detected in the Dounan deposits. The braunites are generally of black color in hand specimen with a hardness value of 6 and they constitute oolites and pisoliths, or spherulites and oncolites but commonly are found in association with different materials (e.g. quartz, albite, calcite and biofragments) as nuclei. Everywhere, the first generation braunite formed earliest as oolites/pisolites or spherulites in the paragenetic sequence. In early diagenesis, the grains were deformed, elongated and dimensionally oriented parallel to the banding or layers in the ore. This braunite is generally of dark grey-brown color under the microscope, sometimes grading into lilac (in oil) and it is invaded by later minerals. The second generation braunite is much lighter brownish grey in color and is undeformed with well-developed pseudo-octahedron crystals under the scanning electron microscope. It has formed everywhere at the expense of first generation braunite, apparently through recrystallization or replacement. The two generations of braunite vary widely in size. In sedimentary and even in early diagenetic ores, it is usually extremely fine grained and the grain size increases with the evolution of sedimentation from colloform to subhedral- or euhedral-granular ($< 5 \mu - 0.01 \text{ mm}$).

Both chemical and electron microprobe analyses indicate that the Dounan braunite belongs to the normal braunite type (or braunite I), with about 10% SiO_2 , and is not braunite II, with 4.4% SiO_2 (Roy, 1981), as seen in Table 4.6 and Table V.4. Comparably, the chemistry of the Dounan braunite is similar to those of the Wafangzi Mn deposit of China (Fan, et al., 1988) and Indian syngenetic manganese deposits (Roy, 1966), but the latter two contain much more Fe_2O_3 (~5 times) than the former, which probably led to a different $\alpha\text{-Mn}_2\text{O}_3$ structure. In terms of the che-

Table 4.6 Chemical analyses of braunite from Dounan and comparison with Wafangzi Mn deposits, China.

No. (%)	MnO ₂	MnO	Mn*	Mn ₂ O ₃	Fe ₂ O ₃	Al ₂ O ₃	SiO ₂	MgO	CaO	S	P ₂ O ₅	CO ₂	total
D-46-M1 molecular number	50.10 .5763	36.91 .5204	61.12	87.01	0.83 .0052	1.15 .0113	10.14 .1688	0.84 .0208	0.00	0.03 .0009	0.027 .0009	0.14 .0032	100.17
D-60-M2 molecular number	49.52 .5679	36.61 .5161	59.81	86.13	0.90 .0056	0.67 .0066	11.03 .1836	0.87 .0216	0.12 .0021	0.00 .0000	0.01 .0005	0.42 .0095	100.15
Wafangzi molecular number	46.18 .5321	34.14 .4827	55.90	80.32	3.95 .2470	0.56 .0055	9.95 .1656	0.40 .0199	1.50 .2850		0.04 .0003	1.70 .0386	99.89

* not involved in calculation; the samples have the common prefix 958; the data of Wafangzi braunite from Fan et al (1988).

mical calculation, the formula of Dounan braunite can be written as $(\text{Mn}^{2+}_{1.0} \text{Mn}^{4+}_{0.92} \text{Si}^{4+}_{0.08})_{2.0} \text{O}_3$ or $\text{Mn}(\text{Mn}, \text{Si}) \text{O}_3$ (Liu, et al., 1984). Importantly, the X-ray scanning photographs (Plate 4.10, Figs. 41a, b and c) of the braunite show that Mn, Si and Fe elements are distributed in an overlapping manner in the mineral. Since the X-ray powder (XRD) analysis does not show spectral lines of quartz and iron minerals, Si and Fe must exist as isomorphous mixtures together with Mn in the Dounan braunite.

4.4.2.2 MANGANITE

Manganite has been detected in Dounan Mn oxides and is rarely present in braunite ooliths/pisoliths or in carbonate matrix where it occurs as crypto- and micro-crystalline grains ($< 1 \mu - 0.02 \text{ mm}$), or occasionally as acicular or columnar subhedral or euhedral grains (up to 0.36 mm). The manganite is generally light brownish grey to grey to yellow green and has internal reflection of dark-red color. All the characteristics, together with XRD analysis (Tables 4.3a and 4.3b), illustrate that Dounan manganite is very similar to the standard mineral, and the formula should be expressed as $\text{Mn}(\text{OH})_2 \cdot \text{MnO}_2 \cdot \text{H}_2\text{O}$ or $\text{Mn}_2\text{O}_3 \cdot \text{H}_2\text{O}$.

4.4.2.3 CALCIORHODOCHROSITE

In natural Mn carbonates (ideally MnCO_3), manganese is readily substituted by calcium and divalent iron, and pure MnCO_3 is very rare in nature (Huebner, 1969). A number of workers (e.g. Krieger, 1930; Wayland, 1942; Gryaznov, 1955; all cited by Deer *et al.*, 1963) suggest a complete solid solution series between calcite and rhodochrosite. Goldsmith (1959) experimentally determined the subsolidus relations for the $\text{CaCO}_3 - \text{MnCO}_3$ system and indicated the absence of natural minerals in the isomorphous series between compositions of 50 and approximately 80 mol% MnCO_3 . Thus, the entry of calcium in the structure of the Dounan rhodochrosite is easily explained and the formula of calciorhodochrosite can be written as $(\text{Mn}, \text{Ca}) \text{CO}_3$.

After braunite, calciorhodochrosite has considerable importance in the Dounan Mn ores, particularly in Mn carbonate ores, and can be found throughout the deposits. Commonly, this mineral occurs in the ooliths and pisoliths as paragenetically concentric laminae (generally together with braunite concentric laminae) or in the matrix as euhedral microcrystals in unsorted or banded and Mn carbonate ores. The handspecimen shows grey, dark-grey or dark-red colours with a grey streak. Under the microscope the mineral is generally of grey colour, and shows microcrystalline granular ($< 2 \mu - 0.03 \text{ mm}$) texture in the rhombohedral structure of the trigonal system, and with a refractive index of 1.726 ± 0.002 .

The chemical analysis (Table 4.7) of this mineral shows that it contains more CaO and SiO_2 than normal rhodochrosite. Based on the chemical and electron microprobe analysis of the

Plate 4.10 X-ray scanning photographs of Dounan Mn minerals, after Zhang et al (1979) and Liu et al (1984).

Fig. 41a: Distribution of Mn from braunite; 45 μ x 45 μ ; 16 seconds.

Fig. 41b: Distribution of Si from braunite; 45 μ x 45 μ ; 80 seconds.

Fig. 41c: Distribution of Fe from braunite; 45 μ x 45 μ ; 40 seconds.

Fig. 42a: Distribution of Mn from calciorhodochrosite; 360 μ x 360 μ ; 16 seconds.

Fig. 42b: Distribution of Ca from calciorhodochrosite; 360 μ x 360 μ ; 50 seconds.

Fig. 42c: Distribution of Fe from calciorhodochrosite; 360 μ x 360 μ ; 40 seconds.

Fig. 42d: Distribution of S from calciorhodochrosite; 360 μ x 360 μ ; 40 seconds.

Fig. 42e: Distribution of Si from calciorhodochrosite; 360 μ x 360 μ ; 80 seconds.

Fig. 42f: Distribution of Mg from calciorhodochrosite; 360 μ x 360 μ ; 80 seconds.

Plate 4.10

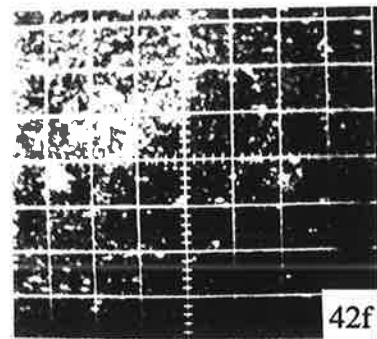
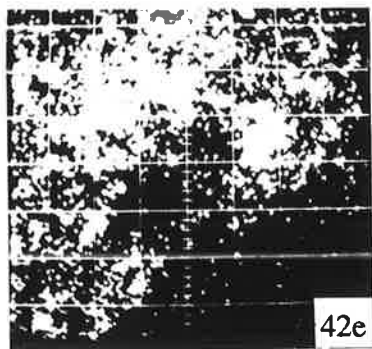
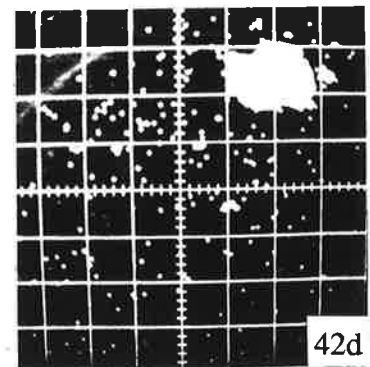
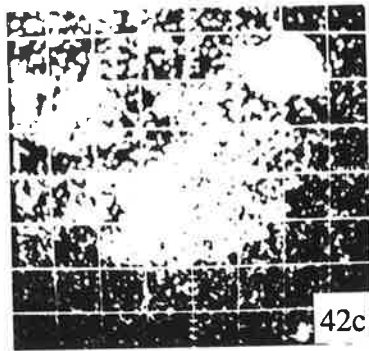
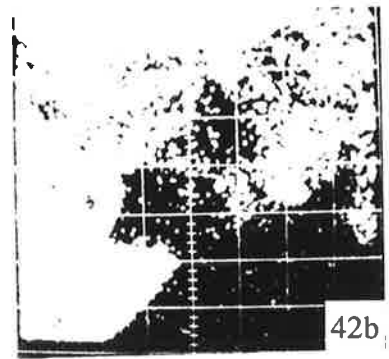
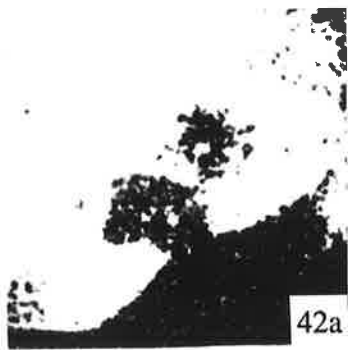
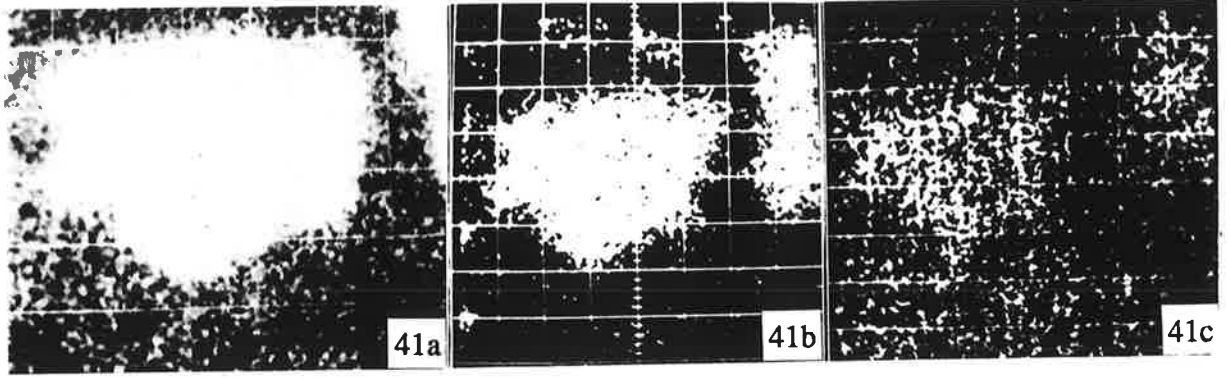


Table 4.7 Chemical analyses of calciorhodochrosite / rhodochrosite from Dounan Mn deposits

No. (%)	Mn	CaO	MgO	T Fe	SiO ₂	Al ₂ O ₃	mineral
D-142-M3	20.23	15.77	5.64	1.59	11.20	2.01	calciorhodochrosite
D-143-M4	20.71	15.74	5.52	1.60	11.33	2.05	calciorhodochrosite
D-144-M5	20.94	15.50	5.46	1.70	11.37	2.06	calciorhodochrosite
* The samples have the common prefix 958.							
* M-R18	45.30	2.79	2.12	0.20	0.00	0.60	rhodochrosite
* calculated MnCO ₃ = 94.81% (data from Liu et al., 1984).							

mineral, the calculated contents (Liu et al., 1984) of carbonates can be worked out: MnCO₃ 48.99%, CaCO₃ 30.97%, MgCO₃ 17.60%, FeCO₃ 2.91, and the ratio of MnCO₃ : CaCO₃ = 1.32 : 1 or 3.97 : 1 (Table V.4). The X-ray scanning diagrams (Plate 4.10, Figs. 42a, b, c, d, e and f) of the calciorhodochrosite show that Mn and Ca have overlapping distributions as isomorphous mixtures; the overlapping distributions of Fe and S probably indicate the presence of pyrite; whereas the scattering of Mg and Si may imply dolomite and quartz. Thus, the mineral belongs to the isomorphous series between CaCO₃ (calcite) - MnCO₃ (rhodochrosite), so called calciorhodochrosite, and is characterized by higher relief and Mn content (Mn 20-35%) and lower CaO content CaO 5-20%) than calcite. It also has higher CaO and lower Mn contents than rhodochrosite. Rarely, relatively pure rhodochrosite can also be detected in the Dounan deposits (Mn 35-48%, MnCO₃ > 80%, CaO < 5%, Tables 4.7 and V.4). Detailed study of this mineral is still awaited, though pure rhodochrosite is rare in the Dounan deposits.

4.4.2.4 MN-CALCITE / MN-BEARING CALCITE

Mn-calcite (Mn > 12%) and Mn-bearing calcite (Mn < 12%) mainly occur in unsorted or banded Mn oxide and Mn carbonate ores, mostly occurring with calciorhodochrosite, and also has been found to be both sedimentary or diagenetic in origin in the deposits. In hand specimen it is similar to calciorhodochrosite and it is difficult to distinguish them. This mineral is generally of grey colour under the microscope, and occurs in both Mn oxide and carbonate oolites/pisolites and in matrix as colloform, crypto- or micro-crystalline euhedral-granular. However, the second generation of the minerals is coarser in size and occurs as euhedral rhombohedral crystals. Also, Mn and Ca elements occur in isomorphous series, and the minerals exhibit a refractive index of 1.700. There is not much controversy about this mineral structure and composition, and most workers agree with a formula expressed as (Ca, Mn) CO₃.

4.4.2.5 SUPERGENE OXIDIZED MINERALS

About four manganese oxide minerals constitute the Dounan supergene ores restricted to supergene oxidized zones at or near the surface. Since they are of much less importance in the formation of the Dounan deposits, only brief descriptions of these minerals is given below.

1) *Psilomelane*

The handspecimen commonly shows black or steel black colour, but is generally grey under the microscope, and with dark brown internal reflection. Psilomelane occurs as crypto- or micro-crystalline aggregates, occasionally with colloform texture, and sometimes it constitutes ooliths/pisoliths (0.4-0.8 mm), massive or banded structures. The formula is expressed as $m\text{MnO} \cdot \text{MnO}_2 \cdot n\text{H}_2\text{O}$. In Dounan supergene ores, psilomelane is most abundant in the surficial oxidation crust. Braunite is found to be altered to this higher oxide quite often; although rare, the mineral which is most readily altered is hausmannite.

2) *Pyrolusite*

Pyrolusite is rare and present only as a supergene oxidation product of primary Mn oxides, and it abounds in colloidal ores of the surficial oxidation crust. The handspecimen shows black color and earthy structure with a low hardness. The mineral is generally of brown color under the microscope and occurs as crypto- or micro-crystalline euhedral forms in foliated textures. Braunite is found to be altered to this higher oxide (and to psilomelane). Several chemical analyses of pyrolusite from different supergene oxidized ores suggest the formula is MnO_2 (Liu et al (1984).

3) *Nsutite*

Nsutite appears mostly in the surficial oxidation crust developed on primary Mn carbonates and poorly crystalline MnO_2 with a natural occurrence of $\gamma\text{-MnO}_2$. Thus, nsutite is predominant in supergene ores derived from Mn-carbonate protore (Roy, 1981). The handspecimen shows dark brown color and earthy structure with poor hardness (~1.5). Its low specific gravity (~1) leads to its being able to float on the surface of water and it has strong water absorption. Generally, the mineral is of grey-brown color and colloform texture under the microscope, and can be expressed in formula as $\text{MnO}_2 \cdot n\text{H}_2\text{O}$ (Liu et al., 1984).

4) *Hausmannite*

Hausmannite has rarely been detected and only locally in the surficial oxidation crust (e.g. test pits K608 of Gake, B201 of Baigu and K735 of Milike; Zhang et al., 1979). It is present as well-microcrystallized grains (0.001 - 0.05 mm) and shows light blue-brownish grey colors under the microscope. Chemically, the composition of analyzed Dounan hausmannite is generally close to that of Mn_3O_4 with only trace substitution by other elements (Table 4.8), which is extremely

Table 4.8 Electron microprobe analyses of Dounan hausmannite (from Liu et al., 1984).

No. (%)	Mn ₃ O ₄	MnO*	Mn*	O*	FeO	CaO	SiO ₂	MgO	Na ₂ O	total
B-R9	100.90	93.84	72.68	7.06	0.10	---	---	---	---	101.00

* calculated based on Mn₃O₄

similar to the standard mineral (MnO 93.01% and O 6.99%, Liu et al., 1984). Thus, the formula of Dounan hausmannite can reasonably be expressed as Mn₃O₄.

4.4.2.6 GANGUE MINERALS

1) Calcite

Calcite, as the main gangue mineral in the deposits, is abundant in all Dounan orebodies. It occurs as microcrystalline grains (0.001 - 0.06 mm) in the Mn oxides mostly as matrix, or as fragments or cements in the Mn carbonates, sometimes as nuclei in oolites and pisolites. The refractive index is 1.658.

2) Quartz (and/or Chalcedony)

Quartz (and/or chalcedony), like calcite, occurs throughout the deposits as a main gangue mineral, particularly in the manganese oxides. It commonly shows microcrystalline sedimentary grains (0.02 - 0.20 mm) and occurs sometimes as nuclei in oolites and pisolites.

3) Albite

Albite has been detected as a primary gangue mineral mostly in unsorted and banded Mn oxide ores, and commonly as microcrystalline colloidal grains, sometimes as nuclei in oolites and pisolites.

4) Hydromica

Hydromica rarely occurs in unsorted and banded Mn oxide ores, commonly as micro-flakes (< 5 μ) on the surfaces of quartz or carbonate minerals.

5) Dolomite

Rare dolomite occurs mainly in banded manganese oxide ores as microcrystalline granular masses (0.001- 0.1 mm), with a refractive index of 1.690.

6) Chlorite

Chlorite is a very rare gangue mineral in the deposits, and is limited in occurrence to the matrix of oolites/pisolites as colloform and crypto- or micro-crystalline textures.

4.5 Ore Phases

4.5.1 Conception and General Features

Here, the concept of ore phase refers to an association of ore minerals, closely distributed in the orebody and formed under the same (or similar) physical and geochemical (environmental) conditions during sedimentation and post-deposition events. Thus, two main ore phases can be separated: i.e. primary and supergene ore phases. However, the primary ore phases will be emphasized here because they comprise about 97% of the total reserves of the Dounan manganese deposit; they can be divided into three ore phases: i.e. Mn oxides, Mn carbonates and mixed type ore phases. The Mn oxide phase is an association mainly composed of various primary Mn oxide (braunite) ores formed in oxidizing or weakly reducing environments; the Mn carbonate phase mainly consists of various primary manganese carbonate (e.g. calciorhodochrosite and Mn-calcite) ores formed in weakly reducing environments; whereas the transitional (or mixed) ore phase is made up of both Mn oxide and Mn carbonate ores formed in environments ranging from weakly oxidizing to weakly reducing. The boundaries between the ore phases are generally not sharp.

The ore phases of the Dounan Mn deposits occur in a roughly zonal arrangement in orebodies. Commonly, the Mn oxide ores occur in the central parts, then the transitional type ores distributed surrounding the Mn oxides, and finally in outer zones by the Mn carbonate phase (Wang, 1981; Liu et al., 1984; Figs. 4.2 and 4.3). The zonal distribution of primary ore phases, in fact, reflects an evolution of the three ore phase zones from oxidation, to interaction and to reduction. Of these the (pure) Mn oxide ore phase developed poorly and only in some large scale orebodies (e.g. V1 and V8) and represents only a very small proportion (~4%); the reduced ore phase also shows a restricted distribution (~26%); whereas the transitional (or mixed) phase developed very well in orebodies (~70%). The supergene ore phase occurs only in a few local outcrops of primary orebodies. Interestingly, such transitional manganese ore main ore type the almost unique to the Dounan Mn deposits, and is rarely reported not only in China but also elsewhere.

4.5.2 Primary Ore Phases

4.5.2.1 Microphases of Ores

1) Microphases of Manganese Oxide Ores

The Mn oxide ore phase is observed throughout the Gake and Baigu areas and also around the Kata area, and commonly occurs in the central parts or upper parts in vertical section of

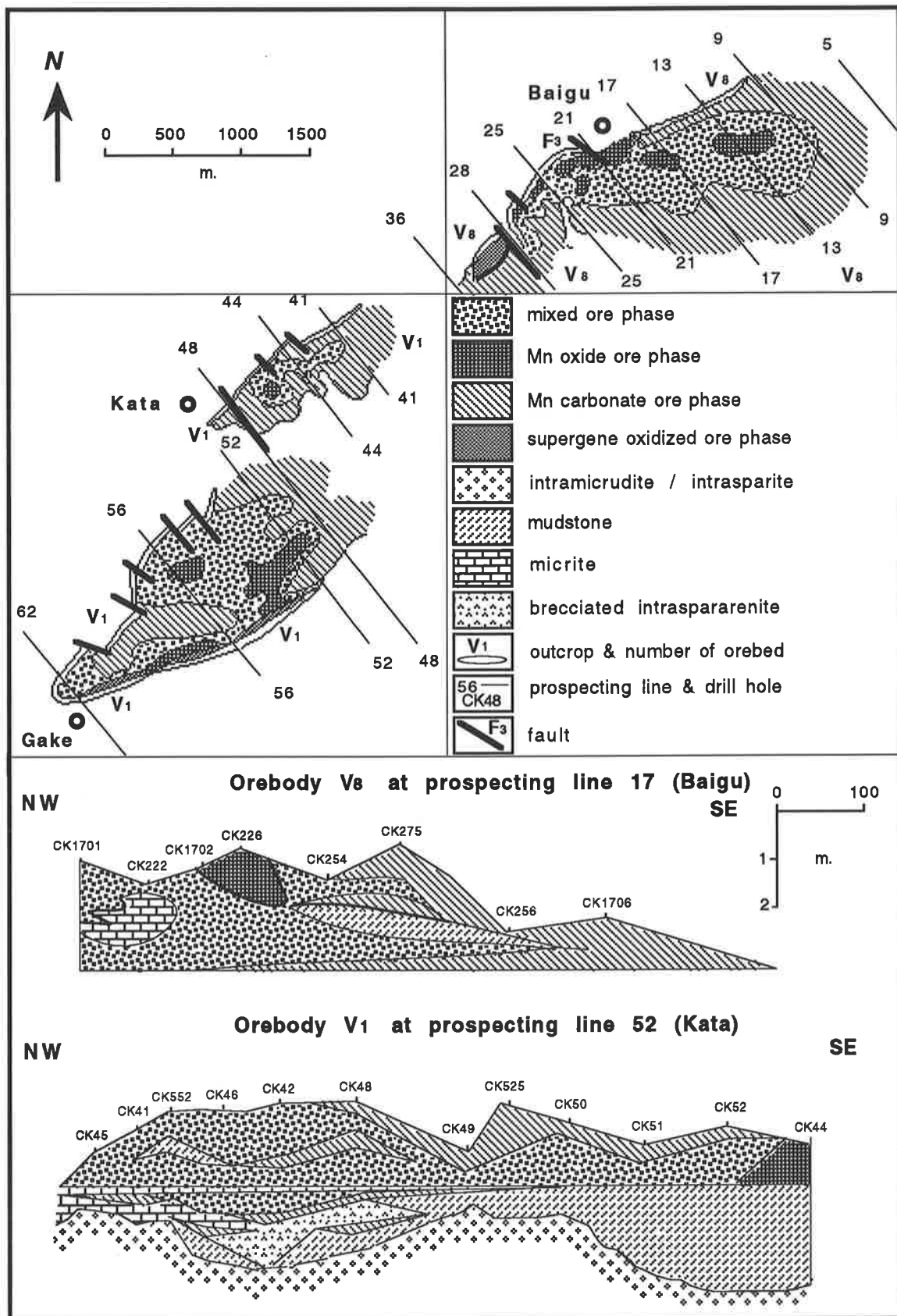


Fig. 4.2 Distribution of ore phases of main orebods of Dounan deposits (modified after Liu et al., 1984).

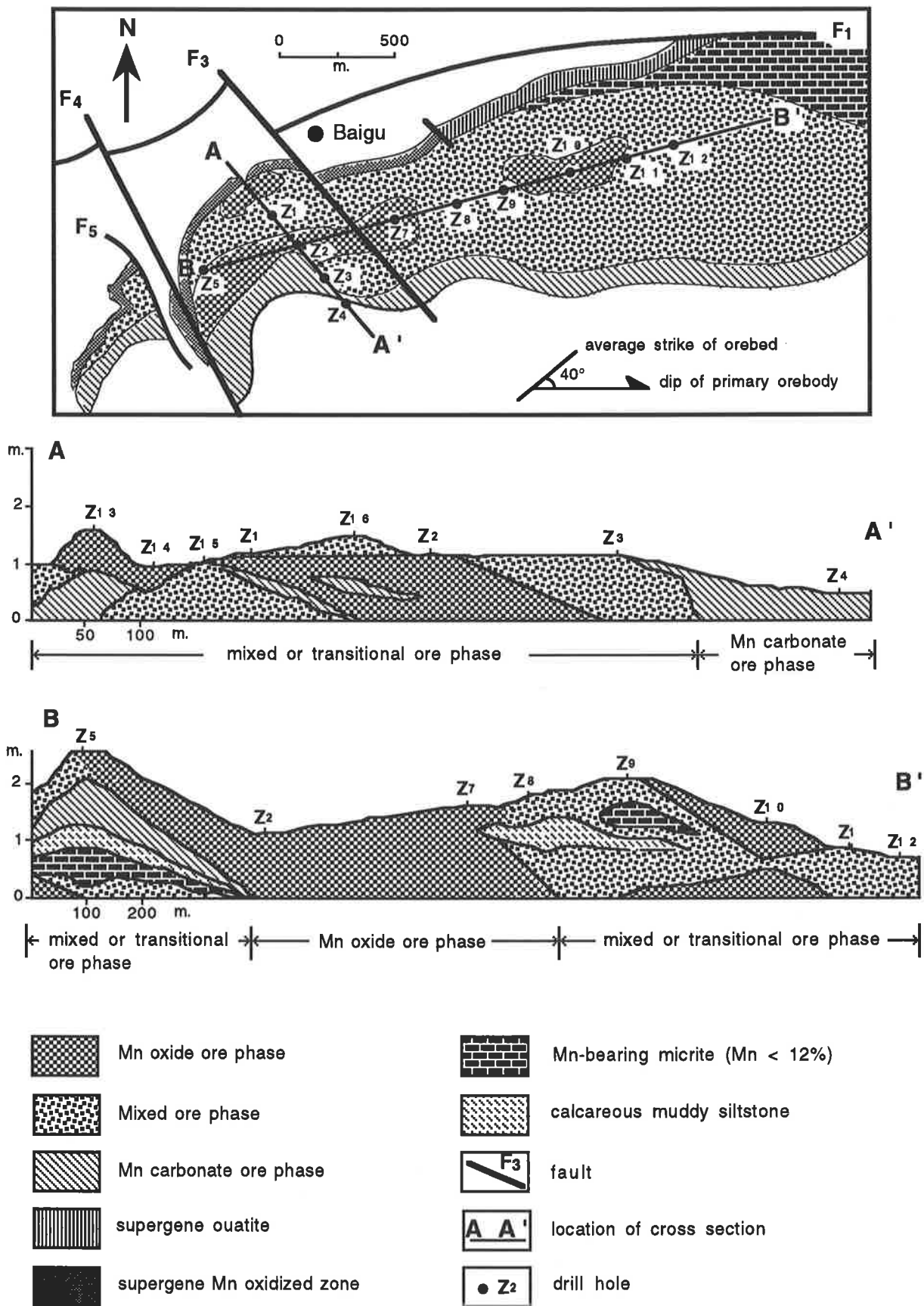


Fig. 4.3 Distribution and cross sections of ore phases of Dounan orebed V₈ (modified after Wang, 1981).

orebodies (Figs. 4.2 and 4.3). Generally, several sedimentary cycles of normal and inverse grading (Fig 4.4) can be recognized in this ore phase. The ores are mainly composed of oolitic and pisolitic braunite and minor calciorhodochrosite, and show black or brownish black colours. Figure 4.4 gives an example of the phase texture. Roughly, there are three cyclothems (including first normal followed by inverse grading) in the vertical sequence of the orebody V₁, and they all show complete development from coarse to fine and again to coarse oolitic and pisolitic textures, reflecting energy and environmental variations. However, inverse grading in the upper cyclothem indicates a relatively low energy environment.

2) *Microphases of Transitional Ores*

The transitional ore phase is found throughout the deposits surrounding and underlying the Mn oxide ore phase, and generally dominates in the deposits (Figs. 4.2 and 4.3). This phase is mainly composed of three primary ore types, i.e. deformed (braunite) oolites/pisolites, banded or unsorted ores and oolitic/pisolitic braunite and calciorhodochrosite, intercalated with minor Mn-bearing intraclastic micrite. Statistically, the ratio of thickness of these three ores in the main orebodies is 2.9 : 3.8 : 1.0 (Liu et al., 1984). Thus, calcareous Mn oxide ores and minor Mn carbonate ores dominate in the transitional ore phase, and their proportion is about 6.7 : 1.0. Similarly to the Mn oxide ore phase, the transitional ore phase generally consists of several cyclothems defined by normal and inverse grading. For instance, the ore phase texture of orebody V₈ shows three cyclothems (Fig. 4.5, S₁₆₋₁₄, S₁₃₋₁₁ and S₁₀₋₈) in the vertical profile. These possibly reflect variations of Mn oxides vs Mn carbonates, or between oxidation and reduction, or between low and high energy environments.

3) *Microphases of Manganese Carbonate Ores*

The Mn carbonate ore phase generally occurs surrounding or underlying the transitional ore phase and is also less abundant than the latter. This ore phase is mainly composed of Mn carbonates and minor braunite, commonly with dark-red (or grey) colour and oolitic and pisolitic textures. This ore phase can be found throughout the deposits, e.g. orebody V₂ in Gake and Kata areas, orebody V₃₊₂ in Daaazi and Milike areas, and orebodies V₆, V₇ and V₉ in Baigu area, and represents relatively reducing facies. Commonly, the ore phase composed of calciorhodochrosite ooliths, sands, biofragments and minor braunite ooliths/pisoliths shows fragmental or brecciated and inverse grading fabrics, or constitutes unsorted ores when containing more braunite ooliths/pisoliths. Laterally, the Mn carbonate ore phase in some cases changes into the transitional ore phase, or into Mn-bearing oolitic/pisolitic micrite (Mn 4-12%), considered to be a poor quality ore zone.

4.5.2.2 *Vertical Variation of Ore Phases*

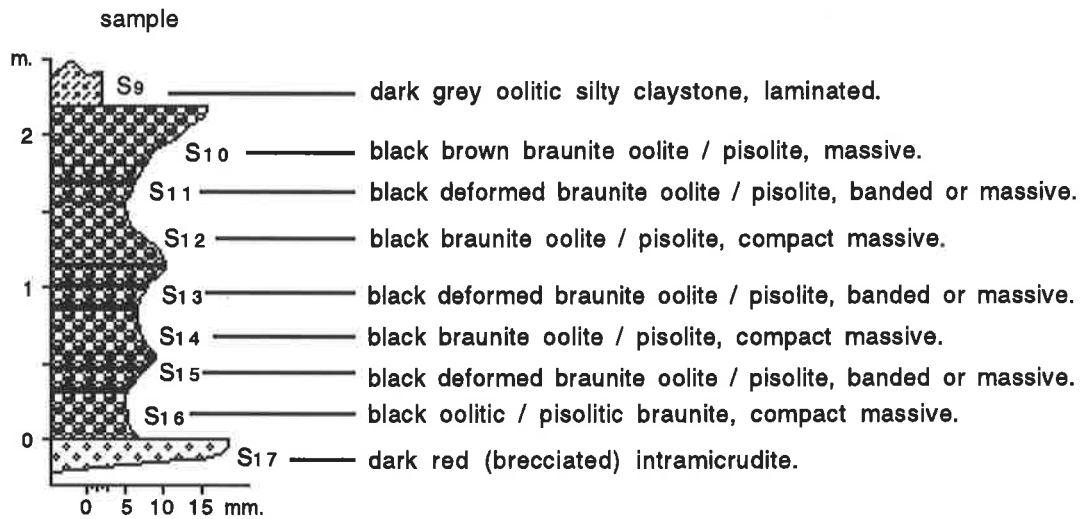


Fig. 4.4 Vertical profile of orebed V₁, drill hole CK566, Gake area.

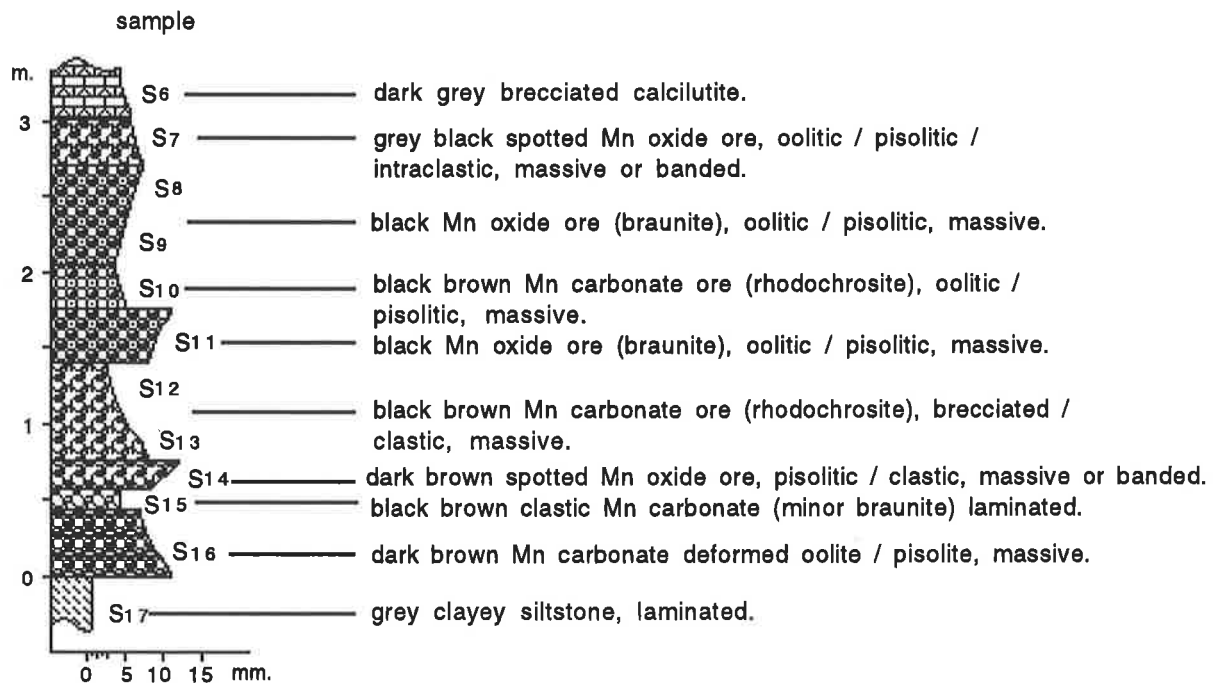


Fig. 4.5 Vertical profile of orebed V_a, drill hole CK2501, Baigu area.

In vertical sections of individual main orebodies, the variation of ore phase exhibits close relationships with regressive cyclothem sedimentation. The Mn carbonate ore phase developed well in the initial period of regression. Further continuous regression led to shallower water, a rise of the redox interface, and shrinkage of the sedimentary basin, in which the transitional ore phase accumulated. Still further regression led to progressively shallower environments and a smaller depositional basin, or even the development of several depositional sub-basins in which the Mn oxide ore phase precipitated.

In the lower (T2f4-1) Mn-bearing series, orebeds V1 (including accompanying orebodies) and V2 commonly show the features of Mn oxide and transitional ore phases; whereas the younger orebeds V3, V3+1 and V3+2 (or V4) mainly occur as Mn carbonate and transitional ore phases. In the upper (T2f5-2) Mn-bearing series, orebed V5 mainly consists of Mn carbonates; orebeds V6 and V7 are generally composed of the transitional ore phase; orebed V8 shows both Mn oxide and transitional features; higher still, Mn carbonate and minor transitional ore phases dominate in orebeds V9 and V10. Thus, although the Dounan Mn deposits are mainly characterized by the transitional ore phase, Mn carbonate ore phases mostly developed at the beginning of regressive cyclothem sedimentation, whereas Mn oxide phases are typically formed at the end of regressive cycles.

In addition, the vertical variation of Dounan ore phases is also characterized by the complex microphase textures of the transitional ore phase and relatively simple microphase textures of Mn carbonate and Mn oxide ore phases. For instance, the cross section of orebody V1 located at prospecting line 52 in Gake area (Fig. 4.2) shows that the orebody consists of all three ore phases, of which the Mn carbonate and Mn oxide ore phases occur as lenticular or wavy bedded bodies; whereas the transitional ore phase is irregularly stratiform with gangue intercalations. The section of orebody V8 selected from prospecting line 17 is complex and exhibits a down-dip variation from lenticular Mn oxide ore phase to wavy bedded transitional ores and then to wavy stratiform Mn carbonate ore phase (Fig. 4.2). Furthermore, the zonally distributed ore phases of orebody V8 show that the Mn oxide ore phase mainly occurs in the central parts; the outer margins are mainly characterized by Mn carbonate ore phases; whereas the transitional ore phase is generally in an intermediate position (Fig. 4.3), which indicates an evolution toward shallow water and a shrinking depositional basin during regression.

4.5.2.3 *Horizontal Distribution of Ore Phases*

The ore phases of the Nikopol manganese deposit in the Ukraine and the Chiatura deposit of the Republic of Georgia show an obvious zonal distribution related to environment of deposition, i.e. Mn oxide ore phase in the littoral area with a mixed ore phase in the shallow marine area and an Mn carbonate ore phase in deeper water. However, Bolton and Frakes (1985) found inversely graded pisolite at Chiatura and interpreted this as indicating marine regression. The development

of ore phases in individual deposits in the world should differ due to their different geological conditions. The ore phases of the Dounan Mn deposits probably resulted from the evolution of (basin) sedimentation from reduction to oxidation during the deposition of individual orebodies. Thus, the horizontal distribution of Dounan ore phases in a zonal distribution parallel to the coast, to some extent, is different from those of the Nikopol and Chiatura deposits; also, the Mn oxide phase at Dounan does not belong to the littoral zone but shows high energy features of the intertidal area. The Dounan deposits represent Mn accumulation in very shallow environments during dynamic regression and in this sense only do they differ from Nikopol and Chiatura.

1) Ore Phases of Lower Ore-bearing Series

In orebody V₁ of the Gake and Kata areas, the Mn oxide and transitional ore phases occur from place to place, but the Mn carbonates dominate in the area between Gake and Kata and even to the eastern area of Kata, occasionally changing laterally into Mn-bearing micrite or other rocks (Fig. 4.2). The distribution of orebody V₂ generally is smaller than that of orebody V₁, and it mostly occurs as mixed (including minor Mn carbonate) ore phase. Although smaller-scale orebodies such as V₃, V₃₊₀ and V₃₊₂ exhibit similar distributions, they mostly show discontinuously lenticular bodies, which probably resulted from changed shapes and depths of depositional sub-basins due to the continuous supply of sediments and/or insufficient supply of manganese.

2) Ore Phases of Upper Ore-bearing Series

After deposition of the lower Mn-bearing series, the regional regression led to migration of any Dounan ore-forming environments towards the east. Following the next transgression, orebodies V₅, V₆, V_{7a} and V_{7b}, V₈, V₉ and V₁₀ were deposited in an offlapping arrangement indicating the subsequent regional regression.

As the distribution of sedimentary ore phases is generally controlled by lithofacies-paleogeographic environment relationships, it is possible to search for blind deposits in terms of the zonal law. The variation of Dounan ore phases allows a reasonable genetic interpretation. The depositional basin was characterized by relatively deep water with accumulation of manganese beneath the redox interface during the initial period of regression, and the reducing to weakly reducing environments led to accumulation of Mn carbonates. Further continuous regression led to shallow environments characterized by intertidal high energy, weak oxidation and weak reduction; the evolution of sediments controlled by the redox interface led to the mixed ores. Finally, the shallowing and shrinking depositional basin was characterized by oxidation or weak oxidation, when, given sufficient manganese supply, Mn oxides were deposited during the final period of regression.

4.5.3 *Supergene Oxidized Ore Phases*

The formation and distribution of Dounan supergene ore phases were generally controlled by abundant rainfall of subtropical climates contributing abundant dissolved manganese to the basin, by redox conditions and was also influenced by the abundance of Mn in the source area and by geological structures. However, the underground water level also played an important role in the development of the supergene ores.

1) *Relations between Supergene Ore Phases and Natural Morphology*

Morphology and the location of primary orebodies are very important to the formation and development of Dounan supergene ores. Generally, secondary oxidation of ores develops to greater depth when the orebeds dip in the same direction as the slopes on the upper parts of mountains, but shows poor development in valleys and when the orebeds dip toward mountains slopes. The best examples of Dounan supergene ore phases are distributed in such advantaged areas, such as prospecting lines 56-60 of the Gake area and 28-30 of the Baigu area, all with secondary oxidation extending to about 70-90 meters depth.

2) *Relations between Supergene Ore phases and Faults*

Dounan supergene ores are also controlled by the faults. Generally, the strike faults show larger effect on the secondary oxidation of primary ores than the dip faults. Groundwater percolating down along the fractured zone of strike faults contributed to the development of large supergene oxidized zones. For example, fault F30 located in prospecting lines 53-55 of the Gake area intersects a supergene oxidized zone to depths of about 100 m; fault F3 on the other hand in the Baigu area played only a minor role in the formation of supergene ores.

4.6 *Discussion*

The petrological and mineralogical examination of ores and associated gangues demonstrates that all primary and diagenetic products are stratigraphically controlled in their formation. Aspects governing the secondary overprinting of the deposits, diagenetic recrystallization, mobilization and precipitation processes are, to some extent, examined. However, when the descriptions and data of this chapter are compared, a picture emerges that reflects the presence of significant diagenetic processes, though the sedimentary process dominates in the Dounan Mn deposits. This means in general terms that the diagenetic mechanisms result in the following mineralogical and geological relationships:

- changes of ore textures and structures;
- recrystallization and replacement of ores and gangues, as well as their microfabrics;
- development of similar sequences of the primary products.

According to the composition and fabrics as well as phases of ores and gangues, three main ore types are identified:

- Mn oxide ores mainly occurring in upper parts of orebodies;
- transitional (or mixed) ores dominating in orebodies;
- Mn carbonate ores generally appearing in lower parts of orebodies.

Although these ore types often grade into each other and cannot be separated clearly, there are also materials that are typical for specific places.

The most widely distributed manganese products in the deposits are apparently Mn oxide (including deformed and compact massive) oolites/pisolites. Braunite shows its strongest enrichments in the Mn oxide ores, whereas other manganese minerals are subordinate or (trace) rare in these materials. Deeper down the section of the orebody, calciorhodochrosite and/or Mn-calcite increase in unsorted and banded Mn oxide ores, and are most prominent in Mn carbonate ores.

All mentioned ores most commonly developed in rich quartz silts or muddy materials, and in Ca-rich carbonate materials, and thus, the sequence of paragenesis with quartz (minor feldspar) and calcite (minor dolomite), which are the main mixed materials of mudstone, siltstone and limestones at Dounan, indicates a sedimentary geochemical control over the formation of these ores. Additionally, the higher oxygen concentrations in porewater in Mn-bearing series near the upper parts of orebodies may play a significant role during diagenetic precipitation of Mn oxides. However, as similar parageneses exist below the ore, the availability of oxygen may be much less effective in the mineralogical control of secondary precipitates than expected.

Mn oxides in the deposits are dominated by braunite, and these ores are generally more prominent in the upper parts of the orebodies. Clayey and silty materials from the overlying layers can provide Si to the higher parts of the ore, and brecciated or oolitic/pisolitic limestones from the underlying beds are easily available for interaction with precipitation processes in producing diagenetic carbonates. Unsorted or banded and Mn carbonate ores from lower parts of orebodies support the above findings. Additionally, the supergene products are dominated by psilomelane or nsutite and they are closely associated with quartz or clay materials, or both.

Ores in stratigraphically intermediate positions can contain relatively complex minerals (e.g. braunite, manganite, calciorhodochrosite, Mn-calcite and gangues) occurring in both Mn oxides and carbonates and in ooliths/pisoliths and matrix. Ooliths/pisoliths mainly composed of braunite occur together with the main Mn carbonate matrix, these ores show unsorted or banded structures. These mixing/transitional ore types composed of co-existing Mn oxide and Mn carbonate materials suggest a transition of depositional environments towards Mn oxides from Mn carbonates, as ores of this type are dominated by Mn oxides.

XRD and chemical analyses also confirm that the abundance of calciorhodochrosite generally increases with increasing depth in the orebody, opposite to the behavior of braunite. The

geochemical stabilities of these two minerals are apparently linked, but the presence of one or the other phase does not explain which of the minerals is replaced. However, under the microscope, CL and SEM, it is evident that both formed in early and late stages and that they replaced each other. Also, the ore minerals recrystallized from poorly crystalline manganese phases. Examples for this process can be found in most ore types and at any position in the sections. Although less evident than in the case of (compact massive) Mn oxide oolite/pisolite, alteration is commonly apparent in oolites and pisolites, which possess mottled cemented patches consisting mainly of relatively coarse calciorhodochrosite. This contrasts strongly with findings in which primary materials are normally dominated by crypto- or micro-crystalline Mn minerals. Through a stabilization process, brought about by the availability of certain minerals (e.g. pyrite), the latter might represent a late diagenetic stage in the development of the mineralization.

Considering initial precipitates and their successors formed through diagenesis, the mineralogical history of the Dounan deposits may have proceeded in the following steps (Fig. 4.6):

- crystalline clastic (detrital) phases, formed in presedimentation stages: quartz, feldspar and mica;

Fig. 4.6 Paragenetic sequence of Mn oxide and carbonate and gangue minerals of Dounan ores

mineral \ stage	presedimentation	syndimentation	diagenesis	supergeneration
quartz				
feldspar				
mica				
manganite				
braunite				
calciorhodochrosite				
Mn-calcite				
Mn-bearing calcite				
calcite				
dolomite				
albite				
chlorite				
pyrite				
limonite				
hausmannite				
psilomelane				
pyrolusite				
nsutite				

- poorly crystalline phases, as primary depositional products;
- recrystallized or replacement phases, evident in many ores of the deposit, mainly formed during diagenesis;
- psilomelane (or pyrolusite) and nsutite, replacement products from braunite and Mn carbonate minerals, in supergene environments.

Recrystallization is also evident in gangue minerals such as calcite and authigenic albite, which replace Mn ores. Commonly, Mn oxide oolites/pisolites are deformed or destroyed by diagenetic processes that first act on deforming braunite-rich ooliths/pisoliths, selectively remobilizing these grains and replacing them with other phases, and excluding the Mn carbonate-rich matrix.

Evidence of processes which led to gangue replacing manganese minerals is very common, and often, the mobilized manganese reprecipitates as diagenetic products. These processes prevail in Mn oxide and transitional ores. Many diagenetic ores develop in the same location and the dissolved manganese has its highest concentration in the same orebody where the replacement reactions work. Since diagenetic enrichment of Mn oxides is likely to occur in the same orebody, only short distances of horizontal and vertical transport are indicated.

As mentioned above, calcite is the main gangue mineral to replace manganese ores. Typically, calciorhodochrosite is much more affected than braunite, which often remains as a residual matrix mineral. Braunite also seems to replace other manganese minerals and gangue minerals, but polished and thin sections clearly illustrate that some braunite, together with calcite, represents the latest stage of diagenesis in the mobilization reactions which led to the removal of both manganese and calcium. This observation is particularly important, because it provides direct evidence for the remobilization of calcareous (and perhaps siliceous) minerals through braunite precipitation. That this mechanism sustains some processes responsible for the secondary enrichment of manganese will be discussed later

This short discussion emphasizes the importance of detailed petrological and mineralogical studies of ores and associated rocks in providing a wealth of information on primary sedimentation and diagenetic processes. The following chapter on the geochemistry of the samples, analyzes the relationships among the various elements, and it also examines whether the broad history of the deposits as described above is also reflected in the geochemical data.

Chapter 5 Geochemistry

5.1 Introduction

One of the main tasks of this study is the geochemical characterization of the different ores and associated rocks at the Dounan deposit. Until recently, geochemical analyses on these materials either focused on larger areas of the deposit (Zhang et al., 1979) or on individual minerals (Liu et al., 1984). Thus, a close examination of the primary and secondary products is necessary to investigate primary and diagenetic oxidation and reduction processes occurring in the orebodies; information on the nature of trace elements in specific materials also assists mine planning operations. The geochemical characteristics of the Dounan deposits are Additionally compared with those of other ore deposits elsewhere to identify possible genetic relationships in ore formation.

All ore types and rocks identified were the subject of detailed sampling procedures. First, two main stratigraphical sections were sampled at closely spaced intervals (10-20 cm in ores, 40-50 cm in rocks; see also Chapter 2). Secondly, with the exception of a few rare supergene ores (e.g. psilomelane and nsutite ores), which did not provide sufficient materials (nearly mined out), at least 3-10 samples of each ore and rock type were collected to provide 5 or more "pure" samples for each individual set. An overview of the elements present and the respective analytical techniques is given in Table 5.1.

Major, minor and trace elements were analyzed by wet chemistry at the Yunnan Geological Laboratory Center and X-Ray Fluorescence (XRF) at the University of Adelaide. Rare Earth Elements were examined by Isotopic Dilution Mass Spectrometry (IDMS, University of Adelaide) because of their extremely low concentrations (Appendix V, Tables V1-3; for method see Appendix I.1). A large number of Mn minerals were analyzed by Electron Microprobe Analysis (EMPA), and oxygen and carbon isotopes were determined by Stable Isotopic Analysis (SIA). Loss On Ignition was determined for all samples.

Table 5.1 Elements and methods used for geochemical characterization.

Method	Samples	Elements
Chemical analysis	12	Mn, Fe, S, P, Ca, Mg, Si, Al, K, Na, CO ₂ , H ₂ O.
XRF	38	Si, Al, Fe, Mn, Mg, Ca, Na, K, Ti, P, S, Sr, Ba.
XRF/AA	47	Y, Sr, Rb, Nb, Zr, Th, Pb, U, Ga, Zn, Ni.
IDMS	18	La, Ce, Nd, Sm, EU, Gd, Dy, Er, Yb (for REEs).
EMPA	117	MnO/MnO ₂ , FeO, CaO, MgO, K ₂ O, Na ₂ O, Al ₂ O ₃ , SiO ₂ , TiO ₂ , Cr ₂ O ₃ .
SIA	36	O, C (for stable isotopes).
LOI	38	H ₂ O, CO ₂ .

The Rare Earth Elements were normalized with European shale (Haskin and Haskin, 1966) to simplify comparison of multi-element patterns; the deviations of Ce and Eu from the overall trend (anomalies) were calculated from the normalized values. Average element abundances and concentration ranges of ores and rocks are provided in the respective sections.

5.2 Chemical Characterization of Ores and Rocks

The following section discusses the three major components of the deposit, Mn-, Ca/Mg-, and Si/Al-phases, which in places incorporate specific elements. Major, minor, and trace element abundances (including the Rare Earths) for individual ore and rock types are also dealt with. Information gained from composition patterns of these materials is used to determine whether it is possible at the present stage of investigation to establish a common origin for each element.

5.2.1 Inter - Element Correlations

First, the materials dominating in the deposit are examined for their role in concentrating the various elements. Three main groups were visually identified on the basis of their major constituent (Table 5.2); these groups are the Mn ores (both Mn oxides and Mn carbonates), carbonate rocks with a calcium carbonate dominance, and clay/silt-rich materials. Since the diagenetic products commonly occur in close association, trends are observed. Examination of the results relied on a visual cross-comparison of all samples and elements under investigation. Below, the mentioned groups are discussed together to determine general elemental relationships within, and between, ores and rocks; later, ores and gangues are discussed separately.

The tabulated elements illustrate the relatively complex nature of the materials, because many elements occur in more than one particular group. Manganese, calcium and silica all are good examples of the difficulties arising from such multiple element correlations. Nearly all elements identified with calcium and silica also occur in the Mn phases (of both Mn oxides and Mn

Table 5.2 Visual cross-correlation of major and trace elements in 97 samples; underlined elements appear in more than one group; elements in brackets show weak correlations.

main element group	associated major and trace elements
Mn	Ba, <u>Ca</u> , Ce, Co, Cu, Eu, <u>Fe</u> , Ga, <u>Gd</u> , K, La, <u>Mg</u> , Mo, Na, Nb, Ni, P, Pb, <u>Rb</u> , <u>Sc</u> , <u>Si</u> , Sm, <u>Sr</u> , (Ti), <u>U</u> , V, <u>Y</u> , Yb, Zn.
Ca, Mg	<u>Fe</u> , <u>Ga</u> , <u>Gd</u> , <u>Rb</u> , S, <u>Sc</u> , <u>Sr</u> , <u>Th</u> , (U), <u>Y</u> .
Al, Si	<u>Fe</u> , <u>Gd</u> , <u>Sc</u> , <u>Si</u> , <u>Th</u> , <u>Ti</u> , Zr.

carbonates). However, this finding does not surprise, because both calcium and silica phases are present within the ore, often as detritals; the general question about the host minerals for specific elements remains unanswered. The same applies to combinations of calcareous with clay/silt-rich materials. This means that this relatively simple and broad scheme does not provide sufficient detailed information and that small-scale differentiations, such as among ore types or minerals, are necessary.

However, a few generalizations can clearly be made. Interestingly, many of the elements that might be expected to occur in conjunction with Mn, such as Fe, Ti (dominantly occurring in braunite), does not show an unambiguous relation to manganese, although these elements appear in the manganiferous group. Thus, variations within different ore types can weaken generalizations. Occasionally, elements with a weak correlation to one of the main groups show a much better relation to other elements, which, in turn, correlate well with the respective major group. Such behaviour is frequently observed and was used to establish the element associations.

Calcium serves as example for the observation above (Fig. 5.1a). The data in the regression plot for Ca and Mn show a strong negative correlation and the same can be said about elements such as Mg or Fe. Such relationships may reflect either reactions during sedimentation or chemical replacement between different generations. However, these elements show very poor correlation to elements dominating the gangues (Fe/Ca, Fig. 5.1b). Significantly, elements like Ni, Co, or Cu (deep sea ferromanganese nodules) seem to correlate well with Mn (Fig. 5.1c), whereas they correlate poorly with elements sited in presedimentary mineral, such as U in zircon (Fig. 5.1d), which indicates that the manganese sedimentation bears some similarity to that of marine manganese nodules. Therefore, a combination of Ca with other elements produces recognizable patterns, which may be attributed to replacement between the manganiferous and calcareous groups in a successive diagenetic step.

Elements associated with Ca are less well correlated within the group and they also occur in the two other main groups. However, a strong relationship is obtained from Mn and Si (Fig. 5.1e). The data in the regression plot for Mn and Si scatter widely but show slight negative correlation; the same relationship exists between Mn and elements such as Al, Ti, or Zr. This finding is later used in the interpretation of different generations and diagenetic process, but is not discussed further here. The clay/silt-rich group (alumina/silica) generally exhibits relatively low trace

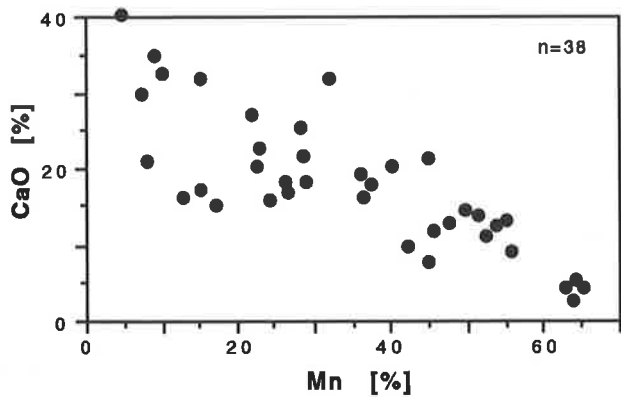


Fig. 5.1a: Correlation of Mn and CaO in ores and rocks

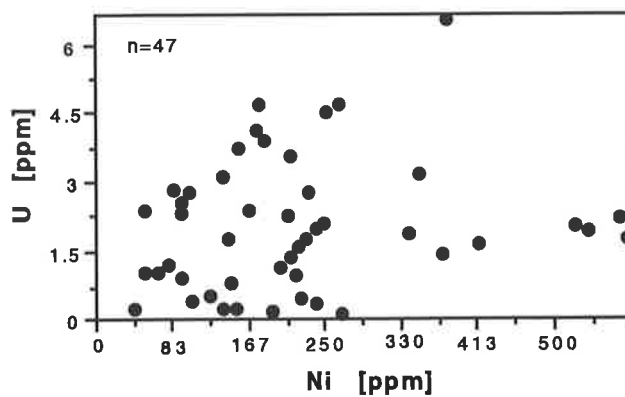


Fig. 5.1d: Correlation of Ni and U in ores and rocks

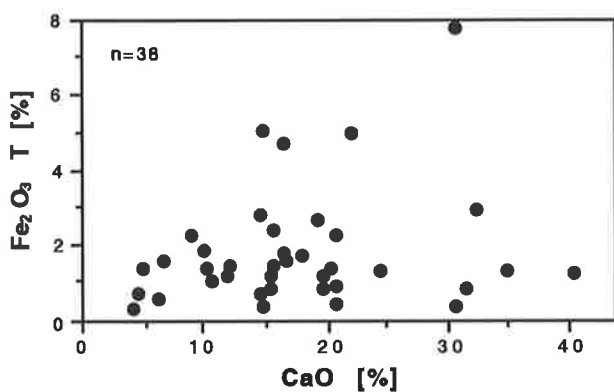


Fig. 5.1b: Correlation of CaO and total Fe₂O₃ in ores and rocks

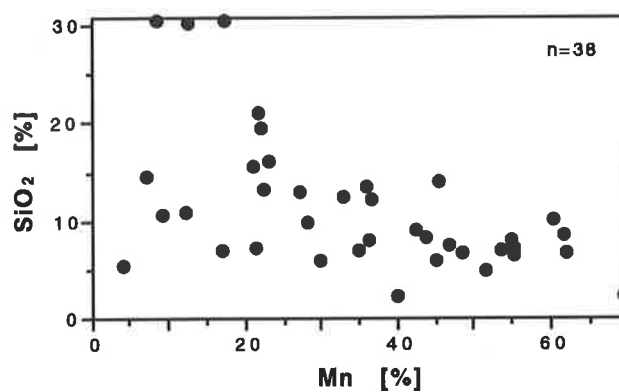


Fig. 5.1e: Correlation of Mn and SiO₂ in ores and rocks

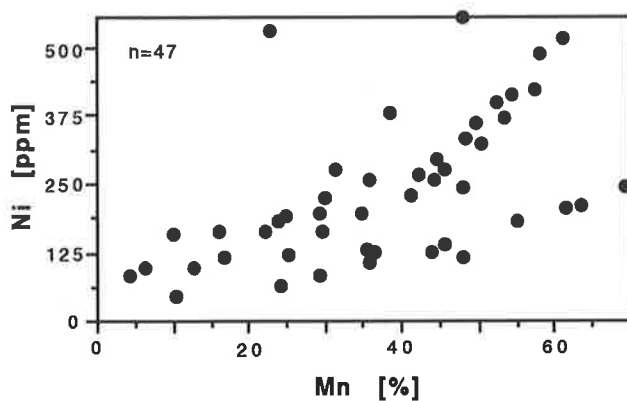


Fig. 5.1c: Correlation of Mn and Ni in ores and rocks

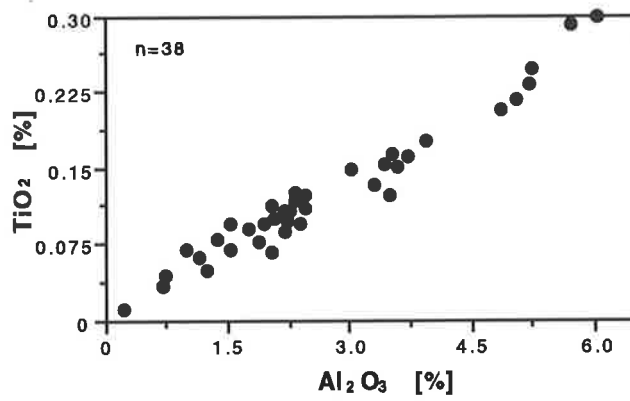


Fig. 5.1f: Correlation of Al₂O₃ and TiO₂ in ores and rocks

Fig. 5.1 Correlations of components in Dounan ores and rocks.

element concentrations. Well developed positive regression patterns are identified for elements such as Ti or Zr vs Al (Fig. 5.1f). These good correlations are generally associated with gangues containing quartz and feldspar.

5.2.2 Bulk Composition of Ores and Rocks

Below, major, minor and trace element abundances of manganese ores and associated gangues are separated into three main groups (major plus minor, trace elements, REEs); for simplicity, the groups are further sub-divided into four sets, as follows:

- Mn oxide (including deformed and compact massive) oolites/pisolites, often with both carbonate and clay/silt-rich matrix;
- Mn carbonate (calciorhodochrosite and Mn-calcite) oolites/pisolites;
- transitional (unsorted and banded) type ores;
- Mn-bearing clayey siltstone or silty claystone and carbonate rocks.

For each ore and rock type the average is plotted; elements are plotted in order of the respective atomic number. Statistical data, such as mean, maximum, minimum, sample number (n), and standard deviation, are provided in Tables 5.3-5.5 in the respective sections.

5.2.2.1 Major and Minor Elements

(1) Chemical Analyses

The major and minor elements vary in abundance in the ores (Table 5.3). Based on this result, the chemistry of the Dounan manganese ores exhibits the following characteristics:

- Mn shows negative correlation with total content of gangue elements;
- The contents of P and S are extremely low (desireable in ores);
- MnO₂ content increases with ore quality (grade), which contrasts to MnO;
- roughly, Fe, CO₂ and H₂O vary inversely with Mn content.

A statistical treatment of the row data was attempted (correlation matrix, Tables 5.4a-c), but multiple regressions for many elements made it necessary to visually compare each main parameter against all others. In Mn oxide ores, MnO₂ shows slightly positive correlations with SiO₂, Na₂O, S, and P but has negative correlations with other elements (Table 5.4a). MnO shows positive correlations with MgO and CO₂ and negative correlations with SiO₂ and Al₂O₃. (MnO₂+MnO) exhibits negative correlations with most elements except CO₂, Na₂O and P. These relationships indicate that Mn⁴⁺ dominates the braunite and has a close relationship with Si, sometimes replacing Mn carbonates in secondary enrichment. In transitional (e.g. unsorted and banded) ores, MnO₂ and MnO show negative correlations with CaO, MgO (slight positive in MnO), Al₂O₃ (slight positive in MnO₂) and S but slightly positive correlations with others (Table 5.4), which probably correlates with transitionally variable environments of co-existing

Table 5.3 Chemical analyses of major and minor elements [%].

sample	Al ₂ O ₃	CaO	CO ₂	Fe	H ₂ O	K ₂ O	MgO	Mn*	MnO ₂	MnO	Na ₂ O	P	S	SiO ₂
D-46	1.61	15.60	16.97	1.12	1.46	0.10	2.64	33.25	26.25	21.25	0.31	0.100	0.072	11.14
D-50	1.55	1.78	7.22	0.96	4.35	1.50	0.72	53.04	78.78	4.20	0.16	0.043	0.004	3.78
D-60	1.87	16.27	23.02	1.22	1.35	0.17	2.70	32.97	27.07	20.50	1.47	0.056	0.088	10.30
D-65	2.39	24.29	15.85	1.83	1.16	0.39	3.29	18.92	6.20	6.46	0.71	0.074	0.216	15.29
D-82	2.09	21.19	21.61	1.42	1.50	0.15	4.21	22.48	14.88	27.81	0.59	0.087	0.068	9.28
D-167	2.48	22.95	23.40	1.99	1.57	0.17	3.69	15.10	7.67	4.31	0.58	0.065	0.156	14.85
D-187	1.96	19.74	22.02	1.52	1.50	0.17	2.96	25.87	17.71	18.95	0.41	0.052	0.096	11.65
D-194	2.21	18.53	15.93	1.50	1.82	0.10	3.20	27.21	19.76	12.61	0.32	0.061	0.100	11.54
D-212	2.10	21.78	21.73	1.36	1.59	0.68	2.77	22.41	21.51	11.39	0.44	0.043	0.112	11.62
D-227	2.27	22.62	17.91	1.93	1.58	0.17	4.79	16.53	7.60	20.72	0.46	0.065	0.176	12.80
D-228	2.90	19.11	19.72	1.91	1.85	0.31	3.34	19.06	12.03	14.79	0.65	0.091	0.104	16.88
D-231	2.60	24.54	19.34	1.05	1.43	0.48	3.16	14.94	8.20	12.59	0.58	0.061	0.176	15.03

- Mn* resulting in calculated average value; from MnO + MnO₂
- all samples have the common prefix 958;
- respective ore or rock types see Appendix IV;
- data analyzed in the laboratories of the Geological Bureau of Yunnan Province.

Table 5.4a Correlation matrix of composition of manganese oxide ores.

	Al ₂ O ₃	CaO	CO ₂	Fe	H ₂ O	K ₂ O	MgO	Na ₂ O	P	S	SiO ₂
MnO ₂	-0.68	-0.80	-0.13	-0.84	-0.40	-0.0003	-0.81	0.43	0.07	0.01	0.20
MnO	-0.37	-0.14	0.28	-0.23	-0.62	-0.54	0.56	0.27	0.68	0.92	-0.84
MnO ₂ +MnO	-0.80	-0.67	0.15	-0.79	-0.81	-0.47	-0.08	0.58	0.64	-0.79	-0.59

Table 5.4b Correlation matrix of composition of transitional (or mixed) ores.

	Al ₂ O ₃	CaO	CO ₂	Fe	H ₂ O	K ₂ O	MgO	Na ₂ O	P	S	SiO ₂
MnO ₂	0.89	-0.89	0.30	0.07	0.87	0.02	-0.20	0.08	0.73	-0.95	0.63
MnO	-0.01	-0.36	-0.32	-0.06	0.45	-0.14	0.60	-0.63	0.09	-0.26	-0.38
MnO ₂ +MnO	0.25	-0.56	-0.19	-0.04	0.64	-0.12	0.46	-0.52	0.28	-0.50	-0.14

Table 5.4c Correlation matrix of composition of manganese carbonate ores.

	Al ₂ O ₃	CaO	CO ₂	Fe	H ₂ O	K ₂ O	MgO	Na ₂ O	P	S	SiO ₂
MnO ₂	-0.76	-0.87	0.15	-0.64	0.07	-0.19	-0.65	0.18	-0.04	-0.80	-0.70
MnO	-0.52	-0.49	0.10	-0.39	0.03	-0.44	0.21	0.09	0.32	-0.64	-0.61
MnO ₂ +MnO	-0.76	-0.81	0.15	-0.61	0.06	-0.36	-0.28	0.16	0.16	-0.86	-0.82

Table 5.5: Statistics of major and minor elements; [%].

	Al	Ba	Ca	Fe	K	Mg	Mn	Na	P	S	Si	Sr	Ti
Compact massive Mn oxide oolite/pisolite													
mean	1.35	0.55	6.68	1.04	0.22	1.50	63.01	0.11	0.16	0.03	9.19	0.04	0.09
maximum	2.32	0.13	12.78	1.56	0.56	2.30	69.82	0.20	0.18	0.08	12.73	0.07	0.12
minimum	0.77	0.02	4.36	0.65	0.01	0.39	53.57	0.03	0.09	0.01	2.63	0.02	0.07
n	8	8	8	8	8	8	8	8	8	8	8	8	8
std. dev.	0.66	0.04	3.14	0.40	0.14	0.58	5.46	0.06	0.04	0.03	4.83	0.02	0.02
Mn oxide oolite/pisolite													
mean	1.91	0.16	13.85	1.28	0.19	2.24	48.27	0.16	0.14	0.13	10.47	0.05	0.10
maximum	3.41	0.33	18.20	2.27	0.41	4.52	55.54	0.54	0.29	0.22	17.03	0.07	0.17
minimum	0.68	0.02	7.46	0.61	0.02	0.79	36.73	0.02	0.09	0.02	8.37	0.03	0.03
n	10	10	10	10	10	10	10	9	10	9	10	10	10
std. dev.	0.96	0.17	3.02	0.60	0.15	1.14	5.58	0.18	0.04	0.08	2.92	0.02	0.07
Mn oxide deformed oolite/pisolite													
mean	2.12	0.03	15.59	1.26	0.18	2.54	42.32	0.34	0.20	0.03	11.49	0.05	0.10
maximum	3.15	0.03	21.36	1.80	0.52	4.62	45.03	0.47	0.29	0.04	15.58	0.07	0.16
minimum	1.05	0.02	10.81	0.68	0.01	0.70	35.73	0.26	0.10	0.01	7.49	0.03	0.05
n	5	5	5	5	5	5	5	5	5	5	5	5	5
std. dev.	0.74	0.01	4.25	0.40	0.45	1.37	3.85	0.07	0.06	0.01	2.88	0.01	0.05
Unsorted Mn oxide ores													
mean	1.24	0.03	21.95	1.00	0.13	2.72	33.15	0.23	0.15	0.07	6.10	0.07	0.08
maximum	1.86	0.04	29.01	1.27	0.19	4.08	40.77	0.41	0.16	0.10	8.28	0.10	0.11
minimum	0.49	0.02	15.60	0.85	0.01	1.15	22.62	0.03	0.14	0.04	3.06	0.03	0.05
n	4	3	4	4	4	4	4	3	4	4	4	4	4
std. dev.	0.57	0.01	5.50	0.19	0.08	1.20	7.69	0.16	0.01	0.03	2.22	0.04	0.03
Banded Mn oxide ores													
mean	3.13	0.04	21.14	1.72	0.42	5.00	26.40	0.73	0.16	0.05	14.44	0.05	0.15
maximum	5.52	0.06	33.37	2.60	1.08	7.84	37.07	1.52	0.33	0.09	23.16	0.07	0.24
minimum	1.82	0.02	11.44	1.00	0.12	2.12	17.55	0.07	0.10	0.02	7.49	0.03	0.10
n	7	7	7	7	7	7	7	7	7	7	7	7	7
std. dev.	1.27	0.01	6.18	0.52	0.31	2.41	5.84	0.55	0.08	0.02	6.38	0.02	0.05

Table 5.5 (continued): Statistics of major and minor elements; [%].

	Al	Ba	Ca	Fe	K	Mg	Mn	Na	P	S	Si	Sr	Ti
Mn carbonate (calciorhodochrosite) oolite/pisolite													
mean	3.90	0.03	16.87	2.97	0.75	3.46	25.57	0.47	0.19	0.26	16.08	0.03	0.21
maximum	4.62	0.03	19.95	5.20	1.01	4.13	28.98	0.92	0.29	0.73	17.58	0.04	0.26
minimum	2.97	0.02	14.91	1.70	0.47	2.64	23.27	0.27	0.12	0.04	14.00	0.03	0.15
n	5	5	5	5	5	5	5	5	5	5	5	5	5
std. dev.	0.70	0.01	1.50	1.39	0.26	0.55	1.32	0.22	0.06	0.28	1.50	0.01	0.05
Mn carbonate (Mn-calcite) oolite/pisolite													
mean	1.65	0.05	33.30	0.91	0.20	1.75	18.39	0.16	0.09	0.03	8.55	0.05	0.09
maximum	3.09	0.06	35.14	1.57	0.41	2.84	33.26	0.35	0.10	0.03	12.54	0.06	0.15
minimum	0.23	0.05	31.42	0.27	0.01	0.65	10.11	0.04	0.07	0.02	4.25	0.04	0.03
n	3	3	3	3	3	3	3	3	3	3	3	3	3
std. dev.	1.35	0.01	1.84	0.65	0.20	0.97	8.08	0.12	0.01	0.01	4.08	0.01	0.06
Mn-bearing clayey siltstones													
mean	5.78	0.03	18.02	4.18	1.00	2.82	13.39	1.13	0.12	0.03	30.31	0.06	0.29
maximum	6.43	0.04	21.82	5.22	1.29	3.27	17.55	1.18	0.14	0.97	30.74	0.07	0.33
minimum	5.12	0.02	15.99	2.63	0.74	2.53	8.01	1.05	0.11	0.03	29.99	0.03	0.25
n	4	4	4	4	4	4	4	4	4	4	4	4	4
std. dev.	0.56	0.01	2.87	1.05	0.27	0.41	3.06	0.05	0.02	0.39	0.42	0.01	0.04
Mn-bearing oolitic/pisolitic limestones													
mean	2.02	0.02	35.44	4.14	0.34	2.84	8.48	0.13	0.14	1.05	10.55	0.08	0.09
maximum	2.32	0.02	43.81	8.14	0.41	3.47	11.81	0.19	0.19	3.86	13.60	0.09	0.10
minimum	1.84	0.01	30.41	1.16	0.22	2.03	5.28	0.10	0.07	0.10	5.94	0.07	0.07
n	4	4	4	4	4	4	4	4	4	4	4	4	4
std. dev.	0.31	0.01	7.37	3.36	0.11	0.72	3.11	0.03	0.06	0.91	3.00	0.01	0.01

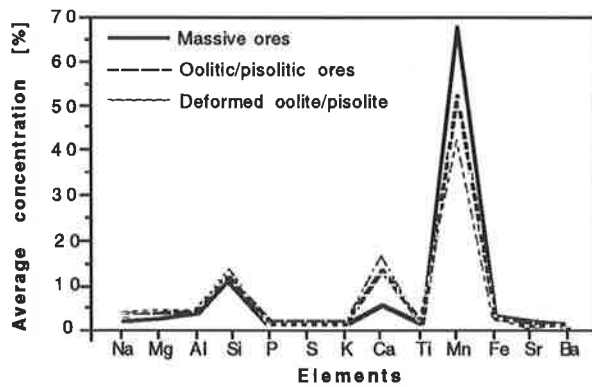


Fig. 5.2a Major and minor element concentrations in Mn oxide ores.

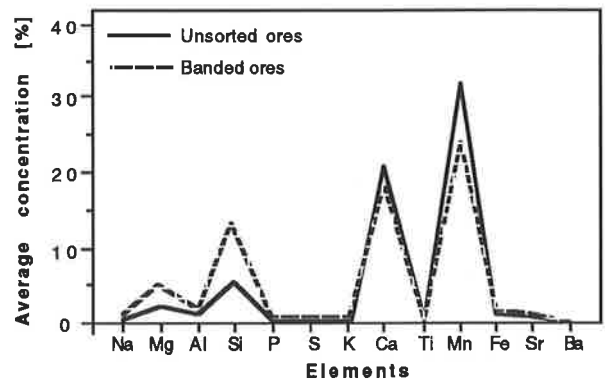


Fig. 5.2b Major and minor element concentrations in transitional (or mixed) Mn oxide ores.

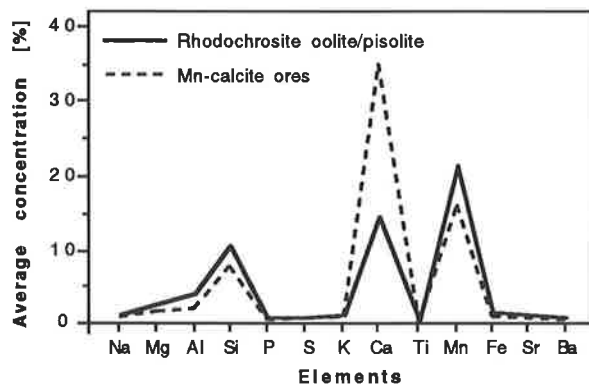


Fig. 5.2c Major and minor element concentrations in Mn carbonate ores.

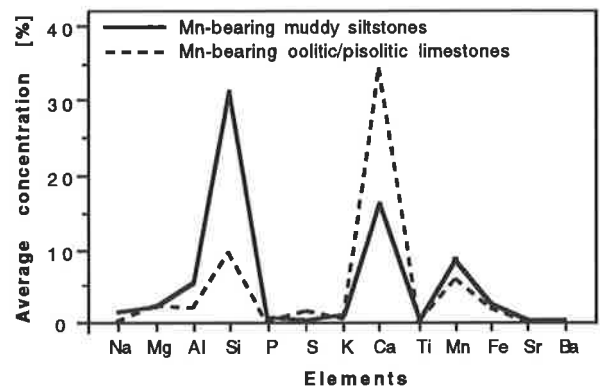


Fig. 5.2d Major and minor element concentrations in Mn-bearing rocks.

weak oxidation dominated by fine clastic rocks and weak reduction characterized by carbonates. The MnO_2 and MnO of Mn carbonates generally exhibit negative correlations with SiO_2 , Al_2O_3 , and CaO but positive correlations with CO_2 and Na_2O (Fig. 5.4c), which illustrates the close relationship between Mn carbonates and Mn^{2+} and CO_2 , and a reverse relationship with Ca.

On average, the supergene ores (e.g. sample 958-50, Table 5.3) are enriched in Mn (170%), Fe (210%), SiO_2 (150%), and Al_2O_3 (230%), but are depleted in CaO (18%), MgO (38%), P (71) and S (33%) relative to primary Mn oxides. This probably resulted from acid conditions during formation of Mn oxidized ores.

(2) XRF/AA Analyses

Although different in ore type (possibly also in mineralogy and petrology), compact massive Mn oxide oolite/pisolite, Mn oxide oolite/pisolite and Mn oxide deformed oolite/pisolite exhibit remarkable similarities in their major/minor element concentration patterns (Fig. 5.2a; compare also Table 5.5). The curves of both compact massive and deformed oolites/pisolites are almost identical to those of Mn oxide oolite/pisolite. The largest variations are observed for Ca and Mn (main calciorhodochrosite and braunite components). Compact massive oolite/pisolite shows concentration of Mn which is larger than those of both Mn oxide oolite/pisolite and deformed oolite/pisolite, whereas the latter two contain about twice or three times as much Ca as compact massive ore and also are slightly more enriched in Al and Si.

The plot for transitional ores shows concentrations and patterns comparable to the previous group (Fig. 5.2b). Both the unsorted and banded Mn oxide ores show lower Mn-concentrations and higher Ca-concentrations than those of the previous group, which reflects the increase of calciorhodochrosite and the decrease of braunite in these ores. The higher Si-concentrations relative to unsorted or banded Mn oxide ores indicate an increase in the supply of silty materials (quartz). Mg in banded ores is of little importance though it exhibits slightly higher levels than in other ores. All other elements approximate those of the Mn oxide group.

Although the ores dominated by calciorhodochrosite and Mn-calcite are both Mn carbonates, they show a few important differences in the Al-, Si-, Ca- and Mn-concentrations (Fig. 5.2c). The calciorhodochrosite ore possesses slightly higher Al-, Si- and Mn-concentrations, whereas Mn-calcite ores show much higher Ca-concentration, with other elements similar to each other and to the previous groups, which suggests that Mn-calcite ore probably formed in relatively more reducing environments (somewhat deeper water) than calciorhodochrosite ore, which also contains slightly more terrigenous material.

The remaining ores and rocks are strongly dominated by quartz and calcite (Fig. 5.2d). Si shows high concentrations and the ratio of the Si/Al peaks is approximately 6 in Mn-bearing clayey siltstones. This indicates that the silica may mainly come from presedimentary quartz grains. Significant levels of Ca in the ores reflect that a certain amount of carbonate was deposited together with terrigenous clastic materials. Additionally, the silica exhibits significant levels in Mn-bearing intraclastic carbonate rocks; Mn is of little importance in both rock types, suggesting that the ore-containing series mainly formed in weakly oxidizing to reducing environments.

5.2.2.2 Trace Elements

The trace elements (TEs) allow a further separation of ore and rock types. In general, the abundance of the TEs is similar in different ore types, but some individual elements (Ni, Zn, Rb, Sr and Zr) show variations, and all ore types are characterized by a sharp peak for Sr (Figs 5.3a-d; see also Table 5.6). High concentrations are also observed for Ni and Zn in all ores and gangues (110-350 ppm). The highest concentration of Ni occurs in Mn oxide (deformed) oolites/pisolites, and it decreases to unsorted (or banded) ores and then to Mn carbonate ores and Mn-bearing rocks, all of which show a parallel decrease in Mn.

In contrast, increasing concentrations are observed for Zn from Mn oxide ores to transitional ores, Mn carbonate ores through to Mn-bearing rocks, while Mn decreases. Rb, Sr, Zr and even Ga show the same trend as Zn. For other elements the curves of all ore and rock types are comparable, and elemental concentrations are similar, though the trace elements concentrations

Table 5.6: Statistics of trace elements in ores and rocks; [ppm].

	Ga	Nb	Ni	Pb	Rb	Sr	Th	U	Y	Zn	Zr
Compact massive Mn oxide oolite/pisolite											
mean	3.5	2.4	264.7	10.7	15.1	366.9	9.7	3.3	7.1	116.2	18.1
maximum	5.3	4.0	402.6	15.5	22.4	654.8	11.7	7.1	14.1	186.6	35.5
minimum	1.4	1.1	216.2	7.2	5.7	158.7	7.7	1.5	3.1	54.4	6.5
n	5	5	5	5	5	5	5	5	5	5	5
std. dev.	1.6	0.6	69.0	2.9	7.2	261.7	2.0	2.0	3.7	46.2	11.4
Mn oxide oolite/pisolite											
mean	3.0	2.6	348.0	11.5	11.7	421.4	7.0	2.6	12.1	180.2	25.4
maximum	5.5	5.2	928.3	26.5	25.1	660.1	10.6	5.0	24.4	446.7	49.6
minimum	0.3	1.4	110.6	2.4	5.2	212.2	4.9	1.1	7.1	41.6	10.5
n	10	10	10	10	10	10	10	9	10	10	10
std. dev.	1.6	1.1	217.7	7.0	7.4	113.8	1.7	1.1	4.9	121.4	12.3
Mn oxide deformed oolite/pisolite											
mean	3.7	2.9	297.1	12.2	14.1	477.3	7.3	3.1	15.4	155.8	23.7
maximum	4.4	4.3	523.0	20.9	33.7	717.6	8.4	4.7	24.3	233.7	44.6
minimum	2.8	2.1	168.1	8.0	5.0	275.2	5.5	2.2	10.0	117.0	10.0
n	5	5	5	5	5	5	5	5	5	5	5
std. dev.	0.6	0.9	183.2	4.7	10.3	186.1	1.1	1.1	4.9	40.6	12.2
Unsorted Mn oxide ores											
mean	1.7	2.0	156.3	10.3	11.5	521.4	6.1	1.4	7.4	122.0	19.3
maximum	2.1	2.6	254.1	14.5	15.6	916.2	6.7	2.1	8.7	164.8	30.4
minimum	0.8	1.3	76.9	7.4	5.5	283.8	5.7	0.7	6.6	56.0	4.7
n	4	4	4	4	4	4	4	4	4	4	4
std. dev.	0.6	0.5	73.5	3.0	4.3	281.1	0.4	0.6	0.9	53.4	10.8
Banded Mn oxide ores											
mean	3.9	3.3	197.7	14.8	22.5	406.9	5.4	1.3	14.0	151.1	34.6
maximum	7.4	5.4	562.3	30.5	57.6	627.3	8.0	2.8	22.1	327.0	61.5
minimum	1.2	2.1	51.9	6.5	6.4	267.9	2.8	0.2	7.4	39.0	16.4
n	7	7	7	7	7	7	7	7	7	7	7
std. dev.	3.1	1.7	168.5	8.7	17.7	112.7	1.7	0.9	7.1	96.7	14.9

Table 5.6 (continued): Statistics of trace elements in ores and rocks; [ppm].

	Ga	Nb	Ni	Pb	Rb	Sr	Th	U	Y	Zn	Zr
Mn carbonate (calciorhodochrosite) oolite/pisolite											
mean	5.5	5.1	159.1	10.9	41.7	274.0	7.8	1.7	14.8	152.3	61.1
maximum	5.8	6.4	221.4	13.6	54.5	320.5	9.6	2.0	18.4	241.3	73.1
minimum	5.0	3.9	85.6	9.8	29.2	233.4	5.6	1.2	11.3	67.9	39.7
n	5	5	5	5	5	5	5	5	5	5	5
std. dev.	0.3	0.9	65.7	1.6	11.9	49.6	1.4	0.3	2.5	68.7	13.1
Mn carbonate (Mn-calcite) oolite/pisolite											
mean	3.6	2.5	122.0	14.7	19.1	470.4	5.5	2.2	11.2	113.7	21.9
maximum	4.2	4.9	171.4	25.8	28.1	569.5	7.4	3.8	21.0	172.9	35.4
minimum	3.0	0.5	49.3	7.8	4.9	355.2	4.1	0.2	3.4	33.0	3.6
n	2	3	3	3	3	3	3	3	3	3	3
std. dev.	0.6	1.8	52.5	8.0	9.8	88.5	1.4	1.8	10.4	59.1	13.4
Mn-bearing clayey siltstones											
mean	11.5	7.8	119.3	12.1	79.6	339.5	9.8	2.3	26.2	192.0	107.6
maximum	18.9	13.1	197.9	18.9	140.2	647.8	13.6	5.0	46.4	352.6	174.2
minimum	7.4	5.3	61.1	6.0	40.0	106.2	7.8	0.2	16.6	77.5	67.5
n	6	6	6	6	6	6	6	6	6	6	6
std. dev.	5.5	2.9	45.9	6.1	34.0	222.5	2.5	2.3	13.9	100.5	33.6
Mn-bearing oolitic/pisolitic limestones											
mean	3.1	2.3	127.5	10.0	19.6	702.0	5.7	0.7	11.9	169.9	23.2
maximum	5.2	3.3	219.8	15.0	24.4	940.6	7.1	1.3	15.0	522.8	34.6
minimum	1.4	1.1	49.3	7.4	11.2	486.5	4.1	0.1	8.5	33.0	5.8
n	5	5	5	5	5	5	5	5	5	5	5
std. dev.	1.3	0.7	75.5	2.7	5.8	146.9	1.2	0.5	2.8	141.3	15.0

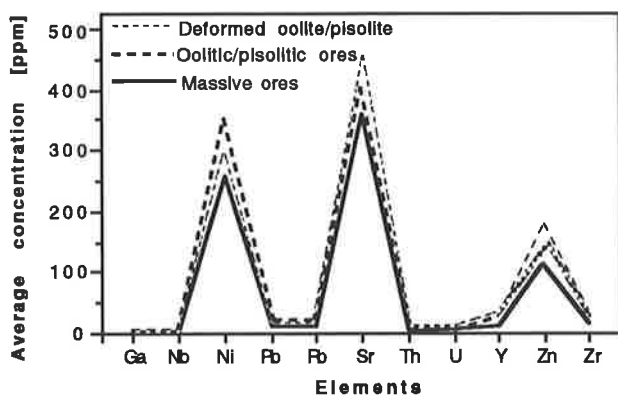


Fig. 5.3a: Trace element concentrations in Mn oxide ores.

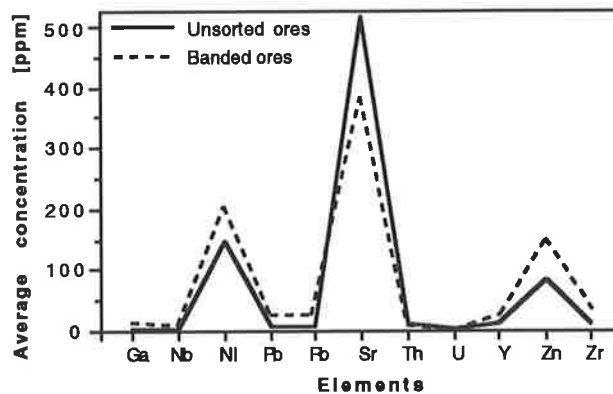


Fig. 5.3b : Trace element concentrations in transitional (or mixed) Mn oxide ores.

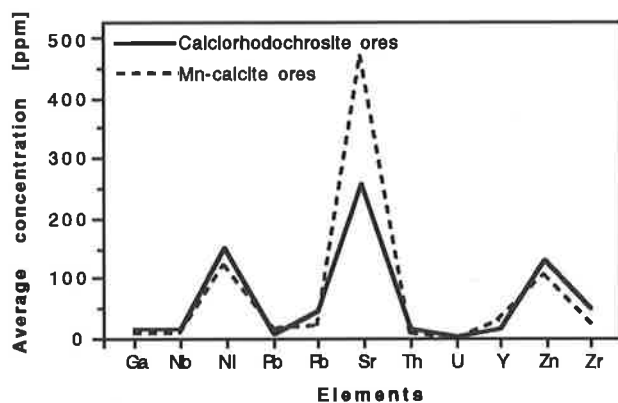


Fig. 5.3c: Trace element concentrations in Mn carbonate ores.

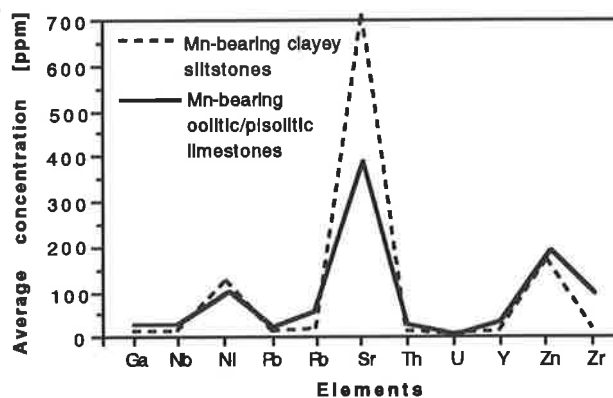


Fig. 5.3d: Trace element concentrations in Mn-bearing hosted rocks.

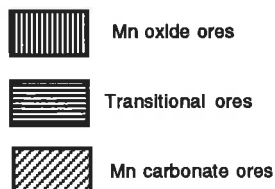
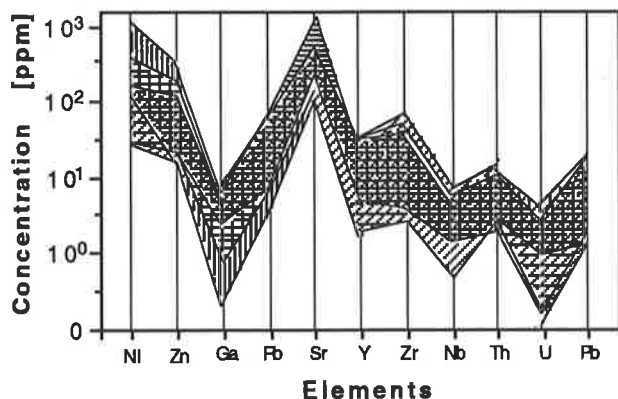


Fig. 5.3e: Trace element range of all samples of manganese ores.

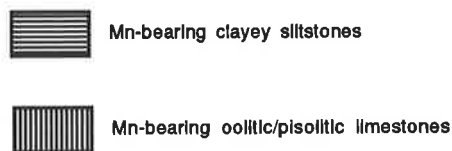
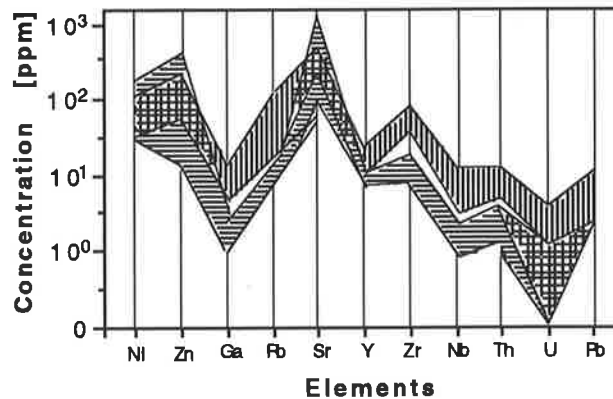


Fig. 5.3f: Trace element range of all samples, concentrations in Mn-bearing rocks.

described above vary considerably in different ore and rock types. Significantly, Zr gains importance in poor quality ores and silt/clay-rich products where it reaches levels similar to Ni (Fig 5.3d).

In an overview, ranges of the respective materials are compared (Figs. 5.3e-f). Although the Mn oxide ores show less variability in their trace element composition than the transitional ores which, in turn, show smaller variations in their trace element composition than the Mn carbonate ores (Fig. 5.3e), the patterns for TEs of the three ore types are similar. Some of the Mn oxide ores show marked depletions in Ga, whereas some of the transitional and carbonate ores are depleted in U. However, all Mn-ores contain relatively high concentrations of Ni and Sr.

Clayey siltstones and oolitic/pisolitic limestones can also be considered as "end-members" in the sense that they contain different dominant gangue minerals (in association with Mn-ores). These materials appear in almost any possible combination as gangue or within ore (Fig. 5.3f, see also Chapter 4). Probably as a result of this, the trace element concentrations of both rock types are generally similar to those of the Mn-ores, and as gangue they "dilute" bulk sample compositions of ores with lower trace element levels (e.g. Ni) or in the case of relatively high trace element concentrations (e.g. Zn, Zr), they may superimpose their signature upon ores.

Both rock types associated with Mn-ores contain a number of elements in concentrations near the upper limits observed. The ranges of clayey siltstone and oolitic/pisolitic limestone overlap for the lighter elements (Ni and Zn, Rb-Y) and also for U. The trace elements of clayey siltstone dominate over those of oolitic/pisolitic limestone.

5.2.2.3 *Rare Earth Elements*

The geochemistry of the rare-earth elements (REEs) has for some years been of interest to those involved in the study of deep-sea ferromanganese nodules and encrustations (Goldberg et al., 1963; Piper, 1974; Glasby, 1973; Fleet, 1983; De Baar et al., 1985; Calvert et al., 1987; Hein et al., 1988). But for shallow-marine continental margin and epicontinental seas, there are few data concerning the distribution of REEs in manganiferous deposits (Glasby, 1973; Ingri and Pontér, 1987; Pracejus et al., 1990). Typically, these deposits show much lower concentrations of REEs compared to deep-sea deposits and commonly the Ce anomaly is weak or absent. Similarly, there are very few data on the distribution of REEs in ancient sedimentary manganese oxide deposits (Grasselly and Pantó, 1988; Pracejus et al., 1990). These deposits possess REE concentrations comparable to the Dounan deposit, the Ce anomaly is generally positive and the Eu anomaly negative. These and other studies indicate that an understanding of the geochemistry of the REEs may be an useful aid in the determination of the processes and environment of deposition and possible sources of elements in the deposits (e.g. Elderfield et al., 1981). Thus, the first data on the rare-earth element geochemistry of Mn ores from the Dounan Mn deposit in

Yunnan of China are presented in this text, also the observed patterns of shale-normalized ores are compared with other manganese and ferromanganese deposits. Since the manganese ores were expected to contain very low REE concentrations, it was only possible to analyze the ores by a complex analytical technique, Isotope Dilution Mass Spectrometry (IDMS), a technique generally regarded as being the most accurate for REE analysis (Thirwall, 1981).

Studies of the REE contents of sedimentary rocks (Haskin et al., 1966, 1968; Wildeman and Haskin, 1973; Wildeman and Condie, 1973; Cullers et al., 1974) have shown remarkably little variation, attesting to the powerful homogenizing ability of most sedimentary processes. However, Ce (+3, +4) and Eu (+2, +3) are an exception because these elements appear in different valencies, which make them more mobile (Piper and Graef, 1974). Since the REE contents of clastic sedimentary rocks are likely to reflect changing REE compositions of crustal source regions (Jakes and Taylor, 1974), chemical sediments are likely to provide the best evidence as to behavior of the REE in the sedimentary environment through time. Therefore, a depletion or enrichment of the REEs in the various primary or secondary materials may reflect sedimentary or diagenetic processes much better than the elements discussed earlier. Rare earth data on the manganese ores are valuable in that they give additional boundary conditions for any hypothesis of Mn ore genesis. In particular, five factors can be considered:

- the absolute REE abundance, which is dependent on the rate of deposition of the REE from seawater;
- the REE distribution pattern, which gives some indication of the mode of uptake of the REE into the manganese ore structure from seawater;
- the La/Yb (or $\Sigma\text{LREE}/\Sigma\text{HREE}$) ratio, which probably is a reflector of alkalinity (pH) of the environment;
- the cerium enrichment (Ce/La ratio), which is a possible redox indicator; and
- the Ce and Eu anomalies, which are also referred to as redox indicators because of their multiple oxidation states.

An overview of statistical data is given in Table 5.7. Because of the difficulties of analysis, this work was limited to the study of 18 Mn ore and rock samples.

A comparison of the total ΣREE content of calciorhodochrosite oolite/pisolite with those of Mn oxides (Table 5.7) indicates a twofold enrichment in the former relative to the latter. This provides evidence as to the important role played by redox environments in the concentration of REEs. However, the recrystallized Mn-calcite shows similar ΣREE to the Mn oxides, which in part probably results from alteration events after sedimentation. Presumably, the Mn carbonate phases played a more important role in the primary enrichment of REE than the Mn oxide phases, however, a further decrease of the REE content in recrystallizing Mn carbonate results from the later changes. When comparing the ΣREE content of the various ore types, some regularity among the environments of the basin and the ΣREE content of the samples of sections is apparent. ΣREE is 63 ppm in Mn carbonate; in the overlying transitional ores, it is 35 ppm; still higher, in the Mn oxide deformed oolite/pisolite, total REE content is 30 ppm; and

Table 5.7a: Statistics of Rare Earth Elements in ores and associated rocks; [ppm].

	La	Ce	Nd	Sm	Eu	Gd	Dy	Er	Yb	ΣREE
Compact massive Mn oxide oolite/pisolite										
mean	2.49	6.25	2.23	0.46	0.10	0.57	0.55	0.36	0.43	13.44
maximum	3.07	7.22	3.14	0.98	0.22	1.05	1.22	0.74	0.64	18.28
minimum	1.92	5.18	1.27	0.12	0.02	0.29	0.08	0.16	0.22	9.16
n	3	3	3	3	3	3	3	3	3	3
std. dev.	0.59	1.05	0.92	0.37	0.06	0.35	0.52	0.28	0.27	4.23
Mn oxide oolite/pisolite										
mean	4.68	6.67	3.59	0.76	0.17	0.98	0.92	0.60	0.53	18.90
maximum	5.74	7.01	4.74	1.12	0.21	0.99	1.25	0.73	0.82	22.61
minimum	3.42	6.11	2.45	0.20	0.11	0.97	0.53	0.42	0.14	14.35
n	3	3	3	3	3	3	3	3	3	3
std. dev.	0.96	0.40	1.03	0.40	0.03	0.01	0.30	0.13	0.28	4.30
Mn oxide deformed oolite/pisolite										
mean	6.95	12.89	4.47	0.88	0.20	0.86	0.79	0.45	0.39	27.88
maximum	7.12	13.89	5.01	0.89	0.26	0.97	0.99	0.52	0.41	30.06
minimum	6.62	11.57	3.91	0.88	0.12	0.73	0.45	0.35	0.37	25.11
n	3	3	3	3	3	3	3	3	3	3
std. dev.	0.07	0.96	0.45	0.01	0.06	0.10	0.32	0.07	0.02	2.79
Unsorted Mn oxide ores										
mean	6.44	12.92	5.42	1.18	0.27	1.21	1.16	0.67	0.60	29.87
maximum	7.52	14.59	5.82	1.98	0.29	1.54	1.76	0.70	0.66	34.59
minimum	5.23	11.35	5.03	0.45	0.25	0.82	0.70	0.62	0.57	25.02
n	3	3	3	3	3	3	3	3	3	3
std. dev.	0.98	1.50	0.40	0.70	0.02	0.35	0.58	0.04	0.04	4.12
Mn carbonate (calciorhodochrosite) oolite/pisolite										
mean	13.64	27.40	9.41	2.26	0.48	2.24	2.23	1.33	1.24	60.23
maximum	14.53	27.95	9.81	2.38	0.51	2.48	2.30	1.83	1.44	63.23
minimum	12.55	26.45	8.66	2.12	0.45	1.96	2.11	0.96	0.96	56.22
n	3	3	3	3	3	3	3	3	3	3
std. dev.	0.99	0.60	0.50	0.13	0.03	0.25	0.15	0.40	0.20	3.01
Mn carbonate (Mn-calcite) oolite/pisolite										
mean	2.15	4.32	1.72	0.40	0.10	0.57	0.61	0.38	0.32	10.57
maximum	2.25	4.72	1.92	0.48	0.14	0.87	0.67	0.53	0.35	11.93
minimum	1.97	3.66	1.34	0.31	0.07	0.38	0.52	0.34	0.29	8.88
n	3	3	3	3	3	3	3	3	3	3
std. dev.	0.10	0.55	0.27	0.08	0.03	0.25	0.07	0.17	0.03	1.23

Table 5.7b: Statistics of ratios, anomalies and enrichment ratios in REE*.

	Ce / La	La / Yb	$\frac{\sum \text{LREE}}{\sum \text{HREE}}$	LREE enrichment La/Sm	HREE enrichment Yb/Sm	Cerium anomaly	Erbium anomaly
Compact massive Mn oxide oolite/pisolite							
mean	1.27	0.60	6.37	1.51	2.24	+0.02	-0.01
maximum	1.33	0.86	10.35	2.50	3.50	+0.02	-0.01
minimum	1.20	0.42	3.95	0.54	1.46	+0.01	-0.02
n	3	3	3	3	3	3	3
std. dev.	0.06	0.22	3.25	0.11	1.21	0.00	0.00
Mn oxide oolite/pisolite							
mean	0.72	0.69	5.21	0.81	1.21	-0.02	+0.02
maximum	1.00	1.41	5.64	0.93	1.67	+0.01	+0.02
minimum	0.64	0.56	4.91	0.57	0.50	-0.04	+0.02
n	3	3	3	3	3	3	3
std. dev.	0.28	0.12	0.41	0.12	0.37	0.01	0.00
Mn oxide deformed oolite/pisolite							
mean	0.94	1.42	10.32	1.39	1.00	+0.01	0.00
maximum	1.00	1.45	12.90	1.42	1.00	+0.02	+0.04
minimum	0.88	1.42	9.60	1.33	1.00	0.00	-0.04
n	3	3	3	3	3	3	3
std. dev.	0.06	0.01	0.62	0.03	0.00	0.01	0.00
Unsorted Mn oxide ores							
mean	1.01	0.89	7.41	1.50	1.57	+0.01	-0.03
maximum	1.08	1.06	9.93	3.00	2.83	+0.02	+0.06
minimum	0.94	0.76	6.06	0.63	0.74	0.00	-0.06
n	3	3	3	3	3	3	3
std. dev.	0.07	0.11	2.24	0.21	0.72	0.01	0.00
Mn carbonate (calciorhodochrosite) oolite/pisolite							
mean	1.01	0.87	10.54	1.08	1.22	+0.04	-0.02
maximum	1.06	1.07	10.90	1.10	1.33	+0.05	-0.01
minimum	0.97	0.80	10.01	1.06	1.00	+0.03	-0.03
n	3	3	3	3	3	3	3
std. dev.	0.04	0.08	0.42	0.02	0.14	0.01	0.01
Mn carbonate (Mn-calcite) oolite/pisolite							
mean	1.13	0.50	4.50	0.93	1.84	+0.01	-0.01
maximum	1.20	0.56	4.80	1.25	2.25	+0.01	+0.03
minimum	1.00	0.45	4.18	0.71	1.43	+0.01	-0.03
n	3	3	3	3	3	3	3
std. dev.	0.07	0.06	0.30	0.19	0.41	0.00	0.01

* Data sources as for Table V. 3; all REE contents are shale-normalized, with exception of $\sum \text{LREE} / \sum \text{HREE}$ ratio; Ce anomaly = $\text{Ce}_n / (\frac{2}{3}\text{La}_n + \frac{1}{3}\text{Nd}_n)$; Eu anomaly = $\text{Eu}_n / (\frac{2}{3}\text{Sm}_n + \frac{1}{3}\text{Gd}_n)$.

at the top, in Mn oxide oolite/pisolite, the ΣREE is 20 ppm. A decrease from bottom to top of the orebody is therefore apparent.

The unnormalized REE concentration patterns are used to differentiate some of the ore types. Generally, both the Mn oxides and Mn carbonates show decreases in concentrations from the light and middle REEs (LREE, i.e. La, Ce, Nd/Sm, Eu and Gd) towards the heavy REEs (HREE, i.e. Dy, Er and Yb), with the strongest drop in concentrations between Ce and Sm (Figs. 5.4a-b). Most ores are depleted in Eu relative to the concentration of neighboring elements and are enriched in Gd and Ce. However, strong differences among the respective ore types are observed. Mn oxides exhibit almost identical patterns for the HREEs (Fig. 5.4a). The average is characterized by a moderately steep pattern ($\Sigma\text{LREE}/\Sigma\text{HREE}=7.39$, Table 5.6b and Figs. 5.4a-b) and a small negative europium anomaly (~-0.05) and a slight positive cerium anomaly ($\sim+0.07$) (Table 5.7b). A pronounced Ce enrichment occurs in the Mn oxide deformed oolite/pisolite and a relatively small enrichment characterizes the Mn oxide oolite/pisolite and compact massive Mn oxide ores. This fact can probably be used to chemically distinguish the deformed oolitic/pisolitic ores from other Mn oxides.

A variety of Mn carbonate and unsorted ore types show REE patterns similar to those of Mn oxides (Fig. 5.4b). However, REE concentrations of some of these ores are relatively high compared with Mn oxide materials. Calciorhodochrosite oolite/pisolite, in particular, possesses extreme enrichment of the LREEs, which is unequalled by any other ores of the deposit. Unsorted Mn oxide ores display patterns very similar to that of Mn oxide oolite/pisolite, they have higher Ce concentrations. Though the Mn-calcite oolite/pisolite exhibits a positive Ce anomaly, the Ce concentration is the lowest of all ore types. Thus, although magnitudes differ, the Mn oxides and Mn carbonates display patterns that are identical to each other.

When the relationships between various ore or gangue minerals and the REE contents are examined, it becomes clear that two minerals play a dominant role in concentrating REEs. Calciorhodochrosite and Mn-calcite seem to be enriched in most of the REEs and its abundance correlates particularly well with La, Eu, Nd and Sm (Figs. 5.5a-b). Braunite, in contrast, is not enriched in most of the REEs and also has pronounced negative correlations with La, Eu, Nd and Sm (Figs. 5.5b-c). However, depending on the ore type, La_n/Yb_n values (where n refers to shale-normalized ratio), which indicate relative behavior of LREEs to HREEs, remain in the range ~ 0.50 to ~ 1.42 from all ore types (Table 5.7b), overlapping with estimated average terrigenous input (~ 1.3 ; Sholkovitz, 1990). Also, La/Yb ratios exhibit similar behavior relative to the abundance of Mn carbonate and Mn oxide minerals in rock samples (Figs. 5.5d-e), which reflects a similar mode of mineralization. Ce is concentrated in both braunite and calciorhodochrosite, but it is not concentrated in Mn-calcite oolitic/pisolitic ores, for which the concentrations of Eu and Ce (Fig. 5.5f) do not exhibit obvious increases or decreases when the abundance of manganese minerals varies. Both Eu and Ce anomalies vary within a small range ($+0.05$ to -0.05), which probably suggests a stable precipitation environment. The calculated

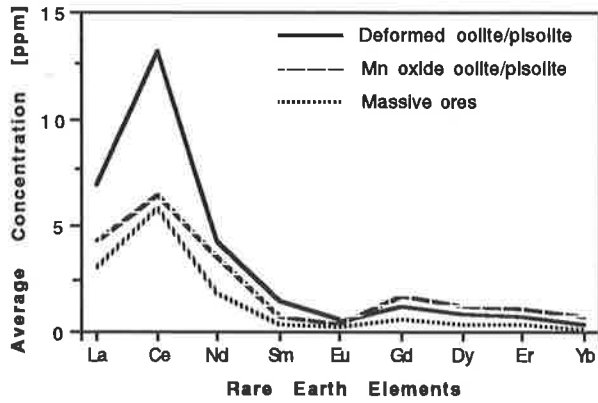


Fig. 5.4a: Mean REE concentration patterns of Mn oxides

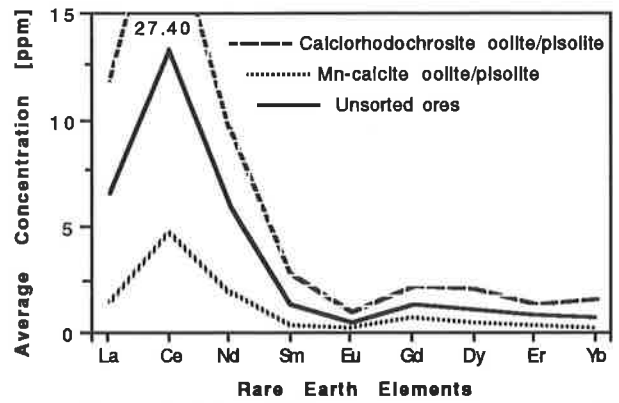


Fig. 5.4b: Mean REE concentration patterns of Mn carbonates and unsorted ores

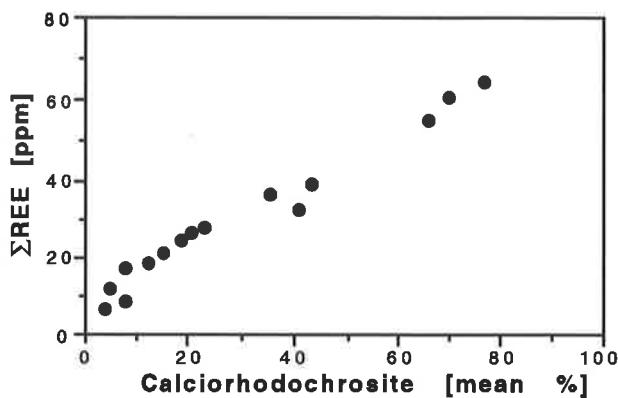


Fig. 5.5a: Scatter plot of total REE and calciorhodochrosite content

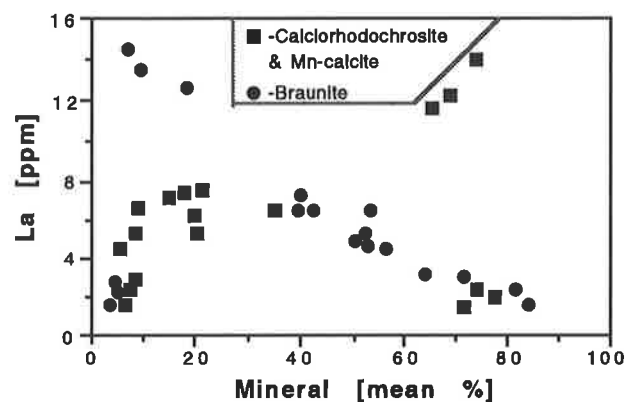


Fig. 5.5b: Scatter plot of Mn minerals and La

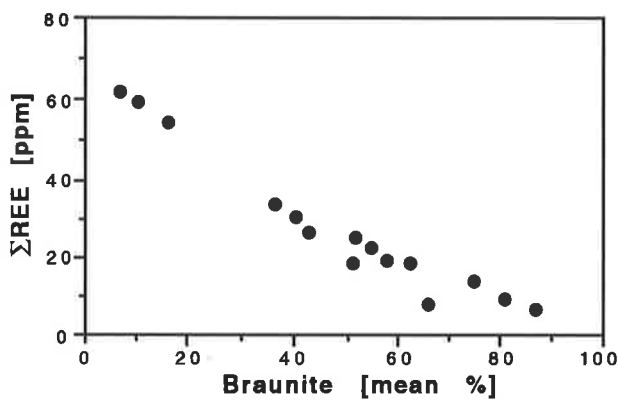


Fig. 5.5c: Scatter plot of total REE and braunite content.

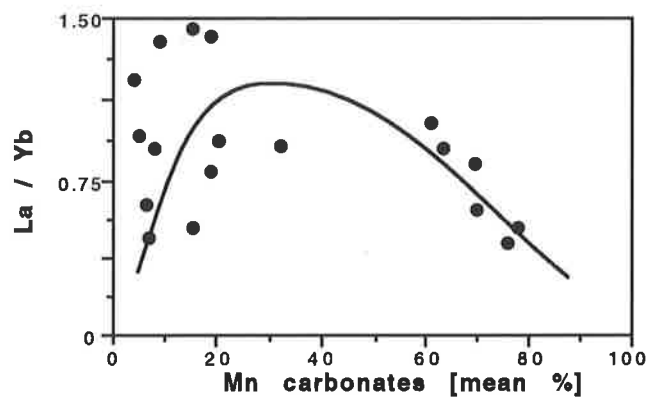


Fig. 5.5d: Scatter plot of calciorhodochrosite content and La/Yb ratio.

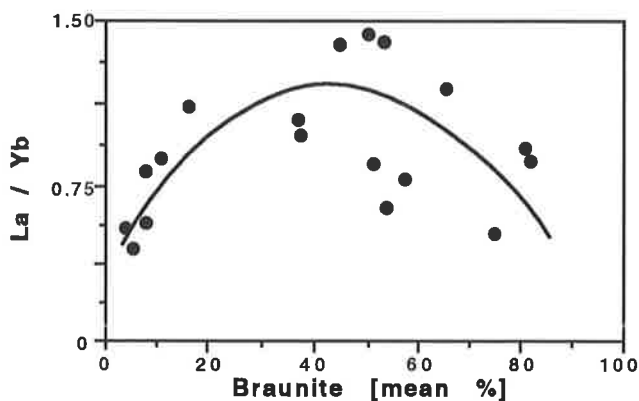


Fig. 5.5e: Scatter plot of braunite content and La/Yb ratio.

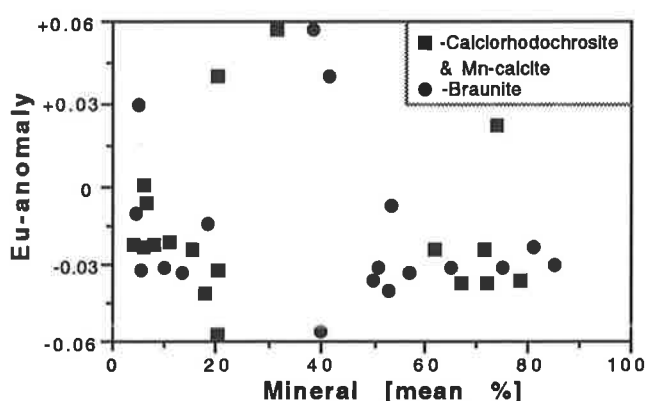


Fig. 5.5f: Scatter plot of Mn minerals and Eu-anomaly.

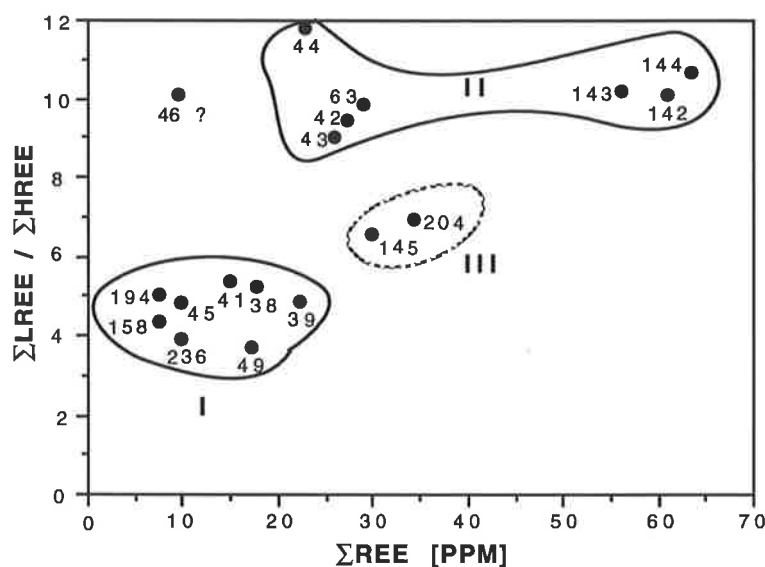


Fig. 5.6 Scatter plot of ΣREE and $\Sigma\text{LREE}/\Sigma\text{HREE}$; sample numbers are indicated at the side of the respective points; all samples have the common prefix 958. Group I - oxides; Group II - carbonates; Group III - transitional ores.

anomalies for Eu and Ce show the deviation of the respective element from the interpolated values between the adjacent elements. The direction of this deflection is indicated by plus or minus signs [$\text{Eu}_{[\text{anomaly}]} = \text{Eu}^* - (1/2 \text{Sm}^* + 1/2 \text{Gd}^*)$; $\text{Ce}_{[\text{anomaly}]} = \text{Ce}^* - (2/3 \text{La}^* + 1/3 \text{Nd}^*)$; * shale-normalized element].

La is the strongest alkaline element in REEs, as alkalinity decreases with increasing atomic number of REEs (Zhao, 1978). Thus, a highly alkaline environment is favorable for LREE enrichment; whereas HREEs are enriched in more acidic environments. The REE concentrations and $\Sigma\text{LREE}/\Sigma\text{HREE}$ ratio of the ores seem to depend strongly on the ore type and possibly on the of depositional environments. $\Sigma\text{LREE}/\Sigma\text{HREE}$ ratios of the Dounan Mn ores exhibit a positive correlation with the ΣREE concentrations in Figure 5.6, in which three groups can be observed. Group I shows both lower ΣREE concentrations and $\Sigma\text{LREE}/\Sigma\text{HREE}$ ratios, considered to be slightly alkaline to acidic ores mainly composed of Mn oxides, except for sample 958-46 (massive Mn ore). The latter shows a low value of ΣREE concentration but a high ratio $\Sigma\text{LREE}/\Sigma\text{HREE}$ probably resulting from diagenetic influence. Group II exhibits relatively high ΣREE concentrations and $\Sigma\text{LREE}/\Sigma\text{HREE}$ ratios and mainly consists of alkaline REE in Mn carbonate and some transitional banded ores. Group III shows medium behavior between groups I and II, and is made up of transitional unsorted ores. The two samples of Mn-calcite ore included here unexpectedly fall in group I, probably due to secondary change or sampling. Most differences between the groups in Figure 5.6 probably result from different precipitation environments or pH/Eh values.

The several ore types show similar Ce/La ratios (~ 1 ; Table 5.7b) which indicates that they did not form in greatly different environments, but rather under similar redox conditions, which is in accord with the observations and interpretations in previous chapters. That the highest Ce/La ratio of the Mn oxides is associated with the highest Ce/La ratio of the Mn carbonates suggests that the sediments are influenced by the same processes and that Ce is oxidized to the tetravalent state not only in the Mn oxides but also in the Mn carbonates by the same mechanism (Glasby

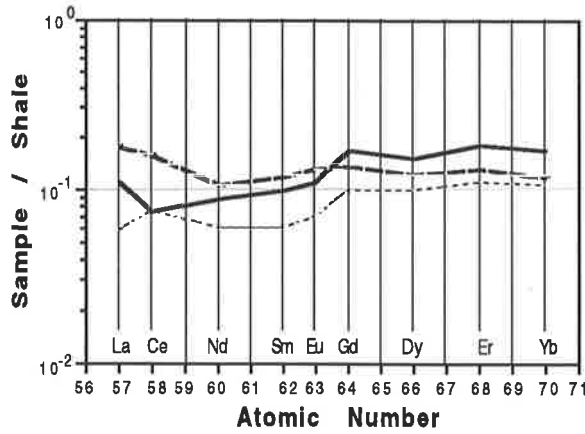


Fig. 5.7a Shale-normalized REE-patterns of Mn oxides.

— Mn oxide oolite/pisolite;
 - - - Mn oxide deformed oolite/pisolite;
 ····· Massive Mn oxide oolite/pisolite.

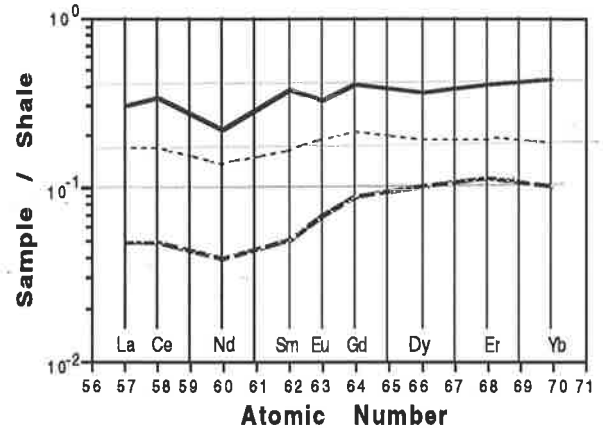


Fig. 5.7b Shale-normalized REE-patterns of Mn carbonates & unsorted ores.

— Calciorhodochrosite oolite/pisolite;
 - - - Mn-calcite oolite/pisolite;
 ····· Unsorted ores.

et al., 1987). However, the moderate increase in Ce/La from Mn oxides (0.72) to Mn carbonates (~1.13) may be due to increased reduction during sedimentation, with a corresponding increase in transitional ore. One can judge the Ce/La ratio for the terrigenous component from the Ce and La levels in the terrigenous suspensate (Gordeyev, 1983) and in terrigenous sediments in inland and marginal seas, as well as in the biogenic-terrigenous sediments in shelf zones (Volkov and Fomina, 1973; Brongersma-Sanders et al., 1980). The Ce/La ratios in terrigenous materials are similar to those in shale (Piper, 1974) and are ~2, substantially higher than for ocean water (0.1-0.5; Dubinina and Volkov, 1986), so the REE in terrigenous material may raise Ce/La in the sediment.

5.2.3 Shale-normalized REE-Patterns

The shale-normalized REEs (Haskin and Haskin, 1966) of all ore types from Dounan Mn deposit are very similar to each other, with calciorhodochrosite oolite/pisolite showing a strong Σ REE concentration and Mn-calcite oolite/pisolite exhibiting lower Σ REE concentration (Figs. 5.7a-b). Significantly, most REE patterns of the Dounan ores exhibit the slightly positive Ce anomalies which are generally regarded as of primary marine or early diagenetic origin. The exception is Mn oxide oolite/pisolite, which has the characteristic negative Ce anomaly typical of sea water (e.g. Elderfield and Sholkovitz, 1987).

The LREE and HREE are slightly enriched in calciorhodochrosite oolite/pisolite and unsorted ores. REEs of all ore types show comparable patterns in both IREE and HREE, but the concentration of LREE is moderately lower in the Mn oxide and Mn-calcite oolites/pisolites (Figs. 5.7a and b). The heavier elements display less fractionation than the light elements. The normalized REE concentrations of the ores decrease gradually from La to Nd, then increase

slightly to Er and again decrease slightly to Yb, with the exception of calciorhodochrosite oolite/pisolite in which from Nd to Yb the normalized concentrations increase slightly (Fig. 5.7b).

As with the elements discussed above, the REE concentrations of the ores strongly depend on the ore type. Mn oxide ores exhibit comparable concentrations of the entire group of the Rare Earths (Σ REE). A similar correlation between the shale-normalized REE-patterns of individual ore types is also observed, with the exception of a slight difference in Ce anomalies. The concentrations from Nd to Gd of Mn oxide oolite/pisolite seems to increase slightly more rapidly than those of other Mn oxide ores (Fig. 5.7a). The Mn carbonates and unsorted Mn oxide ores show extremely similar patterns to those of Mn oxides though the ores differ in their appearance and mineralogy. Although calciorhodochrosite and Mn-calcite oolites/pisolites also show similar shale-normalized REE-patterns, the former exhibits an increasing concentration of the entire group of the Rare Earths (Σ REE), whereas the latter shows a decreasing concentration of Σ REE and a larger LREE depletion than other ores. Also, note from Table 5.7b that the REE patterns for both Mn oxides and Mn carbonates are slightly more enriched in heavy REE compared to light REE, with the exception of Mn oxide deformed oolite/pisolite which is slightly enriched in light REE.

Both Mn oxides and Mn carbonates as well as the transitional types (unsorted and banded ores) show surprisingly similar REE patterns to each other, though some ores possess small differences, e.g. a slight positive Ce anomaly (+0.04) in massive Mn oxide ore, a smaller negative Ce anomaly (-0.02) in Mn oxide oolite/pisolite and a weak negative Eu anomaly (-0.03) in rhodochrosite oolite/pisolite (Table 5.7b and Figs. 5.7a-b). Elderfield and Sholkovitz (1987) concluded that Ce is significantly enriched in pore waters by diagenesis in the interfacial cycling process of seawater-sediment-porewater in the zone of Mn and Fe dissolution/precipitation, near the interface relative to Nd, its REE neighbor. Hence, the difference in the Ce anomalies of the ores probably reflects a development from sedimentation to early diagenesis, and must, therefore, reflect enhanced Ce mobilization and cycling, which is restricted to near the sediment-water interface. The Ce enrichment in most ores and the Ce negative anomaly in Mn oxide oolite/pisolite, as observed in this study, also favor the conclusion that sea water is the probable source for the REE in the Mn ores. Thus, an analysis of the normalized REE patterns from Dounan Mn ores demonstrates that though the ores differ in their appearance and mineralogy, the behavior of REEs is comparable for all ores.

5.2.4 Electron Microprobe Analysis (EMPA)

It is well-known that the crystal chemistry and genesis of Mn carbonate minerals are relatively simple. However, the mineral braunite, of general composition $\text{Mn}^{2+} \text{Mn}^{3+}_6 \text{SiO}_{12}$ (Fleischer, 1987) exists in two polytype forms, normal braunite (or braunite I) which corresponds to chemical composition $3\text{Mn}_2\text{O}_3 \cdot \text{MnSiO}_3$, with about 10% SiO_2 and a rarer form, braunite II, which

appears to contain essential calcium and iron, much less SiO_2 (about 4%) and has an ideal formula $\text{Ca}(\text{Mn}_{12}\text{Fe}_2)_3 + \text{SiO}_{24}$ (De Villiers, 1980). The existence of other elements, such as magnesium, barium, and boron in the mineral has been reported by Frenzel (1980). For braunite, both the crystal chemistry and the genesis are not only complex but unresolved. Thus, it is necessary to examine the microanalysis of minerals so that more genetic information about the deposit can be provided. The microanalyses of all Mn minerals from Dounan are listed in Table 5.8a-b.

Electron microprobe analysis from a number of areas of five basic morphologies of braunite indicate that all braunites from different ore types belong to the normal braunite type, with about 10% of SiO_2 , and are not braunite II, with 4.4% SiO_2 as defined by De Villiers and Herbstein (1967). An exception is the braunite from some Mn carbonate samples with ~20% SiO_2 , which probably results from secondary changes. The analyses also suggest that:

- calcium, at about 0.5-2.5% CaO, is a constant feature of all the analyses, with the exception of the braunite from Mn carbonate, in which braunite carries considerably more calcium (~7-15% CaO);
- in five basic morphologies of braunite, the braunite from massive ore possesses the highest Mn concentration (at 74-78% $\text{MnO}_2 + \text{MnO}$); from deformed or unsorted ores it contains high manganese (at 65-78% $\text{MnO}_2 + \text{MnO}$); the braunite of Mn oxide oolite/pisolite shows relatively low Mn concentration (at 50-70% $\text{MnO}_2 + \text{MnO}$); the braunite from Mn carbonate, however, contains the lowest manganese (at 30-37% $\text{MnO}_2 + \text{MnO}$);
- the braunite from Mn oxide and carbonate oolites/pisolites contains iron and magnesium which are largely absent from other ore types;
- other elements, (Al, Ca, Mg, and Si) are constant features of all braunite analysis.

The deviation of the analytical totals from 100% for braunite is probably due to the presence of different valencies of manganese present, which cannot be determined by electron microprobe analysis.

Recently, Abs-Wurmbach et al (1983) identified coupled isomorphous exchanges between Mn^{3+} , Fe and Mn^{2+} and Ca in braunite, and discussed the calcium end-member, neltnerite ($\text{Ca Mn}^{3+}_6 \text{SiO}_{12}$). Frenzel (1980) lists values of CaO ranging from 1.2 to 4.3% in braunite. On the basis of the above it appears that the Dounan braunite contains calcium in its structure but, in the massive and deformed Mn oxide oolites/pisolites, at least, there is little evidence that Ca has exchanged with Fe. Nevertheless, the braunite from Mn carbonate contains relatively more Ca and Si, which probably resulted from diagenetic changes.

Variation in the manganese content of braunites from the different ore types strongly suggests that primary braunite, identified by primary textures or structures, has relatively low manganese concentration, whereas high concentration Mn braunite probably formed during diagenetic enrichment. Thus suggestion is supported by the fact that relatively low-Mn braunite is found in well-developed concentric rings in Mn oolites/pisolites, while high-Mn braunite occurs in poorly-developed concentric rings (due to recrystallization or replacement). Reprecipitation or

Table 5.8a: Microanalysis of braunite from the Dounan ores [wt.%].

Area	MnO/ MnO ₂ *	FeO	CaO	MgO	K ₂ O	Na ₂ O	Al ₂ O ₃	SiO ₂	TiO ₂	Cr ₂ O ₃	Total
Mn oxide deformed oolite / pisolite [sample No. 958-40]											
1	78.67	nd.	1.07	0.28	nd.	nd.	1.19	10.11	0.34	0.05	97.71
2	75.85	0.06	0.79	0.04	0.10	nd.	1.01	9.34	0.22	nd.	87.41
3	74.57	nd.	0.91	1.32	0.03	nd.	1.26	10.31	0.03	nd.	88.42
4	66.24	nd.	1.04	0.89	0.02	0.01	1.65	10.24	3.19	nd.	83.27
5	64.50	nd.	7.46	0.77	nd.	0.19	1.83	8.86	nd.	nd.	83.60
6	53.54	0.49	2.49	1.93	0.02	nd.	1.69	23.10	0.23	nd.	83.51
7	62.29	nd.	1.38	1.58	0.06	0.17	1.24	15.79	nd.	nd.	82.50
8	65.39	nd.	1.01	0.76	0.01	0.01	1.82	10.30	2.18	nd.	81.48
9	67.93	1.36	1.93	1.30	0.27	nd.	2.72	12.29	0.02	nd.	87.82
10	71.62	2.58	1.23	1.00	0.03	0.09	2.09	11.45	1.00	nd.	91.08
11	77.43	0.32	1.67	0.47	0.05	nd.	1.39	10.53	nd.	nd.	91.86
12	78.46	0.10	0.51	0.05	0.04	0.15	1.12	8.20	0.04	0.04	88.80
Mn oxide oolite / pisolite [sample No. 958-43]											
13	59.35	0.24	9.97	0.88	0.27	nd.	2.20	8.77	nd.	nd.	81.68
14	71.11	1.10	1.36	0.45	0.29	nd.	3.17	11.60	0.14	nd.	89.21
15	69.46	nd.	1.08	2.82	0.01	nd.	1.96	12.52	0.10	nd.	87.95
16	54.87	0.02	0.65	0.42	0.12	nd.	1.10	7.26	0.08	0.09	64.60
17	72.47	0.20	3.10	0.15	0.10	nd.	1.82	9.88	0.28	nd.	87.25
18	71.24	2.49	1.64	0.55	0.02	0.14	1.68	10.53	0.29	0.02	88.60
19	59.74	1.37	11.65	0.73	nd.	nd.	0.82	8.31	0.27	nd.	82.89
20	69.70	nd.	2.89	1.92	nd.	0.01	1.00	11.93	0.17	0.15	87.73
21	50.92	0.36	12.35	3.75	0.08	0.06	1.91	12.11	0.06	nd.	81.58
Massive Mn oxide oolite / pisolite [sample No. 958-39]											
22	77.84	nd.	0.71	0.17	nd.	0.01	1.72	9.62	nd.	nd.	90.08
23	76.87	nd.	0.85	0.63	0.08	0.32	1.53	10.47	0.10	0.10	90.93
24	76.52	0.24	1.09	0.23	0.08	nd.	2.08	10.57	0.14	nd.	90.94
25	73.86	0.27	1.07	1.60	nd.	nd.	1.33	10.09	0.11	nd.	88.27
26	74.50	nd.	0.75	0.98	nd.	nd.	1.65	10.87	0.14	0.02	88.91
27	74.45	nd.	0.92	0.60	0.07	0.26	1.41	9.99	0.04	0.09	87.82
28	78.30	nd.	0.77	0.07	nd.	0.10	0.85	9.70	0.56	nd.	90.25
29	74.17	nd.	2.95	0.24	nd.	nd.	1.87	9.69	0.01	nd.	88.93
30	73.63	0.49	1.01	0.87	0.05	nd.	1.83	11.13	0.24	0.03	89.27
Unsorted Mn oxide oolite / pisolite [sample No. 958-145]											
100	76.66	0.37	1.21	0.01	0.01	nd.	1.55	9.99	0.18	nd.	89.98
102	76.13	0.23	1.40	0.22	0.07	0.40	1.91	10.67	0.04	nd.	91.08
104	70.48	1.30	1.67	1.85	0.01	0.11	2.35	12.55	0.20	nd.	90.34
106	73.59	0.97	2.42	nd.	0.03	0.10	1.89	10.53	0.31	0.01	89.86
110	71.82	2.00	1.97	1.36	0.02	nd.	2.85	11.74	0.17	0.24	92.16
112	75.65	0.65	1.77	0.20	nd.	nd.	2.00	11.15	0.09	nd.	91.49
114	76.01	0.71	1.75	0.58	0.11	0.11	1.99	11.09	0.03	nd.	92.37
116	74.35	nd.	1.68	1.01	0.19	0.25	2.80	11.87	nd.	0.03	92.17
Mn carbonate (calciohodochrosite) oolite / pisolite [sample No. 958-144]											
79	36.44	0.88	7.08	2.85	0.15	nd.	1.97	22.27	0.04	0.05	71.71
80	30.30	0.05	15.78	2.54	0.05	nd.	1.75	14.66	nd.	nd.	65.13
87	32.35	nd.	15.19	2.46	0.05	nd.	1.77	13.66	nd.	nd.	65.48
88	37.49	0.81	7.07	2.85	0.15	nd.	2.00	22.30	0.03	0.05	72.75

* oxide stoichiometry expressed as MnO / MnO₂; nd. = not detected.

Table 5.8b: Microanalysis of Mn carbonate minerals from the Dounan ores [wt.%].

Area	MnO*	FeO	CaO	MgO	K ₂ O	Na ₂ O	Al ₂ O ₃	SiO ₂	TiO ₂	Cr ₂ O ₃	Total
Calciorhodochrosite from calciorhodochrosite oolite/pisolite [sample No. 958-65]											
31	52.56	nd.	5.53	1.27	0.11	0.10	0.29	0.32	nd.	0.07	60.24
32	45.38	nd.	11.66	0.86	0.08	0.09	0.87	8.96	0.21	nd.	68.11
33	44.98	nd.	9.87	1.15	0.18	nd.	0.71	2.00	0.29	nd.	59.18
34	43.50	0.18	11.56	0.73	0.31	nd.	0.49	2.58	0.02	nd.	59.37
35	41.89	nd.	16.31	0.75	nd.	nd.	0.34	0.06	0.08	nd.	59.40
36	35.77	1.08	9.62	2.49	1.37	nd.	5.64	10.48	nd.	nd.	66.04
37	29.36	0.12	20.96	2.35	0.62	0.21	2.26	4.04	0.12	nd.	60.03
38	26.72	0.82	21.61	2.36	0.72	nd.	3.65	6.19	nd.	nd.	62.07
39	21.44	0.17	19.69	7.77	0.47	0.31	6.04	9.74	0.11	nd.	65.73
40	28.05	nd.	24.56	0.56	0.02	nd.	0.51	2.29	nd.	nd.	56.08
41	29.82	nd.	26.96	0.78	nd.	nd.	0.85	1.42	nd.	nd.	59.83
42	37.12	nd.	18.43	1.31	0.14	nd.	1.03	0.82	0.10	nd.	58.95
43	41.92	0.10	20.97	2.04	nd.	0.10	2.32	6.22	0.11	nd.	73.78
44	42.98	0.13	14.39	0.27	nd.	nd.	0.30	0.01	nd.	nd.	58.09
45	45.36	nd.	12.25	0.45	0.09	0.44	0.34	0.39	0.10	nd.	59.41
46	47.32	1.31	16.32	1.58	0.15	nd.	1.57	8.67	0.24	nd.	77.16
47	53.01	1.59	12.87	1.87	0.07	0.05	2.34	8.43	0.23	nd.	80.44
73	46.16	nd.	11.17	0.32	0.01	nd.	0.24	0.29	0.09	nd.	58.28
74	31.73	1.11	23.96	2.10	0.12	0.09	1.21	3.10	0.32	nd.	63.74
76	24.88	0.39	27.55	0.80	0.07	nd.	0.64	3.66	0.13	nd.	58.13
77	26.75	0.29	20.17	1.62	0.14	0.28	1.10	11.75	0.12	nd.	62.22
78	36.60	0.25	21.78	1.15	0.09	0.28	0.90	7.35	0.06	nd.	68.46
81	44.46	nd.	11.62	0.20	0.01	0.18	0.31	0.45	nd.	nd.	57.24
82	44.02	nd.	10.27	1.77	0.17	0.15	1.41	3.52	0.10	nd.	61.40
83	44.62	0.03	10.75	1.71	0.15	0.19	0.83	2.31	0.08	nd.	60.67
84	45.82	nd.	11.76	1.15	0.15	0.19	0.89	2.19	0.08	nd.	63.23
85	45.12	nd.	10.56	1.82	0.19	0.15	1.49	2.55	0.10	nd.	61.98
86	45.56	nd.	12.65	0.25	0.01	0.15	0.35	0.47	nd.	nd.	59.44
89	37.65	0.20	21.80	1.15	0.08	0.28	0.91	7.10	0.06	nd.	69.23
90	27.65	0.22	20.10	1.60	0.15	0.25	1.00	9.65	0.15	nd.	60.77
91	28.98	0.33	26.51	0.85	0.08	0.01	0.60	3.20	0.12	nd.	60.68
93	32.73	nd.	23.92	2.20	0.13	0.06	1.25	3.00	0.33	nd.	63.86
94	46.18	nd.	11.15	0.34	0.01	nd.	0.22	0.29	0.08	nd.	58.29
Mn-calcite/Mn-bearing calcite from Mn-calcite oolite/pisolite [sample No. 958-142, 143 & 144]											
48	19.67	nd.	32.81	0.90	0.24	0.07	1.29	2.91	0.01	nd.	57.91
49	17.09	nd.	37.44	0.69	nd.	nd.	0.66	0.46	nd.	nd.	56.35
50	14.81	nd.	38.86	1.04	nd.	0.01	0.39	0.06	nd.	nd.	55.27
51	13.68	nd.	42.17	0.69	0.04	0.05	0.72	0.19	0.26	nd.	57.79
52	13.95	nd.	37.63	2.00	0.17	nd.	0.40	0.18	0.19	nd.	54.51
53	14.23	0.01	38.45	0.66	0.07	nd.	0.59	0.36	nd.	nd.	54.37
54	19.98	nd.	35.57	1.18	nd.	0.13	0.72	0.82	0.10	nd.	58.40
55	20.63	0.27	30.78	1.16	0.16	0.05	0.96	1.39	0.06	nd.	55.45
56	10.52	nd.	42.20	1.16	0.19	0.01	0.88	1.35	0.09	nd.	56.40
57	7.80	nd.	46.36	0.72	0.11	0.09	0.61	0.11	nd.	nd.	55.80
58	5.15	nd.	47.05	0.68	0.03	0.01	0.58	0.53	0.03	nd.	54.05
59	3.34	nd.	50.09	0.79	0.71	0.43	0.52	0.23	0.07	nd.	56.18
60	2.43	nd.	54.07	0.94	0.09	nd.	0.71	0.22	0.09	nd.	58.55
61	1.91	nd.	51.59	0.48	nd.	0.01	0.54	0.23	0.24	nd.	55.00
62	1.75	nd.	50.04	1.05	0.04	nd.	0.63	0.22	0.19	nd.	53.92
63	1.33	nd.	50.94	0.97	nd.	0.16	0.15	0.20	0.18	nd.	54.29
64	1.86	nd.	49.90	1.16	0.01	nd.	0.34	0.18	0.16	nd.	53.60
65	2.43	nd.	51.32	0.57	0.10	0.12	0.61	0.38	0.04	nd.	55.58
66	4.43	nd.	48.35	1.06	0.19	1.81	0.39	0.96	0.27	nd.	57.46
67	4.91	nd.	47.27	1.34	0.01	0.43	0.67	0.81	0.20	nd.	55.63
68	6.51	0.38	40.24	4.17	0.34	0.10	3.26	5.38	0.18	nd.	60.55
69	10.54	nd.	33.43	8.85	nd.	nd.	0.42	0.21	0.09	nd.	53.53

* oxide stoichiometry expressed as MnO; nd. = not detected.

replacement during diagenesis (Fig. 5.8a) may also explain the absence of Fe and Mg in Mn-rich braunite (e.g. from massive Mn oxide ore).

Microanalyses from a number of analytical areas within Mn carbonate minerals suggest that most areas belong to calciorhodochrosite, with about 10-25% CaO, and only a few are rhodochrosite, with <10% CaO. A few of the minerals are Mn-calcite or Mn-bearing calcite which are identified by low Mn content in calcite (~12% MnO, Table 5.8b). The analyses also reveal:

- large variations in Mn content (21-53% MnO) in a single sample (perhaps indicating an environmental change from primary to diagenetic processes);
- similarly, large differences of Ca content (since Ca correlates negatively with manganese content, an isomorphic replacement is suggested);
- magnesium, at 0.3-2.5% MgO, is a constant feature in primary samples (which might reflect derivation from seawater and a small stable apply of clastic materials);
- positive correlation of Si and Al in the minerals indicates a stable input of terrigenous materials.

Although it is very difficult to distinguish Mn-calcite from Mn-bearing calcite either in hand-specimen or under microscopy, the separation by EMPA is efficient through Mn content, with the former having 14-22% MnO and the latter 1.5-11% MnO in the minerals. Like calciorhodochrosite, the Ca and Mn are negatively correlated in both minerals, again reflecting isomorphic exchange. But Si and Al, together with Mg, are constant features of all analysis, and the minerals are lacking in Fe, which probably reflects a small difference of environment and material input between the Mn carbonate minerals. Deviations of the analytical totals from 100% for Mn carbonate minerals probably reflects the presence of CO₂ as a volatile component, which cannot be detected by EMPA.

Elemental distributions within the main Mn minerals show various patterns with genetic significance. The manganese distribution in braunite from Mn oxide deformed oolite/pisolite generally exhibits low Mn content in the central area of the grain, but with relatively high Mn concentration on the grain margin. Si and Ca do not show much variation, except for the core of the grain. The strong suggestion is that formation of the grain probably resulted from different processes, i.e. the margin may result from recrystallization and secondary enrichment (Fig. 5.8a; Plate 5.1, Fig.1). Commonly, the elemental distributions (e.g. Mn, Ca, Si) in the braunite grains from both Mn oxide oolite/pisolite and massive ores are relatively homogeneous, although there is a difference in Mn concentration between the two types, probably reflecting an environmental (e.g. primary and diagenetic) difference (Figs. 5.8b-c; Plate 5.1, Figs. 2-3). Mn-calcite and Mn-bearing calcite show increasing Mn and decreasing Ca to the margin, a surprisingly low trace of Si and a lack of Fe (Fig. 5.8d; Plate 5.1, Fig. 4a), which imply overprinting processes of recrystallization or replacement. Similarly, the zonal distribution of elements in calciorhodochrosite also strongly supports the suggestion of overprinting processes throughout primary and diagenetic stages (Fig. 5.8e; Plate 5.1, Fig. 4b). The difference in Si and Fe contents between

Plate 5.1 Analytical area diagrams of electron microprobe analysis of Dounan Mn minerals and ooliths.

Fig. 1: Analyzed area of braunite from Mn oxide deformed oolite/pisolite; sample 958-42; Gake area.

Fig. 2: Analyzed area of braunite from Mn oxide oolite/pisolite; sample 958-39; Gake area.

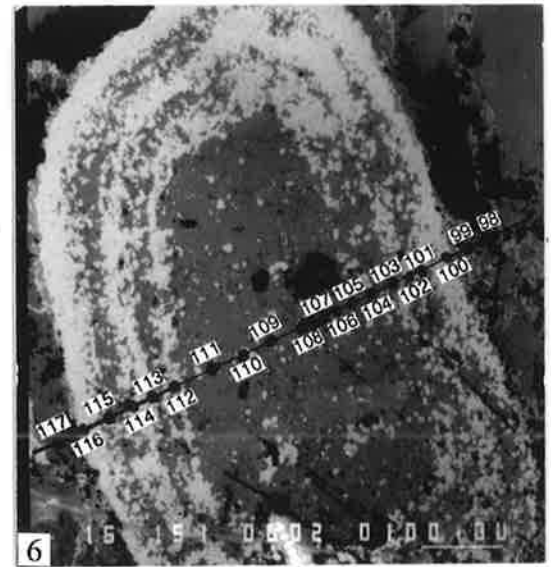
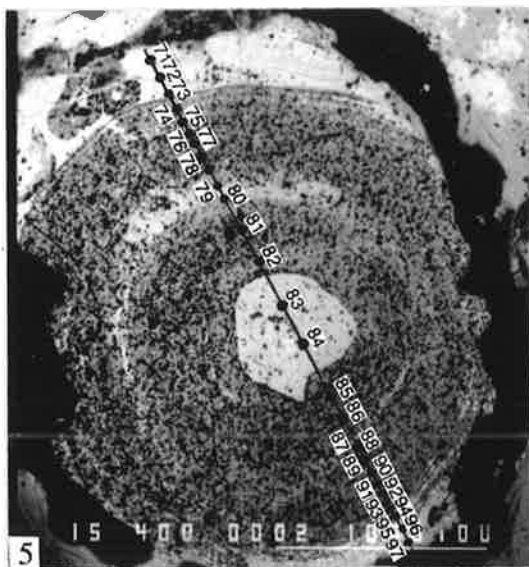
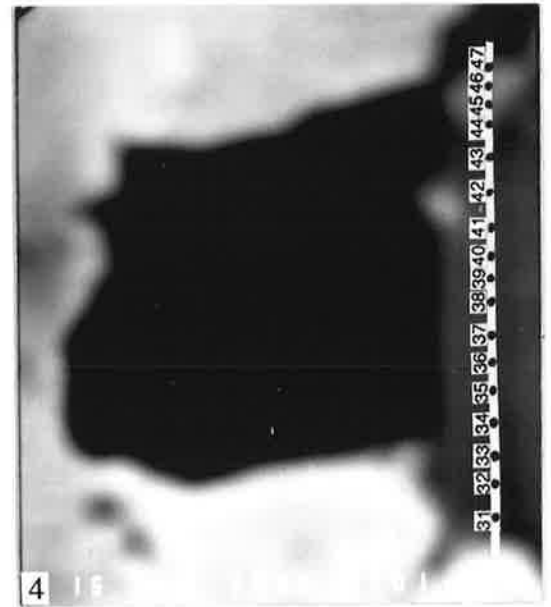
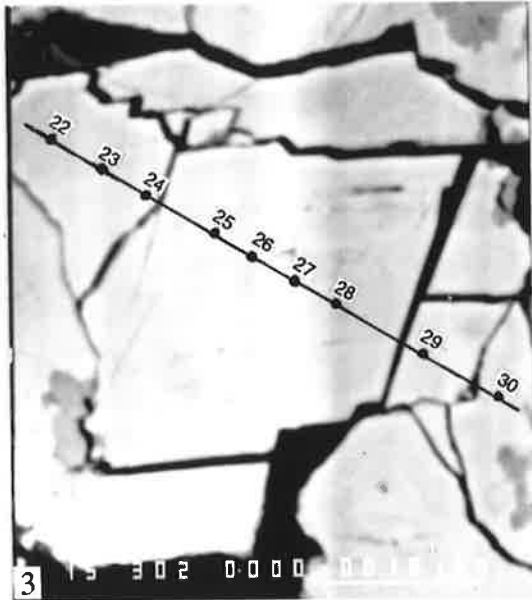
Fig. 3: Analyzed area of braunite from massive Mn oxide oolite/pisolite; sample 958-46; Gake area.

Fig. 4: Analyzed area of calciorhodochrosite from Mn carbonate ore; sample 958-142; Baigu area.

Fig. 5: Analyzed area of calciorhodochrosite oolith from Mn carbonate ore; sample 958-143; Baigu area.

Fig. 6: Analyzed area of braunite oolith from Mn oxide deformed oolite/pisolite; sample 958-43; Gake area.

Plate 5.1



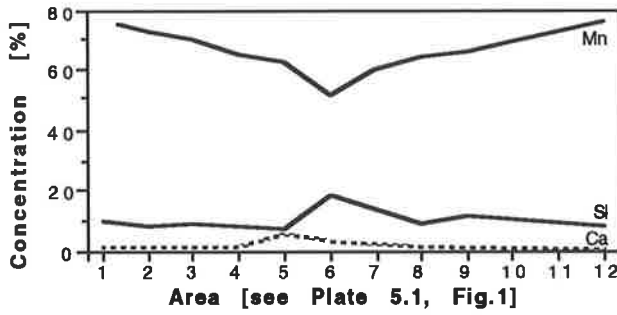


Fig. 5.8a: Distribution of elements in braunite; No. 42.

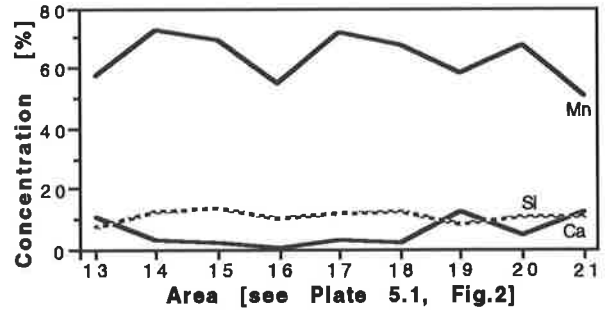


Fig. 5.8b: Distribution of elements in braunite; No. 39.

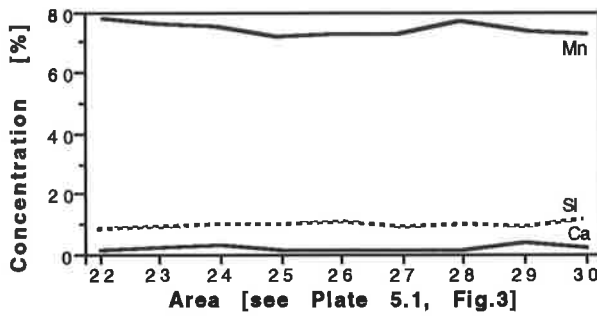


Fig. 5.8c: Distribution of elements in braunite; No. 46.

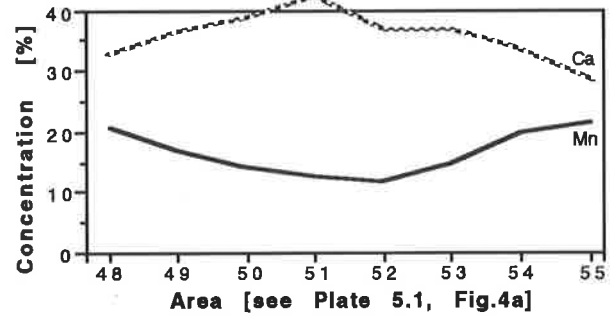


Fig. 5.8d: Distribution of elements in Mn-calcite; No. 142.

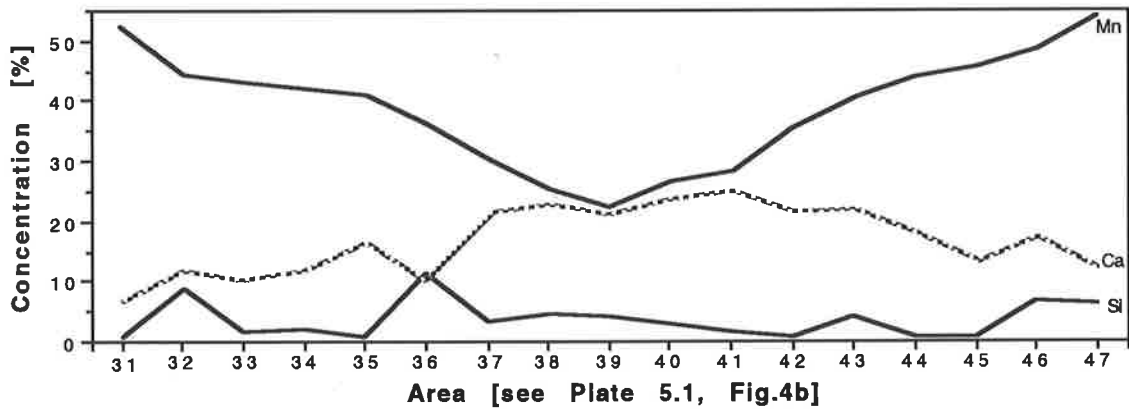


Fig. 5.8e: Distribution of elements in calciorhodochrosite; No. 142.

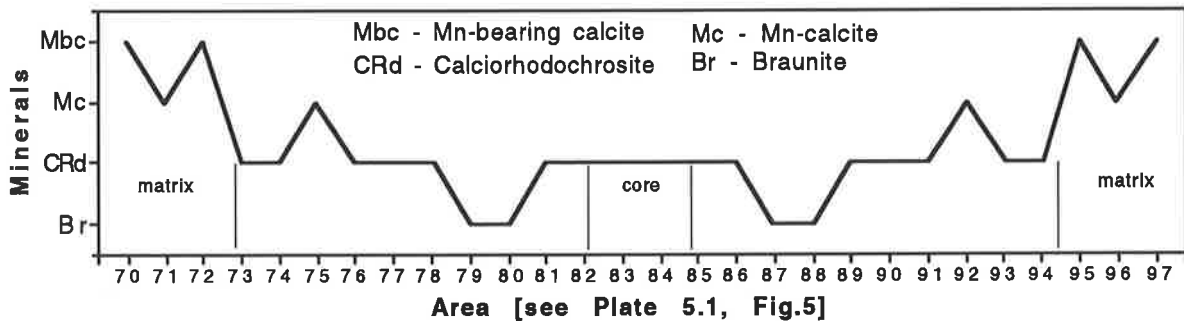


Fig. 5.9a: Distribution of minerals in calciorhodochrosite oolith; No. 143.

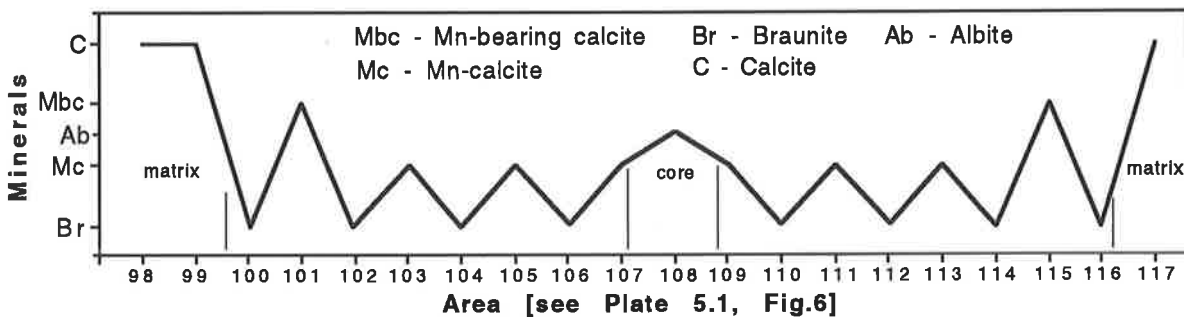


Fig. 5.9b: Distribution of minerals in braunite oolith; No. 43.

* the Area number see Tables 5.8 & V.4; all samples (No.) have the common prefix 958.

calciorhodochrosite and Mn-calcite probably indicate different microenvironments and material input.

In order to understand the mechanism of oolith/pisolith formation, two respective (calciorhodochrosite and braunite) ooliths were microanalyzed by EMPA in detail (crossing ooliths). The calciorhodochrosite oolith consists of calciorhodochrosite, minor braunite and Mn-calcite, with matrix composed of Mn-calcite and Mn-bearing calcite (Fig. 5.9a; Plate 5.1, Fig. 5). The concentric laminae composed of different materials show normal relationships without any secondary changes (e.g. replacement), suggesting that the minerals represent primary products. The angular nature of the nucleus, however, reflects an earlier time of formation and a different environment. Importantly, the alternating concentric laminae consisting of the three minerals indicate frequent fluctuation between weakly oxidizing and reducing microenvironments during the precipitation of the oolith. The braunite oolith, on the other hand, is mainly composed of braunite and minor Mn-calcite or Mn-bearing calcite laminae, with a nucleus composed of albite and cryptocrystalline calcite matrix (Fig. 5.9b; Plate 5.1, Fig. 6). Similarly, the concentric laminae also exhibit primary continuous relationships, but most Mn carbonate laminae were replaced by braunite laminae, suggesting a secondary enrichment.

5.2.5 Isotopic Characteristics of Ores and Rocks

5.2.5.1 Introduction

Within the past few years isotopic analysis has come to be an increasingly important tool in the study of sedimentary or diagenetic events, supplementing the more traditional approach based on structural and textural relationships and trace element analysis. The carbon and oxygen isotopic compositions of Dounan Mn ores and associated rocks are here considered with a view to evaluating the relative importance of primary and diagenetic processes in the genesis of the ores and rocks. Many interesting primary and diagenetic problems present themselves in the Dounan area but isotopic investigations have been not undertaken previously. The lack of isotopic analysis in earlier investigations of Dounan geology makes it difficult to give a reasonable genetic interpretation on Dounan Mn deposits, especially as regards primary and diagenetic processes, i.e. environmentally controlled differences in isotopic composition. The present research is an outgrowth of previous work elsewhere and is intended to demonstrate the extent to which isotopic criteria are applicable to environmental studies of Dounan ores and rocks.

Keith and Weber (1964) suggested that three factors may control or change the carbon and oxygen isotopic composition of carbonates: (1) Isotopic composition of sea water (including effects from dissolved material together with the food web of the local environment of deposition), (2) Isotopic fractionation by carbonate-forming organisms and the magnitude of their bulk contribution to carbonate sediments, (3) Diagenetic and subsequent isotopic exchange and the selective dissolution and precipitation of carbonates in sediments and consolidated rocks.

Usually, environmental interpretations or classifications can reasonably be based on isotopic analyses only for sample groups in which environment-controlled differences are large in comparison with those which result from factors under categories (2) and (3) above (Keith and Weber, 1964).

5.2.5.2 *Sample Selection*

The problem of separating environmental differences from other variables was approached by analysing only selected samples which could be readily classified into primary or diagenetic categories. The distinction was made on the basis of relationships between minerals composing ores and rocks, on relationships between oolite/pisolite and matrix, or between concentric laminae of different material in oolites/pisolites. In assembling the preferred group of specimens, the writer eliminated all samples of questionable depositional environments and also avoided dolomites. In most cases the sample selections were of course dependent on the studies described earlier Chapter 2 (Stratigraphy), Chapter 3 (Orebeds) and Chapter 4 (Petrology and Mineralogy).

All samples, from two ore-bearing stratigraphic sections previously examined by X-ray diffraction (XRD) and X-ray fluorescence (XRF), were selected from both oolites and matrix in oolitic/pisolitic Mn-bearing carbonates (including Mn carbonate oolites/pisolites). The samples from Mn oxide oolites/pisolites (including deformed, unsorted or banded, and massive ores) were taken not only from matrix but also from carbonate concentric rings (e.g. calcite, Mn-bearing calcite, Mn-calcite or calciorhodochrosite) between braunite concentric laminae. Carbon and oxygen isotopic compositions of both Mn oxides and carbonates as well as associated rocks from Dounan Mn deposits were determined by standard stable isotope methods, and the data are reported relative to PDB. Sample preparation, analytical background and procedure, analytical equipment as well as analytical results are listed in Appendices I and V.

5.2.5.3 *Isotopic Features*

The complete data set for both carbon and oxygen is presented in the normal δ notation with reference to PDB in Table 5.9, columns 3 and 4. Most samples are similar in composition to those of biolimestones (comprising those from corals, algae, foraminifera and bryozoa), which exhibit a range of carbon isotopic composition from +1.4 to -8.4 mil and oxygen isotopic composition from -3.1 to +7.1 per mil (Keith and Weber, 1964). The oxygen isotopic equilibrium fractionation between carbonate and water is a function of temperature. For calcite the relationship is given by

$$T = 16.9 - 4.21(\delta_c - \delta_w) + 0.14(\delta_c - \delta_w)_2$$

(Craig, 1965) where $(\delta_c - \delta_w)$ is the measured difference in $\delta^{18}\text{O}$ between calcite and water and is used here in the same sense as originally defined by Epstein et al. (1953). An isotopic

Table 5.9 Isotopic composition, inferred temperatures and depth of precipitation, Dounan ores and rocks.

Sample description	No.	$\delta^{18}\text{O}$ PDB	$\delta^{13}\text{C}$ PDB	T ($^{\circ}\text{C}$)*	CO_2 (%)	Depth (m)#
Group I 'Primary' samples						
Mn oxide ooliths/pisoliths	958-74	-3.21	+0.66	26.2	79.31	-
	958-73	-3.95	-2.67	29.5	41.50	-
	958-41	-3.67	-1.03	28.0	57.78	-
	958-46	-3.76	-2.18	28.8	62.28	-
	958-49	-3.79	-3.57	28.9	82.32	-
	958-192	-3.82	+0.78	28.9	91.12	-
Mn-bearing limestone	958-169	-3.65	+0.56	28.0	84.18	-
Unsorted Mn ores	958-61	-3.77	-1.29	28.3	66.26	-
	958-145	-3.47	-1.81	27.1	64.42	-
	958-204	-3.79	-0.94	28.9	68.82	-
Group II 'Early diagenetic' samples						
Mn oxide deformed oolites/pisolites	958-40	-4.50	-2.65	32.3	57.60	13
	958-42	-4.56	-3.55	32.6	64.61	18
	958-43	-4.46	-3.65	32.1	62.21	10#
	958-62	-4.38	-1.98	31.7	56.21	4
				Mean	32.1	
Group III 'Diagenetic' products						
Banded Mn ores (Mn oxides/carbonates)	958-44	-4.92	-3.59	34.51	62.49	85
	958-63	-5.09	-2.07	35.4	44.01	185
	958-64	-4.78	+1.58	33.8	70.81	60
	958-172	-4.07	+2.14	33.4	55.32	46
	958-233	-5.89	-3.62	40.0	37.23	280
	958-245	-5.97	-3.56	40.2	35.52	288
	958-246	-5.29	-3.57	36.3	33.46	160
	958-65	-5.88	-5.18	39.5	69.63	263
Mn carbonate oolites/pisolites	958-142	-4.80	+5.81	33.9	34.99	64
	958-143	-4.96	-3.26	34.6	33.21	89
	958-144	-5.97	-5.25	40.2	47.47	288
	958-45	-7.77	-4.67	50.6	31.79	664
	958-236	-7.24	-4.19	47.7	30.31	554
	958-47	-7.28	-3.83	47.7	39.63	554
Mn oxide oolites/pisolites (matrix)	958-171	-4.86	+2.55	34.2	52.23	75
	958-232	-5.69	-4.73	38.6	30.79	231
	958-234	-5.79	-3.55	40.2	36.34	295
	958-244	-5.94	-3.52	40.0	33.12	280
	958-38	-7.45	-4.96	48.7	26.35	589
Massive Mn oxide ores (ooliths/pisoliths)	958-39	-6.96	-4.87	45.8	28.24	486
	958-194	-7.21	-4.82	47.3	28.22	540
	958-205	-6.89	-5.76	45.4	28.34	472

* T calculated for water, $\delta^{18}\text{O} = -1.2$ per mil.

Depth values calculated assuming: temperature at base of sulphate reduction zone 32.1°C . Depth of base of sulphate reduction zone 10 m. Thermal gradient 28°C per km. No depth values given for primary (surface water) precipitation carbonates.

composition of -1.2‰ , the value for pre-glacial oceans (Shackleton and Kennett, 1975), has been assumed for both seawater and porewater. The isotopic equilibrium temperature, T , and depth of precipitation for each sample are listed in Table 5.9, columns 5 and 6.

As regards Dounan, all $\delta^{18}\text{O}$ values are negative, with the lowest values being recorded from the compact massive Mn oxide oolite/pisolite and Mn carbonate oolites/pisolites; a small number of the $\delta^{13}\text{C}$ results are slightly positive. No significant differences are apparent within Group I, between Mn oxide oolite/pisolite, Mn-bearing oolitic/pisolitic limestones and unsorted ores; Group II, between Mn oxide deformed oolite/pisolite and banded ores; nor in Group III, between Mn carbonates and Mn oxide oolite/pisolite (matrix) and massive Mn oxide ores. Results from Group I of primary origin show narrow ranges for both carbon and oxygen; all samples are very similar, with $\delta^{13}\text{C}$ close to zero and moderately negative $\delta^{18}\text{O}$ indicating a small range in temperature of 25° - 29°C . Attention was concentrated on the Mn oxide oolite/pisolite in which a number of interesting differences occur in both carbon and oxygen isotopes between grains and matrix. Those of the ooliths/pisoliths contain primary information, whereas those of the matrix show secondary exchange. Second, four samples of Mn oxide deformed oolite/pisolite exhibit similar values of both $\delta^{13}\text{C}$ and $\delta^{18}\text{O}$, but with slightly higher temperatures (about 32°C). The third category, consisting of banded, massive and Mn carbonate ores, post-date compaction of Mn oxide oolite/pisolite. They have strongly negative $\delta^{18}\text{O}$ values reaching a maximum of -7.77 , by far the lowest value found in the whole study, and a much wider scatter for carbon ($\delta^{13}\text{C}$) than in other groups, from the highest value of $+5.81\text{‰}$ to the lowest of -5.76‰ , and a wider range of temperature (34° - 50°C). It is important to distinguish the primary Mn oxide ooliths/pisoliths, often with moderately negative $\delta^{18}\text{O}$ and $\delta^{13}\text{C}$ quite close to zero, from the secondary matrix of Mn oxide oolite/pisolite, which is associated with later changes. The latter has strongly negative $\delta^{18}\text{O}$. Commonly, Mn carbonates show strongly negative values for both $\delta^{18}\text{O}$ and $\delta^{13}\text{C}$.

Stratigraphic variation of $\delta^{13}\text{C}$ is readily evident and correlates well with the percentage of manganese (Okita et al., 1988); a moderate negative correlation exists between Mn content and $\delta^{13}\text{C}$ values for most data from two ore-bearing sections at Dounan (Figs. 5.10a-b and 5.11). Isotopic analyses of carbonate minerals in concentric rings of ooliths/pisoliths from Mn-bearing carbonate or unsorted ores and Mn oxide oolite/pisolite show $\delta^{13}\text{C}$ values of around 0‰ PDB (Table 5.9, Group I), consistent with the assumed isotopic value of normal seawater. During early diagenesis, carbonate precipitation utilized carbon mainly from seawater HCO_3^- in agreement with results from Hungary (Polgári et al., 1991).

5.3 Discussion

5.3.1 Relationships between Trace Elements and REEs in Different Materials

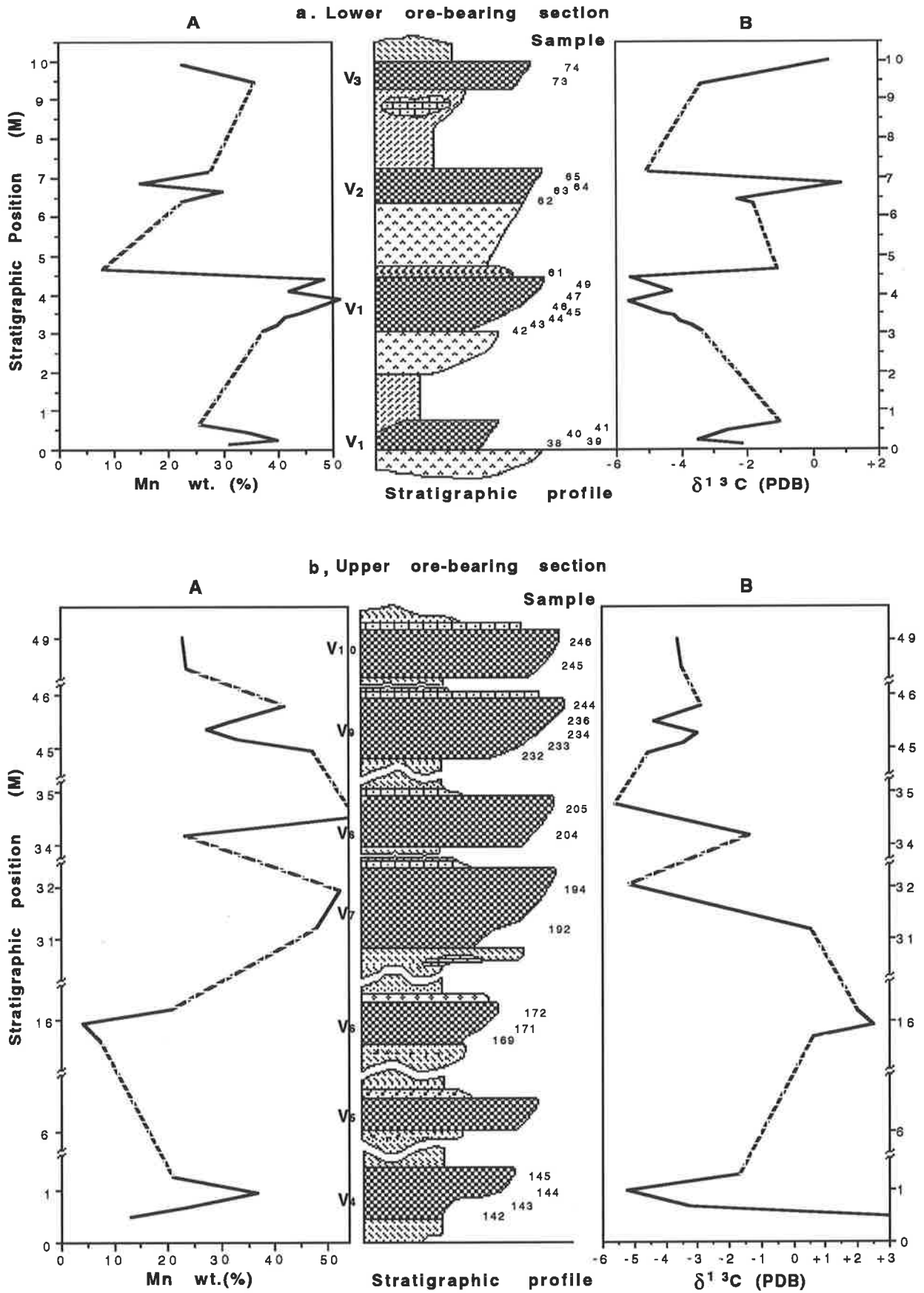


Fig. 5.10: Stratigraphic profile of (A) Mn content and (B) $\delta^{13}C$ values of bulk ore samples from **a** lower (T2f4-1, Gake mine-field) and **b** upper (T2f5-2, Baigu mine-field) ore-bearing sections of the Dounan Mn deposits; data from Tables 5.9 and V.5; dashed lines = no data; the three main ore horizons are labelled V1 - V9 (see Chapter 3). Note the correlation of high Mn content with more negative $\delta^{13}C$ values.

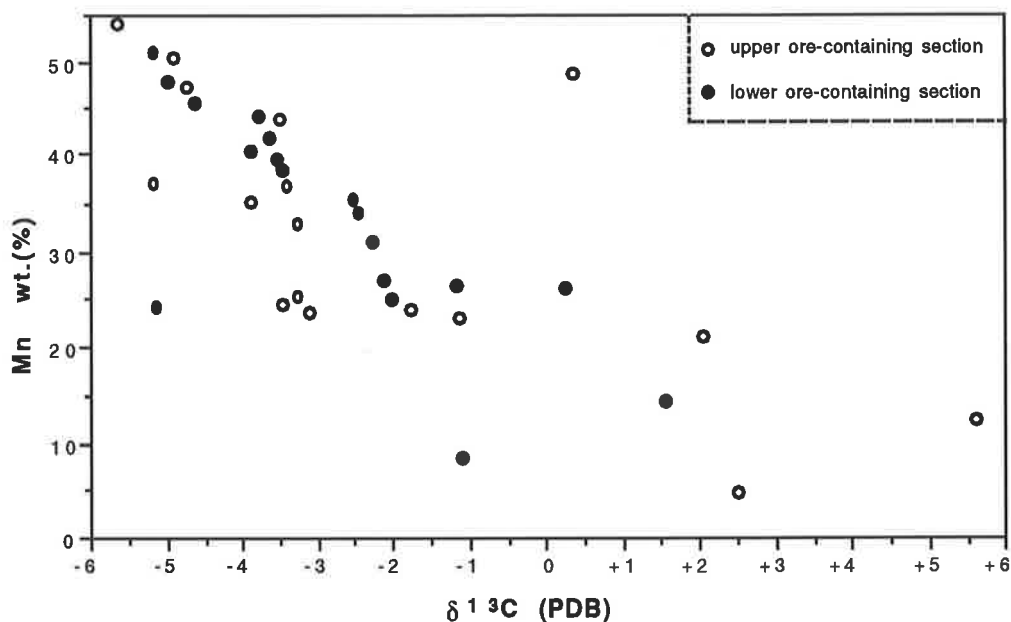


Fig. 5.11
Scatter plot
of Mn content
versus $\delta^{13}\text{C}$
values for the
combined lower
and upper
ore-containing
series samples.

An examination of the major element concentrations in oolites/pisolites, the dominant ore type of the deposits shows that these ores are remarkably similar. Similar patterns are exhibited by most primary and diagenetic products, and therefore, these elements cannot be used to distinguish ore and rock types from each other. Only between Mn oxides and Mn carbonates, or between primary/diagenetic Mn ores and supergene Mn ores, which show variable elemental concentrations (e.g. Mn, Ca), is it possible to separate the materials.

In contrast, the trace elements can help to differentiate some of the ore types, mainly on the basis of strong variations in the Ni and Sr contents. Striking differences are noted among Mn oxides, Mn carbonates and transitional ores, the ores possessing increasingly dominant Ni-peaks with increasing manganese (e.g. from Mn carbonates to transitional ores to Mn oxides). With the exception of Sr and sometimes Ni, which often show an elevated abundance, most of the other elements are distributed relatively evenly. Gradual elemental changes from one ore type to the next are probably due to small variations in the mineralogy of the materials.

It has also been shown that multi-element patterns of the REEs (not normalized) can readily be used to chemically distinguish some of the ore types. For instance, Mn oxide oolite/pisolite and calciorhodochrosite oolite/pisolite possess distinct differences in the Ce content, although the concentrations are generally very similar for all the other Rare Earths. The shapes of REE patterns are comparable, with the exception of strong variations for Ce, and to a lesser extent for Gd. When the samples are shale-normalized a clearer picture emerges. All ore types possess shale-normalized REE patterns that are slightly enriched in the LREEs, but Mn carbonates seem to have slightly more LREEs when compared with Mn oxides. Nevertheless, the overall patterns of the ores do not exhibit large variations. On the other hand, the normalized patterns of all ore types are comparable in the HREEs, but the patterns diverge slightly for the LREEs and IREEs. This behavior, where associated minerals show a preferential uptake of LREE, IREE, or HREE,

indicates fractionation by various mineral phases (Goldberg, 1965). This results from the electron charge properties of the REEs (lanthanide contraction: decreasing ionic radii with increasing atomic number).

Strong negative or positive correlations between Σ REEs and braunite, or calciorhodochrosite, suggest that continuous environmental changes within tidal flats are responsible for the formation and changes of the ores from Mn oxides to transitional ores to Mn carbonates and for a consequent enrichment or depletion of REEs. This is strongly supported by the positive correlations between Σ REEs and Σ LREEs/ Σ HREEs ratios (Fig. 5.6), which suggest that variations in pH and redox reactions between Mn and O or CO_3^{2-} are responsible for the formation of different ore types. The primary Mn minerals such as braunite and calciorhodochrosite show important REE patterns for manganese ores during sedimentation at Dounan; the patterns did not change much during diagenesis due to the special stability of REEs. Variations in sedimentary conditions began with the dissolution/reduction of tetravalent Mn-oxides and their reaction with CO_3^{2-} during the initial period of marine regression. The resulting Mn carbonate phases can preferentially contain relatively more REEs, which definitely led to a relative decrease or dilution of REEs in the sea water. The REEs still available in the sea waters were incorporated, in turn, into new transitional ore phases and finally, into Mn oxide phases under progressive regression. Thus the Mn oxide phases contain relatively less REEs than transitional ores which in turn have less REEs than Mn carbonates.

Diagenesis resulted in recrystallization and slight replacement, but the concentrations and patterns of REEs from different ore types exhibit only slight variations, probably because diagenetic changes were only slight, but also because of the stronger stability of REEs (Haskin and Haskin, 1966). The small Eu and Ce anomalies of the ores support this interpretation because Ce and Eu are the most mobile members of the REE group, and a general decrease of these elements in buried deeper parts of the orebody can be linked to prolonged reaction times that result from an increasing availability of interstitial or pore waters, which thus enable the redox reactions to take place (Pracejus, 1989 and Pracejus et al., 1990). As with the REEs, other trace elements also do not show strong fractionation between primary ores and diagenetic products.

Generally, the REE-pattern of an ore-bearing series is not an exact indicator of the pattern in contemporaneous sea water (Fryer, 1977). The Dounan ore-bearing series probably was subjected to a kind of special mineralizing fluid (as seawater containing dissolved elements due to various factors) which could precipitate the ores by chemical processes in suitable sedimentary environments. Therefore, the REE-patterns of an ore-bearing series can be explained in the following ways: (1) they may be representative of the enriched solution; (2) they may result from the REE-patterns of contemporaneous sea waters; or (3) they may represent a mixture of both REE-patterns. In addition, the REE-pattern can also be affected by other factors such as the type and amount of terrigenous sediments, local and regional pH and Eh values and depth of basin. Although every sort of sediment has its own geological background and various factors

contribute to its REE-pattern, in most cases, the mixture of mineralizing fluid and contemporaneous sea water gives rise to an ore-forming solution. Thus, its REE abundance and patterns reflect its conditions of formation in the local environment (Zhao, 1978).

5.3.2 Vertical Variation of Rare Earth Elements

For the Dounan Falang Formation, variation of REEs with depth is strongly influenced by a number of lithologically repeating sedimentary cycles. However, the calculated depths of burial based on the stable isotope analysis (Table 5.9) of the ore-bearing profiles permit some discussion. The REE profiles show slightly increasing concentrations with increasing depth (Fig. 5.12). They attain values up to ~3 times surface seawater concentrations within 90 m depth. The largest REE enrichment is for Ce derived from Mn carbonate. There is an indication that REE concentrations level off in still deeper samples (down to ~500 m). The Mn carbonates are probably mobile under diagenesis, as enhanced by the elevated porewater concentrations, but the "solid-phase" (i.e. the deeper buried sediments, >90 m) data are insensitive to diagenetic mobility.

Elderfield and Sholkovitz (1987) and Sholkovitz et al. (1989) studied REEs in the pore waters of modern nearshore sediments of Buzzards Bay and concluded that the REEs are mobile during early diagenesis, leading to greatly enhanced concentrations in pore waters (2-10 times?), but more deeply buried sediments are characterised by a lack of variation in REE. This implies significant dissolved REE fluxes, both internal to the sediment system and across the sediment-seawater interface, verifying suggestions that REEs can take part in diagenetic mobilization reactions. Several lines of evidence at Dounan show that ores, including REEs, underwent diagenetic reformation. Assuming equilibrium at all depths, pore water concentrations of all the REEs must have increased slightly with increasing depth, to reach values which are only 1-3 times upper seawater concentration at the interface sediments, indicating a significant participation of REEs in diagenetic mobilization reactions.

The fractionation of REEs during diagenesis is treated in element-element diagrams to illustrate the changes in relative abundances of REEs; these provide the most direct and convincing evidence for diagenetic fractionation (Sholkovitz et al., 1989). Figure 5.13 shows Yb, Er, Eu, and Nd concentrations plotted against La concentrations for both sedimentary and diagenetic samples. La was chosen because it is the lightest REE while Eu represents a MREE, and Er and Yb are HREEs. La-Nd and La-Eu plots show linear relationships throughout the samples while La-Er and La-Yb plots display more irregular patterns. Large reversals in the La-Er and La-Yb plots occur between sedimentary and diagenetic samples, where removal of the LREEs and MREEs exceeds that of HREEs (Fig. 5.12), although with fewer data points. The shapes of the La-Er and La-Yb curves indicate small-scale removal of LREEs and MREEs below the seawater-sediment interface (0-4 m), a phenomenon described in previous sections.

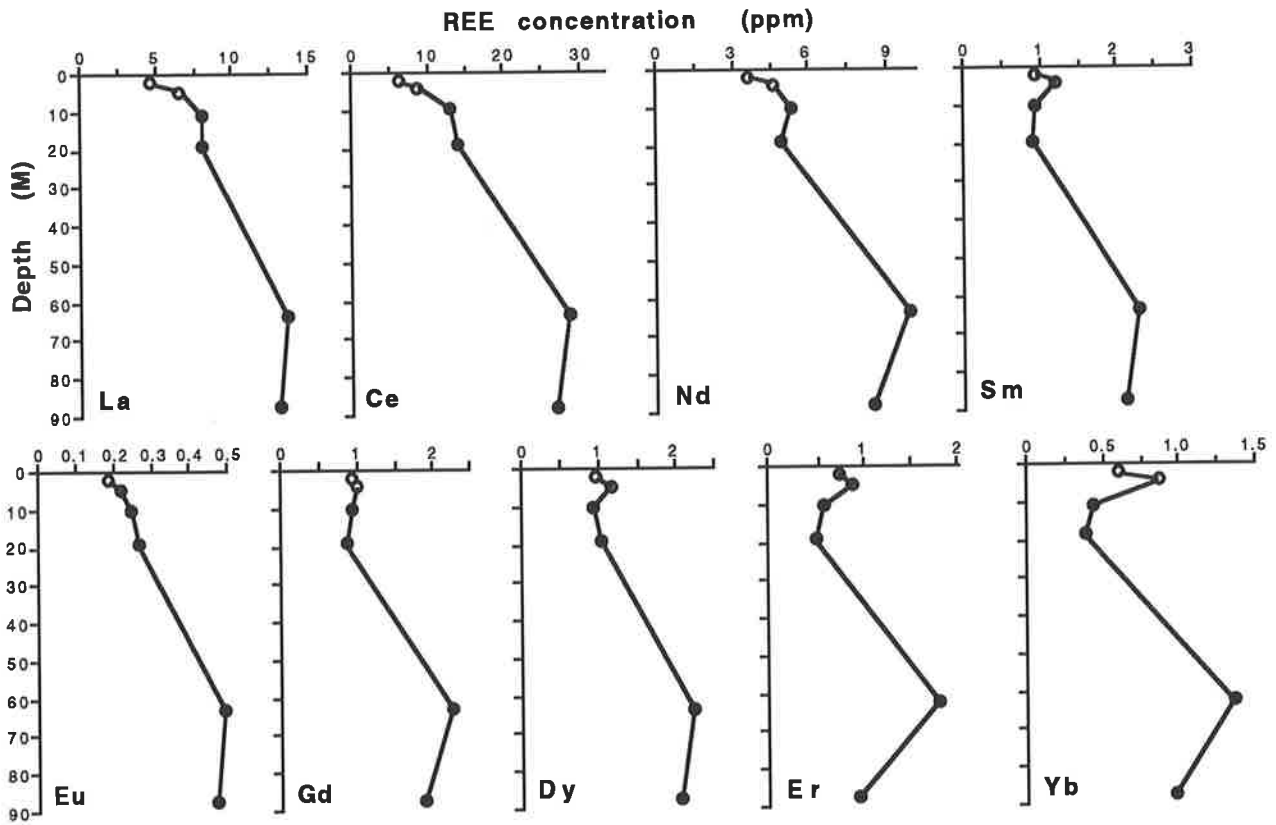


Fig. 5.12 REE concentration profiles in sedimentary Mn materials and early diagenetic materials. Open circles represent synsedimentary Mn sediment and closed circles early diagenetic products. Depths are calculated from stable isotopic data (see Table 5.9); sample numbers are ordered from the surface (46, 49, 42, 43, 142 and 143, which have the common prefix 958).

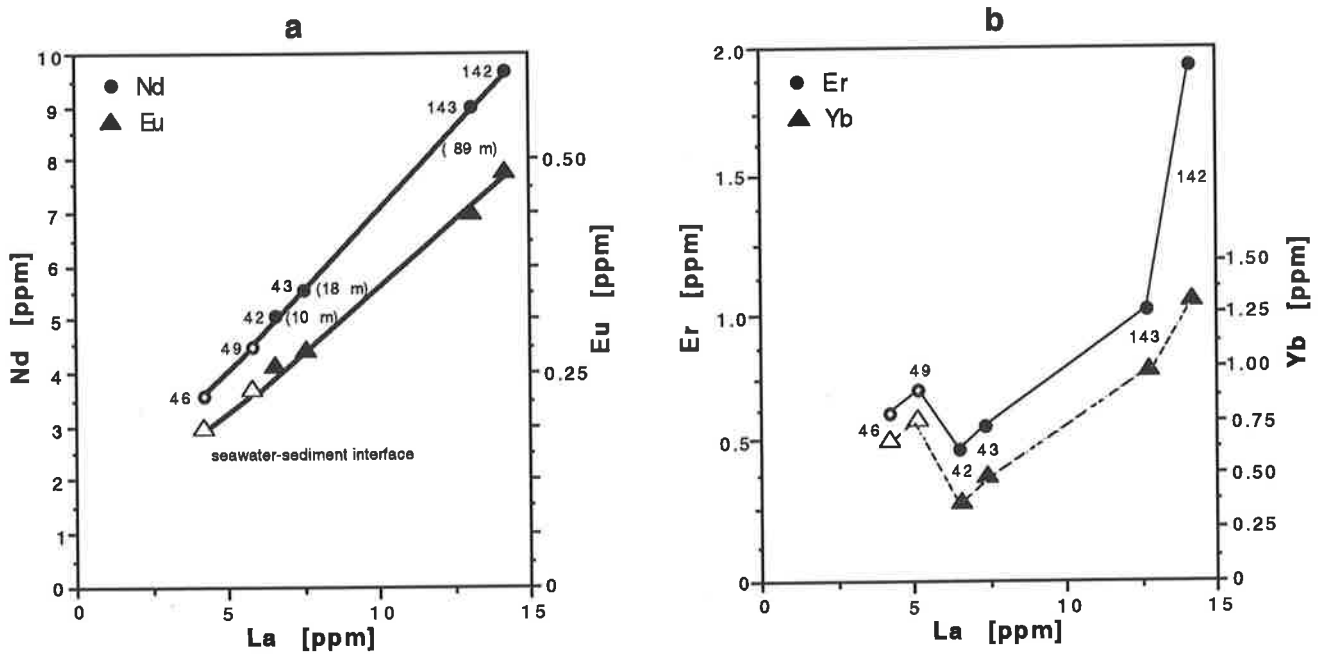


Fig. 5.13 a) La-Nd and La-Eu plots for Dounan sedimentary and early diagenetic samples. Depth horizons are indicated at left down to the depths as calculated by isotopes. The sample numbers beside points are the same as Figure 5.13. b) La-Er and La-Yb plots as per (a). Open symbols refer to sedimentary samples and solid symbols to early diagenetic samples.

To further quantify fractionation over the samples, one can consider $(La_n)/(Yb_n)$ for a LREE/HREE comparison, $(La_n)/(Sm_n)$ for a LREE/MREE comparison and $(Yb_n)/(Sm_n)$ for a HREE/MREE comparison (Table 5.7b). A value of 1 means that a diagenetic sample has the same relative abundance of REE as does the sedimentary (primary) sample. Deviations from 1 indicate that there is fractionation relative to bottom water and sediment composition. Hence the pore waters were significantly fractionated relative to the mean sediment composition (Sholkovitz et al., 1989); they are enriched in HREE (Yb) relative to MREE (Sm) and LREE (La) when normalized to sediment.

5.3.3 Comparison of REE Patterns from Dounan with Other Mn (Oxide) Deposits

The Rare Earth Elements were chosen for this comparison, because of redox control on REE abundance and the availability of comparable data from other deposits. Most of the trace elements on the other hand are often difficult to compare, because the spread of elements varies from study to study.

Since repeated mobilization and reprecipitation cannot be demonstrated in the ores of Dounan, primary minerals are easily recognized. Eu anomalies (and similarly Ce) of the initial precipitates (Fryer, 1977) have not been overprinted by events after sedimentation, and these ores can be used for comparison. Mineral-specific incorporation of REEs (and also TEs) into the lattice of primary phases and fractionation of the various elements in subsequent diagenesis can produce patterns that cannot be ascribed to supergene concentration or to errors of sampling. It is therefore possible to compare the Dounan ores with other deposits that are still close to their initial geochemical composition. Also, it was demonstrated that though some deposits have been influenced by supergene processes at the surface (e.g. Figs. 4.2-3), individual ore and rock types within a stratigraphic section maintain a comparable shale-normalized REE signature. The various ores are compared on this basis.

The most important features for comparison are the pronounced REEs anomalies (variations in the Ce and Eu content) of the Dounan ores (Fig. 5.14). These anomalies are characteristic of the geochemical environment in which the manganese oxides and carbonates developed, and the type of the anomaly (positive, negative) reflects the thermodynamic conditions during the formation of the ores (Piper, 1974; Elderfield and Greaves, 1981; Ingri and Pontér, 1987; De Carlo and McMurtry, 1990).

Calvert et al. (1987) pointed out that the rare earth elements (REE) in ferromanganese nodules are evidently supplied by at least two sources. Sea water (the hydrogenous source) provides what may be regarded as the background supply of REE, while diagenetic reactions in the bottom sediments provide an additional supply (Elderfield et al., 1981). In addition, Piper (1974) was concerned primarily with the biogenic and authigenic phases of marine sediments, those

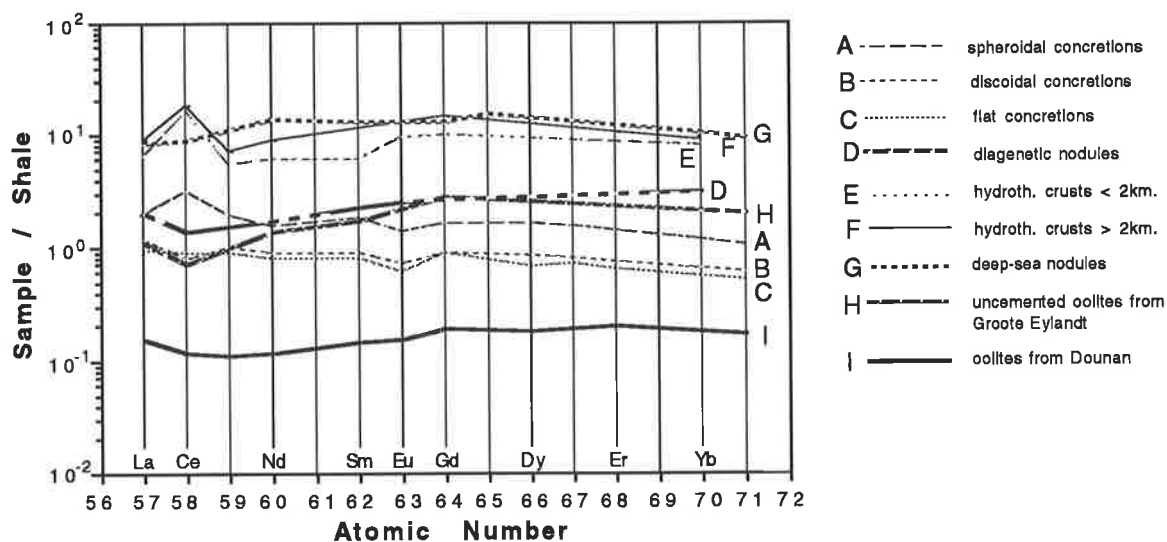


Fig. 5.14 Comparison of shale-normalized REE patterns of various manganese oxides:

- deep sea marine nodules (after Piper 1974);
- marine crusts formed by hydrothermal processes from water depths <2000 m (averages from De Carlo and McMurtry, 1990);
- marine crusts formed by hydrothermal processes from water depths >2000 m (averages from De Carlo and McMurtry, 1990);
- marine nodules associated with diagenetic processes (from Elderfield and Greaves, 1981);
- shallow water marine nodules (flat, discoidal and spheroidal concretions; taken from Ingri and Pontér, 1987);
- oolitic ores from Groote Eylandt of Australia (average values from Pracejus et al., 1990); and
- oolitic ores from Dounan Mn deposits (average values from this study).

phases that have formed directly from seawater. The major biogenic source of marine sediments is CaCO_3 tests of planktonic organisms (Turekian, 1965).

It is known that most marine nodules showing negative anomalies precipitated mainly under the influence of hydrothermal processes (e.g. Rankin and Glasby, 1979; De Carlo and McMurtry, 1990), and some were formed by diagenetic processes (Elderfield and Greaves, 1981; Calvert et al., 1987). It is unlikely the Dounan ores accumulated under hydrothermal conditions, because there is no evidence of any Triassic volcanic activity in the region. Although diagenetic formation in precisely the same way as in marine nodules is not very plausible, given the nearshore marine environments of deposition, and the morphological and petrological features (e.g. cross-bedding, normal/inverse grading) also argue against a purely diagenetic origin, the shape of the shale-normalized REE patterns of the Dounan ores are very similar to those of diagenetic nodules. However, REE concentration levels of the Dounan ores are lower than those of diagenetic nodules (Fig. 5.14).

Piper (1974) describes marine nodules from water depths greater than 3000 m that show extraordinary similarities to a few Dounan ore samples (massive Mn oxide ore); though the REE concentration differs, they possess similar patterns. From the previous chapters, it is known that Dounan ores developed in shallow marine environments, so the similarities are puzzling. The Groote Eylandt ores of Australia recently examined by Pracejus (1989) and Pracejus, et al.

(1990) exhibit shale-normalized REE patterns very similar to the Dounan ores, though they also possess different REE concentrations. Importantly, from sedimentological studies (Bolton, 1981; Frakes and Bolton, 1984), it is known that the ores at Groote Eylandt also developed in shallow marine environments, so in this case the similarities are very significant.

Discoidal and flat concretions from the Gulf of Bothnia (Ingri and Pontér, 1987) collected from water depths of 70 to 120 m possess patterns which are, to some extent, similar to the Dounan ores, though the REE concentrations differ. The shape of the curves for the IREEs and HREEs is nearly horizontal for concretions, whereas the Dounan ore patterns increase towards Gd. However, the pattern for concretions also shows negative anomalies for both Ce and Eu. On the other hand, spheroidal concretions from the same area but in water depths of about 50 to 70 m show strong positive Ce anomalies. Assuming that diagenetic processes did not completely overprint the initial REE pattern, the discoidal and/or flat concretions might represent in some aspects a modern analogue of the Dounan ores, and also of the Groote Eylandt ores (15-50 m deep, Cretaceous), which also formed under shallow-marine conditions.

Grasselly and Pantó (1988) recently examined the REE geochemistry of the Jurassic Mn-deposits at úrkút, Hungary, and found positive Ce anomalies, negative Eu anomalies, and enriched LREEs, which show extraordinary similarities to a few Dounan ore samples (massive ores), though the levels of individual REEs in the úrkút ores are an order of magnitude higher than in the Dounan ores. This suggests not only significant similarities but also differences in the development and subsequent alteration of the deposits.

Some authors suggest the use of Ce/La ratio for an assessment of the rate of Ce depletion in the sediments, which then can be taken as an indicator for the redox conditions during formation of the ores (e.g. Dubinina and Volkov, 1986; Glasby, et al., 1987). Similarly, Grasselly and Pantó (1988) come to the same conclusion in their examination of the úrkút deposits. According to them, the Ce/La ratio is an expression for the rate of Ce depletion in sediments. They suggest that a low Ce/La ratio (0.12) indicates that Ce and a large part of the REE are associated with hydrogenous iron-and manganese hydroxides and are adsorbed from sea water. In the case of the East Pacific Rise, on the other hand, the hydrothermal activity decreases with distance from the rise, while the carbonate and biogenic components in the sediment increase. The Ce/La ratio correspondingly increases to a value of 1.45. With an increase in the amount of terrigenous components, the Ce/La ratio further increases and in the pelagic clays of the Pacific Ocean, the ratio is on average 2.32. In some places it can reach a value of 3 or even more. In Dounan, the Ce/La ratio varies between 1.22 - 2.70 (Table 5.7b). In light of the above, the carbonate, biogenic and terrigenous sources of REE all may also have played important roles.

The La/Yb ratios (Table 5.7b) are fairly similar in the different ore types, in which these ratios range from 0.50-1.42. This indicates that the fractionation of light and heavy REEs here is not

higher or lower compared to mean value (0.83) for the total Dounan area (1.00, respectively), and mainly originated through depositional effects (Zhao, 1978).

The possibility that the ore minerals have only been changed slightly during diagenetic processes, and that these phases may have kept most of the initial REE signatures, leads to the conclusion that in terms of the REE geochemistry a present-day analogue to the Dounan manganese ores can probably be found in the shallow-water marine nodules of the Gulf of Bothnia (discoidal and flat concretions from depths between 70 and 120 m). These Mn-oxides, chemically but also not physically similar to the Groote Eylandt ores, bear the closest REE resemblance to the ores examined here. Besides the strong similarities to diagenetic nodules, sedimentological and petrological or mineralogical studies of the Dounan deposits suggest that the ores, to greater or lesser extent, underwent diagenesis. However, the redox conditions within the sediments where these nodules developed may have been comparable to the geochemical environment of the ores.

5.3.4 *Application of Isotopic Analysis*

As Hudson made clear in his review (1977), significant departures of $\delta^{13}\text{C}$ and $\delta^{18}\text{O}$ from zero result from different processes. Negative or falling oxygen values relate to increased temperature, the introduction of meteoric water or diagenetic reactions, while carbon fluctuations relate to the presence of organic matter and the different isotopic types of CO_2 produced by various organic reactions. Generally, calcareous sediments deposited in near-shore or transitional marine environments may be affected by isotopically light carbon and oxygen from continental sources (Weber and Woodhead, 1970). The isotopic data presented here throw light on several important geological questions.

The negative correlation between manganese content and carbon isotope ratio (Fig. 5.11) is attributed to coupled manganese oxyhydroxide reduction and organic matter oxidation, as has been described by Okita (1987), Okita and Shanks (1988), and Okita et al. (1988) for other sedimentary Mn deposits. This process is a bacterially mediated diagenetic reaction that can take place near the sediment-water interface (Polgári et al., 1991). The negative $\delta^{13}\text{C}$ values further support the involvement of organic matter in the mineralization process.

Carbon in carbonate minerals formed in sedimentary environments can be derived from seawater, from dissolution of pre-existing carbonate, and from degradation of organic matter. Carbon produced from organic matter will be isotopically very light, whereas the other two sources are typically near 0‰ (Polgári et al., 1991). Thus, the simplest explanation for isotopically light to medium values at Dounan is that the CO_2 produced by organic matter mixed moderately with fluids having a signature of $\sim 0\text{‰}$ (i.e. seawater). Also, the moderate variation in $\delta^{13}\text{C}$ values implies that mixing with normal seawater or porewater having an assumed $\delta^{13}\text{C}$ value near 0‰

must have occurred in only moderately varying proportions. The mixing ratio was less (i.e. 1:1 for a $\delta^{13}\text{C}$ value of -2) for the most negative values. However, for the smallest negative values at Dounan, it is likely that there was a small contribution of near 0‰ normal seawater, which may reflect semi-closed-system conditions at the time of precipitation. In contrast, some samples (Table 5.9, Group I) have $\delta^{13}\text{C}$ values near 0‰, within the range of normal seawater.

As mentioned, the sources of 0‰ HCO_3^- include normal seawater and the dissolution of biogenic skeletal carbonate. There is no reason to believe that seawater in the Dounan basin was lacking in bicarbonate, because carbonate deposits are abundant in the vicinity of the mineralization. Thus, the negative $\delta^{13}\text{C}$ values further indicate a moderate lack of communication between the mineralizing fluid (the porewater) and seawater-derived bicarbonate or large input from organic C. For the most negative $\delta^{13}\text{C}$ carbonates, the system was probably semi-closed.

In the study of sedimentary and diagenetic processes, much emphasis is placed on thermally-induced reactions but little on several other processes which equally affect source rock potential. These are more important at shallower burial depths and also lead to diagenetic cementation which can affect both hydrocarbon migration and reservoir properties (Irwin et al., 1977). Curtis (1977) proposed that several different depth-related zones could be recognized within burial sequences and that kinetic controls (notably rate of burial) dictated the relative importance of each zone in determining the extent and style of diagenetic modification. Curtis (1977) and Irwin et al. (1977) have put forward the model (Fig. 5.15) of depth zonation in sedimentary burial sequences with particular reference to the generation of carbon dioxide. Note the nonlinear depth scale which exaggerates the depth span of shallower zones. Bacterial processes dominate in zone 1, 2, and 3.

It should be noted that unstable primary carbonates ($\delta^{13}\text{C}$ ~0 per mil PDB) might dissolve and add carbon of intermediate isotopic composition to the porewater reservoir in which case the above trends might be blurred (Curtis, 1977). This is supported convincingly by data from the Dounan ores and rocks. Isotopically, the ores and rocks can be roughly divided into three groups (Table 5.9) which mostly show normal relationships between $\delta^{13}\text{C}$ and $\delta^{18}\text{O}$ (Fig. 5.16), and the samples of all groups appear to define two/three parallel isotopic trends which shift successively towards lower $\delta^{18}\text{O}$ -values. These features suggest that carbon and oxygen from different sources contributed, to variable extents, to the minerals.

Fig. 5.16 is a plot of $\delta^{18}\text{O}$ PDB against $\delta^{13}\text{C}$ PDB. The calcite precipitation temperature scale is given. The isotopic composition of the first group (primary ores) is very much that to be expected for precipitation from marine reservoir bicarbonate in warm surface waters ($\delta^{13}\text{C}$ ~ zero, $\delta^{18}\text{O}$ ~-3.3‰ corresponding to approximately 25° - 29° C). Bearing in mind that some of the samples contain minor diagenetic carbonate, the range is small.

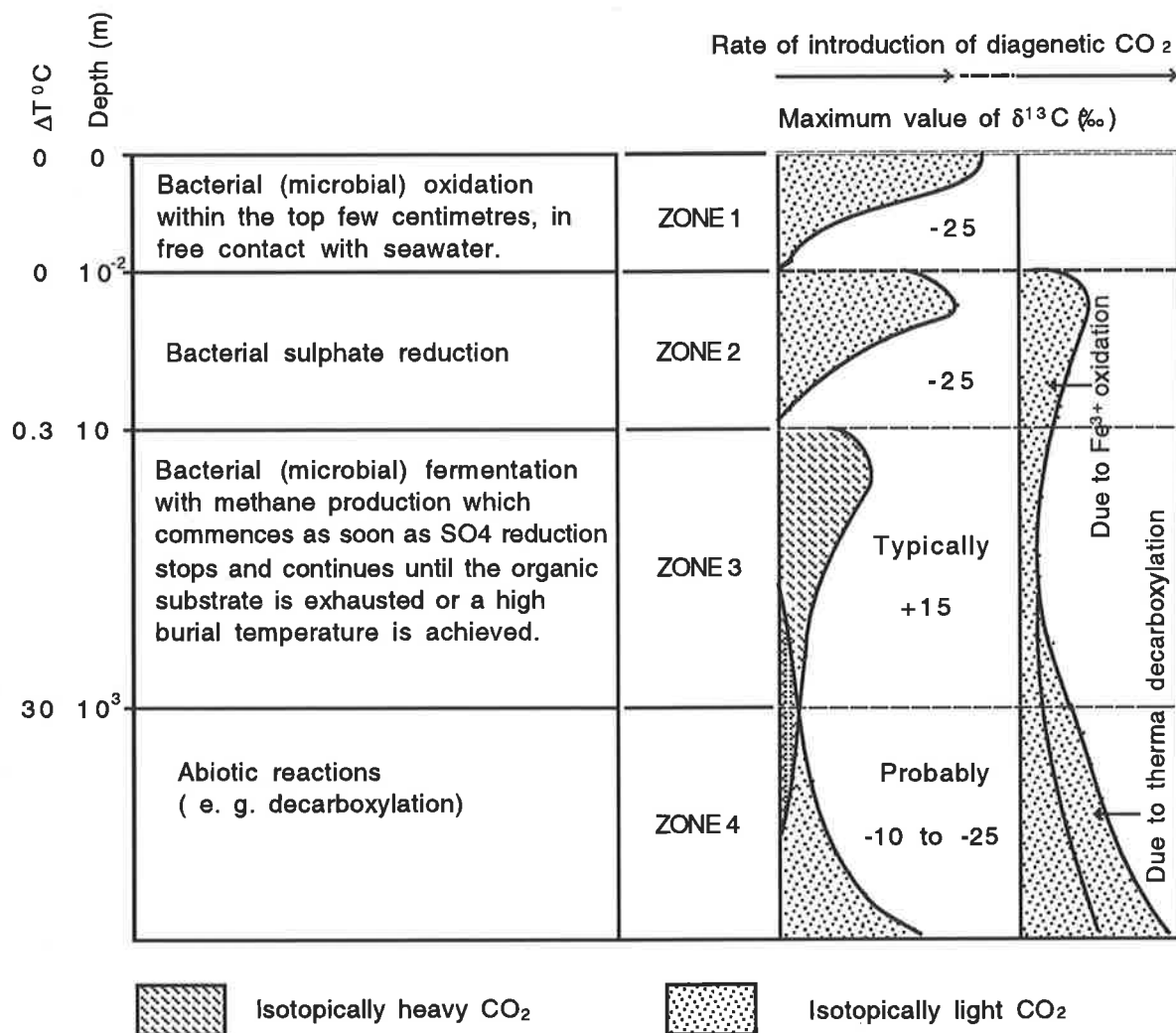


Fig. 5.15 Sources and isotopic composition of diagenetic carbon dioxide in depth-related diagenetic zones (from Irwin et al., 1977).

The Mn deformed oxide oolites/pisolites show little different isotopic ratios with $\delta^{13}\text{C} \sim -3\text{‰}$ and $\delta^{18}\text{O} \sim -4.5\text{‰}$ corresponding to a slightly higher precipitation temperature $T \sim 32^\circ\text{C}$. It seems reasonable to suggest that they precipitated close to the sediment-water interface largely from carbon dioxide produced by sulphate-reducing bacteria (Zone 2, Fig. 5.15). The isotopes indicate therefore that diagenetic segregation of CaCO_3 must have begun shortly after deposition of sediment and before there had been much time to modify the isotopic composition of the seawater. The involvement of such bacteria during concretion development has been discussed by Raiswell (1976). The thermal gradient within the marine water column is in the reverse direction to that within buried sediments: the sediment-water interface must lie close to the mean temperature within the total water plus sediment column. The presence of pyrite in these samples has already been noted, though iron and sulfur contents (Table 5.5) indicate that syngenetic pyrite formation was limited by the amount of available Fe and S.

The third category is remarkable for its wide range of both carbon and oxygen isotopic ratios. Carbon ranges from very heavy to light and oxygen isotopic ratios indicate precipitation

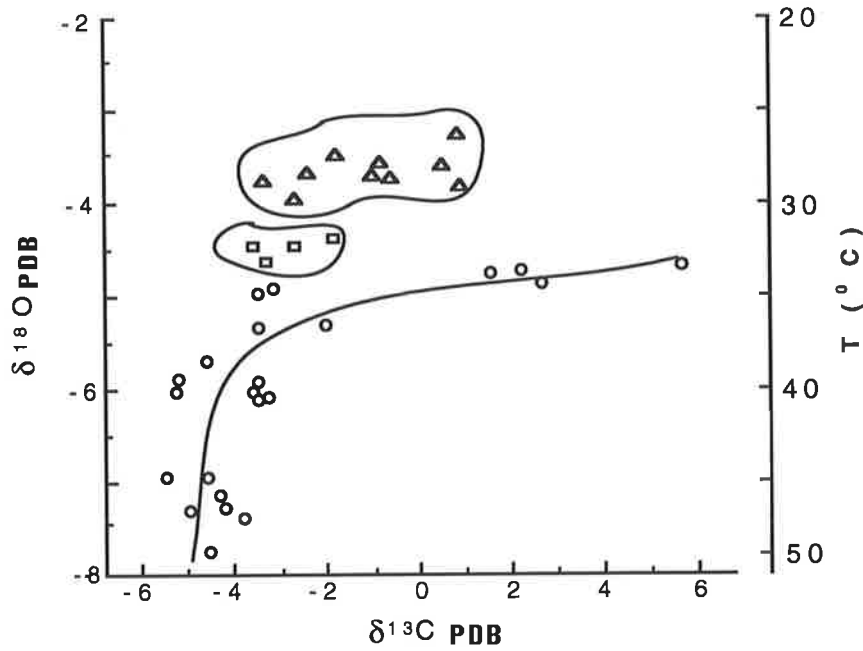


Fig. 5.16 Plot of oxygen isotope ratio against carbon isotope ratio for all samples. Triangles represent primary ores/rocks (group I), squares early diagenetic products (group II), circles diagenetic ores/rocks (the third category). The temperature scale relates to fractionation of calcite with seawater of $\delta^{18}\text{O} = -1.2$ per mil.

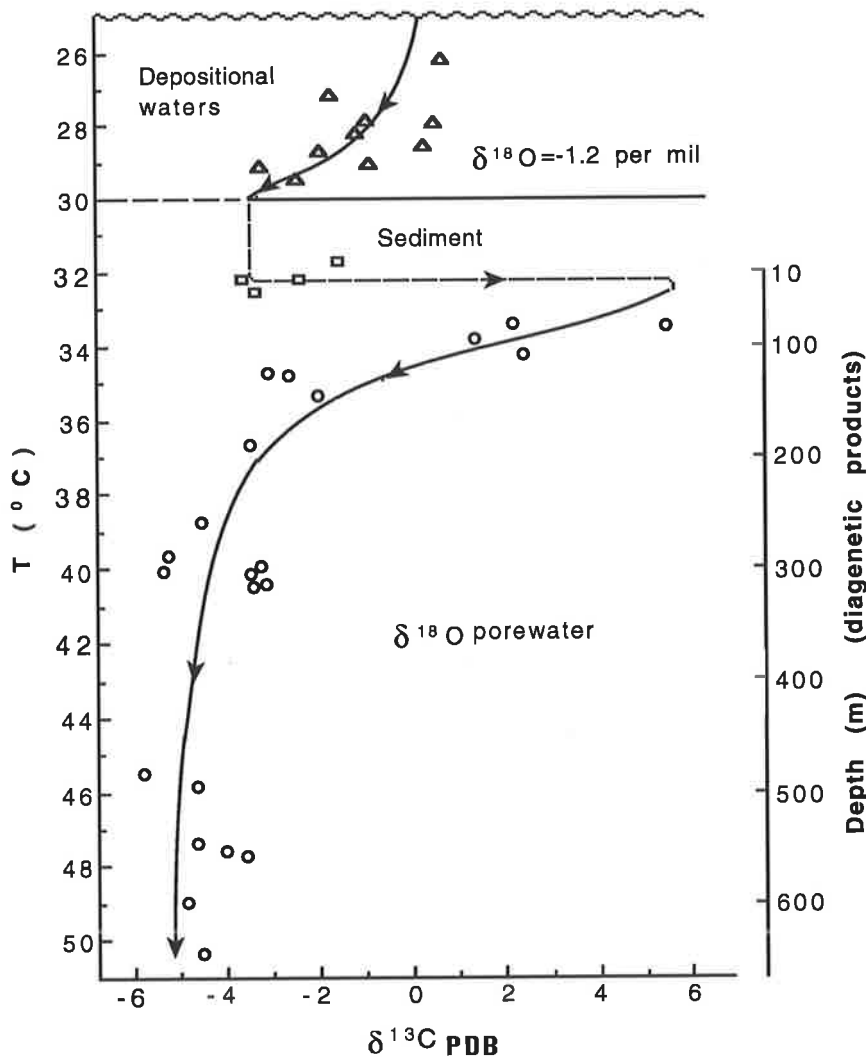


Fig. 5.17 Plot of calculated precipitation temperatures for Dounan Mn ores/rocks against carbon isotope ratio. Primary ores/rocks are shown associated with depositional waters, diagenetic ores/rocks with sediment porewaters. Precipitation pathway is indicated showing passage through zone 2 (sulphate reduction) to zone 3 (fermentation-heavy C, Fig. 5.15) to zone 4 at the base where light carbon isotope ratios are again encountered. For discussion of porewater isotope composition and precipitation depth estimates see text. Symbols as for Fig. 5.16.

temperatures from 34° C to 51° C. Most remarkable of all is the very strong correlation between the two sets of data: heaviest $\delta^{13}\text{C}$ being precipitated at the lowest temperatures. The obvious first interpretation is that these carbonates started to precipitate at some depth below the sediment-water interface from porewaters supersaturated with ^{13}C -rich bicarbonate and that precipitation continued to much greater burial depths where porewater bicarbonate was very much poorer in ^{13}C , in fact enriched in ^{12}C relative to marine reservoir bicarbonate. All these data can be matched easily with the zonal model in Figure 5.15. The lower temperature ore samples precipitated near the top of zone 3 where fermentation processes introduced ^{13}C -rich bicarbonate from organic matter. The gradual and systematic changeover to ^{12}C -rich carbonates with depth of precipitation reflect changes to fermentation downwards through zone 3 into zone 4. Although some ores (e.g. massive ores) contain minor calcite and it is possible that some primary calcite dissolved to contribute bicarbonate to the porewater pool, the observed trend is so well developed that the writer must conclude that bicarbonate derived from organic matter was the principle source for both diagenetic Mn oxides and Mn carbonates. These low $\delta^{18}\text{O}$ values may result either from recrystallization or solid-state exchange of oxygen with a solution whose $\delta^{18}\text{O}$ value differs from the original solution from which the carbonate precipitated.

From this discussion it is felt that the isotope data strongly support the view that distinctive depth-related zones of diagenesis, as shown in Figure 5.15, persisted within the sediment column during Dounan Falang times. This work underlines the importance of diagenetic reactions in being responsible for significant modification of organic matter and the production of massive amounts of carbonate cement. There remains the intriguing and possibly important prospect of being able to determine the depth of precipitation assuming a particular thermal gradient.

The precipitation temperature data (Table 5.9, column 4) indicate relatively coherent changes between Groups 1, 2, 3, and 4. The major isotopic effect of diagenesis on porewater is depletion of ^{18}O associated with formation of diagenetic minerals enriched in that isotope. This applies to clay minerals as well as carbonates (Irwin et al., 1977). The main accompanying physical effect is reduction of pore space and upward expulsion of water. At depth one would expect diagenetic minerals to be formed in equilibrium with isotopically light, modified connate water. Measurements on porewater in samples recovered from the Deep Sea Drilling Project (Lawrence et al., 1975; Perry et al., 1976) show a systematic reduction of $\delta^{18}\text{O}$ with depth by a maximum of 3 per mil at 300 m. This was attributed to diagenetic reactions. This depletion should prevail at all depths below a mixing zone open to the effectively infinite seawater reservoir. The Dounan Falang sediments were probably deposited much more rapidly than those referred to above and such that the "mixing zone" was relatively limited in extent and effective for a shorter time with respect to any individual sediment unit. It should be noted that enrichment of ^{18}O in formation water by exchange with isotopically heavy rocks (Clayton et al., 1966) is a quite different effect from that produced by precipitation of diagenetic minerals. By assuming the temperature of the base of the sulphate-reaction zone is 32.1° C, its depth to be 10 m and a thermal gradient of 28° C per km [a value used in Curtis, 1977], precipitation depths can be calculated and these are

listed in Table 5.9, column 6. In Figure 5.17, the various carbonate samples are plotted as $\delta^{13}\text{C}$ against precipitation temperature. Primary ore/rock samples are plotted separately since they formed within the depositional environment.

Estimates of burial depths for precipitation of diagenetic minerals suggest values ranging to 0.7 km. This means that all these carbonates precipitated relatively early during diagenesis and they almost certainly predated liquid hydrocarbon formation or migration. The trend depicted in Figure 5.17 represents a time sequence for precipitation of carbonates at any particular sediment horizon. Carbonates precipitated from depositional waters obviously constitute the first component. Shortly after burial sulphate reduction promoted precipitation of early diagenetic carbonate, rich in ^{12}C and reflecting slightly higher temperatures. The next carbonates to form did so at similar temperatures but had extremely different carbon isotope ratios with ^{13}C enrichment in consequence of fermentation reactions. Thereafter, successively later carbonates reflect higher precipitation temperatures and the increasing influence of abiotic and decarboxylation reactions (^{12}C -rich bicarbonate input).

Isotopically, the precipitation temperature of the Dounan Mn ores seems to be little higher than that of some modern marine environments. Frakes and Francis (1988) concluded that the geological literature reveals existence of ice-rafted deposits for every period of the Phanerozoic Era except the Triassic. Also, for the Middle Triassic, in its entirety the earth was warmer than now (Frakes, 1979; Frakes et al., 1992). But, the low palaeolatitude (23° - 25°N) of the Dounan area indicates that the precipitation temperature was likely and significant.

Other isotopic properties of Dounan Mn ores/rocks are given in Figure 5.18. Calcite and calciorhodochrosite differ little, most notably in $\delta^{18}\text{O}$. Two features of the data are of particular interest: (1) calciorhodochrosite $\delta^{18}\text{O}$ values as a group are nearly constant over the range of calciorhodochrosite compositions, averaging -5 per mil. A statistical test of the uncertainty of

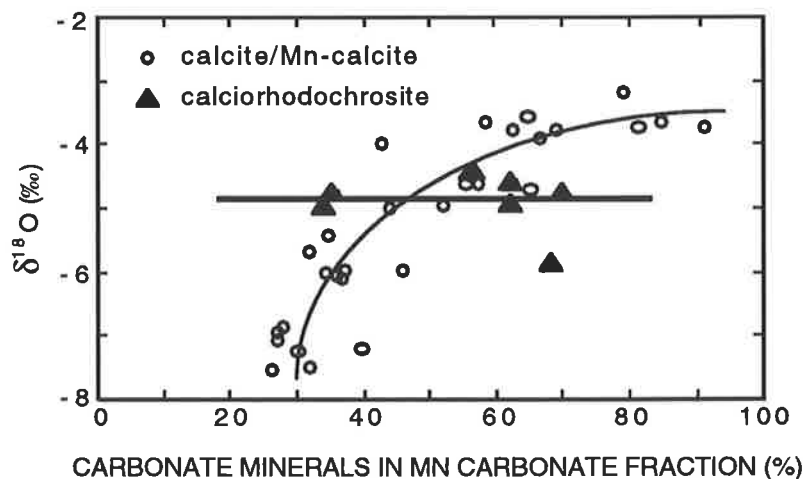


Fig. 5.18
Oxygen-isotope
composition of calcite
/ Mn-calcite and
calciorhodochrosite,
versus percentage of
carbonate minerals, in
Dounan Mn ores.

this line indicates that its slope is close to zero; (2) calcites coexisting with calciorhodochrosites have $\delta^{18}\text{O}$ values that are distinctly "lighter" and "heavier" by ~ 2 and ~ 3 per mil, (and somewhat "lighter" and "heavier" $\delta^{13}\text{C}$ values).

Any interpretation of the calcite in these ores/rocks should account for the variations of calcite $\delta^{18}\text{O}$ and $\delta^{13}\text{C}$, but these changes apply to the "total" calcite undifferentiated as to its various forms: Mn-calcite, Mn-bearing calcite, and fossils. With an increase in braunite, calcite and calciorhodochrosite are less abundant. This increase in the proportion of braunite (i.e. decrease in the calcite) correlates well with the trend towards "lighter" $\delta^{18}\text{O}$ values for "total" calcite (Fig. 5.18). This change may result from the evolution from primary to early and late diagenetic processes in the study area. Perhaps careful apportionment of "bulk" isotopic composition, among the Dounan ore/rock constituents that contribute to the "bulk" values, would show that many ores/rocks in fact contain isotopic vestiges of their origins; their primary marine character may not have been wholly erased during diagenesis. Commonly, carbonate cement of Mn oxides was most likely precipitated early in diagenesis, from seawater circulating through pores. Lack of compaction features in the Mn oxide/carbonate oolites/pisolites implies very early lithification, and such lithification must have involved the introduction of relatively large volumes of cement. Analogy with tracts of recent shallow marine lime-mud suggests that this lithification occurred slightly (perhaps as deep as a few meters) below the sea floor (Philip, 1968).

Before or after early diagenesis (perhaps both) the original unreplaced ooliths/pisoliths became partly cemented by CaCO_3 precipitated in pores by seawater. The resultant partly lithified but still-permeable ores/rocks consisted mainly of Mn deformed oxide/carbonate oolites/pisolites having an estimated $\delta^{18}\text{O}$ between -4 and -5 per mil. Unreplaced ores in the more permeable rocks later underwent marked changes in $\text{O}^{18} : \text{O}^{16}$ and in $\text{C}^{13} : \text{C}^{12}$ during a long and probably complex sequence of diagenetic events that began in Falang time. The net changes in calcite of these ores/rocks were toward depletion in the "heavy" isotopes, probably accomplished by precipitation of CaCO_3 from formation waters containing less oxygen 18 and possibly less carbon 13 than seawater contained. Where cementation was sparse, compaction played an important role; the result was massive Mn oxide oolitic/pisolitic ores.

The most negative $\delta^{13}\text{C}$ values observed from similar marine sedimentary deposits from Molango, Mexico (Okita, 1992; Okita et al., 1988), Gabon (Hein et al., 1989) and úrkút (Polgári et al., 1991) are around -15 to -20% . These values are generally more negative than those of Dounan ores, though several similarities in geochemical and mineralogical characteristics (e.g. rhodochrosite as major Mn carbonate mineral, a lack of pyrite in the ore beds, correlation of manganese content with negative carbon isotope values) exist between the Dounan and other sedimentary manganese deposits. However, the $\delta^{18}\text{O}$ values vary, with values from these deposits being generally higher/lower than the values for the Dounan deposits. These carbon isotope differences probably reflect different sedimentation and diagenetic effects that resulted from local geothermal and tectonic histories of the different depositional basins. The above authors

interpreted their carbon isotopic data to indicate that manganese carbonate precipitated from a carbonate reservoir (closed-system, Polgári et al., 1991) that was significantly fractionated by the addition of ^{12}C -enriched carbonate. The most probable source of this isotopically light component was from the degradation of organic matter (Okita et al., 1988). However, the light carbon isotopic component from Dounan was probably characterized by mixing between organic matter and normal seawater or porewater. Carbonates isotopically depleted in C^{13} and O^{18} , such as those reported by Pfeifer et al. (1988), may reflect a somewhat more oxygenated environment of formation, or a lower organic matter content of the sediment. Significantly lower $\delta^{18}\text{O}$ values, such as those reported by Tassé and Hesse (1984) for authigenic carbonates in Cretaceous black shale, probably reflect formation during relatively deeper burial.

Thus, the ores/rocks associated with the Dounan Mn deposits appear to have been substantially depleted in C^{13} and O^{18} during Falang stage mineralization of the Middle Triassic by diagenetic decarbonation, but some ores/rocks still display primary normal marine isotopic ratios. Mn-calcites, calciorhodochrosites, Mn-bearing calcites and gangue calcites in the ore deposits show a variety of isotopic compositions, which suggests various sources of carbon and oxygen, and deposition over a range of temperatures. Probably, organic (e.g. bacteriogenic) and/or inorganic (e.g. decarbonation) sources played a major role at Dounan.

PART III

INTERPRETATION AND CONCLUSIONS

Chapter 6 Genesis of the Manganese Deposits

6.1 Introduction

Aspects of the Dounan manganese deposits-stratigraphy, sedimentation, paleoenvironments, the mode of occurrence of orebeds, mineralogy, petrology, texture and paragenesis of the manganese orebodies and associated host rocks, have already been discussed in the previous sections. The results obtained from these investigations will now be examined critically to decipher the mode of origin of the manganese deposits. The following key points will be considered in this connection:

- paleotectonics and paleogeomorphology;
- relationships between ores and rock units;
- relationships between ore beds and syngenetic sediments;
- evolution of the Mn sedimentary basin and environments;
- paleoclimate and paleogeography during Mn deposition;
- normal and relict sedimentary textures (indicating the operation of both syngenetic and diagenetic processes);
- biological or microbial activity;
- geochemistry of the Mn deposits;

Note: no trace of hydrothermal, volcanogenic and metamorphic sediments or minerals have been found in either the manganese ore-bearing horizons or in other strata of the Falang Formation).

In view of the fact that sedimentation plays an important role in the accumulation of ore-forming elements in the Dounan basin, all major ore and rock types (excepting those which are distinctly supergene) contribute in some way to this enrichment, and therefore, diagenetic mechanisms need a careful assessment as to their ability to alter primary ores. The dominant type of diagenesis also determines the strength of overprinting and if this is marked it can be used to

discern some of the main mineralization processes and to improve geological and geochemical exploration to identify the best target areas.

As mentioned before, braunite is the dominant Mn mineral in the Dounan deposits. Till now arguments on the origin of braunite still continue. However, the different genetic views, e.g. sedimentary-metamorphic (Zhang et al., 1979), sedimentary (Su, 1983), metamorphic (Yue, 1985), lack strong evidence to support their points of view due to the absence of detailed research work (e.g. geochemistry, microanalysis). Generally because braunite is so characteristic of the meta-sedimentary manganese ores of India, irrespective of the grade of metamorphism (Roy, 1966), and of similar diagenetic to metamorphosed rocks in South Africa and South America, the mineral is commonly considered to be a metamorphic reaction product. It is also a common manganese mineral in manganese-bearing base-metal veins, in association with fluorite, barite and carbonate, which may be the ancient equivalents of present-day hydrothermal emanations at oceanic spreading centers (Roy, 1981). Both modes of origin are of elevated temperature and/or variable confining pressure. There is also a small number of reports which suggest that braunite may have developed at low temperature and pressure, in the supergene weathering zone of manganese deposits (Hewitt, 1972) or as product of diagenesis of manganese-bearing sediment (Roy, 1981). A few researchers (Ostwald and Bolton, 1990) have recently presented detailed reports on diagenesis of braunite. In most of these reported cases the evidence for braunite development under normal surface temperature and pressure is not very good. Therefore, the discovery of braunite showing a range of morphologies, textures, and geochemistry (e.g. REE and isotopes) in sedimentary rocks of the Triassic manganese deposits of Dounan, China, allowed the postulated low-temperature origin of braunite to be examined, thus adding to the knowledge of the mineralogy of this mineral.

In this chapter a detailed discussion is given on dissolution, transport, and precipitation processes, including their "diagenetic variation potential". The evidences of sedimentary and diagenetic activities of Dounan manganese ores/rocks are examined first, because the understanding of mineralizing mechanisms should be based on such evidence which have direct implications for the formation or alteration of manganese ores. A discussion of these initial conditions is vital for the understanding of complex geochemical, mineralogical, and biological mechanisms.

6.2 Evidence of Sedimentary and Diagenetic Activity

The formation of manganese and associated materials in the deposits has been interpreted to be related to sedimentary and diagenetic processes on the basis of previous descriptions such as relationships between ore and rock units, lithofacies or on the environmental controls on manganese ores and associated rocks, but also on the typical sedimentary and diagenetic fabrics, replacement features, and the geochemical characteristics. Further direct or indirect evidence for

both sedimentary and diagenetic mineralizing mechanisms can also come from consideration of the conditions of metallogenesis, as follows.

6.2.1 Paleotectonics and Paleogeomorphology

6.2.1.1 Regional Tectonic Position and Features of Dounan Area

The Triassic sedimentary area of southeastern Yunnan, China, is located in the western part of the Yunnan-Guizhou-Guangxi sedimentary province, and it is surrounded by the northern Niu-shoushan Oldland, western Kangdian Oldland, southwestern Ailaoshan Rise and southern Yuebei Oldland, which are characterized by a number of different paleogeomorphological conditions which led to complex lithofacies zones, e.g. intertidal flats, barrier, shelf and slopes (Figs. 1.2, 1.3; 2.24 and 2.25).

In terms of the analysis of Triassic Falang Formation and regional tectonics of southeastern Yunnan (Chapter 1), the eastern boundary of the Yuebei Oldland was approximately controlled by the Wen-Ma fault during Falang sedimentation and in the southeast, this, together with the Ailaoshan Rise, extends towards southern Vietnam (Figs. 1.2 and 1.3, Zhang et al., 1979). The areas surrounding these oldlands were apparently affected by NW-SE faults which were characterized by down-to-basin movements on the east, and by larger fault displacements in the south relative to the northern area. Thus, also taking into account the analysis of lithofacies-paleogeography (Chapter 2), the paleogeomorphology of Yuebei and Ailaoshan oldlands was characterized by higher southern parts and lower northern areas. Their northern boundary with the southeastern Yunnan Triassic basin is approximately located along the Ming-Su arcuate fault. The Dounan marine sub-basin is located on the northern margin of the Yuebei Oldland, in the southern area of the southeastern Yunnan basin.

6.2.1.2 Features of Dounan Marine Basin (Yanzijiao-Dounan-Laowu)

The main structural outline of the southeastern Yunnan Triassic basin is characterized by a series of NW-SE rises and sub-basins. For instance, the Geju and Dounan sub-basins are separated by the Kaiyuan-Yanshi rise (Fig. 2.25), and the complex paleotectonic, and the resulting paleogeomorphology, of the southeastern Yunnan basin thus controlled the formation and development of the Dounan marine sub-basin. Activity on the NW-SE Wen-Ma fault led to the development of another structural system, i.e. the SW-NE Ming-Su arcuate fault and the Dounan arcuate syncline. The Dounan Triassic sub-basin and syncline therefore are the products of regional tectonic movements, and sedimentation there was also controlled by tectonics. Obviously, the Dounan sub-basin had restricted connections to the open sea due to the presence of the Shanjia old island as well as barrier facies during the Triassic age.

6.2.1.3 Mn Formation Controls of Paleotectonic and Paleogeomorphology

Previous analysis showed that paleotectonics and paleogeomorphology controlled the formation and evolution of the Dounan sub-basin which in turn controlled the development of sedimentary environments and sedimentation of Triassic strata (e.g. Zhang et al., 1979; Liu et al., 1984). Facies associations of Falang Formation sediments in the Dounan sub-basin demonstrate the co-existence of fine terrigenous clastic and intraclastic carbonate sediments, indicating that the Yuebei Oldland was characterized by both physical and chemical weathering and a relatively stable erosional state. Low stream gradients and slow transportation is suggested by the fine-grained gradients and deep chemical weathering is indicated by the chemically precipitated sediments of the basin. Constant subsidence controlled the transportation of materials from rivers. A number of well-developed Mn orebeds reflect the repetition of similar sedimentary environments, indicating control of paleoenvironments for Mn deposition through repetitious subsidence. The paleogeography of the Dounan area led to development of a complex of shallow marine environments including those characterized by both low and high energy. The stratigraphic analysis also revealed a series of small transgressive/regressive events associated with Mn sedimentations. These characteristics can be illustrated by the following lines of evidence:

- Considering the Ming-Su fault as the southern paleo-coastline of the marine basin, basin sediments accumulated approximately 2-6 km from the paleo-coastline, and the basin area 4-5 km from the coast-line was most favorable for Mn deposition (Liu et al., 1984); the Yanzijiao, Dounan and Laowu Mn deposits are all located within this area;
- Normally/inversely graded textures reflect transgressive/regressive events;
- The variation of grainsize indicates shallow environments with relatively high energy;
- Primary Mn oxides, the predominant orebodies, contain extremely low S and P, also reflecting shallow, brackish and slightly oxidizing environments;
- The petrology of the ore-bearing series implies a shallow depositional environment;
- The vertical sequence (from Mn carbonates to Mn oxides) suggests a regressive development.

6.2.2 Stratigraphic and Textural Features

6.2.2.1 Relations between Orebodies and Enclosing Rocks

1) In all areas under consideration in this text, the manganese orebodies are conformably interbedded with and folded along with their country rocks as sedimentary layers, and, in each case, they exhibit similar structural attitudes to those of the enclosing lithic units. There is not a single instance in the whole area along the Dounan Mn belt or the fairly widespread deposits of the Yanzijiao, Dounan and Laowu districts, where the orebodies (excepting those which are distinctly supergene), discordantly cut across the enclosing rocks. All stratigraphic observations in the

Dounan area indicate that the manganese orebodies and the enclosing rocks were formed as part of the same sedimentary sequence and were later folded together (Chapters 2 and 3).

2) The manganese orebodies of the southwestern Dounan area, scattered as they are over a larger area (e.g. Gake, Kata), occupy more than three definite stratigraphic horizons (i.e. orebeds V₁₋₁ - V₃₊₂ in the lower ore-containing section, T_{2f4-1}, Chapters 2 and 3). Similarly, the orebeds in the northeastern part of Dounan area (e.g. Baigu), are also confined to at least seven horizons (i.e. orebeds V₄ - V₁₀ in T_{2f5-2}) in the upper ore-containing series. All are orebodies interbedded with associated terrigenous clastic rocks and intraclastic carbonate rocks, which together with the manganese ore deposits, are also entirely confined to the Falang Formation. This restricted nature of the orebodies to definite stratigraphic horizons establishes their formation as part of the Falang sedimentary sequence.

3) Significantly, the sharp contact relationships between the manganese orebodies and enclosing or intercalated intraclastic carbonates and mudstones/siltstones, suggest that both ore and carbonate units were originally laid down as chemical sediments, which is also indicated by the micritic textures of the carbonates. Mudstones/siltstones were deposited as detrital sediments.

4) Generally, the thickness of orebeds is positively correlated to that of the Mn-bearing series which in turn is positively correlated with that of the Falang Formation sediments. In the thicker Falang Formation, the Mn-bearing series are better developed, that is, orebodies are thicker and there are more of them. This suggests sufficient material input to maintain stable sedimentary environments.

5) The orebodies and intraclastic (Mn-bearing) limestones are most intimately associated and interbedded each other, and both sharp and gradational contacts are seen. Intercalations within orebodies invariably exhibit a mode of occurrence similar to that of the orebodies, and from field study it is clear that their modes of formation were also similar. The manganese oxide in the orebody occurs alone when manganese carbonate is not present, but when carbonate is intercalated, they are intimately interbedded with the latter. The major orebodies are all made up of braunite, and together with the observations of the relationships between Mn oxides and Mn-bearing carbonate intercalations, it is clear that they are not derived from the Mn-bearing intercalations but, apparently, were formed by the same process (e.g. chemical precipitation) as a separate entity.

6) The spatial distribution of the Dounan Mn orebodies probably are indicative of not only complex paleogeography but also of a regressive evolution of the Dounan Mn sedimentary basin (Chapter 3). This is strongly supported by the fact that manganese horizons occur at regular intervals and by their offlapping geometry.

6.2.2.2 *Information on the Primary Sedimentary Origin of Mn Ores*

- 1) The manganese orebodies are always associated with unequivocal syngenetic sediments. Conformable structural attitudes with such rocks indicate that the manganese ores were also originally laid down as syngenetic sediments.
- 2) Importantly, banding occurs both on a macro- and a micro-scale; these are in the form of bands rich in braunite and others rich in carbonate minerals. This banding represents the original sedimentary nature of the manganese ores. Similar banding within Mn carbonates and between braunite and siltstones is also noticeable where calciorhodochrosite and Mn-calcite, or braunite, concentrate in certain bands and gangue minerals or rocks in others. This apparently indicates compositional banding in the original sediments.
- 3) Again importantly, concentric laminae of ooliths/pisoliths consist of either braunite-rich and Mn carbonate minerals-rich, or single braunite or Mn carbonate minerals. This represents the original sedimentary structure of the manganese oolites/pisolites.
- 4) The preponderance of manganese oxides in the Dounan ores, together with relatively minor manganese carbonates, and the presence of banding and concentric laminae composed of both Mn oxides and Mn carbonates, indicates that the chemical sedimentation originally took place mainly under slightly oxidizing to reducing conditions.
- 5) In all the manganese ore-bearing horizons discussed in this text, no trace of volcanogenic sediments have been found. There is also no evidence or indication that any volcanic or pneumatolytic activity played any part in the deposition of the ores, nor of other Triassic sediments in the Dounan area.
- 6) Similarly, in all the manganese ore-bearing horizons, including the Triassic sedimentary sequence of the Dounan area, there is also no evidence or indication of any metamorphic or hydrothermal activity which might have played a role in the history of formation of the Dounan ores or Falang sediments (e.g. Figs. 2.13, 2.16, 2.18, 2.20).
- 7) The nature of the Dounan Falang Formation sediments shows that Mn deposition was associated with both clastic and carbonate sediments, rather than development of either clastic rocks or carbonates.
- 8) Extremely similar geochemistry of different ore-bearing sequences reflects similar development of sedimentary environments.

6.2.2.3 *Variation in Diagenetic Effects*

Diagenetic variation does not seem to have been extreme in the Dounan sequence. For instance, diagenetic vein structures are rare and small in scale and therefore could not have affected the stratigraphic sections pervasively. On the other hand, diagenetic textures or structures exist in ores/rocks throughout the sequence, demonstrating that diagenesis played a major role in altering the mineralogy.

6.2.3 *Lithofacies-Paleogeographic Conditions*

It is well-known that lithofacies-paleogeographic conditions are the most important factors controlling the sedimentation of sedimentary manganese deposits. Thus, the following aspects are considered below: lithofacies and Mn deposition; lithofacies of the Mn-bearing series; paleogeographic evolution of the Mn-bearing series; lithofacies-paleogeographic controls on Mn deposition and evolution of the sedimentary basin and Mn series.

6.2.3.1 *Relationship between Lithofacies and Mn Deposition*

The detailed study of sedimentary lithofacies in Chapter 2 allows division of the Dounan Falang Formation into seven major facies: (1) limestone facies; (2) (Mn-bearing) siltstone facies; (3) (Mn-bearing) clayey siltstone facies; (4) (Mn-bearing) silty claystone facies; (5) Mn-bearing mudstone-limestone facies; (6) Mn-bearing intraclastic limestone-mudstone facies; and (7) Mn-bearing intraclastic limestone-muddy siltstone facies, of which the last two facies [(6) and (7)] are most intimately associated with Mn deposition. Generally, the Dounan Falang lithofacies is characterized by two noticeable cases: 1) Mn-free sediments exhibit simple or unique lithofacies; 2) Mn-bearing units always developed in complex lithofacies associations composing both terrigenous clastic rocks and intraclastic limestones. This indicates that lithofacies exerted an important control on the formation of the deposits.

6.2.3.2 *Lithofacies of Mn-bearing Series*

The lithofacies of the lower Mn-bearing series is composed of mudstones (45%), limestones (28%), clayey siltstones (20%), and manganese ores (~5%), classified as a siltstone-carbonate-mudstone lithofacies of Mn-bearing series (i.e. the so called Mn-bearing argillaceous facies, Liu et al., 1984). In relative contents, the lithofacies of the upper Mn-bearing series consists of clayey siltstone (64%), intraclastic limestones (22%), mudstones (9%), and manganese ores

(~5%), classified as a mudstone-carbonate-clayey siltstone Mn-bearing lithofacies (i.e. the so called Mn-bearing argillaceous siltstone facies, Liu et al., 1984).

6.2.3.3 Paleogeographic Evolution of Mn-bearing Series

Based on the analysis of sedimentary environment and isopachs, the detailed paleoenvironmental and paleogeographic studies by Liu et al., (1984) show that the paleo-coastline of the Dounan sub-basin was located approximately 20-30 km south of the Yanzijiao-Dounan-Laowu zone during initial Falang sedimentation. However, by the beginning of Mn deposition, the paleo-coastline had moved towards the north and northeast and was located about 5-10 km from Yanzijiao-Dounan-Laowu, evidently indicating a marine regression. The nearshore paleogeographic environments gradually developed as favorable to ore formation, i.e. tidal flat-lagoon-barrier-slope-open marine (Figs. 2.23, 2.24 and 2.25). By the Niaoge stage of the Late Triassic, after a major marine transgression, the coast-line had already migrated to nearby Dounan, leading to littoral coarse terrigenous sediments over the Baigu area. This fact indicates transgressive/regressive sedimentation for the Dounan manganese sequence.

6.2.3.4 Lithofacies-Paleogeographic Control to the Mn Deposits

Paleoenvironmental analysis indicates that the sedimentary environments of the Dounan Mn-bearing series were characterized by tidal flats with barrier island, and the implied hydrodynamic variation indicates that deposition of the manganese sediments was intimately associated with high energy tidal sedimentation. Mn-free sediments, on the other hand, were mostly deposited in lower energy lagoonal or open marine conditions, thus the occurrence of multiple Mn horizons in vertical profile reflects a cyclic recurrence of similar Mn mineralizing environments. It is known that lithofacies and paleogeography are generally controlled by sedimentary environment and paleotectonics. Thus, the intimate relations between manganese deposition and paleotectonic and paleogeographic environment suggest that facies development controlled or influenced the formation and distribution of the Dounan manganese deposits. These conditions of Mn ore formation have not been reported from modern environments: that is, there is no modern analogue for the Dounan ores. Similarly, there is no strictly comparable ancient deposit.

6.2.3.5 Evolution of the Mn Sedimentary Basin and Mn-bearing Series

The Dounan sub-basin lay approximately parallel to the paleo-coastline along the northern margin of the Yuebei Oldland, and accumulated clastic and Mn materials from the oldland. The shape and size of the basin varied depending on paleomorphologic and paleogeographic changes

(transgression-regression related to subsidence, sediment supply and sea-level change). Initially, the sedimentary basin was larger during the first ore-forming period than in the second or following ore-forming periods. Further, the thickness and extent of the different orebeds vary as well as their shape (stratiform-lenticular), seemingly also related to the evolution of regressive Mn sedimentation.

Figure 6.1 shows an overview of lithofacies and isopach variation of the lower Mn-bearing series (e.g. the first Mn-depositional cycle). The Mn sedimentary area was composed of several small depocenters (individually ~1000 m long and 500 m wide). Commonly, manganese deposition took place in the shallow parts or between the depocenters, whereas the deeper central parts were manganese-poor depositional areas (with thinner Mn horizons or without Mn deposition) probably due to the unfavorable environmental conditions (e.g. pH/Eh) for manganese precipitation.

The distribution of T2f4-1 Mn-bearing argillaceous facies is controlled by micro-paleogeomorphology within the basin, as well as by the occurrence of mixed clastic and chemical sediments. The lithofacies isopach variation (Fig. 6.1) shows that the shallow northeastern part (probably tidal flat behind barrier) and the southeastern part (perhaps intertidal flat) contain better developed manganese than the deep central part (e.g. CK303) of the marine depocenter; the lithofacies includes clayey siltstone, silty claystone, carbonate-mudstone, and mudstone-carbonate facies in a trend from SW to NE. Thus, based on the available information, the zonal variation of lithofacies from SW to NE reflects a restricted tidal environment with barrier island. In addition, the lenticular siltstone facies also suggests complex micro-paleogeomorphology and material input. However, the contact between Geju Formation limestone (T2g) and T2f4-3 sediments (e.g. CK3902) indicates the absence of the lower Mn-bearing deposition, implying the presence of a rise or barrier. Towards the northeast (Baigu area), the lithofacies vary from mudstone-limestone to limestone without any manganese deposition, a reflection of unique lithofacies developed in relatively deep water.

Similarly, the lithofacies isopach variation of the upper Mn-bearing series near Baigu implies the presence of two small depocenters, i.e. a southwestern sub-basin about 1900 m long and 600-1000 m wide; and a northeastern one about 1300 m by 500-800 m, generally showing horizontal basement with local irregularities (Fig. 6.2). The manganese again was deposited in areas of mixed lithofacies of both clastic and carbonate rocks.

6.2.4 Paleoclimate

For the overview of the globe, the initial Triassic climates were characterized by a warm, drying-out period which may have lasted until the middle Jurassic (Frakes et al., 1992). During the

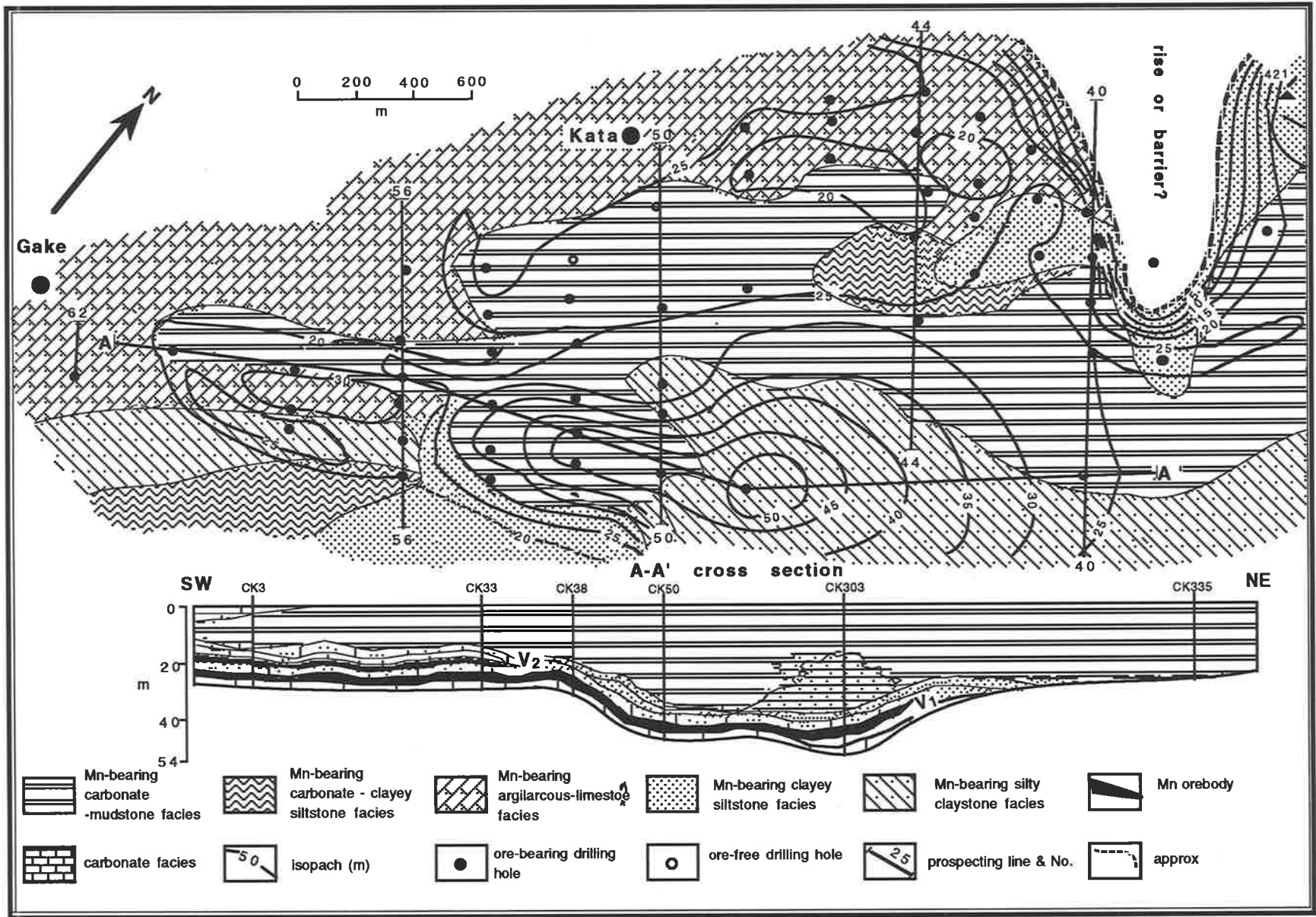


Fig. 6.1 Lithofacies-isopach map of Lower Mn-bearing series (T₂f₄₋₁) of the Dounan Mn deposits (modified after Liu, et al., 1984).

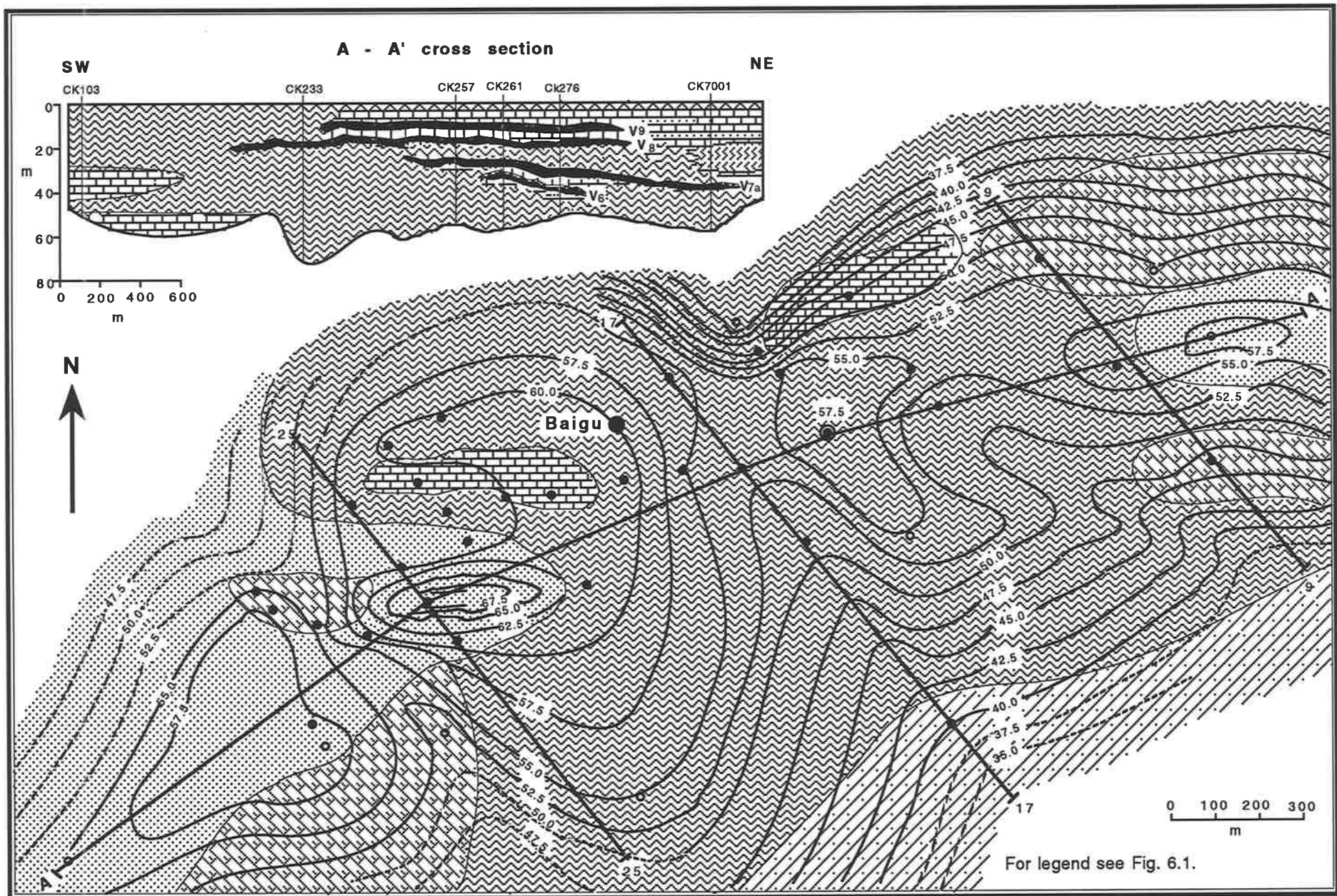


Fig. 6.2 Lithofacies-isopach map of Upper Mn-bearing series (T₂fs-2) of the Dounan Mn deposits (modified after Liu, et al., 1984).

Triassic, southeastern Yunnan was located in mid latitudes ($\sim 33^\circ - 35^\circ \text{ N}$) and was characterized by dolomites concentrated in the Middle Triassic (e.g. Baixian section, Chapter 2). These may represent an evaporitic phase, formed as temperatures rose over much of the low latitudes of the globe (Fig. 6.3, Frakes, 1979). The sediment types and fossil assemblages as well as the oxygen isotopes of sediments may reveal some characteristics of paleoclimate in or near the Dounan basin. Also, in studying the paleoclimate of any area, land or sea, it is most important to know the paleolatitude, as this contributes more than any other factor to regional climate conditions (Frakes, 1979). The Triassic latitudes of the Dounan area did not differ much from those of today (Fig. 6.3).

The Middle Triassic interval features a dominance of dolomite deposition in the Baixian area, to the southeast of the Dounan area, and worthy of note is the fact that the Dounan sediments show a dominance of red-bed deposition in some horizons (e.g. T_{2f3-2}) which may represent evaporitic times.

Though there exist red-bed units, it is not yet possible to assign climatic conditions to the Triassic red beds. However, since evaporitic carbonates are concentrated in the Middle Triassic both here and in the Sichuan basin to the north (Fig. 6.4, Wang et al., 1985), it appears that this was a time of increased aridity relative to the early and late Triassic (Frakes, 1979). Frakes (1979) concluded that global climates during the Mid-Triassic probably were as dry as at present, and probably drier, and that the rock distributions also indicate climates at least as warm as at present. As shown in Figure 6.3, Triassic coral reefs extend almost to 35° N latitude, suggesting that temperatures of low-latitude water masses approximated or slightly exceeded those of the present. Mid-Triassic reefs distributed in the northern part of southeastern Yunnan (Fig. 2.24) strongly support this suggestion.

Although Triassic paleotemperatures have not been widely assessed quantitatively, some idea of temperature conditions can be gained from oxygen and deuterium isotope composition of cherts. (Karhu and Epstein, 1986); these yield a range of about $25-27^\circ \text{ C}$ for the subtropics. The trend in these data is towards increasing temperatures in the Middle Triassic. Isotopically, the precipitation temperature of the Dounan sediments of the Mid-Triassic seems to be a little higher ($25^\circ-30^\circ \text{ C}$, Chapter 5) than that of modern marine environments at these latitudes. The Dounan paleotemperatures suggest that the low mid-latitudes were only moderately warmer than present, and significantly cooler than the Karhu and Epstein maxima.

Manganese materials could be dissolved in acidic surface waters, and transported to the basin, where they were deposited in weakly oxidizing and alkali NE shallow marine waters to form sedimentary Mn oxides or minor Mn carbonates (Frakes and Bolton, 1992). The warm and humid paleoclimate and weakly oxidizing atmosphere played important roles in the dissolution, transportation and deposition of manganese.

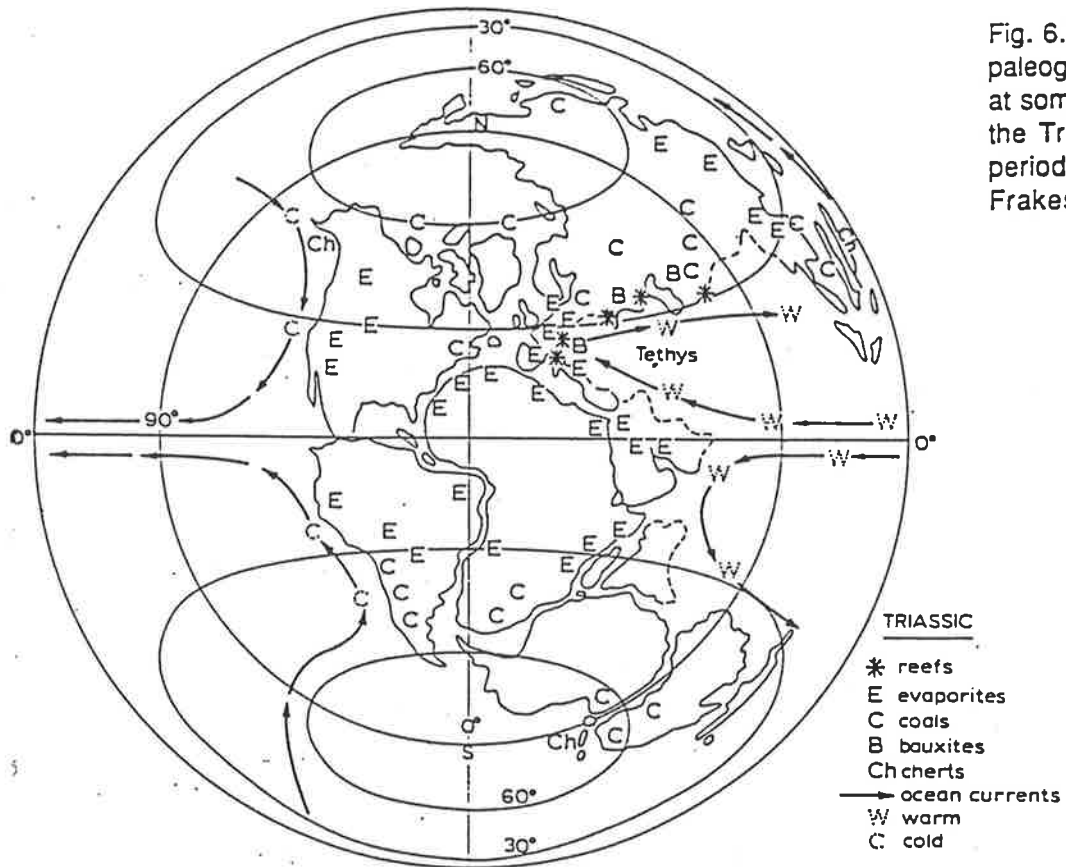


Fig. 6.3 Global paleogeography at some time in the Triassic period (from Frakes, 1979).

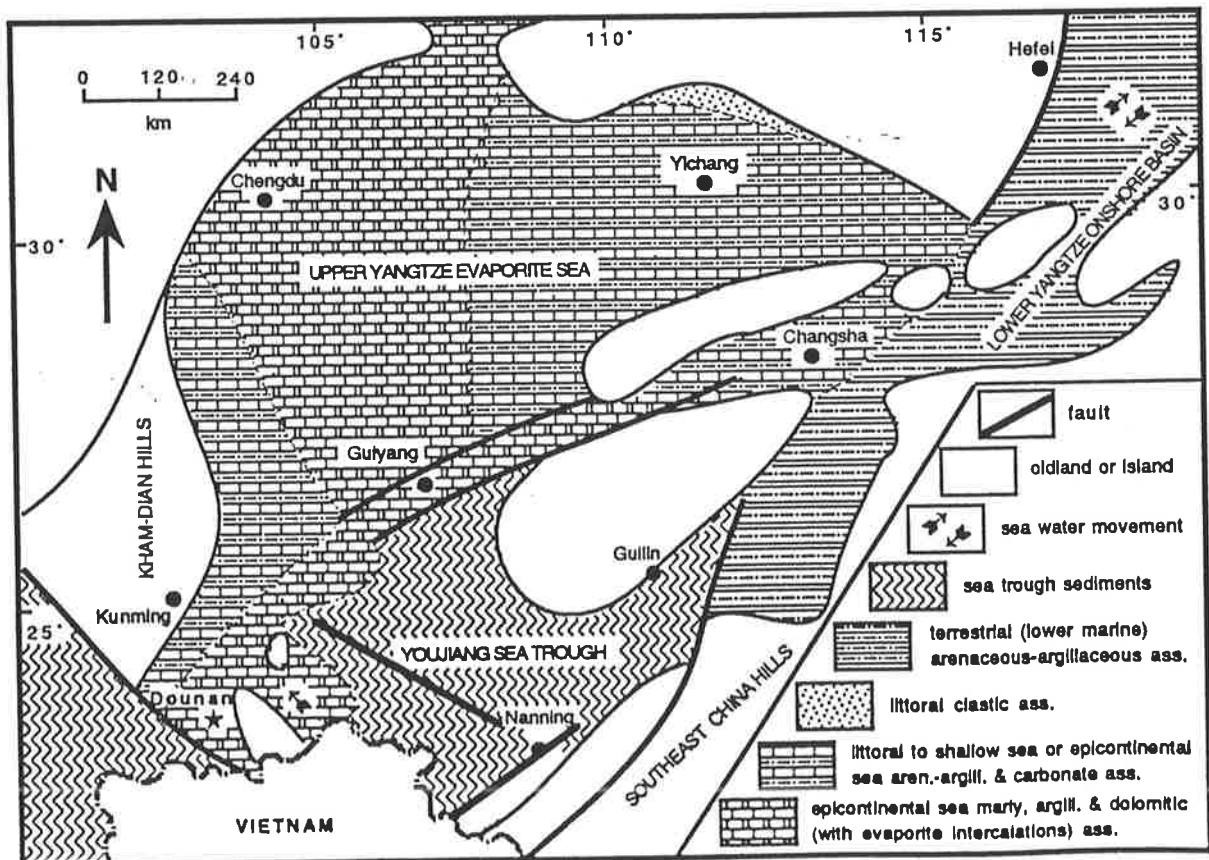


Fig. 6.4 Palaeogeography of the middle Triassic of south China (modified after Wang et al., 1985).

6.2.5 Environmental Conditions of Mn Mineralization

6.2.5.1 Mineral and Rock Indicators

Although few authigenic minerals are identified in the Dounan ores/rocks, they are, to some extent, significant in environmental analysis. For instance, the glauconite occurring in the Dounan clayey siltstone or silty claystone is sometimes considered as a typical shallow marine indicator, mostly formed in relatively low energy environments (e.g. open sea or lagoon); the presence of trace collophanite in the mudstones suggests deeper environments (e.g. open sea); whereas the occurrence of pyrite and bivalvia fossils probably indicates a reducing environment (e.g. lagoon) (e.g. Blatt et al., 1980).

In addition, stromatolites and oncolites are also specific authigenic products of sedimentation (e.g. Hoffmann, 1973), though they do not exactly belong to mineral types. These are apparently also environmental indicators of lower intertidal or upper subtidal zones. Importantly, the co-existence of Mn oxides and Mn carbonates (e.g. unsorted and banded ores) strongly suggests that they formed in varying levels of oxygen depletion, thus also indicating environmental changes.

6.2.5.2 Relations between Ore Phases

Commonly, the vertical distribution of the Dounan ore phases, e.g. Mn carbonates, Mn oxides and transitional type, also reflects an evolution of primary Mn sedimentary environmental changes (Figs. 4.2, 4.3). This evolution apparently developed from reduction to transition and to oxidation, or towards shallow environments due to regression. However, the major concentration of transitional Dounan ores relative to "pure" Mn oxides and Mn carbonates suggests that the transitional weakly oxidizing-weakly reducing environments characterized by varying levels of water anoxia controlled the formation of the Dounan Mn deposits. Also, normal and inverse grading in the ore phases obviously indicate small changes in energy levels related to transgression/regression.

The vertical variation of individual major orebodies, from Mn carbonates to transitional type and to Mn oxides, exhibits an obvious relationship with regressive cyclothemic sedimentation, which suggests that Mn carbonate phase developed in the initial period of regressive Mn mineralization, whereas further regression led to the change of ore phases towards transitional and Mn oxide ores. This is also strongly supported by the horizontal distribution of the ore phases in which changes from Mn carbonate to transitional and to Mn oxide phases apparently indicate the progressive shallowing and shrinkage of the depositional basin during the regression.

6.2.5.3 *Primary Fabric Indicators*

Sedimentary fabrics are one of the most important and significant environmental indicators. At Dounan, various primary sedimentary fabrics reflect a relatively complex set of sedimentary environments. Generally, the normal and inverse variations in grain size of ores/rocks indicate not only a change of energy or environment but also provide information on transgression or regression. Commonly, the massive bedding occurring in the Dounan fine terrigenous sediments suggests rapid sedimentation in low energy slope or open sea environments. Laminations and small scale low-angle cross-bedding in the fine clastic or carbonate sediments probably indicate low energy lagoonal or upper subtidal environments. Importantly, various high energy intertidal fabrics occur in the orebeds include such typical intertidal fabrics as oolites/pisolites and tabular and lenticular cross-beddings.

The contacts of the concentric laminae of oolites/pisolites are sharp except where replacement and mixture of the components occur. The collo- or crypto-crystalline textures probably resulted from collo-chemical sedimentation of manganese. There is little doubt that the grains of oolites/pisolites, spherulites and oncolites are the primary products of sedimentation. In addition, the fragmental and brecciated structures also exhibit syndimentary features possibly caused by high energy tidal waves.

6.2.5.4 *Diagenetic Fabric Indicators*

Although the examination of the Dounan fabrics by a number of methods (e.g. macro- and microscopy, CL and SEM) generally lead to syndimentary interpretations, the changing nature of some fabrics suggests the presence of diagenetic variations. Admixing and/or replacement is indicated by contact relationships between the concentric laminae of Mn oolites/pisolites; the Mn-oxide or -carbonate interlaminae often disappear due to replacement or recrystallization. In many samples, grains of ore or gangue minerals are observed to be partially or totally transformed to others. Relatively coarse grains of Mn minerals generally formed along the contact between crypto- and micro-crystalline Mn concentric laminae, and the perfect euhedral crystals of braunite and rhombohedral crystals of Mn carbonate minerals in sharp contact with carbonate gangues indicate changes to higher temperatures of diagenetic processes. Particularly, the observed conversion to braunite from Mn carbonate minerals by further reaction with available silica generally occurred along the grain margins or crystallographic planes. Thus, a diagenetic change from the sedimentary stage can be recognized in the Dounan Mn ores/rocks, though it played a less important role than sedimentation in the formation of the deposits.

6.2.5.5 *Eh-pH Relations of Manganese Formation*

Since the precipitation of Mn minerals is mainly controlled by environmental factors, such as Eh and pH, the different Mn minerals may reflect various precipitating velocities. Braunite is the major manganese mineral in the deposits and is a water-free manganese compound. Hem (1972) observed a system containing biocarbonate species activity. Besides introducing a large field of stability for MnCO_3 , there is also a solute complex, MnHCO^{+3} , whose effect is important. This will be discussed in detail later.

From the Eh-pH diagrams (see Figs. 6.6 and 6.8) and related calculations, it is possible to generalize about the relative importance of different chemical controls on solubilities and to speculate briefly about the manner in which Mn materials might most readily become available, through increased solubility, for uptake by plants or utilization by animals (Hem, 1972). Thus, the compositional controls on the environmental system are not of negligible significance. This is strongly supported by the fact that the explanation of the presence of Dounan manganocalcite or calcium in rhodochrosite is, to some extent, limited by the relationships in Figures 6.8-6.8 (see later discussion in **6.5 Sedimentation Processes**). Therefore, the precipitation of Mn minerals is apparently controlled by dissolved manganese activity in marine water as well as the physical and chemical fields of stability.

However, where composition is invariant, environmental conditions (e.g. Eh and pH) must play the dominant role in manganese precipitation. The solubility of manganese may be changed by changes in either pH or Eh (Hem, 1972). In addition, Hem (1972) noted that solubility can be altered from values given under normal conditions (25° C and 1 atm) by changes in temperature or pressure. However, the effects under near-surface conditions (e.g. diagenesis) are probably substantially smaller than those indicated for pH/Eh. Thus, the chemical nature of the environment remains as the critical factor in precipitation of these essential ore-forming materials.

6.2.5.6 *Redox Interface Controls on Precipitation Environments*

Based on the discussion above, the position of the redox interface (that is, the top of the oxygen-depleted zone) during the deposition of Dounan manganese ores can be characterized by the following three situations:

- 1) when the redox interface is located below the sediment-water interface, the precipitation of manganite and braunite suggests oxidizing and neutral (weakly acid or alkaline) environments;
- 2) when the redox interface is approximately coincident with the sediment-water interface, co-deposition of braunite and Mn carbonate minerals (e.g. unsorted and banded ores), indicates weakly oxidizing transitional environments;

3) when the redox interface is located above the sediment-water interface, the precipitation of Mn carbonate minerals reflects a weakly reducing alkaline environment.

Therefore, the discussion of Dounan environments generally explains the formation of the primary manganese ores. Mn oxides were probably formed in the oxidizing pH-neutral phases, whereas the unsorted and banded ores as well as the ooliths/pisoliths composing both Mn oxide and carbonate concentric rings probably resulted from varying levels of oxygen depletion and/or other varying environmental conditions. For instance, environments featuring low tidal action were characterized by oxidation or weakly oxidizing neutral conditions, whereas the hightidal activity developed weakly reducing alkaline environments which tended to increase the possibility of forming Mn carbonates or concentric rings in oolite/pisolites. In addition, biological activity may also have indirectly affected the formation of the ores, through affecting micro-environments (see following discussion).

6.2.6 *Biological Activity*

The biological characteristics and their relationships with Mn ores in the Dounan deposits were described in Chapter 2 (Table 2.7 and Plates 2.3 and 2.4). Here the discussion emphasizes their possible direct or indirect influence on manganese precipitation.

6.2.6.1 *Biological Influences on the Mn Environments*

It is known that many natural waters are subject to pH/Eh changes caused by photosynthesis and other biological factors (Hem, 1972). For instance, the biological activity of algae on intertidal flats can be increased due to the input of fresh water (decreased alkalinity and salinity), which in turn can lead to decreasing pH; Eh can also decrease because of increased utilization of algae by invertebrate animals. In most cases, the effects of grazing are much less important than the effects of increased photosynthesis by plants in tidal flats, so that the Eh changes may be negligible. In any case these environments appear to have been favorable for the precipitation of braunite. In the subtidal zone photosynthesis plays a less important role due to lesser plant densities and deeper water. The environments are relatively alkaline because $\text{Ca}(\text{HCO}_3)_2$ is abundant in marine water and they are weakly reducing below the zone of mixing because of oxygen utilization by animals. Manganese carbonates form in these environments, particularly in estuaries (Calvert and Price, 1972). It is in such environments that the Dounan manganese deposits were formed. Biological activity thus contributed to the local environments of the Dounan manganese deposition in general; there may also have been biological effects in catalyzing precipitation of Mn on the micro-scale within ooliths/pisoliths, though this is difficult to establish.

6.2.6.2 *Environments of Dounan Oncolites and Stromatolites*

Abundant algae or oncolite and stromatolite structures mineralized by manganese ores (e.g. Plate. 2.3, Figs. 1a-d and 2a-b) indicate that algal activity was of some importance in the formation of the manganese ores. Generally, the micrite oncolites, braunite oncolites or stromatolites are considered to have formed in very similar environments (e.g. lower intertidal or upper subtidal zones) due to algal or other biological activity (e.g. Hoffmann, 1973). The microstromatolite structures in the Dounan ores and rocks appear to have formed in very shallow environments, though they are not as abundant as oncolites. Oncolites formed from microstromatolites due to tidal action and, perhaps, other environmental changes. This is strongly indicated by the fact that many inner textures of oncolites are characterized by micro-stromatolites (e.g. Plate. 2.3, Figs. 1a-d and 2a-b).

6.2.6.3 *Influence of Biological Activity on Mn Mineralization*

It is known that oncolites, stromatolites and biogenetic sedimentary structures result from activity of blue algae (e.g. Hoffmann, 1973). Blue algae have two important habits in forming oncolites and stromatolites: (1) the precipitation of carbonate in or on algal crusts involves both photosynthesis and bacterial decomposition, which changes the local environment (e.g. pH changes due to the absorption of CO_2 from sea water) and leads to CaCO_3 or MnCO_3 precipitation; (2) the sticky colloidal algal crusts secreted from blue algal cells possess the ability to catch materials or fragments from the water, and of course, to adsorb manganese colloidal suspensions. Thus, in the colloidal chemical precipitation of manganese, biological (particularly algal) action has importance not only for changing the micro-environment but also for concentrating manganese materials. The presence of algal materials in the Dounan manganese oolites /pisoliths (or oncoliths) strongly support the existence of primary sedimentary braunite.

In summary, biological mineralization at Dounan operated through at least three processes:

- 1) adsorption of colloidal manganese materials on the growing algal surfaces;
- 2) absorbing manganese materials from marine water as nutrient, leading to Mn enrichment. The statistics by Trudinger (1976) show that some marine plants (particularly bacteria and algae) exhibit a strong ability to absorb manganese (2.6×10^4 enrichment in plants relative to sea water);
- 3) changing the sedimentary micro-environment (e.g. pH and Eh), thus leading to the chemical deposition of various manganese compounds.

6.2.6.4 *Biological Mineralization in Diagenesis*

The fact that many biological fossils are replaced or filled by braunite or manganese carbonate minerals (e.g. Plates 2.3 and 2.4) is strong evidence for diagenetic changes in the Dounan Mn ores. Though this can not directly provide the proofs that biological activities played a significant role in concentrating manganese materials during diagenesis, it provides indirect information that the Dounan ores experienced changes after deposition. The fossils as the nuclei of Mn oolites /pisolites, in particular, are replaced or filled by manganese minerals, suggesting that these Mn oolites/pisolites experienced a "long-term" evolution from sedimentation to diagenesis.

6.2.7 Geochemical Conditions

6.2.7.1 General Geochemical Natures of Manganese

Manganese (atomic number 25) is the 12th most abundant element and is represented in nature by +2, +3 and +4 multi-valence states which make it easy to be dissolved in anoxygenous environments and transported as low-valence ion (+2) or its compounds. Oxidation can lead to precipitation as +3 or +4 valence Mn oxides.

Calculations of the average abundance of manganese in the earth's crust show values close to 1000 ppm (1000 ppm, Goldschmidt, 1954; 950 ppm, Krauskopf, 1967; 1060 ppm, Ronov and Yaroshevsky, 1972). A calculated average Mn-content for sedimentary rocks in general is 0.056% (Beus, 1976). However, the manganese coefficient of concentration (i.e. the lowest Mn mining tenor / Mn Clark value = $30 / 0.1 = 300$) is very high compared to those of some other elements, e.g. 20 times higher than that of iron and 40 times higher than that of aluminium, though the average abundance (Clark value) in the earth's crust or in sedimentary rocks is relatively low, which leads to many mineable manganese deposits. In addition the similar ionic radius of Mn^{2+} (0.91Å), those of Ca^{2+} (1.08Å) and Mg^{2+} (0.80Å), means these elements may easily replace each other in an isomorphous series; this in part probably explains the occurrence of the Dounan Mn carbonate minerals. Thus, the geochemical nature of manganese itself is apparently one of the important factors in manganese mineralization.

6.2.7.2 Geochemistry of Manganese during Sedimentation

The migration and deposition of manganese are affected by complex factors such as tectonic movements, source materials, sedimentary conditions, paleoclimate, biologic development, and CO_2 content in the atmosphere. Numerous estimates have been made of Mn-content in surface waters (e.g. Roy, 1981) and it has been shown that under most conditions manganese is under-saturated with respect to oxide precipitation in groundwater, river, lake and seawater. According

to Crerar et al (1980), the soluble inorganic components of natural waters occur in the following relative order of abundance:



As manganese geochemistry, as with iron, in sedimentary environments is governed by oxidation and reduction (Maynard, 1983), the formation of a valuable manganese deposit appears to require that two general conditions be met: manganese must be concentrated to at least 200 times its average crustal abundance and iron cannot be concentrated to any appreciable degree from its average crustal abundance of about 5 percent (Force and Cannon, 1988). The concentration of Mn in seawater mostly varies between 0.1 and 8.0 ppb (Roy, 1981). While Alexandrov (1972) estimated that over 90% of the manganese introduced by rivers into the sea is in the form of suspension, Hood (1972) observed that manganese occurs in seawater mostly as Mn^{2+} ion, in part complexed with organic matter, and that particulate manganese is restricted to the surface water column devoid of colloidal MnO_2 . Crerar and Barnes (1974) estimated that approximately 10% of the total manganese in seawater is colloidal or particulate, that another 10% is organically complexed and that the remainder consists of Mn^{2+} and simple inorganic complexes. Sapozhnikov (1970) assumed that in an ore deposition process, dissolved manganese is the main source of the metal. For Dounan Triassic Mn deposits, manganese probably was transported by surface or subsurface waters into the sea, mainly in the form of Mn^{2+} ion but with minor colloidal or particulate suspension, probably with trace organic complexes. It was deposited under changing environmental conditions either as Mn carbonates or as Mn oxides depending on fluctuations in the sedimentary environments (e.g. varying levels of oxygen depletion). Dissolved manganese from the regional weathering cycle probably was the main source of the metal in the basin (see later discussion).

6.2.7.3 *Relations between Manganese and Other Major or Minor Elements*

The widely varying negative correlations between Mn and Ca or Si probably indicate not only variations in the redox conditions of Dounan sedimentary environments (e.g. Eh, but including pH), but also isomorphic replacement between the elements (Fig. 5.1). Also, the good correlations between Mn and some trace elements such as Ni, Co and Cu, may suggest Mn sedimentation similar to that of modern marine manganese nodules (Frakes, 1982). However, the correlation matrix of elements in Dounan ores (Table 5.4) suggests that Mn^{+4} dominates the braunite and has a close relationship with Si, whereas Mn^{+2} mainly occurs in Mn carbonate minerals and shows a close relationship to Ca. The former pairing probably represents an isomorphic relationship between Mn^{+4} and Si^{+4} in braunite, whereas the latter indicates an isomorphic replacement between Mn^{+2} and Ca^{+2} in Mn carbonate minerals. Variation in major and minor elements such as Mn, Si, and Ca in different ore types could also reflect varying inputs of materials and different sedimentary environments (Fig. 5.2).

Although the abundances of the trace elements in different ore types are similar, some elements (e.g. Sr, Ni, Rb, Zn, Zr) to some extent vary independently (Fig. 5.3). The decreasing trend of Ni with decreasing Mn and negative correlations between Mn and other trace elements such as Sr, Zn, Rb and Zr, probably reflect varying material sources and sedimentary environments during manganese deposition (Jin and Li, 1981). This possibly indicates an interactive effect of terrigenous clastic and intraclastic carbonate materials, or oxidizing and reducing environments.

Significantly, in terms of the microanalyses of Dounan Mn minerals (Chapter 5), the paragenesis of two kinds of braunite (i.e. normal braunite I with ~10% SiO₂ in Mn oxides and the 'braunite' in the Mn carbonates with more Ca (7-15%) and Si (15-22%)) suggests interactive sedimentation in varying levels of oxygen depletion. In addition, the element distributions within Mn minerals (Figs. 5.8a-e) indicate the co-existence of both primary and diagenetic phases. Similarly, the distribution of Mn oxide and carbonate minerals in the oololiths /pisoliths also indicates a syngenetic relationship during the sedimentation of varying levels of oxygen depletion in the water column.

6.2.7.4 REE Evidence of Mn Mineralization

The REE study has yielded significant results for understanding the genesis of Dounan Mn ores (Chapter 5). Several results, such as on the abundance and pattern of REEs, normalized REEs, Ce and Eu anomalies, and special REE ratios, carry very important genetic information neglected in previous works. Comparison of Σ REE content among the different ore types (Table 5.7) provides evidence as to the important role played by redox environments in the concentration of REEs. The small range of both Eu and Ce anomalies in various Dounan Mn ores indicates a stable Mn sedimentary (mineralizing) environment. The nature of sedimentary environments reflected in the diagram of Σ REE against Σ LREE/ Σ HREE (Fig 5.6) is closely related to and seems to control the petrology and geochemistry of the different Mn ore types. Differences apparently result from varying parameters of the sedimentary (mineralizing) environments (e.g. pH, Eh and alkalinity).

The similar Ce/La ratios (Table 5.7) from various ore types indicate that the ores formed in broadly similar redox conditions, suggesting that the same factor controls the Ce enrichment in both Mn oxides and carbonates (Glasby et al., 1987). Most shale-normalized REE patterns (Figs. 5.7a-b) of the Dounan ores show slightly positive Ce anomalies, which are regarded as signaling primary marine or early diagenetic sediments (e.g. Elderfield and Sholkovitz, 1987). The similarity of patterns in different ore types also means that though the ores differ in their appearance and mineralogy, the behavior of their REEs were comparable, suggesting similar shallow marine genesis for all.

The Ce anomalies suggest that sea water probably was the source for REEs in the ores. Piper (1974) suggested that this enrichment of Ce in Mn nodules with complementary depletion of Ce in the sea water can be considered as positive evidence in support of a precipitative origin of the REEs in manganese nodules. Because Ce mobilization and cycling is restricted to near-bottom sea water, the Ce enrichment in most Dounan ores as observed in this study (Chapter 5) favors the conclusion that sea-water was the main source for the REEs in the Mn ores. This implies that perhaps the ores are hydrogenous, that is, they precipitated directly from sea-water (Sunit, 1979). However, smaller Ce anomalies in some transitional and Mn carbonate samples compared to the Mn oxides are interpreted as due to formation in less oxidizing conditions.

REE evidence suggests that continuous environmental changes within tidal flats are responsible for the formation of the ores and changes in their character. This mode of origin has been documented in Chapter 5 (5.3 Discussion), in which sedimentary and diagenetic effects were recognized. Although diagenesis did not affect Dounan ores in precisely the same way as in marine nodules, various characteristics of the mineralogy and petrology argue against a purely diagenetic origin. Given that the shape of the shale-normalized REE patterns of the Dounan ores are very similar to those of diagenetic nodules (Fig. 5.14), however, the processes influencing materials are comparable in the two types of deposit. The same condition can be applied to Groote Eylandt ores (Cretaceous) which exhibit shale-normalized REE patterns very similar to those of the Dounan ores; the former is regarded as having formed in shallow-water marine environments. Similarly, the discoidal and/or flat concretions from the shallow marine Gulf of Bothnia might represent in some geochemical aspects a modern-day analogue for both the Dounan and Groote Eylandt ores.

6.2.7.5 *Isotopic Evidence of Mn Mineralization*

Although there exists an overprinting of primary minerals by diagenetic ores (Chapters 4 and 5), careful selection of samples made it possible to obtain both primary and diagenetic information from oxygen and carbon isotopic analysis (see following discussion). A few samples show very similar results, with $\delta^{13}\text{C}$ close to zero, moderately negative $\delta^{18}\text{O}$ and a small range in temperature (25° - 29° C). These apparently represent primary Mn sedimentation, which is consistent with other field and laboratory studies. Also, stratigraphic variation of $\delta^{13}\text{C}$ is readily evident and correlates positively with manganese content (Fig. 5.10), thus probably reflecting an evolution from sedimentation to diagenesis during marine regression. CO_2 was produced by decaying organic matter and this was mixed moderately with fluids having $\delta^{13}\text{C}$ of about 0‰ (i.e. sea-water) for the Dounan ores. This model provides a sedimentary interpretation of variations in isotopic composition in a semi-closed-system (Chapter 5.3 Discussion).

Relations between $\delta^{13}\text{C}$ and $\delta^{18}\text{O}$ (including calcite precipitation temperature; Fig. 5.16) and between $\delta^{13}\text{C}$ and depth (Fig. 5.17) also show the evolution of Dounan Mn ores from sedimentary to diagenetic conditions. The further correlation between oxygen isotopes and Mn carbonate content (Fig. 5.18) shows the changes that resulted from diagenetic processes.

6.2.7.6 Diagenetic Variation

The negative correlations between Mn and Si or Ca to some extent probably reflect replacement between the elements after sedimentation. Therefore, a combination of Ca with either element produces recognizable patterns which may be attributed to the replacement between the manganeseiferous and calcareous or siliceous groups in the diagenetic stage. This is strongly supported by the inferred isomorphic relationships between Mn^{+4} and Si^{+4} in braunite, and between Mn^{+2} and Ca^{+2} in Mn carbonate minerals, and by obvious enrichment of manganese with corresponding decreases of Si or Ca in some rich ores (e.g. massive ores). The isomorphic replacement between the elements thus is viewed as an important factor in redistribution of manganese during diagenesis. Though some trace elements (e.g. Ni, Sr, Zn) show differences in their abundance, they probably are not important as guides to diagenesis. (e.g. negative relationship between Mn and Ni). The similarity of ΣREE concentrations between Mn oxides and recrystallized manganocalcite probably indicates a widespread change after sedimentation.

The range of Ce anomalies in Dounan ores is considered to reflect the change from sedimentation to early diagenesis, through enhanced Ce mineralization and cycling of enriched in diagenetic pore waters (Elderfield and Sholkovitz, 1987). However, small Ce anomalies in some transitional and Mn carbonate samples as compared to the Mn oxides are interpreted as due to their formation in less oxidizing conditions. This implies that perhaps some Mn ores were formed during post-depositional periods (Sunit, 1979). In addition, the slightly enriched REEs apparently characterized the pore waters relative to sea water and were probably mobilised during early diagenesis; significant fluxes are indicated. This is also supported by the fractionation of REE during diagenesis, which is treated in element-element diagrams (Figs. 5.13a-b), providing the most direct and convincing evidence for fractionation during diagenesis (Sholkovitz et al., 1989).

The REE features of the úrkút manganese ores (Jurassic) and the Dounan Mn ores exhibit not only significant similarities but also differences in the development and subsequent alteration of the two deposits. However, though the possibility exists that ore minerals have been slightly changed during diagenetic processes, these phases may have retained most of the initial REE concentrations.

Isotopically, significant departures of $\delta^{13}\text{C}$ and $\delta^{18}\text{O}$ (Table 5.9) from zero result from different processes, for example, decreasing oxygen values relate to increased temperature and/or diagenetic reactions (Hudson, 1977). Some samples (e.g. Mn-rich oxides and carbonates) exhibit a wide scatter for both carbon and oxygen as well as higher temperature ranges (32° to 50° C); this is interpreted as representing increasing diagenesis down section. Second, the negative correlation between manganese content and the carbon isotope ratio (Fig.5.11) suggests that this process is a bacterially mediated diagenetic reaction that took place near the sediment-water interface, in agreement with Polgrári et al (1991). The correlations between $\delta^{13}\text{C}$ and $\delta^{18}\text{O}$ (Fig.5.16) suggest that carbon and oxygen from different sources contributed, to a variable extent, to the minerals (Chapter 5.3 Discussion). Thus, the deeper Dounan ores/rocks appear to have been conclusively depleted in ^{13}C and ^{18}O during Falang stage mineralization by diagenetic decarbonation, while shallower ores/rocks still display primary normal marine isotopic signals.

Mineralogically, the microanalyses of Mn minerals show that braunites from different ore types contain manganese in variable amounts, suggesting that the braunites formed in different environments or underwent varying degrees of diagenesis. For instance, the Mn-rich minerals usually underwent diagenetic changes leading to secondary Mn enrichment because of recrystallization and isomorphic replacement of elements (Chapter 5). Importantly, the element distribution in Mn mineral grains (Figs 5.8a-e) suggests that some grains experienced at least two (forming and reforming) stages. This is strongly supported by the secondary enrichment or dilution of some elements in the margins of mineral grains.

6.3 Source Materials and Weathering Processes

The various mineralizing conditions of the Dounan Mn deposits have been discussed in the previous section. However, source materials are also one of the important factors in mineralization. The Dounan ores/rocks, in particular, are characterized by relatively complex components, including terrigenous clastic and carbonate sediments as well as manganese materials, which indicates complex material sources. Information from this and previous works are generally enough to outline the source materials of the Dounan deposits, though more detailed work on this aspect is required.

6.3.1 Source of Gangues

As described before, the Dounan Mn deposits formed in variable sedimentary environments which yielded Mn-bearing terrigenous clastic and carbonate rocks characterized by ~65% clayey siltstone, ~30% mudstone, ~5% intraclastic carbonates and manganese orebeds. Terrigenous clastic rocks are generally composed of quartz, clay and minor feldspar, as well as traces of

muscovite, biotite, zircon, apatite, and rutile, which indicate that they were derived from crystalline erosional oldlands. Their final form as sediments is influenced by energy levels and sediment flux. Terrigenous clastic materials of Dounan are generally cemented by calcareous cement, including large amounts of micritic, minor sparry calcites, and other chemical (e.g. manganese) materials, ultimately derived from porewaters and dissolution of carbonate minerals both from within the sequence and from the source area.

Generally, sedimentary carbonate materials are derived from detrital components of marine organisms or as a result of chemical precipitation from seawater. Some elements with similar chemical properties, such as Ca, Mg, Mn and Fe came mainly from erosional oldlands, while HCO_3^- or CO_3^{2-} of seawater interacted in the formation of Dounan carbonates. The intraclastic textures of many Dounan carbonates suggests that they had already experienced mechanical resedimentation after primary chemical deposition (see Chapter 4, textures or structures).

6.3.2 Source of Manganese

Despite the lack of detailed and systematic work, the suggestion of an oldland source for the Dounan manganese materials is commonly accepted by most workers (e.g. Zhang et al., 1979; Wang, 1981; Su, 1983; Liu et al., 1984). The No.2 Geological Brigade of Yunnan Geological Bureau (1983) investigated the regional distribution of manganese deposits across provinces around the Dounan area and suggested oldland sources of the Dounan manganese materials, which is evidenced by the following points:

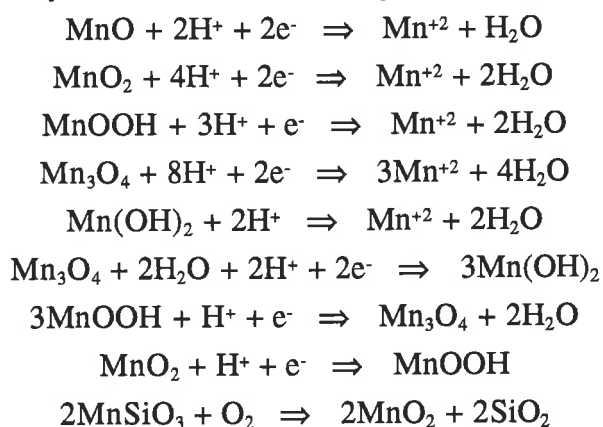
- the existence of pre-Devonian Mn-rich granite gneiss, biotite schist and hornblende gneiss of Yuebei Oldland to the south: these could be expected to contain Mn in excess of crustal abundance;
- the presence of thin manganese layers and Mn-bearing sandstones in the Donggangling Formation and underlying Pozhen Formation (Upper Devonian), in the Yuebei Oldland;
- Upper Permian Omei Shan basalt of Yuebei Oldland, which contains manganese (MnO ~5.18%) in Datie of the Qiubei area, and Mn (0.28%) in Dehou of the Wenshan area;
- Geju Formation limestone of Middle Triassic age contains manganese (Mn0.10%) in Dounan drill core CK3902;
- Precambrian basalt and Mn and Fe-rich slate of the Kangdian Oldland;
- very low Fe and low Fe/Mn ratio of the Dounan ores, reflecting no trace of a contemporaneous volcanic source;
- suitable (e.g. warm and humid) paleoclimate.

Thus, the Yuebei Oldland probably was the main and important source land for Dounan manganese materials. This is also supported by the fact that the Dounan basin lies adjacent to the northern margin of the Oldland, and intertidal fabrics of the ores indicate deposition near the

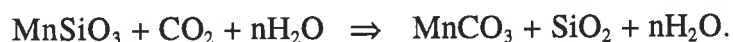
coastline. Also, erosional or weathering events before the Falang Formation (possibly intervening between deposition of the Geju and Falang Formations) allowed sufficient decomposition and transport of Mn or Mn-bearing materials. In addition, the low phosphorous in the Dounan ores probably supports this point of view too, because the rocks of the Yuebei Oldland also generally are extremely low in phosphorous. The Baixian Mn ores contain relatively high P which probably was derived from the Kangdian Oldland. The total reserves of the Dounan deposits are not so large as to preclude derivation of much of the Mn from seawater itself, in a manner similar to that proposed by Frakes and Bolton (1984).

6.3.3 Weathering Processes

Based on many previous studies of three main Mn weathering concentrations from the Dounan Oldlands, i.e. manganolite or rhodonite (MnSiO_3 , from silicate), pyrolusite and manganite (MnO_2 and MnOOH from older-sediments), and other sources such as MnO from the Omei basalt and MnCO_3 from pre-existing Mn-carbonate sediments, the mobilization or dissolution processes of manganese materials from the oldlands might be outlined. A number of chemical reactions can oxidize / or reduce / dissolve manganese materials of various valencies under natural conditions. However, under certain conditions the solubility of these materials can increase considerably. Generally, the thermodynamic stability fields for manganese oxides and hydroxides become relatively small under the following chemical reactions:



However, reactions between Mn silicate and carbon dioxide can also separate Mn from silicate:

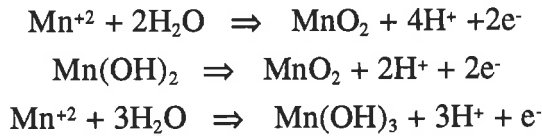


The MnCO_3 , together with that from Mn carbonate sediments, could further be changed into Mn bicarbonate due to its much higher dissolution than Mn carbonate (e.g. Mn carbonate solubility 6.5×10^{-3} g/100g water at 25° C, whereas Mn bicarbonate is mostly dissolved at 25° C):



Similarly, aqueous chemical systems that contain manganese proceed from dissolved ionic species towards more or less refined particulates and colloids occurring as suspended loads. Below, the main independent half-cell reactions of Mn illustrate the processes and compounds,

in which $\text{Mn}(\text{OH})_2$ and some Mn^{+2} oxidize to Mn^{+4} (MnO_2 particulates), other Mn^{+2} reacts to form Mn^{+3} [$\text{Mn}(\text{OH})_3$, colloids], and all reactions produce free electrons:



Important controls on manganese solubility include the level of oxygen present and the acidity of the depositional environment (see Figs. 6.6-6.8, Hem, 1972). Aside from physical removal by erosion from bedrock and soils, manganese is removed mainly through chemical processes in which ground water dissolves Mn-bearing minerals in at least mildly reducing conditions (Frakes and Bolton, 1992). They considered that Mn is then carried down the soil profile and moved laterally by groundwater eventually to the ocean, where it occurs in both oxidized particulates and in dissolved state Mn^{+2} , some of the latter as components in dissolved organic matter. Mn is efficiently stripped from the source region by chemical weathering because of its high degree of mobility and enriches oceans by a factor of river waters.

Also, Frakes and Bolton (1992) concluded that abundant rainfall (a climatic factor) is conducive to deep chemical weathering of the bedrock, and humid climates foster the growth of extensive vegetation which yields decomposition products to soil, and ultimately, to surface runoff.

6.4 Transport Processes

Examination of transport mechanisms here focuses mainly on manganese, since the formation of gangue minerals is mainly of interest for the mechanical or chemical conditions of terrigenous clastic and carbonate rocks and also reflects the relatively simple transport mechanisms of rock materials. Earlier several geochemical and biochemical processes were described that are able to produce manganese ores and associated rocks. It was also demonstrated that all dissolution and transport processes depend directly on the availability of surface/subsurface waters, river systems and seawater. Therefore, good drainage systems (e.g. rivers) between the erosional oldland and the marine basin are prerequisites. Without water, any mechanism that could lead to the dissolution, transport and sedimentation or even diagenesis of manganese is unlikely.

6.4.1 Transport of Detrital Sediments

From the nature of Dounan detrital sediments (mainly fine grained siliciclastics) it is apparent that most detrital materials were transported as suspended load (e.g. clay or silt) by surface waters. These detrital materials from the oldlands were mainly produced by physical and chemical (e.g. erosional or weathering) processes and were further reformed by various geological

(e.g. physical and geochemical) agents during transport in surface waters. When they arrived in the marine basin, they were mainly deposited by mechanical-sedimentary differentiation by grainsize (from coarse to fine) towards the offshore.

6.4.2 *Transport of Carbonate Materials*

The carbonate gangue materials were derived from parent materials which were mainly decomposed by chemical weathering processes and transported to the sea as bicarbonates. The solubility of bicarbonate is much higher (nearly one hundred times) than that of carbonate at 25° C:



In addition, seawater and the activity of organisms can also supply some cations for carbonate materials (Ca^{+2} , Mg^{+2} , and $\text{CO}_3^{=}$).

6.4.3 *Transport of Manganese*

Generally, dissolved manganese can be transported either in divalent ionic form, in complexes or as suspended particulates, or colloids, though many viewpoints on the transport of manganese have been presented. Laxen et al., (1984) demonstrated that for a pH < 7.5 ($\text{Eh} \approx 0$) in river waters, essentially all Mn in the fraction < 0.0015 μm is present as reduced Mn^{+2} -species, which seems to indicate that particulates do not play a significant role in oxic freshwater and that they are not in equilibrium with dissolved manganese. However, Ye (1961) and Fu (1963) considered that the ore-forming materials of Fe and Mn deposits can be transported in mechanically-suspended particulates and colloids which are easily precipitated when transported to the sea, and therefore they would experience only short transport from oldlands (see *Ore Deposits*, published by Geological Publishing House of China, 1978). Strakhov (1969) observed that over 50% of dissolved Fe and Mn of the Diniebo River were transported in organic complexes; the remainder as suspended load including adsorbed particulates and various colloids. In addition, Sapozhnikov (1970) and Strakhov (1969) assumed that dissolved manganese is the main source of Mn for ore deposits and manganese can be transported as humic acid and other metallo-organic complexes such as bicarbonate complexes in slightly acidic surface waters and anaerobic groundwaters, and as sol of $\text{Mn}(\text{HO})_3$ stabilized by adsorbed organic substances.

In places with a high input of organic matter, manganese is complexed by various biogenic compounds, such as amino-, carboxyl-, sulphur-, or phosphorus-containing groups with high molecular weights. Putilina and Varentsov (1980) stated that in the presence of these compounds Mn can increase dramatically in concentration, whereas Mn^{+2} is oxidized much faster without the protective mechanisms of the phases mentioned (Hallberg et al., 1979). The formation of chelate

complexes thus enable freshwaters to carry high amounts of manganese in a relatively stable condition over large distances.

Frakes and Bolton (1992) considered that during transport, manganese can be concentrated in surface waters relative to iron through selective precipitation of iron as oxide coatings along the banks of streams and on coasts in stream beds, and that dissolved iron hydroxide can be absorbed on clays, leading to the separation of manganese and iron during transport. The sedimentary process involves derivation of manganese and other elements in basinal water mainly from the weathering zones on the continents by transport through surface and ground waters. The average Mn/Fe ratio of the earth's crust is 0.017 (Krauskopf, 1967; Ronov and Yaroshovsky, 1972), and thus, the process of formation of an Mn deposit with high Mn/Fe ratios involves separation of the two elements at different stages during derivation from source rocks, transport, deposition and early diagenesis (Roy, 1981).

Depending upon the nature of the weathering process, manganese and iron may be leached simultaneously from the source rocks or there may be preferential leaching of manganese with respect to iron because of its larger ionic size, lower ionic potential and enzymatic microbial reduction (by *Bacillus*, *Thiobacillus thiooxidans*, *Coccus*, *Yeast* etc, Roy, 1981). A severe hot and acid climate in the weathering zone has been considered by some (Mohr, 1965; Varentsov, 1964; Frakes and Bolton, 1992) to be responsible for the release of manganese from terrestrial rocks. The solubility of manganese is considerably higher than that of iron and aluminium for any given Eh and acid pH (Roy, 1981). Organic reactions, such as simple organic decay, may be catalytically accelerated by bacteria, indirectly leading to manganese dissolution (Crerar et al., 1972). Mn-specific soil bacteria may also lead to dissolution and leaching of the element (Perkins and Novielli, 1962). Borchert (1970) concluded that manganese and iron are derived from the rocks in the continental weathering zone principally through humic acid solutions.

Manganese is geochemically mobile and it migrates in surface and ground waters. As mentioned before, manganese may migrate in solution, as particulates and as organic complexes in variable proportions or as a sol of colloids. Mn is one of the most reactive metals in river water (Turekian, 1971), and in estuaries precipitation of manganese oxyhydroxides may lead to removal of other metals through adsorption. Therefore, separation of Fe and Mn by differential solubility and mobility is controlled by multiple parameters. Transport of Mn in ionic solution in stream waters over great distances is difficult in an oxygenated environment and in such a case the element migrates principally in metallo-organic complexes or in colloidal suspension (Roy, 1981).

Contrary to freshwaters, manganiferous oxyhydroxide particulates seem to dominate in the marine environment, where they may be associated with organic molecules or bacteria (Van Der Sloot et al., 1988). Although particulates generally tend to flocculate in strong electrolytes,

manganese seems to have a surprisingly long residence time in the sea (~20 years; Bishop and Fleisher, 1987). Despite this, large quantities of the river load at Groote Eylandt are removed from solution through precipitation processes (Pracejus, 1989).

Although manganese materials are polysourced and transported by various agents, the terrigenous manganese was mainly transported by surface and subsurface waters and its transport was affected by the nature of paleoatmosphere and hydrosphere. The early evolution of atmosphere and hydrosphere during the Precambrian was characterized by being CO₂-rich and O₂-poor, illustrated by calculations of O₂ and CO₂ partial pressures (e.g. Holland, 1984; Kasting, 1987). Under these conditions, dissolved manganese could be transported in divalent ionic or bicarbonate complexes. After the Cambrian, with increasing bioactivity, CO₂ decreased in the atmosphere and hydrosphere while O₂ increased, implying that long-distance transporting power of dissolved manganese was less common due to increased oxidation of manganese (from Mn⁺² to Mn⁺³ or Mn⁺⁴). The transport of dissolved manganese was, to a great extent, substituted by the mechanically suspended loads of Mn particulates (MnO₂) and colloids [Mn(OH)₃].

Transport also takes place within marine basins after Mn input from rivers, but tidal action plays an important role (Frakes and Bolton, 1992). In the form of tidal currents, erosional agents, including algae (or bacteria) moves particulates to where they could form Mn ooliths/pisoliths, or spheruliths and oncoliths. Meanwhile a certain proportion of particulates are transported farther seaward for short distances to be redeposited and cemented by carbonates. Dounan ancestral manganese therefore was mostly transported as suspended and adsorbed particulates and colloids, with minor amounts in divalent ionic form or in complexes within the marine basin, which can strongly be supported by the fact that the Dounan ores are mostly composed of Mn oxide ooliths/pisoliths (some nuclei apparently made of adsorbed particulates), or spheruliths and oncoliths (algal action) with colloform textures.

The two dominant mechanisms of manganese mobilization at Dounan were pH controlled dissolution processes and redox reactions of Mn oxides or Mn silicate and Mn carbonates; the two are distinctly different in their physico-chemical parameters. Redox reactions produce their own electrochemical environments (electron transfer, pH, etc.). pH variations frequently occur as a result of environmental changes and then the pH alone may affect the solubility of Mn-bearing minerals. Once local surface waters reached river systems, redox reaction processes were interrupted, and the waters equilibrated with the new environment. The resulting stabilization of Mn compounds affected Mn particulates and colloids in transported loads. However, at a pH of about 8.0, reached when tidal seawater mixed with riverwaters, the new geochemical environment enhanced Mn precipitation.

In the sea, the manganese was again influenced by Eh and pH conditions. The manganese concentration increased as pH increased and Eh decreased. This means that Eh/pH controlled

processes led first to the destruction of previously stable compounds and then to precipitation of manganese. The type of precipitate was determined by the electrochemical parameters that dominate this environment; this is discussed in the following section.

The descriptions above illustrate that manganese mobilization, transportation and precipitation processes can be distinguished easily. Thus, Mn-water relationships are grouped into three major sets:

- Mn materials not in equilibrium with their surroundings and with diffuse trends; examples as in ores, silicates, basalt, etc.;
- Mn transported load in rivers at equilibrium, in response to Eh/pH control mechanisms;
- Mn load adjusts to new equilibrium in seawater, responding to Eh/pH control mechanisms.

6.5 Sedimentation Processes

Chemically controlled sedimentation is responsible for the formation of the vast majority of manganese deposits in Recent and ancient geological sequences (Roy, 1981). The presence at Dounan of dominant primary ores and rocks illustrates active deposition of sedimentary minerals. The major sources of materials have been identified as fluids derived from exogenous weathering of pre-existing rocks. Many of these primary phases change their geochemical environments, for instance by influencing the pH and/or Eh, and thus, the formation of one particular ore phase has direct implications for the stability or instability of other co-existing phases. The various primary products (including fabrics) of different ore phases observed in the Dounan deposits support this view and it is demonstrated below that most of the precipitation processes can be explained in relatively simple terms. Most of the chemical equations were discussed earlier, including some reverseable reactions.

Only limited studies have been made on river water-seawater interaction as it affects manganese deposition. Graham et al., (1976) observed that most of the Mn in Narragansett Bay is particulate though in most rivers feeding the bay the Mn is in a dissolved state, and the mixing of river water (pH 6-8) with seawater leads to a rise in pH, favouring metal adsorption. Strongly pH-dependent processes play a major role in determining the distribution of manganese in a dissolved or particulate state in natural waters (Roy, 1981).

Sea water in the coastal zone is usually deeper than freshwater and less homogeneously mixed, salinity may increase to at least that of seawater, alkaline environments become prevalent, and transport is no longer unidirectional (as in rivers), due to wave and tidal effects (Frakes and Bolton, 1992). It has been illustrated by experimental and field work that when river water mixes with seawater, there is a marked and sudden flocculation or coagulation of dissolved river constituents beginning at salinities of about 15 per mil. Sholkovitz (1976; Sholkovitz et al.,

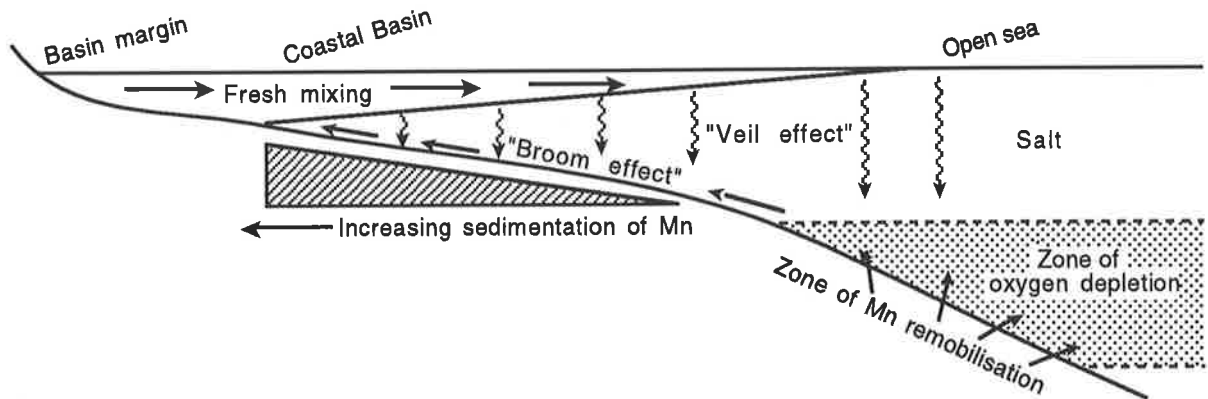


Fig. 6.5 Manganese sedimentation in the coastal zone of an intracratonic basin, showing operation of the "veil" effect in retaining Mn from saline mixing, and the "broom" effect in pushing particulate Mn shoreward through tidal activity. After Frakes and Bolton (1984).

1978), for instance, found that total flocculates of manganese amounted to 90 to 100 percent of the dissolved river load, thus indicating a very efficient tool for removing metals in coastal environments.

Also, Frakes and Bolton (1984, 1992) suggested that this saline mixing (the "veil" effect; Fig. 6.5) might therefore be expected to generate coastal manganese orebodies. Reduced interstitial waters are more abundant and remobilization of metals to the sediment-water interface is common. In these near-shore environments, organic matter is often abundant in the sediments and its decomposition will lead to the consumption of O_2 and the liberation of CO_2 . Mn may become mobile in the form of $MnHCO_3^+$, and eventually precipitate as $MnCO_3$ in slightly more reduced (deeper) levels rather than as Mn oxides; marine regression can lead to a great oxygenation and the consequent precipitation of Mn oxides/carbonates

The Dounan deposits show evidence of having precipitated where the interface between deep water of relatively low Eh and shallower water of high Eh intersected shallow-marine substrates. Water column interfaces are loci of precipitation because they juxtapose waters with dissolved elements in differing concentrations. Mixing processes, or diffusion, across the interface will cause precipitation, including biochemical precipitation, if a supersaturated fluid is generated, i.e., the concentration of a compound in one body of water exceeds the effective solubility in the other. The amount of precipitation is proportional to the degree of mixing and of effective supersaturation (Force and Cannon, 1988). For manganese, a particularly sharp solubility gradient exists along oxidation-reduction interfaces in water columns, as in the Black Sea. Anoxic water may have dissolved manganese contents many times than that of oxidized water. Changes of Eh/pH and P_{CO_2} are other important influences on manganese solubility and locally occur along these interfaces. Where a water column is stratified such that near-surface water is oxic and lies above an anoxic water body, manganese will precipitate on the oxic side as oxide or on

the slightly oxygen deficient side as carbonate; these particulates will dissolve as they fall into the deeper, more anoxic water (Brewer and Spencer, 1974).

6.5.1 Precipitation of Mn Oxide Minerals

Enrichments of manganese sited in the Dounan stratigraphy in the form of oolites/pisolites, or concretions indicate the presence of sedimentary processes operating in geochemically variable environments (e.g. Eh, pH). Manganese was mostly transported into the Dounan shallow marine basin in the dissolved state. The precipitation of Mn as oxides was far more important than that of Mn carbonate minerals, the former following the latter during regression. This is because the shallow intertidal-flat environments lay above the level of water anoxia. Particulates were supplied to the flats by wave action, which also gave rise to mechanical formation of graded bedding in ooliths/pisoliths and spheruliths.

The gradually increasing concentration of Mn in solution in the basin as a result of continuous Mn supply from freshwater led to phase changes in the Mn-Si-O₂ (or CO₂)-H₂O system. Precipitation of most of the Mn load on the substrate above the level of water anoxia resulted from slight changes in Eh and pH. During this process, intense movement of particles occurs on/near the substrate due to high energy tidal movements. Ooliths/pisoliths or spheruliths form through accretion of particulates, with grain-size variations resulting from tidal energy variation during the tidal cycle. These grains were gradually cemented by argillaceous, calcareous and/or Mn oxide cements. The oxides (braunite, manganite) in such deposits can form by several reactions at normal surface temperature:



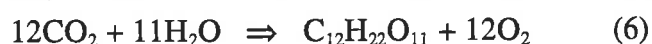
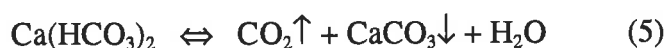
Higher oxide particulates of manganese (MnO₂), admixed with silica may yield braunite in higher fo₂ according to reaction (1), which indicates that if braunite can form at a suitable oxygen fugacity, it may appear at low temperature (Roy, 1981). Braunite may also form from Mn bicarbonate solution by admixture with silica at higher fo₂ (reaction 2) at a lower temperature, because bioactivity (e.g. algae) absorbed CO₂, leading to decomposition of Mn bicarbonate. Commonly, manganese colloidal dehydration can lead to precipitation of manganite based on reaction (3). However, the reaction (4) between Mn colloidal suspension and SiO₂ is possible at a higher fo₂ and lower temperature because of the presence of colloform braunite, though this has not been demonstrated in natural deposits.

In a series of phase-equilibria studies of the manganese-water system at room temperature and pressure, Hem (1963, 1972; Fig. 6.6) showed areas of stability for solids and solubility of Mn as well as their dominant solute forms. When the concentration of Mn^{+2} and/or Mn^{+4} in the marine water reached 0.5-5.0 ppm, and SiO_2 species activity equivalent to $2 \times 10^{-5} - 2 \times 10^{-7}$ M is considered, a stability field for braunite is introduced under the geochemical conditions of $Eh = \sim 0.2v.$ and $pH = \sim 8$. This field lies in the zone between $MnSiO_3$ and Mn_2O_3 (Fig. 6.7, Krauskopf, 1957). Such an explanation is consistent with the formation of Dounan braunite, in which the Mn and Si exhibit isomorphous mixture (Chapter 4). The stability boundary of MnO_2 shows a bulge as a consequence of the complexing effect.

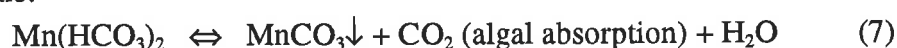
6.5.2 Precipitation of Mn Carbonate Minerals

Based on Figure 6.6, a carbonate complex is introduced in Figure 6.8 (Hem, 1963, 1972) where bicarbonate species activity equivalent to 2000mg/l HCO_3^- ($10^{-1.48}$ mol/l) is present in the system, i.e. a large stability field for $MnCO_3$ is introduced accompanied by the solute complex $MnHCO_3^+$, whose effect is of considerable importance. However, when calcium activity is available in the environment, it must lead to the formation of calciorhodochrosite, Mn-calcite or Mn-bearing calcite depending on the amount of calcium introduced. It has also been suggested that manganese associates with calcium in preference to iron in reducing conditions during the formation of carbonates (Michard, 1969). During late transgression, in the earliest period of Mn mineralization, the sedimentary environment was reducing (CO_2 -rich and O_2 -poor); the higher pH ($\sim 7.8-8.8$) and lower Eh ($\sim 0v.$) would lead to the precipitation of Mn carbonates below the anoxia interface.

The continuous accumulation of Mn bicarbonate and Mn^{+2} in solution in the basin would lead to significant precipitation of Mn carbonates. In addition, algal activity could play an important role in the precipitation of carbonates. Algal activity absorbed CO_2 and HCO_3^- from seawater in photosynthesis, leading to higher pH and carbonate saturation. In experiments (Laboratory Center of Hunan, China, 1985), one mol of CO_2 derived from the water medium can lead to one mol of $CaCO_3$ precipitation, whereas at least 12 mols of CO_2 are required to meet the need of 1 mol of chlorophyll formed from vegetation. The molecular weight of $C_{12}H_{22}O_{11}$ is 343, whereas that of $CaCO_3$ is 100, so the ratio between them is $343 : 100 \times 12 = 1 : 3.5$, i.e. every gram of chlorophyll yielded from vegetation can lead to 3.5 gram $CaCO_3$ precipitate, as expressed by the following reactions:



When the concentration of Mn^{+2} dominates over Ca^{+2} in a basin of algal activity, the reaction should become:



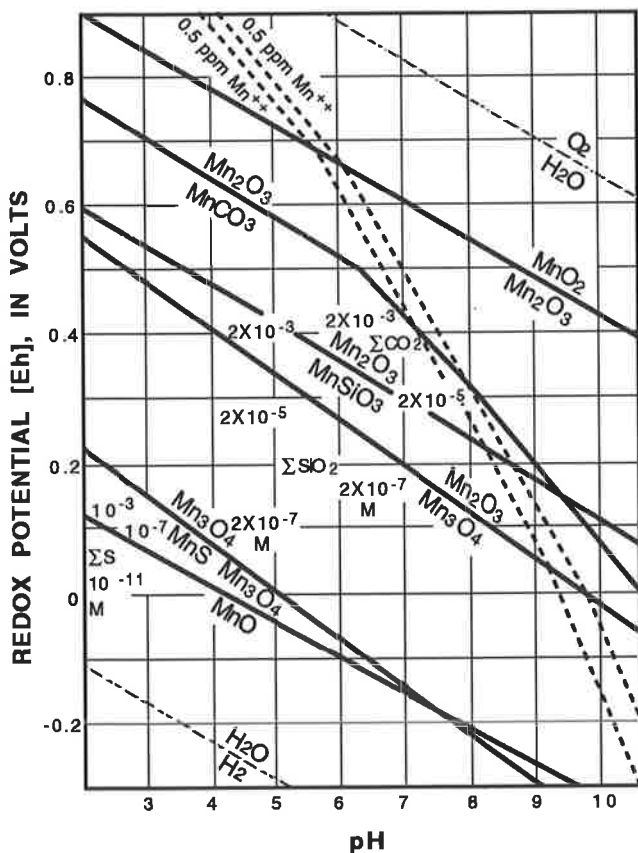
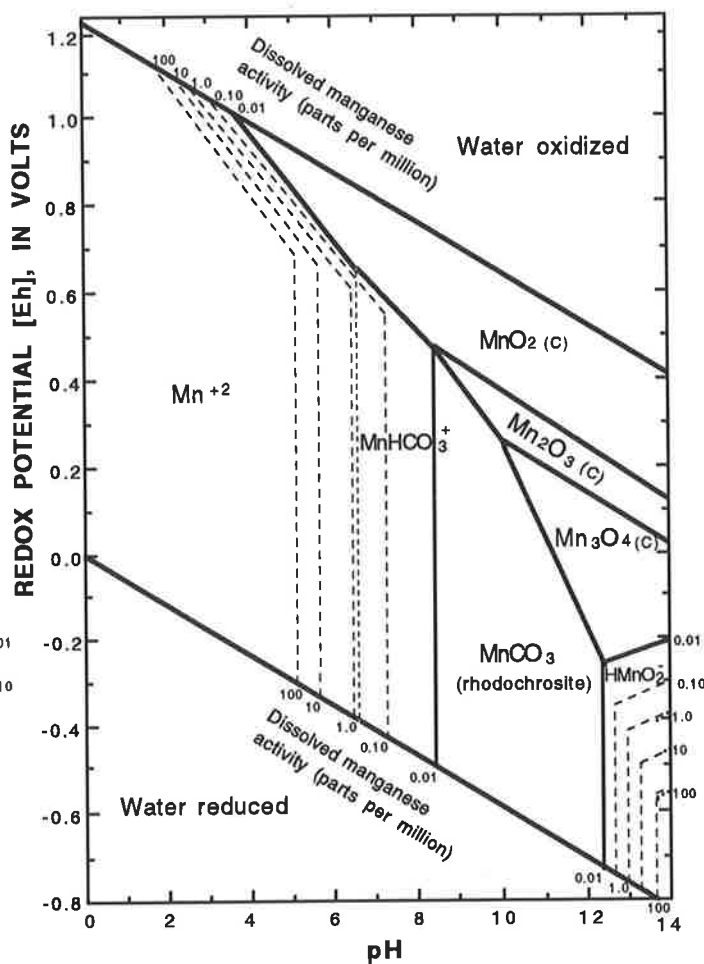
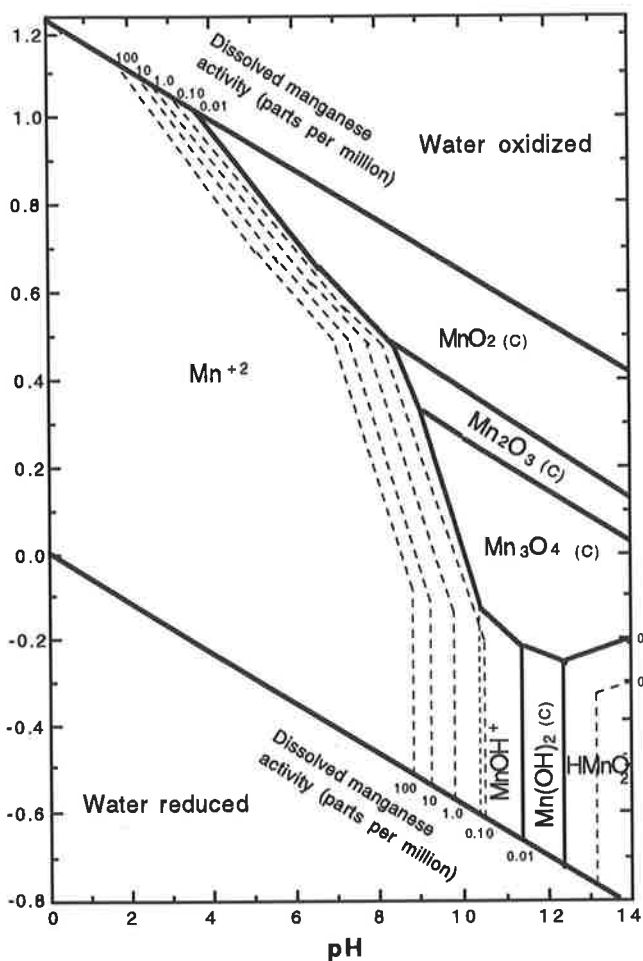


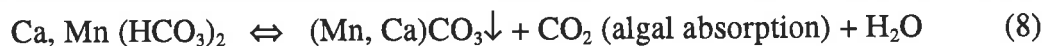
Fig. 6.6	Fig. 6.8
Fig. 6.7	location of figures

Fig. 6.6 Fields of stability of solids and solutes and solubility of manganese as functions of pH and redox potential at 25°C and one atm. in the system Mn-H₂O. (Reproduced from Hem, 1972, *Geological Society of America Bulletin*, vol. 83, p. 448, Fig. 5).

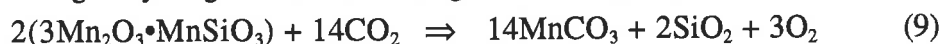
Fig. 6.7 Eh-pH diagram for anhydrous Mn compounds at 25°C and 1 atm. Solid lines are boundaries of stability fields; each line separates the field of an oxidized form (above) from that of a reduced form (below). Cross-bars on vertical lines show positions of field boundaries at lower concentrations of carbonate, sulphide, and silica. Dash-dot lines are limits of possible redox potentials in water solution. Dashed lines are "isoconcentration" lines, draw through points where the concentration of Mn²⁺ in equilibrium with the oxides is 5 ppm and 0.5 ppm respectively; from Krauskopf, 1957.

Fig. 6.8 Fields of stability of solids and solutes and solubility of manganese as functions of pH and redox potential at 25°C and 1atm. in the system Mn-CO₂-H₂O; bicarbonate species activity 2,000 mg/l as HCO₃⁻. (Reproduced from Hem, 1972, *Geological Society of America Bulletin*, vol. 83, p. 448, Fig. 6).

However, owing to their similar geochemical natures, Mn^{+2} and Ca^{+2} commonly are formed in isomorphous mixture series between $MnCO_3$ - $CaCO_3$, thus a corresponding reaction follows as:



Depending on the amount of calcium introduced, the Mn carbonate minerals, such as calciorhodochrosite, manganocalcite and Mn-bearing calcite could form. In addition, reducing reactions between particulate braunite and CO_2 probably took place, particularly under reduction conditions during early diagenesis, also leading to $MnCO_3$ precipitation:



In Figures 6.6-6.8, the stability boundary of MnO_2 is distorted somewhat due to the complexing effects. When the dissolved manganese activity is concentrated between 0.1 - 0.01 ppm, the Eh value is -0.2 - +0.2 volt and pH is about 8, Mn carbonate compounds would precipitate to form various Mn carbonate minerals. However, because alkalinity (or pH) apparently did not vary greatly, the precipitation of Dounan unsorted ores mainly depended on variation of Eh (see following discussion).

6.5.3 Precipitation of Transitional (or Mixed) Mn Ores

Based on the above explanation of Mn oxide and Mn carbonate precipitation, it seems not to be difficult to work out the mineralizing picture of the transitional ores. Although redox reactions rarely take place between Mn oxides and Mn carbonates directly (Eq. 9), their respective redox reactions lead to a situation where the newly forming Mn oxide or Mn carbonate minerals either consume or increase the concentration of O_2 , H^+ or CO_3^{2-} ions in the solution, which means that the pH and Eh change frequently, i.e. the depth to water anoxia changed from time to time. Thus, during redox reactions the generally large Mn oxide stability field develops above the level of water anoxia dictated by the f_{O_2} or f_{CO_2} and the developing pH. The Mn carbonate stability field generally replaces that of the Mn oxides due to the levels of water anoxia expanding upward. When the stability fields of the Mn oxide and Mn carbonate systems (Fig. 6.8) are superimposed, it can be seen that the redox reaction theory supports the field and laboratory observations; not only the micro-concentric laminae composed of both Mn oxide and Mn carbonate in oololiths and pisoliths, but also the macro-banded or unsorted transitional Mn ores, can developed under frequently changing geochemical environments. The frequency of change mainly depends on the period of redox reaction but also on the level of water anoxia, which may be controlled by sea level (Frakes and Bolton, 1984, 1992). For instance, whether manganese oxide oololiths/pisoliths are fixed above or near the level of water anoxia, no doubt depends strongly on the availability of oxygen; however, when the anoxia level rises due to sea-level rise, the grains are cemented by rapid precipitation of Mn carbonates under reducing conditions. This, therefore, is the suggested mechanism for formation of the transitional Mn ores.

6.5.4 *Precipitation of Gangues*

The stabilities of terrigenous clastic minerals in mechanical sedimentary systems are not considered here, because the predominant species (clay and silts) remain little altered during the precipitation processes. Although this seems to simplify the discussion, at least silica is known to form Mn polymers (braunite). However, this mechanism results in relatively complex interactions among Si^{+4} , Mn^{+2} , Mn^{+4} and O^{-2} ions during chemical precipitation rather than among solid compounds like quartz and braunite minerals.

Since Ca and Mg co-exist in most carbonate samples, these elements are discussed together. In the carbonate precipitation system, the fact that calcium always dominates in shallow marine conditions leads to the conclusion that pure Mg minerals such as dolomite are generally less abundant than calcite under normal sedimentary conditions. It is also deduced that the Mg deficiency in seawater to some extent is reflected in the much lower availability of these phases in minerals. Additionally, excess calcium inputs further decrease the Mg potential through the formation of carbonate gangues. Thus, the development of carbonate gangues in the presence of surplus dissolved calcium results in the suppression of stable magnesium phases, which explains the scarcity of minerals like dolomite in the deposits. During precipitation of carbonate gangues, CO_3 -ions are consumed and the H^+ and O_2 concentrations in the solution increase, which means that the pH becomes more acidic (Eqs. 8 and 9), which again leads to Mn oxide precipitation due to the changing redox conditions. This sequence also can be used to explain the formation of banded and unsorted Mn ores.

6.5.5 *Growth Rate and Environment of Mn Ooliths/Pisoliths*

The syngenetic elements such as Cu, Co, Ni, etc in manganese accumulations have been used to examine the structural growth rate by many workers (Michard, 1969; Krauskopf, 1956; Goldberg, 1954; Bender et al., 1970; Dasch et al., 1971; Piper, 1972; Dymond et al., 1973; Sayles and Bischoff, 1973, etc.). Generally, precipitation of Mn^{+2} from aqueous solution is catalyzed by surfaces of ferric oxyhydroxide as well as by calcite, silica, feldspathic sand and freshly precipitated MnO_2 (Morgan, 1967; Morgan and Stumm, 1965; Michard, 1969; Hem, 1964; Jenkins, 1973; Crerar and Barnes, 1974). Theoretically, catalysis can also be provided by micro-organisms (Sorokin, 1972; Greenslate et al., 1973; Piper and Williamson, 1977; Dugolinsky et al., 1977; and many others).

As described before (Chapter 5), the Dounan Mn ooliths/pisoliths contain many minor or trace elements such as Si, Ca, Al, Mg, Fe, Ni, Co, Cu, Pb and B, and are closely associated with clastic silicate grains and calcite. Sorem et al. (1978) pointed out the presence of abundant clastic

silicate grains in Mn-rich layers of deep-sea nodules and visualized that the fine-grained silicates present in such boundary layers might significantly catalyse precipitation of Mn oxides rich in Ni and Cu. The rate constants for oxidation reactions for calcite, $\text{Fe}(\text{OH})_3$ and MnO_2 are consistent with manganese nodule accretion rates of $10 \text{ mm} / 10^6 \text{ years}$ (Michard, 1969) in present-day basins. Trace elements such as Zn, Cu, Pb, Bi, Cd, Ni, Co, Hg, Ag, Mo, W and V are very undersaturated in seawater and have relatively short mean residence times. Krauskopf (1956) showed that these elements may be adsorbed successfully on to hydrated colloidal MnO_2 at pH 7.7-8.2 and 20°C .

However, the distributional concentrations of elements depend on the rate of accretion of manganese nodules or crusts and of selective chemisorption and autocatalytic oxidation on active surfaces (Morgan; 1967; Varentsov, 1972, 1976; Varentsov and Pronina, 1973, 1976; Varentsov et al., 1979; Hey, 1978; Murray and Brewer, 1977). They observed that the rather rapid accretion rate of $0.3\text{-}1000 \text{ mm} / 10^3 \text{ years}$ of manganese nodules occurs commonly in shallow marine environments. A comparison of the syngenetic elements of the Dounan Mn ooliths/pisoliths with those of both fresh water localities and ocean shows that Cu and Co concentrations of the Dounan ooliths/pisoliths have intermediate values, whereas Ni content is the lowest. This suggests that though Mn^{+2} or Mn^{+4} ions possess relatively strong chemisorption properties, they can only adsorb small amounts of undersaturated trace elements from seawater because of the rather rapid rate of accretion of the ooliths/pisoliths (Table 6.1). As for the Dounan ores, some trace element compositions may be controlled by the geochemistry of rocks in the source area, a possibly which requires more study.

6.5.6 Hydrodynamic Conditions of Forming Mn Ooliths/Pisoliths

Table 6.1 Comparison of syngenetic elements (mean) of Dounan Mn ooliths/pisoliths with other places (modified after Liu et al., 1984).

Area	Position	Mn	Fe	Co	Cu	Ni	Zn	Mn/Fe
Dounan Mn deposits	braunite ooliths/pisoliths (orebody V ₁)	61.12	0.90	0.03	0.01	0.01		67.91
	braunite ooliths/pisoliths (orebody V ₈)	59.81	0.50	0.015	0.006	0.015		119.61
	Mn-bearing carbonate ooliths/pisoliths (top of orebody V ₁)	>5	0.50	0.05	0.005	0.015		>10
Lacustrine environment (Callender & Bowser, 1976)	Mn nodules from fresh water	33.00	16.50	0.0196	0.0014	0.0296	0.1665	2.00
Average value of Mn nodules from the Ocean (Murray & Brewer, 1977)		16.17	15.60	0.298	0.256	0.488		1.03

Since the conditions of formation of the Dounan Mn ooliths/pisoliths, to some extent, have been discussed previously (Chapter 2), the discussion here focuses on the hydrodynamic conditions of forming Mn ooliths/pisoliths. As described before, the Dounan Mn ooliths/pisoliths exhibit various types in part depending on their shapes and nuclei, reflecting complex hydrodynamic processes. The discussion of Dounan Mn ooliths/pisoliths can be separated, on the basis of their characteristics as follows:

1) Spherical ooliths/pisoliths with single nucleus mainly composed of braunite; generally formed in high energy intertidal zone, owing to tidal action. The environments were similar to those in which calcite ooliths/pisoliths form. Plentiful concentric laminae generally reflect rapid rate of accretion growth under high energy conditions.

2) Spherical ooliths/pisoliths without nuclei (e.g. spherulith) mainly consisting of braunite and commonly formed in tidal race environments. The lack of a visible nucleus, in some cases possibly due to the vagaries of section cutting, indicates either comparatively low energy environments incapable of transporting coarse material or a lack of supply of coarse material.

3) Ovoid ooliths/pisoliths with single nucleus made up of both braunite and Mn carbonate minerals mainly formed in low-tidal zone. With moderate energy levels, this sort of oolith/pisolith commonly develops near the oxic-anoxic interface, which fluctuated to cause alternating precipitation of oxides and carbonates.

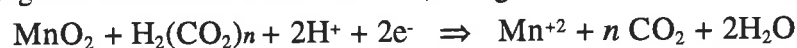
4) Ovoid ooliths/pisoliths with polynuclei generally experienced two kinds of hydrodynamic conditions, i.e. the previous ooliths/pisoliths formed in high energy disturbed or tidal race environments and were then transported to relatively low energy environments where ovoid oolith/pisolith growth was renewed.

5) Malformed or broken-ooliths/pisoliths commonly distributed among braunite ooliths/pisoliths at random. Generally, this type of oolith/pisolith results from intensive movement due to tides or waves in the intertidal zone, leading to sub-spherical or broken ooliths/pisoliths.

However, recent experimental works (Momoi et al., 1992) has shown that spherules or ooliths of manganese synthesized in gel at room temperature and pressure can be formed also in the quiet geological environment, although the synthesized spherules are very similar to natural manganese micronodules and oolites in their textures. The experimental results suggest that the fluctuating diffusion of manganese in gel also yields similiary texture to natural manganese oolites. The cause for the fluctuation of diffusion is an important unsolved problem.

6.5.7 *Biological Influence on the Precipitation of Mn Ooliths/Pisoliths*

Biological activity during formation of Mn ores can be an important mechanism for accumulating Mn in a wide range of sedimentary basins (Hariya and Kikuchi, 1964; Brockamp, 1976). The participation of microorganisms in the processes of solution and deposition of manganese and iron compounds in hydrogenous systems has been suspected for a long time (Thiel, 1925; Butkevitch, 1928; Zappfe, 1931; Kindle, 1935; Bandopadhyay, 1989). The biological influence on growth and composition of manganese nodules in the Central Pacific (Sorokin, 1972) and in areas of high organic productivity such as the northeast equatorial Pacific is well recognized (Greenslate et al., 1973; Piper and Williamson, 1977; Dugolinsky et al., 1977; and many others). Some studies (Zhang et al., 1979; Su, 1983; Liu et al., 1984) conclude that microbiota have taken part in the metallogenesis of the Dounan deposits, and others have demonstrated that microorganisms are able to influence ore formation under laboratory conditions (Madgwick, 1987). The biogenetic organic acids reduce Mn^{+4} to Mn^{+2} , being oxidized themselves to CO_2 and water.



Investigations indicate that reducing capacities of bacteria generally seem to be stronger than those of algae, but the latter can adsorb CO_2 from the system, catalysing the reduction of manganese dioxides. However, the co-existence of bacteria and algae improves the overall strength of the reaction process (Merz and Madgwick, 1982), such an improvement resulting from the addition of algae or other organic energy sources for the bacteria (e.g. yeasts, molasses). In a number of cases an electron transfer process between organics and Mn oxides is coupled to the intermediate formation of organo-metallic complexes (Marshall, 1979). Organisms or evidence of biological activity during Dounan manganese mineralization (Chapter 2) suggest reducing capabilities under microaerobic to anaerobic conditions.

It was demonstrated that biological processes apparently took part in or influenced the mineralization of Dounan primary ores (Chapter 2). The introduction of organic acids into a basin can lead to a pH-dependent manganese reduction that parallels inorganic precipitation processes. This means that the activities of organisms may play a catalysing role in decomposing or reducing MnO_2 particulates into braunite or other Mn carbonate minerals. Wendt (1974) showed that colonies of sessile foraminifera and diverse organisms are present within and attached on deep-sea manganese nodules and crusts at all depths. The abrupt changes noticed in foraminiferal content in the growth history of manganese nodules apparently represent changes in the microbiological and sedimentary environment. Wendt (1974) also concluded that encrusting organisms may contribute substantially to the growth of manganese nodules and crusts.

The role of bacteria in the development of manganese nodules has been emphasized by many workers such as Ehrlich (1963, 1964, 1966, 1972, 1975), Silverman and Ehrlich (1964), Ehrlich et al., (1972, 1973), Ghilose and Ehrlich (1974), and Trimble and Ehrlich (1968, 1970). The predominance of biological structures in some of the Dounan Mn ooliths/pisoliths, or even in

matrix, strongly suggest relationships between the activity of microorganisms and the growth of these manganese grains, despite the lack of evidence for bacteria. For instance, the occurrence of micro-ooliths/pisoliths attached to the internal part of the tests of invertebrate fossils (Plates, 2.3-2.4) suggest at least local organic control of grain formation.

Krumbein (1971) claimed that precipitation of manganese in concentric rings may be induced by fungi. Monty (1973) concluded that filament-type bacteria produced the very fine and regular lamellar structure with characteristic stromatolitic undulations and also turbiate and columnar structures in manganese nodules from the Blake Plateau and he suggested that Recent manganese nodules are thus "oceanic stromatolites". The micro-columnar structures and oncoliths exhibited by the Dounan manganese ooliths/pisoliths (e.g. Plate 2.3, Figs. 2a-b) also closely resemble stromatolites. Similar structures in ultrafine scale have been described from the Jurassic northern Limestone Alps and have been interpreted as of biological origin (Xavier and Klemm, 1976).

Manganese ooliths/pisoliths intimately associated with undisputed algal stromatolites (*Collembia*) occur in Mn-bearing stratigraphic horizons in the Triassic Dounan manganese areas of China. Similarly, they can also be found in different stratigraphic layers in the Precambrian (> 1845 Ma) Kisenge-Kamata manganese belt of Zaire (Doyen, 1973) and also in the Precambrian Mn stromatolites of south Australia (Williamson, 1987); and Jenkyns (1970) reported an association of nodular manganese deposits with algal stromatolites in Jurassic red limestones of the Tethyan region. Nevertheless, it is yet to be ascertained whether such associations are casual or causal in terms of direct organic contribution to manganese ore deposition. Additionally, Merz and Madgwick (1982) showed that Mn reducing capabilities of microorganisms are enhanced by the addition of organic nutrients (e.g. decomposing leaf litter). Recently, Pracejus et al (1988) studied the importance of microorganisms in the formation of Groote Eylandt manganese ores. Thus, humic compounds may be more important in sustaining biological processes than as direct Eh/pH regulators.

6.5.8 *Depositional Mechanism of Ore Phases*

According to the data of most sedimentary manganese deposits (e.g. Nikopol/Chiatura, former USSR), the sedimentary distribution of ore phases is generally characterized by three ore phase zones from coast to sea: Mn oxides (psilomelane and pyrolusite), manganite and Mn carbonate zones. Although the Dounan ore phases are, to some extent, different from those of known Mn deposits in the world (Chapter 4), their depositional mechanisms are similar. This means that the formation and distribution of ore phases are apparently controlled by similar factors such as sedimentary environment and associated sediments. However, at approximately 30 km distance from the paleocoast the basin depth was 2-30 meters (Liu et al., 1984), and various factors

indicate that the environment contained low levels of free oxygen. These suggest a general alkaline geochemical environment and slight oxidation to slight reduction, which therefore led to a specific Dounan Mn ore phase distribution in which the transitional ore phase dominates in deeper environments, with relatively undeveloped Mn oxide and Mn carbonate ore phases. However, the presence of minor manganite ooliths probably indicates a very poorly developed manganite facies to shoreward from the braunite zone; a manganite ore phase zone near the paleocoast in the Tangde area (Liu et al., 1984). At Dounan, nearshore facies have been extensively eroded. A general oxide to carbonate transition from nearshore to offshore is therefore suggested, as at Chiatura/Nikopol and Groote Eylandt.

The variation of the Dounan ore phases, both vertically and horizontally (Chapter 4) resulted from transgression/regression which led to varying levels of water anoxia. An offlapping Mn sedimentation or ore phase zoning is apparent because of these changes (Fig. 6.9). For instance, the Mn carbonates, with minor unsorted and oxide ores, usually dominated in the initial period; this was followed by the evolution of regressive sedimentation, the transitional ore phase showing relative importance in the second period of Mn mineralization, and oxides towards the end of regression. The vertical variation of ore phases (Fig. 6.9) therefore represent a transition from transgressive to regressive facies in sequence. Texturally, both normal and inverse grading also reflect the overall regression.

Although the oxide facies is mostly of primary origin, the carbonate facies is altered as a result of early diagenesis. The carbonate facies may predominate even where both facies are stable, because manganese oxide precipitation can be extremely slow, where oxide and/or carbonate show evidence of oxygenated bottom water (Force and Cannon, 1988). Primary sedimentary ooliths/pisoliths are also common in this facies (e.g. transitional ores), in and adjacent to ore. Since the deposits lack a "pure" Mn oxide phases (e.g. psilomelane, pyrolusite or manganite), in fact, variation in the ore phases, dominantly composed of mixed or transitional ores (Figs. 4.2 and 4.3), reflect the frequency of varying levels of water anoxia during regression. The geochemical environment underwent complex changes, leading to complex interbedding of ores. The three ore phases, sometimes together with gangue intercalations, overlie each other in the ore-body (Fig. 4.3), but scouring resulting from rapid sea-level change during Mn sedimentation locally leads to the absence of one of the three ore phases. Finally, the termination of the sedimentary basin owing to continuous accumulation of sediments and regression led to the end of manganese sedimentation.

6.6 Remobilization Processes and Secondary Enrichment in Diagenesis

It is generally considered that in hemipelagic environments and areas of high organic productivity in the oceans and shallow seas, where organic matter is abundant in basin floor

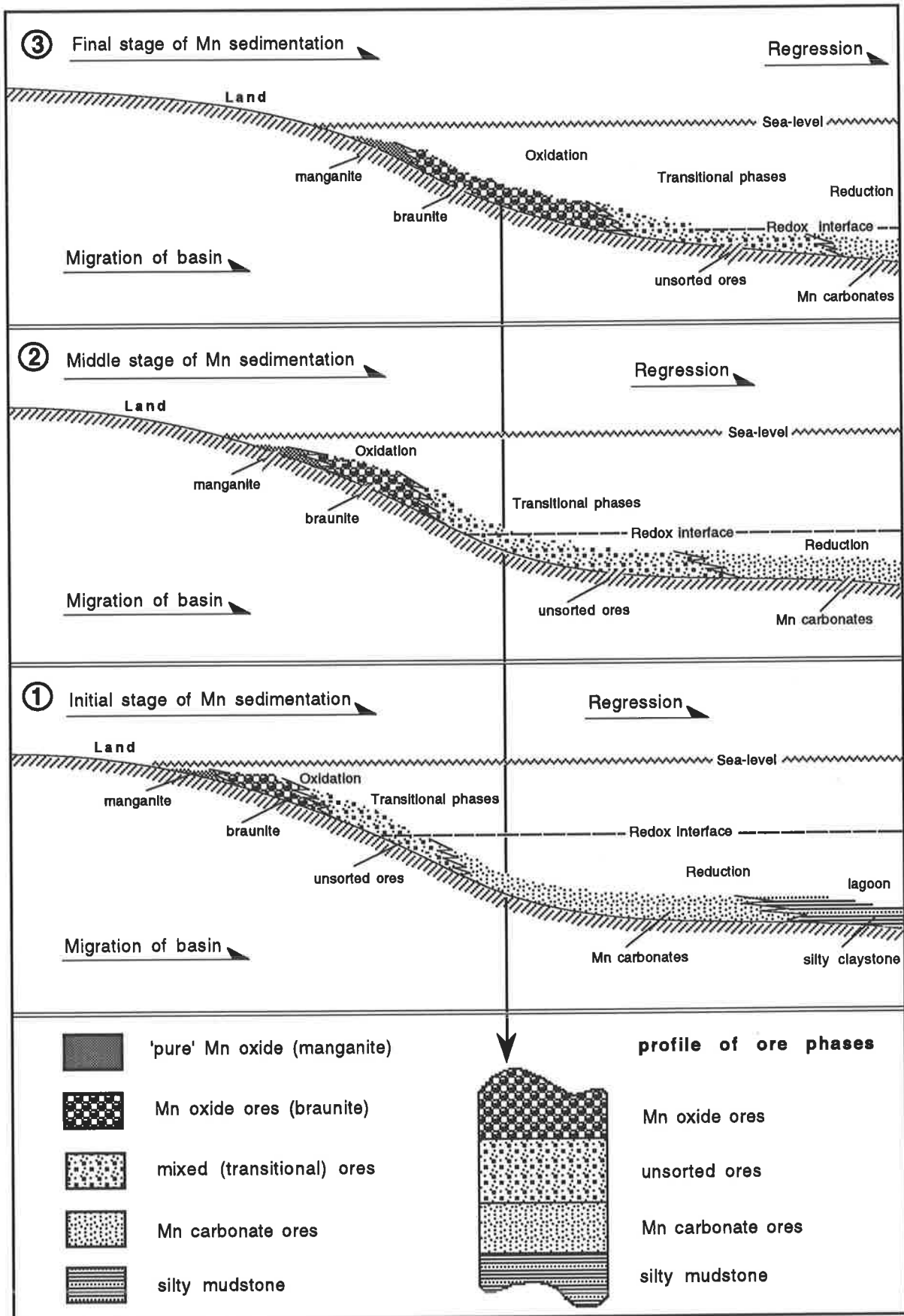


Fig. 6.9 Depositional mechanism sketch map of Dounan ore phases.

sediments, the supply of Mn to the sediment-water interface by diagenetic remobilization is most important and is widespread (e.g. Roy, 1981). When nodules and crusts with varying amounts of Fe, Mn and other minor elements are buried in sediments rich in organic matter, or when Mn-oxide particulates are already present in the sediments, in the reducing and/or acid environments created by the decomposing organic matter and the consumption of oxygen, Mn^{+4} and Fe^{+3} in the solids are reduced to Mn^{+2} and Fe^{+2} . These are easily dissolved in interstitial water and tend to be transported upwards in compacting sediments along the chemical potential gradients towards the alkaline and/or oxygenated zone (Bezrukov, 1960; Wangersky, 1963; Lynn and Bonatti, 1965; Manheim, 1965; Price, 1967; Strakhov, 1966; Li et al., 1969; Calvert and Price, 1970, 1972; Price and Calvert, 1970; Glasby, 1972; Crerar and Barnes, 1974; Robbins and Callender, 1975; and many others). In areas of relatively high heat flow, diagenetic remobilization of metals may be accelerated (Boström, 1967; Raab, 1972).

6.6.1 *Dissolution of Quartz and Calcite*

As mentioned before, quartz, calcite and their hydrated forms are closely associated with Mn oxide and Mn carbonate minerals and also with their secondary Mn products. Numerous recombinations of ionic compounds result in various diagenetic changes such as collocrystallization, recrystallization and replacement, depending on the geochemical environment. Under the same thermodynamical conditions, crystals, particularly coarse and highly crystalline ones, are more stable than non-crystal phases; crystalline materials strongly dominate over all diagenetic products. Although the crystallinity and micro-replacement illustrate a history of diagenesis, the lack of diagenetic minerals in some deposits suggests that pressure solution and temperature probably play important roles in diagenesis. This is strongly supported by the occurrence of deformed ooliths/pisoliths and the disappearance of concentric laminae of ooliths/pisoliths in compact massive ores.

Quartz and calcite recrystallinity are examined to determine the major dissolved Si- and Ca-species. Previous studies indicate quartz and calcite interact in many ways with associated Mn minerals, although they are often regarded as relatively immobile phases. It has, for instance, been illustrated that both quartz and calcite invade manganese minerals through micro-pipe systems, and replace previous Mn or gangue minerals. Also quartz and calcite are replaced by manganese. Moreover, stable isotopes from various types of Dounan ores/rocks imply that these two minerals are mobilized at somewhat higher pressure and temperature than surface geochemical conditions. Therefore, the discussion focuses on dissolution processes associated with relatively high temperature and pressure as well as low pH values.

6.6.1.1 *Thermodynamics of the Si-H₂O System*

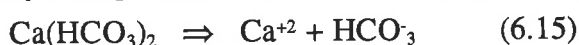
Pracejus (1989) observed that in long-term experiments, sediment samples indicate an increasing removal of dissolved silica from $\text{SiO}_2\text{-H}_2\text{O}$ solutions at surface temperature and pressure. The only hydrated silica compound detected was H_4SiO_4



The dissolved silica mainly comes from terrigenous clastic silts, but when the water contains dissolved calcium or manganese, the following mineral pairs are possible in the system $\text{Si-H}_2\text{O}$: quartz/braunite and braunite/calcite or Mn-bearing calcite (Fig. 6.7). The mobility of quartz is consistently low over a large pH range (Kittrick, 1969) and thus, variations in pH most probably do not play a direct role in the dissolution of this mineral. This is also supported by the co-existence of quartz and carbonate minerals.

6.6.1.2 Thermodynamics of the $\text{Ca-CO}_2\text{-H}_2\text{O}$ System

The stability fields of calcite and dissolved species are determined by Eqs. (6.13-16)



Ca^{+2} and HCO_3^- dominate in porewaters associated with the deposits (ores, rocks, porewaters), whereas HCO_3^- seems to gain importance with increasing acidity in the porewater due to the changes of physical and chemical conditions, including any contributions from biological activity. If the system, therefore, contains any calcium, the pH of the water indicates that $\text{CaH}^+\text{CO}_3^+$ is present (Fig. 6.8). In mixed chemical systems, however, which for instance contain dissolved silica or manganese, other phases form (see following sections).

As with quartz, a pH control over the dissolution of calcite also seems to be insignificant; Figure 6.8 depicts only small variations within a large pH range at surface conditions. Probably much more effective in the remobilization of calcite are the higher temperature and pressure as well as the dehydration of this mineral.

6.6.2 Dissolution of Manganese Oxides

A number of chemical reactions can reduce/dissolve tetra- and trivalent manganese oxides under diagenetic conditions. These minerals have long been considered to be very stable in oxygenated

waters, only to become unstable under oxygen deficient conditions in the presence of reducing agents. The presence of extensive secondary ore types examined in previous chapters documents the fact that large quantities of manganese (e.g. from Mn-bearing calcite or previous Mn minerals) were available for enrichment of diagenetic materials.

6.6.2.1 Alteration of Braunite

As discussed under Mn transport and sedimentation processes, the Mn oxides are generally highly insoluble in aqueous solutions. However, under certain conditions (e.g. higher temperature or pressure) the solubility of these minerals can increase considerably. The manganese oxide orebodies are "diagenetic" and not "diagenetic", in the sense that diagenesis only modified the mineralogical crystallinity and texture of the pre-existing ores and had a considerable role in their enrichment. Thus, the dissolution processes and products reflect the initial chemical and mineralogical composition of the sediments, modified by the variable intensity of diagenesis. The pre-existing Mn oxide minerals such as manganite and braunite, therefore, can be dissolved under higher diagenetic temperature and pressure through Eqs. (6.17-23).



However, dissolution is largely related to small increases in temperature and pressure, which led to extensive recrystallization as seen in incompletely dissolved microcrystals.

6.6.2.2 Redox Reactions between Carbonate Phases and Manganese Oxides

During the course of this study, it became obvious that redox reactions between braunite and carbonates are probably the most powerful mobilization processes in diagenesis. Reactions of manganese oxides and carbonates with other phases (e.g. Si, Ca, etc.), with rising temperature, have been studied in natural and synthetic systems (Roy, 1964a, b, 1968, 1972, 1973, 1974; Huebner, 1969; Peters et al., 1973, 1974; Coutinho et al., 1976; Candia et al., 1975). Although evidence of these reactions is very common in the deposits, they have not been recognized and described before. These reactions are discussed and put into a theoretical framework below:



This reaction has been suggested for Buritirama (Pará, Brazil) and Alagna (Pennine nappe, Alps) deposits, which, however, were all classified as related to metamorphism. Thus far, stability con-

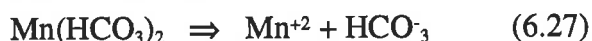
siderations for braunite and carbonate minerals have been separated, but it will be demonstrated that when these minerals appear in an aqueous system under rising temperature and pressure, they will interact. Then, the "normal" Eh/pH conditions for the stability of both tetravalent and divalent manganese compounds are no longer valid, and the reaction of manganese continues to reach an overall equilibrium (Eq. 6.24). This is examined in more detail for its role in replacement processes in the section on diagenetic precipitation.

Here, emphasis is directed towards manganese solution. An almost continuous supply of divalent manganese from pressure solution of carbonates guarantees the basis for further redox reactions (see following section). As Mn minerals with lower valences are considered to be less stable, the higher valence oxides are concentrated under diagenetic conditions. This is strongly supported by the fact that braunite is dominant over Mn carbonate minerals in many of the diagenetic ores.

The above process (Eq. 6.24) can lead to an initial removal of braunite and Mn carbonate minerals in succession, once new redox equilibria form. That the latter reduction processes are less dominant in the deposit follows from the relative enrichment of braunite during the development of the diagenetic ores. Eventually, however, considerable parts of former ores are recrystallized and replaced by secondary materials. This vast amount of previous manganese is available for the formation of diagenetic ores nearby the deposits.

6.6.3 Dissolution of Manganese Carbonates

The Mn-CO₂-H₂O and Si-Mn-CO₂-H₂O systems exhibit importance in the dissolution of manganese carbonates. As with calcite in the Ca-CO₂-H₂O system, the stability fields of Mn carbonates and dissolved species are also simply determined by Eqs. (6.25-28).



Therefore, the dissolving mechanism is very similar to that of calcite in the Ca-CO₂-H₂O system. But since the composition of natural rhodochrosite deviates considerably from the pure end-member in the isomorphous CaCO₃-MgCO₃-FeCO₃-MnCO₃ series, the decarbonation temperature varies according to composition (lower when FeCO₃ is present, higher when CaCO₃ is present, with total pressure and the presence of H₂O in the fluid phases; Roy, 1981).

However, when the Mn-CO₂-H₂O system occurs with the Si-H₂O system, leading to a relatively complex Si-Mn-CO₂-H₂O system, redox reactions between Mn oxides and carbonates

can take place. Also, the Si-Mn-CO₂-H₂O system enhances the transformation of Mn carbonate to Mn oxide phases under many diagenetic conditions.

6.6.4 *Biological Activity*

Microbial reduction of manganese oxides can be an important mechanism for mobilizing Mn in a wide range of contemporary sediments, including anaerobic/aerobic terrestrial freshwater and marine environments (Hariya and Kikuchi, 1964; Stone, 1987; Adams and Ghiorse, 1988). It is likely that microorganisms have been active over geological time, despite the paucity or lack of direct evidence preserved in the rock record. Though studies of Dounan diagenesis have not focused on biogenic reactions so far and it is difficult to assess the overall importance of the biota, it has been demonstrated that microorganisms are able to remobilize the ores under laboratory conditions (Madgwick, 1987).

However, it still needs to be demonstrated that microbiological processes preferentially mobilize the thermodynamically least stable manganese oxides or carbonates in the Dounan deposits, though some organisms (e.g. algae, foraminifera, bivalves, ammonoids and bioclastic debris being naturally resident on/in Dounan manganese ores show improved reducing capabilities under microaerobic to anaerobic conditions during diagenesis) can be found in Dounan diagenetic ores. If they do cause mobilization, the introduction of organic acids into the porewater system leads to a pH-dependent manganese reduction that parallels inorganic dissolution processes. However, such biologically controlled processes might not be indicated by the Dounan oxides, because in most parts of the deposits increasing diagenetic effects and cementation of the ore results in even greater braunite dominance rather than increases in Mn carbonate minerals (Mn⁺²). This is despite the fact that the ores show that Mn carbonate minerals replace the thermodynamically stable braunite. This means that most of the latter mineral is not remobilized by the biological processes, and that a biota-controlled dissolution of the ores cannot fully explain the observed diagenetic succession of the major manganese oxides. Therefore, biological activities probably play only a small role in the diagenetic enrichment of Dounan Mn ores. Given that textural evidence for biological activity during diagenesis is rare, it can be concluded that this process is very limited in the deposits.

6.6.5 *Pressure Solution*

The basic concept for this process is that at point contacts between grains pressures mainly induced by overburden load and depending on depth can develop and result in preferential dissolution of the material at the point of stress. Immediately adjacent, precipitation occurs in open pores or at places with less pressure, e.g. along the margins of grains. Additionally, the presence

of thin clay films can speed up the transfer of dissolved material to open pore spaces via the provision of diffusion paths (Pettijohn et al., 1987).

Pressure solution is a very important mechanism for mobilizing Mn in a very wide range of sediments, and there is evidence indicating that this type of mobilization process took place in Dounan orebodies (e.g. Plate 4.1, Fig. 3b; Plate 4.4, Fig. 15). This can also be strongly supported by abundant evidence that recrystallization of grains and deformation of oolites/pisolites leads to the disappearance of concentric rings of oolites/pisolites and development coarse crystals in the massive or deformed oolites/pisolites (Chapter 4).

Nordstrom and Munoz (1985) demonstrated that it is possible to obtain reasonably good results from simplified calculations using their theoretical model on the pressure solution of quartz together with data from Walther and Helgeson (1977). They showed the assumption that the molecular volumes are not functions of pressure and temperature is relatively good for lower pressure. They also state that at higher temperature, changes in the actual mol volume become more apparent. This suggests that for ambient conditions of the manganese orebody, the temperature control is negligible, molecular volumes are approximately constant, and the main factor for pressure solution is the overall pressure. Fortunately, the simple manganese mineralogy, together with some particular diagenetic structures, structural homogenities, mineral recrystallization, etc., suggest an extremely similar situation and therefore, the simplified theoretical approach can easily be applied to the Dounan diagenetic ores.

The above mechanism of intergranular pressure solution, which is often believed to be the dominant process of pressure solution, is nonetheless 7 to 9 orders of magnitude smaller than a different type of mobilization described by Tada et al. (1987). They propose a "plastic deformation plus free-face pressure solution", which is especially effective when the grain contact area is very small (early compaction of sediment). Intergranular pressure solution can gain importance in the late stages of compaction. As the overburden of the deposits and the deposits themselves possess very high density, it can be expected that pressures large enough to induce any type of pressure solution are abundantly reached. Diffuse, extremely fine impregnations of both clastic material and cryptocrystalline carbonates in the matrix of the oolitic/pisolitic ores occur frequently and they may have resulted from this mechanism, leading to limited dissolution and immediate recrystallization surrounding the primary grains.

6.7 Transport of Dissolved Manganese in Porewater

Examination of transport mechanisms in porewater focuses only on manganese, since the dissolution of gangue minerals is mainly of interest for the reduction/re-mobilization of Mn ores. However, gangue minerals are again examined for their role in replacement processes. Several

geochemical and biochemical processes were described that are able to reform manganese ores and associated rocks. It was also demonstrated that all dissolution processes depend directly on the availability of porewaters. Without water, any mechanism that could lead to the redistribution of manganese is unlikely. However, the very high density of the ores and associated rocks indicates that the deposits presently possess low permeabilities. Thus, these dissolution processes may act for short time intervals and over very small distances, and the recrystallization of grains gains more importance than replacement under the pressure solution process.

The two dominant mechanisms of manganese liberation at Dounan are overburden pressure and temperature controlled dissolution processes; pH and redox reactions between Mn oxides and carbonates play relatively minor roles and they are distinctly different in their physico-chemical parameters. For instance, redox reactions produce their own electrochemical environments (electron transfer, pH, etc.), largely due to the induced changes of pressure, temperature and even pH. Acidification of the water on the other hand, be it biologically or mineralogically mediated, is generally more positive. Such pH variations frequently occur as a result of environmental changes and then the pH alone may affect the solubility of minerals.

Theoretically, pressure solutions are probably not in equilibrium with surrounding materials. Once the pressure solutions join porewaters to generate new ore-forming solutions under constant pressure and temperature, ongoing dissolution processes are interrupted, and the waters equilibrate with the new environment, forming element patterns that reflect the respective mobilization (or precipitation) reactions. The manganese concentration in porewaters generally increases with increasing pH by this stage, and Mn reaches equilibrium and stabilizes in solution. Such stabilization of Mn compounds may be the result of silicate and/or bicarbonate complexes that can develop through the activities of changing pressure, temperature, pH and in bacterial activity. This interpretation is first supported by the fact that the diagenetic products are also composed of the same Mn minerals (e.g. braunite) as primary ores without any new products, although now relatively coarsely crystalline.

During anoxic diagenesis, iron is fixed in pyrite during sulfate-reducing diagenetic reactions under low Eh conditions, and manganese is remobilized toward the sediment-water interface by diffusion or by upward-moving pore fluids. Where the overlying seawater also has a sufficiently low Eh to support high manganese solubility, manganese remains in solution and contributes to the increasing reservoir of dissolved manganese (Force and Cannon, 1988). The manganese concentration in the porewater solution begins to decrease with increasing pH and decreasing pressure and temperature due to the initiation of recrystallization. This means that Eh/pH controlled processes result in the destruction of the previously stable complexes and manganese is removed from solution. As with the primary ores, the type of precipitate is determined by the geochemical or electrochemical parameters that dominate the environment; this is discussed in the following section.

The processes described above can be distinguished easily. Thus, the porewaters during diagenesis are grouped into two major sets:

- (pressure) solutions not in equilibrium with their surrounding and with diffuse trends; derived from ores, associated rocks, and original porewaters, and
- (ore-containing) solutions at equilibrium, depicting Eh/pH or redox control mechanisms; derived from Mn-bearing porewaters.

When the second group is examined, it is possible to determine the type of process that dominates the mobilization of manganese. This has serious implications for the detection of diagenetic ores, because diagenetic ores of the deposits similar to others do not have a strong Eh control. In such a case, redox processes in the orebody may be of minor importance for the formation of secondary ores, and recrystallization will be the important process for the formation and enrichment of diagenetic ores.

6.8 Fixation Processes During Diagenesis

Although there is not much experimental information on diagenetic precipitation processes, the presence of many diagenetic ores and rocks illustrates active deposition of secondary products. Many of these newly formed phases change their geochemical environment, for instance by influencing the pH, and thus, the formation of one particular mineral has direct implications for the stability or instability of co-existing phases (Merino and Ransom, 1982). Various replacement products are observed in the Dounan deposits, and it is demonstrated below that most of the precipitation and replacement processes can be explained in relatively simple terms.

The position of the interface between oxidized and reduced ambience controls the redeposition of manganese which may take place within the sediments near the sediment-water interface or within the overlying stratified water column. A part of the Mn^{+2} migrating upwards in the bicarbonate form may lose its mobility in the layers of decreased P_{CO_2} , leading to deposition of $MnCO_3$ below the oxic-anoxic boundary according to the reaction: $xCaCO_3 \rightarrow yMnCO_3 \rightarrow (Ca_x - yMn_y)CO_3 + yCa_2$ (Boström, 1967). The formation of Mn-carbonates during diagenesis has been recorded from the hemipelagic areas of the oceans, shallow seas and freshwaters by many workers (e.g. Zen, 1959; Manheim, 1961; Lynn and Bonatti, 1965; Rossmann and Callender, 1968; Calvert and Price, 1970; etc.)

Mn^{+2} is separated from Fe^{+2} during the upward diffusion owing to its high mobility and the affinity of Fe to form organic complexes as well as FeS_2 (Cheney and Vredenburg, 1968) within the reduced sediments in marine basins. At Dounan, this is demonstrated by the presence of pyrite formed during the diagenetic alteration of iron-poor manganese oolites/pisolites. Mn does not form metallo-organic complexes easily (Callender and Bowser, 1976), and the dissolved

Mn^{+2} migrates upwards to the oxygenated zone (generally the sediment-water interface) and is precipitated as Mn^{+4} -rich oxides (e.g. braunite).

6.8.1 Reprecipitation of Si- and Ca-Minerals

The stabilities of minerals and ions in the Si-H₂O and Ca-CO₂-H₂O systems are not redox-dependent, because all species retain their valency state during dissolution or precipitation. Thus, redox reactions with other elements need not be considered (Eqs. 6.10-16). This serves to simplify the discussion, particularly for silica which can result in complex polymers, but such mechanisms that could retard or increase the development of equilibrium with stable phases are not discussed, because of a general lack of data from Dounan. Instead, attention is focused on element interaction during reprecipitation.

The fact that quartz silt always dominates in the gangue leads to the conclusion that pure Si minerals, such as quartz, are generally less mobile than carbonates under present-day as well as diagenetic conditions. In any case, the fact that there are hardly any secondary Si minerals (quartz) in the massive or deformed oolites/pisolites suggests another important conclusion: that limited dissolved Si ions are consumed to form braunite as isomorphous additions. This leads to increased H⁺ concentration in the solution, which means that the pH becomes more acidic (Eqs. 6.11-12), and few Si ions are precipitated as quartz. Thus, the development of secondary braunite in the presence of limited dissolved silica results in the suppression of stable silicic phases, which explains the scarcity of Si-rich minerals like quartz in the diagenetic ores.

Transformation reactions between the initial unstable Ca precipitate (bicarbonate) and Ca-carbonate display strong dependencies on the presence of HCO₃⁻ and CO₃⁼ ions and on the pH variation (Eqs. 6.13-16). Generally, most of these processes were examined in alkaline media and at elevated temperature, and, for kinetic reasons, the transformations are then likely to be rapid. However, the transformation of Ca-bicarbonate to more crystalline phases (calcite) is strongly retarded in the presence of high concentrations of manganese, which seems to result from the isomorphous relationship between Ca⁺² and Mn⁺² ions owing to their similar geochemical nature. When the concentration of manganese is low enough to allow transformations to proceed, the development of calcite is promoted and the formation of Mn-bearing calcite or Mn-calcite is hindered. Manganese shows the same effect in enhancing the transformation of bicarbonates to Mn-bearing calcite, Mn-calcite and even calciorhodochrosite (see following section).

Both of the above observations are indeed valid for the Dounan diagenetic ores. In the same Mn oxide orebody, where braunite dissolution products are abundant, quartz can be observed occasionally. Similarly, in Mn carbonate parts of the orebody and within the Mn carbonate orebody itself, where Mn-calcite or calciorhodochrosite dominates strongly, calcite can be found

occasionally. A fascinating relationship is thus revealed, in which the two main gangue components of the deposits, Si and Ca, are seen to be interdependent in their formation and destruction during diagenesis:

- dissolved silica favours both braunite and quartz, depending on the geochemical conditions of formation;
- dissolved calcium facilitates the transformation of bicarbonate to calcite and Mn-bearing calcite, depending on the amount of manganese introduced.

6.8.2 Reprecipitation of Mn Minerals

At several places in the deposits it can be seen that orebodies have been reformed, and even replaced by secondary materials, though such changes are mostly detected under microexamination. The following sections examine the diagenetic precipitation conditions for this secondary enriched manganese. Manganiferous cementation occurs in many diagenetic ores, and low grade ores are thus enriched by these diagenetic products.

6.8.2.1 Reprecipitation of Mn During Redox Reaction between Mn Oxides and Carbonates

That redox reactions between Mn oxides and carbonates result in the dissolution of Mn was demonstrated above. However, the basic principle of such a redox reaction is that parallel to the reduction of one reaction partner the other must precipitate (Eq. 6.24). This leads to a situation where the newly forming Mn carbonate mineral takes the place of the dissolving Mn oxide, or vice versa (Plate 4.5, Fig. 19e). Mn oxide and carbonate dominate their geochemical environments during their interaction, which mostly took place in the transitional ores.

During redox reactions the generally large MnCO_3 stability field extends further towards the boundary dictated by the available Mn^{+2} and $\text{CO}_3^{=}$ concentrations and by developing pH (due to poor Eh effect on diagenesis); this is opposite to the stability gap that forms for braunite and other tetra- or tri-valent manganese oxides (Fig. 6.7). When the stability diagrams of both Mn oxide and carbonate systems are superimposed, it seems that the thermodynamic theory supports the field and laboratory observations (Figs. 6.7-6.8). The superimposed area in which both braunite and Mn carbonate minerals are unstable is covered by both braunite and rhodochrosite. Therefore, a redox reaction between Mn oxide and carbonate under the diagenetic conditions at Dounan always results in incomplete replacement in both directions, as long as tetra- or tri-valent and divalent manganese is available.

6.8.2.2 Reprecipitation of Mn as Oxides

Enrichment of manganese in the massive and deformed oolites/pisolites indicates the operation of diagenetic processes involving solutions carrying dissolved Mn. Since dissolved manganese is generally transported only for very small distances, reprecipitation should obviously take place nearby. This mechanism is particularly visible in the recrystallized ooliths/pisoliths and in crystalline grains (e.g. Plate 4.5, Figs. 19b-d and f; Plate 4.7, Figs. 27-30), which show recrystallized margins based on the primary grains. Porewaters carry dissolved Mn around primary grains and precipitate most of their load adjacent to the grains. When intense fluid movements occur in the primary ores, the ore-bearing solutions in such positions are abundant and cement the ooliths/pisoliths to form compact massive oolites/pisolites.

That manganese in braunite is fixed at or near previous dissolution positions indicates an abundance of oxygen and silica, a suggestion supported by the fact that there is nearly no other reaction to consume them (Eqs. 6.17-23). Ore minerals from the massive ores are all braunite and mostly crystalline, caused by slow precipitation of the oxide. The CO₂ from dissolved calcite (gangue) also contributed to the precipitation processes in the system through a buffering of the porewaters. This effect appears to have stabilized the pH at a suitable value, thus preventing stronger acidification reactions which could enhance the dissolution of manganese oxides. The appearance of incomplete dissolution and recrystallization on the same grains supports this view. Ores of this type mostly are located at the base of orebodies (e.g. V1, V7 or V8), but they often disappear in upper parts of the ore-bearing sections (e.g. orebodies V3 and V9). However, the absence of carbonate in this type of ore is probably related to two factors: (1) the relatively small amounts of organic matter present to yield CO₂, and (2) the comparatively high content of dissolved oxygen in bottom and/or pore waters (Frakes and Bolton, 1992).

6.8.2.3 *Reprecipitation of Mn as Carbonates*

Similar to the Mn oxides, the alteration processes of Mn carbonates affects the manganese phases, where Mn⁺² is liberated into solution from the primary minerals, but also where CO₃⁼ or HCO₃⁻ is concentrated (Eqs. 6.25-28); nevertheless, the pH also controls the precipitating processes (Fig. 6.8). Minerals coupled to transformation (e.g. from Mn-bearing calcite to Mn-calcite or to calciorhodochrosite, or even to rhodochrosite) during their formation increase the amount of manganese in the rocks, thus leading to secondary enrichment of the ores.

6.8.2.4 *Microbial Influence on Mn Reprecipitation*

Because microorganisms can enhance the oxidation of Mn⁺², the influence of bacteria or algae on precipitation reactions has been noted by some workers in recent years (e.g. Chapnik et al.,

1982; Burdige and Kepkay, 1983). Diem and Stumm (1984) reported that Mn did not precipitate from sterile solutions even in the presence of relatively high oxygen levels, implying the need for catalysis. Such catalytic reactions have, for instance, been observed on the surfaces of dormant bacterial spores (Nealson and Tebo, 1980; Rosson and Nealson, 1982) or in association with exopolymers (extracellular oxidation; Ghiorse, 1986). Experimentally, the oxidation of manganese is also strongly influenced by particulates acting as surface catalysts (Morgan, 1964). Adams and Ghiorse (1988) observed that in natural systems, organisms of the *leptothrix* family often catalyze manganese oxidation. The decay of organic matter also contributes to diagenetic growth of Mn minerals both above and within sediment (Frakes and Bolton, 1992). Other publications refer to these bacteria as *metallogenium*, so that it can thus be assumed that organisms of the *metallogenium* type are active.

Unfortunately, it is difficult to assess the role of organics in the deposits, because of very limited data, i.e. at present, the concentration and distribution of microorganisms in the Dounan orebody is unknown, although many types of biota were identified (e.g. algae, bivalves, Zhang et al., 1979; Liu et al., 1984). Therefore, extensive research is needed, before a qualified assessment of the biological influence on diagenetic precipitation processes can be made, but microbia at least to some extent, influenced the Mn remobilization and reprecipitation during diagenesis.

6.8.2.5 Reprecipitation Dependency upon Mineralogy of Substrate Rocks

It was noted in numerous instances above (Chapter 4) that depending upon the type of substrata, different manganiferous deposits develop. For instance, in contrast to primary products, braunite forms less readily in the presence of quartz (e.g. in massive ores), whereas Mn carbonate minerals overprint Mn ores in cases where little or no silicic materials are associated. This clearly illustrates that diagenetic precipitation processes are at least partly controlled by the materials in which the precipitation occurs.

It has been demonstrated in the example of manganiferous precipitates above, that the type of mineral formed strongly depends on the presence of various other dissolved elements. From the chemical similarities either between Mn^{+4} and Si^{+4} , or between Mn^{+2} and Ca^{+2} it would appear that comparable dependencies are possible in the case of manganese precipitation. This seems to support the findings above, but so far, research on this aspect is very limited (Ebinger and Schulze, 1989) and thus, this proposed relationship remains tentative.

The replacement of quartz and calcite, Mn oxides and carbonates also results from chemical/mineralogical interactions between Mn-carrying solutions and specific substrate rocks. Manganiferous silicate complexes, under natural conditions, are likely to form in more acid environments containing abundant dissolved manganese. Once these complexes dehydrate, silica is mo-

bilized and Mn oxides develop, as the dissolution of silica produces an increase in alkalinity, which in turn forces more manganese to precipitate. Similar reactions may apply to the replacement of calcite by Mn minerals. The main Mn mineral, braunite, is direct evidence for the existence of such Mn-Si complexes in the deposits. Therefore, this mechanism apparently provides a mechanism for the replacement of quartz and calcite by Mn oxides and carbonates.

6.9 Discussion

This Chapter has described sedimentary dissolution, transport and precipitation, and diagenetic remobilization and reprecipitation processes, and it also discussed arguments for and against the existence of these mechanisms based on the evidence of sedimentary and diagenetic activities discussed initially. Although the mineralogy, geochemistry, and in some cases, the mode of origin of many Phanerozoic sedimentary manganese orebodies are fairly well known the effects of the important variables represented by changing ocean chemistry, sea level, and climate on ore formation are only recently being considered. Frakes and Bolton (1992) discussed the mode of origin of several important orebodies of Phanerozoic age and indicated that variation in ocean chemistry, sea level, and paleoclimate have strongly influenced the deposition of sedimentary manganese over time. They pointed out that the cycle of manganese involves weathering, transport, deposition, and alteration, all of which are, to some extent, influenced by ocean geochemistry, sea level, and climate. Processes of ore formation in the Dounan area will now be discussed in the light of these larger concepts. Finally, since the Dounan sedimentary braunite is apparently a rare occurrence, it is necessary to give a genetic overview of the mineral. In the final section an overview of the dominating processes is given in context with geochemical and geological models.

6.9.1 Discussion of Mn Sedimentation

An examination of the dissolution, transport and sedimentation allowing the primary precipitation of both Mn oxides and Mn carbonates as well as their mixed products, the transitional ores, under specific geochemical conditions reveals that the most likely minerals to form are those of the MnOOH , $\text{Mn}(\text{Mn},\text{Si})\text{O}_3$ or $\text{Mn}_2\text{O}_3 \cdot \text{MnSiO}_3$, and $(\text{Mn},\text{Ca})\text{CO}_3$ groups (e.g. manganite, braunite, calciorhodochrosite or Mn-calcite). These minerals are stable at relatively narrow Eh/pH intervals ($\text{Eh} \approx +0.1 - +0.3$, $\text{pH} \approx 7.8 - 8.8$; see Figs. 6.6-6.8).

Where Mn is dissolved in freshwater from oldlands, Eh/pH controlled processes dominate. From the oldlands and associated surface and subsurface waters, manganese is dissolved by physico-chemical processes. Although detrital materials are also liberated and transported, dissolution appears to be the most effective process to liberate Mn from bedrocks of oldlands. As so-

lutions from groundwater reach equilibrium with river water, the geochemical parameters of these waters should favour the precipitation of tetravalent Mn oxides, once the concentrations are high enough. However, the development of chelate complexes, colloidal suspension and particulates in river waters protects much manganese from rapid oxidation or precipitation and the concentration of Mn^{+2} increases, thus enabling large amounts of manganese to travel large distances as dissolved load (Frakes and Bolton, 1992).

As the solutions reach equilibrium with the seawater, the geochemical parameters of these waters should favour the precipitation of Mn oxides or carbonates, once the concentrations of manganese are high enough and other geochemical conditions (e.g. Eh/pH) are suitable. In seawater the geochemistry changes dramatically and much of the dissolved Mn is forced out of solution. Under these circumstances, manganese precipitates in the form of Mn oxyhydroxides, Mn oxides or carbonates, such as manganite, braunite or rhodochrosite.

Frakes and Bolton (1992) concluded that variations in ocean chemistry, sea level, and the rainfall factor in climate are all important in controlling the formation of sedimentary manganese orebodies. They considered that weathering rate at which dissolved Mn is removed from the bedrocks of oldlands is governed by the amount of rainfall, through indirect controls on vegetation and hence on water acidity and also the rate at which Mn is transported in surface and ground waters is determined by rainfall, and therefore high rainfall and low sea level are the most favorable conditions for removing and transporting Mn from source area.

Deposition of manganese is also affected, to a variable extent, by ocean chemistry, sea level, and climate (Frakes and Bolton, 1992). As seen in transgressive-regressive relations in Figure 6.10 (Frakes and Bolton, 1984), high sea level leads to the formation of oxygen-depleted basin waters through increased organic productivity and the accumulation of manganese in solution; whereas falling of sea level makes waters become oxygenated, leading to precipitation of the metal, first as carbonates, and with increasing oxygenation, as transitional ores and oxides (Frakes and Bolton, 1992).

6.9.1.1 The Influence of Ocean Chemistry on Ore Formation

In view of understanding the formation of Mn ore, the importance of oxygen and carbon as two important elements of seawater and their significant variations over time have been emphasized by Frakes and Bolton (1992). They considered that variation in the chemical composition of both atmosphere and the ocean are influenced by past variations in the carbon cycle, and the record of $\delta^{13}C$ in ocean sediments and glacial ice can be used to study this history. In the isotopic studies of the Dounan Mn deposits, the range of $\delta^{13}C$ from slightly positive to negative carbon isotopic values (+3 to -6) suggests sedimentary-diagenetic formation of the ores, pro-

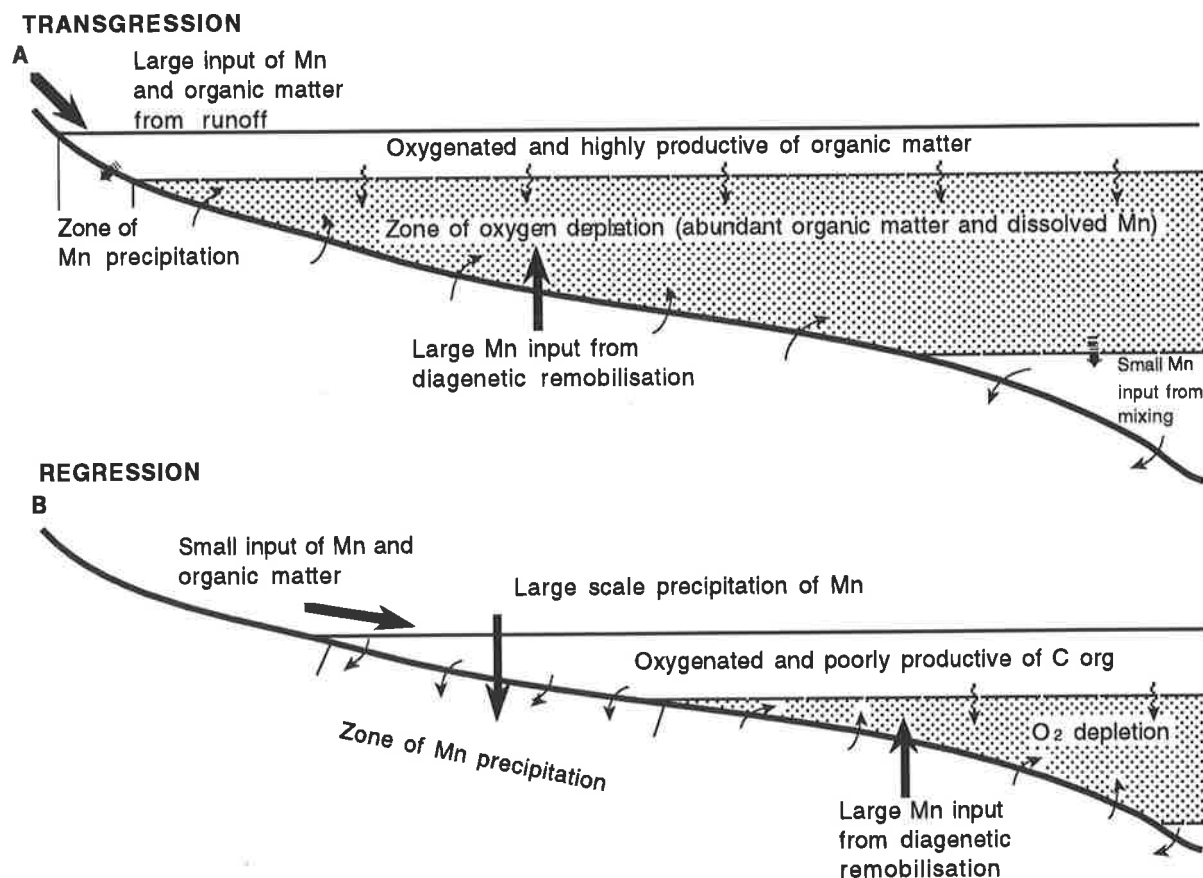


Fig. 6.10 A. Relationships at a basin margin during marine transgression, showing zone of oxygen depletion and dissolved Mn enrichment impinging on the bottom and inferred movements of Mn. B. Relationships during marine regression, showing abundant diagenetic remobilization and precipitation of Mn in reducing and oxidizing zones, respectively. After Frakes and Bolton (1984).

bably through both organic and inorganic pathways. More negative values seem to characterize Mn enriched ore types, probably reflecting an input of isotopically light carbon from organic matter during diagenetic alteration of buried Mn oxides. Formation of the original oxides suggests changes in oxygen levels within the basin environments prior to any diagenesis, whereas the diagenetic alteration itself is consistent with postdepositional oxygen depletion (Frakes and Bolton, 1992).

On the other hand, the increased Mn concentrations (approximately from 5% to 50% Mn) slightly preceded or coincided with a positive excursion of about 2.5 per mil in the carbon isotopic record in the carbonate fraction of the Dounan Mid-Triassic Mn-bearing sequence, whereas the diagenetic samples of the same sequence show a fall of 4.5 per mil at the level of greatest Mn enrichment (about 55% Mn; Figs. 5.10-5.11). All analyzed samples in Dounan show negative correlation with $\delta^{13}\text{C}$.

The isotopic character of the Dounan Mn deposits may, however, reflect the basinal history of fluctuating oxygenation and oxygen depletion on short time scales. Frakes and Bolton (1992) explained that Mn sedimentation is to be expected to peak at the end of anoxic events or in their

late stages, as ocean waters representing dilute ore-forming solutions are affected by widespread oxic conditions capable of supplying manganese to the sediment column. They also considered, however, that some of the major manganese orebodies of the Phanerozoic coincide roughly with the times of increased anoxia, such as the deposits at Groote Eylandt (Albian-Cenomanian, Australia) and Imini-Tasdremt (Cenomanian-Turonian, Morocco), whereas others appear to be related to at least local or regional stages of oxygen depletion (e.g. Oligocene deposits in the Ukraine and Georgia).

6.9.1.2 Sea Level Influence on Ore Formation

As the formation of trapping estuaries and other coastal inlets is strongly controlled by sea level, relative sea level plays an important role in the generation of sedimentary Mn deposits (Frakes and Bolton, 1984, 1992). They pointed out that eustatic highstand in the past would have led to formation of estuaries, fjords, bays, and inlets, and possibly led to more abundantly accumulation of manganese in coastal environments where manganese included in particulate flocs or aggregates is moved by tides and river inflow and eventually settles and may be buried as part of the sediment pile. Also, marine transgression (high sea level) brings about a tendency of anoxic conditions and reduced sedimentation rates. With lower rates of sediment input, there is less dilution of the Mn component in potential ore beds.

Stratigraphic sequences formed under low sedimentation rates during highstands usually contain large amount of organic matter as a consequence of sea-floor anoxia thought to originate from increased rates of supply of organic matter from surface waters (Pedersen and Calvert, 1990). At such times, metals being soluble in reducing environments can be trapped by the restricted basin (Cannon and Force, 1983; Frakes and Bolton, 1984; Bolton and Frakes, 1985). Manganese may form particulates, oolites, pisolites, nodules, and disks as a result of the availability of oxygen in aerated near-shore locations; this can also result if there is a substantial change in the oxygen levels in the basin (Frakes and Bolton, 1992). They (1984, 1985) found evidence of marine regression concurrent with Mn oolite-pisolite deposition at Groote Eylandt and Chiatura (U.S.S.R) and attributed ore accumulation to renewed oxygenation of basins having restricted access to the open sea (Fig. 6.10), this is extremely similar to or coincident with the case of the Dounan deposits. They explained that rising anoxia resulted from abundant soil organic matter, delivered to the basin as the sea transgressed over the land, leading to oxygen consumption. In regression, the reservoir of dissolved manganese suddenly gained access to oxygen and precipitated to form oxide ores (Fig. 6.10).

6.9.1.3 Paleoclimatic Influence on Ore Formation

Frakes and Bolton (1992) considered that rainfall is the most important climate parameters in the formation of a sedimentary Mn orebody, because Mn solubility usually depends on Eh and pH, which vary significantly in surface and ground waters. Generally, humid climate is favorable for manganese being mobilized from bedrock and soil and transported, because of the availability of waters. Also, such humid climates are characterized by acid ground waters deriving from extensive vegetation growth, in which manganese is most mobile (Frakes and Bolton, 1992).

The Mid-Triassic Mn deposits of Dounan lay in somewhat higher than latitudes their present locations, that is, about 33° to 35° north. Mid-Triassic climates were characterized by remarkable warmth and equability (see 6.2.4). The best interpretation is that deep weathering in the Triassic (represented by the dark grey T2g limestone and T2f1-2 mudstone facies) built up a reservoir of dissolved Mn in the seaway; this then provided a source for precipitation in the Mid-Falang stage. This, together with other examples from Groote Eylandt of Australia and Nikopol/Chiatura of former USSR, discussed by Frakes and Bolton (1992), demonstrate the relative importance of rainfall relative to paleotemperature. These localities were all characterized by humid conditions while ores were forming; the temperature conditions varied greatly. Although Dounan and Groote Eylandt experienced a warming precisely at the time of ore accumulation, the Paratethys region of the former U.S.S.R. underwent a marked cooling. This leads to the conclusion that supply of Mn through chemical weathering, and not the temperature conditions, is the crucial factor in determining whether an orebody could form (Frakes and Bolton, 1992).

6.9.2 Mn Secondary Enrichment in Diagenesis

During the course of this chapter a diversity of mechanisms leading to the remobilization or reprecipitation of Mn oxide and carbonate ores and associated rocks was examined. It is likely that these processes have affected or reformed the orebodies at Dounan at early to late stages of the diagenetic history of the deposits. These processes were of major importance to the secondary enrichment of the deposits. Significantly, the redox reaction between Mn oxide and carbonate seems to be much more prevalent than all other mechanisms. A combination of several remobilization or reprecipitation processes can nevertheless enhance the overall effect, and it is the co-existence of such reactions that probably drove the continuous reformation of the ores.

The following example illustrates that a combination of different processes may also result in a decreasing effectiveness of the system. If chemical and redox reactions as well as microorganisms are working in parallel to dissolve the ore, then organo-metallic or chemical complexes of both oxide and carbonate are likely to form. These compounds, however, lead to a general decrease of dissolved ionic species of ore-forming elements (e.g. Mn, Si, O, CO₂). It is mentioned above that the pH of the redox process is a function of the activities of Mn of different valences and that with increasing Si concentration the geochemical environment becomes more acid. A

complex development reducing the concentration of dissolved Si thus results in an increasing alkalinity, because less Si is available for redox reactions. This also means that less manganese is remobilized through the interplay of these mechanisms. Although increased effectiveness could be expected, there is a general decrease when these particular processes act together.

It is evident that many diagenetic processes depend on each other to operate, and most require the availability of porewater which can stabilize or destabilize certain phases. Therefore, a generalized reformation path for the dominant minerals (calcite, quartz, multi-valent Mn oxide and carbonate) is outlined to demonstrate the interdependence of the phases. Quartz was shown to precipitate from solution mainly during diagenesis when abundant Si is available. This results in an acidification of microenvironments, which in turn leads to the reduction of braunite on a small scale and its successive replacement by other minerals. The oxidation of Mn^{+2} to braunite (Mn^{+3} or Mn^{+4}) is the main factor for dissolution of Mn carbonate, because this dominating redox reaction imposes specific geochemical conditions on the environment. It must be repeated that only tetra (or minor tri-) valent manganese oxides (braunite) participate in the described redox reactions; lower valency minerals (e.g. Mn-calcite) are passive under these conditions.

Once Mn^{+2} enters solution, the transformation of calcite or Mn-bearing calcite to Mn-calcite or calciorhodochrosite predominates. Because $MnCO_3$ is isostructural with calcite, up to 15% or more of the Ca in this mineral can be substituted by Mn. The formation of more stable calcareous phases, such as calcite, is suppressed by the presence of Mn^{+2} . It must be noted here that some observations also point to a comparable dependency of various Mn minerals upon other ions (e.g. $Si \rightarrow$ braunite). However, the stability of the $CaCO_3$ - $MnCO_3$ series mostly depends on the relative Ca^{+2} and Mn^{+2} concentrations in the solution and on the geochemical conditions, leading to a series of carbonate minerals, i.e. calcite - Mn-bearing calcite - Mn-calcite - calciorhodochrosite - even rhodochrosite. However, in most cases, oxygen in pore waters decreases with depth in the sediment pile and reducing conditions exist at shallow depth. In this zone, Mn^{+2} is remobilized in interstitial water and diffuses with it either laterally or upward. On traversing the redox gradient, dissolved manganese will precipitate immediately where conditions are sufficiently oxidizing (Frakes and Bolton, 1992).

It is unclear whether the formation of carbonates, as described above, is the only mechanism to reduce braunite, although there is a lack of direct evidence for other processes. However, it can be assumed that, for instance, microorganisms participate in the dissolution of braunite in at least some places of diagenetic variation, where additional organic nutrients are available. It is also possible that organisms or manganiferous silica complexes, contribute to the remobilization of silica and manganese from quartz and braunite. These ionic species then precipitate again, when their geochemical environment changes. Although Mn oxide mainly reprecipitates during redox and chemical reactions, microbial influences on the manganese oxyhydroxides (e.g. $MnOOH$) cannot be excluded. Similarly, bacteria such as *Metallogenium* may contribute to the succession

of Mn minerals at Dounan, which is also affected by rapid reprecipitation through oxygen-rich porewater and the mixing of porewaters due to pressure solution. Field observations indicate that whatever reprecipitation processes is active, it is strongly characterized by the removal of concentric laminae and reformation in ooliths/pisoliths.

During diagenesis, the trace metals, Ni, Co, Cu and Pb may react with organic matter within the sediments to form stable chelates, or they may be captured (particularly Ni, Cu, Co) by Fe-sulphides (in marine basins) and thus immobilized (Bonatti et al., 1972; Cheney and Vredenburg, 1968). Thus, in general, diagenetically-formed manganese deposits register much higher ratios of Mn/Fe, Mn/Ni, Mn/Co and Mn/Cu when compared to pure hydrogenous deposits in the oceans (Bonatti et al., 1972; Calvert and Price, 1970; Price and Calvert, 1970; Glasby, 1973, Glasby et al., 1971; Summerhayes and Willis, 1975 and others) and are related strongly to the composition of interstitial waters rather than that of basinal water. The Dounan case of higher Mn/Fe, Mn/Co, Mn/Ni, and Mn/Cu probably result from this mechanism.

6.9.3 *Interaction of Processes*

Studies in present-day marine and lacustrine basins have clearly demonstrated that in most cases no single source or mechanism, by itself, could give rise to the manganese deposits (Roy, 1981). In some marine basins the presence or relative importance of biogenic, terrigenous and other (e.g. volcanogenic) sources, or their conjunction, is extremely difficult to estimate. Boström (1976) maintained that most of the Fe and Mn in Pacific deep-sea sediments was derived from terrigenous and biological sources. Nevertheless, Roy (1981) concluded that in the pelagic parts of the ocean, metals may be derived both from the basinal water (enriched by terrigenous or biological contribution) and from other sources such as endogenous fluids. Again, in the hemipelagic areas of the oceans and in shallow seas and lakes, the metals may be contributed by both the basinal water above and the interstitial water below, often at the same time (Glasby et al., 1971; Raab, 1972; Calvert and Price, 1977, Dugolinsky et al., 1977). The Dounan case is very similar to the latter cases. The actual mechanism of accretion of the ooliths/pisoliths may be attributed to inorganic scavenging through chemisorption and autocatalytic oxidation, or to biological processes involving microorganisms, or to both. In fact, the productivity of certain microorganisms (which ultimately oxidize Mn^{+2}) may be dependent on environments created by inorganic and physical processes in the basin; on the other hand, biological productivity may also create an environment in which inorganically controlled solution, migration or deposition of Mn can take place. The source of metals and the mechanism of formation of sedimentary Mn deposits are, therefore, multivariate, and in many cases the products represent their cumulative effect (Roy, 1981).

Strakhov (1969) suggested that nonvolcanogenic-sedimentary deposits of the Al-Fe-Mn triad in the older geological sequences were mainly formed under humid conditions in various climates, ranging from the tropical to the temperate. The Mn oxides were deposited during minimum terrigenous influx as in the case of deposits in present-day basins. This agrees with the established increase in mobility of the Al-Fe-Mn triad in subdued tectonic activity when mechanical denudation declines and chemical activity increases, as well as with the mixed sedimentary formation of the Dounan manganiferous sequence. Away from the continental drainage area, deposition of Mn was minimal in siltstone and increasingly dominant in the sequence of silty claystones - intraclastic limestones throughout the Falang stage of the Mid-Triassic. That the processes of formation of sedimentary Mn deposits recognized in present-day basins might have been operative in older geological ages is indicated by a number of ancient deposits dating back to at least the Cambrian (Roy, 1981), though the reports of modern braunite deposits are lack.

Strakhov (1966) recognized a diagenetic contribution in the formation of ancient sedimentary Mn deposits and termed such deposits sedimentary-diagenetic. The Mid-Triassic Mn deposits at Dounan show abundant evidence of diagenetic modification of the primary Mn oxides and carbonates. Since the diagenetic modification is limited in parts of the deposits, the sequence of changes has been retained in the recrystallization and replacement records of the mineralogy. Similarly, the lower Oligocene deposits of Nikopol type (see Chapter 7), also demonstrate diagenetic modification of the Mn⁺⁴-bearing oxides to rhodochrosite through manganite (Strakhov, 1966; Strakhov and Shterenberg, 1966). Owing to the diagenetic modification in limited parts of these deposits, the sequence of changes has been retained in the mineralogical record of the orebodies. Thus, the Mn-carbonate ores may form either by direct precipitation from basinal water or (more probably?) by precipitation from interstitial water through diagenetic recycling in reduced sediments. Such ores, generally with high Mn/Fe ratios, are sometimes closely associated with reduced sediments rich in carbonaceous matter.

6.9.4 Genetic Overview of Dounan Braunite

The mineral braunite was first described by Haidinger (1831) and its general composition is now recognized as $Mn^{2+} Mn^{3+}_6 SiO_{12}$ (e.g. De Villiers, 1975; Moore and Araki, 1976; Fleischer, 1987; Fleischer and Mandarino, 1991). Although the mineral has been known and studied both naturally and experimentally for over 160 years by many workers (e.g. Aminoff, 1930; Byström and Mason, 1943; Krishnan and Banerjee, 1939; De Villiers, , 1945 and 1951; Muan, 1959a, b; De Villiers and Herbstein, 1967; Huebner, 1967; Abraham and Schreyer, 1975; Hino et al., 1978; Abs-Wurmbach, 1980; Dasgupta and Manickavasagam, 1981b; Abs-Wurmbach et al., 1983 and many others), the details of both its crystal chemistry and genesis remain unresolved.

The mineral exists in two polytypes. Normal braunite (or braunite I), being close to the chemical formula $3\text{Mn}_2\text{O}_3 \cdot \text{MnSiO}_3$ with about 10% of SiO_2 (Frenzel, 1980), may occur as an important mineral in manganese ores and manganese-rich rocks (e.g. S.W. Africa, De Villiers, 1951; India, Roy, 1966; China, Su, 1983; Western Australia, Ostwald and Bolton, 1990; North Africa, USSR, Brazil, Roy, 1980a), whereas the low-silica (~4% SiO_2) braunite II described by De Villiers and Herbstein (1967) is a rarer form and has an ideal formula $\text{Ca}(\text{Mn}_{12}\text{Fe}_2)^{3+}\text{SiO}_{24}$ (De Villiers, 1980). The valence of manganese in the formula of braunite I is not completely clear. In terms of the magnetic measurements of Krishnan and Banerjee (1939) and of the structural investigations of Byström and Mason (1943), both Mn^{2+} and Mn^{4+} could exist and the formula could be written $3\text{Mn}^{2+}\text{Mn}^{4+}\text{O}_3 \cdot \text{MnSiO}_3$, in which silica possibly replaces the Mn^{4+} diadochically, in view of the considerably fluctuating SiO_2 -content (Frenzel, 1980). The existence of other elements such as Fe, Mg, Ca and Ba in braunite has been reported by Frenzel (1980), who also suggested the possibility of Mn^{3+} existing in the mineral, particularly as braunite and bixbyite precipitate almost simultaneously or shortly after each other.

Because braunite occurs ubiquitously in the metamorphosed manganese oxide ores in different Precambrian formations of India (Roy, 1966, 1981; Dasgupta and Manickavasagam, 1981a, b; Ostwald and Nayak, 1993), and in similar diagenetic to metamorphosed rocks in South Africa and South America, the mineral is commonly considered to be a metamorphic reaction product. Braunite also occurs as a common manganese mineral in Mn-bearing base-metal veins, associated with fluorite, barite and carbonate, and which may be equivalent to present day hydrothermal emanations at oceanic spreading centres (Roy, 1981). Experimental results of both natural and synthetic braunites (Muan, 1959a, b; Huebner, 1967; Hino et al., 1978; Abs-Wurmbach et al., 1983) and both the above modes of origin require elevated temperature and/or variable confining pressure. A few reports have suggested that braunite may have formed at low temperature and pressure, either in the supergene zone of manganese deposits (Hewitt, 1972), or as a diagenetic product in rare instances (Roy, 1981; Roy et al., 1990; Ostwald, 1982; Ostwald, 1992; Ostwald and Bolton, 1990; De Villiers, 1983; Miyano and Beukes, 1987), or very rarely as a primary ones (Serdyuchenko, 1980; Su, 1983). However, the reported evidence for braunite developing under normal surface temperature and pressure mostly is not very good (Ostwald and Bolton, 1990).

However, the discovery of braunite showing a range of morphologies and textures in sedimentary rocks of the Dounan Mid-Triassic manganese deposits of China (e.g. Zhang et al., 1979; Wang, 1981; Su, 1983; Liu et al., 1984; Zhong, 1986) suggests primary sedimentary/diagenetic origin. Contrary to the popular belief that a large proportion of braunite in ore deposits are oxidation products of the manganese silicate minerals under metamorphism (Roy, 1966), examination of the Dounan braunite occurrences by numerous analytical methods satisfy the sedimentary-diagenetic interpretation, yielding a generalised picture of the behavior of the manganese mi-

nerals under varying sedimentary and diagenetic conditions. The Dounan manganese oxide and carbonate mineralization exhibits a consistent pattern of strata of braunite and carbonate minerals, conformable with layers of enclosing admixtures of fine terrigenous clastic and carbonate rocks. The existence of abundant fossils both within the braunite oololiths/pisoliths and in the Mn carbonate matrix or in the enclosing clastic and carbonate sediments indicates that the manganese oxides and carbonates are the products of marine sedimentary processes (Roy, 1981).

The Dounan braunite occurrences show no evidence, either petrological, mineralogical or textural, of a metamorphic or hydrothermal origin, as discussed by Roy (1981). Neither do the occurrences show any evidence of volcanism or metamorphism, as indicated by the host rock mineralogy (Table 4.3). Field studies in the area confirm this (Zhang et al., 1979; Liu et al., 1984). Various interpretations of the stratigraphic, petrological and mineralogical, geochemical characteristics of the Dounan braunite discussed in this text stress its primary origin and its occurrence within sediments of a transgressive/regressive cycle. Also, the presence of marine fossils both within the braunite and in the enclosing sediments (Plates 2.3 and 2.4) indicate that the manganese oxide is the product of marine sedimentary processes.

Various investigations show that braunite is universally present in manganese ores of all mine-areas of Dounan, from sedimentary to diagenetic stages. Concentric laminations of accretionary Mn oxide/carbonate oololiths/pisoliths are characteristic both in macro- and microscale, and contacts of the laminae are generally sharp except where replacement and admixture of the components occur. The braunite and Mn carbonate mineral interlaminations are often obscured by recrystallization. Commonly, these manganese minerals, constituting both oololiths/pisoliths and matrix, retain evidence of both primary precipitation and diagenetic recrystallization or replacement.

In the initial stage of recrystallization, aggregates show an obvious crystallizing evolution from collo- or cryptocrystalline to polycrystalline textures, whereas in the final stage the outer form and the interlaminations of the grains are obliterated and very fine but discrete grains of braunite, calciorhodochrosite, Mn-calcite, etc. have evolved. These latter minerals were also transformed to other generations of manganese oxide or carbonate phases by replacement during diagenesis. The evidence of conversion from one mineral to another is mostly retained frozen in the ores. Such conversion usually started from the contact planes of concentric laminae of pre-existing phases. In many samples, grains of ore or gangue minerals are observed to be partially or totally transformed to others (see Plate 4.5, Fig. 19e). Relatively coarse grains generally formed along the contacts of concentric laminae, occurring as euhedral crystals in sharp contact with Mn carbonate minerals (see Plate 4.8, Fig. 34d). Thus, the typical sedimentary and diagenetic textures and structures of the ores, including oolitic/pisolitic types, laminations, cross-bedding, normal and inverse grading, in the total absence in the ores of metamorphic and hydrothermal textures, indicate a sedimentary-diagenetic origin of Dounan braunite ores.

Various interpretations of the stratigraphic occurrence of Dounan sequence (Zhang et al, 1979; Liu et al., 1984) stress its occurrence within sediments of transgressive/regressive cycles. As mentioned earlier, The manganese horizons of the Dounan sub-basin succession, appears to have been deposited during minor transgressive/regressive cycles. As such, the deposition of manganese in such a sequence is consistent with similar marine transgressive/early regressive manganese deposits described elsewhere (Cannon and Force, 1983; Frakes and Bolton, 1984). Ooliths/pisoliths comprising concentrically zoned braunite and Mn carbonate appear to be a response to varying levels of water anoxia. The Dounan deposits appear to belong to the better-known proximal manganese oxide-distal manganese carbonate model of Stanton (1972). The results of this study point to the braunite being either a primary constituent of the sediment or a diagenetic enrichment. A primary origin for the Dounan braunite has been postulated by Su (1983).

However, Su (1983) considered that both braunite and Mn carbonates at Dounan were primary sediments and that diagenetic effects are lacking. When the descriptions and data of this study are compared, a picture emerges that reflects the presence of significant diagenetic process, though the sedimentary process dominates in the Dounan deposits. This means in general terms that the diagenetic mechanisms result in the following mineralogical and geochemical relationships: (a) changes of ore textures or structures, (b) recrystallization and replacement of ore and gangue minerals, as well as their microfabrics, (c) development of similar sequences of the primary products, (d) secondary enrichment of manganese. Su (1983) considered the braunite ooliths/pisoliths to be biogeochemical in origin, on the basis of their enclosed filamentous microorganisms (bacteria and/or microalgae), and he developed a conceptual model of decaying shallow marine organics precipitating Mn on suspended clay particles in coastal embayments. However, this biogeochemical model for braunite formation must be considered speculative, particularly as there appears to have been no reports in the literature of braunite formation by microorganisms under laboratory conditions (Ostwald and Bolton, 1990). On the other hand, organic matter seems not to be abundant enough at Dounan to affect braunite formation, though the direct or indirect influence of bioactivity on formation of the Dounan braunite, as described previously, can be accepted. However, the geochemical activities of various microorganisms found at Dounan (see Table 2.7 and Plates 2.3 and 2.4) are at least associated with the physiological processes of manganese extraction from solution, even very dilute ones: with manganese oxidation and concentration in and around plant cells; with changes in the oxygen, CO₂, HCO₃ and H₂S regimes in interstitial and bottom waters (in conditions of syngensis) (Serdyuchenko, 1980).

Another example of a sedimentary origin for braunite has been reported by Serdyuchenko (1980), on the basis of the occurrence of the mineral in stratiform bodies in Precambrian rocks. He considered that the braunite facies were the products of coastal lagoons and evaporite flats, as

distinct from deeper-water, off-shore, marine-manganese carbonate sediments (rhodochrosite facies). He also quoted the experimental work of Listova to validate his model for braunite sedimentation, in which the braunite begins to precipitate from seawater at pH of 7.80-9.95 and Eh of 430 mV, although there is a salinity effect. Such a facies sequence appears to be similar to the Dounan case of proximal manganese oxide-transitional variety- distal manganese carbonate model (Stanton, 1972). This concept has apparently received larger confirmation.

The braunite mechanism in diagenesis was first suggested by De la Hunty (1966) in relation to the Manganese Group braunite occurrence in Western Australia. He described the braunite texture being consistent with concretionary growth in a sedimentary medium (Berner, 1980) and considered that the braunite nodules may have been converted from early diagenetic carbonate. However, Ostwald and Bolton (1990) suggested that the nodules grew as concretions within the unconsolidated sediment, which included accumulations of decaying biological material, on the basis of the traces of apatite found in the nodules examined. In addition, Miyano and Beukes (1987) introduced another diagenetic origin for braunite in Mamatwan-type manganese deposits in South Africa. However, the diagenetic change of Dounan braunite differs, to some extent, from those of the above cases, with straight forward secondary enrichment of primary braunite by recrystallization and replacement.

Supergene effects are rarely visible on the surfaces of weathered outcrops of Dounan manganese ore bodies, where pyrolusite, psilomelane, nsutite, and minor hausmannite are common. These minerals, together with some typical supergene textures, suggest alteration of earlier braunite and manganese carbonates. Considering initial precipitates and their successors formed through diagenetic and supergene processes, the mineralogical history of the Dounan deposits may have proceeded in the four steps with their characteristic mineral assemblages shown in Figure 6: (1) crystalline clastic (detrital) phases, formed in presedimentation stages; (2) poorly crystalline phases, as primary depositional products; (3) recrystallizing or replacing phases, evident in many ores of the deposits, formed during diagenesis; (4) supergene products converted from sedimentary-diagenetic materials.

The genesis of braunite has been described by Ramdohr (1969) and Roy (1981). Ramdohr (1969, p.966) states "The known occurrences indicate very different conditions of formation. Braunite is not at all rare in manganese ores formed at very low temperatures or which probably even formed through enrichment by lateral secretion involving surface water. It may here well have formed from a psilomelane-gel or from other similar manganese ore minerals. Braunite of all other localities formed at high temperatures and, at times, high pressures." Nevertheless, Roy (1981, p.35) describes "Braunite is a common mineral in metamorphosed sedimentary manganese oxide-silicate rocks (gondite). In some cases braunite has been suspected to have formed during diagenesis of Mn-oxide deposits. It is fairly common in hydrothermal deposits." Research on the Dounan manganese deposits has not confirmed the conclusions of Ramdohr

(1969) and Roy (1981) as to diagenetic, metamorphic and hydrothermal vein braunite, but it suggests a mode-of-origin as shallow marine sedimentary-diagenetic manganese deposits, formed in P-T conditions of sedimentary and diagenetic regimes in the total absence of hydrothermal/volcanogenic input and metamorphism. An attempt to simulate such processes in the laboratory under normal surface conditions would greatly enhance knowledge of low temperature braunite genesis.

Chapter 7 The Mineralization Model

7.1 Introduction

Above, detailed investigations focused on various aspects of the Mn oxide or carbonate orebodies to determine the type and geological history of overall ores and associated rocks at Dounan, Yunnan Province of China. Some of the presedimentary mobilization/transportation and sedimentary precipitation processes are now combined to produce a genetic model of the dominant primary depositional mechanisms of formation of the Dounan primary ores. Diagenetic remobilization and reprecipitation processes are then joined to yield another genetic model for the secondary enrichment mechanisms operating in the deposits. A sedimentary development concept and a diagenetic reaction cycle are examined and the following discussion puts primary and secondary products into context within an idealized stratigraphic section and mineralizing model. A comparison of the Dounan manganese orebody with other deposits assists in the definition of general concepts and their applicability to deposits with similar mineralogy and mode of origin.

7.2 Primary and Secondary Evolution of Dounan Ores and Rocks

7.2.1 Sedimentary Development of Primary Ores and Rocks

The subtropical conditions at Dounan in the middle Triassic created strongly changing geochemical environments affecting pre-existing Mn ores and Mn-bearing rocks in oldland source area through physical and chemical weathering. It is certain that weathering processes are influenced by such variations, because most weathering mechanisms directly depend on surface water to operate (e.g. Frakes and Bolton, 1992). Thus, it can be expected that mobilization, transportation and precipitation generally follow climatic as well as geochemical patterns. However, as the decomposition of the materials proceeds much slower than the weather changes, the geochemical

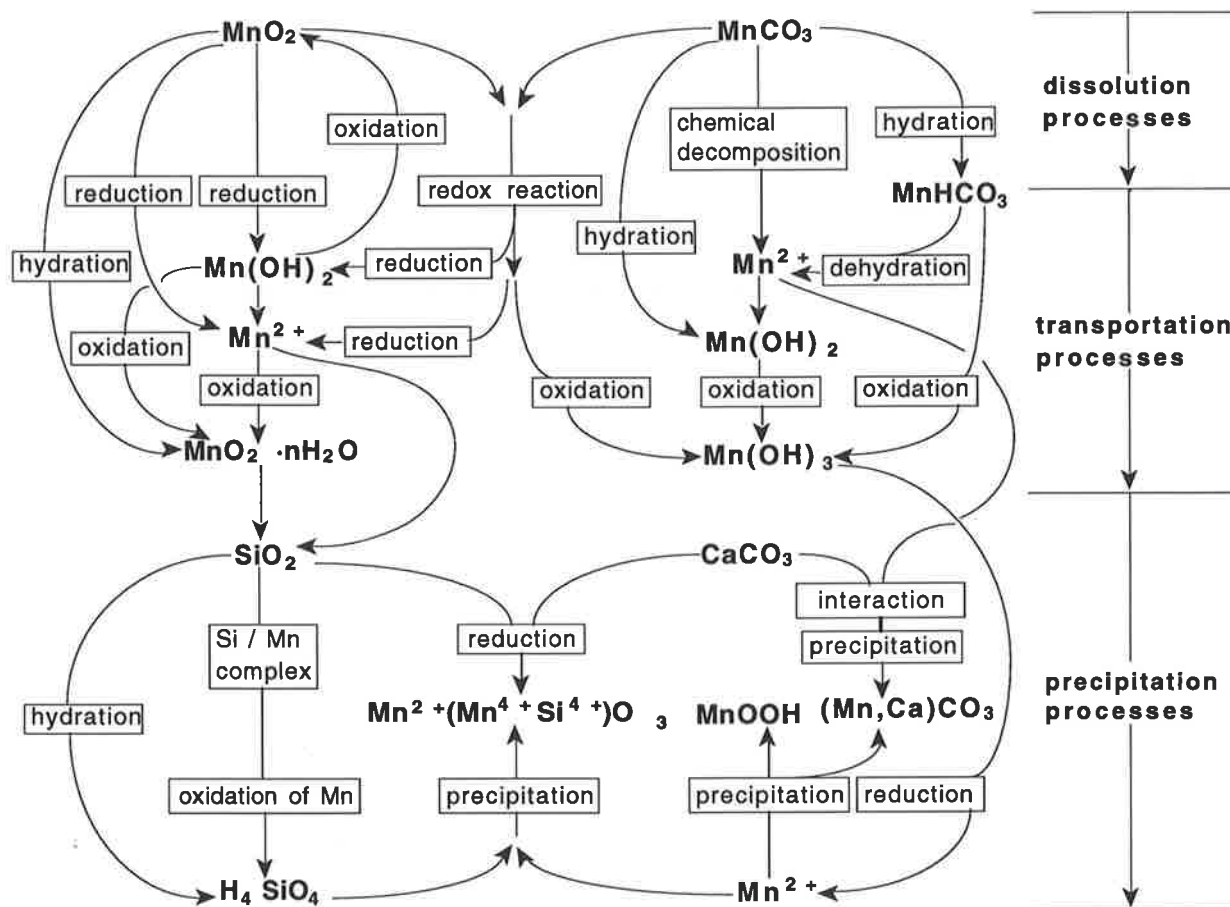


Fig. 7.1 Model of mobilization, transportation and precipitation paths for primary ore and gangue minerals in the weathering-sedimentary environment of Dounan.

reactions are likely to continue into the dry season. Mn was transported in solution in equilibrium to the sedimentary basin, where precipitation processes dominated.

The following model illustrates the mobilization, transport and precipitation processes as well as interactions between the main ore and gangue minerals of the deposits (Fig. 7.1). Processes relevant for the formation of each specific phase are summarized by a keyword such as oxidation, but mechanisms such as biogenic influences, are not described separately; further information is provided in the previous section. The model does not distinguish between different valency Mn oxides from oldland, because of their similar behaviors during mobilization processes and because of a lack of data. Contrasting with this necessary simplification for manganese, manganite is taken to represent the MnOOH mineral for an examination in aging processes of the later manganese precipitates.

Abundant surface water is necessary to start the model mechanisms for the formation of primary ore and gangue minerals. Therefore, the humid climate or wet season weather make Mn ores or Mn-bearing materials of the bedrock easily soluble by various chemical processes such as redox reactions and hydration. Manganese is liberated from unstable phases under the

influence of abundant water and other weathering processes. This dissolution of manganese materials from bedrock resulted from acidification of the aqueous system. The pH becomes low enough to decompose, reduce or oxidize pre-existing Mn materials to form various relatively stable loads (e.g. $\text{MnO}_2 \cdot n\text{H}_2\text{O}$, $\text{Mn}(\text{OH})_3$, Mn^{+2} , MnHCO_3^+) in river and/or subsurface waters, which transport them into the depositional basin. The dissolved manganese can either 1) form semi-stable manganese hydroxide, 2) be oxidized through contact with oxygen to a manganese dioxide gel suspension, 3) form stable $\text{Mn}(\text{OH})_3$ colloidal suspensions by redox reactions, 4) occur as ionic Mn^{+2} , or combine with HCO_3^- , forming bicarbonates. Many studies suggest that these are the main dissolution processes for transport. Additionally, experimental works (Momoi et al., 1992) have shown that the spherules or oolites of manganese oxide are easily synthesized in gel at a room temperature or lower and at one atmospheric pressure, which are very similar to nature manganese micronodules and oolites. Transport is followed by interaction between various dissolved elements or materials in the basin, leading to the precipitation of primary Mn ore and gangue minerals by various geochemical reactions.

The availability of dissolved silica and tetra-, tri-, and di-valent manganese in water is the major factor for the precipitation of braunite in the Dounan basin, although other parameters such as biological activity and Eh/pH cannot be neglected. Owing to restraints on the dehydration or precipitation of $\text{Mn}(\text{OH})_3$, however, only limited manganite precipitates. As in the formation of braunite, dissolved Mn^{+2} can precipitate in the formation of stable Mn-carbonate directly from the dehydration of manganese bicarbonates or from chemical reactions between Mn^{+2} and $\text{CO}_3^{=2}$ in the solution under a reducing environment. However, the presence of CaCO_3 or Ca^{+2} in the solution leads to a complex MnCO_3 - CaCO_3 series. This varying control of manganese and calcium over all Mn-carbonate phases is a clear indication of the continuous interaction of the various Mn-carbonate minerals examined so far, depending on their relative concentrations in the solution; otherwise different Mn-carbonate minerals (e.g. rhodochrosite) would have developed at Dounan.

7.2.2 *Cyclic Mobility of Diagenetic Products*

After the manganese materials are buried, the diagenetic conditions again create a strongly changing geochemical environment affecting both ores and rocks through the presence of pore or interstitial waters, and slowly rising temperature and pressure. It is certain that diagenetic processes are influenced by such variations, because all examined changing mechanisms directly depend on interstitial water, rising temperature and pressure to operate. Thus, it can be expected that diagenetic cycles generally follow the influences of diagenetic conditions such as pore or interstitial waters, pressure, temperature and microbial activity.

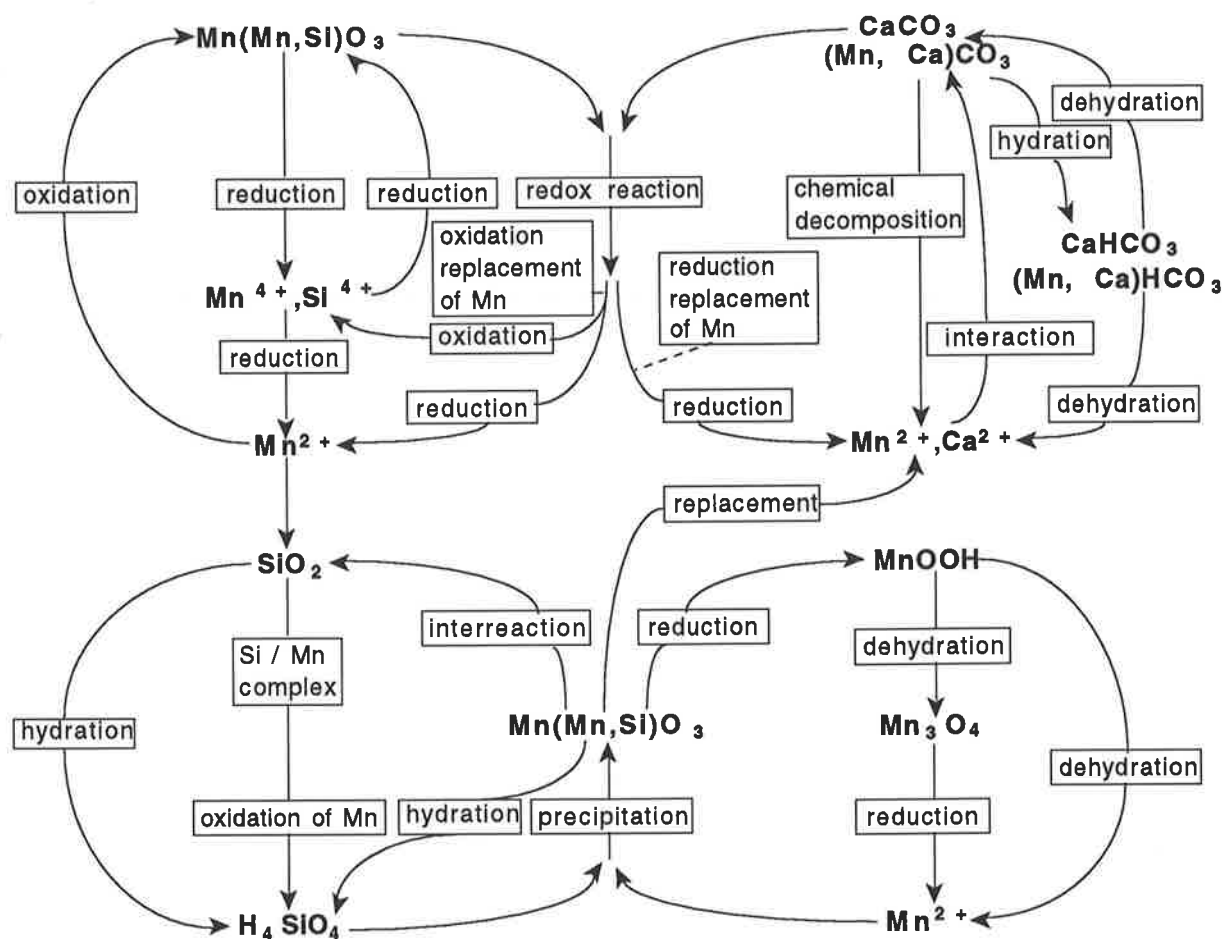


Fig. 7.2 Model of remobilization and reprecipitation paths for dominant diagenetic ore and gangue minerals in the buried environment of Dounan.

Figure 7.2 describes the model of remobilization and reprecipitation, illustrating interactions between the main ore and gangue minerals. Similar to those of primary ores and rocks, the processes relevant for the diagenetic formation of each specific phase are also summarized by a keyword such as hydration and oxidation, and biogenic mechanisms are not described separately. The model does not distinguish between different divalent Mn and/or Ca carbonates, because these minerals behave similarly during remobilization and reprecipitation processes. Although manganite ($MnOOH$) is rare in the deposits, it is incorporated in the model as a precursor for braunite during the alteration of Mn oxides.

To start the model mechanisms operating in the deposits during diagenesis, abundant interstitial water and rising temperature and pressure are needed. Therefore, the beginning of overburden load sets the parameters for all further geochemical reactions. Silica and manganese previously liberated from unstable phases co-precipitate as braunite under the influence of reduction. This Si-Mn oxide formation results in an increased acidification of the aqueous system with pressure solution developing in the vicinity of the newly formed mineral. Locally again, the pH becomes lower to further hydrate or reduce braunite to Mn^{4+} , Si^{4+} and Mn^{2+} . This mobilized manganese can either form semi-stable manganiferous silica complexes, or it can be oxidized through con-

tact with oxygen, or it can take part in redox reactions with carbonates. If braunite is remobilized through the formation of carbonate minerals, and many findings suggest that this is the main reduction process for this phase, the successive carbonate mineral development leads to the replacement of braunite by carbonates (see Plate 4.4, Fig. 19a; Plate 4.5, Figs. 19b-g, Plate 4.7, Figs. 27-33).

The availability of divalent manganese and calcium carbonates is the major factor for the reduction of tetravalent manganese in the Dounan deposits, although other processes such as microbial interactions with the ore may be involved. Nevertheless, redox reactions with carbonates seem to outlast other mechanisms, because carbonate replacements of Mn oxides are commonly found in the diagenetic ores. During the reaction, manganese predominantly dissolves as Mn^{+2} . Parallel to the reduction of Mn^{+4} , Mn^{+2} dissolved from Mn carbonates is oxidized and it precipitates at the reaction site, replacing braunite. This phase is also unstable and it alters to the generally more crystalline minerals of the same $Mn(Mn,Si)O_3$ group, i.e. recrystallization of braunite. The presence of divalent carbonate minerals in solution promotes a further alteration to braunite. This strong dominance of braunite over all diagenetic Mn phases is a clear indication of the continuous interaction of the minerals examined so far; otherwise different diagenetic minerals would have developed at Dounan.

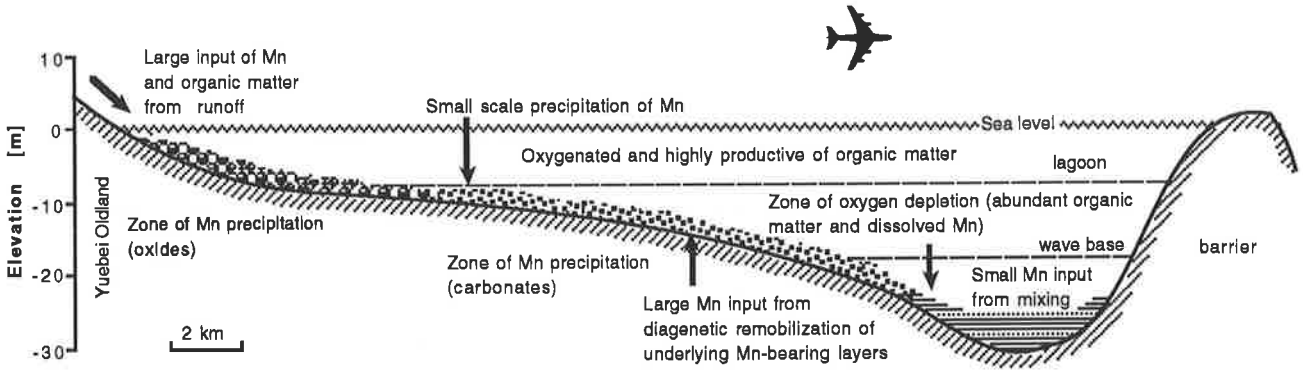
As in recrystallized braunite, dissolved divalent manganese can reprecipitate in the formation of Mn-Ca carbonate series under alkaline reducing microenvironments, due to successive reprecipitation of braunite, or they can reprecipitate surrounding primary grains by recrystallization. Thus, low-grade Mn carbonate ores are upgraded to economically significant concentrations. Nevertheless, the transformation or replacement to braunite from Mn carbonates, in particular, play a much more important role in upgrading the low-grade Mn ores to the high-grade Mn ores.

7.3 The Profile of Mineralization

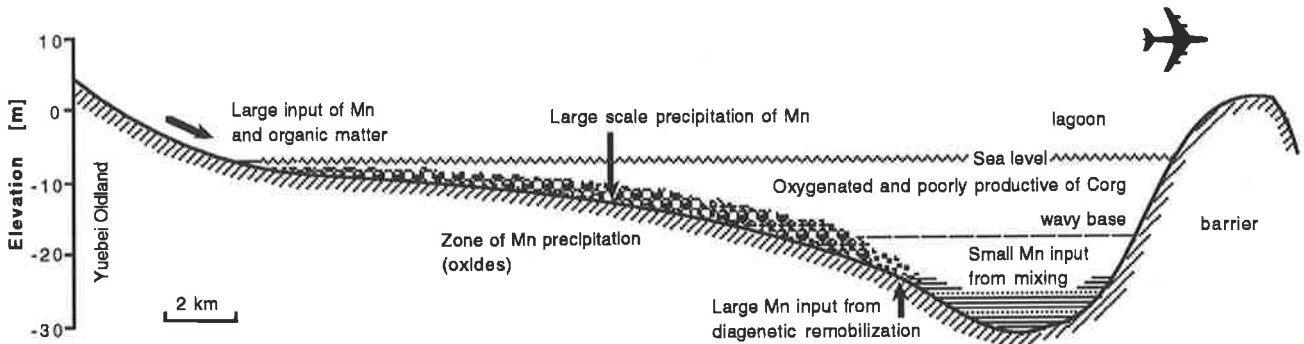
Contrary to detailed stratigraphic profiles and facies examined earlier, the following cross sections are greatly generalized to provide the geological context for the sedimentary-diagenetic manganese orebodies at Dounan (Fig. 7.3a). Secondary features of ores and associated rocks are shown in part IV of the Figure. The dominant directions of interstitial water or pressure solution movement associated with secondary processes are indicated by arrows (Fig. 7.3b; ref. to Pracejus, 1989).

Various suspensions in river waters such as Mn^{+2} , $Mn(OH)_3$ suspensoid and $MnO_2 \cdot nH_2O$ particulates or gel were transported into the shallow marine basin, in which the precipitation of primary Mn ores and associated minerals took place due to changes in the geochemical environments. During the transgression, high sea level enhanced the formation of oxygen-depleted

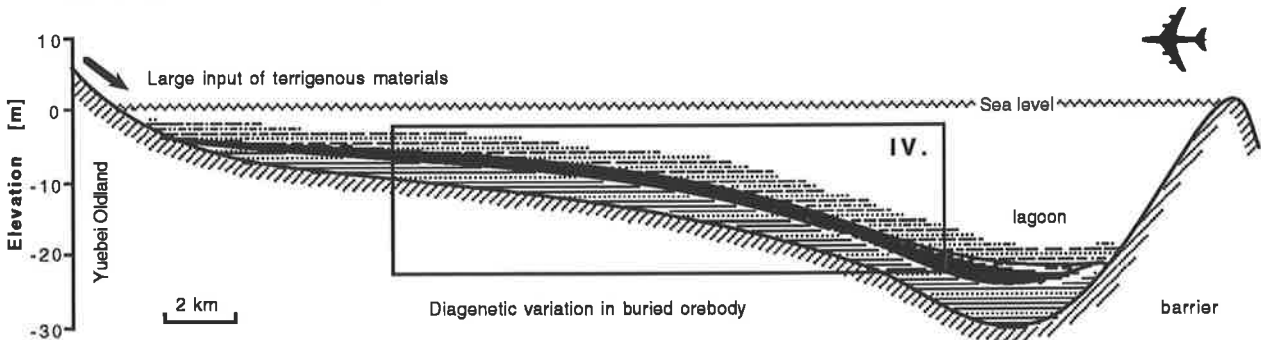
I. SEDIMENTATION OF MN CARBONATE OOLITES/PISOLITES DURING INITIAL REGRESSION



II. DEVELOPMENT OF MN OXIDE OOLITES/PISOLITES DURING REGRESSION



III. MANGCRETE EVOLUTION UNDER BURIED CONDITIONS



IV. ENLARGED SEGMENT

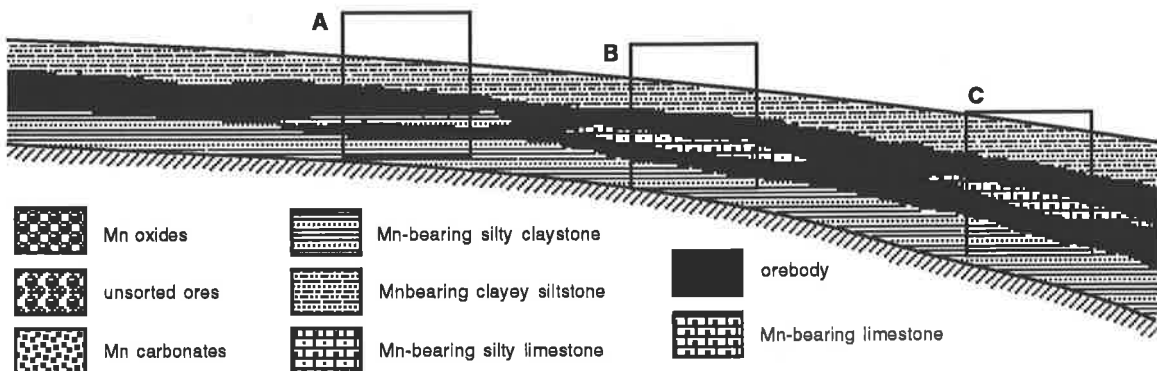


Fig. 7.3a: Idealized history of the Dounan Mn deposits; I. sedimentation of Mn carbonate oolites/pisolites during initial regression; II. development of Mn oxide oolites/pisolites during regression; III. buried variation; IV. enlarged segment of III; IV. details of IV. in Fig. 7.3b.

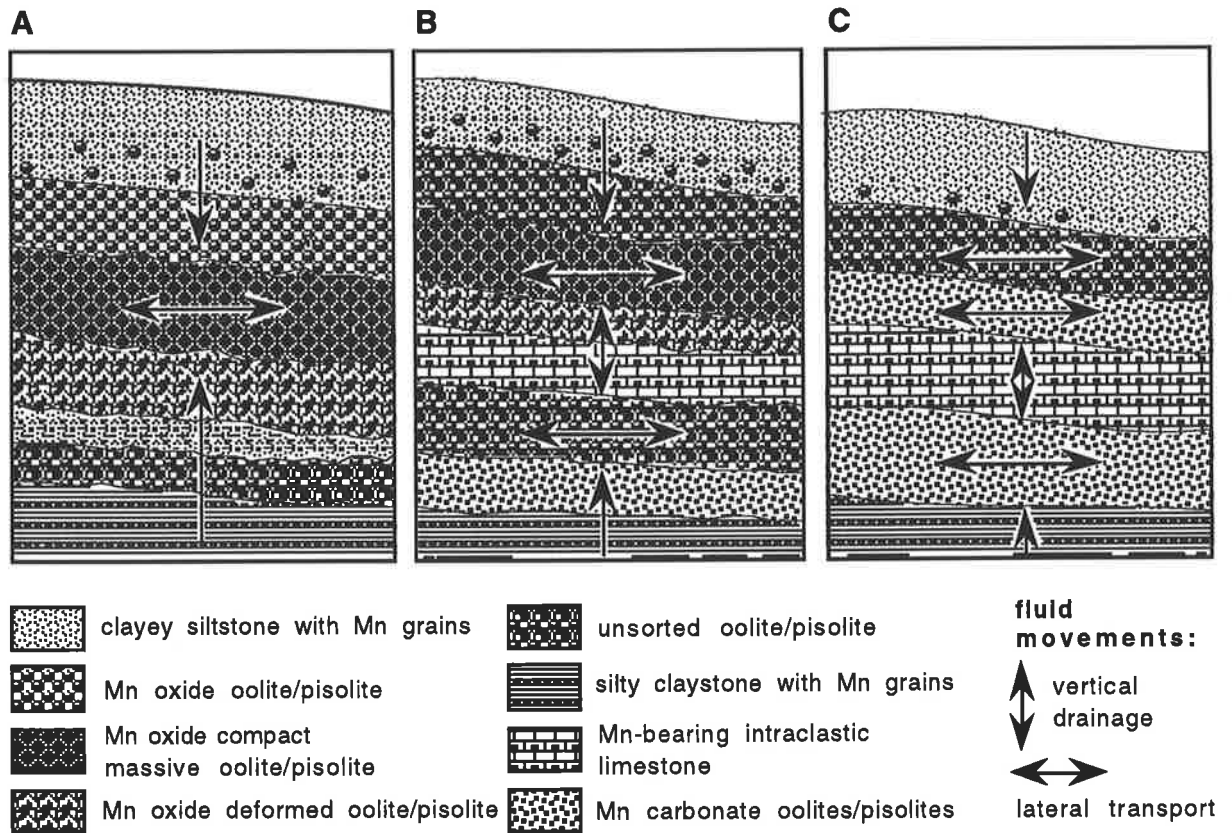


Fig. 7.3b Detailed sections of Fig.7.3a, IV; the capital letters correspond to the outlined geological positions of the previous figure; for explanation see text.

basin waters through increased organic productivity and led to the accumulation of manganese in solution (see Fig 6.10, after Frakes and Bolton, 1984). When the sea level is at peak or beginning to fall, i.e. at the initial period of regression, waters became oxygenated, leading to precipitation of manganese, first as the dominant Mn carbonates, and then with increasing oxygenation towards the coast, as minor Mn oxides (Fig. 7.3a, I). Thus, the dissolved manganese was concentrated in relatively anoxic waters of the basin during transgression and precipitated as carbonates and oxides during regression (Frakes and Bolton, 1984). The high energy tidal action in oxidation zone led to the accumulation of dominant braunite oololiths/pisoliths, whereas Mn carbonates precipitated mainly in deeper zones of reduction exhibit relatively few oololiths/pisoliths; instead, spheruliths and oncoliths dominated probably due to relatively low energy effects. Inverse grading in the ore was generated by increasing energy levels during basin shallowing. The transitional ores formed during the period of change from high to low sea level.

When relative sea level is low, regression enhances the formation of oxygenated basin waters, leading to precipitation of the dominant Mn oxides (Fig. 7.3a, II). The high-energy and chemical precipitating processes in the oxidation zone leads to strongly dominant braunite oolites/pisolites, with minor Mn carbonates located farther away towards the sea. Particularly, transitional environmental conditions lead to the development of the dominant ore type of the Dounan deposits, i.e transitional ores formed in the environment of varying levels of water anoxia. The

oxidizing environments seems to have been of more importance in the formation of transitional ores than reducing ones, because the Mn carbonate minerals occur only as cements. It is the regular variation between Mn oxide and Mn carbonate laminae either in concentric laminae in oolites/pisolites or in banded ores that evidently reflect fluctuating environmental changes. Additionally, the dominant inverse grading in the orebody suggests a general regressive effect during Mn deposition.

As sedimentation evolves, the ore develops as a stratiform body within an offlapping sedimentary sequence (Fig. 7.3a, III). The close contact of the ore with underlying Mn-bearing silty claystones and overlying Mn-bearing clayey siltstones as well as the intercalations of Mn-bearing intraclastic limestones (Fig. 7.3a, IV) suggests that many parts of the deposits are exposed to geochemical reactions associated with these clay- or lime-rich rocks during diagenesis. Also, as the orebody is buried, it undergoes various diagenetic geochemical reactions. In particular, the geothermal gradient and the overburden load can induce various physical and geochemical variations. Additionally, the mudstones below and siltstones above the ore form impermeable horizons, and interstitial waters must move through the ores. Also, pressure solution induced by overburden sediments provides extremely favorable conditions for the continuous activity of diagenetic alteration and enrichment processes.

In Figure 7.3b, sections of the buried profile are examined individually, starting near the margin and moving into the basin. It should be noted that the natural profile of mineralization does not necessarily contain all the features illustrated in one locality. "Multiple profiles" occur commonly in the form of repeated cycles of mineralizations. Incomplete mineralizing sections occur where local factors, inhibited development.

Where various Mn oxide ores/unsorted ores and overlying siltstones/underlying mudstones occur together in the shallow part of the basin, diagenetic Mn enrichment leads to development of compact massive oolite/pisolite (Fig. 7.3b/A). The orebody mainly consists of Mn oxide oolite/pisolite, deformed and massive oolites/pisolites as well as minor unsorted ores with sizes ranging from oolites to pebbles. Below and above the orebody, mudstones and siltstones generally contain manganiferous spherulites and Mn concretions which are stratigraphically distributed. Also, intercalations composing silty claystone contain relatively more manganese than elsewhere. The diagenetic ores from this part are related to recrystallization processes, where oxidation is the main controlling factor. The Mn-bearing solutions derived from both upper and lower horizons, infiltrate the Mn oxide oolite/pisolite layers which are highly porous and permeable. The solution moves laterally within the Mn oxide oolite/pisolite horizon and eventually reprecipitates Mn oxide, reforming some layers of Mn oxide oolite/pisolite into compact massive ores.

Further into the basin, the transitional zone develops, consisting of the unsorted ore phase and displaying relatively dense cementation of predominantly Mn carbonates (Fig. 7.3b/B). Commonly, Mn-bearing intercalations composed of intraclastic limestone occur in the orebody, through which water can move readily by vertical drainage, to unsorted ore horizons. The Mn-bearing solutions moving upward to the Mn oxide oolite/pisolite layer reprecipitates Mn by the same process as in the case of Figure 7.3b/A under oxidation. Solutions draining to lower unsorted or Mn carbonate oolites/pisolites horizons also move laterally along these horizons, and mainly reprecipitate as both braunite and Mn carbonate minerals by recrystallization or replacement. Development of braunite in this section strongly depends on the availability of oxygen. This secondary ore generally decreases in quantity with increasing depth. At depth, the extent of the process is obvious, because these horizons permanently contain water and replacement reactions are continuously in process.

Further again into more reducing areas of the basin, Mn carbonates develop when primary Mn ores are replaced by dense secondary Mn-phases, which overprint initial structures and textures (Fig. 7.3b/C). Sparite cemented mangcretes can grade into good quality ores. The Mn-bearing solutions derived vertically from both overlying and underlying Mn-bearing rocks as well as Mn-bearing intercalations of intraclastic limestone, move laterally within Mn carbonate oolite/pisolite due to relatively large permeabilities. It seems that recrystallization plays more an important role than replacement in this part, where the cementation is usually associated with coarser grains. Carbonate ores commonly underlie primary unsorted ores, and thus alteration of the latter ores mainly derives from diagenetic processes mobilizing manganese from overlying layers or within its own horizons of the section, and reprecipitating the materials within the lower layers. At the contacts between the Mn carbonates and intercalated Mn-bearing limestone, calcium can replace primary Mn-ores, thus, creating "Ca-oolites/pisolites". Such liberated manganese is reprecipitated within Mn carbonate ores as recrystallized products, up grading primary ores into high quality.

7.4 The Model of Mineralization

The stratigraphic characteristics of Dounan section reflect alternations between terrigenous clastic and carbonate (intraclastic) sedimentary environment. It is in such mixed environments that the mixed Mn-bearing rock association formed, and where later diagenesis led to secondary enrichment of primary ores. Based on the genetic analysis above, an idealized model of mineralization through the Dounan manganese deposits can be established (Fig. 7.4), which includes the following processes and controls:

- the high degree of mobility of manganese, particularly through redox or other chemical processes, insures that it can change phase during weathering, transport, deposition, and diagenesis;

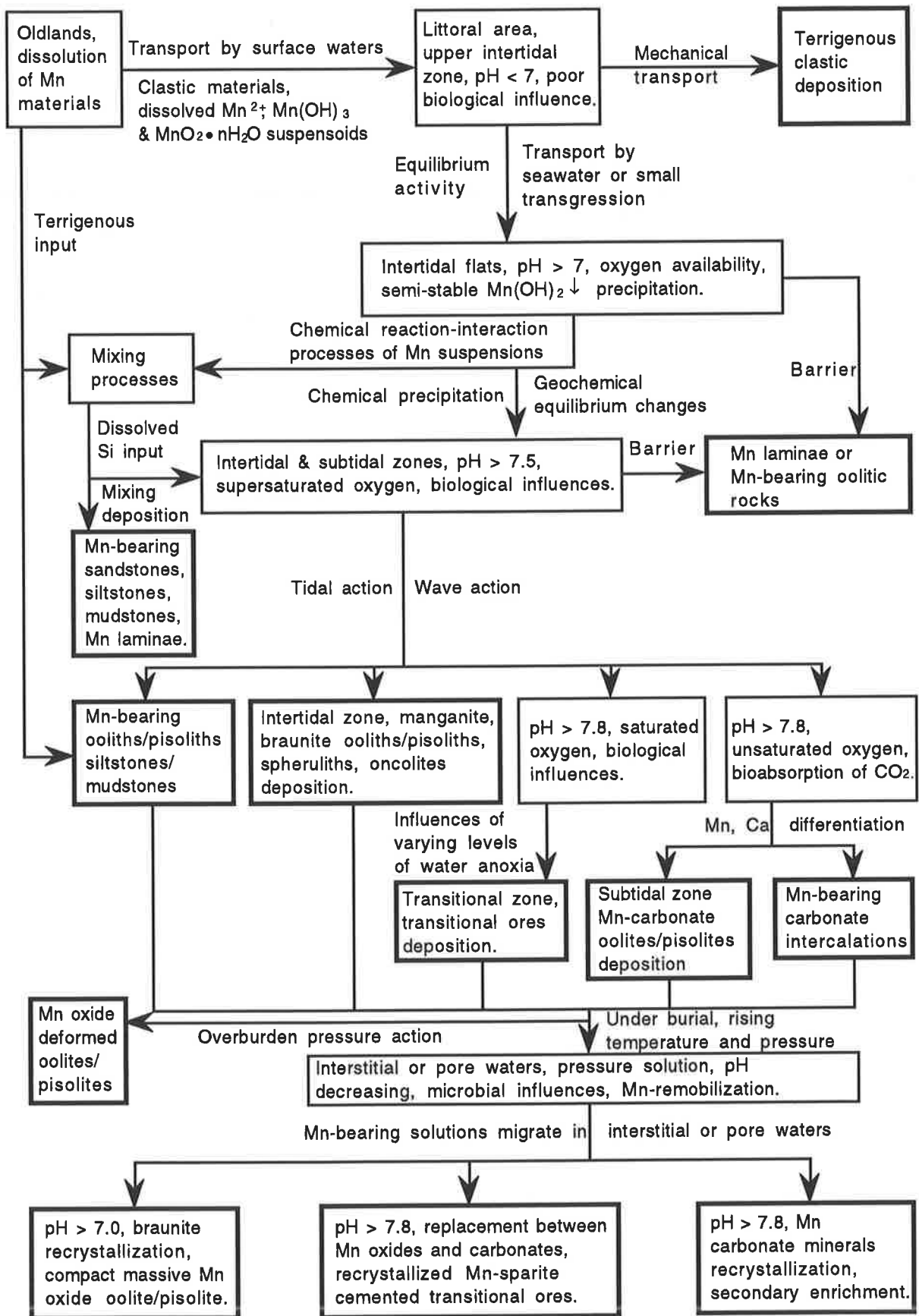


Fig. 7.4 Idealized model of mineralization through the Dounan manganese deposits.

- manganese materials were derived from (mainly Yuebei) oldlands and transported to the marine basin by surface and subsurface waters;
- in the littoral or supratidal area, only Mn-bearing or Mn-free terrigenous clastic rocks were deposited, probably due to low pH and poor biological influence;
- farther into the basin, the environmental conditions on intertidal flats were favorable for dissolved Mn to precipitate, but in the deeper areas of the barrier-lagoon only Mn oolite/pisolite-bearing rocks formed, probably due to low concentrations of Mn and unfavorable environmental conditions (e.g. pH/Eh, biological influence);
- various Mn oolites/pisolites mainly resulted from tidal action of variable energy;
- varying levels of water anoxia were responsible for the formation of transitional ores, including alternating concentric laminae composed of both Mn oxides and carbonates in oolite/pisolite;
- variations in microenvironmental conditions led to the formation of different ore phase;
- very early diagenesis was in the form of deformation of unconsolidated oolites/pisolites due to overburden load;
- after the Mn deposits and associated rocks were laid down, they were affected by early diagenetic processes; various buried Mn ores and associated rocks were remobilized and reprecipitated in the same mineral assemblages as primary ores, but with increased Mn concentrations;
- under diagenetic influences, many primary ores were partly or entirely converted to deformed or massive Mn oxide oolites/pisolites; others were little altered and survived as primary Mn oxide oolite/pisolite;
- with higher intensity diagenetic conditions, there was very little apparent change in the mineralogy of the deposits, although there may have been slight changes in the composition of some of the Mn carbonate minerals (e.g. from Mn-bearing calcite to Mn-calcite or to calciorhodochrosite). Braunite and Mn carbonate minerals became coarser in texture in the zones of intense diagenesis, but they do not appear to be more abundant in deformed oolites/pisolites than in primary ores. Reactions through a fluid phase best explain the observed relations of the primary ores and diagenetic products;
- thus, during chemical weathering, manganese was solubilized in acid, reducing conditions and carried in surface and subsurface waters to the coastal zone, where many of the exploitable ore-bodies formed in slightly reducing (carbonate ores) to oxidizing (oxide ores) conditions. The deposits show compositional zoning and display evidence of having been deposited in shallow-marine environments following accumulation of a dilute ore solution within the basin. Manganese was precipitated when the environments of the basin became oxidized, apparently during early stages of marine regressions (Frakes and Bolton, 1992).

7.5 Review of Sedimentary and Diagenetically Influenced Mn-Deposits

An idealized section through the orebody and the genetic model of Dounan Mn deposits were developed above to demonstrate that the sedimentary-diagenetic processes consistently produce distinct ore and rock types. Below, a few other manganese deposits of the "non-volcanogenic-sedimentary-type" (Roy, 1981), which include the Dounan ores, are discussed to examine whether the same primary ore/rock types and secondary features appear elsewhere under similar primary /diagenetic conditions, and whether formation conditions can be generalized.

In view of the fact that the syngenetic manganiferous ores of Dounan have, to some extent, been changed during diagenesis, it is pertinent to compare them with those deposits in other parts of the world that have undergone the same or similar modes of formation and transformation, and even have similar main ore minerals. In this respect, the mineralogical assemblage of the ores and associated rocks, grade of diagenesis and the nature of the changing ores/rocks may have to be critically examined. Consequently, the scope and aim of this section is limited to a critical analysis of the nature of the syngenetic sedimentary manganese formations of the world, whether they have undergone secondary changes or not, and to indicate the position of the Dounan ores among them. Such sedimentary (or diagenetic) manganese formations occur in different parts of the world, e.g. Brazil, U.S.A., Australia, Ghana, Namibia, Madagascar, Sweden, the former U.S.S.R., India, Japan, China, etc. The bulk of developed deposits consist of oxide or carbonate minerals or both and these have generally been assigned to origins related to redox conditions during sedimentation or early diagenesis.

However, in only a relatively small number of Mn deposits have syngenetic sedimentary ores developed further to yield diagenetic minerals; in most cases primary ores have been metamorphosed to variable degrees. Recently, a few descriptions of manganese occurrences from Western Australia (Ostwald and Bolton, 1990) and China (e.g. Fan et al., 1988; Su, 1983) indicate that similar mineralizing patterns can be explained by syngenetic and diagenetic models identical or comparable to those at Dounan. It is worth noting that the assemblage of braunite-Mn carbonate minerals-calcite-quartz is very rarely described in context with sedimentary-diagenetic processes. This suggests that geochemical reactions or conditions like those discussed earlier are probably unusual, but that the proposed model section may prove to be useful in other deposits when additional studies are made.

7.5.1 Nikopol, Ukraine and Chiatura, Georgia

The sedimentological characteristics and the development of the giant manganese deposits at Nikopol and Chiatura are described by Varentsov and Rakhmanov (1980). The genesis of the two deposits is said to be very similar. The ores contain primary Mn oxides and Mn carbonates, both as oolites/pisolites set in massive matrix. In some localities, among the patches of manganese oxides there are relics of poorly or strongly oxidized carbonate ore. Gryaznov and

Danilov (1980) suggested a transformation of the primary manganese hydroxides to Mn-carbonates under reducing conditions. The manganiferous sediments were deposited in the shallow western parts of the manganiferous paratethys seaway and the ores accumulated under conditions of slow terrigenous sedimentation. Bolton and Frakes (1985) presented a model of oxidation-reduction interface controlling the formation of ores for the Chiatura deposit, and they found that primary sedimentary pisolites and oolites, locally in graded units, form much of the oxide facies ore at Chiatura. Also, Force and Cannon (1988) have observed apparently primary pisolites in specimens of ore from Nikopol.

Later, as a result of diagenetic processes acting in the presence of relatively large amounts of organic matter, Mn oxides were transformed to carbonates. From these initial ores/rocks, supergene hydrated Mn oxides and carbonates formed supergene ores, all of which can be seen in the Dounan deposits; the mineral assemblages differ somewhat (e.g. dominant manganite as Mn oxide at Nikopol, braunite at Dounan). The coincident appearance of the main manganiferous products and mineralization indicates the existence of similar geochemical environments to those described earlier from Dounan; the slight differences in the mineral assemblages probably reflect different sources of material or different depositional microenvironments. Thus, the ores of both Nikopol/Chiatura and Dounan occur in sedimentary-diagenetic and secondary oxidized deposits; the exception is that primary processes were predominant at Dounan. However, it has been noted that the carbonate ore of Nikopol/Chiatura were formed during diagenesis when primary accumulations of manganese oxides were combined with CO₂ produced by decomposition of organic matter in a relatively reducing environment (Varentsov and Rakhmanov, 1980).

7.5.2 *Groote Eylandt, Australia*

The Groote Eylandt manganese oxide deposits of northern Australia primarily consist of pyrolusite and cryptomelane. The manganese ore is considered to be a shallow (15-50 m water depth) marine sediment, which predominantly accumulated as accretionary ooliths/psisoliths, with later modification during diagenesis (Slee, 1980; Varentsov, 1982; Bolton and Frakes, 1988; Frakes and Bolton, 1984; Bolton et al., 1988); supergene alterations later overprinted the ores (Ostwald, 1980; Varentsov and Golovin, 1987; Pracejus, 1989; Pracejus et al., 1988). A number of sedimentary-diagenetic ores/rocks are comparable in many aspects with the depositional profile observed in Dounan, although the Mn mineral assemblage of Dounan is different. According to Frakes and Bolton, deposition was in two separate subbasins; oxide facies accumulated in the first subbasin at shallow depth, and carbonate facies at greater depth (> 90 m) in anoxic to dysaerobic water of the second subbasin. The second subbasin has an estuarine facies also containing manganese oxides. Recently, Ostwald (1990) suggested that these pisoliths and ooliths satisfy specific criteria for biogenetic origin and thus they appear to be manganese oxide oncolites. He considered that this deduction is consistent with the presence of a variety of

manganese-oxide structures interpreted as stromatolitic in origin in the orebody. Dounan ores contain similar structures but some of them have been interpreted as resulting from colloform precipitation, probably not involving biological activity.

There are many similarities between the two deposits in terms of mineralizing mechanisms, although there exist some differences in ore and rock types. Because the climatic and geochemical conditions were very similar, the precipitating tracks for the formation of primary phases seem to be the same as well. The differences of ore and rock types probably resulted from the different sources of materials and forming environments between the two deposits. Thus, the following manganese minerals reported from the Groote Eylandt deposits are absent or very rare in the Dounan primary ores: pyrolusite, cryptomelane, manganite. In addition to common recrystallization and replacement, some new products of diagenesis at Groote Eylandt may have formed by the replacement of clayey sands and sandy clay (Slee, 1980), suggesting more complex mineral assemblage in primary ores than at Dounan.

7.5.3 *Molango, Mexico*

The Molango manganese deposit in Mexico is by far the largest known Mn deposit in North America. Reduced facies manganese carbonate deposits of Jurassic age form a large deposit in Hidalgo exposed over an area 20 by 50 km. The best published descriptions are currently abstracts by Alexandri et al. (1985), Okita et al. (1986) and Okita (1992). Similar to Dounan, the Jurassic sequence is folded but not metamorphosed. The ore, a sedimentary manganese carbonate rock, is mostly barren of fossils, but adjacent beds yield fossils which show that the deposit is Oxfordian to Kimmeridgian (Late Jurassic) and accumulated under marine conditions. The ore horizon forms part of a shallow-marine sequence. The ore is 1- to 9-m-thick layer and typically contains 27 percent Mn. The bottom half of the formation consists of finely laminated dark carbonate with about 2 to 3 percent organic carbon and 0.5 to 4 percent pyrite. Fine laminations and cotted textures suggest deposition in a restricted marine environment.

Ore is underlain by a carbonate unit about 1 m thick that is low in manganese, and by a shell lag at the top of the underlying Santiago Formation. Ore itself consists of finely laminated dark carbonate rock with a pelletal to intraclastic texture and consists essentially of rhodochrosite with minor talc-chlorite. Ore is overlain by similar-looking laminar dark carbonate with progressively less Mn going up section. Rhodochrosite rocks (ore) and the rhodochrosite fraction of two phases assemblages show $\delta^{13}\text{C}$ values of -14 to -9 per mil, whereas values for Kutnohorite [$\text{CaMn}(\text{CO}_3)_2$] are -4 to -7 per mil and for Mn calcite, -2 to 0 per mil. Passing upward from ore, a storm concentration of large bivalve shells and oolitic structures occur, and a massive oolite bed is present toward the top of the formation. However, no primary oxide facies manganese deposits have been found in the district. The fauna and admixed ooids of the carbonate ore are

consistent with deposition just below a water column oxidation-reduction interface (Force and Cannon, 1988). Textural and carbon isotope evidence shows that manganese carbonate is early diagenetic, formed by replacement of calcareous sediments. The recent study (Okita, 1992) suggested that the deposits formed as a very early diagenetic product of Mn oxide reduction coupled with sulfide and organic carbon oxidation. Although the deposits only contain the protore for supergen Mn oxide facies, the geochemical environment and mineralization can at least be compared with those of Dounan Mn carbonates.

7.5.4 *úrkút / Eplény, Hungary*

Similar to many other manganese deposits, the ores in the *úrkút* basin primarily consisted mainly of rhodochrosite and manganocalcite with possibly smaller amounts of additional primary oxides in the northern part of the basin (Szabó and Grasselly, 1980; Grasselly and Pantó, 1988). Manganese in the sedimentary basin of *úrkút* originally accumulated as carbonate during the Upper Liassic. The carbonate ores have been oxidized, eroded and redeposited. Since the deposits contain many sulfides, such as pyrite, the geochemical environment and source of materials of primary ores is certainly much different to those previously discussed. Layered (laminar) manganese oxides in the *úrkút* deposits resulted from *in situ* oxidation of primary carbonates and they are most probably not comparable to the Mn oxides at Dounan.

According to Polgári et al. (1991), the $\delta^{13}\text{C}$ values of the *úrkút* carbonates show a negative linear correlation with Mn contents and a negative exponential correlation with total organic carbon contents. These relations suggest that the deposit was produced by early diagenetic precipitation of manganese carbonate. Thus, the mineralization was a consequence of bacterially mediated diagenetic reductions. Oxygen-deficient water in the depositional basin acted as a carrier and reservoir for Mn^{+2} before its deposition. This is, to some extent, similar to isotopic features of Dounan Mn deposits.

7.5.5 *Braunite Mn Deposits of India, West and North Africa, Former USSR, and Brazil*

From the studies of Indian Mn deposits by Roy (1966, 1980) and Dasgupta et al. (1992), manganese ore deposits of India are all restricted to the Precambrian formations and almost occur as syngenetic bed in the metamorphosed sequences. The Mn oxide ores are generally composed of braunite, bixbyite, jacobsonite, hollandite, and hausmannite. These ores are devoid of any manganese carbonates and were laid down as syngenetic oxide sediments. India seems to exhibit ore types similar to some ores at Dounan (e.g. braunite), although its mineralogical assemblage is, to most extent, different to that of Dounan. However, the reaction processes of various metamor-

phic degrees have implied that it is impossible completely to compare the deposits with those of Dounan.

However, Dasgupta et al (1992) recently concluded that the sediments were deposited in a stable shelf environment, and the oxide ores were formed when anoxic bottom water enriched in Mn^{+2} was welled up on the continental margin and mixed with oxygenated surface water; Mn carbonates were diagenetically derived from oxides by reaction with calcareous partings in isolated pools under evaporative conditions, whereas Mn silicate admixtures were produced as a consequence of influx of detritus during sedimentation. This interpretation is, to some extent, similar to that of Dounan. The majority of the sedimentary-metamorphic Mn deposits of other countries, on the other hand, consists of Mn carbonates and carbonate-silicate rocks (e.g. Brazil, West and North Africa, former U.S.S.R., Roy, 1980; Brazil, Urban et al., 1992). The exceptions are those of Dounan are not sedimentary-metamorphic in origin, though most of the also contain braunite as main Mn mineral. This preferential association of Mn carbonate with carbonaceous horizon in these countries reflects either a direct sedimentation of manganese as carbonate in reducing condition or diagenetic change of Mn oxide to carbonate in the presence of organic matter now represented by carbonaceous horizons, which probably similar to the case of Dounan.

Similarly, diagenetic features are prominently displayed by these manganese deposits and associated rocks. Differently, the extensively metamorphosed manganese orebodies/rocks of these countries have been investigated in detail in respect of their mineralogy and texture. Thus, it has been established that these syngenetic manganese oxide sediments were subjected to reduction during metamorphism and a low oxide assemblage resulted in the metamorphosed orebodies. However, any metamorphic evidences or associated features are not found in Dounan area.

7.5.6 Manganese Group of Western Australia

Recently, the diagenetic braunite in sedimentary rocks of the Proterozoic manganese group in western Australia are described by Ostwald and Bolton (1990). Braunite occurs in shale as flattened concretions which post-date the shale sedimentation and pre-date lithification, According to them, the braunite may have grown as concretions in the still-moist sediment by reaction between Mn^{+2} , liberated from older manganese oxides by decay of trapped organic remains, and silica, and polycrystalline braunite resulted from recrystallization of an older generation of braunite of undefined genesis, most of which can be comparable with diagenetic products of Dounan. Both two braunite occurrences show no evidence, either mineralogical or textural, of a hydrothermal or metamorphic origins, as discussed by Roy (1966, 1980, 1981). Also, various interpretations of the stratigraphic occurrence of the Manganese Group stress its occurrence within sediments of a transgressive/regressive cycle, although the early manganese mineralization can only be surmised, probably including manganese carbonates and oxides (Ostwald and Bolton,

Table 7.1 Comparison of sedimentary-diagenetic products from different localities.

Products	Localities						
	Dounan China	Nikopol/ Chiatura USSR	Groote Eylandt Australia	Molango Mexico	Úrkút Basin Hungary	Deposits of India,USSR, S.W. Africa, Brazil	Mn Group of Western Australia
Ooliths/pisoliths or spheruliths	*	*	*	(*)	(*)	*	(*)
Primary fabricas	*	*	*	*	*	*	n.d.
Mixing concentric rings between Mn oxides and carbonates	*	n.d.	n.d.	n.d.	n.d.	n.d.	n.d.
Transitional ores	*	n.d.	n.d.	n.d.	n.d.	n.d.	n.d.
Deformed ooliths/pisoliths	*	n.d.	n.d.	n.d.	n.d.	*	(*)
Massive mangcrete	*	*	*	n.d.	*	*	(*)
Mn carbonates	*	*	*	*	*	(*)	(*)
Biological influence	*	*	*	*	*	n.d.	n.d.
Synsedimentary deposition	*	*	*	*	*	*	*
Redeposition	*	n.d.	n.d.	n.d.	*	n.d.	n.d.
Diagenetic changes	*	*	*	*	*	*	*
Microbial influence	*	*	*	*	*	*	*
Supergene overprint	*	*	*	*	*	*	n.d.
Metamorphism	n.d.	n.d.	n.d.	n.d.	n.d.	*	n.d.
Braunite	*	n.d.	(*)	n.d.	n.d.	*	*

* the information are mentioned, for their relevance in sedimentary-diagenetic processes at Dounan; n.d. = not described.

1990). The similar appearance of diagenetic braunite developments indicates the existence of the similar diagenetically mineralizing mechanisms described earlier from Dounan.

7.5.7 General Comparison of Sedimentary-Diagenetic Products in Different Areas

When all the information about sedimentary-diagenetic products from the discussed localities are considered, the following comparison emerges (Table 7.1). Most of the marine manganese deposits described herein show a spectrum from oxidizing to reducing depositional conditions. Several deposits show two members of the spectrum in zonal relations. Carbonate facies manganese deposits can apparently be oxic, dysaerbic, or reduced, whereas oxide facies deposits are everywhere oxic. All the deposits, from any part of the spectrum, have several features in common: (1) shallow-marine sedimentary deposition with oolites/pisolites, unrelated or probably only indirectly related to volcanism; (2) deposition at margins of basins; (3) little clastic dilution; (4) mostly diagenetic alteration. Sedimentary and diagenetic products and features from Dounan can be detected in most other deposits. Ooliths/pisoliths, massive mangcrete, Mn carbonates,

primary fabrics and precipitation, diagenetic changes, and supergene overprint, etc. are commonly found in many places. Deformed grains seem to be restricted to early diagenetic deposits, and only the redeposition of Mn grains is restricted to Dounan and Úrkút deposits, although the materials are not directly comparable, whereas metamorphism is common to be seen in the man-ganese deposits of India, Brizal, West and North Africa, South Africa and Madagascar, in which braunite dominates. It is very interesting and significant to see that mixing concentric rings of ooliths/pisoliths composing both braunite and Mn carbonate minerals, transitional ore phase, and biological influence in sedimentation are only associated with Dounan primary ores, also, obviously, only Dounan braunite play a dominant role in the formation of primary manganese ores, which has significantly added to the knowledge of the mineralogy of braunite.

7.6 Discussion

The genetic model above illustrates that many of the sedimentary-diagenetic processes are interdependent and that the source materials and geochemical environments effectively control the formation or reformation of associated phases. The best example for this dependence is the promotion of braunite development by the presence of dissolved Mn and Si in oxidation zone. If for instance the precipitation of minerals in relatively slight reduction or oxidation such as Mn carbonate and transitional phases are supported instead, chemical or redox reactions between Mn, Si, O and carbonates will certainly be less prevailing in the deposits, because less tetravalent Mn and Si as well as O would be available from these environments due to their reduction. With the evolution of regressive Mn sedimentation, the interactions of microenvironments lead to specific three ore phases at Dounan, this can also be strongly supported by the Dounan transitional sedimentary products which are considered a response to vary levels of water anoxia. Thus, a deposit similar to Dounan but which lacks one of the main factors (e.g. different valent dissolved Mn, Si, O, Eh/pH, wave action, biological activity, etc.), thus inhibiting any of the necessary processes, is unlikely to develop prominent primary units.

As most of these deformed and massive oolites/pisolites as well as recrystalline Mn carbonates are bound to specific (buried) geological positions, it is possible to generalize the description of various diagenetic features and materials. In some aspects, the diagenetic mangcrete profile recognized in this study also seems to be applicable to other deposits. Although elsewhere protores and remobilization processes can be totally different, the final products are partly similar to the secondary ores described from Dounan (e.g. the Manganese Group of western Australia; Oswald and Bolton, 1990). The mangcrete model should, therefore, be applicable to a wide variety of other diagenetic manganese deposits with necessary adaptations to additional remobilization and reprecipitation processes.

The above review of available literature for comparison shows that most of the important sedimentary-diagenetic manganiferous formations of the world were originally laid down as syngenetic sediments. The manganese formation of Dounan has been conclusively proved to be synsediments and most of the earlier workers subscribe to this view. However, the study of this text evidently emphasizes secondary enrichment besides the synsedimentation of the manganiferous sequence, and conclusively excludes the possibility of metamorphic effect. In case of compared deposits of manganiferous rocks and associated ores, the most occurrences of Mn oxides, which have a common mineral assemblage such as pyrolusite and cryptomelane, are generally considered as sedimentary (or-diagenetic) products and that they were formed in similar environments; whereas the Mn oxides mainly composing braunite are commonly and universally described as metamorphic products and few examples of diagenesis. Such a conclusion is, however, rather too generalized and may lead to misconception because the view of synsedimentary braunite is first suggested by the Dounan case to be donated to the knowledge of the mineralogy of braunite.

Chapter 8 Résumé and Conclusions

According to the descriptions and discussions in previous chapters, the genetic history of the manganese ore deposits discussed in this text may now be summarized as follows:

- The Dounan Triassic sedimentary basin lie on the southern margin of southeastern Yunnan marine sedimentary province, southerly facing to Yuebei Oldland which through different geological times contains abundant Mn-rich ores/rocks, probably constituting the sources of Dounan manganese materials. Structurally, the long-term evolution of the Dounan syncline leads to the formation of the Dounan Triassic marine basin.
- The stratigraphy of the Dounan Mn deposits exhibits both clearly defined and unmetamorphosed primary ore and rock units. These manganese ore deposits have been shown to be completely restricted to two Mn-bearing horizons in the stratigraphic sequence of the Dounan Falang Formation, both associated with the association of carbonate-terrigenous clastic rocks. The orebodies are strictly conformable with enclosing members in the Falang Formation, and there is no any macroevidence of post-depositional events in the formation. The examination of the Dounan sequence and its environment indicates that the primary sedimentary mineralization could play a more important role in the genesis of the Dounan Mn deposits than other secondary events such as diagenetic processes. The sedimentary environmental evolution of Dounan Falang Formation suggests that both two manganese horizons formed in transgressive /regressive cycles, developed mainly in intertidal-subtidal areas with high energy. Also, biological activity may play a considerable role in the formation of the Dounan Mn ores. This fact is emphasized by the participation of biota in the mineralization of the Dounan Mn deposits.
- Examinations of the orebeds indicate that all manganese ores and associated rocks occur as stratiform or bedded-like layers, showing clear conformable relations with their enclosing rocks.

The lateral distribution gaps of the ore units between neighboring mine-areas probably are indicative of upwell basements or sub-basin events during the deposition of the Dounan Mn deposits or an interruption of the manganese input. Over ten Mn orebeds occurring in regularly vertical intervals and laterally imbricate distribution not only suggest that they formed in similar geochemical environments but also indicate a regressive migration of the mangiferous sedimentary basin respectively, which is also strongly supported by dominantly reverse gradings in the orebodies. Structurally, all orebeds are controlled in the Dounan syncline and their thickness generally become considerable thinner or even disappearing with increasing depth, reflecting an importance or significance of oxygen availability in the basin during mangiferous sedimentation. The timing and spatial distributions of the two ore-containing series (T2f4-1 and T2f5-2) also indicate a regressive process of the Falang Formation. Sharp contact relations between manganese orebodies and intraclastic limestones indicate that both these formations were probably laid down as chemical sediments under wave actions.

- Petrological and mineralogical examinations indicate a relatively small number of minerals representing the bulk of ores and associated rocks. Braunite is by far the most common manganese oxide with trace manganite, followed by small amounts of calciorhodochrosite and Mn-calcite as well as Mn-bearing calcite. Similarly, calcite and quartz dominate the gangue minerals. Thus, the mineralogy of ores suggests that the original deposition took place mainly under both oxidizing and slightly reducing as well as their transitional environments and no sulfide phase of manganese was found. The "pure" rock (e.g. pure carbonate or clastic) phases are generally less important within the deposits, although they often form the underlying or overlying units. The orebodies were generally laid down in association with clastic and calcareous rocks. The dominance of Mn oxidic minerals in defined stratigraphic positions of orebody points to a selective geochemical environment that supports the development of these minerals in dependence on the concentration of oxygen or biological activity with the evolution of regression. Significantly, the typical paragenesis directly depend on the presence of particular environment. Mn carbonates, for instance, predominantly cement Mn oxide oololiths/pisololiths, or the mixing concentric rings are composed of both braunite and Mn carbonate minerals. Thus, this paragenesis of Mn minerals occurring commonly in the deposits, probably indicates a frequency of varying levels of water anoxia. Significantly, many of secondary microfabrics strongly suggest the presence of diagenetic processes, though the sedimentary processes dominate in the formation of the deposits. The diagenetic mechanisms mainly resulted in three mineralogical and geological relationships, i.e. changes of textures and structures, recrystallization and replacement developments of similar parageneses to the primary products.

- Major, minor and trace element analyses of ore and associated rock samples show a moderate or strong differentiation of most elements within the orebody or depending on the ore/rock types. Generally, the elements decrease (e.g. Mn, Si) with increasing depth, though some elements (e.g. Ca) generally increase downwards. The Rare Earth Elements possess particularly

marked variations reflecting enrichment processes in lower horizons of orebody or in diagenetic products. However, the most of the REEs features and their various ratios indicate a possible source from both terrigenous materials and seawater, whereas the secondary changes are probably carried out in porewaters. The similar shale-normalized patterns between Dounan oolites /pisolites and Groote Eylandt uncemented oolites/pisolites and diagenetic nodules suggest significantly similar evolving processes. The Electron Microprobe analysis of the Mn minerals indicates that some minerals indeed experienced different processes from primary deposition to secondary enrichment. The isotopic analysis of carbon and oxygen apparently demonstrates the presence of both primary and diagenetic processes, and rising temperature with depth during diagenesis.

- The above mentioned features and processes were determined to be the main mechanisms for the formation of both Mn oxides and carbonates in the deposits. Other mechanisms leading to the mobilization of Mn are of subordinate nature due to the lack of data. From all available evidences, the bulk of the Dounan Mn orebodies are considered to be of undoubted sedimentary-diagenetic origin. However, the most evidences indicate syngenetic sedimentary nature, relatively small amount of the diagenetic informations, especially on a micro-scale, exhibited by braunite-rich or well crystalline ores, indicates a secondary enrichment. The diagenesis affected all lithic units due to overburden load, but the intensity of diagenesis is best indicated by the Mn oolites /pisolites because of their containing much more interstitials than other units, favouring for pore-water or pressure solution activity. Thus, it is assumed that the manganese orebodies had also suffered identical change under influences of pressure and rising temperature during diagenesis. Additionally, supergene processes only play an unimportant role in the formation of the deposits, which is indicated by only about 2% supergene ores of the total ore reserves.
- It was demonstrated that manganese deposits elsewhere show sedimentary-diagenetic products comparable to those at Dounan, although the geological history of these deposits is different to the petrological and mineralogical assemblages or microenvironments examined in this study. Therefore, the "mineralization model" is suggested as an initial idea for more elaborate future models that incorporate mineralizing mechanisms adjusted to local or global conditions.
- A series of methods has been developed to assist in the analysis of the braunite origin. Though it has been known for over 160 years, in fact, details of both its crystal chemistry and genesis remain unresolved. Only because of its reported metamorphic association from India, South Africa, South America, etc. the mineral is commonly considered to be a metamorphic reaction product. However, few recent studies suggest that braunite may have developed at low temperature and pressure as a product of a manganese-containing sediment diagenesis. Significantly, the discovery of primary sedimentary braunite in Dounan of China has added to the knowledge of the mineralogy of this mineral.

References

- Abraham, K. and Schreyer, W., 1975. Minerals of the Viridine Hornfels from Darmstadt, Germany. *Contrib. Mineral. Petrol.*, 49: 1-20.
- Abs-Wurmbach, I., 1980. Miscibility and Compatibility of Braunitz, $Mn^{2+} Mn^{3+}_6O_{18}/SiO_4$ in the System Mn-Si-O at 1 Atm. in Air. *Contrib. Mineral. Petrol.*, 71: 393-399.
- Abs Wurmbach, I., Peters, T., Langer, K. and Schreyer, W., 1983. Phase Relations in the System Mn-Si-O: An Experimental and Petrological Study. *Neues. Jahrb. Mineral Abh.*, 146: 258-279.
- Adams, A.E. and Schofield, D., 1983. Recent Submarine Aragonite, Magnesian Calcite, and Hematite Cements in a Gravel from Islay, Scotland: *Journal of Sedimentary Petrology*, 53: 417-421.
- Adams, L. F. and Ghiorse, W., 1988. Oxidation State of Mn in the Mn Produced by *Leptothrix discophora* SS-I. *Geochim. Cosmochim. Acta*, 52: 2073-2076.
- Alexandri, R., Jr., Force, E.R., Cannon, W.F., Spiker, E.C. and Zantop, H., 1985. The Sedimentary Manganese Carbonate Deposits of the Molango District, Mexico [abs.]. *Geol. Soc. America Abstracts with Programs*, 17: 551.
- Alexandrov, E.A., 1972. Manganese: Element and Geochemistry. In: *Encyclopedia of Geochemistry and Environmental Sciences* (R.W. Fairbridge, ed.). Van Nostrand Reinhold Co., New York-Toronto-London-Melbourne, pp. 670-671.
- Aminoff, G., 1930. Lattice Dimensions and Space Group of Braunitz. *Kungl. Svenska Vetenskapsakademiens Handlingar* 3, Ser. 9: 14-22.
- Arthur, M.A., Jenkyns, H.C., Brumsack, H.J. and Schlanger, S.O., 1990. Stratigraphy, Geochemistry and Paleocyanography of Organic Carbon-rich Cretaceous Sequences. In: *Cretaceous Resources, Events and Rhythms* (R.N.Ginsburg and B.Beaudoin, eds.): Dordrecht, Kluwer Academic Pub., pp. 75-119.
- Bandopadhyay, P.C., 1989. Proterozoic Microfossils from Manganese Orebody, India. *Nature*, 339: 376-378.
- Barwis, J.H., 1978. Stratigraphy of Kiawah Island Beach Ridges. *Southeastern Geology*, 9: 111-122.
- Bender, M.L., Ku, T.L. and Broecker, W.S., 1970. Accumulation Rates of Manganese in Pelagic Sediments and Nodules. *Earth Planet. Sci. Lett.*, 8: 143-148.
- Berner, R.A., 1980. *Early Diagenesis: A Theoretical Approach*. Princeton Univ. Press, 241 pp.
- Beus, A.A., 1976. *Geochemistry of the Lithosphere*. Mir Publishers Moscow, 366 pp.
- Bezrukov, P.L., 1960. Sedimentation in the Northwestern Part of the Pacific Ocean. 21st Int. Geol. Congr., 10: 39-49.
- Bishop, J.K.B. and Fleisher, M.Q., 1987. Particulate Manganese Dynamics in Gulf Stream Warm-core Rings and Surrounding Waters of the N.W. Atlantic. *Geochimica et Cosmochimica Acta*, 51: 2807-2825.
- Blatt, H., Middleton, G.V. and Murray, R., 1980. *Origin of Sedimentary Rocks*; 2nd ed., Prentice-Hall Inc., Englewood Cliffs, New Jersey, 782 pp.
- Bolton, B.R., 1981 (unpublished). An Investigation of Groote Eylandt Manganese Deposits. Report to B.H.P. Co. Let., 52 pp.
- Bolton, B.R. and Frakes, L.A., 1985. Geology and Genesis of Manganese Oolite, Chiatura, Georgia, U.S.S.R. *Geological Society of America Bulletin*, 96: 1398-1406.
- Bolton, B.R. and Frakes, L.A., 1988. A Shallow-water, Marine Manganese Deposit: Groote Eylandt, Australia. In: *Proceedings of the Sixth Quadrennial IAGOD Symposium Held in Tbilisi, USSR, September, 6-12, 1982* (T.V. Janelidze and A.G. Tvalchralidze, eds.): Stuttgart, Schweizerbart.
- Bolton, B.R., Frakes, L.A. and Cook, J.N., 1988. Petrography and Origin of Inversely Graded Manganese Pisolite from Groote Eylandt, Australia. *Ore Geology Reviews*, 4: 47-69.
- Bonatti, E., Kraemer, T. and Rydell, H.S., 1972. Classification and Genesis of Submarine Iron-manganese Deposit. In: *Ferromanganese Deposits on the Ocean Floor* (D.R.Horn, ed.). National Science Foundation Washington, D.C., pp. 159-166.
- Borchert, H., 1970. On the Ore Deposition and Geochemistry of Manganese. *Miner. Deposita*, 5: 300-314.
- Boström, K., 1967. The problem of Excess Manganese in Pelagic Sediments. In: *Researches in Geochemistry* (P.H. Abelson, ed.). Jhon Wiley and Sons Inc., New York, 2: 421-452.
- Boström, K., 1976. Particulate and Dissolved Matter as Sources for Pelagic Sediments. *Acta Univ. Stockholm., Stockholm Contrib. Geol.*, 30: 17-79.
- Brewer, P.C. and Spencer, D.W., 1974. Distribution of Some Trace Elements in the Black Sea and Their Flux between Dissolved and Particulate Phases. *Am. Assoc. Petroleum Geologists Mem.*, 20: 137-143.
- Brockamp, O., 1976. Dissolution and Transport of Manganese by Organic Acids and Their Role in Sedimentary Mn Ore Formation. *Sedimentology*, 23: 579-586.
- Brongersma-Sanders, M., Stephan, K.M., Kwee, T.G. and DeBruin, M., 1980. Distribution of Minor Elements in Cores from the Southwest Africa Shelf with Notes on Plankton and Fish Mortality. *Marine Geol.*, 37: 91-132.
- Burdige, D.G. and Kepkay, P.E., 1983. Determination of Bacterial Mn Oxidation Rates in Sediments Using an in-situ Dialysis Technique. I. Laboratory Studies. *Geochim. Cosmochim. Acta*, 47: 1907-1916.
- Butkevitch, E.S., 1928. The Formation of Iron and Manganese Deposits and Role of Microorganisms in the Latter. *Verh. Wiss. Meeresinst. Moscow*, 3: 63.
- Byström, A. and Mason, B., 1943. The Crystal Structure of Braunitz $3Mn_2O_3 \cdot MnSiO_3$. *Ark. Kem. Min. Geol.*, 16B, 15: 1-18.
- Callender, E. and Bowser, C.J., 1976. Fresh-water Manganese Deposits. In: *Handbook of Strata-bound and Stratiform Ore Deposits* (K.H.Wolf, ed.). Elsevier, Amsterdam, 7: 341-394.
- Calvert, S.E. and Price, N.B., 1970. Composition of Manganese Nodules and Manganese Carbonates from Loch Fyne, Scotland. *Contrib. Min. Petrol.*, 29: 215-233.
- Calvert, S.E. and Price, N.B., 1972. Diffusion and Reaction Profiles of Dissolved Manganese in the Pore Water of Marine Sediments. *Earth Planet. Sci. Lett.*, 16: 245-249.
- Calvert, S.E. and Price, N.B., 1977. Geochemical Variation in Ferromanganese Nodules and Associated Sediments from the Pacific Ocean. *Mar. Chem.*, 5: 48-74.
- Calvert, S.E., Piper, D.Z. and Baedeker, P.A., 1987. Geochemistry of Rare Earth Elements in Ferromanganese Nodules from DOMES Site A, Northern Equatorial Pacific. *Geochimica et Cosmochimica Acta*, 51: 2331-2338.
- Candia, M.A.F., Peter, Tj. and Valarelli, J.V., 1975. The Experimental Investigation of the Reaction $MnCO_3 + SiO_2 = MnSiO_3 + CO_2$ and $MnSiO_3 + MnCO_3 = Mn_2SiO_4 + CO_2$ in CO_2/H_2O Gas Mixtures at a Total Pressure of 500 Bars. *Contrib. Min. Petrol.*, 52: 261-266.
- Cannon, W.F. and Force, E.R., 1983. Potential for High-grade Shallow Marine Manganese Deposits in North America. In: *Unconventional Mineral Deposits*, W.C.Shanks (Editor). *Soc. Min. Eng.*, pp. 157-189.

- Chapnik, S.D., Moore, W.S. and Nealson, K.H., 1982. Microbiologically Mediated Manganese Oxidation in a Fresh Water Lake. *Limnol. Oceanogr.*, 27: 1004-1014.
- Charles, E., Barker and Otto C. Kopp, 1991. Luminescence Microscopy and Spectroscopy. Text for Short Course No. 25. Sponsored by SEPM, U.S.A., V pp.
- Cheney, E.S. and Vredenburg, L.D., 1968. The Role of Iron Sulfides in the Diagenetic Formation of Iron-poor Manganese Nodules. *J. Sed. Pet.*, 38: 1363-1365.
- Clayton, R.N., Friedman, I., Graf, D.L., Mayeda, T.K., Meents, W.F. and Shimp, N.F., 1966. The Origin of Saline Formation Waters. 1. Isotopic Composition. *J. Geophys. Res.* 71: 3869-3882.
- Coutinho, J.M.V., Candia, M.A.F. and Valarelli, J.V., 1976. Mineralogical Study of the Main Manganese Carbonate-silicate Protores (Queluzites) from Brazil and Their Weathering Products. (Abstract), Symposium 104.3, "Geology and Geochemistry of Manganese." 25th Int. Geol. Congr., Abstracts 3: 764-765.
- Craig, H., 1965. The Measurement of Oxygen Isotope Palaeotemperatures. In: Stable Isotopes in Oceanographic Studies and Palaeotemperatures (E. Tongiorgi, ed.), 3: 1-16.
- Crerar, D.A., Cormick, R.K. and Barnes, H.L., 1972. Organic Controls on Sedimentary Geochemistry of Manganese. *Acta. Mineral. Petrogr.*, 20: 217-226.
- Crerar, D.A. and Barnes, H.L., 1974. Deposition of Deep-sea Manganese Nodules. *Geochim. Cosmochim. Acta*, 38: 279-300.
- Crerar, D.A., Cormick, R.K. and Barnes, H.L., 1980. The Geochemistry of Manganese: an Overview. In: *Geology and Geochemistry of Manganese* (I.M. Varentsov and G. Grassely, eds.). E.Schweizerbartsche Verlagsbuchhandlung Stuttgart, 1: 293-334.
- Cseh-Németh, J., Konda, J. Grasselly, Gy. and Szabó, Z., 1980. Sedimentary Manganese Deposits of Hungary. In: *Geology and Geochemistry of Manganese* (I.M. Varentsov and GY. Grasselly, eds.). E. Schweizerbartsche Verlagsbuchhandlung, Stuttgart, 2: 119-222.
- Cullers, R.L., Yeh, L.-T., Chaudhuri, S. and Guidotti, C.V., 1974. Rare Earth Elements in Silurian Pelitic Schists from N.W. Maine. *Geochim. Cosmochim. Acta*, 38: 389-400.
- Curray, J.R., 1964. Transgressions and Regressions. In: *Papers In Marine Geology - Shepard Commemorate Volume* (R.C. Miller, ed.). New York, MacMillan and Company, pp. 175-203.
- Curtis, C.D., 1977. Sedimentary Geochemistry: Environments and Processes Dominated by Involvement of an Aqueous Phase. *Phil. Trans. R. Soc. London*, 286A, 353-372.
- Czerniakowski, L.A., Lohmann, K.C. and Wilson, J.L., 1984. Closed-system Marine Burial Diagenesis: Isotopic Data from the Austin Chalk and Its Components. *Sedimentology*, 31: 863-877.
- Dasch, E.J., Dymond, J.A. and Heath, G.R., 1971. Isotopic Analysis of Metalliferous Sediment from the East Pacific Rise. *Earth Planet. Sic. Lett.*, 13: 175-180.
- Dasgupta, H.C. and Manickavasagam, R.M., 1981a. Regional Metamorphism of Non-calcareous Manganiferous Sediments from India and the Related Petrogenetic Grid for a Part of the System Mn-Fe-Si-O. *J. Petrol.*, 22: 263-396.
- Dasgupta, H.C. and Manickavasagam, R.M., 1981b. Chemical and X-ray Investigation of Braunite from the Metamorphosed Manganiferous Sediments of India. *N Jahrd Mineral Abh.*, 142: 149-160.
- Dasgupta, S., Roy, S. and Fukuoka, M., 1992. Depositional Models for Manganese Oxide and Carbonate Deposits of the Precambrian Sausar Group, India. *Econ. Geol.*, 87: 1412-1418.
- Dasgupta, S., Sengupta, P., Battacharya, P.K., Fukuoka, M., Roy, S. and Mukherjee, M., 1989. Mineral Reactions in Manganese Oxide Rocks: P-T-X Phase Reactions. *Econ. Geol.*, 84: 434-443.
- De Baar, H.J.W., Bacon, M.P., Brewer, P.G. and Bruland, K.V., 1985. Rare-earth Elements in the Pacific and Atlantic Oceans. *Geochim. Cosmochim. Acta*, 49: 1943-1959.
- De la Hunty, L.E., 1966. Manganese Nodules in Middle Proterozoic Shale in the Pibara Goldfield, Western Australia. *West. Aust. Geol. Surv. Ann. Rep.*, 1965: 65-68.
- De Carlo, E.H. and McMurtry, G.M., 1990. Rare Earth Element Geochemistry of Seamount Ferromanganese Deposits from the Hawaiian Archipelago. *Geochimica et Cosmochimica. Acta*.
- De Villiers, J.E., 1945. Some Minerals Occuring in South African Manganese Deposits. *Trans. Geol. Soc. S. Africa*, 48: 17-26.
- De Villiers, J.E., 1951. The Manganese Ores of Otjosondu, South West Africa. *Trans. Geol. Soc. S. Africa*, 54: 89-98.
- De Villiers, J.E., 1983. The Manganese Deposits of Griqualand West, South Africa: Some Mineralogical Aspects. *Econ. Geol.*, 78: 1108-1118.
- De Villiers, J.P.R., 1975. The Crystal Structure of Braunite with Reference to its Solid Solution Behavior. *Am. Mineral.* 60: 1098-1104.
- De Villiers, J.P.R., 1980. The Crystal Structure of Braunite II and Its Relation to Bixbyite and Braunite. *Am. Mineral.*, 65: 756-765.
- De Villiers, J.P.R. and Herbstein, F.H., 1967. Distribution between Two Members of the Braunite Group. *Am. Mineral.*, 52: 20-30.
- Deer, W.A., Howie, R.A. and Zussman, J., 1963. *Rock-forming Minerals, Non-silicates*. Vol. 5, Longmans, London, 371 pp.
- Dickson, J.A.D., 1965. A Modified Staining Technique for Carbonates in Thin Section. *Nature*, 205: 587.
- Diem, D. and Stumm, W., 1984. Is Dissolved Mn²⁺ Being Oxidized by O₂ in Absence of Mn-bacteria or Surface Catalysts? *Geochim. et Cosmochim. Acta*, 48: 1571-1573.
- Dorobek, S.L., 1987. Petrography, Geochemistry, and Origin of Burial Diagenetic Facies, Siluro-Devonian Helderberg Group (Carbonate Rocks), Central Appalachians. *Am. Assoc. Petroleum Geologists Bulletin*, 71: 492-514.
- Dorr, J.V.N., Geolho, I.S. and Horen, A., 1956. 20th Internat. Geol. Congr., Sympos. Sobre Yacimientos de Manganese, 3: 279-364.
- Doyen, L., 1973. The Manganese Ore Deposit of Kiseng-Kamata (Western Katanga). Mineralogical and Sedimentological Aspects of the Primary Ores. In: *Ores in Sediments* (G.C. Amstutz and A.J. Bernard, eds). VIII Int. Sed. Congr., Heidelberg, pp. 93-100.
- Dubinina, A.V. and Volkov, I.I., 1986. Rare Earth Elements in East Pacific Rise Metalliferous Sediments. *Geokhimija*, 5: 645-662.
- Dugolinsky, B.K., Margolis, S.V. and Dudley, W.C., 1977. Biogenic Influence on Growth of Manganese Nodules. *J. Sed. Pet.*, 47: 428-445.
- Dymond, J., Corliss, J.B., Heath, G.R., Field, C.W., Dasch, E.J. and Veeh, H.H., 1973. Origin of Metalliferous Sediments from the Pacific Ocean. *Geol. Soc. Amer. Bull.*, 84: 3355-3372.
- Ebinger, M.H. and Schulze, D.G., 1989. Mn-substituted Goethite and Fe-substituted Groutite Synthesized at Acid pH. *Clays and Clay Minerals*, 37/2: 151-156.

- Ehrlich, H.L., 1963. Bacteriology of Manganese Nodules. *Appl. Microbiol.*, 11: 15-19.
- Ehrlich, H.L., 1964. Microbial Transformations of Minerals. In: *Principles of Applications in Aquatic Microbiology* (H. Heukelekian and M.C. Dondreo, eds.). John Wiley and Sons, New York, pp. 43-60.
- Ehrlich, H.L., 1966. Reactions with Manganese by Bacteria from Marine Ferromanganese Nodules. *Devs. Ind. Microbiol.*, 7: 279-286.
- Ehrlich, H.L., 1972. The Role of Microbes in Manganese Nodules Genesis and Degradation. In: *Ferromanganese Deposits on the Ocean Floor* (D.R. Horn, ed.). National Science Foundation, Washington, D.C., pp. 63-70.
- Ehrlich, H.L., 1975. The Formation of Ores in the Sedimentary Environment of the Deep Sea with Microbial Participation: the Case for Ferromanganese Concretions. *Soil Sci.*, 119: 36-41.
- Ehrlich, H.L., Ghirose, W.C. and Johnson II, G.L., 1972. Distribution of Minerals in Manganese Nodules from the Atlantic and the Pacific Oceans. *Devs. Ind. Microbiol.*, 13: 57-65.
- Ehrlich, H.L., Yang, S.H. and Mainwaring Jr. J.D., 1973. Bacteriology of Manganese Nodules VI. Fate of Cooper, Nickel, Cobalt and Iron during Bacterial and Chemical Reduction of Manganese (VI). *Z. Allg. Microbiol.*, 13: 39-48.
- Einsele, G., 1992. Sedimentary Basins: Evolution, Facies, and Sediment Budget, Springer-Verlag, Berlin, 628 pp.
- Elderfield, H. and Greaves, M.J., 1981. Negative Cerium Anomalies in the Rare Earth Element Patterns of Oceanic Ferromanganese nodules. *Earth and Planetary Science Letters*, 35: 163-170.
- Elderfield, H. and Sholkovitz, E.R., 1987. Rare Earth Elements in the Pore Waters of Reducing Nearshore Sediments. *Earth Planet Sci. Lett.*, 82: 280-288.
- Elderfield, H., Hawkesworth, C.J., Greaves, M.J. and Calvert, S.E., 1981. Rare Earth Element Geochemistry of Oceanic Ferromanganese Nodules and Associated Sediments. *Geochim. Cosmochim. Acta*, 45: 513-528.
- Epstein, S., Buchsbaum, H.A., Lowenstam, H.A. and Urey, H.C., 1953. Revised Carbonate-water Isotopic Temperature Scale. *Geol. Soc. Am. Bull.*, 64: 1315-1326.
- Fan Delain, Zhao, D.F., Jiang, W., Wang, J. and Yin, L., 1988. Wafangzi Ferro-manganese Ore Deposit and Observed Stops in Chaoyang County, Liaoning Province. Guide Book, International Symposium on Sedimentology Related to Mineral Deposits. Beijing, China, 14 pp.
- Faure, G., 1986. *Principles of Isotope Geology* (Second Ed.). New York, 589 pp.
- Fleet, A.J., 1983. Hydrothermal and Hydrogenous Ferromanganese Deposits: Do They Form a Continuum? The Rare-Earth Element. In: *Hydrothermal Processes at Seafloor Spreading Centers* (P.A. Rona, K. Boström, L. Loubier and K.L. Smith, eds.). Plenum Press, New York, N.Y., pp. 535-555.
- Fleischer, M., 1987. Glossary of Mineral Species. *Mineralogical Record Publ.*, 227 pp.
- Fleischer, M. and Mandarino, J.A., 1991. Glossary of Mineral Species. *The Mineralogical Research*, Tucson, USA, 257 pp.
- Folk, R.L., 1959. Practical Petrographic Classification of Limestones. *Bull. Am. Petrol. Geol.*, 43: 1-38.
- Folk, R.L., 1962. Spectral Subdivision of Limestone Types. In: *Classification of Carbonate Rocks* (W.E. Ham Ed.). *Mem. Am. Ass. Petrol. Geol.*, 1: 62-84.
- Force, E.R. and Cannon, W.F., 1988. Depositional Model for Shallow Marine Manganese Deposits around Black Shale Basins. *Econ. Geol.*, 83: 93-117.
- Frakes, L.A., 1979. *Climates Throughout Geologic Time*. Elsevier, Amsterdam, 310 pp.
- Frakes, L.A., 1982. Metal Chemistry of Manganese Nodules from the Cape Leeuwin Field, Southeast Indian Ocean Marine Geology, 47: M1-M10.
- Frakes, L.A. and Bolton, B.R., 1984. Origin of Manganese Giants: Sea Level Change and Anoxic-oxic History. *Geology*, 12: 83-86.
- Frakes, L.A. and Bolton, B.R., 1992. Effects of Ocean Chemistry, Sea Level, and Climate on the Formation of Primary Sedimentary Manganese Ore Deposits. *Econ. Geol.* 87: 1207-1217.
- Frakes, L.A. and Francis, J.E., 1988. A Guide to Phanerozoic Cold Polar Climates from High-latitude Ice-rafting in the Cretaceous. *Nature*, 333: 547-549.
- Frakes, L.A., Francis, J.E. and Syktus, J.I., 1992. *Climate Modes of the Phanerozoic*. Cambridge, Cambridge Univ. Press, 274 pp.
- Frank, J.R., Carpenter, A.B. and Oglesby, T.W., 1982. Cathodoluminescence and Composition of Calcite Cement in the Taum Sauk Limestone (Upper Cambrian, Southeast Missouri). *Journal of Sedimentary Petrology*, 52: 631-638.
- Frenzel, G., 1980. Manganese Ore Minerals. In: *Geology and Geochemistry of Manganese* (I.M. Varentsov and G. Grasselly, eds.), Vol.1, Schweizerbart, Stuttgart, pp. 25-157.
- Fryer, B.J., 1977. Rare Earth Evidence in Iron-formations for Changing Precambrian Oxidation States. *Geochim. Cosmochim. Acta*, 41: 361-367.
- Fu, J., 1963. Cited in: *Ore Deposits* (in Chinese). Geological Publishing House of China, 1978.
- Garrels, R.M. and Christ, C.L., 1965. *Solutions, Minerals and Equilibria*. Harper & Row, New York, pp. 405.
- Geller, S., 1971. Structures of $\alpha\text{-Mn}_2\text{O}_3$ ($\text{Mn}_{0.983}\text{Fe}_{0.017}\text{O}_3$) and $(\text{Mn}_{0.37}\text{Fe}_{0.63})_2\text{O}_3$ and Relation to Magnetic Ordering. *Acta Cryst. B* 27: 821-828.
- Ghirose, W.C., 1986. Applicability of Ferromanganese-depositing Microorganisms to Industrial Metal Recovery Processes. *Biotechnol. Bioeng. Symp.*, 16: 141-148.
- Ghirose, W.C. and Ehrlich, H.L., 1974. Effects of Sea Water Cations and Temperature on Manganese Dioxide-reductase Activity in a Marine *Bacillus*. *Appl. Microbiol.*, 28: 785-792.
- Gies, H., 1975. Activation Possibilities and Geochemical Correlations of Photoluminescing Carbonates, Particularly Calcites. *Mineralium Deposita*, 10: 216-227.
- Ginsburg, R.N., 1971. Landward Movement of Carbonate Mud: New Model for Regressive Cycles in Carbonates (Abstract). *Am. Assoc. Petrol. Geol. Bull.*, V. 55 i 340.
- Glasby, G.P., 1972. Why Manganese Nodules Remain at the Sediment-water Interface. *N.Z. Jour. Sci.*, 20: 187-190.
- Glasby, G.P., 1973. Mechanism of Enrichment of the Rarer Elements in Marine Manganese Nodules. *Mar. Chem.*, 1: 105-125.
- Glasby, G.P., Tooms, J.S. and Cann, J.R., 1971. The Geochemistry of Manganese Encrustations from the Gulf of Aden. *Deep-sea Res.*, 18: 1179-1187.
- Glasby, G.P., Gwozdz, R., Kundendorf, H., Friedrich, G. and Thijssen, T., 1987. The Distribution of Rare Earth and Minor Elements in Manganese Nodules and Sediments from the Equatorial and S.W. Pacific. *Lithos.*, 20: 97-113.
- Glover, E.D., 1977. Cathodoluminescence, Iron and Manganese Content and the Early Diagenesis of Carbonates [Ph.D. dissertation]; Madison. The University of Wisconsin, 444 pp.
- Goldberg, E.D., 1954. Marine Geochemistry. I. Chemical Scavengers of the Sea. *J. Geol.*, 62: 249-265.
- Goldberg, E.D., 1965. Minor Elements in Sea Water. In: *Chemical Oceanography* (J.P. Riley and G. Skirrow, eds.), 1: 163-169.

- Goldberg, E.D., Koide, M., Schmitt, R.A. and Smith, R.H., 1963. Rare-earth Distribution in the Marine Environment. *J. Geophys. Res.*, 68: 4209-4217.
- Goldschmidt, V.M., 1954. *Geochemistry*. Oxford University Press. 730 pp.
- Goldsmith, J.R., 1959. Some Aspects of the Geochemistry of Carbonates. In: "Researches in Geochemistry" (P.H. Ableson, ed.), Jhon Wiley and Sons Inc., New York. Vol. 1, pp. 336-358.
- Gordeyev, V.V., 1983. Rechnoy Stok V Okeane I Cherey Yego Geokhimii [River Runoff into the Oceans: Geochemical Aspects], Nauka, Moscow.
- Graham, W.F., Bender, M.L. and Klinkhammer, G.P., 1976. Manganese in Narragansett Bay. *Limnol. Oceanogr.*, 21: 665-673.
- Grasselly, GY. and Pantó, GY., 1988. Rare Earth Elements in the Manganese Deposit of Úrkút (Bakony Mts., Hungary). *Ore Geology Reviews*, 4: 115-124.
- Greenslate, J.L., Frazer, J.Z. and Arrhenius, G., 1973. Origin and Deposition of Selected Transition Elements in the Seabed. In: *The Origin and Distribution of Manganese Nodules in the Pacific and Prospects for Exploration* (M.Morgenstein, ed.). An International Symposium Organized by the Valdivia Manganese Exploration Group and the Hawaii Institute of Geophysics, pp. 45-69.
- Grill, E.V., 1978. The Effect of Sediment-water Exchange on Manganese Deposition and Nodule Growth in Jervis Inlet, British Columbia. *Geochim. et Cosmochim. Acta*, 42: 485-495.
- Grover, G.Jr. and Read, J.F., 1983. Paleoaquifer and Deep Burial Related Cements Defined by Regional Cathodoluminescent Patterns, Middle Ordovician Carbonates, Virginia: *Am. Assoc. Petrol. Geol. Bull.*, 67: 1275-1303.
- Gryaznov, V.I. and Danilov, I.S., 1980. Oxidized Ores of Nikopol Deposit. In: *Geology and Geochemistry of Manganese* (I.M. Varentsov and GY. Grasselly, eds.). E. Schweizerbartsche Verlagsbuchhandlung Stuttgart, 2: 99-133.
- Haidinger, W., 1831. Mineralogical Account of the Ores of Manganese. *Trans. R. Sco. Edinburgh*, 11: 119-142.
- Hallberg, R.O., Bubela, B. and Ferguson, J., 1979. Metal Chelation in Sedimentary Systems. *Geomicrobiology Journal*, 2/2: 99-113.
- Hariya, Y. and Kikuchi, T., 1964. Precipitation of Manganese by Bacteria in Mineral Springs. *Nature*, 202: 416-417.
- Harper, C.W., 1984. Improved Methods of Facies Sequence Analysis. In: *Facies Models, Second Edition* (Roger G. Walker, ed.). Geoscience Canada, Reprint Series I, pp. 11-14.
- Haskin, M.A. and Haskin, L.A., 1966. Rare Earths in European Shales: A Redetermination. *Science*, 154: 507-509.
- Haskin, L.A., Haskin, M.A., Frey, F.A. and Wildman, T.R., 1968. Relative and Absolute Terrestrial Abundances of the Rare Earths. In: *Origin and Distribution of the Elements* (L.M. Ahrens, ed.), Pergamon Press, pp. 889-912.
- Haskin, L.A., Wildeman, T.R., Frey, F.A., Gollins, K.A., Keedy, C.R. and Haskin M.A., 1966. Rare Earths in Sediments. *J. Geophys. Res.*, 71: 6091-6105.
- Hein, J.R., Schwab, W.C. and Dawis, A.S., 1988. Cobalt and Platinum-rich Ferromanganese Crusts and Associated Substrate Rocks from the Marshall Islands. *Mar. Geol.*, 78: 255-283.
- Hein, J.R., Bolton, B.R., Pacome, N., Mckirdy, D. and Frakes, L.A., 1989. Chemical, Isotopic and Lithologic Associations within the Moanda Manganese Deposit, Gabon: 4th Field Workshop, IGCP Project No.226, Veszprem, Hungary.
- Hem, J.D., 1963. Chemical Equilibria and Rates of Manganese Oxidation. *U.S. Geol. Surv. Water Suppl. Paper 1667-A*, 17: 1-64.
- Hem, J.D., 1964. Deposition and Solution of Manganese Oxides. *U.S. Geol. Surv. Water Suppl. Paper 1667B*: 1-42.
- Hem, J.D., 1972. Chemical Factors That Influence the Availability of Iron and Manganese in Aqueous Systems. *Geol. Soc. Am. Bull.*, 83: 443-450.
- Hemming, N.G., Meyers, W.J. and Grams, J.C., 1989. Cathodoluminescence in Diagenetic Calcites: the Roles of Fe and Mn as Deduced from Electron Probe and Spectrophotometric Measurements. *Journal of Sedimentary Petrography*, 59: 404-411.
- Hewitt, D.F., 1972. Manganite, Hausmannite and Braunite: Features, Models of Origin. *Econ. Geol.*, 67: 83-102.
- Hewitt, D.H. and Fleischer, M., 1960. Deposits of Manganese Oxides. *Econ. Geol.*, 55: 1-55.
- Hey, M.H., 1978. Thirtieth List of New Mineral Names. *Min. Mag.* 42: 521-532.
- Hino, H., Minato, T. and Kushakaba, Y., 1978. Hydrothermal Synthesis of Braunite in the System Manganite (MnOOH)-Silica (SiO₂), Hausmannite (Mn₃O₄)-Silica (SiO₂) and Pyrolutite (MnO₂)-Silica (SiO₂) (2,500 bars). *Mem. Fac. Eng. Kyoto Univ.*, 40: 16-29.
- Hoffmann, H.J., 1973. Stromatolites. *Earth-Science Reviews*, 9: 339-373.
- Holland, H.D., 1984. *The Chemical Evolution of the Atmosphere and Oceans*. Princeton: Princeton University Press, 582 pp.
- Hood, D.W., 1972. Seawater Chemistry. In: *Encyclopedia of Geochemistry and Environmental Sciences* (R.W. Fairbridge, ed.). Van Nostrand Reinhold Co., New York, pp.1062-1070.
- Hudson, J.D., 1977. Stable Isotopes and Limestone Lithification. *Journal of Geol. Soc. London*. 133: 637-660.
- Huebner, J.S., 1967. Stability Relations of Minerals in the System Mn-Si-C-O. Ph D thesis. The Johns Hopkins University, Baltimore, USA, pp 279.
- Huebner, J.S., 1969. Stability Relations of Rhodochrosite in the System Manganese-Carbon-Oxygen. *Amer. Mineral*, 54: 457-481.
- Ingri, J. and Pontér, C., 1987. Rare Earth Abundance Patterns in Ferromanganese Concentrations from the Gulf of Bothnia and the Barents Sea. *Geochimica et Cosmochimica Acta*, 51: 155-161.
- Irwin, H., Curtis, C.D. and Colerman, M., 1977. Isotopic Evidence for Source of Diagenetic Carbonates Formed during Burial of Organic-rich Sediments. *Nature*, 269: 209-213.
- Jakes, P. and Taylor, S.R., 1974. Excess Europium Content in Precambrian Sedimentary Rocks and Continental Evolution. *Geochim. Cosmochim. Acta*, 38: 739-746.
- Jenkins, S.R., 1973. Effect of Selected Cation Concentration on Coagulation and Adhesion to Silica Surfaces of δ MnO₂. *Environ. Sci. Technol.*, 7: 43-47.
- Jenkyns, H.C., 1970. Fossil Manganese Nodules from the West Sicilian Jurassic. *Eclog. Geol. Helv.*, 63: 741-774.
- Jenkyns, H.C., 1988. The Early Toarcian (Jurassic) Anoxic Events: Stratigraphic, Sedimentary and Geochemical Evidence. *Amer. J. Sci.*, 288: 101-151.
- Jin, S. and Li, H., 1981. Generalization of Genetic Mineralogy. Changchun Univ. of Earth Sciences, China (in Chinese).
- Karhu, J. and Epstein, S., 1986. The Implication of the Oxygen Isotope Records in Coexisting Cherts and Phosphates. *Geochim. Cosmochim. Acta*, 50: 1745-1756.

- Kasting J.F., 1987. Theoretical Constraints on Oxygen and Carbon Dioxide Concentrations in the Precambrian Atmosphere. *Precambrian Res.* 34: 205-229.
- Keith, M.L. and Weber, J.N., 1964. Isotopic Composition and Environmental Classification of Selected Limestones and Fossils. *Geochim. Cosmochim. Acta*, 28: 1282-1816.
- Kindle, E.M., 1935. Manganese Concretions in Nova Scotia Lakes. *Trans: Roy. Soc. Can.*, 29: 163-180.
- Kittrick, J.A., 1969. Soil Minerals in the Al_2O_3 - SiO_2 - H_2O System and a Theory of Their Formation. *Clays and Clay Minerals*, 17: 157-167.
- Klingsberg, C. and Roy, R., 1959. Stability and Interconvertibility of Phases in the System Mn-O-OH. *Amer. Mineral.* 44: 819-838.
- Krauskopf, K.B., 1956. Factors Controlling the Concentrations of Thirteen Rare Metals in Sea Water. *Geochim. Cosmochim. Acta*, 9: 1-34.
- Krauskopf, K.B., 1957. Separation of Manganese from Iron in Sedimentary Processes. *Geochim. Cosmochim. Acta*, 2: 61-84.
- Krauskopf, K.B., 1967. Introduction to Geochemistry. McGraw-Hill, New York, 721 pp.
- Krishnan, K.S. and Banerjee, S., 1939. Magnetic Studies on Braunite $3Mn_2O_3 \cdot MnSiO_3$. *Z. Krist.* 101: 507-511.
- Krumbein, W.E., 1971. Manganese-oxidising Fungi. *Naturwissenschaften*, 58: 56-57.
- Lawrence, J.R., Gieskes, J.M. and Broecker, W.S., 1975. Oxygen Isotope and Cation Composition of DSDP Pore Waters and the Alteration of Layer II Basalts. *Earth Planet. Sci. Lett.* 27:1-10.
- Laxen, D.P.H., Davis, W. and Woof, C., 1984. Manganese Chemistry in Rivers and Streams. *Geochimica et Cosmochimica Acta*, 48: 2107-2111.
- Leeder, M.R., 1982. *Sedimentology: Process and Product*. George Allen and Unwin, London, 344 pp.
- Li, Y.H., Bischoff, J.L. and Mathieu, G., 1969. The Migration of Manganese in the Arctic Basin Sediment. *Earth Planet Sci. Lett.*, 7: 265-270.
- Liebhafsky, H.A. and Pfeiffer, H.G., 1971. X-Ray Techniques. In: *Modern Methods of Geochemical Analysis* (R.E. Wainnerdi and E.A. Uken, eds.). Plenum Press, New York, pp. 245-270.
- Liu, B. and Zheng, Y., 1985. The Basis and Methods of Lithofacies-Paleogeography. Geological Publishing House, Beijing, China, 442 pp.
- Liu, G. et al. of No.2 Geological Brigade of Yunnan Geological and Mineral Resources Bureau., 1984. Typical Deposit Research Report of Dounan Mn Deposits, Yanshan County, Yunnan Province, Geological and Minerals Bureau of Yunnan Province (in Chinese), 126 pp.
- Liu, Z., 1985. Geological Characteristics of Dounan Manganese Deposits, Yunnan Province. In: *Symposium on Geology of Manganese Ore Deposits in China*. Geological Publishing House, Beijing, China (in Chinese) pp. 247-265.
- Long, J.V.P. and Agrell, S.O., 1965. The Catho-luminescence of Minerals in Thin Section. *Mineralogical Magazine*, 34: 318-326.
- Lynn, D. and Bonatti, E., 1965. Mobility of Manganese in Diagenesis of Deep Sea Sediments. *Mar. Geol.*, 3: 457-474.
- Machel, H.G., 1985. Cathodoluminescence in Calcite and Dolomite and Its Chemical Interpretation: *Geoscience Canada*, 2: 139-147.
- Machel, H.G., Mason, R.A., Mariano, A.N. and Alfonso Mucci., 1991. Causes and Measurements of Luminescence in Calcite and Dolomite. In: *Luminescence Microscopy and Spectroscopy* (C.E. Barker and O.C. Kopp, eds.), Text for Short Course No.25, SEPM, U.S.A., pp. 9-23.
- Machel, H.G. and Burton, E.A., 1991. Factors Governing Cathodo-luminescence in Calcite and Dolomite and Their Implications for Studies of Carbonate Diagenesis. In: *Luminescence Microscopy and Spectroscopy* (C.E. Barker and O. C. Kopp, eds.), Text for Short Course No.25, SEPM, U.S.A., pp. 37-57.
- Madgwick, J.C., 1987. Microbial Processing of Manganese. *Australian Journal of Biotechnology*, 1/2: 41-43.
- Major, R.P., 1991. Cathodoluminescence in Post-Miocene Carbonates. In: *Luminescence Microscopy and Spectroscopy* (C.E. Barker and O.C. Kopp, eds.), Text for Short Course No.25, SEPM, U.S.A., pp. 149-153.
- Major, R.P. and Wilber, R.J., 1991. Crystal Habit, Geochemistry, and Cathodoluminescence of Magnesian Calcite Marine Cements from the Lower Slope of Little Bahama Bank. *Geol. Soc. Amer. Bull.*, 4: 461-471.
- Manheim, F.T., 1961. A Geochemical Profile in the Baltic Sea. *Geochim. Cosmochim. Acta*, 25: 52-70.
- Manheim, F.T., 1965. Manganese-iron Accumulations in the Shallow Marine Environment. In: *Symp. Marine Geochemistry*, Rhode Island. Univ. Narragansett Marine Lab., Occasional Publ., 3: 217-276.
- Marshall, D.J., 1988. *Cathodoluminescence of Geological Materials: an Introduction*. Winchester, MA: Allen & Unwin, 146 pp.
- Marshall, K.C., 1979. Biogeochemistry of Manganese Minerals. In: *Biogeochemical Cycling of Mineral-forming Elements* (P.A. Trudinger and D.J. Swaine, eds.). Elsevier, Amsterdam, pp. 253-292.
- Mason, B., 1943. Mineralogical Aspects of the System FeO - Fe_2O_3 - MnO - Mn_2O_3 . *Geol. Fören. Förhandl.* 65: 97-180.
- Maynard, J.B., 1983. *Geochemistry of Sedimentary Ore Deposits*. Springer-Verlag New York Inc., 305 pp.
- McIntosh, J.L., Farag, J.S. and Snee, J.K., 1975. Groote Eylandt Manganese Deposits. In: *Economic Geology of Australia and Papua New Guinea - 1. Metals* (C.L. Knight, Ed.), Australas. Inst. Min. Metall. Monograph 5, pp. 815-821.
- Mercz, T.I. and Madgwick, J.C., 1982. Enhancement of Bacterial Manganese Leaching by Microalgal Growth Products. *Proc. Australas. Inst. Min. Metall.*, 283: 43-46.
- Merino, E. and Ransom, B., 1982. Free Energies of Formation of Illite Solid Solutions and their Compositional Dependence. *Clay and Clay Minerals*, 30: 29-39.
- Meyers, W.J., 1974. Carbonate Cement Stratigraphy for the Mississippian Lake Valley Formation. Sacramento Mountains, New Mexico: *Journal of Sedimentary Petrology*, 44: 1078-1088.
- Meyers, W.J. and James, A.T., 1978. Stable Isotope of Cherts and Carbonate Cements in the Lake Valley Formation (Mississippian), Sacramento Mountains, New Mexico. *Sedimentology*, 25: 105-124.
- Miall, A.D., 1984. *Principles of Sedimentary Basin Analysis*. Springer, New York, 490 pp.
- Michard, G., 1969. Kinetics of Manganese Oxidation on the Seafloor. *Trans. Amer. Geophys. Union*, 50: 349.
- Miyano, T. and Beukes, N.J., 1987. Physicochemical Environments for the Formation of Quartz-free Manganese Oxide Ores from the Early Proterozoic Hotazel Formation, Kalahari Manganese Field, South Africa. *Econ. Geol.*, 82: 706-718.
- Mohr, P.A., 1965. Genetic Problems of Some Sedimentary Manganese Carbonate Ores. *Contrib. Geophys. Observatory, Haile Sellasie University, Addis Ababa*, A-5: 1-22.
- Momoi, H., Nakamoto, M. and Kamata, K., 1992. Synthesis of Manganese Oxide Spherules in Gels - An Approach to Understand Growing Process of Manganese Nodules. *Mining Geology*, 42(3): 155-163.
- Monty, C., 1973. Les Nodules De Manganèse Sont Des Stromatolithes Océaniques. *C.R. Acad. Sci. Paris*, 276: 3285-3288.

- Moore, L.J., Moody, J.R., Barnes, I.L., Gramich, J.W., Murphy, T.J., Paulsen, P.J. and Shields, W.R., 1973. Trace Determination of Rubidium and Strontium in Silicate Glass Standard Reference Materials. *Anal. Chem.*, 45: 2384-2387.
- Moore, P.B. and Araki, T., 1976. Braunite: its Structure and Relationship to Bixbyite and Some Insights on the Generalization of Fluorite Derivative Structures. *Am. Mineral.* 61: 1226-1240.
- Morgan, J.J., 1964 (unpublished). Chemistry of Aqueous Manganese II and IV. PhD. Dissertation, Harvard University, Cambridge, MA., pp.224.
- Morgan, J.J., 1967. Chemical Equilibria and Kinetic Properties of Mn in Natural Waters. In: Principles and Application in Water Chemistry (S.D. Faust and J.V. Hunter, eds.). Wiley, New York, pp.561-624.
- Morgan, J.J. and Stumm, W., 1965. Colloid-chemical Properties of Manganese Dioxide. *J. Colloid Sci.*, 19: 347-359.
- Muan, A., 1959a. Phase Equilibria in the System Manganese Oxide - SiO₂ in Air. *Amer. J. Soc.* 257: 297-315.
- Muan, A., 1959b. Stability Relations among Some Manganese Minerals. *Am. Mineral.* 44: 946-960.
- Murray, J.W. and Brewer, P.G., 1977. Mechanism of Removal of Manganese, Iron and Other Trace Metals from Seawater. In: Marine Manganese Deposits (G.P. Glasby, ed.). Elsevier Scientific Publishing Company, Amsterdam pp.291-326.
- Nealson, K.H. and Tabo, B., 1980. Structural Features of Manganese Precipitating Bacteria. *Origins of Life*, 10: 117-126.
- Niemann, J.C. and Read, J.F., 1988. Regional Cementation from Unconformity Recharged Aquifer and Burial Fluids, Mississippian Newman Limestone, Kentucky: *Journal of Sedimentary Petrology*, 58: 688-705.
- Nordstrom, D.K. and Munoz, J.L., 1985. Geochemical Thermodynamics. The Benjamin / Cummings Publishing Co., Inc., California, 477 pp.
- No.2 Geological Brigade of Yunnan Geological and Mineral Resources Bureau, 1983 (unpublished). The report of Regional Manganese Deposits Investigation across Provinces (in Chinese), 326 pp.
- Okita, P.M., 1987. Geochemistry and Mineralogy of the Molango Manganese Orebody, Hidalgo State, Mexico [PhD. Diss.]: University of Cincinnati, 362 pp.
- Okita, P.M., 1992. Manganese Carbonate Mineralization in the Molango District, Mexico. *Econ. Geol.* 87: 1345-1366.
- Okita, P.M. and Shanks, W.C. III., 1988. $\delta^{13}\text{C}$ and $\delta^{34}\text{S}$ Trends in Sedimentary Manganese Deposits, Molango (Mexico) and Taojiang (China): Evidence for Mineralization in a Closed System: IAS International Symposium on Sedimentology Related to Mineral Deposits (Abstracts), Beijing, China, pp.188-189.
- Okita, P.M., Maynard, J.B. and Martinez-Vera, A., 1986. Molango: A Giant Sedimentary Manganese Deposit in Mexico [abs.]. *Am. Assoc. Petroleum Geologists Bull.*, 70: 627.
- Okita, P.M., Maynard, J.B., Spiker, E.C. and Force, E.R., 1988. Isotopic Evidence for Organic Matter Oxidation by Manganese Reduction in the Formation of Stratiform Manganese Carbonate Ore. *Geochim. et Cosmochim. Acta*, 52: 2679-2685.
- Ostwald, J., 1980. Aspects of the Mineralogy, Petrology and Genesis of the Groote Eylandt Manganese Ores. In: *Geology and Geochemistry of Manganese* (I.M. Varentsov and G.Y. Grasselly, eds.). E. Schweizerbartsche Verlagsbuchhandlung, Stuttgart, 2: 149-182.
- Ostwald, J., 1982. Some Observations on Mineralogy and Genesis of Braunite. *Min. Mag.*, 46: 506-507.
- Ostwald, J., 1990. The Biochemical Origin of the Groote Eylandt Manganese Oxide Pisoliths and Oololiths, Northern Australia. *Ore Geology Reviews*, 5: 469-490.
- Ostwald, J., 1992. Mineralogy, Paragenesis and Genesis of the Braunite Deposits of the Mary Valley Manganese Belt, Queensland, Australia. *Mineral Deposita*, 27: 326-335.
- Ostwald, J. and Bolton, B.R., 1990. Diagenetic Braunite in Sedimentary Rocks of the Proterozoic Manganese Group, Western Australia. *Ore Geology Reviews*, 5: 315-323.
- Ostwald, L. and Nayak, V.K., 1993. Braunite Mineralogy and Paragenesis from the Kajlidongri Mine, Madhya Pradesh, India. *Mineral Deposita*, 28: 153-156.
- Pauling, L. and Shappell, M.D., 1930. The Crystal Structure of Bixbyite and the C Modifications of Sesquioxides. *Z. Krist.* 75: 128-142.
- Pedersen, T.F. and Calvert, S.E., 1990. Anoxia vs. Productivity: What Controls the Formation of Organic-carbon-rich Sediments and Sedimentary Rocks? *Am. Assoc. Petroleum Geologists Bull.*, 74: 454-466.
- Perkins, E.C. and Novielli, F., 1962. Bacterial Leaching of Mn-ores. U.S. Bur. Mines, Rep. Invest. 6102, 11.
- Perry, E.A., Jr., Gieskes, J.M. and Lawrence, J.R., 1976. Mg, Ca and O¹⁸/O¹⁶ Exchange in the Sediment-Pore Water System, Hole 149, DSDP. *Geochim. Cosmochim. Acta*, 40: 413-423
- Peters, Tj., Schwander, H. and Tromsdorff, V., 1973. Assemblages among Tephroite, Pyroxmangite, Rhodochrosite, Quartz: Experimental Data and Occurrences in the Rhetic Alps. *Contrib. Min. Petrol.*, 42: 325-332.
- Peters, Tj., Valarelli, J.V. and Candia, M.A.F., 1974. Petrogenetic Grids from Experimental Data in the System Mn-Si-C-O-H. *Revta. Bras. Geociencias*, 4: 15-27.
- Pettijohn, F.J., Potter, P.E. and Siever, R., 1987. Sand and Sandstone (2nd Edition). Springer Verlag, Berlin, 553 pp.
- Pfeifer, H.-R., Oberhänsli, H. and Epprecht, W., 1988. Geochemical Evidence for a Sedimentary Hydrothermal Origin of Jurassic Iron-manganese Deposits at Gonzen (Sargans Helvetic Alps, Switzerland). *Marine Geology*, 84: 257-272.
- Philip, W.C., 1968. Marine Diagenesis of Shallow Marine Lime-Mud Sediments: Insights from δO^{18} and δC^{13} Data. *Science*, 161: 1130-1132.
- Piper, D.Z., 1972. Rare Earth Elements in Manganese Nodules from the Pacific Ocean. In: *Ferromanganese Deposits on the Ocean Floor* (D.R. Horn, ed.). Nat. Sci. Found, Washington, D.C. pp. 123-130.
- Piper, D.Z., 1974. Rare Earth Elements in the Sedimentary Cycle: A Summary. *Chem. Geol.*, 14: 285-304.
- Piper, D.Z. and Graef, P., 1974. Gold and Rare-earth Elements in Sediments from the East Pacific Rise. *Mar. Geol.* 17: 287-297.
- Piper, D.Z. and Williamson, M.E., 1977. Composition of Pacific Ocean Ferromanganese Nodules. *Mar. Geol.*, 23: 285-303.
- Polgári, M., Okita, P.M. and Hein, J.R., 1991. Stable Isotope Evidence for the Origin of the Úrkút Manganese Ore Deposit, Hungary. *Journal of Sediment. Petrol.*, 61/3: 384-393.
- Popp, B.N., Anderson, T.F. and Sandberg, P.A., 1986a. Brachiopods as Indicators of Original Isotopic Compositions in Some Paleozoic Limestones. *Geol. Soc. Amer. Bull.* 97: 1262-1269.
- Popp, B.N., Podosek, F.A., Brannon, J.C., Anderson, T.F. and Pier, Jean., 1986b. $^{87}\text{Sr}/^{87}\text{Sr}$ Ratios in Permo-Carboniferous Sea Water from the Analyses of Well-preserved Brachiopod Shells. *Geochim. Cosmochim. Acta*, 50: 1321-1328.
- Pracejus, B., 1989 (PhD. Diss). Nature and Formation of Supergene Manganese Deposits on Groote Eylandt, N.T. Australia. Adelaide University of South Australia. 231 pp.
- Pracejus, B., Bolton, B.R. and Frakes, L.A., 1988. Nature and Development of Supergene Manganese Deposits, Groote Eylandt, Northern Territory, Australia. *Ore Geology Reviews*, 4: 71-98.

- Pracejus, B., Bolton, B.R., Frakes, L.A. and Abbot, M., 1990. Rare Earth Element Geochemistry of Supergene Manganese Deposits from Grooto Eylandt, Northern Territory, Australia. *Ore Geology Reviews*, 5: 239-314.
- Pratt, L., Force, E.R. and Pomeroy, B., 1991. Coupled Manganese and Carbon-isotopic Events in Marine Carbonates at the Cenomanian-Turonian Boundary. *Jour. Sed. Petrology*, 61: 370-383.
- Price, N.B., 1967. Some Geochemical Observations on Manganese-iron Oxide Nodules from Different Depth Environments. *Mar. Geol.*, 5: 511-538.
- Price, N.B. and Calvert, S.E., 1970. Compositional Variation in Pacific Ocean Ferromanganese Nodules and its Relationship to Sediment Accumulation Rates. *Mar. Geol.*, 9: 145-171.
- Putilina, V.S. and Varentsov, I.M., 1980. Interaction between Organic Matter and Heavy Metals in the Waters of Recent Basins - A Review of the Current State of the Problem. *Chem. Erde.*, 39: 298-310.
- Raab, W., 1972. Physical and Chemical Features of Pacific Deep Sea Manganese Nodules and their Implications in the Genesis of the Nodules. In: *Ferromanganese Deposits on the Ocean Floor* (D.R. Horn, ed.). Nat. Sci. Found., Washington, D.C., pp.31-49.
- Raiswell, R., 1976. The Microbiological Formation of Carbonate Concentrations in the Upper Lias of N.E. England. *Chem. Geol.* 18: 227-244.
- Randohr, P., 1969. *The Ore Minerals and their Intergrowths*. Vol.2. Pergamon, New York, 966 pp.
- Rankin, P.C. and Glasby, G.P., 1979. Regional Distribution of Rare Earth and Minor Elements in Manganese Nodules and Associated Sediments in the Southwest Pacific and Other Localities. In: *Marine Geology and Oceanography of the Pacific Manganese Province* (J.L. Bischoff and D.Z. Piper, eds.). Plenum Publishing Corporation, pp.681-697.
- Reading, H.G., 1978. *Sedimentary Environments and Facies*. Blackwell, Oxford, 557 pp.
- Reeder, R.J., 1991. An Overview of Zoning in Carbonate Minerals. In: *Luminescence Microscopy and Spectroscopy* (C.E. Barker and O.C. Kopp, eds.), Text for Short Course No.25, SEPM, U.S.A., England, pp. 77-81
- Reeder, R.J. and Paquette, J., 1989. Sector Zoning in Natural and Synthetic Calcites. *Sedimentary Geology*, 65: 239-247.
- Reinson, G.E., 1984. Barrier-Island and Associated Strand-Plain Systems. In: *Facies Models, Second Edition* (R.G. Walker, ed.). Geoscience Canada Reprint Series I, pp. 119-140.
- Robbins, J.A. and Callender E., 1975. Diagenesis of Manganese in Lake Michigan Sediments. *Amer. J. Sci.*, 275: 512-533.
- Ronov, A.B. and Yaroshevsky, A.A., 1972. Earth's Crust Geochemistry. In: *Encyclopedia of Geochemistry and Environmental Sciences* (R.W. Fairbridge, ed.). Van Nostrand Reinhold Co., New York, pp.243-254.
- Rossmann, R. and Callender, E., 1968. Manganese Nodules in Lake Michigan. *Science*, 162: 1123-1124.
- Rosson, R.A. and Nealson, K.H., 1982. Manganese Bacteria in Marine Manganese Cycle. In: *The Environment of Deep Sea* (W.G. Ernst and J.G. Moriss, eds.). Prentice Hall, N.J., pp. 201-216.
- Roy, S., 1964a. Mineralogical Trend with Regional Metamorphism in the Manganese Ore Deposits of Madhya Pradesh and Maharashtra, India, 22nd. Int. Geol. Congr., 5: 493-509.
- Roy, S., 1964b. Recent Studies on the Phase-equilibrium Relations of Manganese Minerals and their Implications on the Mineralogical Trend of Natural Ore Deposits. In: *Advancing Frontiers of Geology and Geophysics* (A.P. Subramanian and S. Balakrishna, eds.). Indian Geophysical Union, Hyderabad, pp. 249-261.
- Roy, S., 1966. *Syngenetic Manganese Formations of India*. Jadavpur. University. Press, Calcutta, 219pp.
- Roy, S., 1968. Mineralogy of the Different Genetic Types of Manganese Deposits. *Econ. Geol.*, 63: 760-786.
- Roy, S., 1972. Metamorphism of Sedimentary Manganese Deposits. *Acta Mineral. Petrogr.*, 20: 313-324.
- Roy, S., 1973. Genetic Studies on the Precambrian Manganese Formations of India with Particular Reference to the Effects of Metamorphism. In: *Genesis of Precambrian Iron and Manganese Deposits*. Unesco, Earth Sciences, 9: 229-242.
- Roy, S., 1974. Petrology of the Metamorphosed Manganese Silicate Rocks. *Qt. J. Geol. Min. Meta. Soc. India*, Golden Jubilee Volumes, 46: 267-290.
- Roy, S., 1980a. Manganese Ore Deposits of India. In: *Geology and Geochemistry of Manganese* (I.M. Varentsov and GY. Grasselly, eds.). E. Schweizerbartsche Verlagsbuchhandlung, Stuttgart, 2: 237-264.
- Roy, S., 1980b. Genesis of Sedimentary Manganese Formation: Processes and Products in Recent and Old Geological Ages. In: *Geology and Geochemistry of Manganese* (I.M. Varentsov and GY. Grasselly, eds.). E. Schweizerbartsche Verlagsbuchhandlung, Stuttgart, 2: 13-44.
- Roy, S., 1981. *Manganese Deposits*. Academic Press. London, 458 pp.
- Roy, S., 1992. Environments and Processes of Manganese Deposition. *Econ. Geol.* 87: 1218-1236.
- Roy, S., Dasgupta, S., Bhattacharya, P.K., Majumdar, N., Fukuoka, M. and Banerjee, H., 1986. Petrology of Mn Silicate-Carbonate-Oxide Rock of Sausar Group, India. *N. Jb. Min. Mn.*, 12: 561-568.
- Roy, S., Bandyopadhyay, P.C., Perseil, E.A. and Fukuoka, M., 1990. Late Diagenetic Change in Manganese Ores of the Upper Proterozoic Penganga Group, India. *Ore Geology Reviews*, 5: 341-357.
- Sapozhnikov, D.G., 1970. Geological Conditions for the Formation of Manganese Deposits of the Soviet Union. In: *Manganese Deposits of Soviet Union* (D.G. Sapozhnikov, ed.). Israel Program for Scientific Translations, Jerusalem, pp. 9-33.
- Sayles, F.L. and Bischoff, J.L., 1973. Ferromanganese Sediments in the Equatorial East Pacific. *Earth Planet Sci. Lett.*, 19: 330-336.
- Scherer, M. and Seitz, H., 1980. Rare Earth Element Distribution in Holocene and Pleistocene Corals and their Redistribution during Diagenesis. *Chem. Geol.*, 28: 297-289.
- Schieber, J., 1988. Redistribution of Rare Earth Elements during Diagenesis of Carbonate Rocks from the Mid-Proterozoic Newland Formation, Montana, U.S.A. *Chem. Geol.*, 69: 111-126.
- Schlanger, S.O. and Jenkyns, H.C., 1976. Cretaceous Oceanic Anoxic Events: Causes and Consequences. *Geol. Mijnb.*, 55: 179-184.
- Serdyuchenko, D.P., 1980. Precambrian Biogenic-sedimentary Manganese Deposits. In: *Geology and Geochemistry of Manganese* (I.M. Varentsov and GY. Grasselly, eds.). E. Schweizerbartsche Verlagsbuchhandlung, Stuttgart, 2: 61-88.
- Shackleton, N.T. and Kennett, J.P., 1975. Palaeotemperature History of the Cenozoic and the Initiation of Antarctic Glaciation: Oxygen and Carbon Isotopic Analysis in DSDP Sites 277, 279, and 281, In Initial Reports of the Deep Sea Drilling Project, 24: 243-755.
- Shackleton, N.J., Hall, M.A., Line, J. and Cag Shixi, 1983. Carbon Isotope Data in Core V19-30 Confirm Reduced Carbon Dioxide Concentration of the Ice Age Atmosphere. *Nature*, 306: 319-322.
- Sholkovitz, E.R., 1976. Flocculation of Dissolved Organic and Inorganic Matter during the Mixing of River Water and Seawater. *Geochim. et Cosmochim. Acta*, 40: 831-845.

- Sholkovitz, E.R., 1990. Rare Earth Elements in Marine Sediments and Geochemical Standards. *Chem. Geol.*, 88: 333-347.
- Sholkovitz, E.R., Boyle, E.A. and Price, N.B., 1978. The Removal of Dissolved Humic Acids and Iron during Estuarine Mixing. *Earth Planet. Sci. Lett.*, 40: 130-136.
- Sholkovitz, E.R., Piepgras, D.J. and Jacobsen, S.B., 1989. The Pore Water Chemistry of Rare Earth Elements in Buzzards Bay Sediments. *Geochim. et Cosmochim. Acta*, 53: 2847-2856.
- Silverman, M.P. and Ehrlich, H.L., 1964. Microbial Formation of Minerals. *Adv. Appl. Microbiol.* 6: 153-206.
- Slee, K.J., 1980. Geology and Origin of the Groote Eylandt Manganese Oxide Deposits, Australia. In: *Geology and Geochemistry of Manganese* (I.M. Varentsov and GY. Grasselly, eds.). E. Schweizerbartsche Verlagsbuchhandlung, Stuttgart, 2: 125-148.
- Sorem, R.K., McFarland, W.A. and Fewkes, R.H., 1978. Nature and Significance of a Diffuse Sediment-water Interface "Boundary layer" In East Pacific Manganese Nodules Deposits. (Abstract). IAGOD 5th Symposium, Snowbird, U. S.A., *Abstracts*, 178 pp.
- Sorokin, Yu.I., 1972. Role of Biological Factors in the Sedimentation of Iron, Manganese and Cobalt in the Formation of Nodules. *Oceanology*, 12: 1-11.
- Stanton, R.L., 1972. *Ore Petrology*. McGraw-Hill, New York, N.Y., 713 pp.
- Stone, A.T., 1987. Microbial Metabolites and the Reductive Dissolution of Manganese Oxides: Oxalate and Pyruvate. *Geochim. et Cosmochim. Acta*, 51: 919-925.
- Strakhov, N.M., 1966. Types of Manganese Accumulation in Present Day Basins: their Significance in Understanding of Manganese Mineralization. *Int. geol. Rev.*, 8: 1172-1196.
- Strakhov, N.M., 1969. "Principles of Lithogenesis", Vol.I. Consultants Bureau, New York, 609 pp.
- Strakhov, N.M. and Shterenberg, L.E., 1966. Problems of Genetic Types of Chert Deposit. *Int. Geol. Review*, 8: 549-558.
- Su Junhua, 1983 (10). Dounan Manganese Deposits; Braunite of Sedimentary Origin. *Bulletin of the Institute of Mineral Deposits, Chinese Academy of Geological Sciences (in Chinese), Series III*: 33-49.
- Summerhayes, C.P. and Willis, J.P., 1975. Geochemistry of Manganese Deposits in Relation to the Environment around Southern Africa. *Mar. Geol.*, 18: 159-173.
- Sundby, B., Silverberg, N. and Chesselet, R., 1981. Pathways of Manganese in an Open Estuarine System. *Geochim. et Cosmochim. Acta*, 45: 293-307.
- Sunit, K.A., 1979. Rare Earth Element Patterns in Manganese Nodules and Micronodules from Northwest Atlantic. *Geochim. et Cosmochim. Acta*, 43: 1105-1115.
- Szabó, Z. and Grasselly, GY., 1980. Genesis of Manganese Oxide Ores in the Úrkút Basin, Hungary. In: *Geology and Geochemistry of Manganese* (I.M. Varentsov and GY. Grasselly, eds.). E. Schweizerbartsche Verlagsbuchhandlung Stuttgart, 2: 223-236.
- Tada, R., Maliva, R. and Siever, R., 1987. A New Mechanism for Pressure Solution in Porous Quartzose Sandstone. *Geochim. et Cosmochim. Acta*, 51: 2295-2301.
- Tassé, N. and Hesse, R., 1984. Origin and Significance of Complex Authigenic Carbonates in Cretaceous Black Shales of the Western Alps. *Journal of Sediment. Petrol.*, 54: 1012-1027.
- Thiel, G.A., 1925. Manganese Precipitated by Microorganisms. *Econ. Geol.*, 20: 301.
- Thirlwall, M., 1981. A Triple-filament Method for Rapid and Precise Analysis of Rare-earth Elements by Isotope Dilution. *Chem. Geol.*, 35: 155-166.
- Trimble, R.B. and Ehrlich, H.L., 1968. Bacteriology of Manganese Nodules III. Reduction of MnO_2 by Two Strains of Nodules Bacteria. *Appl. Microbiol.*, 16: 695-702.
- Trimble, R.B. and Ehrlich, H.L., 1970. Bacteriology of Manganese Nodules IV. Induction of MnO_2 -reductase System in a Marine Bacillus. *Appl. Microbiol.*, 19: 966-972.
- Troup, B.N. and Bricker, O.P., 1975. Processes Affecting the Transport of Materials from Continents to Oceans. *Am. Chem. Soc. Symposium Ser.*, 18: 133-151.
- Trudinger, P.A., 1976. Experimental Geomicrobiology in Australia. *Earth Sci. Review*, 12: 259-278.
- Tucker, M.E. and Wright, V.P., 1990. *Carbonate Sedimentology*. Blackwell Scientific Publications, Oxford London, 482 pp.
- Turekian, K.K., 1965. Some Aspects of Geochemistry of Marine Sediments. In: *Chemical Oceanography, II* (J. Riley and G. Skirron, eds.). Academic Press, London, pp. 81-126.
- Turekian, K.K., 1971. Rivers, Tributaries and Estuaries. In: *Impingement of Man on the Oceans* (D.W. Hood, ed.). Wiley-Interscience, 9-74 pp.
- Urban, H., Stribny, B. and Lippolt, H.J., 1992. Iron and Manganese Deposits of the Urucum District, Mato Grosso Do Sul, Brazil. *Econ. Geol.* 87: 1375-1392.
- Van Der Sloot, H.A., Hoede, D., Hamberg, G., De Lange, G.J. and Sophiah, S., 1988. Suspended Manganese-Rich Particles in Kau Bay, Halmahera (Eastern Indonesia). *Mar. Geol.*, 82: 251-259.
- Varentsov, I.M., 1964. "Sedimentary Manganese Ores". Elsevier Publishing Co. Amsterdam, 119 pp.
- Varentsov, I.M., 1972. Geochemical Studies on the Formation of Iron-manganese Nodules and Crusts in Recent Basins. I. Eningi-Lampi Lake, Central Karelia. *Acta. Mineral. Petrogr.*, 22: 363-382.
- Varentsov, I.M., 1976. Geochemistry of Transition Metals in the Processes of Ferromanganese Ore Formation in Recent Basins. (Abstract). Symposium 104.3, "Geology and Geochemistry of Manganese". 25th Int. Geol. Congr., Abstracts, 3: 798-799.
- Varentsov, I.M., 1982. Groote Eylandt Manganese Oxide Deposits, Australia. *Chem. Erde.*, 41: 157-173.
- Varentsov, I.M. and Pronina, N.V., 1973. On the Study of Mechanism of Iron-manganese Ore Formation in Recent Basins: the Experimental Data on Nickel and Cobalt. *Miner. Deposita*, 8: 161-178.
- Varentsov, I.M. and Pronina, N.V., 1976. Experimental Study of Processes of Ferromanganese Ore Formation in Recent Basins: Data on Iron, Manganese, Nickel and Cobalt. (Abstract). Symposium 104.3, "Geology and Geochemistry of Manganese". 25th Int. Geol. Congr., Abstracts, 3: 749.
- Varentsov, I.M. and Rakhmanov, V.P., 1980. Manganese Deposits of the USSR (A Review). In: *Geology and Geochemistry of Manganese* (I.M. Varentsov and GY. Grasselly, eds.). E. Schweizerbartsche Verlagsbuchhandlung, Stuttgart, 2: 319-392.
- Varentsov, I.M. and Golovin, D.I., 1987. The Manganese Ore Deposit of Groote Eylandt, Northern Australia: K-Ar Age of Cryptomelane Ores and Aspects of their Genesis. *Doklady Akademmi Nauk SSSR*, 294/1: 203-207.

- Varentsov, I.M., Bakova, N.V., Dikov, Yu.P., Gendler, T.S. and Giovanoli, R., 1979. On the Model of Mn, Fe, Ni, Co Ore Formation In Recent Basins: Experiments with the Synthesis of Me-hydroxide Phases on Mn_3O_4 . *Miner. Deposita*, 14: 281-296.
- Veizer, Jan, 1983. Trace Elements and Isotopes in Sedimentary Carbonates. In: *Carbonates* (R.J. Reeder, ed.) : Mineralogy and Chemistry, *Reviews in Mineralogy*, Mineral. Soc. Amer., 11: 265-299.
- Volkov, I.I. and Fomina, L.S., 1973. New Data on the Geochemistry of the Rare Earths in the Pacific Ocean Sediments. *Geochim. Intl.*, 19: 1178-1187.
- Walker, G. and Burley, S.D., 1991. Luminescence Petrography and Spectroscopic Studies of Diagenetic Minerals. In: *Luminescence Microscopy and Spectroscopy* (C.E. Barker and O.C. Kopp, eds.), Text for Short Course No. 25, SEPM, U. S.A., pp. 83-95.
- Walker, R.G., ed., 1979. *Facies Models*; Geosci. Can. Reprint Series I, 211 pp.
- Walker, R.G., 1984. General Introduction: Facies, Facies Sequences and Facies Models. In: *Facies Models*, Second Edition (R.G. Walker). *Geoscience Canada*, Reprint Series I, 1-10 pp.
- Walther, J.V. and Helgeson, H.C., 1977. Calculation of the Thermodynamic Properties of Aqueous Silica and the Solubility of Quartz and its Polymorphs at High Pressures and Temperatures. *Am. J. Sci.*, 277: 1315-1351.
- Wang, H.Z. et al. of Institute of Geology, Chinese Academy of Geological Sciences; Wuhan College of Geology, 1985. *Atlas of the Palaeogeography of China*. Cartographic Publishing House, Beijing, China.
- Wang, W., 1981. Dounan Type-Transitional Ore Phase-Rich Manganese Ores. *Geology and Prospecting* (in Chinese), 3: 20-25.
- Wangersky, P.J., 1963. Manganese in Ecology. In: *Radioecology* (V. Schultz and A.W. Klement Jr., eds.). Reinhold, New York. pp. 499-508.
- Weber, F., 1970. Genesis and Supergene Evolution of the Precambrian Sedimentary Manganese Deposit at Moanda (Gabon). *Earth Sciences*, 9: 307-322.
- Weber, J.N. and Woodhead, P.M.J., 1970. Carbon and Oxygen Isotope Fractionation in the Skeletal Carbonates of Reef-building Corals. *Chem. Geol.* 6: 93-117.
- Wendt, J., 1974. Encrusting Organisms in Deep-sea Manganese Nodules. *Int. Assoc. Sediments., Spec. Publ.*, 1: 437-447.
- Wildman, T.R. and Condie, K.C., 1973. Rare Earths in Archean Graywackes from Wyoming and from the Fig Tree Group, South Africa. *Geochim. Cosmochim. Acta*, 37: 439-453.
- Wildman, T.R. and Haskin, L.A., 1973. Rare Earths in Precambrian Sediments. *Geochim. Cosmochim. Acta*, 37: 419-438.
- Williamson, G., 1987 (B. Sc. Diss). *The Geology and Origin of Manganese Deposits at Pernatty Lagoon, South Australia*, Adelaide University of Australia.
- Wilson, J.L., 1975. *Carbonate Facies in Geological History*. Springer-Verlag, Berlin, 471 pp.
- Xavier, A. and Klemm, D.D., 1976. The Ultrastructures of the Pelagic Manganese Nodules from the Pacific Ocean and Implications for their genesis. *25th Int. Geol. Congr. Sect. 8, Abstract*, 2: 359-360.
- Yang, G., 1985. The Geological Features of Manganese Deposits in Yunnan Province. In: *Symposium on Geology of Manganese Ore Deposits in China*. Geological Publishing House, Beijing, China (in Chinese), pp. 227-237.
- Yariv, S. and Cross, H., 1979. *Geochemistry of Colloid Systems*. Berlin, Springer-Verlag, 450 pp.
- Ye, L., 1961. Cited in: *Ore Deposits* (in Chinese). Geological Publishing House of China, 1978.
- Ye, L., Fan, D. and Yang, P., 1988. Characteristics of Manganese Ore Deposits in China. *Ore Geology Reviews*, 4: 99-114.
- Yeats, P.A. and Loring, D.H., 1991. Dissolved and Particulate Metal Distributions in the St. Lawrence Estuary. *Canadian Jour. Earth Sci.*, 28: 729-742.
- Yue, X., 1985. Introduction on Geology of Manganese Ore Deposits In China. In: *Symposium on Geology of Manganese Ore Deposits in China*. Geological Publishing House, Beijing, China (in Chinese), pp.1-11.
- Zappfe, C., 1931. Deposition of Manganese. *Econ. Geol.*, 26: 799-832.
- Zen, E., 1959. Mineralogy and Petrology of Marine Bottom Sediment Samples off the Coast of Peru and Chile. *J. Sed. Pet.*, 29: 513-539.
- Zhang, L., 1985. Geological Introduction of Manganese Deposits in the Southeastern Yunnan Province. In: *Symposium on Geology of Manganese Ore Deposits in China*. Geological Publishing House, Beijing, China (in Chinese), pp. 238-246.
- Zhang, L., Liu, Z., Li, D., Gan, D., Wu, X., Liu, G., Li, Z., Su, Z., Zhou, R. and Zhong, J., 1979. *The Geological Prospecting Report of Gake and Baigu Mine-areas at Dounan*. Yunnan Geological Bureau Press, China (in Chinese), pp.1-79.
- Zhao, Z., 1978 (9). Geochemical Characters of Rare Earth Elements and their Application on the Studies of Rocks and Ore Deposits. *Geology and Geochemistry* (in Chinese), pp. 9-12.
- Zhong, J., 1986. Metallogeny of the Dounan Manganese Deposits. *Geological Review* (in Chinese), 32 (6): 583-588.
- Zwicker, W.K., Groeneveld Meijer, W.O.I. and Jaffe, H.W., 1962. Nsutite-A Wide-Spread Manganese Oxide Mineral. *American Mineralogist*, 47: 246-266.

Appendix I (Methods)

1.1 Sampling Technique

Selected locations of Dounan manganese deposits, Yunnan province of China were stratigraphically logged (see Chapter 2) and sampled, beginning at the base of the Falang Formation to avoid contamination from overlying materials. The samples of Lower Falang Formation were mainly taken from Gake and Kata areas, and the those of Upper Falang Formation were sampled from Baigu Daaazi and Milike areas because of the distribution of the stratigraphy in Dounan area (Fig. 2.22). Sampling intervals of uniform rocks were approximately 2 - 10 m, mainly according to the change of rock type; sampling intervals of uniform ores were approximately 20 - 50 cm, more complex parts of the orebody were sampled at 5 - 20 cm apart. Sub-samples were taken, where necessary, to show local mineralogical and petrological variations.

1.2 Equipment and Sample Preparation

First, every sample was cut a small part for making thin section and polishing section. Second, ores and rocks were broken into chips of a few cm³ with a hand-operated jaw breaker. The instrument was thoroughly cleaned after each sample to prevent contamination from previous material. The samples (about 1 cm³) was taken from each ore type for Scanning Electron Microscopy (SEM) and Electron Microprobe Analysis (EMPA). Then, the samples were ground to a fine powder in a tungsten cabide mill (inner Ø ~ 15cm). Depending on the sample type , the mill was cleaned 5 - 10 times with quartz sand ground to powder and washed with ethanol. Larger samples were then quartered in a sample divider until the remaining sample was reduced to 100 - 200g, small samples were totally retained.

1.3 Rock and Ore Analyses

1.3.1 X-Ray Fluorescence (XRF)

1.3.1.1 Analytical Background

Fused samples or pressed mineral powders are irradiated with X-rays. Elements present in the sample are excited to emit a radiation with an element-specific wavelength. This wavelength together with the respective intensity of the line allow the measurement of a large number of elements.

1.3.1.2 Equipment

A Siemens SRS-1 X-ray Fluorescence instrument of the Department of Geology and Geophysics, Adelaide University, was used to analyse 47 ore and rock samples for trace elements (As, Mo, Pb, Sc, Th, U, W.). All major and minor elements were determined by the same instrument in the quality control laboratory of Department of Geology and Geophysics, Adelaide University.

1.3.1.3 Sample Preparation for Pressed Powder Buttons

10 drops of PVA-solution were added to 5g of the powdered sample and mixed for some minutes. The sample was filled into a plastic cylinder and pressed by hand into a preliminary tablet. This tablet was transferred to a steel cylinder with a slight larger diameter. The empty space between sample and cylinder wall was filled with boric acid (H_3BO_3). The button is finally pressed for some minutes under a pressure of about 50,000 kPa ($\approx 70001b/inch^2$).

1.3.1.4 Sample Preparation for Fusion Beads (for Whole Rock Analysis by XRF)

Vials and crucibles were washed thoroughly with detergent and warm tap water and rinsed thoroughly with tap water and deionised water, then put them in the 110° C oven to dry for loss on ignition (all weighing to be done on the SARTORIUS R200D Dual Range Electronic Balance).

3-4 gms of finely crushed rock and ore powder was placed into clean, dry glass vial which then was put into 100° C oven to dry 3-4 hours. The vial was removed from oven and placed in desiccator and allow to cool to room temperature. The SHARP PC-4502 computer was connected to the SARTORIUS ELECTRONIC BALANCE, and run the loss on ignition program LOG-LOSS. After logged crucible weight, sample was placed into crucible and the new weight

(CRUCIBLE + SAMPLE WT.) was logged in via the hand switch. The weighed crucible was placed into a silica tray and put into the muffle furnace (NEYTECH PROGRAMMABLE FURNACE) for ignition at 960° C for 6 hours and cooling at 200° C for another 6 hours, then removed sample from furnace and allow to cool for 15 minutes then placed in desiccator to cool down to room temperature. To login the ignited weight, the crucible was reweighed the weight was logged (IGNITED CRUCIBLE + SAMPLE WT) using the hand switch. Loss on ignition (L.O.I%) was automatically calculated and stored on the DATA file.

Flux was removed from 500° C furnace and allow to cool down for 15 minutes before placing the platinum dish into a desiccator to cool down to room temperature. The vials cleaned and dried are now ready for sample+flux mixture to be weighed into them. SHARP PC-4502 was connected and run the program LOGWRA to weigh sample+flux mixture. Contents of vial are completely transferred to a Pt/5% Au crucible for fusion by heating above an OXY-PROPANE flam (Temp \cong 1000° C). Crucible is heated for 5 minutes until fusion is complete, then melt is poured into graphite disc and pressed into a glass disc using an aluminium plunger (both disc and plunger kept at a temperature of \cong 230° C). Fused disc is then annealed at 230° C for 30 minutes, then cool down to room temperature. Sample disc is labelled and ready for WHOLE ROCK ANALYSIS BY XRF.

1.3.2 X-Ray Diffraction (XRD)

1.3.2.1 Analytical Background

Randomly oriented mineral grains (powder) are irradiated with X-ray, which are reflected at the lattice of the examined phases. The reflection angle and the peak intensity are mineral specific? and through the Bragg equation ($n*\lambda = 2d*\text{Sin}\theta$) the d-spacings of the mineral is obtained. Tabulated phase data (e.g. ASTM) allow the comparison and identification of the sample spectrum (Liebhafsky and Pfeiffer, 1971).

1.3.2.2 Equipment and Sample Preparation

All samples were analyzed with a Philips diffractometer (PW 1050) at the Department of Geology and Geophysics, Adelaide University, using Coka radiation.

The sample is ground by hand in a agate mortar until it is finely powdered. A small amount is then mixed with methanol, mixed, and poured onto a glass sample holder, to produce a fine coating of the holder. This procedure was applied to all samples to allow direct spectra comparison of small sub-samples with larger samples.

1.3.3 Wet Chemical Analyses

About 130 rock powders (~200g) were prepared for chemical analyses of rocks and ores through Dounan stratigraphy. All major and minor as well as trace elements were determined in the quality control laboratory of No.2 Geological Brigade, Yunnan Geological and Mineral Resource Bureau, China (see also Chapter 5 and Appendix V).

1.3.4 Geochemical Environmental Index

The Geochemical environmental index analyses (Fe^{3+} , Fe^{2+} , $\text{Fe}^{3+}/\text{Fe}^{2+}$, and organic carbon) throughout the Falang Formation of Dounan stratigraphy were determined by No.2 Geological Brigade, the Yunnan Geological and Mineral Resource Bureau, China (see also Chapter 2 and Appendix II).

1.3.5 Scanning Electron Microscopy (SEM)

1.3.5.1 Analytical Background

The scanning electron microscope allows examination of the surface morphology of (solid) rock and ore samples with excellent resolution (down to 40 angstrom units) and at great depth of field (300 times greater than that of a light microscope). Techniques such as back-scattered electron imaging and X-ray analysis allow specimen composition to be determined, and diffraction patterns obtained by electron channelling can provide information about crystal structure and orientation. The electron beam is generated using either a hot tungsten filament or a thermally heated Lanthanum Hexaboride crystal. This filament is the cathode of a sample triode valve commonly termed the "Wehnelt" assembly. The electrons are accelerated (at the accelerating potential) through a series of 'lenses' and apertures and finally as a focused spot are scanned across the surface of the sample. When the electron beam hits the sample several interactions take place. Of these the most important are the generation of SECONDARY ELECTRONS, BACK-SCATTERED ELECTRONS AND X-RAYS. As well Auger (Pronounced O-jay) electrons are produced, cathodoluminescence occurs and some of the primary electron beam are adsorbed in the sample.

1.3.5.2 Equipment and Method

Two scanning electron microscopes - a Siemens ETEC Autoscan and a Philips SEM 505 in the CEMMSA (Center for Electron Microscopy and Microstructure Analysis), Adelaide University,

were used to examine 30 ore and rock samples for their micro-structures and the relationship between different materials. Both instruments are equipped with X-ray analysis facilities, and the Philips instrument also features image processing capabilities.

1.3.5.3 Sample Preparation

The samples must be ensured that they are dry and free from oil and loose particulate matter. It was necessary to section the bulk of the sample to provide a piece [$\sim < 1\text{cm}^3$] for examination that would fit comfortably on a stud or in the examination chamber which is at high vacuum. Samples are mounted on 'studs' using a conducting 'silver-dag', and must have a conducting layer over them to ensure a path for the electrons to return to the ground state. Gold-palladium was used as a standard preparation because it is fine structured and is a good secondary electron emitter.

1.3.6 Electron Microprobe Analyses (EMPA)

1.3.6.1 Analytical Background

The electron microprobe operates on the same principles as the scanning electron microscope, but has been optimized for use as an analytical instrument. Spectrometers operating on either the wavelength or energy dispersive principle are used to measure the characteristic X-rays emitted from a sample under electron irradiation, and a computer provides on-line data reduction. Analyses from micron-sized areas of a sample can be obtained for elements ranging from Boron to Uranium, at levels down to 100 ppm or better.

1.3.6.2 Equipment and Method

The JEOL-733 Superprobe installed in the CEMMSA, Adelaide University, features three dual-crystal wavelength dispersive spectrometers, as well as a keveX energy dispersive X-ray analyser, and may be operated in a variety of modes, from fully computer controlled (unattended) to manual operation.

1.3.6.3 Sample Preparation

Special thin sections or polished sections were made for Electron Microprobe Analyses. Carbon-palladium was used as a standard preparation for a conducting layer.

1.3.7 Cathodoluminescence (CL)

1.3.7.1 Analytical Background

In the vacuum chamber of the CL stage, the electron beam is adsorbed by the surface it hits, much of energy of the incident electron beam is adsorbed by the specimen molecules causing an increase in the energy levels of adsorbing electrons. Normally the excited atoms (also termed Cathodoluminescence centers) return to the ground state by transfer of the excess energy to adjacent atoms by inelastic collisions. Under certain circumstances, the adsorbed energy is re-emitted as light energy in the visible range before these collisions can take place. The conditions for luminescence often occur in impure crystalline substances where the impurities act as the luminescent centers. The intensity of light emitting from any particular point will be proportional primarily to the surface density of luminescent centers. The electron energy is readily adsorbed near the surface, and little luminescence is emitted from below the surface. For instance, manganese is a common activator in minerals and rocks. Iron is a common quencher. This is largely due to the abundance of these trace elements in minerals.

1.3.7.2 Equipment and Method

CL stages use an electron beam to produce Cathodoluminescence in susceptible materials. The CCL 8200 Mk2 stage is used to generate an electron beam reted at 25kV of 250 microamps at the Department of Geology and Geophysics, Adelaide University. This electron beam is capable of producing X-rays from any material it strikes. The stage is designed to adsorb this radiation, but regular periodic inspections are important ensure leaks have not developed. Mini Instruments Ltd makes a compact radiation detector suitable for testing the CL stage. This equipment desgin has been checked for X-ray safety. X-rays production was measured using a Philips monitor type PW 4517 placed directly above the top window. In addition, a simple objective lens set for CL observations would be a 5X and 10X (Nikon M Plan), using Kodak Kodacolor PPC-1600, CF 135 for colour prints.

1.3.7.3 Sample Preparation

Thin sections of rocks and ores are examined in the CL stage and are accommodate with maximum dimension 70 x 80 x/ mm by the CCL 8200 Mk2 stage. The view area is 50 x 70 mm. Optimal details under CL are produced by using high quality polished surfaces. Thin section for CL microscopy uses a cement that is stable at the moderate temperature generated in the sample. Heating and outgassing from the cement can coat the stage window and delay vacuum stabiliza-

tion and extend pump down time. Epoxied or epoxy resins are satisfactory. Cover glass is not used because the electron beam will be adsorbed by it before reaching the sample.

After sample preparation, lubricants, water, fingerprint oils and other volatiles must be removed from the sample because these volatiles will vaporize in the chamber during pump down or CL observation, extending pump down time to operational vacuum levels, and also potentially depositing material on the chamber window. A Freon solvent or alcohol is used as an effective cleaner and dehydrator for samples.

1.3.8 Isotope Analyses

1.3.8.1 Analytical Background

According to Faure (1986), the gas collected from samples are applied to the instrument of carbon dioxide stable isotope measurements. A DELTA value is the Ratio of HEAVY (H) to LIGHT (L) Isotopes in the sample (A), RELATIVE to the Ratio in a REFERENCE (B) as given by the equation:

$$\delta_{A/B} = [(H/L)_A - (H/L)_B] / (H/L)_B \times 1000\text{‰}$$

The calculator gives δ^{46} and δ^{45} values. For the DELTA value δ^{45} , H/L is mass45 / mass44, whereas in the δ^{46} value, H/L is mass46 / (mass44 + mass45). In addition to this, there is a smaller amount of O¹⁷ present, so corrections are made as follows:

$$\delta^{13}\text{C} = 1.0676\delta^{45} - 0.0338\delta^{46}; \text{ the } \delta^{18}\text{O} = 1.0014\delta^{46} + 0.009\delta^{13}\text{C}.$$

These δ values are for the SAMPLE relative to the REFERENCE GAS (usually CIG - Flask), and need to be connected to ∂ for the SAMPLE relative to the STANDARD (P.D.B.). A value is needed for the Reference Gas relative to PDB, and the equation is used:

$$\delta_{A/C} = \delta_{A/B} + \delta_{B/C} + (\delta_{A/B} \cdot \delta_{B/C}) / 1000.$$

Note that $\delta_{A/B} = -1000\delta_{B/A} / (1000 + \delta_{B/A})$, ($\delta_{A/B}$ is not Exactly - $\delta_{B/A}$).

1.3.8.2 Sample Preparation and Equipment

Staining Polish Sections of (Mn-) Carbonate or Oxide Ores/rocks:

The procedure detailed below, adapted from Dickson (1965), has been found generally satisfactory and has been used in preparation of most of the stained sections. Ensure that no dirt or grease adheres to the surface of rock/ore. Two staining solutions were prepared: Alizarin Red S (solution A) - concentration of 0.2g / 100ml of 1.5% hydrochloric acid (15ml pure acide made up to 1 litre with water; Potassium ferricyanide (solution B) - concentration 2g / 100ml of 1.5% hydrochloric acid. Mix solutions A and B in the proportion 3 parts by volum of A to 2 parts of

B. Immerse the section in the mixture of solutions for 30 - 45 seconds. Wash the stained section in running water for a few seconds and the dry it.

Preparation of Carbon Dioxide Samples for Stable Isotope Analyses:

Ensure that the sample tubes are properly clean and dry. Drill about 15 - 30 mg powder from stained section for individual samples (use 15 mg for pure CaCO_3 , if the sample has non-carbonate materials such as braunite, increase the sample weight proportionedly), and then put sample into the side arm of the tube. Fill the sample with acid (~4 ml 100% H_3PO_4) of place drying tube over the top for acid addition and immediately place top on the reaction tube. Connect the tube to the vacuum line for evacuation (evacuate reaction tube before equilibration and mixing). Put all evacuated samples into 25° C water bask for at least 15 minutes. Sift the tube to allow the acid to run into the side arm, and then remove to the water bask for 24 hours. Start up the vacuum line again for collecting sample gas which are applied to the instrument. All samples were analyzed with MICROMASS 602E, ISOGAS mass spectrometer at the Department of Geology and Geophysics, Adelaide University. The data expressed with reference to the universal PDB standard.

1.3.9 REE Analyses by Isotope Dilution

1.3.9.1 Analytical Background

Mass spectrometers can be used to determine the concentration of an element in a sample by means of an analytical technique called isotope dilution (Moore et al., 1973). This method is based on the determination of the Isotopic composition of an element in a mixture of a known quantity of a "spike" with an unknown quantity of the normal element. The spike is a solution (liquid or gaseous) containing a known concentration of a particular element whose isotopic composition has been changed by the enrichment of one of its isotopes. The sample to be analyzed contains an unknown concentration of the element whose isotopic composition is known. Therefore, when a known amount of a sample solution is mixed with a known amount of spike, the isotopic composition of the mixture can be used to calculate the amount of the element in the sample solution. The isotope enrichment is usually done by means of a large electromagnetic separator called a calutron, which is capable of separating the isotopes of an element quantitatively. When the element to be analyzed is nonvolatile, the spike is prepared in the form of a solution whose concentration and isotopic composition are verified separately. A known weight (or volume) of this spike solution is then added to a known weight (or volume) of the sample solution, and mixture is stirred to achieve complete isotopic homogenization. The mixture of the normal element and the spike is then analyzed on a mass spectrometer to determine its isotopic composition. The result, expressed in terms of the ratio of the abundances of two isotopes, is used to calculate the concentration of the element in question in the sample solution.

1.3.9.2 Equipment

The Finnigan MAT261 Mass Spectrometer, with Mass Spectrometer computer, printer, hard disc, load MAT261 program, removing and replacing loaded sample magazines, at the Department of Geology and Geophysics, Adelaide University, were used to analyse 18 ore and rock samples for Rare Earth Elements (La, Ce, Nd, Sm, Gd, Dy, Er, Yb).

1.3.9.3 Sample Preparation or Experimental Procedures

Whole rock/ore analyses were performed on powders. Analyses were performed on 100 - 200 mg of rock/ore powder, plus spike already weighed. For the dissolution of samples, first ~5 drops of 6 N HNO₃ were added to the beaker for trying to wash any sample down off the walls of the beaker then 2 mls HF from dispenser and evaporate to dryness at ~180° C on the clean hot plat in the dissolution fume hood, and then allow to cool; a further 2 mls HF + 1 ml 6 N HNO₃ was added and screw on the cap tightly, and leave this on the hot plate (~150° C) overnight; then open beaker, tapping first to knock down drops on inside of cap, and evaporate to dryness; again added 4 mls 6 N HNO₃ to the solid residue and keep warm (150° C) with cap on until completely dissolved (several hours to overnight), and then evaporate to dryness. For sample splitting and spiking, add 2 N HNO₃ and keep warm (150° C) with cap on until completely dissolved, and then evaporate to dryness. For sample loading, place 1 μ H₃PO₄ (i.e. up to the second notch on pipette) onto a single tantalum filament and evaporate to a small bulk at 1.5A; slowly raise the current until the filament just glows orange (about 2A); turn current back to zero. All the samples were carried out on the MAT261 Mass Spectrometer.

Appendix II (Stratigraphy)

**Table II.1. Sample localities, Sampling Positions in Vertical Section of Falang Formation.
Grainsize [c-clay, s-silt, ss-sand, g-granule, p-pebble].**

Table II.2. Geochemical Environmental Index of Dounan Stratigraphy.

Table II.1 Sample localities, positions and grainsize in vertical section of Falang Formation.

No.	Location	Position	Grainsize	No.	Location	Position	Grainsize
958-I	Gake	T2g	c	958-45	Gake	T2f4-1 (V1)	c-g
958-II	Gake	T2g	c	958-46	Gake	T2f4-1 (V1)	c-p
958-III	Gake	T2g	c	958-47	Gake	T2f4-1 (V1)	c-g
958-1	Gake	T2f1	c-ss	958-48	Gake	T2f4-1 (V1)	c-g
958-2	Gake	T2f1	c-s	958-49	Kata	T2f4-1 (V1)	c-g
958-3	Kata	T2f1	c-s	958-50	Kata	T2f4-1 (V1)	c-g
958-4	Kata	T2f2	s	958-51	Kata	T2f4-1 (V1)	c-g
958-5	Gake	T2f2	s	958-52	Kata	T2f4-1 (V1)	c-p
958-6	Gake	T2f2	c-s	958-53	Daaози	T2f4-1	c-s
958-7	Gake	T2f2	c-s	958-54	Daaози	T2f4-1	s
958-8	Kata	T2f2	c-s	958-55	Daaози	T2f4-1	s
958-9	Kata	T2f2	c-s	958-56	Gake	T2f4-1	c-s
958-10	Gake	T2f3-1	c-s	958-57	Gake	T2f4-1	c-s
958-11	Gake	T2f3-1	c-s	958-58	Gake	T2f4-1	s
958-12	Gake	T2f3-1	c-s	958-59	Gake	T2f4-1 (V2)	c-g
958-13	Gake	T2f3-1	c-s	958-60	Gake	T2f4-1 (V2)	g-p
958-14	Gake	T2f3-1	c-s	958-61	Gake	T2f4-1 (V2)	g-p
958-15	Gake	T2f3-1	c-s	958-62	Gake	T2f4-1 (V2)	g-p
958-16	Kate	T2f3-1	c-s	958-63	Gake	T2f4-1 (V2)	g-p
958-17	Kate	T2f3-1	s	958-64	Gake	T2f4-1 (V2)	g-p
958-18	Kata	T2f3-1	s	958-65	Kata	T2f4-1 (V2)	g-p
958-19	Kata	T2f3-1	s	958-66	Kata	T2f4-1 (V2)	g-p
958-20	Gake	T2f3-2	c-p	958-67	Gake	T2f4-1	g-p
958-21	Gake	T2f3-2	c-p	958-68	Gake	T2f4-1	g-p
958-22	Gake	T2f3-2	c-p	958-69	Gake	T2f4-1 (V3)	s-g
958-23	Gake	T2f3-2	c-p	958-70	Gake	T2f4-1 (V3)	c-g
958-24	Gake	T2f3-2	c-p	958-71	Gake	T2f4-1 (V3)	s
958-25	Gake	T2f3-2	c-p	958-72	Gake	T2f4-1 (V3)	c-g
958-26	Kata	T2f3-2	c-p	958-73	Gake	T2f4-1 (V3)	g-p
958-27	Kata	T2f3-2	c-p	958-74	Gake	T2f4-1 (V3)	s-g
958-28	Kata	T2f3-2	c-p	958-75	Gake	T2f4-1	c-g
958-29	Gake	T2f4-1	c	958-76	Gake	T2f4-1	c-s
958-30	Gake	T2f4-1	c	958-77	Gake	T2f4-1	c-ss
958-31	Kata	T2f4-1	c-s	958-78	Daaози	T2f4-1(V3+1)	c-g
958-32	Kata	T2f4-1	c-s	958-79	Daaози	T2f4-1(V3+1)	s-g
958-33	Gake	T2f4-1	c-s	958-80	Gake	T2f4-1	s
958-34	Gake	T2f4-1	c-s	958-81	Gake	T2f4-1	c-s
958-35	Gake	T2f4-1	c-s	958-82	Gake	T2f4-1(V3+2)	s-g
958-36	Kata	T2f4-1	c-s	958-83	Gake	T2f4-2	c
958-37	Kata	T2f4-1	s	958-84	Gake	T2f4-2	c
958-38	Gake	T2f4-1 (V1)	g-p	958-85	Gake	T2f4-2	c
958-39	Gake	T2f4-1 (V1)	g-p	958-86	Gake	T2f4-2	c
958-40	Gake	T2f4-1 (V1)	g-p	958-87	Gake	T2f4-2	c-s
958-41	Gake	T2f4-1 (V1)	g-p	958-88	Gake	T2f4-2	c-s
958-42	Gake	T2f4-1 (V1)	g-p	958-89	Gake	T2f4-2	c-s
958-43	Gake	T2f4-1 (V1)	g-p	958-90	Gake	T2f4-2	c-g
958-44	Gake	T2f4-1 (V1)	g-p	958-91	Gake	T2f4-2	c-g

Table II.1 Sample localities, positions and grainsize in vertical section of Falang Formation.

No.	Location	Position	Grainsize	No.	Location	Position	Grainsize
958-92	Kata	T2f4-2	c-g	958-139	Milike	T2f5-1	c-ss
958-93	Kata	T2f4-2	c-s	958-140	Milike	T2f5-1	s
958-94	Kata	T2f4-2	c-g	958-141	Baigu	T2f5-1 (V4)	c-g
958-95	Daozi	T2f4-2	s	958-142	Baigu	T2f5-1 (V4)	c-g
958-96	Daozi	T2f4-2	s	958-143	Baigu	T2f5-1 (V4)	c-g
958-97	Daozi	T2f4-2	c-s	958-144	Baigu	T2f5-1 (V4)	c-g
958-98	Gake	T2f4-3	c-s	958-145	Baigu	T2f5-1 (V4)	c-g
958-99	Gake	T2f4-3	s	958-146	Baigu	T2f5-1 (V4)	c-g
958-100	Gake	T2f4-3	s	958-147	Baigu	T2f5-1 (V4)	c-g
958-101	Gake	T2f4-3	c-ss	958-148	Baigu	T2f5-1 (V4)	c-g
958-102	Gake	T2f4-3	c-ss	958-149	Baigu	T2f5-1 (V4)	c-g
958-103	Gake	T2f4-3	c	958-150	Baigu	T2f5-1 (V4)	c-g
958-104	Gake	T2f4-3	c-s	958-151	Baigu	T2f5-2	c-s
958-105	Kata	T2f4-3	c-s	958-152	Baigu	T2f5-2	c-s
958-106	Kata	T2f4-3	c-s	958-153	Baigu	T2f5-2	c-s
958-107	Kata	T2f4-3	c-ss	958-154	Baigu	T2f5-2 (V5)	c-g
958-108	Kata	T2f4-3	c-ss	958-155	Baigu	T2f5-2 (V5)	c-g
958-109	Daozi	T2f4-3	c	958-156	Baigu	T2f5-2 (V5)	c-g
958-110	Daozi	T2f4-3	c	958-157	Baigu	T2f5-2 (V5)	c-g
958-111	Daozi	T2f4-3	c-ss	958-158	Baigu	T2f5-2 (V5)	c-g
958-112	Gake	T2f4-4	c-s	958-159	Baigu	T2f5-2 (V5)	c-g
958-113	Gake	T2f4-4	c-s	958-160	Baigu	T2f5-2 (V5)	c-g
958-114	Gake	T2f4-4	c-s	958-161	Baigu	T2f5-2 (V5)	c-g
958-115	Gake	T2f4-4	c-s	958-162	Baigu	T2f5-2 (V5)	c-g
958-116	Gake	T2f4-4	c-ss	958-163	Baigu	T2f5-2	c-s
958-117	Gake	T2f4-4	c-ss	958-164	Baigu	T2f5-2	c-s
958-118	Gake	T2f4-4	c-s	958-165	Baigu	T2f5-2	c-s
958-119	Kata	T2f4-4	c-s	958-166	Baigu	T2f5-2	c-s
958-120	Kata	T2f4-4	c-s	958-167	Baigu	T2f5-2 (V6)	c-g
958-121	Milike	T2f4-4	c-s	958-168	Baigu	T2f5-2 (V6)	c-g
958-122	Milike	T2f4-4	c-s	958-169	Baigu	T2f5-2 (V6)	c-g
958-123	Daozi	T2f4-4	c-s	958-170	Baigu	T2f5-2 (V6)	c-g
958-124	Daozi	T2f4-4	c-s	958-171	Baigu	T2f5-2 (V6)	c-g
958-125	Daozi	T2f4-4	c-s	958-172	Baigu	T2f5-2 (V6)	c-g
958-126	Baigu	T2f5-1	c-g	958-173	Baigu	T2f5-2 (V6)	g-p
958-127	Baigu	T2f5-1	s	958-174	Baigu	T2f5-2 (V6)	c
958-128	Baigu	T2f5-1	s	958-175	Milike	T2f5-2 (V6)	c-g
958-129	Baigu	T2f5-1	s	958-176	Milike	T2f5-2 (V6)	c-g
958-130	Baigu	T2f5-1	s	958-177	Milike	T2f5-2 (V6)	c-g
958-131	Baigu	T2f5-1	c	958-178	Baigu	T2f5-2	c-g
958-132	Baigu	T2f5-1	c-ss	958-179	Baigu	T2f5-2	c-g
958-133	Baigu	T2f5-1	c-s	958-180	Baigu	T2f5-2	c-g
958-134	Baigu	T2f5-1	c-s	958-181	Baigu	T2f5-2	c-g
958-135	Kata	T2f5-1	c-s	958-182	Milike	T2f5-2	c-g
958-136	Kata	T2f5-1	c-s	958-183	Milike	T2f5-2	c-g
958-137	Kata	T2f5-1	c-ss	958-184	Milike	T2f5-2	c-g
958-138	Milike	T2f5-1	c-ss	958-185	Milike	T2f5-2	c-g

Table II.1 Sample localities, positions and grainsize in vertical section of Falang Formation.

No.	Location	Position	Grainsize	No.	Location	Position	Grainsize
958-186	Baigu	T2f5-2(V7a)	c-g	958-229	Milike	T2f5-2 (V8)	c-g
958-187	Baigu	T2f5-2(V7a)	c-g	958-230	Milike	T2f5-2 (V8)	c-g
958-188	Baigu	T2f5-2(V7a)	c-g	958-231	Baigu	T2f5-2 (V8)	c-g
958-189	Baigu	T2f5-2(V7a)	c-g	958-232	Baigu	T2f5-2 (V8)	g-p
958-190	Baigu	T2f5-2(V7a)	c-g	958-233	Baigu	T2f5-2 (V8)	g-p
958-191	Baigu	T2f5-2(V7a)	g-p	958-234	Baigu	T2f5-2 (V8)	g-p
958-192	Baigu	T2f5-2(V7a)	g-p	958-235	Baigu	T2f5-2 (V8)	g-p
958-193	Baigu	T2f5-2(V7a)	c-s	958-236	Baigu	T2f5-2 (V8)	c-g
958-194	Baigu	T2f5-2(V7a)	g-p	958-237	Baigu	T2f5-2 (V8)	s
958-195	Milike	T2f5-2(V7a)	c-p	958-238	Baigu	T2f5-2 (V8)	c-g
958-196	Milike	T2f5-2(V7a)	c-p	958-239	Baigu	T2f5-2 (V8)	c-g
958-197	Milike	T2f5-2(V7a)	c-g	958-240	Baigu	T2f5-2	c-g
958-198	Milike	T2f5-2(V7a)	c-g	958-241	Baigu	T2f5-2	c-s
958-199	Milike	T2f5-2(V7a)	c-g	958-242	Milike	T2f5-2	c-g
958-200	Milike	T2f5-2(V7a)	c-g	958-243	Baigu	T2f5-2 (V8)	g-p
958-201	Baigu	T2f5-2(V7b)	c-s	958-244	Baigu	T2f5-2 (V8)	g-p
958-202	Baigu	T2f5-2(V7b)	c-g	958-245	Baigu	T2f5-2 (V9)	c-g
958-203	Baigu	T2f5-2(V7b)	c-p	958-246	Baigu	T2f5-2 (V9)	c-g
958-204	Baigu	T2f5-2(V7b)	c-p	958-247	Baigu	T2f5-2 (V9)	c-g
958-204a	Baigu	T2f5-2(V7b)	c-p	958-248	Baigu	T2f5-2 (V9)	c-g
958-204b	Baigu	T2f5-2(V7b)	c-p	958-249	Baigu	T2f5-2 (V9)	c-ss
958-204c	Baigu	T2f5-2(V7b)	c-p	958-250	Baigu	T2f5-2 (V9)	c-s
958-204d	Baigu	T2f5-2(V7b)	c-p	958-251	Baigu	T2f5-2	c-s
958-205	Baigu	T2f5-2(V7b)	g-p	958-252	Baigu	T2f5-2	c-s
958-206	Baigu	T2f5-2(V7b)	g-p	958-253	Baigu	T2f5-2	c-s
958-207	Baigu	T2f5-2(V7b)	g-p	958-254	Baigu	T2f5-2	c-s
958-208	Baigu	T2f5-2(V7b)	c-g	958-255	Milike	T2f5-2	c
958-209	Milike	T2f5-2(V7b)	c-ss	958-256	Milike	T2f5-2	c-s
958-210	Milike	T2f5-2(V7b)	s	958-257	Milike	T2f5-2	c-s
958-211	Milike	T2f5-2(V7b)	c-g	958-258	Milike	T2f5-2	c-s
958-212	Milike	T2f5-2(V7b)	c-g	958-259	Baigu	T2f5-2(V10)	c-g
958-213	Milike	T2f5-2(V7b)	c-g	958-260	Baigu	T2f5-2(V10)	c-g
958-214	Milike	T2f5-2(V7b)	c-g	958-261	Baigu	T2f5-2(V10)	c-g
958-215	Milike	T2f5-2(V7b)	c-s	958-262	Baigu	T2f5-2(V10)	c-g
958-216	Baigu	T2f5-2	c-s	958-263	Baigu	T2f5-3	c-s
958-217	Baigu	T2f5-2	c-s	958-264	Baigu	T2f5-3	c-s
958-218	Baigu	T2f5-2	c-s	958-265	Baigu	T2f5-3	c-s
958-219	Baigu	T2f5-2	c-s	958-266	Baigu	T2f5-3	c-s
958-220	Baigu	T2f5-2	c-s	958-267	Baigu	T2f5-3	c
958-221	Milike	T2f5-2	c-s	958-268	Baigu	T2f5-3	c-s
958-222	Milike	T2f5-2	c	958-269	Baigu	T2f5-3	c-s
958-223	Milike	T2f5-2	c	958-270	Baigu	T2f5-3	c-s
958-224	Milike	T2f5-2	c-g	958-271	Baigu	T2f5-3	c-s
958-225	Baigu	T2f5-2 (V8)	g-p	958-272	Milike	T2f5-3	c-s
958-226	Baigu	T2f5-2 (V8)	g-p	958-273	Milike	T2f5-3	c-s
958-227	Baigu	T2f5-2 (V8)	c-g	958-274	Milike	T2f5-3	c-s
958-228	Milike	T2f5-2 (V8)	g-p	958-275	Milike	T2f5-3	c-s

Table II.1 Sample localities, positions and grainsize in vertical section of Falang Formation.

No.	Location	Position	Grainsize	No.	Location	Position	Grainsize
958-276	Milike	T2f5-3	c-s	958-289	Baigu	T2f6	c-s
958-277	Milike	T2f5-3	c-s	958-290	Milike	T2f6	ss
958-278	Milike	T2f5-3	c-s	958-291	Milike	T2f6	ss
958-279	Baigu	T2f6	ss	958-292	Milike	T2f6	s
958-280	Baigu	T2f6	ss	958-293	Milike	T2f6	c-s
958-281	Baigu	T2f6	ss	958-294	Milike	T2f6	c-s
958-282	Baigu	T2f6	ss	958-295	Baigu	T2f5-2	c-p
958-283	Baigu	T2f6	ss	Grainsize:			
958-284	Baigu	T2f6	ss	c-clay			
958-585	Baigu	T2f6	c-s	s-silt			
958-286	Baigu	T2f6	c-s	ss-sand			
958-287	Baigu	T2f6	c-s	g-granule			
958-288	Baigu	T2f6	c-s	p-pebble			

Table II.2 Geochemical Environmental Index of Dounan Stratigraphy.

No.	strata	Fe ³⁺	Fe ²⁺	Fe ³⁺ /Fe ²⁺	organic C
958-286	T _{2f6}	0.07	0.31	0.23	0.14
958-284	T _{2f6}	0.07	0.35	0.20	0.19
958-282	T _{2f6}	0.09	0.32	0.28	0.16
958-270	T _{2f5-3}	0.67	1.82	0.37	0.65
958-268	T _{2f5-3}	0.67	1.79	0.37	0.63
958-266	T _{2f5-3}	0.69	1.72	0.40	0.65
958-258	T _{2f5-2}	0.03	0.15	0.20	0.02
958-256	T _{2f5-2}	0.06	0.18	0.33	0.07
958-254	T _{2f5-2}	0.07	0.27	0.26	0.06
958-252	T _{2f5-2}	0.54	0.88	0.61	0.42
958-242	T _{2f5-2}	0.08	0.65	0.12	0.40
958-240	T _{2f5-2}	0.66	0.74	0.89	0.11
958-222	T _{2f5-2}	0.09	0.64	0.14	0.44
958-220	T _{2f5-2}	0.68	1.20	0.57	0.11
958-218	T _{2f5-2}	0.72	1.52	0.47	0.15
958-216	T _{2f5-2}	0.79	1.55	0.51	0.17
958-138	T _{2f5-1}	0.79	2.08	0.38	0.43
958-136	T _{2f5-1}	0.74	2.10	0.35	0.44
958-134	T _{2f5-1}	0.72	2.22	0.32	0.43
958-122	T _{2f4-4}	0.81	2.72	0.30	0.48
958-120	T _{2f4-4}	0.52	2.95	0.18	0.49
958-118	T _{2f4-4}	0.66	2.88	0.23	0.51
958-106	T _{2f4-3}	0.77	2.03	0.38	0.47
958-104	T _{2f4-3}	0.79	2.06	0.38	0.46
958-102	T _{2f4-3}	0.72	2.00	0.36	0.44
958-96	T _{2f4-2}	0.19	1.24	0.15	0.16
958-94	T _{2f4-2}	0.29	1.13	0.26	0.15
958-92	T _{2f4-2}	0.22	1.20	0.18	0.14
958-90	T _{2f4-2}	0.21	1.78	0.12	0.16
958-88	T _{2f4-2}	0.30	1.74	0.17	0.14
958-86	T _{2f4-2}	0.36	1.87	0.19	0.12
958-80	T _{2f4-1}	0.24	0.98	0.24	0.09
958-77	T _{2f4-1}	0.25	0.70	0.36	0.10
958-75	T _{2f4-1}	0.29	0.45	0.64	0.13
958-68	T _{2f4-1}	0.35	0.78	0.45	0.12
958-67	T _{2f4-1}	0.24	0.92	0.26	0.09
958-58	T _{2f4-1}	0.75	1.22	0.61	0.21
958-56	T _{2f4-1}	0.66	1.24	0.53	0.08
958-54	T _{2f4-1}	1.24	1.10	1.13	0.12
958-36	T _{2f4-1}	1.54	1.38	1.12	0.11
958-34	T _{2f4-1}	1.56	1.36	1.15	0.10
958-30	T _{2f4-1}	1.55	1.37	1.13	0.11
958-26	T _{2f3-2}	0.15	0.33	0.46	0.07
958-24	T _{2f3-2}	0.32	0.54	0.59	0.07
958-14	T _{2f3-1}	0.34	1.29	0.26	0.09
958-8	T _{2f2}	0.15	0.84	0.18	0.09
958-6	T _{2f2}	0.16	1.66	0.10	0.12
958-5	T _{2f2}	1.99	2.46	0.80	0.13
958-3	T _{2f1}	0.09	0.40	0.30	0.03
958-2	T _{2f1}	0.25	0.82	0.30	0.05
958-1	T _{2f1}	0.60	1.31	0.46	0.09

Appendix III (Orebeds)

Table III.1. Scale, Morphology and Occurrence of Minor (Major see Chapter 3) Orebodies.

Table III.1 Features of minor orebodies of Dounan Mn deposits (modified after Zhang et al., 1979).

orebody	location	ore type major minor	thickness (m)		Mn (%)	
			MAX MID		MAX MID	
V10	Baigu Milike	Mn oxides	1.36		23.44	
		Mn carbonate	1.16		15.89	
V8b	Baigu	Mn carbonate	0.64		34.52	
		Mn oxides	0.50		21.11	
V8a	Baigu	Mn carbonate	1.35		20.29	
		Mn oxides	0.52		12.05	
V5	Baigu Milike	Mn oxides	0.97		43.87	
		Mn carbonate	0.58		26.10	
V4	Baigu Milike	Mn oxides	1.16		41.36	
		Mn carbonate	0.98		32.16	
V3+1	Gake, Baigu, Kata, Milike, Daaози.	Mn oxides	0.33		40.18	
		Mn carbonate	0.32		22.26	
V1-2	Gake	Mn oxides	0.93		21.14	
		Mn carbonate	0.63		15.11	

Appendix IV (Petrology and Mineralogy)

Table IV.1. Ore and Rock Types.

Table IV.1 Ore and rock types.

No.	Rock or ore type	No.	Rock or ore type
958-I	grey micrite	958-49	black Mn oxide oolite/pisolite
958-II	grey micrite	958-50	black Mn oxide oolite/pisolite
958-III	grey micrite	958-51	black Mn oxide oolite/pisolite
958-1	grey calcarenite	958-52	grey oolitic Mn-bearing micrite
958-2	grey calcarenite	958-53	grey clayey siltstone
958-3	grey calcarenite	958-54	grey clayey siltstone
958-4	light grey calcareous siltstone	958-55	grey clayey siltstone
958-5	light grey calcareous siltstone	958-56	grey silty claystone
958-6	grey calcareous clayey siltstone	958-57	grey silty claystone
958-7	grey silty claystone	958-58	grey clayey siltstone
958-8	grey silty claystone	958-59	dark grey Mn-bearing silty claystone
958-9	grey silty claystone	958-60	black massive Mn oxide ore
958-10	grey silty claystone	958-61	dark red unsorted Mn oxide ore
958-11	grey silty claystone	958-62	dark red banded Mn oxide ore
958-12	grey silty claystone	958-63	Mn oxide deformed oolite/pisolite
958-13	grey clayey siltstone	958-64	dark red banded Mn oxide ore
958-14	grey clayey siltstone	958-65	black Mn oxide oolite/pisolite
958-15	grey clayey siltstone	958-66	grey siltstone
958-16	grey silty claystone	958-67	grey clayey siltstone
958-17	grey clayey siltstone	958-68	grey clayey siltstone
958-18	grey siltstone	958-69	dark red banded Mn oxide ore
958-19	grey siltstone	958-70	dark red Mn carbonate ore
958-20	dark red intramicrudite	958-71	calcareous siltstone
958-21	dark red intramicrudite	958-72	dark grey Mn-bearing micrite
958-22	dark red intramicrudite	958-73	black Mn oxide oolite/pisolite
958-23	dark red intramicrudite	958-74	black Mn oxide oolite/pisolite
958-24	dark red intramicrudite	958-75	grey bioclastic debris micrite
958-25	dark red intramicrudite	958-76	dark grey Mn-bearing micrite
958-26	dark red intramicrudite	958-77	grey calcarenite
958-27	dark red intramicrudite	958-78	dark red Mn carbonate ore
958-28	dark red intramicrudite	958-79	dark red banded Mn oxide ore
958-29	grey calcareous claystone	958-80	grey clayey siltstone
958-30	grey calcareous claystone	958-81	grey silty claystone
958-31	grey silty claystone	958-82	dark red unsorted Mn oxide ore
958-32	grey clayey siltstone	958-83	grey silty claystone
958-33	grey clayey siltstone	958-84	grey silty claystone
958-34	grey clayey siltstone	958-85	grey silty claystone
958-35	grey clayey siltstone	958-86	grey silty claystone
958-36	grey clayey siltstone	958-87	grey clayey siltstone
958-37	grey clayey siltstone	958-88	grey clayey siltstone
958-38	black massive Mn oxide ore	958-89	grey clayey siltstone
958-39	black massive Mn oxide ore	958-90	grey calcarenite
958-40	Mn oxide deformed oolite/pisolite	958-91	grey oolitic micrite
958-41	Mn oxide deformed oolite/pisolite	958-92	grey calcareous silty claystone
958-42	Mn oxide deformed oolite/pisolite	958-93	grey calcareous silty claystone
958-43	Mn oxide deformed oolite/pisolite	958-94	grey intrasparite
958-44	black Mn oxide oolite/pisolite	958-95	grey clayey siltstone
958-45	dark red oolitic Mn-bearing carbonate	958-96	grey clayey siltstone
958-46	black Mn oxide oolite/pisolite	958-97	grey silty claystone
958-47	grey oolitic/pisolitic calcarenite	958-98	grey silty claystone
958-48	dark red banded Mn oxide ore	958-99	grey clayey siltstone

Table IV.1 Ore and rock types.

No.	Rock or ore type	No.	Rock or ore type
958-100	grey clayey siltstone	958-151	grey silty claystone
958-101	grey clayey siltstone	958-152	grey silty claystone
958-102	grey calcarenite	958-153	grey silty claystone
958-103	grey silty claystone	958-154	dark red unsorted Mn oxide ore
958-104	grey clayey siltstone	958-155	dark red banded Mn oxide ore
958-105	grey clayey siltstone	958-156	brown Mn-bearing oolitic micrite
958-106	grey clayey siltstone	958-157	dark grey Mn carbonate ore
958-107	grey calcarenite	958-158	dark grey Mn carbonate ore
958-108	grey calcarenite	958-159	dark grey Mn carbonate ore
958-109	grey silty claystone	958-160	dark red unsorted Mn oxide ore
958-110	grey silty claystone	958-161	dark red unsorted Mn oxide ore
958-111	grey calcarenite	958-162	dark grey Mn carbonate ore
958-112	grey clayey siltstone	958-163	grey Mn-bearing clayey siltstone
958-113	grey clayey siltstone	958-164	grey clayey siltstone
958-114	grey clayey siltstone	958-165	grey clayey siltstone
958-115	grey clayey siltstone	958-166	grey Mn-bearing silty claystone
958-116	grey calcarenite	958-167	dark grey Mn carbonate ore
958-117	grey calcarenite	958-168	dark red unsorted Mn oxide ore
958-118	grey calcilutite	958-169	dark grey Mn-bearing intrasparite
958-119	grey clayey siltstone	958-170	dark red banded Mn oxide ore
958-120	grey clayey siltstone	958-171	brown Mn-bearing oolitic micrite
958-121	grey clayey siltstone	958-172	dark red banded Mn oxide ore
958-122	grey clayey siltstone	958-173	blak Mn oxide oolite/pisolite
958-123	grey clayey siltstone	958-174	dark grey Mn-bearing micrite
958-124	grey clayey siltstone	958-175	dark grey Mn-bearing intrasparite
958-125	grey calcarenite	958-176	grey Mn-bearing oolitic mudstone
958-126	grey clayey siltstone	958-177	dark grey Mn-bearing intrasparite
958-127	grey clayey siltstone	958-178	grey Mn-bearing clayey siltstone
958-128	grey clayey siltstone	958-179	grey silty claystone
958-129	grey clayey siltstone	958-180	grey calcilutite
958-130	grey clayey siltstone	958-181	grey silty claystone
958-131	dark grey Mn-bearing micrite	958-182	grey Mn-bearing silty claystone
958-132	grey calcarenite	958-183	grey clayey siltstone
958-133	grey silty claystone	958-184	grey clayey siltstone
958-134	grey silty claystone	958-185	grey silty claystone
958-135	grey clayey siltstone	958-186	grey clayey siltstone
958-136	grey clayey siltstone	958-187	dark red banded Mn oxide ore
958-137	grey calcarenite	958-188	dark red banded Mn oxide ore
958-138	grey calcarenite	958-189	dark red banded Mn oxide ore
958-139	grey calcarenite	958-190	dark red banded Mn oxide ore
958-140	grey clayey siltstone	958-191	blak Mn oxide oolite/pisolite
958-141	dark grey Mn-bearing intrasparite	958-192	blak Mn oxide oolite/pisolite
958-142	dark grey Mn carbonate ore	958-193	grey Mn-bearing silty claystone
958-143	dark grey Mn carbonate ore	958-194	black massive Mn oxide ore
958-144	dark grey Mn carbonate ore	958-195	dark red unsorted Mn oxide ore
958-145	dark red unsorted Mn oxide ore	958-196	dark red unsorted Mn oxide ore
958-146	dark red unsorted Mn oxide ore	958-197	dark red banded Mn oxide ore
958-147	dark red banded Mn carbonate ore	958-198	dark grey Mn-bearing intrasparite
958-148	dark red Mn carbonate ore	958-199	dark grey Mn-bearing intrasparite
958-149	dark red Mn carbonate ore	958-200	dark red Mn carbonate ore
958-150	dark red Mn carbonate ore	958-201	dark grey Mn-bearing siltstone

Table IV.1 Ore and rock types.

No.	Rock or ore type	No.	Rock or ore type
958-202	dark red unsorted Mn oxide ore	958-249	grey calcarenite
958-203	dark red banded Mn oxide ore	958-250	grey clayey siltstone
958-204	dark red unsorted Mn oxide ore	958-251	grey silty claystone
958-204a	dark red unsorted Mn oxide ore	958-252	grey clayey siltstone
958-204b	dark red unsorted Mn oxide ore	958-253	grey clayey siltstone
958-204c	dark red unsorted Mn oxide ore	958-254	grey silty claystone
958-204d	dark red unsorted Mn oxide ore	958-255	grey calcilutite
958-205	black massive Mn oxide ore	958-256	grey silty claystone
958-206	black massive Mn oxide ore	958-257	grey clayey siltstone
958-207	Mn oxide deformed oolite/pisolite	958-258	grey clayey siltstone
958-208	brown Mn-bearing oolitic micrite	958-259	grey Mn-bearing silty claystone
958-209	dark grey Mn-bearing calcarenite	958-260	dark grey Mn carbonate ore
958-210	grey calcareous siltstone	958-261	dark grey Mn carbonate ore
958-211	dark red banded Mn oxide ore	958-262	dark grey Mn-bearing intrasparite
958-212	dark red banded Mn oxide ore	958-263	grey clayey siltstone
958-213	dark red unsorted Mn oxide ore	958-264	grey clayey siltstone
958-214	dark grey Mn-bearing intrasparite	958-265	grey clayey siltstone
958-215	grey clayey siltstone	958-266	grey silty claystone
958-216	grey Mn-bearing silty claystone	958-267	grey calcilutite
958-217	grey silty claystone	958-268	grey silty claystone
958-218	grey clayey siltstone	958-269	grey silty claystone
958-219	grey clayey siltstone	958-270	grey clayey siltstone
958-220	grey Mn-bearing clayey siltstone	958-271	grey clayey siltstone
958-221	grey silty claystone	958-272	grey silty claystone
958-222	grey calcilutite	958-273	grey clayey siltstone
958-223	grey calcilutite	958-274	grey clayey siltstone
958-224	dark grey Mn-bearing intrasparite	958-275	grey silty claystone
958-225	black Mn oxide oolite/pisolite	958-276	grey clayey siltstone
958-226	black Mn oxide oolite/pisolite	958-277	grey silty claystone
958-227	dark red unsorted Mn oxide ore	958-278	grey silty claystone
958-228	dark grey Mn carbonate ore	958-279	light grey fine grain sandstone
958-229	dark red Mn-bearing micrite	958-280	light grey fine grain sandstone
958-230	dark red Mn-bearing micrite	958-281	light grey fine grain sandstone
958-231	dark red unsorted Mn oxide ore	958-282	grey siltstone
958-232	black Mn oxide oolite/pisolite	958-283	grey siltstone
958-233	Mn oxide deformed oolite/pisolite	958-284	grey siltstone
958-234	black Mn oxide oolite/pisolite	958-285	grey silty claystone
958-235	black Mn oxide oolite/pisolite	958-286	grey silty claystone
958-236	dark grey Mn carbonate ore	958-287	grey silty claystone
958-237	grey Mn-bearing calcareous siltstone	958-288	grey silty claystone
958-238	dark red banded Mn oxide ore	958-289	grey silty claystone
958-239	grey Mn-bearing oolitic mudstone	958-290	light grey fine grain sandstone
958-240	grey Mn-bearing oolitic mudstone	958-291	light grey fine grain sandstone
958-241	grey clayey siltstone	958-292	grey siltstone
958-242	dark grey Mn-bearing intrasparite	958-293	grey silty claystone
958-243	black Mn oxide oolite/pisolite	958-294	grey silty claystone
958-244	black Mn oxide oolite/pisolite	958-295	siderite nodule-bearing mudstone
958-245	dark red banded Mn oxide ore		
958-246	dark red banded Mn oxide ore		
958-247	dark red banded Mn oxide ore		
958-248	brown Mn-bearing oolitic micrite		

Appendix V (Geochemistry)

Table V.1. XRF / AA Major and Minor Element Analyses of Ores and Rocks; [%].

Table V.2. XRF Trace Element Analyses of Ores and Rocks; [ppm].

Table V.3. IDMS Rare Earth Element Analyses of Ores and Rocks; [ppm].

Table V.4. Electron Microprobe Analysis; [%].

Table V.5. Stable Isotopic Composition of Ores and Rocks; [PDB].

Table V.1 XRF major and minor element analyses of ores and rocks; [%].

NO.	Al ₂ O ₃	BaO	CaO	TFe ₂ O ₃	K ₂ O	MgO	MnO/MnO ₂	Na ₂ O
958-38	0.77	0.03	6.35	0.67	0.01	1.46	66.41	0.03
958-39	2.19	0.03	5.54	1.47	0.19	2.11	61.67	0.20
958-40	2.22	0.02	12.31	1.24	0.13	3.37	44.98	0.34
958-41	0.89	0.02	14.19	0.66	0.02	2.87	41.00	0.05
958-44	2.04	0.02	10.81	1.33	0.05	4.26	43.53	0.26
958-45	3.09	0.06	35.14	1.57	0.41	2.84	10.11	0.35
958-48	3.38	0.03	11.44	1.64	0.23	5.42	37.07	1.52
958-49	0.68	0.03	14.42	0.61	0.04	0.79	55.54	0.09
958-60	0.91	0.02	4.38	0.86	0.01	2.30	63.58	0.15
958-61	3.06	0.03	21.23	0.88	0.01	1.15	40.77	0.03
958-62	2.01	0.02	17.26	1.61	0.12	7.84	29.08	0.07
958-63	1.05	0.03	21.36	0.68	0.01	0.70	45.03	0.28
958-64	1.82	0.04	33.37	1.00	0.23	4.19	17.55	0.36
958-65	2.97	0.02	19.95	1.70	0.52	4.13	28.98	0.31
958-72	2.32	0.02	30.41	8.14	0.22	3.47	8.36	0.10
958-142	3.47	0.02	17.47	1.92	0.47	3.87	25.04	0.92
958-143	4.62	0.03	15.14	3.07	1.01	2.64	24.97	0.38
958-144	1.86	0.03	4.08	1.27	0.18	4.08	36.06	0.41
958-145	4.52	0.04	14.91	5.20	1.01	3.20	23.27	0.27
958-156	1.90	0.01	32.09	3.11	0.39	3.02	11.81	0.12
958-169	1.84	0.02	43.81	1.16	0.41	2.03	5.28	0.19
958-172	2.38	0.03	24.61	1.34	0.28	2.88	30.25	0.19
958-173	3.41	0.05	10.17	2.02	0.41	2.36	52.66	0.08
958-192	2.15	0.03	7.46	1.31	0.09	2.38	54.90	0.04
958-194	2.32	0.13	12.78	1.56	0.31	1.26	53.57	0.05
958-201	5.78	0.04	16.26	2.63	0.98	3.27	17.75	1.05
958-204	1.38	0.02	29.01	0.85	0.19	2.92	22.62	0.25
958-205	1.20	0.04	4.36	0.65	0.56	0.39	69.82	0.10
958-225	1.41	0.04	18.20	1.03	0.11	4.52	36.73	0.29
958-232	1.95	0.33	15.66	1.19	0.20	1.42	49.73	0.05
958-233	3.15	0.03	17.89	1.80	0.52	1.82	35.73	0.47
958-236	0.23	0.05	31.42	0.27	0.01	0.65	33.26	0.04
958-237	5.12	0.02	21.82	5.22	0.74	2.65	8.01	1.14
958-243	1.93	0.42	15.47	1.18	0.16	1.42	50.25	0.02
958-244	3.08	0.21	8.83	2.27	0.40	2.32	45.97	0.54
958-245	3.68	0.06	21.86	2.10	0.55	2.12	22.79	1.24
958-246	5.52	0.05	18.29	2.60	1.08	2.14	21.67	0.98
958-259	6.43	0.03	15.99	4.68	1.29	2.53	13.49	1.18

Table V.1 XRF major and minor element analyses of ores and rocks; [%].

NO.	P₂O₅	SO₃	SiO₂	SrO	TiO₂	LOI	Total	Mass Abs
958-38	0.18	0.01	10.24	0.02	0.07	7.40	93.64	2.4698
958-39	0.17	0.01	12.73	0.02	0.10	8.48	94.92	2.3260
958-40	0.29	0.03	11.90	0.03	0.10	18.72	95.68	1.8924
958-41	0.21	0.02	8.85	0.04	0.05	20.24	95.11	1.9660
958-44	0.26	0.03	10.98	0.04	0.07	22.61	96.28	1.8181
958-45	0.10	0.02	12.54	0.06	0.15	31.06	97.50	1.1434
958-48	3.33	0.04	14.22	0.03	0.12	22.78	98.22	1.6481
958-49	0.19	0.00	9.21	0.04	0.03	12.58	94.21	2.2422
958-60	0.18	0.03	10.49	0.02	0.09	11.20	94.22	2.3507
958-61	0.14	0.07	3.06	0.04	0.05	26.85	94.80	1.8501
958-62	0.16	0.02	11.29	0.04	0.10	26.63	96.25	1.4649
958-63	0.10	0.01	7.49	0.07	0.05	17.47	94.31	2.0081
958-64	0.12	0.09	7.87	0.05	0.12	31.38	98.20	1.3348
958-65	0.18	0.08	14.00	0.03	0.15	23.53	96.55	1.5180
958-72	0.16	3.86	13.60	0.08	0.10	27.55	98.39	1.0458
958-142	0.12	0.04	15.31	0.03	0.18	28.07	96.92	1.3558
958-143	0.17	0.20	17.41	0.03	0.26	27.50	97.43	1.3381
958-144	0.29	0.73	8.28	0.04	0.24	26.34	97.62	1.2898
958-145	0.16	0.04	17.58	0.03	0.11	27.86	95.96	1.6441
958-156	0.19	0.10	12.12	0.07	0.09	32.43	97.46	1.1453
958-169	0.07	0.13	5.94	0.09	0.07	37.12	98.15	1.0938
958-172	0.12	0.03	7.49	0.05	0.12	25.43	95.20	1.5982
958-173	0.09	0.02	12.06	0.05	0.17	10.64	94.19	2.1162
958-192	0.10	0.04	9.84	0.03	0.12	16.16	94.65	2.1234
958-194	0.18	0.08	9.88	0.06	0.12	11.98	94.27	2.1742
958-201	0.11	0.03	30.20	0.03	0.33	18.87	97.33	1.1751
958-204	0.15	0.10	6.96	0.10	0.08	31.12	95.74	1.4139
958-205	0.09	0.01	2.63	0.07	0.07	12.87	92.86	2.5270
958-225	0.16	0.19	9.32	0.07	0.08	22.92	95.08	1.7103
958-232	0.09	0.17	8.37	0.04	0.10	15.00	94.29	2.0953
958-233	0.15	0.04	15.58	0.04	0.16	18.26	95.64	1.7045
958-236	0.07	0.03	4.25	0.04	0.03	23.62	93.98	1.7722
958-237	0.14	0.15	30.74	0.07	0.25	22.62	98.69	0.9516
958-243	0.09	0.22	8.42	0.04	0.09	14.86	94.53	2.1129
958-244	0.16	0.14	17.03	0.05	0.17	14.17	95.34	1.9045
958-245	0.10	0.05	22.60	0.07	0.17	19.96	97.33	1.3833
958-246	0.11	0.05	23.16	0.05	0.24	21.40	97.32	1.3063
958-259	0.14	0.97	29.99	0.07	0.30	21.68	98.80	1.0491

Table V.3 IDMS rare earth element analyaea of ores and rocks; [ppm].

NO.	La	Ce	Nd	Sn	Eu	Gd	Dy	Er	Yb
958-38	2.48	6.35	2.28	0.28	0.06	0.37	0.35	0.16	0.22
958-39	3.07	7.22	3.14	0.98	0.22	1.05	1.22	0.74	0.64
958-41	3.42	6.11	2.45	0.20	0.11	0.97	0.53	0.42	0.24
958-42	7.05	13.89	4.49	0.88	0.26	0.88	0.99	0.48	0.39
958-43	7.12	13.21	5.01	0.89	0.22	0.97	0.93	0.52	0.41
958-44	6.62	11.57	3.91	0.88	0.12	0.73	0.45	0.35	0.37
958-45	2.23	4.58	1.90	0.41	0.14	0.38	0.64	0.53	0.35
958-46	4.88	6.89	3.68	0.96	0.19	0.98	0.98	0.65	0.63
958-49	5.74	7.01	4.74	1.12	0.21	0.99	1.25	0.73	0.82
958-61	7.25	14.59	5.41	0.45	0.25	0.82	0.70	0.70	0.57
958-142	13.84	27.80	9.81	2.28	0.48	2.28	2.28	1.83	1.34
958-143	12.55	26.45	8.66	2.12	0.45	1.96	2.11	0.96	0.94
958-144	13.53	27.95	9.76	2.38	0.51	2.48	2.30	1.20	1.44
958-145	5.23	11.35	5.03	1.11	0.27	1.54	1.02	0.62	0.57
958-158	1.97	3.66	1.34	0.31	0.07	0.46	0.52	0.34	0.29
958-194	1.92	5.18	1.27	0.12	0.02	0.29	0.08	0.18	0.22
958-204	6.84	12.82	5.82	1.98	0.29	1.27	1.76	0.69	0.66
958-236	2.25	4.72	1.92	0.48	0.10	0.87	0.67	0.38	0.32

Table V.4 Electron microprobe analysis [%].

No.	mr.		Al ₂ O ₃	CaO	Cr ₂ O ₃	FeO	K ₂ O	MgO	MnO	Na ₂ O	SiO ₂	TiO ₂	TOTAL
		CR	0.51	24.65	0	0	0.02	0.56	28.05	0	2.29	0	56.08
40	CRd	NR	0.91	43.96	0	0	0.04	1	50.02	0	4.08	0	100
		12o.	0.128	5.609	0	0	0.005	0.178	5.047	0	0.486	0	11.453
		CR	0.85	26.96	0	0	0	0.78	29.82	0	1.42	0	59.83
41	CRd	NR	1.42	45.06	0	0	0	1.3	49.84	0	2.38	0	100
		12o.	0.201	5.811	0	0	0	0.233	5.082	0	0.286	0	11.614
		CR	1.03	18.43	0	0	0.14	1.31	37.12	0	0.82	0.1	58.95
42	CRd	NR	1.75	31.27	0	0	0.24	2.22	62.97	0	1.39	0.16	100
		12o.	0.257	4.17	0	0	0.038	0.412	6.638	0	0.173	0.015	11.703
		CR	2.32	20.97	0	0.1	0	2.04	41.92	0.1	6.22	0.11	73.78
43	CRd	NR	3.15	28.43	0	0.14	0	2.76	56.81	0.14	8.43	0.15	100
		12o.	0.422	3.461	0	0.013	0	0.467	5.469	0.031	0.959	0.012	10.834
		CR	0.3	14.39	0	0.13	0	0.27	42.98	0	0.01	0	58.09
44	CRd	NR	0.51	24.78	0	0.22	0	0.47	74	0	0.02	0	100
		12o.	0.08	3.499	0	0.024	0	0.092	8.26	0	0.003	0	11.957
		CR	0.34	12.25	0	0	0.09	0.45	45.36	0.44	0.39	0.1	59.41
45	CRd	NR	0.57	20.62	0	0	0.16	0.76	76.36	0.73	0.65	0.16	100
		12o.	0.088	2.906	0	0	0.026	0.148	8.506	0.186	0.085	0.016	11.961
		CR	1.57	16.32	0	1.31	0.15	1.58	47.32	0	8.67	0.24	77.16
46	CRd	NR	2.04	21.15	0	1.69	0.2	2.05	61.33	0	11.23	0.32	100
		12o.	0.273	2.571	0	0.161	0.028	0.346	5.895	0	1.275	0.027	10.576
		CR	2.34	12.87	0	1.59	0.07	1.87	53.01	0.05	8.43	0.23	80.44
47	CRd	NR	2.91	16	0	1.98	0.09	2.32	65.89	0.06	10.48	0.28	100
		12o.	0.393	1.964	0	0.189	0.013	0.396	6.397	0.013	1.201	0.024	10.591
958-142	CR		1.29	32.81	0	0	0.24	0.9	19.67	0.07	2.91	0.01	57.91
48	CM	NR	2.23	56.67	0	0	0.42	1.55	33.96	0.13	5.03	0.01	100
		12o.	0.297	6.859	0	0	0.061	0.261	3.25	0.027	0.569	0.001	11.326
		CR	0.66	37.44	0	0	0	0.69	17.09	0	0.46	0	56.35
49	CM	NR	1.18	66.45	0	0	0	1.22	30.33	0	0.82	0	100
		12o.	0.162	8.341	0	0	0	0.213	3.01	0	0.096	0	11.823
		CR	0.39	38.86	0	0	0	1.04	14.81	0.1	0.06	0	55.27
50	CM	NR	0.71	70.32	0	0	0	1.88	26.8	0.18	0.11	0	100
		12o.	0.098	8.821	0	0	0	0.327	2.658	0.041	0.013	0	11.959
		CR	0.72	42.17	0	0	0.04	0.69	13.68	0.05	0.19	0.26	57.79
51	CM	NR	1.25	72.97	0	0	0.06	1.2	23.67	0.08	0.33	0.44	100
		12o.	0.171	9.049	0	0	0.009	0.207	2.321	0.019	0.038	0.038	11.852
		CR	0.4	37.63	0	0	0.17	2	13.95	0	0.18	0.19	54.51
52	CM	NR	0.73	69.03	0	0	0.31	3.66	25.59	0	0.32	0.35	100
		12o.	0.099	8.554	0	0	0.046	0.631	2.507	0	0.038	0.031	11.905

Table V.4 Electron microprobe analysis [%].

No.	mr.		Al ₂ O ₃	CaO	Cr ₂ O ₃	FeO	K ₂ O	MgO	MnO	Na ₂ O	SiO ₂	TiO ₂	TOTAL
		CR	0.59	38.45	0	0.01	0.07	0.66	14.23	0	0.36	0	54.37
53	CM	NR	1.08	70.72	0	0.02	0.13	1.21	26.17	0	0.67	0	100
		12o.	0.148	8.82	0	0.01	0.019	0.211	2.581	0	0.077	0	11.858
		CR	0.72	35.57	0	0	0	1.18	19.98	0.13	0.82	0.1	58.4
54	CM	NR	1.24	60.9	0	0	0	2.03	34.05	0.22	1.4	0.16	100
		12o.	0.171	7.634	0	0	0	0.353	3.375	0.05	0.164	0.014	11.761
		CR	0.96	30.78	0	0.27	0.16	1.16	20.63	0.05	1.39	0.06	55.45
55	CM	NR	1.73	55.51	0	0.48	0.28	2.09	37.2	0.09	2.51	0.11	100
		12o.	0.237	6.929	0	0.047	0.042	0.363	3.671	0.02	0.292	0.009	11.61
958-143		CR	0.88	42.2	0	0	0.19	1.16	10.52	0.01	1.35	0.09	56.4
56	MC	NR	1.57	74.82	0	0	0.34	2.06	18.65	0.02	2.39	0.15	100
		12o.	0.207	8.985	0	0	0.048	0.345	1.771	0.003	0.286	0.013	11.641
		CR	0.61	46.36	0	0	0.11	0.72	7.8	0.09	0.11	0	55.8
57	MC	NR	1.09	83.09	0	0	0.2	1.29	13.98	0.15	0.2	0	100
		12o.	0.147	10.14	0	0	0.029	0.219	1.348	0.034	0.023	0	11.935
		CR	0.58	47.05	0	0	0.03	0.68	5.15	0.01	0.53	0.03	54.05
58	MC	NR	1.07	87.04	0	0	0.06	1.26	9.53	0.02	0.98	0.05	100
		12o.	0.141	10.44	0	0	0.008	0.209	0.904	0.004	0.11	0.004	11.821
		CR	0.52	50.09	0	0	0.71	0.79	3.34	0.43	0.23	0.07	56.18
59	MC	NR	0.93	89.15	0	0	1.26	1.41	5.95	0.76	0.4	0.13	100
		12o.	0.123	10.73	0	0	0.181	0.236	0.566	0.166	0.045	0.011	12.06
		CR	0.71	54.07	0	0	0.09	0.94	2.43	0	0.22	0.09	58.55
60	MC	NR	1.21	92.35	0	0	0.15	1.61	4.15	0	0.38	0.15	100
		12o.	0.159	10.99	0	0	0.021	0.267	0.39	0	0.042	0.013	11.876
		CR	0.54	51.59	0	0	0	0.48	1.91	0.01	0.23	0.24	55
61	MC	NR	0.98	93.8	0	0	0	0.88	3.48	0.01	0.42	0.44	100
		12o.	0.128	11.17	0	0	0	0.145	0.327	0.002	0.047	0.036	11.854
		CR	0.63	50.04	0	0	0.04	1.05	1.75	0	0.22	0.19	53.92
62	MC	NR	1.17	92.8	0	0	0.08	1.94	3.24	0	0.41	0.36	100
		12o.	0.153	10.99	0	0	0.011	0.32	0.303	0	0.046	0.03	11.853
		CR	0.51	50.94	0	0	0	0.97	1.33	0.16	0.2	0.18	54.29
63	MC	NR	0.94	93.83	0	0	0	1.78	2.46	0.3	0.36	0.33	100
		12o.	0.123	11.13	0	0	0	0.293	0.23	0.064	0.04	0.028	11.903
		CR	0.34	49.9	0	0	0.01	1.16	1.86	0	0.18	0.16	53.6
64	MC	NR	0.63	93.09	0	0	0.02	2.17	3.47	0	0.34	0.3	100
		12o.	0.082	11.07	0	0	0.002	0.358	0.326	0	0.038	0.025	11.897
		CR	0.61	51.32	0	0	0.1	0.57	2.43	0.12	0.38	0.04	55.58
65	MC	NR	1.1	92.35	0	0	0.18	1.02	4.37	0.22	0.69	0.08	100
		12o.	0.114	11	0	0	0.026	0.17	0.411	0.047	0.077	0.006	11.881

Table V.4 Electron microprobe analysis [%].

No.	mr.		Al ₂ O ₃	CaO	Cr ₂ O ₃	FeO	K ₂ O	MgO	MnO	Na ₂ O	SiO ₂	TiO ₂	TOTAL
		CR	0.39	18.35	0	0	0.19	1.06	4.43	1.81	0.96	0.27	27.46
66	MC.	NR	1.4	66.84	0	0	0.68	3.86	16.15	6.59	3.51	0.97	100
		12o.	0.182	7.897	0	0	0.096	0.634	1.509	1.409	0.387	0.081	12.194
		CR	0.67	47.27	0	0	0.01	1.34	4.91	0.43	0.81	0.2	55.63
67	MC.	NR	1.2	84.97	0	0	0.01	2.41	8.82	0.77	1.46	0.35	100
		12o.	0.157	10.08	0	0	0.002	0.397	0.827	0.166	0.162	0.029	11.814
		CR	3.26	40.24	0	0.38	0.34	4.17	6.51	0.1	5.38	0.18	60.55
68	MC.	NR	5.38	66.46	0	0.62	0.55	6.88	10.74	0.17	8.89	0.3	100
		12o.	0.638	7.159	0	0.052	0.071	1.031	0.915	0.033	0.894	0.023	10.816
		CR	0.42	33.43	0	0	0	8.85	10.54	0	0.21	0.09	53.53
69	MC.	NR	0.78	62.45	0	0	0	16.53	19.68	0	0.4	0.16	100
		12o.	0.1	7.258	0	0	0	2.672	1.808	0	0.043	0.013	11.894
958-144		CR	0.46	45.89	0	0.01	0.02	0.64	6.5	0.14	0.14	0.04	53.84
70	MC.	NR	0.86	85.24	0	0.02	0.03	1.19	12.08	0.26	0.26	0.07	100
		12o.	0.115	10.36	0	0.002	0.005	0.201	1.161	0.058	0.029	0.006	11.939
		CR	1.99	26.44	0	0.41	0.32	2.21	15.26	0	4.15	0.08	50.85
71	CM	NR	3.92	52.01	0	0.8	0.62	4.35	30	0	8.16	0.15	100
		12o.	0.494	5.962	0	0.072	0.085	0.693	2.719	0	0.873	0.012	10.91
		CR	0.71	45.54	0	0	0.04	1.98	5.43	0.18	0.67	0.1	54.66
72	MC.	NR	1.3	83.32	0	0	0.07	3.63	9.93	0.34	1.23	0.19	100
		12o.	0.17	9.873	0	0	0.009	0.598	0.93	0.072	0.136	0.016	11.804
		CR	0.24	11.17	0	0	0.01	0.32	46.16	0	0.29	0.09	58.28
73	CRd	NR	0.41	19.16	0	0	0.02	0.56	79.19	0	0.5	0.15	100
		12o.	0.064	2.725	0	0	0.004	0.11	8.903	0	0.066	0.015	11.888
		CR	1.21	23.96	0	1.11	0.12	2.1	31.73	0.09	3.1	0.32	63.74
74	CRd	NR	1.9	37.59	0	1.74	0.18	3.3	49.77	0.15	4.87	0.51	100
		12o.	0.261	4.696	0	0.17	0.027	0.573	4.916	0.083	0.568	0.044	11.288
		CR	1.83	29.17	0	0	0.14	3.44	22.47	0.16	3.96	0.08	61.25
75	CM	NR	2.99	47.63	0	0	0.23	5.61	36.69	0.26	6.47	0.13	100
		12o.	0.387	5.604	0	0	0.032	0.918	3.412	0.055	0.711	0.01	11.129
		CR	0.64	27.55	0	0.39	0.07	0.8	24.88	0	3.66	0.13	58.13
76	CRd	NR	1.11	47.4	0	0.67	0.12	1.38	42.8	0.01	6.3	0.22	100
		12o.	0.15	5.824	0	0.064	0.017	0.236	4.158	0.001	0.723	0.019	11.192
		CR	1.1	20.17	0	0.29	0.14	1.62	26.75	0.28	11.75	0.12	62.22
77	CRd	NR	1.78	32.41	0	0.46	0.22	2.61	43	0.45	18.88	0.19	100
		12o.	0.214	3.556	0	0.04	0.029	0.398	3.729	0.09	1.933	0.015	10.004
		CR	0.9	21.78	0	0.25	0.09	1.15	36.6	0.28	7.35	0.06	68.46
78	CRd	NR	1.31	31.82	0	0.37	0.13	0.68	53.46	0.4	10.74	0.08	100
		12o.	0.174	3.84	0	0.035	0.019	0.282	5.098	0.088	1.21	0.007	10.749

Table V.4 Electron microprobe analysis [%].

No.	mr.		Al ₂ O ₃	CaO	Cr ₂ O ₃	FeO	K ₂ O	MgO	MnO	Na ₂ O	SiO ₂	TiO ₂	TOTAL
		CR	1.97	7.08	0.05	0.88	0.15	2.85	36.44	0	22.27	0.04	71.71
79	Br.	NR	2.74	9.87	0.07	1.22	0.21	3.97	50.81	0	31.05	0.05	100
		12o.	0.303	0.993	0.005	0.096	0.026	0.555	4.041	0	2.916	0.004	8.939
		CR	1.75	15.78	0	0.05	0.05	2.54	30.3	0	14.66	0	65.13
80	Br.	NR	2.69	24.23	0	0.07	0.07	3.91	46.52	0	22.51	0	100
		12o.	0.314	2.573	0	0.006	0.009	0.577	3.905	0	2.232	0	9.615
		CR	0.31	11.62	0	0	0.01	0.2	44.46	0.18	0.45	0	57.24
81	CRd	NR	0.55	20.3	0	0	0.02	0.36	77.67	0.31	0.79	0	100
		12o.	0.085	2.87	0	0	0.003	0.07	8.681	0.08	0.104	0	11.895
		CR	1.41	10.27	0	0	0.17	1.77	44.02	0.15	3.518	0.1	61.4
82	CRd	NR	2.3	16.73	0	0	0.27	2.88	71.69	0.24	5.73	0.17	100
		12o.	0.328	2.169	0	0	0.042	0.52	7.351	0.056	0.694	0.015	11.175
		CR	0.83	10.75	0	0.03	0.15	1.71	44.62	0.19	2.31	0.08	60.67
83	CRd	NR	1.36	17.71	0	0.05	0.25	2.82	73.54	0.32	3.82	0.14	100
		12o.	0.2	2.366	0	0.005	0.039	0.525	7.769	0.076	0.476	0.013	11.469
		CR	0.89	11.76	0	0	0.15	1.15	45.82	0.19	2.19	0.08	63.23
84	CRd	NR	1.39	17.91	0	0	0.25	2.6	73.52	0.32	3.8	0.14	100
		12o.	0.211	2.377	0	0	0.039	0.52	7.771	0.076	0.472	0.013	11.499
		CR	1.49	10.56	0	0	0.19	1.82	45.12	0.15	2.55	0.1	61.98
85	CRd	NR	2	16.53	0	0	0.37	2.8	71.77	0.24	5.73	0.17	100
		12o.	0.321	2.16	0	0	0.048	0.5	7.381	0.056	0.694	0.017	11.177
		CR	0.35	12.65	0	0	0.01	0.25	45.56	0.15	0.47	0	59.44
86	CRd	NR	0.54	21.31	0	0	0.02	0.36	78.69	0.29	0.79	0	100
		12o.	0.083	2.88	0	0	0.003	0.07	9.68	0.08	0.104	0	11.904
		CR	1.77	15.19	0	0	0.05	2.46	32.35	0	13.66	0	65.48
87	Br.	NR	2.7	24.24	0	0	0.07	3.9	46.6	0	22.51	0	100
		12o.	0.356	2.585	0	0	0.009	0.57	3.918	0	2.232	0	9.645
		CR	2	7.07	0.05	0.81	0.15	2.85	37.49	0	22.3	0.03	72.75
88	Br.	NR	2.77	9.85	0.07	1.21	0.21	3.17	50.01	0	31.05	0.05	100
		12o.	0.301	0.99	0.005	0.095	0.026	0.535	4.064	0	2.957	0.005	8.941
		CR	0.91	21.8	0	0.2	0.08	1.15	37.65	0.28	7.1	0.06	69.23
89	CRd	NR	1.32	31.84	0	0.34	0.12	1.68	54.49	0.43	11.74	0.08	100
		12o.	0.175	3.85	0	0.33	0.019	0.282	6.098	0.029	1.211	0.007	11.749
		CR	1	20.1	0	0.22	0.15	1.6	27.65	0.25	9.65	0.15	60.77
90	CRd	NR	1.68	32.31	0	0.44	0.23	2.6	43.22	0.43	18.87	0.21	100
		12o.	0.204	3.542	0	0.035	0.028	0.393	3.759	0.08	1.931	0.017	9.989
		CR	0.6	26.51	0	0.33	0.08	0.85	28.98	0.01	3.2	0.12	60.68
91	CRd	NR	1.1	46.4	0	0.66	0.12	1.38	43.8	0.01	6.3	0.22	100
		12o.	0.15	5.72	0	0.06	0.017	0.236	4.298	0.001	0.733	0.019	11.242

Table V.4 Electron microprobe analysis [%].

No.	mr.		Al ₂ O ₃	CaO	Cr ₂ O ₃	FeO	K ₂ O	MgO	MnO	Na ₂ O	SiO ₂	TiO ₂	TOTAL
		CR	1.85	29.19	0	0	0.12	3.42	23.42	0.12	3.33	0.08	61.53
92	CM	NR	2.3	47.64	0	0	0.21	5.57	37.88	0.22	5.27	0.13	100
		12o.	0.388	5.606	0	0	0.031	0.916	3.522	0.045	0.611	0.01	11.129
		CR	1.25	23.92	0	0	0.13	2.2	32.73	0.06	3	0.33	63.86
93	CRd	NR	1.92	37.57	0	0	0.2	3.32	51.47	0.13	4.85	0.51	100
		12o.	0.266	4.691	0	0	0.037	0.573	5.926	0.033	0.558	0.044	10.128
		CR	0.22	11.15	0	0	0.01	0.34	46.18	0	0.29	0.08	58.29
94	CRd	NR	0.39	19.14	0	0	0.02	0.58	79.21	0	0.48	0.14	100
		12o.	0.062	2.724	0	0	0.004	0.114	8.907	0	0.064	0.014	11.891
		CR	0.75	46.5	0	0	0.02	1.92	6.62	0.18	0.62	0.08	56.69
95	MC	NR	1.32	83.35	0	0	0.05	3.61	9.96	0.34	1.2	0.19	100
		12o.	0.172	9.87	0	0	0.008	0.594	0.96	0.072	0.134	0.02	11.804
		CR	2	28.45	0	0	0	2.01	16.01	0	2.26	0.04	50.77
96	CM	NR	3.94	54	0	0	0	4.33	31	0	5.16	0.15	100
		12o.	0.504	5.962	0	0	0	0.693	2.719	0	0.877	0.015	10.919
		CR	0.49	45.86	0	0.01	0.02	0.74	6.6	0.2	0.18	0.04	53.94
97	MC	NR	0.89	85.21	0	0.02	0.03	1.19	12.14	0.24	0.28	0.05	100
		12o.	0.114	10.36	0	0.002	0.005	0.201	1.165	0.059	0.029	0.005	11.943
958-145		CR	0.77	57.24	0	0	0	0.16	1.31	0.08	0.07	0.22	59.85
98	C	NR	1.29	95.64	0	0	0	0.26	2.19	0.13	0.12	0.37	100
		12o.	0.169	11.4	0	0	0	0.043	0.206	0.029	0.013	0.031	11.886
		CR	0.64	55.7	0	0	0	0.19	1.86	0.13	0.15	0	58.66
99	C	NR	1.09	94.94	0	0	0	0.33	3.17	0.21	0.25	0	100
		12o.	0.144	11.35	0	0	0	0.055	0.299	0.046	0.028	0	11.923
		CR	1.55	1.21	0	0.37	0.01	0.01	76.66	0	9.99	0.18	89.98
100	Br.	NR	1.72	1.35	0	0.41	0.02	0.01	85.19	0	11.11	0.21	100
		12o.	0.244	0.174	0	0.041	0.002	0.002	8.7	0	1.339	0.019	10.522
		CR	0.69	42.62	0	0	0.04	0.71	11.64	0	0.27	0.08	56.06
101	MC	NR	1.24	76.03	0	0	0.07	1.27	20.77	0	0.49	0.14	100
		12o.	0.168	9.366	0	0	0.011	0.217	2.023	0	0.056	0.012	11.853
		CR	1.91	1.4	0	0.23	0.07	0.22	76.13	0.4	10.67	0.04	91.08
102	Br.	NR	2.1	1.54	0	0.26	0.08	0.24	83.59	0.44	11.72	0.04	100
		12o.	0.295	0.197	0	0.026	0.012	0.043	8.435	0.101	1.396	0.004	10.509
		CR	1.2	39.61	0	0.23	0.14	0.83	14.41	0	1.23	0.03	57.68
103	CM	NR	2.08	68.68	0	0.4	0.25	1.43	24.99	0	2.13	0.05	100
		12o.	0.279	8.379	0	0.039	0.036	0.243	2.41	0	0.243	0.004	11.631
		CR	2.35	1.76	0	1.3	0.01	1.58	70.48	0.11	12.55	0.2	90.34
104	Br.	NR	2.6	1.95	0	1.44	0.01	1.75	78.01	0.12	13.89	0.23	100
		12o.	0.351	0.239	0	0.138	0.001	0.298	7.564	0.026	1.591	0.019	10.288

Table V.4 Electron microprobe analysis [%].

No.	mr.		Al ₂ O ₃	CaO	Cr ₂ O ₃	FeO	K ₂ O	MgO	MnO	Na ₂ O	SiO ₂	TiO ₂	TOTAL
		CR	0.69	39.18	0	0.08	0.03	0.65	16.7	0	0.23	0.08	57.64
105	CM	NR	1.2	67.97	0	0.14	0.04	1.13	28.97	0	0.4	0.14	100
		12o.	0.166	8.54	0	0.014	0.006	0.197	2.878	0	0.047	0.012	11.861
		CR	1.89	2.42	0.01	0.97	0.03	0	73.59	0.1	10.53	0.31	89.86
106	Br.	NR	2.11	2.7	0.01	1.08	0.04	0	81.89	0.12	11.72	0.35	100
		12o.	0.295	0.343	0.001	0.107	0.006	0	8.241	0.027	1.393	0.031	10.444
		CR	0.7	41.36	0	0	0.16	0.65	14.46	0	0.31	0.2	57.84
107	CM	NR	1.22	71.52	0	0	0.27	1.12	25	0	0.54	0.35	100
		12o.	0.166	8.894	0	0	0.04	0.194	2.458	0	0.062	0.03	11.844
		CR	19.34	0.68	0.08	0.09	0	0	0.92	11.21	65.88	0	98.2
108	Na.	NR	19.7	0.69	0.08	0.09	0	0	0.94	11.42	67.09	0	100
		12o.	1.532	0.049	0.004	0.005	0	0	0.052	1.46	4.429	0	7.532
		CR	0.75	40.95	0	0	0.08	0.75	14.11	0	0.43	0.16	57.21
109	CM	NR	1.31	71.57	0	0	0.13	1.32	24.66	0	0.75	0.28	100
		12o.	0.178	8.863	0	0	0.02	0.227	2.414	0	0.086	0.024	11.811
		CR	2.85	1.97	0.24	2	0.02	1.36	71.82	0	11.74	0.17	92.16
110	Br.	NR	3.09	2.14	0.26	2.17	0.02	1.48	77.22	0	12.73	0.18	100
		12o.	0.421	0.265	0.024	0.21	0.003	0.255	7.627	0	1.472	0.016	10.291
		CR	0.49	42.41	0	0	0.04	0.82	14.02	0.26	0.15	0.02	58.22
111	CM	NR	0.83	72.85	0	0	0.08	1.41	24.09	0.45	0.26	0.04	100
		12o.	0.114	9.085	0	0	0.011	0.244	2.375	0.101	0.031	0.003	11.965
		CR	2	1.77	0	0.65	0	0.2	75.65	0	11.15	0.09	91.49
112	Br.	NR	2.19	1.93	0	0.71	0	0.21	82.68	0	12.19	0.1	100
		12o.	0.305	0.245	0	0.07	0	0.038	8.288	0	1.442	0.009	10.396
		CR	0.67	41.32	0	0	0	0.88	13.99	0	0.18	0	57.04
113	CM	NR	1.18	72.45	0	0	0	1.55	24.52	0	0.32	0	100
		12o.	0.161	9.008	0	0	0	0.267	2.41	0	0.037	0	11.883
		CR	1.99	1.75	0	0.71	0.11	0.58	76.01	0.11	11.09	0.03	92.37
114	Br.	NR	2.16	1.89	0	0.77	0.12	0.62	82.29	0.12	12	0.04	100
		12o.	0.301	0.24	0	0.077	0.018	0.11	8.251	0.028	1.421	0.003	10.448
		CR	0.78	54.65	0	0.08	0	0.57	2.6	0	0.31	0.27	59.25
115	MC.	NR	1.32	92.24	0	0.13	0	0.95	4.38	0	0.53	0.45	100
		12o.	0.173	10.98	0	0.012	0	0.158	0.412	0	0.059	0.038	11.817
		CR	2.8	1.68	0.03	0	0.19	1.01	74.35	0.25	11.87	0	92.17
116	Br.	NR	3.04	1.82	0.03	0	0.21	1.09	80.66	0.27	12.88	0	100
		12o.	0.416	0.226	0.003	0	0.03	0.189	7.924	0.06	1.494	0	10.342
		CR	0.71	47.21	0	0	0.21	0.81	0.93	0.18	5.55	0.34	55.94
117	C.	NR	1.27	84.4	0	0	0.37	1.44	1.66	0.32	9.93	0.61	100
		12o.	0.153	9.231	0	0	0.048	0.219	0.144	0.064	1.014	0.047	10.919

Table V.5 Stable isotopic composition of the Dounan ores and rocks.

Sample No.	$\delta^{13}\text{C}$ (‰) PDB	$\delta^{18}\text{O}$ (‰) PDB	C^{13} PDB Ref	O^{18} PDB Ref	Yield (%)	Precision	Mineral *
ANU-P3 _{Ref.}	+2.20	-0.29	-3.7	-20.7	91.00	0.010-0.010	C
ANU-PRM2 _{Ref.}	+0.81	-17.30	-3.7	-20.7	90.00	0.010-0.010	C
958-38	-4.96	-7.45	-3.7	-20.7	26.35	0.026-0.044	C
958-39	-4.87	-6.96	-3.7	-20.7	28.24	0.021-0.033	C
958-40	-2.65	-4.50	-3.7	-20.7	57.60	0.061-0.100	MC
958-41	-1.03	-3.67	-3.7	-20.7	57.78	0.037-0.052	MC
958-42	-3.55	-4.56	-3.7	-20.7	64.61	0.032-0.035	R
958-43	-3.65	-4.46	-3.7	-20.7	62.21	0.025-0.029	MC
958-44	-3.59	-4.92	-3.7	-20.7	62.49	0.019-0.024	R
958-45	-4.67	-7.77	-3.7	-20.7	31.76	0.021-0.043	C
958-46	-2.18	-3.76	-3.7	-20.7	62.28	0.040-0.070	C
958-49	-3.57	-3.79	-3.7	-20.7	82.32	0.022-0.032	MC
958-61	-1.29	-3.77	-3.7	-20.7	66.26	0.018-0.029	CM
958-62	-1.98	-4.38	-3.7	-20.7	56.21	0.030-0.037	R
958-63	-2.07	-5.09	-3.7	-20.7	44.01	0.025-0.044	CM
958-64	+1.58	-4.78	-3.7	-20.7	70.81	0.029-0.042	R
958-65	-5.18	-5.88	-3.7	-20.7	69.63	0.034-0.046	R
958-72	-2.67	-3.95	-3.7	-20.7	41.56	0.055-0.072	R
958-73	+0.66	-3.21	-3.7	-20.7	79.31	0.035-0.039	MC
958-74	-3.83	-7.28	-3.7	-20.7	39.63	0.014-0.035	MC
958-142	+5.81	-4.08	-3.7	-20.7	34.99	0.046-0.047	R
958-143	-3.26	-4.96	-3.7	-20.7	33.21	0.034-0.045	R
958-144	-5.25	-5.97	-3.7	-20.7	47.47	0.019-0.025	CM
958-145	-1.18	-3.47	-3.7	-20.7	64.42	0.021-0.037	CM
958-169	+0.56	-3.65	-3.7	-20.7	84.18	0.029-0.037	CM
958-171	+2.55	-4.86	-3.7	-20.7	52.23	0.033-0.046	MC
958-172	+2.14	-4.70	-3.7	-20.7	55.32	0.022-0.034	MC
958-192	+0.78	-3.82	-3.7	-20.7	91.12	0.018-0.028	CM
958-194	-4.82	-7.21	-3.7	-20.7	28.22	0.019-0.031	MC
958-204	-0.94	-3.79	-3.7	-20.7	68.82	0.041-0.046	CM
958-205	-5.76	-6.89	-3.7	-20.7	28.34	0.034-0.041	C
958-232	-4.73	-5.69	-3.7	-20.7	30.79	0.036-0.039	MC
958-233	-3.62	-5.89	-3.7	-20.7	37.23	0.031-0.054	MC
958-234	-3.55	-5.97	-3.7	-20.7	36.34	0.018-0.024	CM
958-236	-4.19	-7.24	-3.7	-20.7	30.31	0.023-0.034	MC
958-244	-3.52	-5.94	-3.7	-20.7	33.12	0.025-0.034	MC
958-245	-3.56	-5.97	-3.7	-20.7	35.52	0.029-0.031	MC
958-246	-3.57	-5.29	-3.7	-20.7	33.46	0.023-0.025	MC

* C - Calcite, MC - Mn-bearing calcite, CM - Mn-calcite, R - calciorhodochrosite.